frontiers | Research Topics

Strategies to overcome metabolic syndrome and related diseases

Edited by
Lin Zhu, Curtis C. Hughey and Bakovic Marica

Coordinated by
William J. Massey

Published in
Frontiers in Physiology
Frontiers in Pharmacology

ISSN 1664-8714
ISBN 978-2-8325-5556-9
DOI 10.3389/978-2-8325-5556-9

About Frontiers

Frontiers is more than just an open access publisher of scholarly articles: it is a pioneering approach to the world of academia, radically improving the way scholarly research is managed. The grand vision of Frontiers is a world where all people have an equal opportunity to seek, share and generate knowledge. Frontiers provides immediate and permanent online open access to all its publications, but this alone is not enough to realize our grand goals.

Frontiers journal series

The Frontiers journal series is a multi-tier and interdisciplinary set of open-access, online journals, promising a paradigm shift from the current review, selection and dissemination processes in academic publishing. All Frontiers journals are driven by researchers for researchers; therefore, they constitute a service to the scholarly community. At the same time, the *Frontiers journal series* operates on a revolutionary invention, the tiered publishing system, initially addressing specific communities of scholars, and gradually climbing up to broader public understanding, thus serving the interests of the lay society, too.

Dedication to quality

Each Frontiers article is a landmark of the highest quality, thanks to genuinely collaborative interactions between authors and review editors, who include some of the world's best academicians. Research must be certified by peers before entering a stream of knowledge that may eventually reach the public - and shape society; therefore, Frontiers only applies the most rigorous and unbiased reviews. Frontiers revolutionizes research publishing by freely delivering the most outstanding research, evaluated with no bias from both the academic and social point of view. By applying the most advanced information technologies, Frontiers is catapulting scholarly publishing into a new generation.

What are Frontiers Research Topics?

Frontiers Research Topics are very popular trademarks of the *Frontiers journals series*: they are collections of at least ten articles, all centered on a particular subject. With their unique mix of varied contributions from Original Research to Review Articles, Frontiers Research Topics unify the most influential researchers, the latest key findings and historical advances in a hot research area.

Find out more on how to host your own Frontiers Research Topic or contribute to one as an author by contacting the Frontiers editorial office: frontiersin.org/about/contact

Strategies to overcome metabolic syndrome and related diseases

Topic editors

Lin Zhu — Vanderbilt University Medical Center, United States

Curtis C. Hughey — University of Minnesota Twin Cities, United States

Bakovic Marica — University of Guelph, Canada

Topic coordinator

William J. Massey — Lerner Research Institute, Cleveland Clinic, United States

Citation

Zhu, L., Hughey, C. C., Marica, B., Massey, W. J., eds. (2025). *Strategies to overcome metabolic syndrome and related diseases*. Lausanne: Frontiers Media SA. doi: 10.3389/978-2-8325-5556-9

Table of contents

frontiers | Frontiers in Physiology

TYPE Editorial
PUBLISHED 02 October 2024
DOI 10.3389/fphys.2024.1501333

OPEN ACCESS

EDITED AND REVIEWED BY
John D. Imig,
University of Arkansas for Medical Sciences, United States

*CORRESPONDENCE
Lin Zhu,
lin.zhu@vumc.org

RECEIVED 24 September 2024
ACCEPTED 26 September 2024
PUBLISHED 02 October 2024

CITATION
Zhu L, Hughey CC, Bakovic M and Massey WJ (2024) Editorial: Strategies to overcome metabolic syndrome and related diseases. *Front. Physiol.* 15:1501333. doi: 10.3389/fphys.2024.1501333

Editorial: Strategies to overcome metabolic syndrome and related diseases

Lin Zhu[1]*, Curtis C. Hughey[2], Marica Bakovic[3] and William J. Massey[4,5]

[1]Division of Endocrinology, Metabolism, and Diabetes, Department of Medicine, Vanderbilt University Medical Center, Nashville, TN, United States, [2]Division of Molecular Medicine, Department of Medicine, University of Minnesota Twin Cities, Minneapolis, MN, United States, [3]Department of Human Health and Nutrition Sciences, College of Biological Science, University of Guelph, Guelph, ON, Canada, [4]Department of Inflammation and Immunity, Lerner Research Institute, Cleveland Clinic, Cleveland, OH, United States, [5]Center for Microbiome and Human Health, Lerner Research Institute, Cleveland Clinic, Cleveland, OH, United States

KEYWORDS

metabolic syndrome (MetS), cardiovascular disease, hypertension, obesity, lipodystrophy, physical activities, adipose tissues

Editorial on the Research Topic
Strategies to overcome metabolic syndrome and related diseases

Metabolic syndrome (MetS) is a cluster of conditions that include increased blood pressure, elevated blood glucose, central obesity, hyperlipidemia, and low HDL cholesterol content (Liang et al., 2021). The diagnosis of MetS requires the presence of three or more of those metabolic conditions. MetS-related diseases include type 2 diabetes, cardiovascular disease, cognitive dysfunction, stroke, and cancers. According to the United States National Health and Nutrition Examination Survey (NHANES) 2011–2018, MetS prevalence increased from 37.6% in 2011–2012 to 41.8% in 2017–2018 among adults aged 20 years or older (Liang et al., 2021). This rising prevalence is concerning because MetS and related diseases would decrease individual life quality and burden the healthcare system (Grundy, 2008). Furthermore, current therapeutic interventions, including pharmaceutical agents and lifestyle modification, mitigate but do not abolish all components of MetS and its co-morbidities. This limitation highlights the importance of improving our understanding of the underlying mechanisms and targets for improving MetS. Welcome to the present Research Topic, which assembles 15 articles, including five review papers, covering nutritional interventions in animal models, clinical trials for management of dyslipidemia, epidemiologic studies regarding environmental factors, and the current understanding of molecular pathways.

It has been reported that up to 87% of individuals with MetS have dyslipidemia (Toh and Lee, 2020). Given this, research into the key factors regulating lipid homeostasis in MetS and its comorbidities has received a vast amount of attention. In this Research Topic, Nauli et al. Explored the effects of sex hormones on the size of intestinal lipoproteins that carry dietary lipids to the periphery (Nauli et al.). Compared to women, men are more prone to central obesity, one of the five conditions that comprise MetS. Using the conscious lymph fistula mouse model, the authors discovered that male mice produced larger intestinal lipoproteins than female mice when intraduodenally infused with lipid emulsion (Nauli et al.). Larger lipoproteins may contribute to central obesity by facilitating increased fat

uptake in visceral abdominal adipose tissue. Further investigations leveraging the Caco-2 cell model showed that testosterone significantly increased the size of lipoproteins in a dose-dependent manner (Nauli et al.). Regarding whole-body cholesterol balance, Banerjee et al. reported that, unlike the Aster-B protein, which plays an essential role in cholesterol transport and downstream esterification, the non-vasicular Aster-C protein (encoded by Gramd1c gene) played a minor role in whole-body cholesterol balance in a sophisticated study including divergent dietary cholesterol and Gramd1c knockout mouse model (Banerjee et al.). The gut hormone glucagon-like peptide-2 (GLP-2) has been shown to play pleiotropic roles in regulating lipid handling in the intestine, which is important for maintaining energy homeostasis and cardiometabolic health. In the review by Mukherjee and Xiao, the authors elucidated the mechanisms of GLP-2 in regulating post-prandial lipid absorption and post-absorptive release of intestinally stored lipids (Mukherjee and Xiao). While further summarizing the role of GLP-2 in metabolic disorders, the authors discussed the opportunities to promote health benefits beyond its current clinical use for treating short-bowel syndrome by manipulating GLP-2 mediated pathways (Mukherjee and Xiao).

MetS is closely linked to dysregulated energy homeostasis. Engaging in daily physical activities has become the first choice in clinics for managing MetS. Physical activities are well known for body weight management by promoting energy expenditure. However, the impact of physical activities on CVD-related HDL function has yet to be further studied. In a human study including healthy lean, obese, and type 2 diabetic subjects, Zhu et al. demonstrated that a short-term high-intensity interval training (HIIT) program improved HDL function depending on metabolic contexts, correlating with improvements in blood lipid profile (Zhu et al.). This study showed that triacylglycerol content in HDL particles may negatively affect the anti-atherogenic function of HDL (Zhu et al.). Furthermore, Sadler et al. quantified the impact of protonophore treatment on whole-body energetics in mice housed at 30°C, a thermoneutral housing that may mask the effects of anti-obesity strategies on energy expenditure (Sadler et al.). They observed that mice housed at 30°C showed reduced basal energy expenditure compared to 24°C controls, and protonophore treatment markedly increased energy expenditure, resulting in reduced adiposity in mice housed at 30°C (Sadler et al.). Nicotinamide N-methyltransferase (NNMT) is involved in energy expenditure by lowering NAD^+ content via catalyzing the methylation of nicotinamide. Sun et al. reviewed the current understanding of the role of NNMT in MetS (Sun et al.). Single nucleotide variants in the NNMT gene are significantly correlated with disturbances in energy metabolism; elevated NNMT gene expression is notably observed in the liver and white adipose tissues of obese individuals (Sun et al.). In animal models, knockdown NNMT expression with RNAi strategies or small molecule inhibitors improved MetS-related diseases (Sun et al.).

Lipodystrophy syndromes are rare diseases, and delays in diagnosis may predispose to the development of severe metabolic complications and end-organ damage. A rapid action plan was developed by Fourman et al. using insights gathered through a series of advisory meetings with clinical experts from multiple countries (Fourman et al.). The Rapid Action Plan includes clinical and family history, physical exams and laboratory criteria, diagnostic tools of imaging and genetic testing, as well as guidelines for the syndrome treatment and management (Fourman et al.). Along with a commentary article by Massey and Zhu, discussions in the Rapid Action Plan highlighted the significant role of adipose tissues in MetS (Fourman et al.; Massey and Zhu). Another clinically relevant research article in this Research Topic is by Bukara-Radujkovic et al. who demonstrated the role of glycemia risk index in managing blood glucose in routine clinical practice by exploring the correlation of traditional parameters, such as HbA1c, and novel parameters, including glycemia risk index and time-in-range, in pediatric patients with type 1 diabetes (Bukara-Radujkovic et al.).

Additionally, Li et al. highlighted the significant role of astrocytes in bridging MetS and cognitive dysfunction (Li et al.). Systemic inflammation and endocrine disruption in MetS may drive neurodegeneration mediated by astrocytes, which sense and integrate metabolic signals with neurological function (Li et al.). In this review, Li and co-authors summarized the alterations in astrocyte phenotypic characteristics in MetS, which could possibly serve as a diagnostic marker or even a therapeutic target for MetS-associated cognitive dysfunction (Li et al.). Furthermore, El-Deen et al. explored the impact of co-administration of apricot kernels and caffeine on MetS in an animal model of diabetes, and Yi et al. showed that acetaminophen administration may improve outcomes in critically ill patients with gout and hypertension (Yi et al.). By analyzing data from the NHANES 2013–2018 survey cycle, Chen et al. observed a negative association between chloroform and type 2 diabetes in older adults in the United States (Chen et al.).

Moreover, Shi reviewed a potential therapeutic target, while Lu et al. reviewed a novel strategy for MetS and related diseases in this Research Topic. Salt-inducible kinases (SIKs) are serine/threonine kinases of the adenosine monophosphate-activated protein kinase family (Shi). Shi summarized the diverse roles of SIKs in sodium sensing and salt intake, vascular remodeling, pulmonary arterial hypertension, cardiac hypertrophy and ischemia, inflammation, fibrosis, and MetS (Shi). Interestingly, SIKs are broadly expressed in relevant metabolic tissues, such as adipose tissues and the liver, and play essential roles in mediating insulin action, lipid metabolism, and energy expenditure (Shi). Pharmaceutical inhibition of SIK activity has shown therapeutic potential in various disease models, including inflammatory and fibrotic diseases (Shi). Genetic variants in SIK genes have also been shown to be linked with alterations in blood lipid panels, however, the potential clinical relevance of SIK for dyslipidemia is yet to be studied further (Shi). Regarding the natural supplements for treating MetS and related diseases, Lu et al. reviewed the role of naringin in treating atherosclerosis (Lu et al.). Naringin is a flavonoid abundantly found in grapefruit and tomatoes. In the liver, naringin can be converted into naringenin by naringinase, which process may be involved in glycemic control (Lu et al.). Lu et al. summarized the anti-atherogenic effects of naringin in lowering blood pressure, improving dyslipidemia, protecting endothelium, and inhibiting vascular smooth muscle cell proliferation and migration (Lu et al.). However, the underlying mechanism is not yet conclusive.

The editor team of this Research Topic would like to thank all the authors, reviewers, and readers who have contributed to this Research Topic. With all your support, we hope this Research Topic may add a piece of the puzzle to the whole picture of MetS while providing a beam of light for future studies in this research field.

Author contributions

LZ: Conceptualization, Writing–original draft, Writing–review and editing. CCH: Writing–review and editing. MB: Writing–review and editing. WM: Writing–review and editing.

Funding

The author(s) declare that financial support was received for the research, authorship, and/or publication of this article. LZ is supported by NIA (K01AG077038). WM is supported by a Cleveland Clinic Global Center for Pathogen and Human Health Research Postdoctoral Fellowship. CCH is supported by the NIDDK (DK136772).

Conflict of interest

The authors declare that the research was conducted in the absence of any commercial or financial relationships that could be construed as a potential conflict of interest.

Publisher's note

References

Grundy, S. M. (2008). Metabolic syndrome pandemic. *Arterioscler. Thromb. Vasc. Biol.* 28, 629–636. doi:10.1161/ATVBAHA.107.151092

Liang, X. P., Or, C. Y., Tsoi, M. F., Cheung, C. L., Cheung, B. M. Y., DoC, P., et al. (2021). The University of Hong Kong, Hong Kong: prevalence of metabolic syndrome in the United States National health and nutrition Examination survey (nhanes) 2011–2018. *Eur. Heart J.* 42. doi:10.1093/eurheartj/ehab724.2420

Toh, S.-A., and Lee, M. H. (2020). "Dyslipidemia in metabolic syndrome," in *metabolic syndrome: a comprehensive textbook ahima* Cham: Springer International Publishing, 1–18.

frontiers | Frontiers in Physiology

TYPE Original Research
PUBLISHED 19 December 2023
DOI 10.3389/fphys.2023.1316982

OPEN ACCESS

EDITED BY
Lin Zhu,
Vanderbilt University Medical Center,
United States

REVIEWED BY
Carrie Wiese,
University of California, Los Angeles,
United States
Katarzyna Piotrowska,
Pomeranian Medical University in
Szczecin, Poland

*CORRESPONDENCE
Andromeda M. Nauli,
andromeda.nauli@wmed.edu

RECEIVED 10 October 2023
ACCEPTED 08 December 2023
PUBLISHED 19 December 2023

CITATION
Nauli AM, Phan A, Tso P and Nauli SM (2023), The effects of sex hormones on the size of intestinal lipoproteins. *Front. Physiol.* 14:1316982. doi: 10.3389/fphys.2023.1316982

The effects of sex hormones on the size of intestinal lipoproteins

Andromeda M. Nauli[1]*, Ann Phan[2], Patrick Tso[3] and Surya M. Nauli[4,5]

[1]Department of Biomedical Sciences, Western Michigan University Homer Stryker M.D. School of Medicine, Kalamazoo, MI, United States, [2]Desert Valley Hospital, Victorville, CA, United States, [3]Department of Pathology and Laboratory Medicine, University of Cincinnati College of Medicine, Cincinnati, OH, United States, [4]Department of Biomedical and Pharmaceutical Sciences, Chapman University, Irvine, CA, United States, [5]Department of Medicine, University of California, Irvine, Irvine, CA, United States

Larger intestinal lipoproteins are more likely to be retained longer in the intestinal wall, allowing more time for their fat to be hydrolyzed and subsequently taken up by the abdominal viscera. Since men generally accumulate more abdominal visceral fat than women, we sought to determine if males produce larger intestinal lipoproteins compared to females. Using the conscious lymph fistula mouse model, we discovered that the male mice indeed produced larger intestinal lipoproteins than the female mice when they were intraduodenally infused with lipid emulsion. We then employed our differentiated Caco-2 cell model with semipermeable membrane system to determine the effects of sex hormones on the size of intestinal lipoproteins. Lipoprotein size was quantitatively measured by calculating the ratio of triglycerides (TG)/Apolipoprotein B (ApoB) and by analyzing their transmission electron micrographs. Our studies showed that while there was no dose-dependent effect of estrogen and progesterone, testosterone significantly increased the size of lipoproteins. When these hormones were combined to resemble the physiological concentrations observed in males and the different ovarian cycle phases in premenopausal females, both the male and luteal groups had significantly larger lipoproteins than the ovulatory group; and the male group also had significantly larger lipoproteins than the follicular group. The ovulatory group secreted a significantly lower amount of TG than the male and luteal groups. ApoB was comparable among all these groups. These findings support our hypothesis that, through their testosterone effects, males are more likely to produce larger intestinal lipoproteins. Larger lipoproteins tend to remain longer in the intestinal wall and may facilitate fat uptake preferentially by the abdominal viscera. Our studies may partly explain why men are more prone to accumulating abdominal visceral fat, which is an independent predictor of mortality.

KEYWORDS

digestion, fat, gender, chylomicron, gut, absorption, VLDL, testosterone

Abbreviations: ANOVA, analysis of variance; ApoB, apolipoprotein B; Caco-2, cancer coli-2; DMEM, Dulbecco's Modified Eagle Medium; DMSO, dimethyl sulfoxide; ELISA, enzyme-linked immunosorbent assay; HDL, high-density lipoprotein; LDL, low-density lipoprotein; SE, standard error; TG, triglyceride; VEGF-A, vascular endothelial growth factor A; VLDL, very low-density lipoprotein.

1 Introduction

It is evident that lipid metabolism, cardiovascular risk factors, and body fat distribution differ between men and premenopausal women (Meloni et al., 2023). Compared to men, premenopausal women have a more favorable lipid profile, characterized by lower total cholesterol, lower low-density lipoproteins (LDL), lower TG, and higher high-density lipoproteins (HDL) (Wang et al., 2011). Although LDL constitutes an important cardiovascular risk factor, its significance appears to be greater in men than in women. Conversely, plasma TG appears to be a significant risk factor in women compared to men (Regitz-Zagrosek et al., 2007).

One of the most apparent sex differences lies in the distribution of body fat, with women predominantly storing fat in the subcutaneous depot and men in the abdominal visceral depot (Grauer et al., 1984). Importantly, the accumulation of abdominal visceral fat is key criterion for diagnosing metabolic syndrome (Grundy et al., 2005). Our previous hypothesis proposed that these sex-based disparities in body fat accumulation are partially attributed to differences in dietary fat absorption (Nauli and Matin, 2019). Specifically, larger intestinal lipoproteins tend to remain longer in the intestinal wall (Takahara et al., 2013), allowing more time for the hydrolysis of their fat content and uptake by the abdominal viscera (Harvey et al., 2005; Escobedo et al., 2016). Since men generally accumulate more abdominal visceral fat than women (Grauer et al., 1984), our study aims to ascertain whether males produce larger intestinal lipoproteins than females. Importantly, studies have also shown that men stored more of their ingested fat in the abdominal viscera than women (Marin et al., 1996; Votruba et al., 2007).

Even though men and women had comparable fat intake as percent of total energy (33.6% and 33.5%, respectively), men consumed more total calories (2,504 kcals) than women (1,771 kcals) (Wright and Wang, 2010). Consequently, men consume more total dietary fat than women. As intestinal cells produce larger lipoproteins when challenged with dietary lipid (Nauli et al., 2006; Nauli et al., 2014), this factor alone can explain why men are more prone to producing larger intestinal lipoproteins. The notion that sex hormones can impact intestinal lipid absorption was initially proposed in the late 1970s by Vahouny et al. (1977), Vahouny et al. (1980). Their studies revealed that female rats exhibited higher VLDL protein production compared to that of male rats, even when both sexes were subjected to the same amount of dietary fat. These studies implied that females predominantly utilize VLDL as their primary gut lipoprotein. Notably, both VLDLs and chylomicrons are both the predominant intestinal lipoproteins, with VLDLs being smaller than chylomicrons.

However, the average size of intestinal lipoproteins between males and females has not been directly compared to date. The primary goal of our current studies is to address this gap. Additionally, we aim to investigate the effect of sex hormones on the size of intestinal lipoproteins.

2 Materials and methods

2.1 Animals

Five female and four male C57BL/6 mice were used. All mice were between 4- and 9-month-old. The animal study was reviewed and approved by the Institutional Animal Care and Use Committee at the University of Cincinnati.

2.1.1 Lymph and duodenal cannulation

The intestinal lymph ducts of the anesthetized mice (ketamine, 80 mg/kg and xylazine, 20 mg/kg) were cannulated with polyvinyl chloride tubing as previously described by Bollman et al. (1948). However, we made the following alterations: the suture of the lymph cannula was replaced by cyanoacrylate glue (Krazy Glue, Itasca, IL, United States) and the tubing was inserted into the duodenum through a fundal incision of the stomach. After the surgery, the mice were intraduodenally infused overnight with 5% glucose in saline at a rate of 0.3 mL/h. The 5% glucose in saline solution was replaced with the prepared lipid infusate (see below) the next morning.

2.1.2 Lipid infusion and lymph collection

Triolein (TG), cholesterol, and egg phosphatidylcholine were dissolved in chloroform. The chloroform-lipid mixture was subjected to a gentle stream of nitrogen gas, and the chloroform-free lipid mixture was then emulsified with sodium taurocholate in phosphate-buffered saline (pH 6.4) and sonicated until the solution appeared homogenous. The lipid emulsion was intraduodenally infused at a constant rate of 0.3 mL per hour into the mice for 6 h. The hourly infusate contained 4 μmol triolein, 0.78 μmol cholesterol, 0.78 μmol phosphatidylcholine, and 5.7 μmol sodium taurocholate in phosphate-buffered saline (Nauli et al., 2006). Lymph samples were collected for 1 hour before lipid infusion (fasting lymph) and for another hour during the 6th hour of lipid infusion (6th hour lymph). These two time points were selected because they represent the fasting and postprandial lymph, respectively. Based on our extensive experience in lymph fistula mouse model (Nauli et al., 2006; Liu et al., 2021), the lymphatic TG transport has usually reached the steady state by the 6th hour of lipid infusion. Only negligible quantity of infused TGs remains in the lumen of the small intestine and colon at the end of our lipid infusion, indicating that almost all of our infused TGs are hydrolyzed and taken up by the enterocytes.

At the end of the 6-h lipid infusion, the estrous cycle of the female animals was determined by vaginal smear/cytology. Afterwards, all the animals were euthanized.

2.1.3 Imaging analysis of the size of intestinal lipoproteins from female and male mice

Both the fasting (not diluted) and 6th hour lymph samples (diluted 1:4 (v/v) with sterile water) were overlaid with carbon-coated formvar film on a 400-mesh copper grid. After drying them with filter paper, the grids were added with 2% phosphotungstic acid (pH 6.0) and redried with filter paper. The samples were then subsequently examined by using a transmission electron microscope (JEOL JEM-1230), and the representative images were captured (Nauli and Whittimore, 2015). The size of the lipoprotein particles (approximately 800 particles per lymph sample) was measured by using Adobe Photoshop software. Unfortunately, analyzing and capturing transmission electron micrographs of intestinal

TABLE 1 The combinations of sex hormones that represent men and different phases of ovarian cycle. Caco-2 cells were incubated with different mixtures of estrogen, progesterone, and testosterone to resemble the physiological concentrations in men and different phases of ovarian cycle.

		Estrogen (pg/mL)	Progesterone (ng/mL)	Testosterone (ng/mL)
Female	Follicular	50	0.1	0.3
	Ovulatory	200	1.0	0.3
	Luteal	150	10	0.3
Male		20	0.1	6.0

lipoproteins were cost prohibitive, allowing us to only have limited number of samples.

2.2 Caco-2 cells

Caco-2 (Cancer Coli-2) cells, which were derived from a 72-year-old Caucasian male suffering from colorectal adenocarcinoma (Fogh et al., 1977), have been characterized both biochemically and microscopically for their ability to produce intestinal lipoproteins (Nauli et al., 2014; Nauli and Whittimore, 2015). Other cells lines, including HT-29 cells derived from a female individual, have not been shown to produce intestinal lipoproteins effectively. As such, we were only able to use Caco-2 cells in these experiments. These cells were purchased from the American Type Culture Collection and were grown at 37°C supplemented with 5% CO_2. The growth media consisted of 15% fetal bovine serum in high glucose Dulbecco's Modified Eagle Medium (DMEM). The experiments were conducted using 13-day post-confluent cells grown on the semipermeable membrane system (6-well plates with polycarbonate membrane inserts, 4.67 cm^2 growth area per insert, 1 μm pore).

2.2.1 Co-treatment of Caco-2 cells with lipid mixture and sex hormones

To study the effects of sex hormones on intestinal lipoprotein secretion, prewashed Caco-2 cells were incubated for 4 h with 1.0 mL of prefiltered lipid mixture (2.0 mM oleic acid, 1.36 mM egg-phosphatidylcholine, and 1.0 mM sodium taurocholate in the growth media) in the apical compartment and 2.0 mL of sex hormone-supplemented growth media in the basolateral compartment. All sex hormones were dissolved in dimethyl sulfoxide (DMSO) to achieve their 1,000x concentrations and were then freshly diluted with the growth media to their desired 1x concentrations. As such, DMSO served as our vehicle control and all groups received the same amount of DMSO. The condition used in these experiments (13-day post-confluence, 2.0 mM oleic acid, 1.36 mM egg-phosphatidylcholine, and the 4-h incubation time) has previously been determined to be the most optimal in producing lipoproteins (Nauli et al., 2014; Nauli and Whittimore, 2015).

For the estrogen studies, the following estradiol concentrations were used: 0, 50, 100, and 200 pg/mL. For progesterone: 0, 0.5, 1, and 10 ng/mL. For testosterone: 0, 3, 6, and 9 ng/mL. To better resemble the physiological condition, we also studied the effects of the combination of these 3 hormones according to their reported concentrations in young normal-weight men and women during follicular, ovulatory, and luteal phase (Sherman and Korenman, 1975) (see Table 1).

2.2.2 Biochemical analysis of the lipoprotein size

At the end of the 4-h incubation, basolateral media were collected and subjected to sodium chloride density gradient ultracentrifugation. Briefly, the collected samples were added with sodium chloride and distilled water to bring their density to 1.2 g/mL and volume to 8.0 mL. The 1.2 g/mL density samples were then gently overlaid with 0.5 mL water (density = 1.0 g/mL) and were spun at 65,000 rpm (429,782 × g) for 24 h at 4°C by using the ultracentrifuge T-1270 rotor. The top 0.5 mL lipoprotein fractions were immediately isolated and analyzed.

The isolated fractions were biochemically analyzed for their TG using the Wako L-type Triglyceride M kit and for their ApoB using our previously described enzyme-linked immunosorbent assay (ELISA) (Nauli et al., 2014). Since there is only one molecule of ApoB per lipoprotein particle (Albers et al., 1996), the relative size of intestinal lipoproteins can be indirectly determined by their TG/ApoB ratio.

2.2.3 Imaging analysis of the size of lipoproteins from sex hormone-treated Caco-2 cells

After the fractions were overlaid with carbon-coated formvar film on a 400-mesh copper grid and negatively stained with 2% phosphotungstic acid (pH 6.0), the size of the lipoprotein particles (approximately 200 particles) from the follicular, ovulatory, luteal, and male groups (n = 3 each) were examined using a transmission electron microscope (JEOL 2800). The representative images were captured and analyzed as described above.

2.3 Statistical analysis

The data shown represent the mean ± standard errors (SE). One-way analysis of variance (ANOVA) was used to determine the statistical significance of three groups or more (Figures 3A–C, Figures 4A–C, Figures 5A–C, Figures 6A–C, Figures 7F). Tukey *post hoc* tests were performed to determine which of the groups were significantly different from one another (Figures 6A, 7F). The two-tailed t-test was used for comparison between two groups (Figures 1D, 2D). Statistical analysis was considered significant if $p < 0.05$. All experiments had n ≥ 3

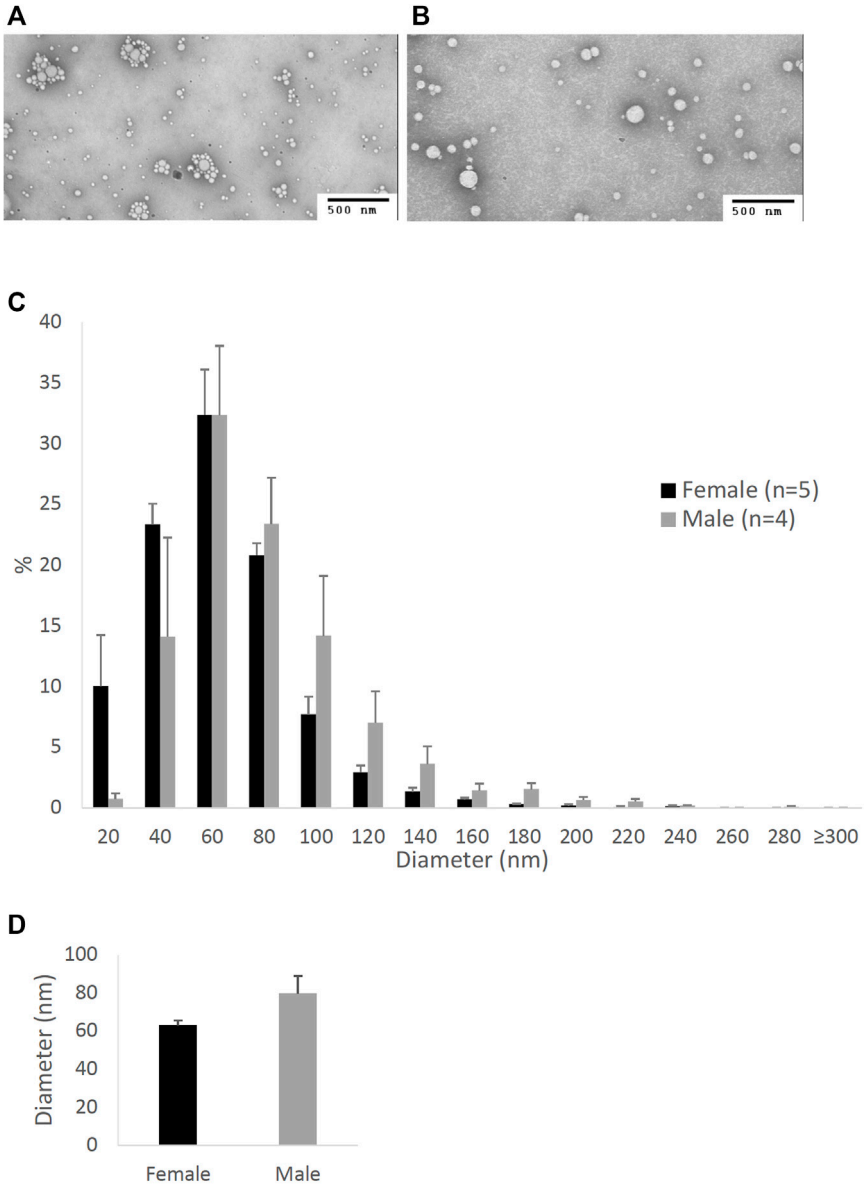

FIGURE 1
Particle size of lipoproteins from the lymph of mice that were intraduodenally infused with glucose/saline solution. Female (n = 5) and male (n = 4) mice were intraduodenally infused with glucose/saline solution and their intestinal lymph was collected for 1 hour. The lipoproteins in the collected lymph were then analyzed by a transmission electron microscope. The representative lipoprotein micrographs of the female **(A)** and male **(B)** mice, their lipoprotein size distribution **(C)**, and their lipoprotein average size **(D)** are depicted. Scale bars are 500 nm. Values are means ± standard errors.

(n represents the total number of inserts for the Caco-2 experiments). To ensure scientific rigor, the Caco-2 experiments were conducted on at least 3 different occasions, i.e., performed on at least 3 different dates.

3 Results

3.1 Lipoprotein size differences between male and female mice during glucose/saline infusion

Figure 1 compares the size of intestinal lipoproteins from the lymph of the male and female mice intraduodenally infused with 5% glucose in saline solution. These fasting lymph samples were collected for 1 hour immediately before lipid emulsion was infused. The representative micrographs of fasting lipoproteins from the female (Figure 1A) and male mice (Figure 1B) are shown. Their lipoprotein size distribution (Figure 1C) shows that female mice (n = 5) produced more lipoproteins with diameters between 20 and 60 nm, whereas male mice (n = 4) produced more lipoproteins larger than 60 nm in diameter. The average diameter of the intestinal lipoproteins of the female mice (63.16 ± 2.46 nm) was not statistically different (p-value = 0.094) from that of the male mice (79.74 ± 9.25 nm) (Figure 1D). Of the 5 female mice, 3 were in estrus, 1 in proestrus, and 1 in diestrus.

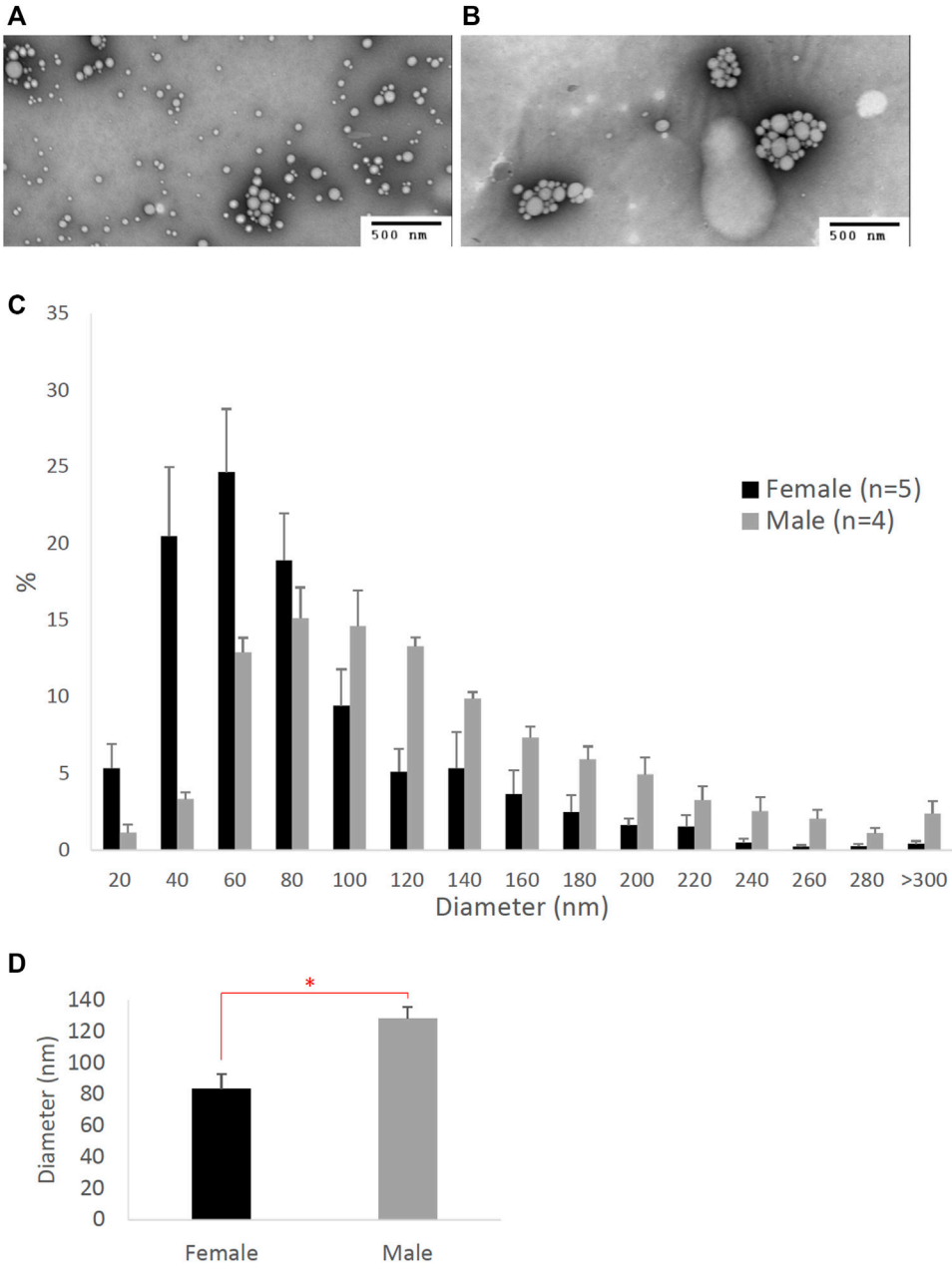

FIGURE 2
Particle size of lipoproteins from the lymph of mice that were intraduodenally infused with lipid emulsion. Female (n = 5) and male (n = 4) mice were intraduodenally infused with lipid emulsion for 6 h and their lipoproteins from the intestinal lymph collected at the 6th hour were analyzed by a transmission electron microscope. The representative lipoprotein micrographs of the female **(A)** and male **(B)** mice, their lipoprotein size distribution **(C)**, and their lipoprotein average size **(D)** are depicted. Scale bars are 500 nm. Values are means ± standard errors. The asterisk sign indicates that p < 0.05 (two-tailed t-test).

3.2 Lipoprotein size differences between male and female mice during lipid infusion

Figure 2 compares the size of intestinal lipoproteins from the 6th-hour lymph of the male and female mice intraduodenally infused with lipid emulsion. As shown, female mice produced smaller intestinal lipoproteins (Figure 2A) than male mice (Figure 2B). Their lipoprotein size distribution (Figure 2C) shows that female mice (n = 5) produced more lipoproteins with diameters between 20 and 80 nm, whereas male mice (n = 4) produced more lipoproteins larger than 80 nm in diameter. As displayed in Figure 2D, the average diameter of the intestinal lipoproteins of the female mice (83.35 ± 9.35 nm) was significantly smaller (p-value = 0.0083) than that of the male mice (128.41 ± 7.28 nm).

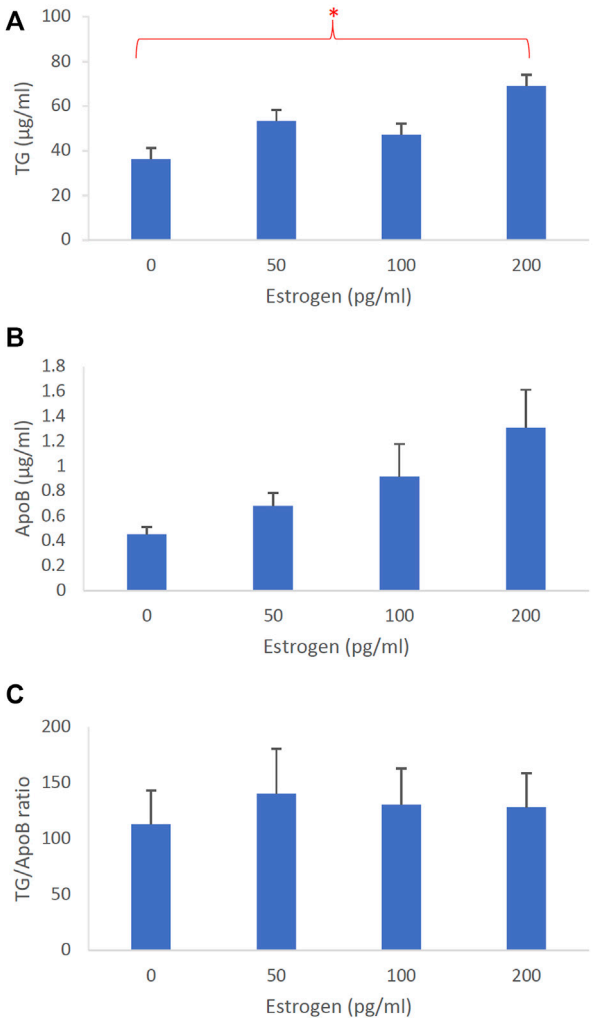

FIGURE 3
The dose-dependent effects of estrogen on intestinal lipoproteins. Using a semipermeable membrane system, the differentiated Caco-2 cells ($n \geq 14$) were incubated for 4 h with lipid mixture in their apical compartment and 0, 50, 100, or 200 pg/mL of estrogen in their basolateral compartment. The lipoproteins were then isolated from their basolateral media by using NaCl gradient ultracentrifugation. The lipoprotein TG **(A)**, ApoB **(B)**, and TG/ApoB ratios **(C)** are depicted. The TG/ApoB ratios represent the sizes of lipoproteins. Values are means ± standard errors. The asterisk sign indicates that $p < 0.05$ (one-way ANOVA).

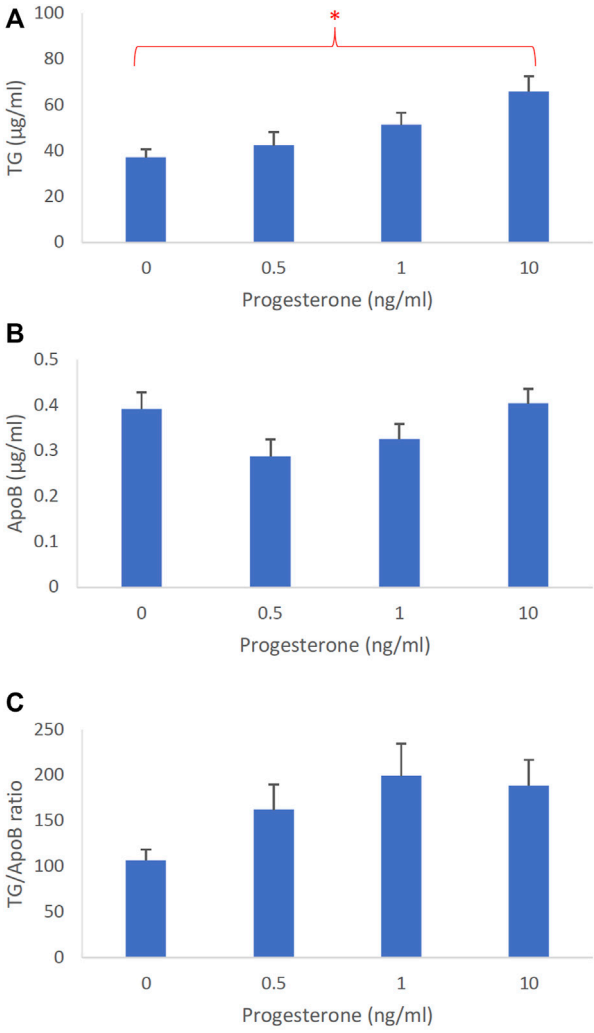

FIGURE 4
The dose-dependent effects of progesterone on intestinal lipoproteins. Using a semipermeable membrane system, the differentiated Caco-2 cells ($n \geq 14$) were incubated for 4 h with lipid mixture in their apical compartment and 0, 0.5, 1, or 10 ng/mL of progesterone in their basolateral compartment. The lipoproteins were then isolated from their basolateral media by using NaCl gradient ultracentrifugation. The lipoprotein TG **(A)**, ApoB **(B)**, and TG/ApoB ratios **(C)** are depicted. The TG/ApoB ratios represent the sizes of lipoproteins. Values are means ± standard errors. The asterisk sign indicates that $p < 0.05$ (one-way ANOVA).

3.3 The dose-dependent effects of sex hormones on TG, ApoB, and TG/ApoB ratio

To determine the effects of sex hormones on the size of intestinal lipoproteins, we utilized our Caco-2 cell model. Figure 3 shows the dose-dependent effects of estrogen on intestinal lipoprotein TG (Figure 3A), ApoB (Figure 3B), and TG/ApoB ratio (Figure 3C) ($n \geq 14$). Estrogen significantly ($p = 0.013$) increased intestinal lipoprotein TG. However, there was a tendency for estrogen to also increase intestinal lipoprotein ApoB ($p = 0.062$). Consequently, the TG/ApoB ratio did not appear to be affected by estrogen ($p = 0.96$), indicating that estrogen did not alter the size of the intestinal lipoproteins. Collectively, these data suggest that estrogen tended to increase the number of lipoprotein particles but did not affect their size ("more of the same size").

The dose-dependent effects of progesterone on intestinal lipoprotein TG, ApoB, and TG/ApoB ratio ($n \geq 14$) are shown in Figures 4A–C, respectively. Progesterone significantly ($p = 0.0026$) increased intestinal lipoprotein TG but did not appear to significantly ($p = 0.064$) affect the ApoB secretion. Since progesterone gradually increased the intestinal lipoprotein TG/ApoB ratios, progesterone was likely capable of increasing–albeit not significantly ($p = 0.086$)–the size of intestinal lipoproteins. These data cooperatively suggest that progesterone tended to increase the size of intestinal lipoproteins by increasing their TG incorporation ("larger but of the same number").

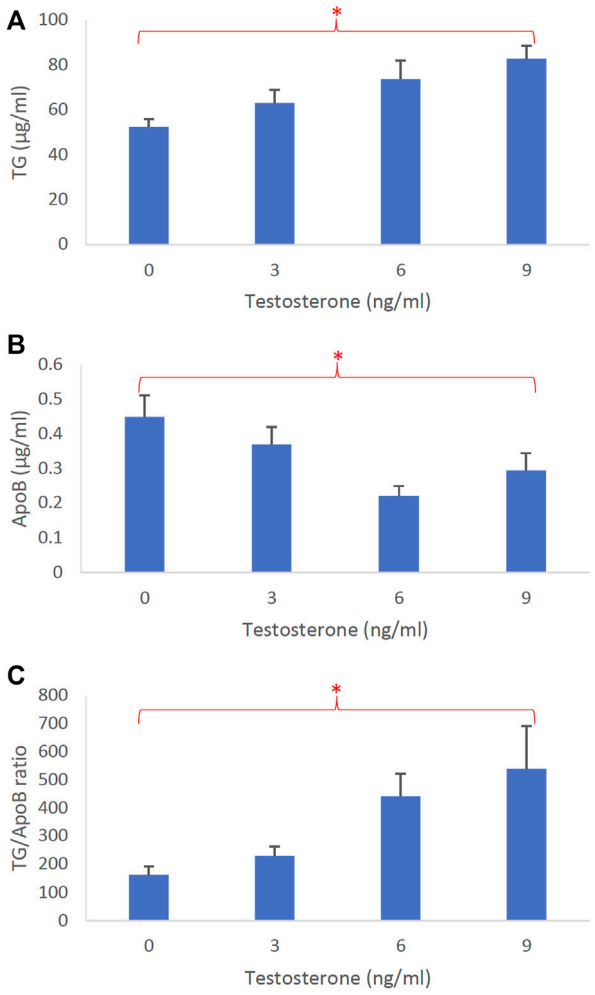

FIGURE 5
The dose-dependent effects of testosterone on intestinal lipoproteins. Using a semipermeable membrane system, the differentiated Caco-2 cells (n ≥ 14) were incubated for 4 h with lipid mixture in their apical compartment and 0, 3, 6, or 9 ng/mL of testosterone in their basolateral compartment. The lipoproteins were then isolated from their basolateral media by using NaCl gradient ultracentrifugation. The lipoprotein TG **(A)**, ApoB **(B)**, and TG/ApoB ratios **(C)** are depicted. The TG/ApoB ratios represent the sizes of lipoproteins. Values are means ± standard errors. The asterisk signs indicate that $p < 0.05$ (one-way ANOVA).

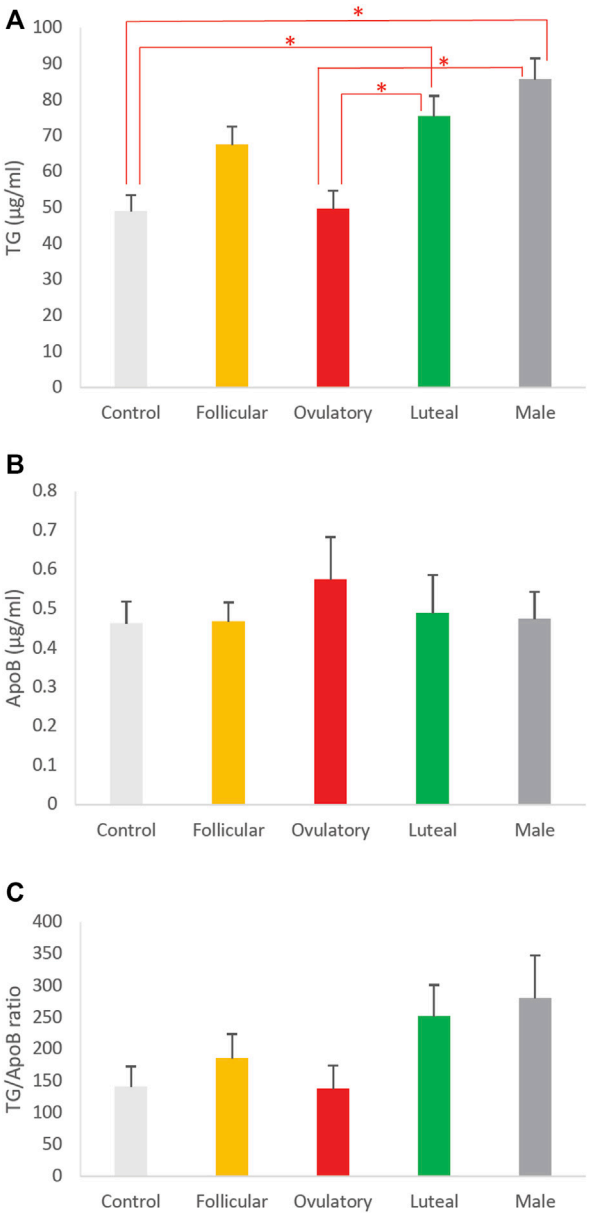

FIGURE 6
The effects of ovarian cycle on intestinal lipoproteins. Using a semipermeable membrane system, the differentiated Caco-2 cells ($n \geq 12$) were incubated with lipid mixture in their apical compartment and sex hormone mixture or vehicle (control) in their basolateral compartment. The concentrations of the sex hormones used resembled those in men and different phases of the ovarian cycle (See Table 1). After 4 h of incubation, the lipoproteins were isolated from the basolateral media by using NaCl gradient ultracentrifugation. The lipoprotein TG **(A)**, ApoB **(B)**, and TG/ApoB ratios **(C)** are depicted. The TG/ApoB ratios represent the sizes of lipoproteins. Values are means ± standard errors. The asterisk signs indicate that $p < 0.05$ (one-way ANOVA; Tukey *post hoc* tests were only performed when one-way ANOVA showed statistical significance).

Figure 5 represents the dose-dependent effects of testosterone on intestinal lipoprotein TG (Figure 5A), ApoB (Figure 5B), and TG/ApoB ratio (Figure 5C) ($n \geq 14$). Testosterone significantly increased TG ($p = 0.0046$) and TG/ApoB ratio ($p = 0.0040$) but decreased ApoB ($p = 0.017$). These data indicate that testosterone led to the production of "fewer but larger" intestinal lipoproteins.

3.4 The effects of ovarian cycle on TG, ApoB, and TG/ApoB ratio

To determine how different phases of ovarian cycle affect the size of intestinal lipoproteins, we examined the combined effects of these 3 hormones based on their concentrations observed in men and women in their follicular, ovulatory, and luteal phase. We also included a control group that consisted of vehicle (DMSO) without any sex hormones. The effects of the ovarian cycle on the intestinal lipoprotein TG, ApoB, and TG/ApoB ratio are shown in Figures 6A–C, respectively. The ovarian cycle had a significant effect on the

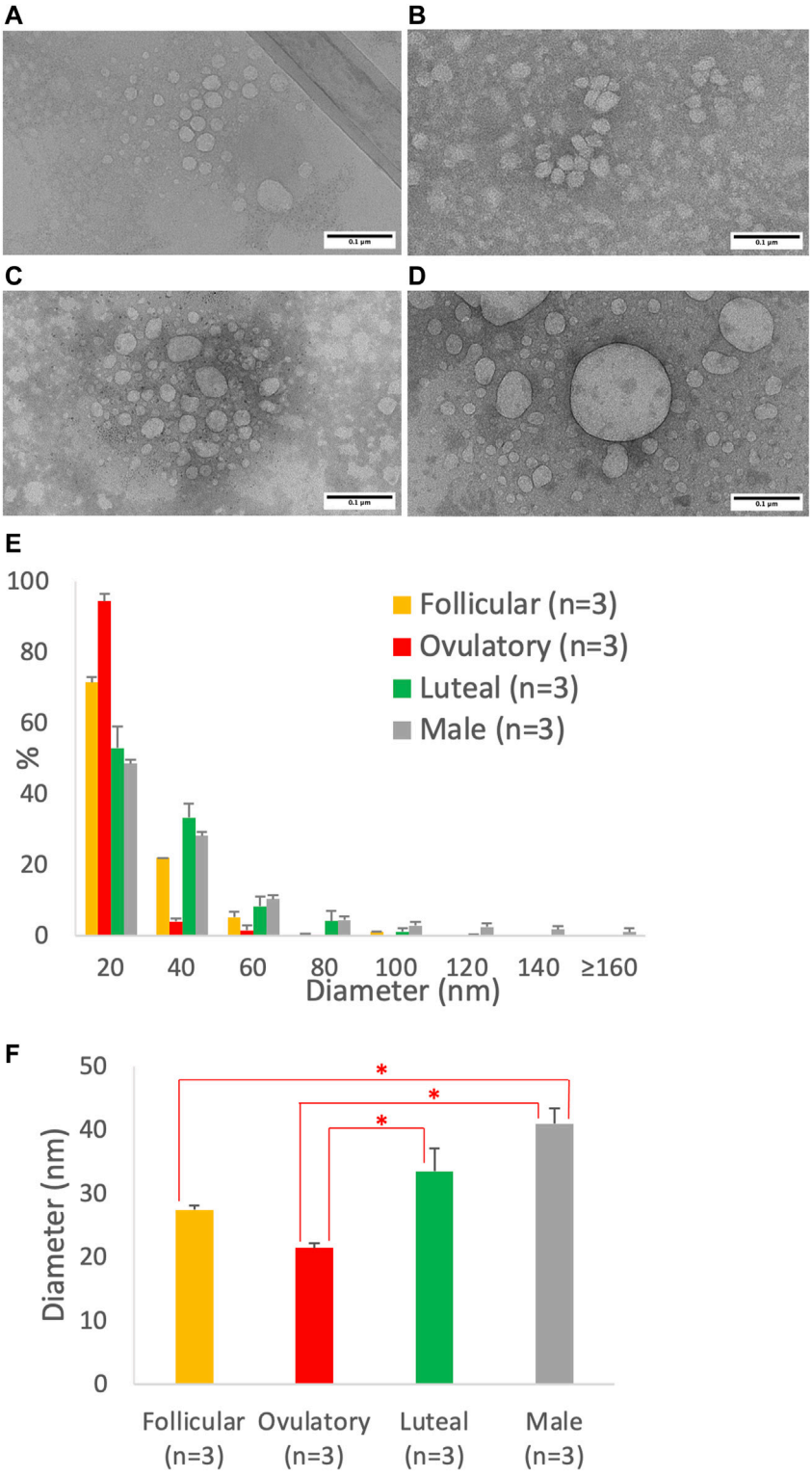

FIGURE 7
Particle size of lipoproteins from Caco-2 cells treated with the combination of sex hormones that resemble men and different phases of ovarian cycle. Using a semipermeable membrane system, the differentiated Caco-2 cells were incubated with lipid mixture in their apical compartment and sex hormone mixture in their basolateral compartment. The concentrations of the sex hormones used resembled those in men and different phases of the ovarian cycle (See Table 1). After 4 h of incubation, the lipoproteins were isolated from the basolateral media by using NaCl gradient ultracentrifugation, and then analyzed by a transmission electron microscope. The representative lipoprotein micrographs of the follicular phase **(A)**, ovulatory phase **(B)**, luteal phase **(C)**, and male **(D)** are depicted. Lipoprotein size distribution **(E)** and average size **(D)** are also presented. Scale bars are 0.1 μm (100 nm). Values are means ± standard errors. The asterisk signs indicate that $p < 0.05$ (one-way ANOVA followed by Tukey *post hoc* tests).

intestinal lipoprotein TG ($p = 0.0000092$) but not on the ApoB ($p = 0.87$) and TG/ApoB ratio ($p = 0.14$).

Tukey *post hoc* tests were subsequently performed to determine which of the groups were significantly different from one another in their intestinal lipoprotein TG secretion. As shown in Figure 6A, the ovulatory group had significantly lower intestinal lipoprotein TG than the luteal ($p = 0.0096$) and male ($p = 0.00010$). Similarly, the control group had significantly lower intestinal lipoprotein TG than the luteal ($p = 0.0073$) and male ($p = 0.000070$). There were no statistical differences between ovulatory and control ($p = 0.99$), ovulatory and follicular ($p = 0.14$), control and follicular ($p = 0.11$), follicular and luteal ($p = 0.84$), follicular and male ($p = 0.12$), and luteal and male ($p = 0.65$).

We did not perform Tukey *post hoc* tests for the effects of ovarian cycle on ApoB and TG/ApoB ratio because their one-way ANOVA tests did not show any significant difference. Next, we compared the size of the intestinal lipoproteins from the follicular, ovulatory, luteal, and male groups by imaging analysis.

3.5 Imaging analysis of the size of lipoproteins from Caco-2 cells treated with different combinations of sex hormones

Using imaging analysis, we compared the size of the intestinal lipoproteins isolated from the follicular (Figure 7A), ovulatory (Figure 7B), luteal (Figure 7C), and male (Figure 7D) groups. The lipoprotein size distribution (Figure 7E) shows that the ovulatory and follicular groups secreted lipoproteins that were mostly 20 nm in diameter. Luteal and male groups were quite similar in their particle size distribution, but male group produced more particles that were larger than 80 nm in diameter. The effect of ovarian cycle on the lipoprotein size was statistically significant ($p = 0.0014$). As shown in Figure 7F, the ovulatory group had smaller lipoproteins than both the luteal ($p = 0.020$) and male ($p = 0.0011$) group. The follicular group also had smaller lipoproteins than the male group ($p = 0.011$). However, there were no statistical differences between ovulatory and follicular ($p = 0.29$), follicular and luteal ($p = 0.28$), and luteal and male ($p = 0.16$).

4 Discussion

It is increasingly clear that abdominal visceral fat is detrimental to health not only in men (Kuk et al., 2006) but also in women (Koster et al., 2015). Men, however, are more likely than premenopausal women to develop abdominal visceral fat (Grauer et al., 1984). The reasons for the sex differences in body fat accumulation remain unclear, but we previously proposed that the small intestine plays several essential roles (Nauli and Matin, 2019). The small intestine is the organ that releases the most amount of TG, predominantly in the form of intestinal lipoproteins, namely VLDL and chylomicron. Large intestinal lipoproteins are more likely to be retained in the intestinal wall (Takahara et al., 2013), allowing their TG to be hydrolyzed and taken up by the abdominal viscera. Indeed, studies have shown that the accumulation of large intestinal lipoproteins in the abdominal wall, caused by the leaky lymphatics, was responsible for the significant gain of abdominal visceral fat (Harvey et al., 2005; Escobedo et al., 2016). Therefore, larger intestinal lipoproteins are likely to contribute to the development of the abdominal visceral fat.

To our knowledge, there has not been any direct comparison of the intestinal lipoprotein size between males and females. Our studies here showed that when they were intraduodenally infused with glucose/saline, female mice produced relatively smaller intestinal lipoproteins than male mice, but their difference was not statistically significant (Figure 1). However, this difference became significant when they were intraduodenally infused with lipid emulsion (Figure 2). Note that these mice were all provided with the same overnight intraduodenal infusion of 5% glucose in saline before being challenged with the same amount of lipid emulsion. Therefore, our data imply that the differences in their intestinal lipoprotein size were partly due to the sex hormones. Since the estrous cycle of mice has different sex hormone profiles than the ovarian cycle of humans, we utilized our Caco-2 cell model to further study the effects of sex hormones and ovarian cycle on the size of intestinal lipoproteins.

All sex hormones, including estrogen, progesterone, and testosterone, increased intestinal TG secretion (Figures 3A, 4A, 5A, respectively). However, only testosterone decreased the intestinal ApoB secretion, resulting in fewer intestinal lipoproteins being produced (Figures 3B, 4B, 5B). These results are consistent with our recently published studies that showed ApoB was not affected by the female sex hormones (Liu et al., 2021). It is important to note, however, that our previous mice studies used different concentrations of sex hormones. Therefore, direct comparisons between these studies should be made with caution.

Conceivably, testosterone also increased the size of intestinal lipoproteins, as evidenced by its significant dose-dependent effect on TG/ApoB ratio (Figure 5C). Progesterone also gradually increased the TG/ApoB ratios from around 100 to 200, but the increase was not statistically significant (Figure 4C). Estrogen did not cause a gradual increase in TG/ApoB ratios as their ratios hovered around 100–150 (Figure 3C). From these experiments, we conclude that testosterone was the sex hormone with the strongest capability of increasing the size of intestinal lipoproteins. It led to the production of "significantly fewer but larger" intestinal lipoproteins. In contrast, estrogen appeared to trigger "slightly more of the same size" of intestinal lipoproteins. Progesterone stimulated "slightly larger but of the same number" of intestinal lipoproteins. In this regard, the testosterone and estrogen effects were rather opposite to each other, and the progesterone effects were somewhat in between those of testosterone and estrogen.

To further investigate the effects of ovarian cycle on intestinal lipoproteins, our Caco-2 cells were exposed to a combination of different sex hormone concentrations resembling those seen in the follicular phase, ovulatory phase, luteal phase, and men (Table 1). As shown in Figure 6A, the control group (vehicle without any sex hormones) had the lowest intestinal lipoprotein TG, followed by the ovulatory, follicular, luteal, and male group. There was, however, no significant difference in the ApoB and TG/ApoB ratio (Figures 6B, C, respectively).

We then analyzed the transmission electron micrographs of the intestinal lipoproteins (Figure 7) and found that the ovarian cycle

had a significant effect on the size of intestinal lipoproteins. The ovulatory group had significantly smaller intestinal lipoproteins than both the luteal and male group; and the follicular group also had significantly smaller intestinal lipoproteins than the male group. The ranking order obtained from the imaging analysis agree with that obtained from the biochemical analysis. The ovulatory group had the smallest intestinal lipoproteins, followed by follicular, luteal, and male group. The calculated TG/ApoB ratios appeared to have more variance than the data obtained from imaging analysis, which may explain why the ovarian cycle showed a statistically significant effect on lipoprotein size measured from the transmission electron micrographs but not from the calculated TG/ApoB ratios.

Collectively, our data indicated that the combination of sex hormones that resemble those found in men produced larger intestinal lipoproteins than the combinations that resemble ovulatory and follicular phase. The sex difference in the intestinal lipoprotein size could partly be attributed to testosterone that drove the production of "larger but fewer" lipoproteins. Progesterone also increased—albeit not significantly—the size of these lipoproteins, possibly explaining why the luteal phase, which had the highest level of progesterone, produced larger lipoproteins than the ovulatory phase.

Our data also indicated that sex hormones in male promoted intestinal TG transport that was more efficient than those in the ovulatory and follicular phase. Since TG is positioned in the core of lipoproteins, larger lipoproteins can feasibly transport more TG. However, larger intestinal lipoproteins may be subjected to longer retention in the intestinal wall, favoring the accumulation of the abdominal visceral fat.

From the evolutionary perspective, it is arguably more advantageous for men to have an efficient intestinal TG secretion and the ability to store their fat in the abdominal viscera. Importantly, the release of the stored fat from the abdominal viscera can reach the liver—the key metabolic organ—more effectively than from the subcutaneous depot (Nauli and Matin, 2019). It is also perhaps more advantageous for women to store fat in their subcutaneous depot as it provides a better insulation to the whole body. This may serve as a critical factor for their survival, especially considering that women have lower muscle mass. Of note, smaller intestinal lipoproteins are more likely to enter the blood capillaries than the lymphatic capillaries (Mansbach et al., 1991; Mansbach and Dowell, 1993). Since the blood circulation has a higher pressure than the lymphatic circulation, the portal transport is associated with less retention of intestinal lipoproteins in the gut, which consequently leads to a more robust dietary fat distribution to the subcutaneous depot.

Our current studies are in general agreement with the previous studies. As indicated above, earlier studies showed that female rats had higher VLDL protein production than male rats (Vahouny et al., 1977; Vahouny et al., 1980). Furthermore, our recently published studies showed that female mice had lower lymphatic TG secretion than male mice, which could partly be due to the estrogen-mediated enhancement of vascular endothelial growth factor A (VEGF-A) signaling (Liu et al., 2021). Enhanced VEGF-A signaling has been shown to prevent the movement of intestinal lipoproteins from the lamina propria of the intestinal villi into their lymphatics (Zhang et al., 2018). In addition, it may facilitate the entrance of smaller intestinal lipoproteins into the lumen of blood capillaries.

It is noteworthy to acknowledge the limitation of our studies. Since Caco-2 cells were originally isolated from a male individual, the sex hormone effects in our studies may be different from studies utilizing cells from a female individual, such as HT-29 cells. Sex hormones may interact with sex chromosomes, resulting in potential differences of sex hormone effects in female- and male-derived cells. Additionally, organizational effects of gonadal hormones, which are permanent, may contribute to sex differences in intestinal lipoprotein size (Blencowe et al., 2022). In our experience, however, HT-29 cells are not effective in secreting lipoproteins. Additionally, primary culture derived from adult intestinal tissues is challenging partly due to the short lifespan (3–5 days) of intestinal epithelial cells (Dutton et al., 2019).

From our studies and those of others, it can be concluded that dietary fat absorption is likely different between men and women. We demonstrated in our current studies that sex hormones that resemble those found in men produced larger intestinal lipoproteins than the sex hormones that resemble those found in the ovulatory and follicular phase. This effect could be explained by the ability of testosterone to induce the production of larger intestinal lipoproteins. Progesterone resembled some of the testosterone effects, possibly explaining why cells in the luteal phase condition produced larger intestinal lipoproteins than cells in the ovulatory phase condition. Since men consume more total dietary fat than women (Wright and Wang, 2010), it is reasonable to speculate that this additional factor can further drive the production of larger intestinal lipoproteins in men. Dietary fat is responsible for the production of larger intestinal lipoproteins (Nauli et al., 2006; Nauli et al., 2014). As such, it will be of great interest to determine the effects of the complex interplay between hormonal fluctuation and dietary fat intake on the size of intestinal lipoproteins. Hormonal changes are not only mediated by ovarian cycle, but also by body fat. As body fat increases, free testosterone level tends to increase in females (Bernasconi et al., 1996) but decrease in males (Fui et al., 2014). It remains to be determined if these changes in free testosterone level can alter the intestinal lipoprotein size.

The effects of the combination of sex hormones that resemble postmenopausal women also warrant further investigation. Postmenopausal women are generally older than premenopausal women. However, studies have shown that postmenopausal women were still more likely to develop metabolic syndrome even when compared with age-matched premenopausal women (Eshtiaghi, Esteghamati, and Nakhjavani, 2010). We have previously postulated that aging closes the gap between men and women in their abdominal visceral fat accumulation (Nauli and Matin, 2019). Aging causes lymphatics to be leakier (Zolla et al., 2015), and consequently promotes lipoprotein retention in the intestinal wall.

The sex differences in abdominal visceral fat accumulation are likely mediated by multiple mechanisms. In men, higher testosterone and higher intake of total fat drive the production of larger intestinal lipoproteins. Large intestinal lipoproteins are more likely to be retained longer in the intestinal wall, promoting abdominal visceral fat accumulation. As aging lymphatics become leakier, the sex differences in the abdominal visceral fat accumulation begin to dwindle. Physical inactivity, which is also associated with aging, further promote leaky lymphatics (Hespe et al., 2016).

Data availability statement

The original contributions presented in the study are included in the article/supplementary material, further inquiries can be directed to the corresponding author.

Ethics statement

The animal study was approved by Institutional Animal Care and Use Committee at the University of Cincinnati. The study was conducted in accordance with the local legislation and institutional requirements.

Author contributions

AN: Conceptualization, Data curation, Formal Analysis, Funding acquisition, Investigation, Methodology, Project administration, Resources, Software, Supervision, Validation, Visualization, Writing–original draft, Writing–review and editing. AP: Data curation, Investigation, Writing–review and editing. PT: Conceptualization, Data curation, Formal Analysis, Funding acquisition, Methodology, Project administration, Resources, Supervision, Visualization, Writing–review and editing. SN: Conceptualization, Funding acquisition, Resources, Visualization, Writing–review and editing.

Funding

The author(s) declare financial support was received for the research, authorship, and/or publication of this article. AN was supported by the pilot grant from the Western Michigan University Homer Stryker M.D. School of Medicine. SN was supported by NIH HL147311 and NIH HL147311-S1.

Acknowledgments

The authors would like to thank Shuqin Zheng (Kallyope, New York, NY) and Qing Yang (University of Cincinnati, Cincinnati, OH) for their assistance in the animal studies; Toshihiro Aoki (University of California, Irvine, CA) for his help with the transmission electron microscope (JEOL 2800); and Marshall B. Ketchum University College of Pharmacy (Fullerton, CA) for their support in some of the data acquisition. Due to space limitation, the authors regret that not all work in this field is cited in this paper.

Conflict of interest

The authors declare that the research was conducted in the absence of any commercial or financial relationships that could be construed as a potential conflict of interest.

The author(s) declared that they were an editorial board member of Frontiers, at the time of submission. This had no impact on the peer review process and the final decision.

Publisher's note

References

Albers, J. J., Kennedy, H., and Marcovina, S. M. (1996). Evidence that Lp[a] contains one molecule of apo[a] and one molecule of apoB: evaluation of amino acid analysis data. *J. Lipid Res.* 37 (1), 192–196. doi:10.1016/s0022-2275(20)37647-1

Bernasconi, D., Del Monte, P., Meozzi, M., Randazzo, M., Marugo, A., Badaracco, B., et al. (1996). The impact of obesity on hormonal parameters in hirsute and nonhirsute women. *Metabolism* 45 (1), 72–75. doi:10.1016/s0026-0495(96)90202-4

Blencowe, M., Chen, X., Zhao, Y., Itoh, Y., McQuillen, C. N., Han, Y., et al. (2022). Relative contributions of sex hormones, sex chromosomes, and gonads to sex differences in tissue gene regulation. *Genome Res.* 32 (5), 807–824. doi:10.1101/gr.275965.121

Bollman, J. L., Cain, J. C., and Grindlay, J. H. (1948). Techniques for the collection of lymph from the liver, small intestine, or thoracic duct of the rat. *J. Lab. Clin. Med.* 33 (10), 1349–1352.

Dutton, J. S., Hinman, S. S., Kim, R., Wang, Y., and Allbritton, N. L. (2019). Primary cell-derived intestinal models: recapitulating Physiology. *Trends Biotechnol.* 37 (7), 744–760. doi:10.1016/j.tibtech.2018.12.001

Escobedo, N., Proulx, S. T., Karaman, S., Dillard, M. E., Johnson, N., Detmar, M., et al. (2016). Restoration of lymphatic function rescues obesity in Prox1-haploinsufficient mice. *JCI Insight* 1 (2), e85096. doi:10.1172/jci.insight.85096

Eshtiaghi, R., Esteghamati, A., and Nakhjavani, M. (2010). Menopause is an independent predictor of metabolic syndrome in Iranian women. *Maturitas* 65 (3), 262–266. doi:10.1016/j.maturitas.2009.11.004

Fogh, J., Wright, W. C., and Loveless, J. D. (1977). Absence of HeLa cell contamination in 169 cell lines derived from human tumors. *J. Natl. Cancer Inst.* 58 (2), 209–214. doi:10.1093/jnci/58.2.209

Fui, M. N., Dupuis, P., and Grossmann, M. (2014). Lowered testosterone in male obesity: mechanisms, morbidity and management. *Asian J. Androl.* 16 (2), 223–231. doi:10.4103/1008-682X.122365

Grauer, W. O., Moss, A. A., Cann, C. E., and Goldberg, H. I. (1984). Quantification of body fat distribution in the abdomen using computed tomography. *Am. J. Clin. Nutr.* 39 (4), 631–637. doi:10.1093/ajcn/39.4.631

Grundy, S. M., Cleeman, J. I., Daniels, S. R., Donato, K. A., Eckel, R. H., Franklin, B. A., et al. (2005). Diagnosis and management of the metabolic syndrome: an American heart association/national heart, lung, and blood institute scientific statement. *Circulation* 112 (17), 2735–2752. doi:10.1161/CIRCULATIONAHA.105.169404

Harvey, N. L., Srinivasan, R. S., Dillard, M. E., Johnson, N. C., Witte, M. H., Boyd, K., et al. (2005). Lymphatic vascular defects promoted by Prox1 haploinsufficiency cause adult-onset obesity. *Nat. Genet.* 37 (10), 1072–1081. doi:10.1038/ng1642

Hespe, G. E., Kataru, R. P., Savetsky, I. L., García Nores, G. D., Torrisi, J. S., Nitti, M. D., et al. (2016). Exercise training improves obesity-related lymphatic dysfunction. *J. Physiol.* 594 (15), 4267–4282. doi:10.1113/JP271757

Koster, A., Murphy, R. A., Eiriksdottir, G., Aspelund, T., Sigurdsson, S., Lang, T. F., et al. (2015). Fat distribution and mortality: the AGES-Reykjavik Study. *Obes. (Silver Spring)* 23 (4), 893–897. doi:10.1002/oby.21028

Kuk, J. L., Katzmarzyk, P. T., Nichaman, M. Z., Church, T. S., Blair, S. N., and Ross, R. (2006). Visceral fat is an independent predictor of all-cause mortality in men. *Obes. (Silver Spring)* 14 (2), 336–341. doi:10.1038/oby.2006.43

Liu, M., Shen, L., Yang, Q., Nauli, A. M., Bingamon, M., Wang, D. Q., et al. (2021). Sexual dimorphism in intestinal absorption and lymphatic transport of dietary lipids. *J. Physiol.* 599, 5015–5030. doi:10.1113/JP281621

Mansbach, C. M., 2nd, and Dowell, R. F. (1993). Portal transport of long acyl chain lipids: effect of phosphatidylcholine and low infusion rates. *Am. J. Physiol.* 264 (6 Pt 1), G1082–G1089. doi:10.1152/ajpgi.1993.264.6.G1082

Mansbach, C. M., Dowell, R. F., II, and Pritchett, D. (1991). Portal transport of absorbed lipids in rats. *Am. J. Physiol.* 261 (3 Pt 1), G530–G538. doi:10.1152/ajpgi.1991.261.3.G530

Mårin, P., Lönn, L., Andersson, B., Odén, B., Olbe, L., Bengtsson, B. A., et al. (1996). Assimilation of triglycerides in subcutaneous and intraabdominal adipose tissues *in vivo* in men: effects of testosterone. *J. Clin. Endocrinol. Metab.* 81 (3), 1018–1022. doi:10.1210/jcem.81.3.8772568

Meloni, A., Cadeddu, C., Cugusi, L., Donataccio, M. P., Deidda, M., Sciomer, S., et al. (2023). Gender differences and cardiometabolic risk: the importance of the risk factors. *Int. J. Mol. Sci.* 24 (2), 1588. doi:10.3390/ijms24021588

Nauli, A. M., and Matin, S. (2019). Why do men accumulate abdominal visceral fat? *Front. Physiol.* 10, 1486. doi:10.3389/fphys.2019.01486

Nauli, A. M., Nassir, F., Zheng, S., Yang, Q., Lo, C. M., Vonlehmden, S. B., et al. (2006). CD36 is important for chylomicron formation and secretion and may mediate cholesterol uptake in the proximal intestine. *Gastroenterology* 131 (4), 1197–1207. doi:10.1053/j.gastro.2006.08.012

Nauli, A. M., Sun, Y., Whittimore, J. D., Atyia, S., Krishnaswamy, G., and Nauli, S. M. (2014). Chylomicrons produced by Caco-2 cells contained ApoB-48 with diameter of 80-200 nm. *Physiol. Rep.* 2 (6), e12018. doi:10.14814/phy2.12018

Nauli, A. M., and Whittimore, J. D. (2015). Using caco-2 cells to study lipid transport by the intestine. *J. Vis. Exp.* 102, e53086. doi:10.3791/53086

Regitz-Zagrosek, V., Lehmkuhl, E., and Mahmoodzadeh, S. (2007). Gender aspects of the role of the metabolic syndrome as a risk factor for cardiovascular disease. *Gend. Med.* 4 (Suppl. B), S162–S177. doi:10.1016/s1550-8579(07)80056-8

Sherman, B. M., and Korenman, S. G. (1975). Hormonal characteristics of the human menstrual cycle throughout reproductive life. *J. Clin. Investig.* 55 (4), 699–706. doi:10.1172/JCI107979

Takahara, E., Mantani, Y., Udayanga, K. G., Qi, W. M., Tanida, T., Takeuchi, T., et al. (2013). Ultrastructural demonstration of the absorption and transportation of minute chylomicrons by subepithelial blood capillaries in rat jejunal villi. *J. Vet. Med. Sci.* 75 (12), 1563–1569. doi:10.1292/jvms.13-0310

Vahouny, G. V., Blendermann, E. M., Gallo, L. L., and Treadwell, C. R. (1980). Differential transport of cholesterol and oleic acid in lymph lipoproteins: sex differences in puromycin sensitivity. *J. Lipid Res.* 21 (4), 415–424. doi:10.1016/s0022-2275(20)39791-1

Vahouny, G. V., Ito, M., Blendermann, E. M., Gallo, L. L., and Treadwell, C. R. (1977). Puromycin inhibition of cholesterol absorption in the rat. *J. Lipid Res.* 18 (6), 745–752. doi:10.1016/s0022-2275(20)41592-5

Votruba, S. B., Mattison, R. S., Dumesic, D. A., Koutsari, C., and Jensen, M. D. (2007). Meal fatty acid uptake in visceral fat in women. *Diabetes* 56 (10), 2589–2597. doi:10.2337/db07-0439

Wang, X., Magkos, F., and Mittendorfer, B. (2011). Sex differences in lipid and lipoprotein metabolism: it's not just about sex hormones. *J. Clin. Endocrinol. Metab.* 96 (4), 885–893. doi:10.1210/jc.2010-2061

Wright, J. D., and Wang, C. Y. (2010). Trends in intake of energy and macronutrients in adults from 1999-2000 through 2007-2008. *NCHS Data Brief.* (49), 1–8.

Zhang, F., Zarkada, G., Han, J., Li, J., Dubrac, A., Ola, R., et al. (2018). Lacteal junction zippering protects against diet-induced obesity. *Science* 361 (6402), 599–603. doi:10.1126/science.aap9331

Zolla, V., Nizamutdinova, I. T., Scharf, B., Clement, C. C., Maejima, D., Akl, T., et al. (2015). Aging-related anatomical and biochemical changes in lymphatic collectors impair lymph transport, fluid homeostasis, and pathogen clearance. *Aging Cell.* 14 (4), 582–594. doi:10.1111/acel.12330

frontiers | Frontiers in Physiology

TYPE Review
PUBLISHED 14 February 2024
DOI 10.3389/fphys.2024.1358625

OPEN ACCESS

EDITED BY
Lin Zhu,
Vanderbilt University Medical Center,
United States

REVIEWED BY
Vincenza Cifarelli,
Saint Louis University, United States
Revathi Sekar,
Helmholtz Association of German Research Centres (HZ), Germany

*CORRESPONDENCE
Changting Xiao,
changting.xiao@usask.ca

RECEIVED 20 December 2023
ACCEPTED 31 January 2024
PUBLISHED 14 February 2024

CITATION
Mukherjee K and Xiao C (2024), GLP-2 regulation of intestinal lipid handling.
Front. Physiol. 15:1358625.
doi: 10.3389/fphys.2024.1358625

GLP-2 regulation of intestinal lipid handling

Kundanika Mukherjee and Changting Xiao*

Department of Anatomy, Physiology and Pharmacology, College of Medicine, University of Saskatchewan, Saskatoon, SK, Canada

Lipid handling in the intestine is important for maintaining energy homeostasis and overall health. Mishandling of lipids in the intestine contributes to dyslipidemia and atherosclerotic cardiovascular diseases. Despite advances in this field over the past few decades, significant gaps remain. The gut hormone glucagon-like peptide-2 (GLP-2) has been shown to play pleotropic roles in the regulation of lipid handling in the intestine. Of note, GLP-2 exhibits unique actions on post-prandial lipid absorption and post-absorptive release of intestinally stored lipids. This review aims to summarize current knowledge in how GLP-2 regulates lipid processing in the intestine. Elucidating the mechanisms of GLP-2 regulation of intestinal lipid handling not only improves our understanding of GLP-2 biology, but also provides insights into how lipids are processed in the intestine, which offers opportunities for developing novel strategies towards prevention and treatment of dyslipidemia and atherosclerotic cardiovascular diseases.

KEYWORDS

glucagon-like peptide-2, neural pathway, intestine, chylomicron, triglyceride

Introduction

Balanced and regulated lipid metabolism is critical for whole-body energy homeostasis and overall health. In certain situations, lipid appearance (dietary lipid absorption in the intestine and lipoprotein production from the liver) is not balanced with its clearance, leading to abnormal levels and characteristics of lipids in the blood circulation (dyslipidemia) (Lewis et al., 2015). Dyslipidemia is common in patients with metabolic disorders (e.g., type 2 diabetes, obesity, and metabolic syndrome) and it increases the risk of atherosclerotic cardiovascular diseases (Lewis et al., 2015; Stahel et al., 2018). It is therefore important to understand the mechanisms of lipid metabolism for developing effective strategies for the prevention and treatment of atherosclerotic cardiovascular diseases.

Dietary lipids (mostly triglycerides, TGs) are processed in the intestine. TGs are absorbed into the intestinal absorptive cells (enterocytes) and packaged into either lipoprotein particles (chylomicrons, CMs) for secretion, or cytoplasmic lipid droplets (CLDs) for storage (Xiao et al., 2019a; Stahel et al., 2020; Zembroski et al., 2021; Ghanem et al., 2022). Following digestion in the small intestinal lumen, the digestion

Abbreviations: ARC, arcuate nucleus; CD36, cluster of differentiation 36; CLD, cytoplasmic lipid droplet; CM, chylomicron; DMH, dorsomedial hypothalamus; DPPIV, dipeptidyl peptidase IV; GLP-2, glucagon-like peptide-2; GLP-2R, glucagon-like peptide-2 receptor; IL-22, interleukin 22; MC4R, melanocortin 4 receptor; NO, nitric oxide; NOS, nitric oxide synthase; NTS, nucleus tractus solitarius; POMC, proopiomelanocortin; PVN, paraventricular nucleus; SBS, short bowel syndrome; TG, triglyceride; VEGF, vascular endothelial growth factor; VEGFR, vascular endothelial growth factor receptor; VIP, vasoactive intestinal peptide; VIPR, vasoactive intestinal peptide receptor.

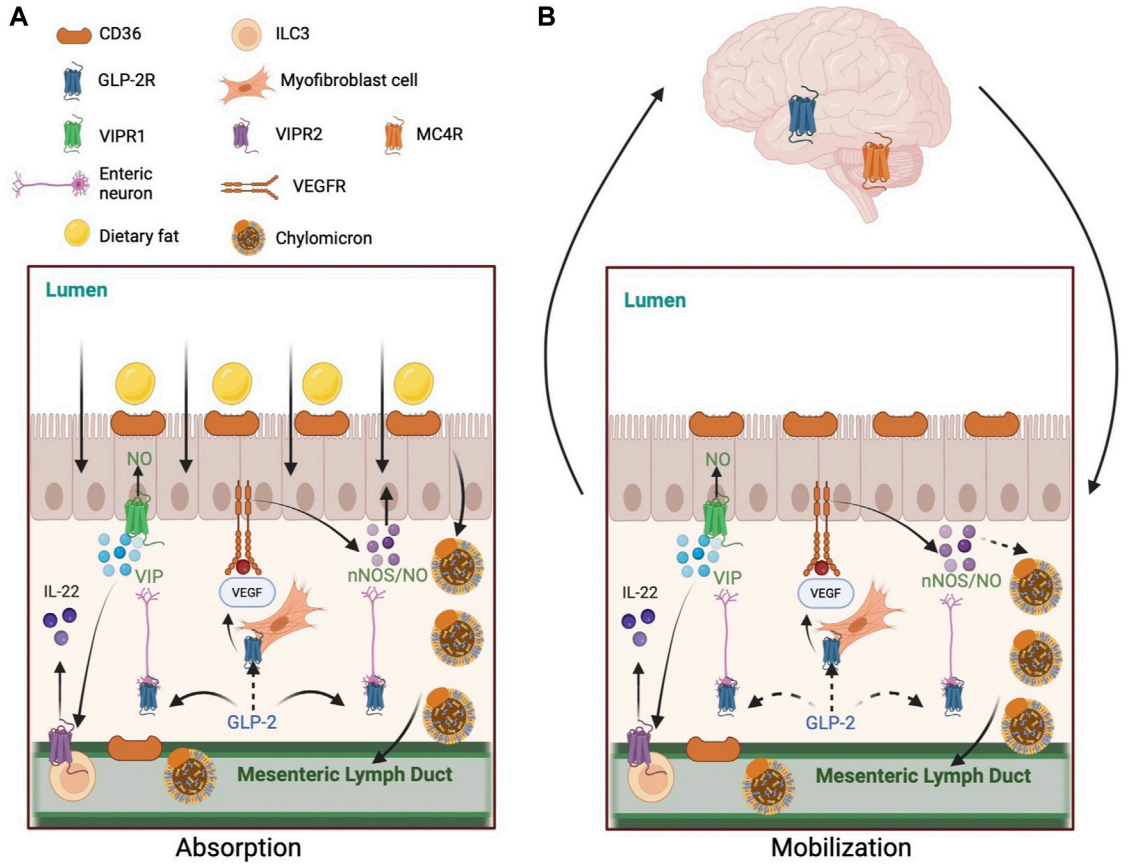

FIGURE 1
Mechanisms of GLP-2 regulation of intestinal lipid handling. **(A)** GLP-2 enhances lipid absorption during postprandial state. 1) GLP-2 increases CD36 glycosylation on the apical membrane of enterocytes. 2) GLP-2 stimulates NO production in NOS-expressing cells, including enterocytes, endothelial cells, and enteric neurons. GLP-2 activates neuronal NOS which subsequently activates protein kinase G. GLP-2 may stimulate VEGF release by myofibroblast to activate VEGFR on enterocytes to enhance lipid absorption directly or indirectly via NO production. GLP-2 increases intestinal blood flow via increased NO production, which may indirectly enhance lipid absorption. 3) GLP-2 stimulates VIP production by enteric neurons. VIP may activate VIPR1 on enterocytes to stimulate NO production and lipid absorption. VIP may also activate VIPR2 on type-3 innate lymphoid cells to release IL-22, which activates IL-22 receptors on enterocytes to enhance lipid absorption. **(B)** GLP-2 promotes the release of intestinally stored lipids during post-absorptive state. 1) GLP-2 stimulated NO production mediates the mobilization of intestinal lipid stores in rodents, but not humans. GLP-2 may stimulate VEGF release by myofibroblast to activate VEGFR on enterocytes to enhance lipid mobilization directly or indirectly via NO production. 2) GLP-2 may enhance lymphatic function by stimulating VEGF release from subepithelial myofibroblasts and longitudinal and circular muscles surrounding the lymphatics. CD36 on lymphatic endothelial cells may respond to GLP-2. 3) A neural pathway involving the CNS also participates GLP-2 mobilization of intestinal lipid stores. This pathway may include GLP-2 activation of its receptors on vagal afferent neurons, central activation of GLP-2R and MC4R, and vagal efferent outflow to the intestine. Solid arrows indicate known pathways. Dashed arrows indicate implicated but not yet elucidated pathways. Abbreviations: CD36, cluster of differentiation 36; GLP-2, glucagon-like peptide-2; GLP-2R, glucagon-like peptide-2 receptor; IL-22, interleukin 22; MC4R, melanocortin 4 receptor; NO, nitric oxide; NOS, nitric oxide synthase; VEGF, vascular endothelial growth factor; VEGFR, vascular endothelial growth factor receptor; VIP, vasoactive intestinal peptide; VIPR, vasoactive intestinal peptide receptor.

products (fatty acids and monoglycerides) are transported across the apical membrane of the enterocytes lining the villi of the intestine. Inside the enterocytes, they are resynthesized into TGs and form lipid droplets at the ER membrane. Most of these lipid droplets are directed to CM synthesis in the ER lumen where lipid-poor apolipoprotein B48 is lipidated to form pre-CMs. Pre-CMs are transported in transport vesicles to the Golgi apparatus for additional processing. Mature CM particles are exocytozed at the basolateral membrane, travel through the lamina propria, enter and transport through the lymphatics, and eventually join the blood circulation via the subclavian veins. CM biosynthesis, assembly and secretion in enterocytes have been extensively studied. It is well documented that CM production is subjected to regulation by nutrients, hormones and nutraceuticals and that CM production is increased in compromised metabolic status (Dash et al., 2015). Although the majority of dietary TGs undergo the CM synthesis and secretion route, some of the lipid droplets at the ER membrane are also used to form CLDs as a transient storage.

Besides immediate secretion of CMs following a meal, the intestine is also capable of retaining a significant portion of dietary lipids for secretion at later times. These two processes of lipid handling in the intestine, namely dietary lipid absorption and post-absorptive release of intestinally stored lipids, have been shown to be affected by various factors. Among these factors, gut hormones glucagon-like peptide-1 (GLP-1) and glucagon-like peptide-2 (GLP-2) have been shown to impact different aspects of these processes, as previously reviewed (Xiao et al., 2015; Stahel et al., 2021). Briefly, GLP-1 suppresses postprandial CM secretion by inhibiting CM

biosynthesis and assembly. In contrast, GLP-2 stimulates CM secretion in both processes, the mechanisms of which remains elusive but begins to be better defined recently. This review aims to summarize current understanding of the mechanisms whereby GLP-2 modulates lipid handling in the intestine, with particular attention to emerging roles of neural pathways.

Post-absorptive lipid storage and release in the intestine

Lipid storage and release in the intestine during post-absorptive state is a phenomenon with renewed recognition lately. Several earlier studies support prolonged lipid retention in the intestine into post-absorptive phase. In healthy, lean individuals, postprandial TG level in plasma rises rapidly, peaks at approximately 3–4 h after a lipid-rich meal, and gradually returns to fasting level after 6–8 h. However, ingestion of a second meal leads to a very early increase in plasma and CM TG, a phenomenon referred to as the "second-meal effect" (Jackson et al., 2001). This is attributed to the release of lipids stored in the intestine that are derived from the previous meal. In a stable isotope tracing study in humans, TGs from an earlier meal appeared in CM within as early as 20 min and up to 18 h after a second fat-rich meal (Chavez–Jauregui et al., 2010). Lipid storage may provide a significant portion of postprandial TG excursion. For example, regarding the second meal effects, it was estimated that ~1/4 TG appearing during a morning meal is derived from the previous dinner (Chavez-Jauregui et al., 2010) and ~1/3 of lunch lipids enter the blood after the onset of dinner (Jacome-Sosa et al., 2021). The exact location and form of lipid stores remain unclear, but CLDs in enterocytes and CMs in extra-enterocyte locations (such as intercellular space, lamina propria, and lymphatics) are likely (Xiao et al., 2019b; Xiao et al., 2020; Syed-Abdul et al., 2022a). In the small intestine, jejunum and duodenum retained abundant lipid droplets after fat ingestion in humans (Robertson et al., 2003; Xiao et al., 2018) and after oil gavage in mice (Hung et al., 2017). Besides a subsequent meal, several other factors have also been shown to release stored lipids from the intestine. Glucose ingestion in humans (Xiao et al., 2019a) or direct delivery of glucose into the upper small intestinal lumen in rats (Stahel et al., 2019) leads to CM output from the intestine. As shown in humans, increased CM output is accompanied by depletion of CLDs, pointing to the utilization of CLD TG as substrates for CM synthesis and secretion (Xiao et al., 2019a). Sham fat feeding (tasting without ingesting fat) similarly increases CM secretion (Chavez-Jauregui et al., 2010), the mechanism of which is not well understood but may invoke a neural circuitry involving taste receptors. The gut hormone GLP-2 has also been shown to cause rapid release of stored lipids from the intestine during post-absorptive state (discussed in more details below).

The physiological significance of intestinal lipid storage and release remains largely speculative. One possibility is that temporary retaining of part of dietary lipids in the intestine attenuates postprandial excursion of plasma TG. Rapid and complete secretion of dietary lipids into blood circulation would create a scenario where other organs may be overwhelmed with lipid overloading and lipotoxicity. In line with this, insulin resistant humans have reduced capacity of lipid storage in the intestine, which contributes to their postprandial lipemia (Jacome-Sosa et al., 2021). It is known that lipoprotein synthesis and secretion persist in fasting state. Post-absorptive release of stored lipids from the intestine may keep CM synthesis and secretory machinery 'oiled' and ready to ramp up with the next incoming meal (Xiao et al., 2020). It is unclear whether altered lipid retention/release in the intestine is the cause or consequence of pathophysiological conditions such as hyperlipidemic states, obesity, metabolic syndrome, and diabetes. Nonetheless, understanding the mechanism of this storage-release dynamics may offer unique opportunities for the prevention and treatment of dyslipidemia and atherosclerotic cardiovascular diseases.

Glucagon-like peptide-2 (GLP-2)

GLP-2 was isolated and sequenced as a 33-amino acid peptide from human and porcine intestine. It belongs to the glucagon family of peptides, encoded by the proglucagon gene, that are majorly produced from the enteroendocrine cells of the intestine. The mammalian prohormone, proglucagon, undergoes tissue-specific posttranslational processing to give rise to GLP-2 in intestine and brain endocrine cells. GLP-2 is co-secreted with glucagon-like peptide-1 (GLP-1) in response to nutrients. Both these peptides are prone to degradation by dipeptidyl peptidase IV (DPPIV), a ubiquitous protease expressed in the intestine and vascular endothelium. Degradation of GLP-2 by DPPIV results in two circulating forms, GLP-2 (1-33) and GLP-2 (3-33).

Sources of GLP-2

GLP-2 is secreted by the enteroendocrine L-cells in distal small intestine and colon. It is a meal responsive hormone with its secretion stimulated by nutrients, mostly fat and glucose (Roberge and Brubaker, 1991; Brubaker and Anini, 2003). Besides intestinal L-cells, GLP-2 is also secreted by the neurons of brainstem (Vrang et al., 2007; 2008; Amato et al., 2016) that innervate the hypothalamic areas including paraventricular nucleus (PVN) and dorsomedial hypothalamus (DMH). GLP-2 immunoreactive fibres are also present in the arcuate nucleus (ARC) and PVN (Tang-Christensen et al., 2000). Since these hypothalamic areas are well-known for the regulation of food intake and energy balance, it is likely that GLP-2 may play important roles in energy balance as a neurotransmitter in these areas (Tang-Christensen et al., 2000).

Physiological functions of GLP-2

GLP-2 is well-known for regulating several physiological functions in the gastrointestinal tract. It was initially identified as an intestinotrophic factor for its promotion of small intestinal growth and repair. Other actions of GLP-2 in the gastrointestinal tract include stimulation of hexose transport and nutrient absorption, suppression of epithelial permeability, increase in mesenteric blood flow, improvement in intestinal barrier function, and reduction in gastrointestinal motility and acid secretion. These findings helped to identify GLP-2 as a possible therapeutic agent for the treatment of gastrointestinal diseases, such as short bowel syndrome (SBS), inflammatory bowel disease, and chemotherapy-induced mucositis. Besides the gastrointestinal tract, GLP-2 also acts centrally to regulate food intake and hepatic glucose metabolism.

Intestinotrophic effects of GLP-2

GLP-2 promotes intestinal growth and repair. Chronic administration of GLP-2 increased small intestinal weight and jejunal crypt-villus height in mice (Drucker et al., 1996; Brubaker et al., 1997). Chronic treatment with GLP-2 also increased villus height and crypt depth in short bowel jejunostomy patients (Jeppesen et al., 2001; 2009). These studies identified GLP-2 as a growth-promoting factor that stimulates intestinal growth and repair and supported the development of GLP-2 as a treatment for SBS. Teduglutide, a DPPIV resistant GLP-2 analogue with a prolonged half-life (~3–5 h) compared to native GLP-2 (~7 min), was approved for the treatment of SBS in 2012. Long-acting GLP-2 analogs, such as apraglutide (half-life 72 h), also exhibit improved efficacy in promoting intestinal growth (Hargrove et al., 2020). Mechanistically, GLP-2 inhibits crypt and enterocyte apoptosis and stimulates crypt cell proliferation, leading to expansion of the mucosal epithelium and increased mucosal surface area (Drucker, 2002), via activation of ErbB signaling (Yusta et al., 2009) and growth factors like insulin-like growth factor-1 (Murali et al., 2012).

GLP-2 in nutrient absorption

GLP-2 increases nutrient absorption. GLP-2 infusion increased glucose and amino acid uptake in total parenteral nutrition-fed piglets (Guan et al., 2003). GLP-2 can increase glucose uptake indirectly by increasing glucagon secretion as GLP-2 receptor (GLP-2R) is expressed in pancreatic alpha cells (De Heer et al., 2007) or through portal drained visceral blood (Guan et al., 2003). Exogenous GLP-2 administration increased absorption of intestine luminal fatty acids (Hsieh et al., 2009). SBS patients suffer from poor nutrient absorption and may require total parenteral nutrition. Administration of GLP-2 or its analogue in these patients improved their overall energy, carbohydrate, fluid and electrolyte absorption (Jeppesen et al., 2001; 2009; Eliasson et al., 2021).

GLP-2 in food intake and gut motility

GLP-2 suppresses food intake and gastric emptying in humans and rodents. Administration of GLP-2 in the brain (intracerebroventricular) decreased food intake in mice (Guan et al., 2012) and rats (Tang-Christensen et al., 2000) and reduced gastrointestinal motility in mice (Guan et al., 2012). These effects require the activation of GLP-2R in proopiomelanocortin (POMC) neurons in the hypothalamus (Guan et al., 2012). Interestingly, GLP-2 actions on food intake were abolished in rats with the loss of GLP-1R (Tang-Christensen et al., 2000). On the contrary, central inhibitory actions of GLP-2 on food intake in mice is increased after loss of Glp-1r signaling (Lovshin et al., 2001). It remains controversy regarding the interplay between GLP-1 and GLP-2 on food intake. In fasted rats, GLP-2 administration into the nucleus tractus solitarius (NTS), where Glp-2r is expressed (Lovshin et al., 2004), resulted in inhibition of food intake, which was abolished by blockade of melanocortin 4 receptor (MC4R) (Sun et al., 2021). These findings indicate that GLP-2 regulates food intake via a central mechanism with GLP-2R and MC4R as important mediators.

Gastric emptying is an essential process in regulating short-term food intake. Intravenous GLP-2 infusion decreases gastric emptying in pigs (Wøjdemann et al., 1998) and humans (Nagell et al., 2004). It has been shown that GLP-2 increases murine gastric capacity by inhibiting gastric fundic tone (Amato et al., 2009). This effect seems to be mediated by vasoactive intestinal peptide (VIP), as VIP receptor (VIPR) desensitization reduced gastric relaxation induced by GLP-2 (Amato et al., 2009). The increased gastric capacity may underline the short-term inhibition of food intake by GLP-2 (Baccari et al., 2022).

Anti-inflammatory function of GLP-2

Anti-inflammatory function of GLP-2 has been shown in various studies. GLP-2R activation reduced the expression of macrophage-dependent cytokines and LPS-induced inflammation in human islets (He et al., 2021). In pigs, chronic administration of GLP-2 also reduced LPS-induced inflammation (Qi et al., 2015). Necrotizing enterocolitis is a severe gastrointestinal disorder in premature infants. In experimental rat model of necrotizing enterocolitis, chronic GLP-2 administration decreased mucosal inflammatory cytokine production (Nakame et al., 2016). Chronic administration of Glp-2r antagonist improved hepatic inflammation in obese mice (Cani et al., 2009). GLP-2 reduced hepatic inflammation and fibrosis in multidrug resistance 2 knockout mice by inactivating hepatic stellate cells and activating intestinal Farnesoid X receptor signaling (Fuchs et al., 2023), while loss of Glp-2r signaling in mice activated hepatic stellate cells and exacerbated diet-induced steatohepatitis (Fuchs et al., 2020). GLP-2 treatment also reduced pro-inflammatory cytokines and crypt cell apoptosis in rats with intestinal inflammation (Sigalet et al., 2007). These anti-inflammatory effects of GLP-2 are mediated by activation of VIP in enteric neurons (Sigalet et al., 2007), highlighting an important role of the enteric neural pathway in this action.

Regulation of blood flow by GLP-2

GLP-2 increases intestinal blood flow in healthy humans (Bremholm et al., 2009; Xiao et al., 2019c) and in patients with SBS (Bremholm et al., 2011). Its enhancement in intestinal blood flow is nitric oxide (NO) dependent, as co-infusion with nitric oxide synthase (NOS) inhibitors attenuated this effect in pigs (Guan et al., 2003), rats (Deniz et al., 2007) and humans (Xiao et al., 2019c). GLP-2R is expressed on enteric neurons expressing VIP and endothelial NOS (Guan et al., 2006). Both VIP and endothelial NOS are well-known for regulating mucosal blood flow. These vasoactive neurotransmitters in the enteric neurons therefore are important mediators in the increase in blood flow by GLP-2.

GLP-2R expression

GLP-2 actions require binding and activating its receptor, GLP-2R, a G-protein coupled receptor and a member of the glucagon-secretin receptor family. In humans and rodents, GLP-2R is predominantly expressed in the gastrointestinal tract and central nervous system. In the intestine, GLP-2R mRNA transcripts are abundant in the lamina propria of the mucosa layer, in the circular and longitudinal muscle layers, and in the nerve plexuses within the duodenum, and the mucosa and nerve plexuses of the jejunum and ileum (Wismann et al., 2017). Regarding specific cell types, GLP-2R is expressed on myofibroblasts (Ørskov et al., 2005), enteroendocrine cells (Yusta et al., 2000) and enteric neurons (Bjerknes and Cheng, 2001; Guan et al., 2006). Notably, enterocytes do not express GLP-2R (Yusta et al., 2000; 2019;

Nelson et al., 2007; Pedersen et al., 2015). GLP-2R is also expressed in the nodose ganglia of vagus nerve (Nelson et al., 2007; Amato et al., 2016), which contains the cell bodies of vagal afferent nerve fibers. The physiological significance of GLP-2R expression in anatomical locations and specific cell types in the intestine has yet to be determined. Centrally, GLP-2R is mostly expressed in DMH and ARC of the hypothalamus and is also located in the brainstem (dorsal motor nucleus of vagus nerve [DMV]) and hippocampus (parabrachial neurons) (Guan, 2014). Since these are major energy balance regulating areas of the brain, it is conceivable that GLP-2 plays important roles in metabolic regulation.

GLP-2 in metabolic disorders

Elevated levels of circulating GLP-2 have been reported in streptozotocin-induced diabetic rats compared with nondiabetic controls (Fischer et al., 1997). Obese subjects also have elevated plasma GLP-2 levels in both fasting and postprandial states, which correlated with increases in hemoglobin A1c and insulin resistance (Verdam et al., 2011; Geloneze et al., 2013). Postprandial plasma GLP-2 level was found to be unaltered in obese subjects compared to normal weight individuals following a fat meal (Higgins et al., 2020). In obese insulin-resistant subjects, postprandial secretion of GLP-2 was blunted (Higgins et al., 2020). Further, circulating levels of GLP-2 are increased in obese subjects following bariatric surgery (Cazzo et al., 2016). Normal GLP-2R signaling may be protective against dysregulated lipid metabolism. In hamsters, GLP-2 actions on increasing plasma TG in insulin resistant states may contribute to postprandial dyslipidemia (Hein et al., 2013). In addition, chronic treatment with a GLP-2R antagonist, GLP-2 (3-33), exacerbated insulin resistance in high-fat fed mice (Baldassano et al., 2015) and hepatic lipid accumulation (Baldassano et al., 2016). On the contrary, high fat-fed GLP-2R knockout mice had reduced hepatic lipoprotein (very-low-density lipoprotein) secretion and similar fasting plasma TG levels as compared to chow-fed mice (Taher et al., 2018). Chronic intraperitoneal GLP-2 administration stimulated very-low-density lipoprotein secretion and increased fasting plasma TG levels in chow-fed but not high fat-fed hamsters (Taher et al., 2018). Chronic administration of GLP-2 reduced inflammation in the brain of obese mice (Nuzzo et al., 2019). Loss of Glp-2r in mice reduces atherosclerosis (Kahles et al., 2023). Finally, patients with myocardial infarction have higher circulating levels of GLP-2, making GLP-2 an early indicator for cardiovascular diseases (Kahles et al., 2023). Although these studies suggest beneficial effects of endogenous GLP-2 against metabolic disorders, it remains unclear whether increased GLP-2 secretion and action is pathological for or a characteristic of metabolic disorders.

Regulation of lipid handling in the intestine by GLP-2

Besides the above-mentioned biological functions, GLP-2 has been shown to play pleiotropic roles in regulating lipid handling in the intestine. Considering the unique aspects of GLP-2's actions in this regard, it is important to make distinctions of its effects on two separate processes, i.e., dietary fat absorption during postprandial state, and the release of intestinally stored lipids during post-absorptive state.

Lipid absorption

GLP-2 enhances lipid absorption in the intestine. In healthy humans, intravenous infusion of GLP-2 increased plasma levels of free fatty acids and TG during meal ingestion, indicating enhanced absorption of luminal lipids (Meier et al., 2006). In mice and hamsters, acute GLP-2 administration enhanced lipid absorption and CM secretion during oral oil gavage (Hsieh et al., 2009). GLP-1, another gut hormone co-secreted with GLP-2 in a 1:1 M ratio from enteroendocrine L cells, decreased lipid absorption in hamsters (Hein et al., 2013). However, when GLP-1 and GLP-2 were co-infused for short-term (30 min), there was increased lipid absorption, suggesting a predominant effect of GLP-2 (Hein et al., 2013). In contrast, prolonged (120 min) co-infusion of GLP-1 and GLP-2 decreased lipid absorption. In addition, inhibition of DPPIV, the enzyme that cleavages GLP-1 and GLP-2, decreased lipid absorption (Hein et al., 2013). This suggests that under normal physiological conditions the actions of GLP-2 predominate to enhance lipid absorption, which is lost under conditions of sustained GLP-1 activity. Overall, studies in humans and rodents show that exogenous GLP-2 enhances dietary lipid absorption, although the physiological significance of this has yet to be determined.

Lipid mobilization

As mentioned above, the intestine withholds a portion of ingested dietary lipids into the post-absorptive state. A unique feature of GLP-2 in intestinal lipid handling is its post-absorptive mobilization of such intestinally stored lipids. In humans, administration of GLP-2 7 h after a fat load increased plasma and CM TG (Dash et al., 2014). The increased CM secretion following GLP-2 is attributed to the release of CM that are "pre-formed" (i.e., not newly synthesized) and reside in locations outside enterocytes, such as intercellular space, lamina propria and mesenteric lymphatics. Several evidence support this notion. Firstly, tracer kinetics data and mathematic modelling did not support enhanced synthesis of new apolipoprotein B48 (apoB48, the structural apolipoprotein on CM); instead, they pointed to increased appearance of apoB48 in blood circulation without the contribution of new apoB48 synthesis. In line with this, GLP-2 did not affect CM biosynthesis pathway in humans (Syed-Abdul et al., 2022b) and CM particle size in lymph fluid in rats (Stahel et al., 2019). Secondly, retinal palmate tracing of dietary lipids supported that the increased TG in plasma and CM originated from the earlier meal (Dash et al., 2014). Mobilization of intestinal lipid stores by GLP-2 during fasting was confirmed in studies with rodents, including mice and hamsters (Hsieh et al., 2015) and rats (Stahel et al., 2019).

Mechanisms of GLP regulation of intestinal lipid handling

The exact mechanisms whereby GLP-2 modulates intestinal lipid handling remains elusive. In the following sections, we summarize direct and indirect evidence that help provide mechanistic insights for both processes of lipid handling.

Postprandial lipid absorption

Several mechanisms have been proposed for GLP-2's enhancement in postprandial lipid absorption. In mice and hamsters, GLP-2 enhances dietary lipid absorption via glycosylation of CD36 (Hsieh et al., 2009). CD36 is a scavenger receptor mediating the transport of fatty acids across the plasma membrane of various cell types, including enterocytes (Nassir et al., 2007). CD36 glycosylation by GLP-2 may provide functional enhancement in fatty acid uptake by the enterocytes. How GLP-2 increases CD36 glycosylation is unknown.

Since GLP-2R is not expressed on the enterocytes where CM biosynthesis occurs, enhanced lipid absorption is likely indirect. One possibility is via GLP-2's effects on the secretion of several hormones, as GLP-2 infusion in humans inhibits ghrelin (Banasch et al., 2006) and stimulates glucagon (Meier et al., 2006) secretion. GLP-2 also stimulates VIP secretion from enteric VIP-expressing neurons (de Heuvel et al., 2012). Enterocytes are known to express VIP receptor (Dharmsathaphorn et al., 1983) and VIP may activate VIPR1 on enterocytes to stimulate NO production (Spessert, 1993; González et al., 1997). As discussed above, GLP-2 exerts anti-inflammatory effects via activation of VIP neurons (Sigalet et al., 2007). In a recent study, it was shown that intestine luminal lipids stimulate VIP-expressing neurons to release VIP, which activates VIPR2 on type-3 innate lymphoid cells to release IL-22 and subsequently IL-22 stimulates enterocytes to enhance lipid absorption (Talbot et al., 2020). It is therefore likely VIP-neurons are an important intermediate cell type that responds to GLP-2 stimulation by secreting VIP to enhance lipid absorption. This intriguing hypothesis remains to be tested in future studies.

Nitric oxide (NO) signaling was suggested to mediate enhanced postprandial lipid absorption by GLP-2. GLP-2-stimulated lipid absorption and CM secretion was blocked by NOS inhibitor in hamsters and endothelial NOS-deficient mice were resistant to GLP-2 stimulation in CM secretion (Hsieh et al., 2015). GLP-2R is expressed on NOS-positive cells (Cinci et al., 2011); therefore, it is conceivable that GLP-2 enhances lipid absorption through stimulating NO production. Importantly, the NO donor S-nitroso-L-glutathione stimulated CM production *in vitro* in primary enterocytes (Hsieh et al., 2015). This indicates that NO production in enterocytes can have a direct effect on lipid absorption. VEGF-C receptor (VEGFR3) signaling is required for lipid absorption along with NO production (Shew et al., 2018). VEGF is released by myofibroblasts which express GLP-2R and VEGF can activate its receptor on the enterocytes (Siafakas et al., 1999). It is possible that a GLP-2-VEGF-NO pathway may be operative for the stimulation of lipid absorption. Several of GLP-2's other actions are underlined by its stimulation on NO production, which may indirectly contribute to GLP-2's effects on lipid absorption. For instance, GLP-2-stimulated increase in intestinal blood flow in pigs was blunted by NOS inhibitor (Guan et al., 2003). NO is a vasodilator, thus increased NO production may lead to increased blood flow. Increased mesenteric blood flow, secondary to increased NO production, might contribute to increased CM secretion by GLP-2; however, a direct link between blood flow and CM secretion has not been established. Local NO production by specific cells may play important roles in mediating GLP-2's effects on intestinal lipid absorption. In a recent study, Grande et al. showed that GLP-2 stimulates dietary lipid absorption and CM production in mice and hamsters via neuronal NOS (nNOS) (Grande et al., 2022). Specifically, loss of nNOS in hamsters and mice ablated GLP-2 enhancement in lipid absorption. The exact nature of this pathway remains unclear, but protein kinase G (PKG) seems to be downstream of nNOS, thus GLP-2 invokes a nNOS-PKG-dependent pathway (Grande et al., 2022).

Post-absorptive release of lipid stores

NO signaling has been proposed to mediate GLP-2's effects on postprandial release of intestinal lipid stores. In hamsters, the NO donor S-nitroso-L-glutathione stimulated, while NOS inhibitor attenuated, the release of stored TGs during post-absorptive stage (Hsieh et al., 2015). In humans, co-infusion of GLP-2 and a NOS inhibitor attenuated GLP-2's effects on stimulating mesenteric blood flow but did not affect its effects on stimulating post-absorptive CM release (Xiao et al., 2019b). The discrepancy may be due to species differences. It is also possible that NO production from specific cell types in the intestinal region, but not systemic NO production, mediates GLP-2's effects on post-absorptive release of intestinally stored lipids. If this being the case, the specific cell type(s) remain undefined. As discussed above, neuronal NOS was shown to underly GLP-2's enhancement in postprandial lipid absorption (Grande et al., 2022). Whether GLP-2 mobilizes intestinal lipid stores via neuronal NOS remains to be studied.

An additional mechanism for GLP-2 to release intestinal lipid stores may involve the modulation of lymphatic functions. Following secretion from the enterocytes, CMs enter the lacteals and transport in the mesenteric lymph ducts before joining the blood circulation. VEGF signaling plays important roles in regulating the contractility, pumping and opening/closing of the lymphatic endothelial wall (Breslin et al., 2007; Choe et al., 2015; Zhang et al., 2018). VEGF, which is expressed on the smooth muscle cells lining the lacteal, is vital for sustained increase in lymphatic contraction and lipid absorption (Syed-Abdul et al., 2022a). It has been shown that GLP-2 promotes intestinal growth through VEGF release from subepithelial myofibroblasts (Bulut et al., 2008). It is possible that increased VEGF release in response to GLP-2 enhances lymphatic functions to promote lipid output. CD36 expression on lymphatic endothelial cells increases from lacteals to collecting vessels and is responsible for maintaining lymphatic integrity and lipid absorption (Cifarelli et al., 2021). An intriguing hypothesis is that VEGF and CD36 are downstream mediators of GLP-2 in mobilizing intestinal lipid stores by regulating lymphatic functions.

Potential neural pathways in mediating GLP-2's effects on intestinal lipids

GLP-2R is expressed on neuronal cells in both the intestine and the brain. In the intestine, it is expressed on the enteric neurons (Bjerknes and Cheng, 2001; Guan et al., 2006). GLP-2R activation on enteric neurons contributes to GLP-2 promotion of intestinal growth and repair (Bjerknes and Cheng, 2001). Centrally, GLP-2R is expressed mostly in the energy balance regulating areas of the brain and several of these areas are innervated by GLP-2 immunoreactive terminal fibres from the brainstem (Larsen et al., 1997; Yusta et al., 2000; Lovshin et al., 2001). CNS GLP-2R signaling has been shown to play significant roles in regulating several

physiological processes, including feeding behavior and gastrointestinal function. Chronic intracerebroventricular infusion of GLP-2 suppressed food intake and increased POMC mRNA in the ARC (Guan et al., 2012). POMC neurons are well-known for regulating energy balance by integrating long-term adiposity and short-term satiety endocrine signals. POMC specific Glp-2r knockout in mice increased food intake and gastric motility (Guan et al., 2012). CNS GLP-2R signaling has also been shown to regulate peripheral metabolism, thus POMC-specific Glp-2r knockout in mice impaired whole-body glucose metabolism and increased hepatic glucose production (Shi et al., 2013).

The importance of central GLP-2/GLP-2R is also highlighted by its link to behavioral and neuropathological conditions. Astrocytes are non-neuronal cells that are abundantly present in the CNS. They are important for homeostasis, defence and regeneration of the CNS and active contribution to pathogenesis of neurodegenerative disorders including Alzheimer's disease. GLP-2 increased proliferation of cultured rat astrocytes (Velázquez et al., 2003). This is in line with higher expression of GLP-2R in younger passages of astrocyte cell culture (with higher capacity of proliferation) compared to older passages of the culture (Velázquez et al., 2022). GLP-2 has also been shown to restore memory and neurogenesis in experimental Alzheimer's disease mouse model (Sasaki-Hamada et al., 2019). Thus, targeting GLP-2/GLP-2R signaling may be beneficial for the treatment of Alzheimer's disease. GLP-2 analogue exhibited neuroprotective properties against Parkinson's disease (Su et al., 2021; Zhang et al., 2021). Central GLP-2 infusion also showed prevention and protection against inflammation-induced memory impairment and anxiety in mice (Iwai et al., 2015).

Intestinal and brain neuronal GLP-2R expression and the regulation of feeding behavior and hepatic glucose metabolism by central GLP-2 signaling strongly suggest a neural network in regulating its effects on intestinal lipid handling. Besides evidence that local neural pathways are involved in GLP-2 enhancement of lipid absorption, post-absorptive mobilization of intestinal lipid stores also involves a neural mechanism. In a recent study, we demonstrated that the full effects of GLP-2 in releasing lipid stores during post-absorptive state requires a neural pathway involving the CNS (Mukherjee et al., 2023). In consistency with previous studies, intraperitoneal administration of GLP-2 during post-prandial period stimulated intestinal lipid output in rats. This was accompanied with activation of POMC neurons in the ARC of hypothalamus. When the gut-brain neural communication was disrupted with subdiaphragmatic vagotomy, GLP-2's effects on intestinal lipid release was blunted. This supports that GLP-2 mobilizes lipid storage in the intestine through both local and central mechanisms. The exact nature of this pathway remains to be defined. MC4R signaling in the hypothalamus is activated by POMC neurons to control feeding and gastric emptying in rats (Guan et al., 2012; Guan, 2014; Sun et al., 2021). GLP- 2R activation in POMC neurons increases vagal outflow by activating MC4R in the brainstem (Guan et al., 2012; Shi et al., 2013). In light of their roles in regulating feeding behavior and hepatic glucose metabolism, CNS GLP-2R and MC4R are likely candidate key players along this pathway. Collectively, a working model for GLP-2 mobilization of lipid stores in the intestine involves both peripheral and central mechanisms, the latter requiring further elucidation.

Concluding remarks and future directions

The intestine is a key organ for lipid handling. Beside the well-recognized role in dietary lipid absorption, it is also increasingly recognized that the intestine is capable of retaining a releasable pool of lipids during post-absorptive period. The regulation of these processes, despite significant advances, remain not fully understood. GLP-2, a gut hormone with a range of biological roles, regulates lipid handling in the intestine, both during dietary lipid absorption and during post-absorptive release of stored lipids. How GLP-2 mediates each of these two processes are being elucidated. However, the exact mechanisms are not fully defined. The current knowledge is that GLP-2 "indirectly" enhances lipid absorption via intermediate GLP-2R-expressing cell(s), that neural pathways are invoked by GLP-2 at least partly in both processes, and that both local and central regulatory mechanisms are likely involved (Figure 1). It is hoped that better understanding of the mechanism whereby GLP-2 regulates lipid handling in the intestine will provide health benefits beyond its current clinical use for the treatment of short-bowel syndrome.

Author contributions

KM: Conceptualization, Visualization, Writing–original draft, Writing–review and editing. CX: Conceptualization, Funding acquisition, Supervision, Writing–original draft, Writing–review and editing.

Funding

The author(s) declare financial support was received for the research, authorship, and/or publication of this article. Research in CX lab is supported by a Saskatchewan Health Research Foundation (SHRF) Establishment Grant, a Natural Science and Engineering Research Council (NSERC) Discovery Grant, a Canadian Institutes of Health Research (CIHR) Project Grant, and College of Medicine Research Awards (CoMRAD) to CX. CX is a recipient of a New Investigator Award and the Henry J. M. Barnett Scholarship from the Heart and Stroke Foundation of Canada. KM is supported by the Department of Anatomy, Physiology, and Pharmacology Devolved Scholarship.

Conflict of interest

The authors declare that the research was conducted in the absence of any commercial or financial relationships that could be construed as a potential conflict of interest.

The author(s) declared that they were an editorial board member of Frontiers, at the time of submission. This had no impact on the peer review process and the final decision.

Publisher's note

References

Amato, A., Baldassano, S., and Mulè, F. (2016). GLP2: an underestimated signal for improving glycaemic control and insulin sensitivity. *J. Endocrinol.* 229, R57–R66. doi:10.1530/JOE-16-0035

Amato, A., Baldassano, S., Serio, R., and Mulè, F. (2009). Glucagon-like peptide-2 relaxes mouse stomach through vasoactive intestinal peptide release. *Am. J. Physiology-Gastrointestinal Liver Physiology* 296, G678–G684. doi:10.1152/ajpgi.90587.2008

Baccari, M. C., Vannucchi, M. G., and Idrizaj, E. (2022). Glucagon-like peptide-2 in the control of gastrointestinal motility: physiological implications. *Curr. Protein Pept. Sci.* 23, 61–69. doi:10.2174/1389203723666220217142935

Baldassano, S., Amato, A., Caldara, G. F., and Mulè, F. (2016). Glucagon-like peptide-2 treatment improves glucose dysmetabolism in mice fed a high-fat diet. *Endocrine* 54, 648–656. doi:10.1007/s12020-016-0871-3

Baldassano, S., Rappa, F., Amato, A., Cappello, F., and Mulè, F. (2015). GLP-2 as beneficial factor in the glucose homeostasis in mice fed a high fat diet. *J. Cell Physiol.* 230, 3029–3036. doi:10.1002/jcp.25039

Banasch, M., Bulut, K., Hagemann, D., Schrader, H., Holst, J. J., Schmidt, W. E., et al. (2006). Glucagon-like peptide 2 inhibits ghrelin secretion in humans. *Regul. Pept.* 137, 173–178. doi:10.1016/j.regpep.2006.07.009

Bjerknes, M., and Cheng, H. (2001). Modulation of specific intestinal epithelial progenitors by enteric neurons. *Proc. Natl. Acad. Sci. U. S. A.* 98, 12497–12502. doi:10.1073/pnas.211278098

Bremholm, L., Hornum, M., Andersen, U. B., Hartmann, B., Holst, J. J., and Jeppesen, P. B. (2011). The effect of Glucagon-Like Peptide-2 on mesenteric blood flow and cardiac parameters in end-jejunostomy short bowel patients. *Regul. Pept.* 168, 32–38. doi:10.1016/j.regpep.2011.03.003

Bremholm, L., Hornum, M., Henriksen, B. M., Larsen, S., and Holst, J. J. (2009). Glucagon-like peptide-2 increases mesenteric blood flow in humans. *Scand. J. Gastroenterol.* 44, 314–319. doi:10.1080/00365520802538195

Breslin, J. W., Gaudreault, N., Watson, K. D., Reynoso, R., Yuan, S. Y., and Wu, M. H. (2007). Vascular endothelial growth factor-C stimulates the lymphatic pump by a VEGF receptor-3-dependent mechanism. *Am. J. Physiology-Heart Circulatory Physiology* 293, H709–H718. doi:10.1152/ajpheart.00102.2007

Brubaker, P. L., and Anini, Y. (2003). Direct and indirect mechanisms regulating secretion of glucagon-like peptide-1 and glucagon-like peptide-2. *Can. J. Physiol. Pharmacol.* 81, 1005–1012. doi:10.1139/y03-107

Brubaker, P. L., Izzo, A., Hill, M., and Drucker, D. J. (1997). Intestinal function in mice with small bowel growth induced by glucagon-like peptide-2. *Am. J. Physiology-Endocrinology Metabolism* 272, E1050–E1058. doi:10.1152/ajpendo.1997.272.6.E1050

Bulut, K., Pennartz, C., Felderbauer, P., Meier, J. J., Banasch, M., Bulut, D., et al. (2008). Glucagon like peptide-2 induces intestinal restitution through VEGF release from subepithelial myofibroblasts. *Eur. J. Pharmacol.* 578, 279–285. doi:10.1016/j.ejphar.2007.08.044

Cani, P. D., Possemiers, S., Van de Wiele, T., Guiot, Y., Everard, A., Rottier, O., et al. (2009). Changes in gut microbiota control inflammation in obese mice through a mechanism involving GLP-2-driven improvement of gut permeability. *Gut* 58, 1091–1103. doi:10.1136/gut.2008.165886

Cazzo, e., Gestic, m. A., Utrini, m. P., Chaim, f. D. M., Geloneze, b., Pareja, j. C., et al. (2016). Glp-2: a poorly understood mediator enrolled in various bariatric/metabolic surgery-related pathophysiologic mechanisms. *Abcd. Arq. Bras. Cir. Dig. (são paulo)* 29, 272–275. doi:10.1590/0102-6720201600040014

Chavez–Jauregui, R. N., Mattes, R. D., and Parks, E. J. (2010). Dynamics of fat absorption and effect of sham feeding on postprandial lipema. *Gastroenterology* 139, 1538–1548. doi:10.1053/j.gastro.2010.05.002

Choe, K., Jang, J. Y., Park, I., Kim, Y., Ahn, S., Park, D.-Y., et al. (2015). Intravital imaging of intestinal lacteals unveils lipid drainage through contractility. *J. Clin. Investigation* 125, 4042–4052. doi:10.1172/JCI76509

Cifarelli, V., Appak-Baskoy, S., Peche, V. S., Kluzak, A., Shew, T., Narendran, R., et al. (2021). Visceral obesity and insulin resistance associate with CD36 deletion in lymphatic endothelial cells. *Nat. Commun.* 12, 3350. doi:10.1038/s41467-021-23808-3

Cinci, L., Faussone-Pellegrini, M. S., Rotondo, A., Mulè, F., and Vannucchi, M. G. (2011). GLP-2 receptor expression in excitatory and inhibitory enteric neurons and its role in mouse duodenum contractility. *Neurogastroenterol. Motil.* 23, e383–e392. doi:10.1111/j.1365-2982.2011.01750.x

Dash, S., Xiao, C., Morgantini, C., Connelly, P. W., Patterson, B. W., and Lewis, G. F. (2014). Glucagon-like peptide-2 regulates release of chylomicrons from the intestine. *Gastroenterology* 147, 1275–1284. doi:10.1053/j.gastro.2014.08.037

Dash, S., Xiao, C., Morgantini, C., and Lewis, G. F. (2015). New insights into the regulation of chylomicron production. *Annu. Rev. Nutr.* 35, 265–294. doi:10.1146/annurev-nutr-071714-034338

De Heer, J., Pedersen, J., Ørskov, C., and Holst, J. J. (2007). The alpha cell expresses glucagon-like peptide-2 receptors and glucagon-like peptide-2 stimulates glucagon secretion from the rat pancreas. *Diabetologia* 50, 2135–2142. doi:10.1007/s00125-007-0761-6

de Heuvel, E., Wallace, L., Sharkey, K. A., and Sigalet, D. L. (2012). Glucagon-like peptide 2 induces vasoactive intestinal polypeptide expression in enteric neurons via phophatidylinositol 3-kinase-γ signaling. *Am. J. Physiology-Endocrinology Metabolism* 303, E994–E1005. doi:10.1152/ajpendo.00291.2012

Deniz, M., Bozkurt, A., and Kurtel, H. (2007). Mediators of glucagon-like peptide 2-induced blood flow: responses in different vascular sites. *Regul. Pept.* 142, 7–15. doi:10.1016/j.regpep.2007.01.002

Dharmsathaphorn, K., Harms, V., Yamashiro, D. J., Hughes, R. J., Binder, H. J., and Wright, E. M. (1983). Preferential binding of vasoactive intestinal polypeptide to basolateral membrane of rat and rabbit enterocytes. *J. Clin. Investigation* 71, 27–35. doi:10.1172/JCI110748

Drucker, D. J., Ehrlich, P., Asa, S. L., and Brubaker, P. L. (1996). Induction of intestinal epithelial proliferation by glucagon-like peptide 2. *Proc. Natl. Acad. Sci. U. S. A.* 93, 7911–7916. doi:10.1073/pnas.93.15.7911

Drucker, D. J. (2002). Gut adaptation and the glucagon-like peptides. *Gut* 50, 428–435. doi:10.1136/gut.50.3.428

Eliasson, J., Hvistendahl, M. K., Freund, N., Bolognani, F., Meyer, C., and Jeppesen, P. B. (2021). Apraglutide, a novel glucagon-like peptide-2 analog, improves fluid absorption in patients with short bowel syndrome intestinal failure: findings from a placebo-controlled, randomized phase 2 trial. *J. Parenter. Enter. Nutr.* 46, 896–904. doi:10.1002/jpen.2223

Fischer, K. D., Dhanvantari, S., Drucker, D. J., and Brubaker, P. L. (1997). Intestinal growth is associated with elevated levels of glucagon-like peptide 2 in diabetic rats. *Am. J. Physiology-Endocrinology Metabolism* 273, E815–E820. doi:10.1152/ajpendo.1997.273.4.E815

Fuchs, C. D., Claudel, T., Mlitz, V., Riva, A., Menz, M., Brusilovskaya, K., et al. (2023). GLP-2 improves hepatic inflammation and fibrosis in Mdr2–/– mice via activation of NR4a1/Nur77 in hepatic stellate cells and intestinal FXR signaling. *Cell. Mol. Gastroenterol. Hepatol.* 16, 847–856. doi:10.1016/j.jcmgh.2023.08.003

Fuchs, S., Yusta, B., Baggio, L. L., Varin, E. M., Matthews, D., and Drucker, D. J. (2020). Loss of Glp2r signaling activates hepatic stellate cells and exacerbates diet-induced steatohepatitis in mice. *JCI Insight* 23 (5), e136907. doi:10.1172/jci.insight.136907

Geloneze, B., Lima, M. M. de O., Pareja, J. C., Barreto, M. R. L., and Magro, D. O. (2013). Association of insulin resistance and GLP-2 secretion in obesity: a pilot study. *Arquivos Brasileiros de Endocrinol. Metabologia* 57, 632–635. doi:10.1590/S0004-27302013000800008

Ghanem, M., Lewis, G. F., and Xiao, C. (2022). Recent advances in cytoplasmic lipid droplet metabolism in intestinal enterocyte. *Biochim. Biophys. Acta Mol. Cell Biol. Lipids* 1867, 159197. doi:10.1016/j.bbalip.2022.159197

González, C., Barroso, C., Martín, C., Gulbenkian, S., and Estrada, C. (1997). Neuronal nitric oxide synthase activation by vasoactive intestinal peptide in bovine cerebral arteries. *J. Cereb. Blood Flow Metabolism* 17, 977–984. doi:10.1097/00004647-199709000-00007

Grande, E. M., Raka, F., Hoffman, S., and Adeli, K. (2022). GLP-2 regulation of dietary fat absorption and intestinal chylomicron production via neuronal nitric oxide synthase (nNOS) signaling. *Diabetes* 71, 1388–1399. doi:10.2337/db21-1053

Guan, X., Shi, X., Li, X., Chang, B., Wang, Y., Li, D., et al. (2012). GLP-2 receptor in POMC neurons suppresses feeding behavior and gastric motility. *Am. J. Physiology-Endocrinology Metabolism* 303, E853–E864. doi:10.1152/ajpendo.00245.2012

Guan, X. (2014). The CNS glucagon-like peptide-2 receptor in the control of energy balance and glucose homeostasis. *Am. J. Physiol. Regul. Integr. Comp. Physiol.* 307, R585–R596. doi:10.1152/ajpregu.00096.2014

Guan, X., Karpen, H. E., Stephens, J., Bukowski, J. T., Niu, S., Zhang, G., et al. (2006). GLP-2 receptor localizes to enteric neurons and endocrine cells expressing vasoactive

peptides and mediates increased blood flow. *Gastroenterology* 130, 150–164. doi:10.1053/j.gastro.2005.11.005

Guan, X., Stoll, B., Lu, X., Tappenden, K. A., Holst, J. J., Hartmann, B., et al. (2003). GLP-2-mediated up-regulation of intestinal blood flow and glucose uptake is nitric oxide-dependent in TPN-fed piglets 1. *Gastroenterology* 125, 136–147. doi:10.1016/s0016-5085(03)00667-x

Hargrove, D. M., Alagarsamy, S., Croston, G., Laporte, R., Qi, S., Srinivasan, K., et al. (2020). Pharmacological characterization of apraglutide, a novel long-acting peptidic glucagon-like peptide-2 agonist, for the treatment of short bowel syndrome. *J. Pharmacol. Exp. Ther.* 373, 193–203. doi:10.1124/jpet.119.262238

He, W., Rebello, O. D., Henne, A., Nikolka, F., Klein, T., and Maedler, K. (2021). GLP-2 is locally produced from human islets and balances inflammation through an inter-islet-immune cell crosstalk. *Front. Endocrinol. (Lausanne)* 12, 697120. doi:10.3389/fendo.2021.697120

Hein, G. J., Baker, C., Hsieh, J., Farr, S., and Adeli, K. (2013). GLP-1 and GLP-2 as yin and yang of intestinal lipoprotein production: evidence for predominance of GLP-2-stimulated postprandial lipemia in normal and insulin-resistant states. *Diabetes* 62, 373–381. doi:10.2337/db12-0202

Higgins, V., Asgari, S., Hamilton, J. K., Wolska, A., Remaley, A. T., Hartmann, B., et al. (2020). Postprandial dyslipidemia, hyperinsulinemia, and impaired gut peptides/bile acids in adolescents with obesity. *J. Clin. Endocrinol. Metab.* 105, 1228–1241. doi:10.1210/clinem/dgz261

Hsieh, J., Longuet, C., Maida, A., Bahrami, J., Xu, E., Baker, C. L., et al. (2009). Glucagon-like peptide-2 increases intestinal lipid absorption and chylomicron production via CD36. *Gastroenterology* 137, 997–1005. doi:10.1053/j.gastro.2009.05.051

Hsieh, J., Trajcevski, K. E., Farr, S. L., Baker, C. L., Lake, E. J., Taher, J., et al. (2015). Glucagon-like peptide 2 (GLP-2) stimulates postprandial chylomicron production and postabsorptive release of intestinal triglyceride storage pools via induction of nitric oxide signaling in male hamsters and mice. *Endocrinology* 156, 3538–3547. doi:10.1210/EN.2015-1110

Hung, Y.-H., Carreiro, A. L., and Buhman, K. K. (2017). Dgat1 and Dgat2 regulate enterocyte triacylglycerol distribution and alter proteins associated with cytoplasmic lipid droplets in response to dietary fat. *Biochimica Biophysica Acta (BBA) - Mol. Cell Biol. Lipids* 1862, 600–614. doi:10.1016/j.bbalip.2017.02.014

Iwai, T., Jin, K., Ohnuki, T., Sasaki-Hamada, S., Nakamura, M., Saitoh, A., et al. (2015). Glucagon-like peptide-2-induced memory improvement and anxiolytic effects in mice. *Neuropeptides* 49, 7–14. doi:10.1016/j.npep.2014.11.001

Jackson, K. G., Denise Robertson, M., Fielding, B. A., Frayn, K. N., and Williams, C. M. (2001). Second meal effect: modified sham feeding does not provoke the release of stored triacylglycerol from a previous high-fat meal. *Br. J. Nutr.* 85, 149–156. doi:10.1079/BJN2000226

Jacome-Sosa, M., Hu, Q., Manrique-Acevedo, C. M., Phair, R. D., and Parks, E. J. (2021). Human intestinal lipid storage through sequential meals reveals faster dinner appearance is associated with hyperlipidemia. *JCI Insight* 6, e148378. doi:10.1172/jci.insight.148378

Jeppesen, P. B., Hartmann, B., Thulesen, J., Graff, J., Lohmann, J., Hansen, B. S., et al. (2001). Glucagon-like peptide 2 improves nutrient absorption and nutritional status in short-bowel patients with no colon. *Gastroenterology* 120, 806–815. doi:10.1053/gast.2001.22555

Jeppesen, P. B., Lund, P., Gottschalck, I. B., Nielsen, H. B., Holst, J. J., Mortensen, J., et al. (2009). Short bowel patients treated for two years with glucagon-like peptide 2: effects on intestinal morphology and absorption, renal function, bone and body composition, and muscle function. *Gastroenterol. Res. Pract.* 2009, 616054–616112. doi:10.1155/2009/616054

Kahles, F., Sausen, M., Quintana, L., Rueckbeil, M., Idel, P., Mertens, R., et al. (2023). GLP-2 predicts cardiovascular outcomes in patients with myocardial infarction and increases atherosclerosis in mice. *Eur. Heart J.* 44 (Suppl 2), ehad655.1429. doi:10.1093/eurheartj/ehad655.1429

Larsen, P. J., Tang-Christensen, M., Holst, J. J., and Ørskov, C. (1997). Distribution of glucagon-like peptide-1 and other preproglucagon-derived peptides in the rat hypothalamus and brainstem. *Neuroscience* 77, 257–270. doi:10.1016/S0306-4522(96)00434-4

Lewis, G. F., Xiao, C., and Hegele, R. A. (2015). Hypertriglyceridemia in the genomic era: a new paradigm. *Endocr. Rev.* 36, 131–147. doi:10.1210/er.2014-1062

Lovshin, J., Estall, J., Yusta, B., Brown, T. J., and Drucker, D. J. (2001). Glucagon-like peptide (GLP)-2 action in the murine central nervous system is enhanced by elimination of GLP-1 receptor signaling. *J. Biol. Chem.* 276, 21489–21499. doi:10.1074/jbc.M009382200

Lovshin, J. A., Huang, Q., Seaberg, R., Brubaker, P. L., and Drucker, D. J. (2004). Extrahypothalamic expression of the glucagon-like peptide-2 receptor is coupled to reduction of glutamate-induced cell death in cultured hippocampal cells. *Endocrinology* 145, 3495–3506. doi:10.1210/en.2004-0100

Meier, J. J., Nauck, M. A., Pott, A., Heinze, K., Goetze, O., Bulut, K., et al. (2006). Glucagon-like peptide 2 stimulates glucagon secretion, enhances lipid absorption, and inhibits gastric acid secretion in humans. *Gastroenterology* 130, 44–54. doi:10.1053/j.gastro.2005.10.004

Murali, S. G., Brinkman, A. S., Solverson, P., Pun, W., Pintar, J. E., and Ney, D. M. (2012). Exogenous GLP-2 and IGF-I induce a differential intestinal response in IGF binding protein-3 and -5 double knockout mice. *Am. J. Physiol. Gastrointest. Liver Physiol.* 302, G794–G804. doi:10.1152/ajpgi.00372.2011

Mukherjee, K., Wang, R., and Xiao, C. (2023). Release of lipids stored in the intestine by glucagon-like peptide-2 involves a gut-brain neural pathway. *Arterioscler. Thromb. Vasc. Biol.* 44, 192–201. doi:10.1161/ATVBAHA.123.320032

Nagell, C. F., Wettergren, A., Pedersen, J. F., Mortensen, D., and Holst, J. J. (2004). Glucagon-like peptide-2 inhibits antral emptying in man, but is not as potent as glucagon-like peptide-1. *Scand. J. Gastroenterol.* 39, 353–358. doi:10.1080/00365520410004424

Nakame, K., Kaji, T., Mukai, M., Shinyama, S., and Matsufuji, H. (2016). The protective and anti-inflammatory effects of glucagon-like peptide-2 in an experimental rat model of necrotizing enterocolitis. *Pept. (N.Y.)* 75, 1–7. doi:10.1016/j.peptides.2015.07.025

Nassir, F., Wilson, B., Han, X., Gross, R. W., and Abumrad, N. A. (2007). CD36 is important for fatty acid and cholesterol uptake by the proximal but not distal intestine. *J. Biol. Chem.* 282, 19493–19501. doi:10.1074/jbc.M703330200

Nelson, D. W., Sharp, J. W., Brownfield, M. S., Raybould, H. E., and Ney, D. M. (2007). Localization and activation of glucagon-like peptide-2 receptors on vagal afferents in the rat. *Endocrinology* 148, 1954–1962. doi:10.1210/en.2006-1232

Nuzzo, D., Baldassano, S., Amato, A., Picone, P., Galizzi, G., Caldara, G. F., et al. (2019). Glucagon-like peptide-2 reduces the obesity-associated inflammation in the brain. *Neurobiol. Dis.* 121, 296–304. doi:10.1016/j.nbd.2018.10.012

Ørskov, C., Hartmann, B., Poulsen, S. S., Thulesen, J., Hare, K. J., and Holst, J. J. (2005). GLP-2 stimulates colonic growth via KGF, released by subepithelial myofibroblasts with GLP-2 receptors. *Regul. Pept.* 124, 105–112. doi:10.1016/j.regpep.2004.07.009

Pedersen, J., Pedersen, N. B., Brix, S. W., Grunddal, K. V., Rosenkilde, M. M., Hartmann, B., et al. (2015). The glucagon-like peptide 2 receptor is expressed in enteric neurons and not in the epithelium of the intestine. *Pept. (N.Y.)* 67, 20–28. doi:10.1016/j.peptides.2015.02.007

Qi, K. K., Wu, J., Deng, B., Li, Y. M., and Xu, Z. W. (2015). PEGylated porcine glucagon-like peptide-2 improved the intestinal digestive function and prevented inflammation of weaning piglets challenged with LPS. *Animal* 9, 1481–1489. doi:10.1017/S1751731115000749

Roberge, J. N., and Brubaker, P. L. (1991). Secretion of proglucagon-derived peptides in response to intestinal luminal nutrients. *Endocrinology* 128, 3169–3174. doi:10.1210/endo-128-6-3169

Robertson, M. D., Parkes, M., Warren, B. F., Ferguson, D. J. P., Jackson, K. G., Jewell, D. P., et al. (2003). Mobilisation of enterocyte fat stores by oral glucose in humans. *Gut* 52, 834–839. doi:10.1136/gut.52.6.834

Sasaki-Hamada, S., Ikeda, M., and Oka, J. I. (2019). Glucagon-like peptide-2 rescues memory impairments and neuropathological changes in a mouse model of dementia induced by the intracerebroventricular administration of streptozotocin. *Sci. Rep.* 9, 13723. doi:10.1038/s41598-019-50167-3

Shew, T., Wolins, N. E., and Cifarelli, V. (2018). VEGFR-3 signaling regulates triglyceride retention and absorption in the intestine. *Front. Physiol.* 9, 1783. doi:10.3389/fphys.2018.01783

Shi, X., Zhou, F., Li, X., Chang, B., Li, D., Wang, Y., et al. (2013). Central GLP-2 enhances hepatic insulin sensitivity via activating PI3K signaling in POMC neurons. *Cell Metab.* 18, 86–98. doi:10.1016/j.cmet.2013.06.014

Siafakas, C. G., Anatolitou, F., Fusunyan, R. D., Walker, W. A., and Sanderson, I. R. (1999). Vascular endothelial growth factor (VEGF) is present in human breast milk and its receptor is present on intestinal epithelial cells. *Pediatr. Res.* 45, 652–657. doi:10.1203/00006450-199905010-00007

Sigalet, D. L., Wallace, L. E., Holst, J. J., Martin, G. R., Kaji, T., Tanaka, H., et al. (2007). Enteric neural pathways mediate the anti-inflammatory actions of glucagon-like peptide 2. *Am. J. Physiology-Gastrointestinal Liver Physiology* 293, G211–G221. doi:10.1152/ajpgi.00530.2006

Spessert, R. (1993). Vasoactive intestinal peptide stimulation of cyclic guanosine monophosphate formation: further evidence for a role of nitric oxide synthase and cytosolic guanylate cyclase in rat pinealocytes. *Endocrinology* 132, 2513–2517. doi:10.1210/endo.132.6.7684978

Stahel, P., Xiao, C., Davis, X., Tso, P., and Lewis, G. F. (2019). Glucose and GLP-2 (Glucagon-Like peptide-2) mobilize intestinal triglyceride by distinct mechanisms. *Arterioscler. Thromb. Vasc. Biol.* 39, 1565–1573. doi:10.1161/ATVBAHA.119.313011

Stahel, P., Xiao, C., Hegele, R. A., and Lewis, G. F. (2018). The atherogenic dyslipidemia complex and novel approaches to cardiovascular disease prevention in diabetes. *Can. J. Cardiol.* 34, 595–604. doi:10.1016/j.cjca.2017.12.007

Stahel, P., Xiao, C., Nahmias, A., and Lewis, G. F. (2020). Role of the gut in diabetic dyslipidemia. *Front. Endocrinol. (Lausanne)* 11, 116. doi:10.3389/fendo.2020.00116

Stahel, P., Xiao, C., Nahmias, A., Tian, L., and Lewis, G. F. (2021). Multi-organ coordination of lipoprotein secretion by hormones, nutrients and neural networks. *Endocr. Rev.* 42, 815–838. doi:10.1210/endrev/bnab008

Su, Y., Zhang, Z., Li, H., Ma, J., Sun, L., Shao, S., et al. (2021). A GLP-2 analogue protects SH-SY5Y and neuro-2a cells against mitochondrial damage, autophagy impairments and apoptosis in a Parkinson model. *Drug Res.* 71, 43–50. doi:10.1055/a-1266-3263

Sun, H., Meng, K., Hou, L., Shang, L., and Yan, J. (2021). Melanocortin receptor-4 mediates the anorectic effect induced by the nucleus tractus solitarius injection of glucagon-like Peptide-2 in fasted rats. *Eur. J. Pharmacol.* 901, 174072. doi:10.1016/j.ejphar.2021.174072

Syed-Abdul, M. M., Stahel, P., Tian, L., Xiao, C., Nahmias, A., and Lewis, G. F. (2022a). Glucagon-like peptide-2 mobilization of intestinal lipid does not require canonical enterocyte chylomicron synthetic machinery. *Biochimica Biophysica Acta (BBA) - Mol. Cell Biol. Lipids* 1867, 159194. doi:10.1016/j.bbalip.2022.159194

Syed-Abdul, M. M., Tian, L., Xiao, C., and Lewis, G. F. (2022b). Lymphatics - not just a chylomicron conduit. *Curr. Opin. Lipidol.* 33, 175–184. doi:10.1097/MOL.0000000000000821

Taher, J., Baker, C., Alvares, D., Ijaz, L., Hussain, M., and Adeli, K. (2018). GLP-2 dysregulates hepatic lipoprotein metabolism, inducing fatty liver and VLDL overproduction in male hamsters and mice. *Endocrinology* 159, 3340–3350. doi:10.1210/en.2018-00416

Talbot, J., Hahn, P., Kroehling, L., Nguyen, H., Li, D., and Littman, D. R. (2020). Feeding-dependent VIP neuron–ILC3 circuit regulates the intestinal barrier. *Nature* 579, 575–580. doi:10.1038/s41586-020-2039-9

Tang-Christensen, M., Larsen, P. J., Thulesen, J., Rømer, J., and Vrang, N. (2000). The proglucagon-derived peptide, glucagon-like peptide-2, is a neurotransmitter involved in the regulation of food intake. *Nat. Med.* 6, 802–807. doi:10.1038/77535

Velázquez, E., Le Baut Ayuso, Y., Blázquez, E., and Ruiz-Albusac, J. M. (2022). Glucose and several mitogenic agents modulate the glucagon-like peptide-2 receptor expression in cultured rat astrocytes. *J. Alzheimers Dis. Rep.* 6, 723–732. doi:10.3233/ADR-220043

Velázquez, E., Ruiz-Albusac, J. M., and Blázquez, E. (2003). Glucagon-like peptide-2 stimulates the proliferation of cultured rat astrocytes. *Eur. J. Biochem.* 270, 3001–3009. doi:10.1046/j.1432-1033.2003.03677.x

Verdam, F. J., Greve, J. W. M., Roosta, S., van Eijk, H., Bouvy, N., Buurman, W. A., et al. (2011). Small intestinal alterations in severely obese hyperglycemic subjects. *J. Clin. Endocrinol. Metab.* 96, E379–E383. doi:10.1210/jc.2010-1333

Vrang, N., Hansen, M., Larsen, P. J., and Tang-Christensen, M. (2007). Characterization of brainstem preproglucagon projections to the paraventricular and dorsomedial hypothalamic nuclei. *Brain Res.* 1149, 118–126. doi:10.1016/j.brainres.2007.02.043

Vrang, N., Larsen, P. J., Jensen, P. B., Lykkegaard, K., Artmann, A., Larsen, L. K., et al. (2008). Upregulation of the brainstem preproglucagon system in the obese Zucker rat. *Brain Res.* 1187, 116–124. doi:10.1016/j.brainres.2007.10.026

Wismann, P., Barkholt, P., Secher, T., Vrang, N., Hansen, H. B., Jeppesen, P. B., et al. (2017). The endogenous preproglucagon system is not essential for gut growth homeostasis in mice. *Mol. Metab.* 6, 681–692. doi:10.1016/j.molmet.2017.04.007

Wøjdemann, M., Wettergren, A., Hartmann, B., and Holst, J. J. (1998). Glucagon-like peptide-2 inhibits centrally induced antral motility in pigs. *Scand. J. Gastroenterol.* 33, 828–832. doi:10.1080/00365529850171486

Xiao, C., Dash, S., Morgantini, C., Adeli, K., and Lewis, G. F. (2015). Gut peptides are novel regulators of intestinal lipoprotein secretion: experimental and pharmacological manipulation of lipoprotein metabolism. *Diabetes* 64, 2310–2318. doi:10.2337/db14-1706

Xiao, C., Stahel, P., Carreiro, A. L., Buhman, K. K., and Lewis, G. F. (2018). Recent advances in triacylglycerol mobilization by the gut. *Trends Endocrinol. Metabolism* 29, 151–163. doi:10.1016/j.tem.2017.12.001

Xiao, C., Stahel, P., Carreiro, A. L., Hung, Y.-H., Dash, S., Bookman, I., et al. (2019a). Oral glucose mobilizes triglyceride stores from the human intestine. *Cell Mol. Gastroenterol. Hepatol.* 7, 313–337. doi:10.1016/j.jcmgh.2018.10.002

Xiao, C., Stahel, P., and Lewis, G. F. (2019b). Regulation of chylomicron secretion: focus on post-assembly mechanisms. *Cell Mol. Gastroenterol. Hepatol.* 7, 487–501. doi:10.1016/j.jcmgh.2018.10.015

Xiao, C., Stahel, P., Morgantini, C., Nahmias, A., Dash, S., and Lewis, G. F. (2019c). Glucagon-like peptide-2 mobilizes lipids from the intestine by a systemic nitric oxide-independent mechanism. *Diabetes Obes. Metab.* 21, 2535–2541. doi:10.1111/dom.13839

Xiao, C., Stahel, P., Nahmias, A., and Lewis, G. F. (2020). Emerging role of lymphatics in the regulation of intestinal lipid mobilization. *Front. Physiol.* 10, 1604. doi:10.3389/fphys.2019.01604

Yusta, B., Huang, L., Munroe, D., Wolff, G., Fantaske, R., Sharma, S., et al. (2000). Enteroendocrine localization of GLP-2 receptor expression in humans and rodents. *Gastroenterology* 119, 744–755. doi:10.1053/gast.2000.16489

Yusta, B., Holland, D., Koehler, J. A., Maziarz, M., Estall, J. L., Higgins, R., et al. (2009). ErbB signaling is required for the proliferative actions of GLP-2 in the murine gut. *Gastroenterology* 137, 986–996. doi:10.1053/j.gastro.2009.05.057

Yusta, B., Matthews, D., Koehler, J. A., Pujadas, G., Kaur, K. D., and Drucker, D. J. (2019). Localization of glucagon-like peptide-2 receptor expression in the mouse. *Endocrinology* 160, 1950–1963. doi:10.1210/en.2019-00398

Zembroski, A. S., D'Aquila, T., and Buhman, K. K. (2021). Characterization of cytoplasmic lipid droplets in each region of the small intestine of lean and diet-induced obese mice in response to dietary fat. *Am. J. Physiol. Gastrointest. Liver Physiol.* 321, G75–G86. doi:10.1152/AJPGI.00084.2021

Zhang, F., Zarkada, G., Han, J., Li, J., Dubrac, A., Ola, R., et al. (2018). Lacteal junction zippering protects against diet-induced obesity. *Science* 361, 599–603. doi:10.1126/science.aap9331

Zhang, Z., Hao, L., Shi, M., Yu, Z., Shao, S., Yuan, Y., et al. (2021). Neuroprotective effects of a GLP-2 analogue in the MPTP Parkinson's disease mouse model. *J. Park. Dis.* 11, 529–543. doi:10.3233/JPD-202318

frontiers | Frontiers in Physiology

TYPE Original Research
PUBLISHED 17 April 2024
DOI 10.3389/fphys.2024.1371096

OPEN ACCESS

EDITED BY
Curtis C Hughey,
University of Minnesota Twin Cities,
United States

REVIEWED BY
Mario Ruiz,
University of Gothenburg, Sweden
Bo Wang,
University of Illinois at Urbana-Champaign,
United States

*CORRESPONDENCE
J. Mark Brown,
brownm5@ccf.org

†These authors have contributed equally to this work and share first authorship

RECEIVED 15 January 2024
ACCEPTED 19 March 2024
PUBLISHED 17 April 2024

CITATION
Banerjee R, Hohe RC, Cao S, Jung BM, Horak AJ, Ramachandiran I, Massey WJ, Varadharajan V, Zajczenko NI, Burrows AC, Dutta S, Goudarzi M, Mahen K, Carter A, Helsley RN, Gordon SM, Morton RE, Strauch C, Willard B, Gogonea CB, Gogonea V, Pedrelli M, Parini P and Brown JM (2024), The nonvesicular sterol transporter Aster-C plays a minor role in whole body cholesterol balance.
Front. Physiol. 15:1371096.
doi: 10.3389/fphys.2024.1371096

The nonvesicular sterol transporter Aster-C plays a minor role in whole body cholesterol balance

Rakhee Banerjee[1,2†], Rachel C. Hohe[1,2†], Shijie Cao[1,2], Bryan M. Jung[1,2], Anthony J. Horak[2], Iyappan Ramachandiran[2,3], William J. Massey[1,2,4], Venkateshwari Varadharajan[1,2], Natalie I. Zajczenko[1,2], Amy C. Burrows[1,2], Sumita Dutta[1,2], Maryam Goudarzi[1,2], Kala Mahen[1,2], Abigail Carter[5], Robert N. Helsley[5,6], Scott M. Gordon[5], Richard E. Morton[3], Christopher Strauch[7], Belinda Willard[7], Camelia Baleanu Gogonea[8], Valentin Gogonea[8], Matteo Pedrelli[9], Paolo Parini[9] and J. Mark Brown[1,2]*

[1]Department of Cancer Biology, Lerner Research Institute of the Cleveland Clinic, Cleveland, OH, United States, [2]Center for Microbiome and Human Health, Lerner Research Institute, Cleveland Clinic, Cleveland, OH, United States, [3]Department of Cardiovascular and Metabolic Sciences, Lerner Research Institute, Cleveland, OH, United States, [4]Department of Inflammation and Immunity, Lerner Research Institute, Cleveland Clinic, Cleveland, OH, United States, [5]Department of Physiology and the Saha Cardiovascular Research Center, University of Kentucky College of Medicine, Lexington, KY, United States, [6]Department of Internal Medicine, Division of Endocrinology, Diabetes, and Metabolism, University of Kentucky College of Medicine, Lexington, KY, United States, [7]Proteomics and Metabolomics Core, Lerner Research Institute, Cleveland Clinic, Cleveland, OH, United States, [8]Department of Chemistry, Cleveland State University, Cleveland, OH, United States, [9]Department of Laboratory Medicine, Karolinska Institute, Huddinge, Sweden

Introduction: The Aster-C protein (encoded by the *Gramd1c* gene) is an endoplasmic reticulum (ER) resident protein that has been reported to transport cholesterol from the plasma membrane to the ER. Although there is a clear role for the closely-related Aster-B protein in cholesterol transport and downstream esterification in the adrenal gland, the specific role for Aster-C in cholesterol homeostasis is not well understood. Here, we have examined whole body cholesterol balance in mice globally lacking Aster-C under low or high dietary cholesterol conditions.

Method: Age-matched *Gramd1c*$^{+/+}$ and *Gramd1c*$^{-/-}$ mice were fed either low (0.02%, wt/wt) or high (0.2%, wt/wt) dietarycholesterol and levels of sterol-derived metabolites were assessed in the feces, liver, and plasma.

Results: Compared to wild type controls (*Gramd1c*$^{+/+}$) mice, mice lacking*Gramd1c* (*Gramd1c*$^{-/-}$) have no significant alterations in fecal, liver, or plasma cholesterol. Given the potential role for Aster C in modulating cholesterol metabolism in diverse tissues, we quantified levels of cholesterol metabolites such as bile acids, oxysterols, and steroid hormones. Compared to *Gramd1c*$^{+/+}$ controls, *Gramd1c*$^{-/-}$ mice had modestly reduced levels of select bile acid species and elevated cortisol levels, only under low dietary cholesterol conditions. However, the vast majority of bile acids, oxysterols, and steroid hormones were unaltered in *Gramd1c*$^{-/-}$ mice. Bulk RNA sequencing in the liver showed

10.3389/fphys.2024.1371096

that *Gramd1c*$^{-/-}$ mice did not exhibit alterations in sterol-sensitive genes, but instead showed altered expression of genes in major urinary protein and cytochrome P450 (CYP) families only under low dietary cholesterol conditions.

Discussion: Collectively, these data indicate nominal effects of Aster-C on whole body cholesterol transport and metabolism under divergent dietary cholesterol conditions. These results strongly suggest that Aster-C alone is not sufficient to control whole body cholesterol balance, but can modestly impact circulating cortisol and bile acid levels when dietary cholesterol is limited.

KEYWORDS

cholesterol, lipoprotein, metabolism, steroid hormone, oxysterol

Introduction

In most mammalian cells the majority of cholesterol resides in the plasma membrane (PM), yet feedback regulation of cholesterol synthesis and metabolism of cholesterol happens at intracellular membranes of the endoplasmic reticulum (ER), mitochondria, and nucleus. Therefore, the trafficking of PM cholesterol to intracellular organelles is tightly controlled to maintain cellular homeostasis. A recently identified family of ER-resident proteins called Asters (Aster-A, -B, and -C) form membrane-membrane contact sites to facilitate the transfer cholesterol away from the PM (Sandhu et al., 2018; Naito et al., 2019; Ferrari et al., 2020; Ferrari et al., 2023; Xiao et al., 2023). Aster-B was first described as a liver X receptor (LXR)-stimulated cholesterol transporter that facilitates PM-to-ER sterol transfer for cholesterol ester (CE) storage in the adrenal gland (Sandhu et al., 2018). More recently, Aster-C was found to be a direct transcriptional target gene for the farnesoid X receptor (FXR) in the liver where it plays a role in reverse cholesterol transport (RCT) (Xiao et al., 2023). Although there is emerging evidence of functional redundancy in some tissues, all three Asters (A, B, and C) have been implicated in both intestinal and hepatic cholesterol trafficking under certain conditions of fasting and re-feeding (Ferrari et al., 2023; Xiao et al., 2023). However, the specific individual role for each Aster protein in regulating whole body

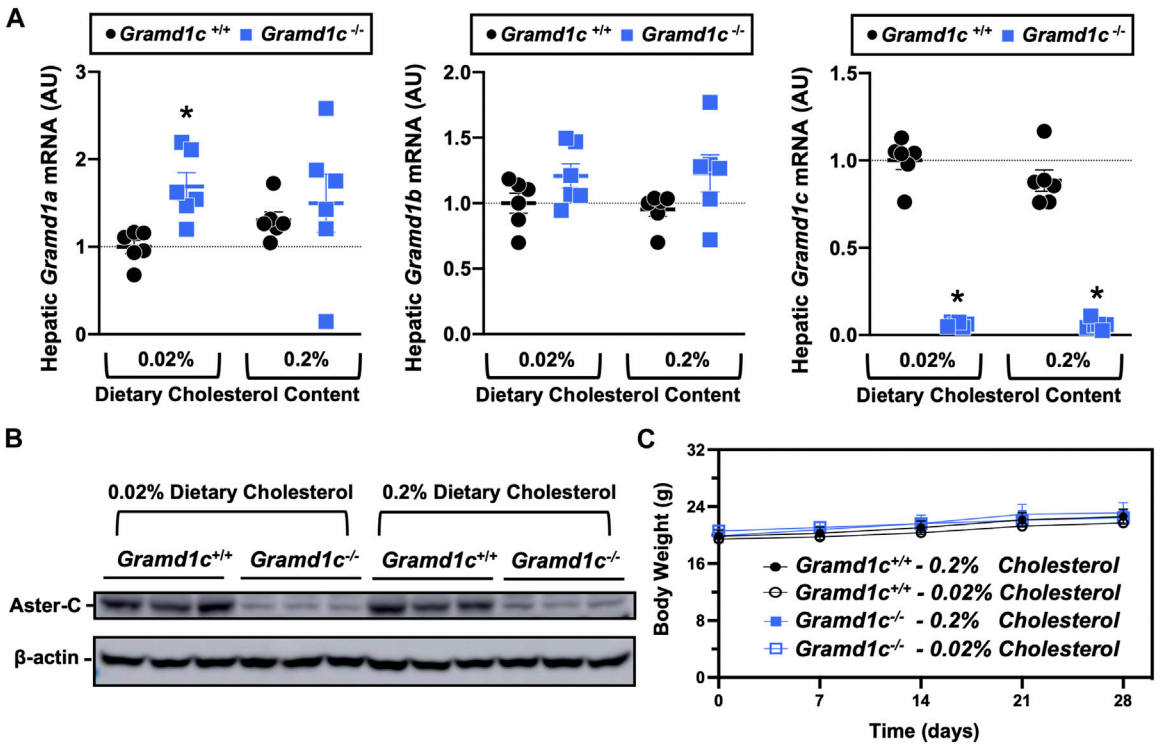

FIGURE 1
Selective loss of *Gramd1c* does not alter body weight. At 8 weeks of age, female wild type (*Gramd1c*$^{+/+}$) or *Gramd1c* knockout mice (*Gramd1c*$^{-/-}$) were switched from standard rodent chow to one of two experimental synthetic diets containing low (0.02%, wt/wt) or high (0.2%, wt/wt) levels of dietary cholesterol. Mice were maintained on these diets over a 4-week period of study. **(A)** The expression of *Gramd1a*, *Gramd1b*, and *Gramd1c* in the liver was quantified via qPCR. **(B)** Western blot in liver lysates from n = 3 mice per group. **(C)** Body weight curves over the 4-week feeding period. Data are presented as mean ± SEM from n = three to six mice per group. There were no statistically significant differences between *Gramd1c*$^{+/+}$ and *Gramd1c*$^{-/-}$ mice on either the low or high cholesterol diets.

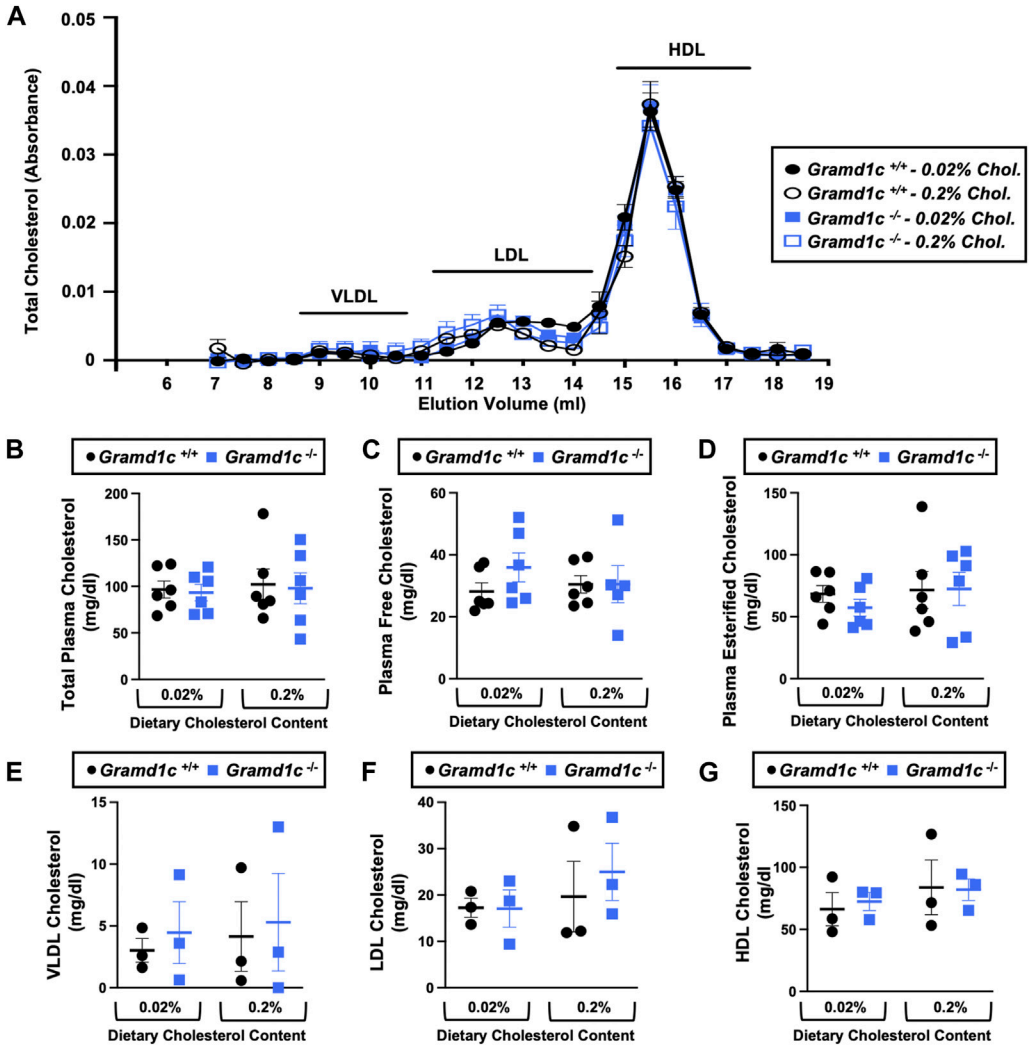

FIGURE 2
Global deletion of *Gramd1c* does not significantly alter circulating lipoprotein cholesterol levels. At 8 weeks of age, female wild type (*Gramd1c*$^{+/+}$) or *Gramd1c* knockout mice (*Gramd1c*$^{-/-}$) were switched from standard rodent chow to one of two experimental synthetic diets containing low (0.02%, wt/wt) or high (0.2%, wt/wt) levels of dietary cholesterol. Mice were maintained on these diets over a 4-week period of study. **(A)** Plasma was subjected to size exclusion chromatography to examine total cholesterol distribution across lipoprotein fractions. **(B–D)** Total plasma cholesterol **(B)**, total plasma free cholesterol **(C)**, and total plasma esterified cholesterol **(D)** levels were determined by gas chromatography-tandem mass spectrometry (GC-MS/MS). **(E–G)** Plasma very low-density lipoprotein (VLDL), low-density lipoprotein (LDL), and high-density lipoprotein (HDL) cholesterol levels. Data are presented as mean ± SEM from n = three to six mice per group. There were no statistically significant differences between *Gramd1c*$^{+/+}$ and *Gramd1c*$^{-/-}$ mice on either the low or high cholesterol diets.

cholesterol balance under conditions of excess dietary cholesterol is not well understood.

Although only 5 years have passed since their original discovery as sterol transporters by Tontonoz and colleagues (Sandhu et al., 2018), there has been rapid progress to understand the relative and tissue-specific roles each ASTER family member plays in cholesterol transport. Each Aster has a cholesterol-binding pocket that is near the N-terminal GRAM domain and are tethered to the ER via a transmembrane domain at the C terminus. The GRAM domain plays a central role in binding the plasma membrane (PM) at PM-ER contact sites where Asters can facilitate nonvesicular transfer of cholesterol to the ER for esterification or feedback regulation of *de novo* cholesterol synthesis via the sterol regulatory element-binding protein cleavage-activating protein (SCAP-SREBP) system (Sandhu et al., 2018). In addition to their roles in cellular cholesterol transport, Aster proteins have also been shown to transport carotenoid lipids (Bandara et al., 2022). Aster-C specifically has also been implicated in regulating autophagosome biogenesis and mitochondrial bioenergetics (Ng et al., 2022; Charsou et al., 2023), but how the lipid transporting function of Aster-C facilitates autophagy is still incompletely understood. One potential clue is that Aster-C has been reported to activate mTORC1 (Zhang et al., 2020), which is a master regulator of nutrient sensing and autophagy. Several recent reports have linked differential expression of *GRAMD1C* to diverse cancers including hepatocellular carcinoma, clear cell renal carcinoma, and breast cancer (Hao et al., 2019; Li et al., 2022; Fan et al., 2023; Gong et al., 2023). Although there is emerging evidence that Aster-C can

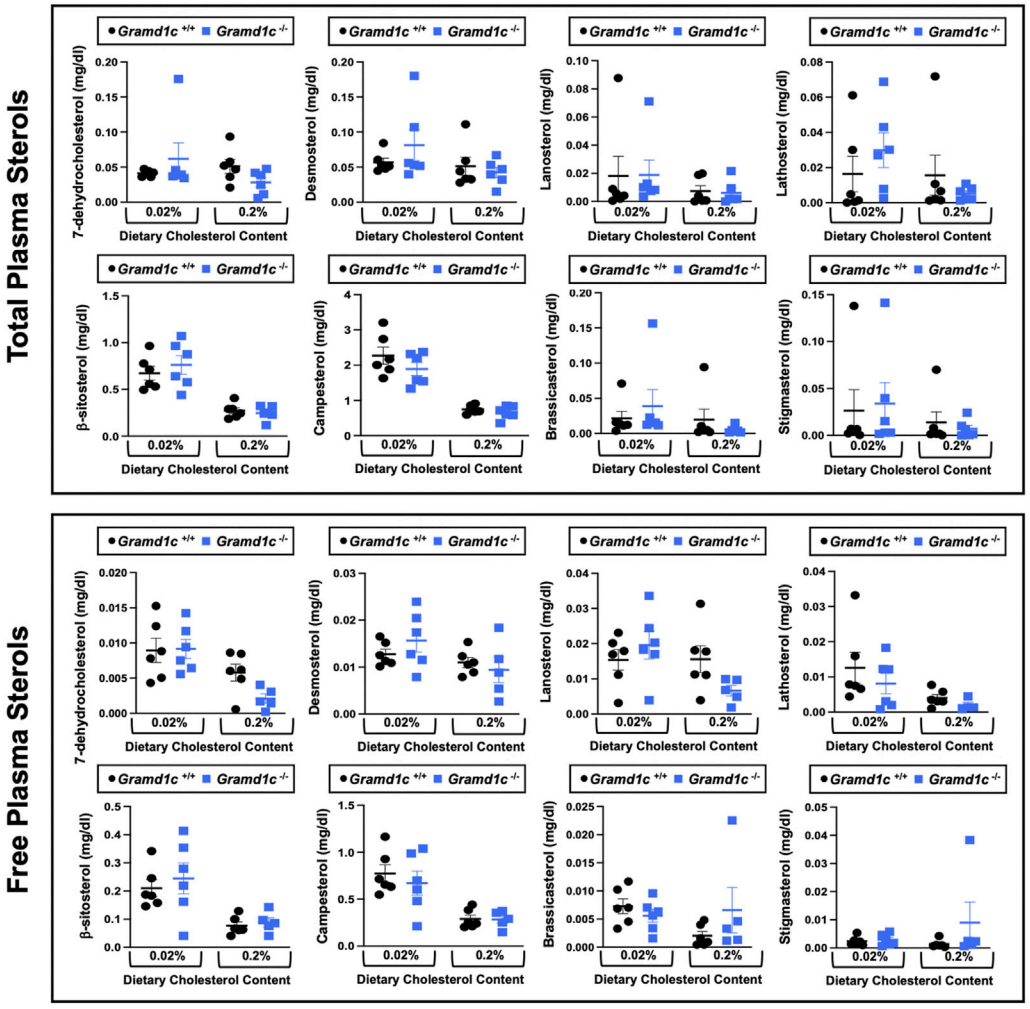

FIGURE 3
Global deletion of *Gramd1c* does not significantly alter circulating levels of various sterols. At 8 weeks of age, female wild type (*Gramd1c*$^{+/+}$) or *Gramd1c* knockout mice (*Gramd1c*$^{-/-}$) were switched from standard rodent chow to one of two experimental synthetic diets containing low (0.02%, wt/wt) or high (0.2%, wt/wt) levels of dietary cholesterol. Mice were maintained on these diets over a 4-week period of study. The total and free levels of a variety of sterols in the liver were quantified by gas chromatography tandem mass spectrometry (GC-MS/MS) in samples with or without alkaline hydrolysis. Data are presented as mean ± SEM from n = five to six mice per group. There were no statistically significant differences between *Gramd1c*$^{+/+}$ and *Gramd1c*$^{-/-}$ mice on either the low or high cholesterol diets.

facilitate sterol transport and potentially signal transduction, the relative role that Aster-C plays in tissue and whole body sterol homeostasis has yet to be defined. Here we address this gap by studying sterol balance in *Gramd1c*-deficient mice under conditions of limited *versus* excess dietary cholesterol.

Methods

Mouse studies

Gramd1c knockout mice were obtained from MMRRC UC Davis, strain 047990-UCD, *C57BL/6N-Atm1Brd Gramd1ctm1a(KOMP)Wtsi/JMmucd.* A breeding colony was developed at the Cleveland Clinic after the mice were genotype confirmed using a commercial partner (Transnetyx, Inc., Cordova, TN, United States). Heterozygous (*Gramd1c*$^{+/-}$) mice were interbred to generate littermate controls. At 8 weeks of age, female wild type (*Gramd1c*$^{+/+}$) or *Gramd1c* knockout mice (*Gramd1c*$^{-/-}$) were switched from standard rodent chow to one of two experimental synthetic diets containing low (0.02%, wt/wt) or high (0.2%, wt/wt) levels of dietary cholesterol. These experimental diets were synthesized by Envigo—Teklad Diets (Madison, WI, United States) and additional information can be found for each of these diets by referencing the following diet numbers: TD.130,104 (low cholesterol diet) and TD.160,514 (high cholesterol diet) from our previous work (Pathak et al., 2020). Mice were maintained on these diets over a period 4 consecutive weeks, and phenotyped as described below for sterol and bile acid homeostasis. In a subset of male mice, we studied liver X receptor-driven alterations in sterol balance. For LXR agonist studies, the LXR agonist GW3965 was suspended in a vehicle containing 1.0% carboxymethylcellulose (CMC) and 0.1% Tween 80. Mice were gavaged with either vehicle or 40 mg/kg GW3965 once daily for a period of seven

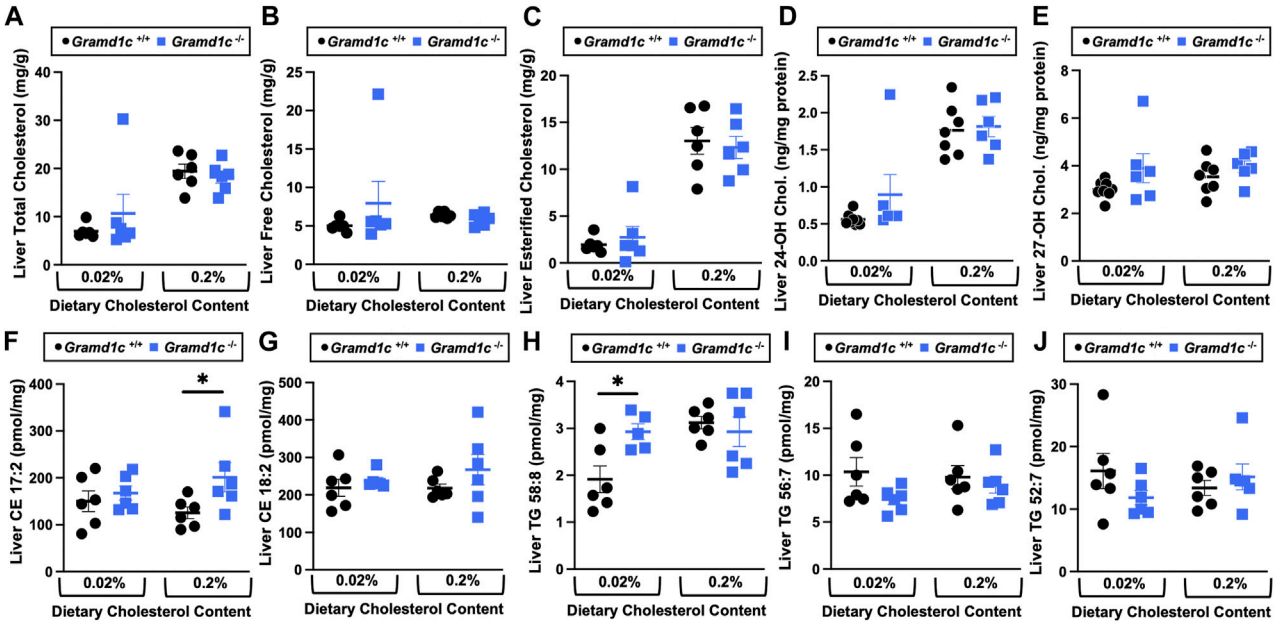

FIGURE 4
The hepatic lipidome is modestly impacted by global deletion of *Gramd1c*. At 8 weeks of age, female wild type (*Gramd1c*$^{+/+}$) or *Gramd1c* knockout mice (*Gramd1c*$^{-/-}$) were switched from standard rodent chow to one of two experimental synthetic diets containing low (0.02%, wt/wt) or high (0.2%, wt/wt) levels of dietary cholesterol. Mice were maintained on these diets over a 4-week period of study. A variety of lipids were quantified by targeted mass spectrometry assays including **(A)** total cholesterol, **(B)** free cholesterol, **(C)** total esterified cholesterol, **(D)** 24-hydoxycholesterol (24-OH Chol.), **(E)** 27-hydroxycholesterol (27-OH Chol.) **(F)** 17:2 cholesteryl ester (CE 17:2), **(G)** 18:2 cholesteryl ester (CE 18:2), **(H)** 58:8 triacylglycerol (TG 58:8), **(I)** 56:7 triacylglycerol (TG 56:7), and **(J)** 52:7 triacylglycerol (TG 52:7). Data are presented as mean ± SEM from n = 6 mice per group. * = significantly different ($p \leq 0.05$) when comparing *Gramd1c*$^{+/+}$ and *Gramd1c*$^{-/-}$ mice within each diet group.

consecutive days. All mice were maintained in an Association for the Assessment and Accreditation of Laboratory Animal Care, International-approved animal facility and all experimental protocols were approved by the Institutional Animal Care and Use Committee (IACUC) of the Cleveland Clinic (IACUC protocol # 00002499 and 00003201).

Standardized necropsy conditions

To keep results consistent, the vast majority of experimental mice were fasted for 4 h (from 9:00 a.m. to 1:00 p.m.) prior to necropsy. At necropsy, all mice were terminally anesthetized with ketamine/xylazine (100–160 mg/kg ketamine-20–32 mg/kg xylazine), and a midline laparotomy was performed. Blood was collected by heart puncture. Following blood collection, a whole body perfusion was conducted by puncturing the inferior vena cava and slowly delivering 10 mL of saline into the heart to remove blood from tissues. Tissues were collected and immediately snap frozen in liquid nitrogen for subsequent biochemical analysis or fixed for morphological analysis.

Quantification of total and free sterols in plasma and liver

To extract total sterols from plasma, an internal standard cocktail in 3 mL of chloroform: methanol (2:1, v/v) solution was added to 20 µL of plasma. The solution was vortexed briefly, and thereafter centrifuged at 3,000 rpm for 15 min for phase separation of the solvents. Lipids dissolved in chloroform form the supernatant layer which was transferred to a fresh glass tube. For extraction of lipids from liver tissues, an internal standard cocktail in 3 mL of chloroform: methanol (2:1, v/v) solution was added to 20–40 mg of liver tissue and mixed well. The reaction mixture was incubated overnight, and the chloroform layer containing lipid was collected in a fresh glass tube. The lipid extracts (from both plasma and liver tissue) were washed twice with water by centrifuging the solution at 3,000 rpm for 15 min. The bottom layer comprising of lipids dissolved in chloroform was collected in a fresh tube and dried under a stream of N_2 gas. To differentiate total *versus* esterified forms of sterols, the dried lipids were resuspended in 100 µL of 0.5 M potassium hydroxide (KOH) and subjected to base hydrolysis for 1 h at 37°C. The reaction was then neutralized by adding 400 ul of 0.25 M hydrochloric acid (HCl). Thereafter, 1 mL of isopropanol: hexane:2 M acetic acid (40:10:1, v/v/v; Solution A) was added to the reaction mixture and vortexed briefly. Another 1 mL of hexane was added to the reaction mixture and the resultant solution was vortexed for ~1 min. The solution was then centrifuged at 2,500 *g* for 5 min at 4°C, the top hexane layer collected in a fresh tube, and dried in a stream of N_2 gas. To ensure complete drying, the lipids were put in a speed vacuum for 1 h, and later resuspended in 50 ul of Sylon™ HTP (HMDS + TMCS + Pyridine; 3:1:9) and incubated the solution at 90°C for 1 h. Thereafter the samples were transferred to glass tubes suitable for gas chromatography. The quantitation of a variety of plant and animal-derived sterols including:

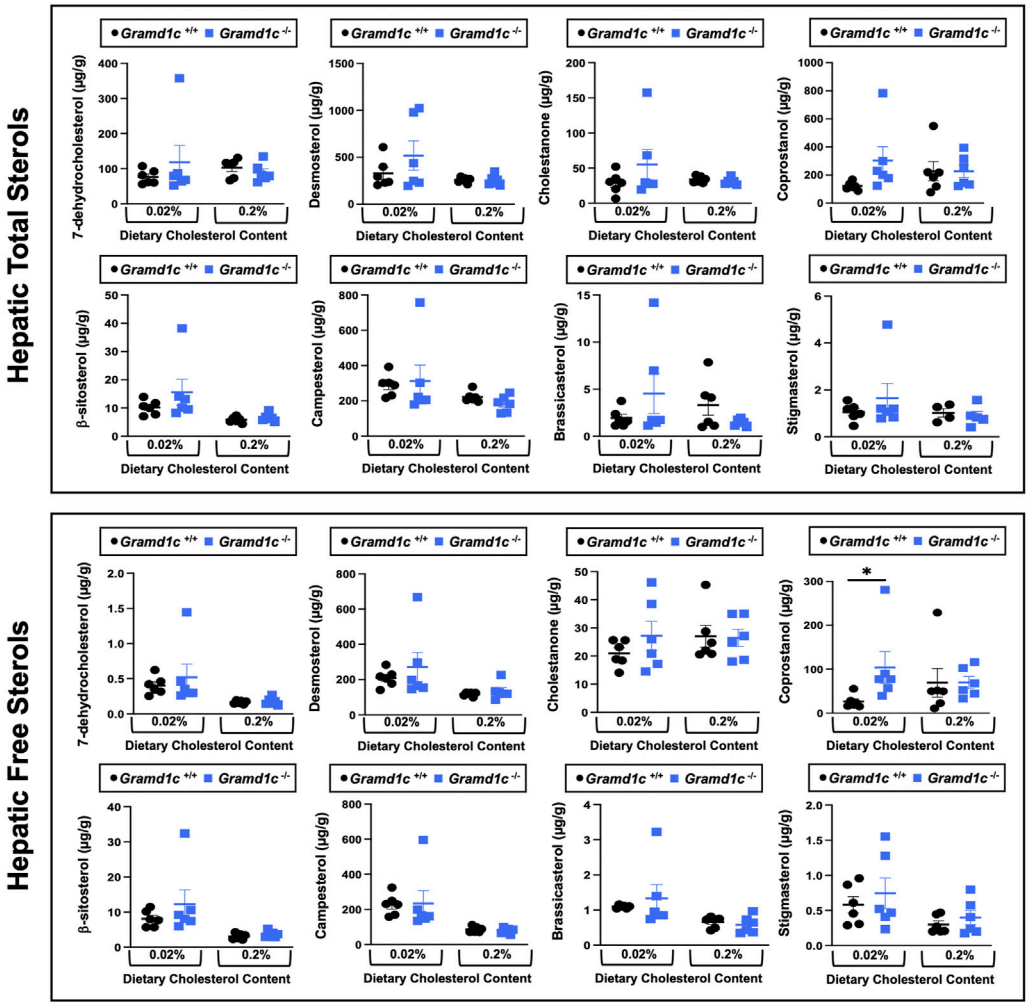

FIGURE 5
Global deletion of *Gramd1c* does not significantly alter levels of various sterols in the liver. At 8 weeks of age, female wild type (*Gramd1c*$^{+/+}$) or *Gramd1c* knockout mice (*Gramd1c*$^{-/-}$) were switched from standard rodent chow to one of two experimental synthetic diets containing low (0.02%, wt/wt) or high (0.2%, wt/wt) levels of dietary cholesterol. Mice were maintained on these diets over a 4-week period of study. The total and free levels of a variety of sterols in the liver were quantified by gas chromatography tandem mass spectrometry (GC-MS/MS) in samples with or without alkaline hydrolysis. Data are presented as mean ± SEM from n = 6 mice per group. There were no statistically significant differences between *Gramd1c*$^{+/+}$ and *Gramd1c*$^{-/-}$ mice on either the low or high cholesterol diets.

7-dehydrocholesterol, brassicasterol, β-sitosterol, campesterol, cholestanone, cholesterol, coprostanol, desmosterol, ergosterol, lanosterol, lathosterol and stigmasterol were performed using isotope dilution gas chromatography-tandem mass spectrometry (GC-MS/MS) by using multiple reaction monitoring (MRM) mode. The absolute quantity of each sterol was determined using calibration curves measured for each analyte. Samples were analyzed by using the Thermo TSQ-Evo triple quadrupole in tandem with the Trace 1,310 gas chromatograph (Thermo Fisher Scientific). Chromatographic separation was achieved by using an Agilent CP-Sil 8 CB fused silica column (50 m × 0.250 mm x 0.25 µm; Agilent Technologies, Santa Clara, CA, United States) coated with 5% phenyl methylpolysiloxane. Each extract was injected (1 µL) in splitless mode for 6 min into PTV (programmable temperature vaporizer) inlet. The PTV program was as follows. Initial temp 80°C for 2 min. Evaporative stage 5°C/min to 85°C for 1 min. Transfer stage 14.5°C/min to 280°C for 5 min with cleaning stage of 14.5°C/min to 300°C for 3 min. Helium as carrier gas flow was 1 mL/min. The GC oven temperature program was as follows. The initial temperature of 150°C was held for 3 min after injection before it was increased up to 280°C at 30°C/min, followed by an increase to 295°C at 10°C/min and then held for 6 min. Argon was used a collision gas. The transfer line, and ion source temperature were set at 310°C and 275°C respectively. The mass spectrometer was tuned to an electron impact ionization energy of 70 eV in MRM mode with the following parent to daughter ion transitions: *m/z 351.3→143.2* for 7-dehydrocholesterol, *m/z 470.4→255.3* for brassicasterol, *m/z 396.4→213.2* for β-sitosterol, *m/z 402.5→219.3* D_6 - β-sitosterol, *m/z 382.4→213.3* for campesterol, *m/z 388.4→213.3* D_6—campesterol, *m/z 386.4→231.2* for cholestanone, *m/z 368.4→213.3* for cholesterol, *m/z 375.4→213.2* D_7—cholesterol, *m/z 370.4→215.3* for coprostanol, *m/z 343.3→253.3* for desmosterol, *m/z 396.65→157.1* for

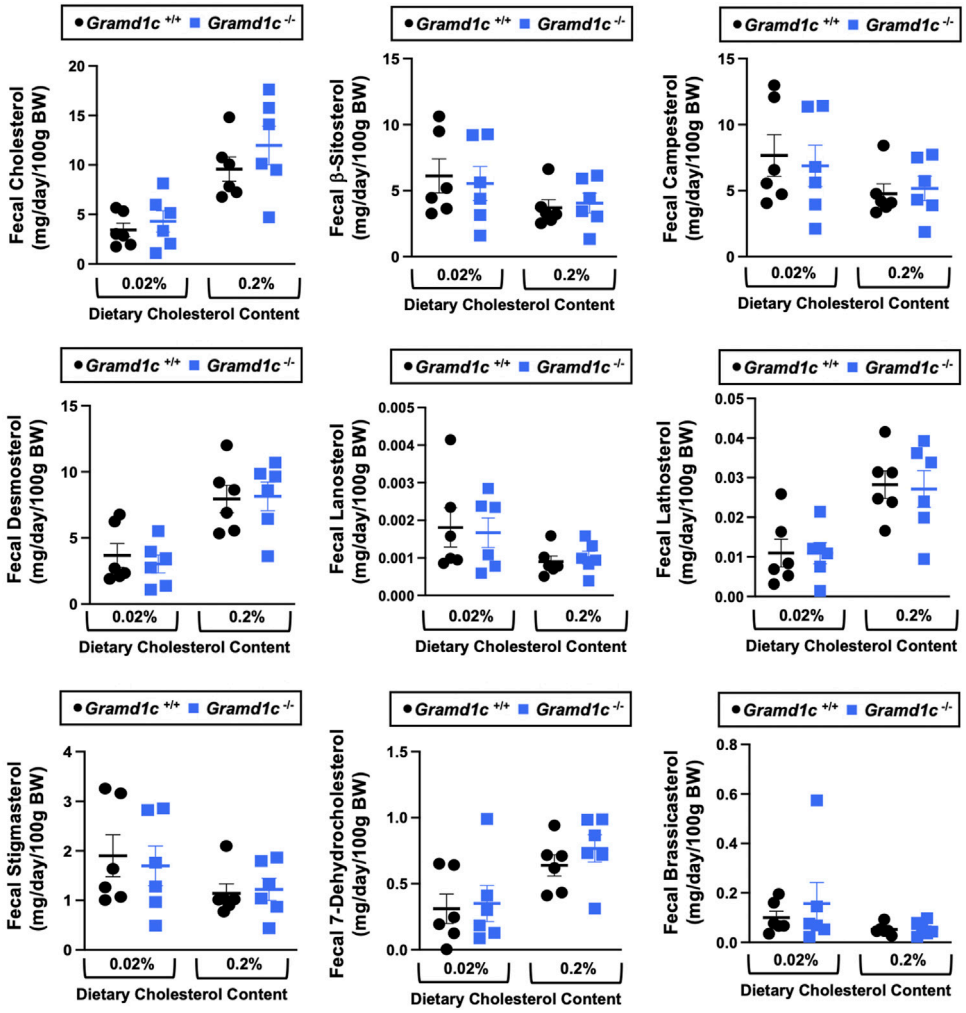

FIGURE 6
Global deletion of *Gramd1c* does not significantly alter fecal sterol loss. At 8 weeks of age, female wild type (*Gramd1c*$^{+/+}$) or *Gramd1c* knockout mice (*Gramd1c*$^{-/-}$) were switched from standard rodent chow to one of two experimental synthetic diets containing low (0.02%, wt/wt) or high (0.2%, wt/wt) levels of dietary cholesterol. Mice were maintained on these diets over a 4-week period of study, and feces were quantitatively collected over the final 72 h for fecal sterol analyses via gas chromatography tandem mass spectrometry (GC-MS/MS). Data are presented as mean ± SEM from n = 6 mice per group. There were no statistically significant differences between *Gramd1c*$^{+/+}$ and *Gramd1c*$^{-/-}$ mice on either the low or high cholesterol diets.

ergosterol, *m/z 394.4→109.2* for lanosterol, *m/z 459→213.3* for lathosterol and *m/z 484.6→169.2* for stigmasterol.

Quantification of fecal neutral sterol excretion

Quantitative fecal excretion of both plant and animal derived sterols were analyzed by GC-MS/MS with MRM. Briefly, after being fed experimental diets for 4 weeks, mice were individually housed in a cage with a wire bottom and was allowed free access to diet and water for 3 consecutive days. After a 3 days fecal collection, the mice were weighed, and the feces were collected, dried in a 70°C vacuum oven, weighed, and crushed into a fine powder. A measured mass (50–100 mg) of feces was placed into a glass tube containing internal standard mixture. The feces were saponified and the neutral lipids were extracted into hexane, and mass analysis of the extracted neutral sterols was conducted by GC-MS/MS with MRM as described above.

Quantification of plasma bile acid levels

Quantification of individual plasma bile acid species was conducted using a quantitative stable isotope dilution LC-MS/MS analytical method as recently described (Choucair et al., 2020). Briefly, stable isotope labeled internal standards (IS) included were: D_4-glycolithocholic acid, D_4-glycoursodeoxycholic acid, D_4-glycodeoxycholic acid, D_4-glycocholic acid, D_4-taurolithocholic acid, D_4-tauroursodeoxycholic acid, D_4-taurochenodeoxycholic acid, D_4-taurodeoxycholic acid, and D_4-taurocholic acid; D_4-lithocholic acid, D_4-chenodeoxycholic acid, D_4-deoxycholic acid, and D_4-cholic acid, and D_4-glycochenodeoxycholic acid. Mouse plasma samples were mixed with ice-cold methanolic IS working solution of internal standard, and were vortexed for

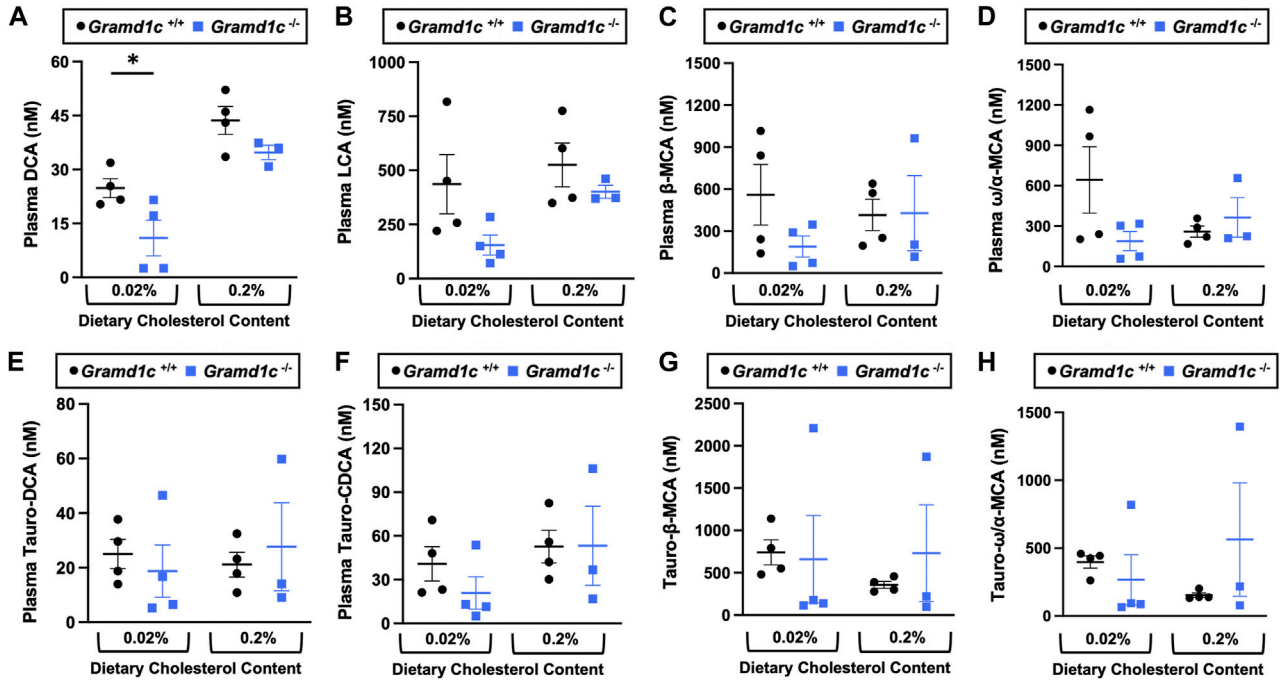

FIGURE 7
The impact of *Gramd1c* deficiency on plasma bile acids. At 8 weeks of age, female wild type (*Gramd1c*$^{+/+}$) or *Gramd1c* knockout mice (*Gramd1c*$^{-/-}$) were switched from standard rodent chow to one of two experimental synthetic diets containing low (0.02%, wt/wt) or high (0.2%, wt/wt) levels of dietary cholesterol. Mice were maintained on these diets over a 4-week period of study. The levels of various bile acids including **(A)** deoxycholic acid (DCA), **(B)** lithocholic acid (LCA), **(C)** β-muricholic acid (β-MCA), **(D)** ω/α-muricholic acid (ω/α-MCA), **(E)** taurodeoxycholic acid (Taura-DCA), **(F)** taurochenodeoxycholic acid (Tauro-CDCA), **(G)** tauro-β-muricholic acid (Taura-β-MCA), and **(H)** tauro-ω/α-muricholic acid (Tauro-ω/α-MCA) were quantified by liquid chromatography-tandem mass spectrometry (LC-MS/MS). Data are presented as mean ± SEM from n = three to four mice per group. * = significantly different ($p \leq 0.05$) when comparing *Gramd1c*$^{+/+}$ and *Gramd1c*$^{-/-}$ mice within each diet group.

10 min and centrifuged (14,000 *g*, 20 min, 4°C). The supernatant was transferred to glass HPLC vials for LC/MS/MS analysis using a 4000 Q-Trap triple quadrupole tandem mass spectrometer (AB SCIEX, MA, United States) equipped with an electrospray ionization source operating in negative ion mode. Mass spectrometry parameters were as follows: ions spray voltage—4200 V, ion source heater temperature 500°C, source gas 1: 35 psi, source gas 2: 45 psi, and curtain gas 35 psi. Nitrogen gas was used for the nebulizer, curtain and collision gas. Analyses were performed using electrospray ionization in negative-ion mode with multiple reaction monitoring (MRM) of precursor and characteristic product ions specific for each monitored bile acid. The HPLC system consisted of four binary pumps (LC-20 AD), autosampler operating at 10°C (Nexera X2 SIL-30AC), controller (CBM-20A) (Shimadzu Scientific Instruments, Inc., MD, United States) and a dual column switching valve system Rheodyne (IDEX Health and Science, MA, United States). Chromatographic separations were performed on a reverse phase columns (Kinetix C18, 2.6 µm, 150 mm × 4.6 mm ID; catalog # 00F-4462-E0; Phenomenex, Torrance, CA). Mobile phase A was 1 mM ammonium acetate and 0.1% acetic acid in methnol:acetonitrile:water (1:1:3; v/v/v) and mobile phase B was 0.1% acetic acid in methanol: acetonitrile:2-propanol (4.5:4.5:1; v/v/v). Samples were injected onto columns equilibrated in 100% A, and separated using a gradient as follows: 0–2 min 0% B; 2–20 min 0%–100% B; 20–28.5 min 100% B. Flow rate was programmed as follows: 0.3 mL/min from 0–20 min, and 0.5 mL/min from 20–28 min. Samples are introduced to the mass spec for analysis from 9–28 min. To eliminate carry over, an extensive washing step alternating between mobile phase A and B was added at the end of each run as follows: 100% A for 28–35 min, then directly switched to 100% B from 36–46 min, and equilibration step of 100% A from 46–60 min. To increase sample throughput 2-fold, a dual chromatographic system was used. At 28 min of the gradient on the first column, the next sample was injected into a second column; thus, during the first column washing and equilibration, the second column is used for BAs separation and diversion to the mass spectrometer for analysis. Calibration curves were built by fitting each analyte concentration (10 different points) to peak area ratios (analyte/internal standard). The limit of detection (LOD) was defined as the lowest concentration of analyte in sample matrix (e.g., serum) that generated a signal-to-noise ratio of ≥3. The limit of quantification (LOQ) was defined as the lowest concentration of analyte in sample matrix that generated a signal-to-noise ratio of ≥10. Recovery was tested by comparing area of deuterated standards added to pooled human serum (mix of ≥10 equal serum aliquots from healthy normal subjects) *versus* methanol, and calculated according to the following formula: % recovery = (average area spiked in serum pool/average area spiked in methanol) x100.

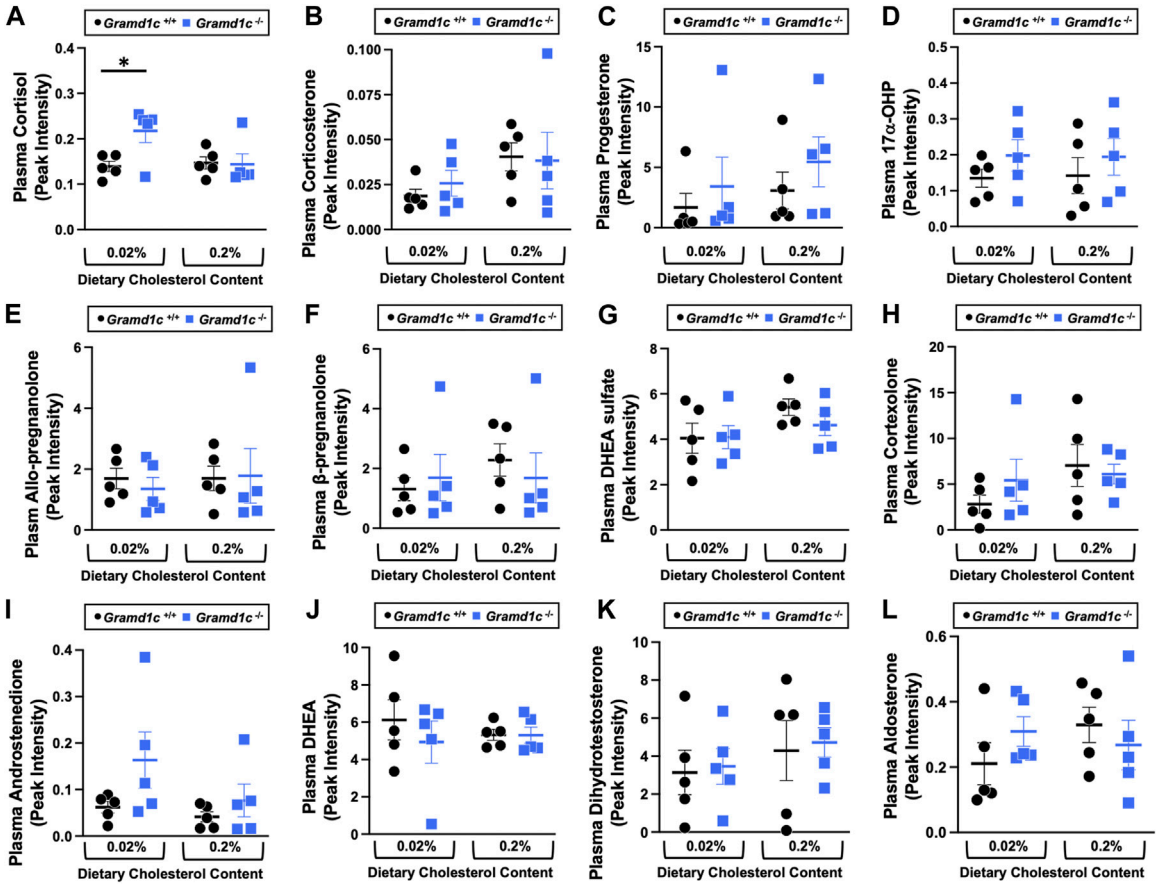

FIGURE 8
The impact of *Gramd1c* deficiency on plasma steroid hormones. At 8 weeks of age, female wild type (*Gramd1c*$^{+/+}$) or *Gramd1c* knockout mice (*Gramd1c*$^{-/-}$) were switched from standard rodent chow to one of two experimental synthetic diets containing low (0.02%, wt/wt) or high (0.2%, wt/wt) levels of dietary cholesterol. Mice were maintained on these diets over a 4-week period of study. The plasma levels of various steroid hormones including **(A)** cortisol, **(B)** corticosterone, **(C)** progesterone, **(D)** 17-α-hydroxyprogesterone, **(E)** allo-pregnanolone, **(F)** β-pregnanolone, **(G)** dehydroepiandrosterone (DHEA) sulfate, **(H)** cortexolone, **(I)** androstenedione, **(J)** dehydroepiandrosterone (DHEA), **(K)** dihydrotestosterone, and **(L)** aldosterone were measured semi-quantitatively by liquid chromatography-tandem mass spectrometry (LC-MS/MS). Data are presented as mean ± SEM from n = 5 mice per group.). * = significantly different ($p \leq 0.05$) when comparing *Gramd1c*$^{+/+}$ and *Gramd1c*$^{-/-}$ mice within the low cholesterol diet.

Quantification of plasma steroid hormone levels

A targeted steroid hormone panel from plasma including extraction was performed by the West Coast Metabolomics Center at the University of California—Davis (Director—Dr. Oliver Fiehn). The extraction protocol was adapted from Pedersen and Newman. 2018. Plasma sample was vortexed and 50 µL of Surrogate Standards of the 3 lipid classes was added along with CDU and vortexed again for 30sec. Samples were centrifuged at 6°C for 5 min at 15,000 g and the supernatant (~240 µL) was transferred into new Eppendorf tube/filter plate Spin Filter (0.1 um) and stored in −20°C until analysis. The samples were run using Thermo Scientific Vanquish Horizon UPLC/SciEx QTrap 6,500+.

Quantification of liver oxysterol levels

Lipids were extracted by addition of 2 mL hexane/isopropanol (3:2, v/v) or chloroform/methanol (2:1, v/v) from the cell monolayers and liver tissue, respectively. 24–25- and 27- hydroxy cholesterol levels were quantified by isotope dilution mass spectrometry as previously described (Dzeletovic et al., 1995). Oxysterol levels were normalized for the total protein content measured using the RC DC™ Protein Assay (BioRad Laboratories Inc., United States) in liver tissue after digestion with NaOH (0.25 mol/L).

Liver targeted metabolomics

The AbsoluteIDQ® p400 HR kit from Biocrates Life Sciences AG was used to obtain targeted quantitative metabolomics data as we have previously described (Osborn et al., 2019). Liver tissue was collected at time of necropsy and samples were prepared according to manufacturer protocol. Briefly, at least 30 mg of each tissue sample was cut and weighed, and kept frozen throughout this protocol. The tissue samples were homogenized and centrifuged at 10,000 × g for 5 min. The supernatant was then collected, 10 µL of which per sample was

10.3389/fphys.2024.1371096

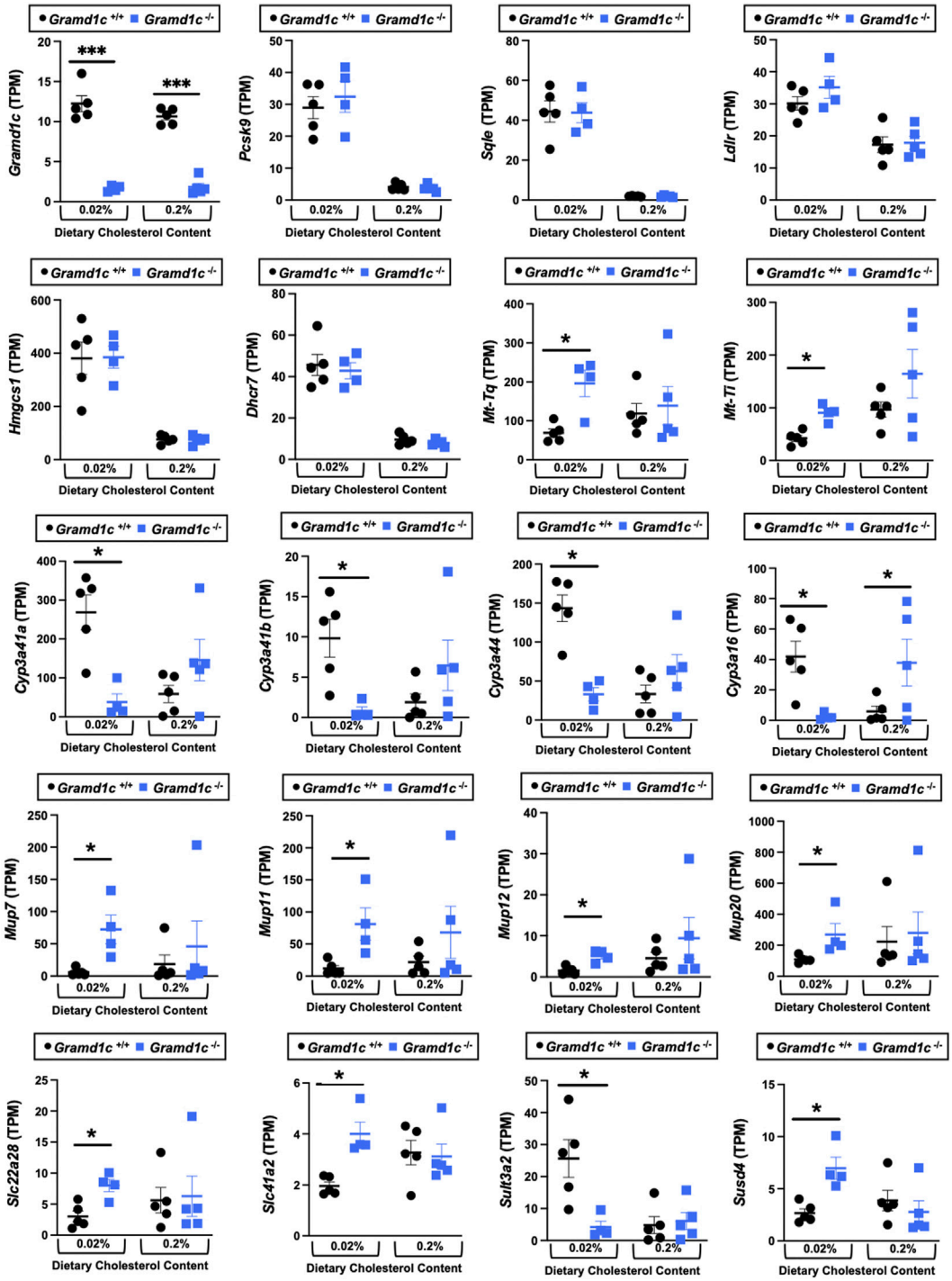

FIGURE 9
Bulk RNA sequencing in the liver of *Gramd1c–/–* mice identifies alterations in a small subset of genes. At 8 weeks of age, female wild type (*Gramd1c*$^{+/+}$) or *Gramd1c* knockout mice (*Gramd1c*$^{-/-}$) were switched from standard rodent chow to one of two experimental synthetic diets containing low (0.02%, wt/wt) or high (0.2%, wt/wt) levels of dietary cholesterol. Mice were maintained on these diets over a 4-week period of study, and thereafter bulk RNA sequencing was performed to identify differentially-expressed genes. Data are presented as mean ± SEM from n = four to five mice per group. * = significantly different ($p \leq 0.05$) when comparing *Gramd1c*$^{+/+}$ and *Gramd1c*$^{-/-}$ mice within each diet group.

loaded onto a 96-well plate containing stable isotope-labeled standards, and processed according to manufacturer protocol. The LCMS analysis was done using specific parameters (both Tune and LCMS methods) per kit manufacturer's recommendations. The assay was performed on a Q-Exactive HF (operated only in positive ESI mode) coupled with a Vanquish UHPLC + focused liquid chromatography as detailed per assay instructions. The manufacturer-provided software, MetIDQ (Biocrates, Life Science AG), was used to provide the peak identification.

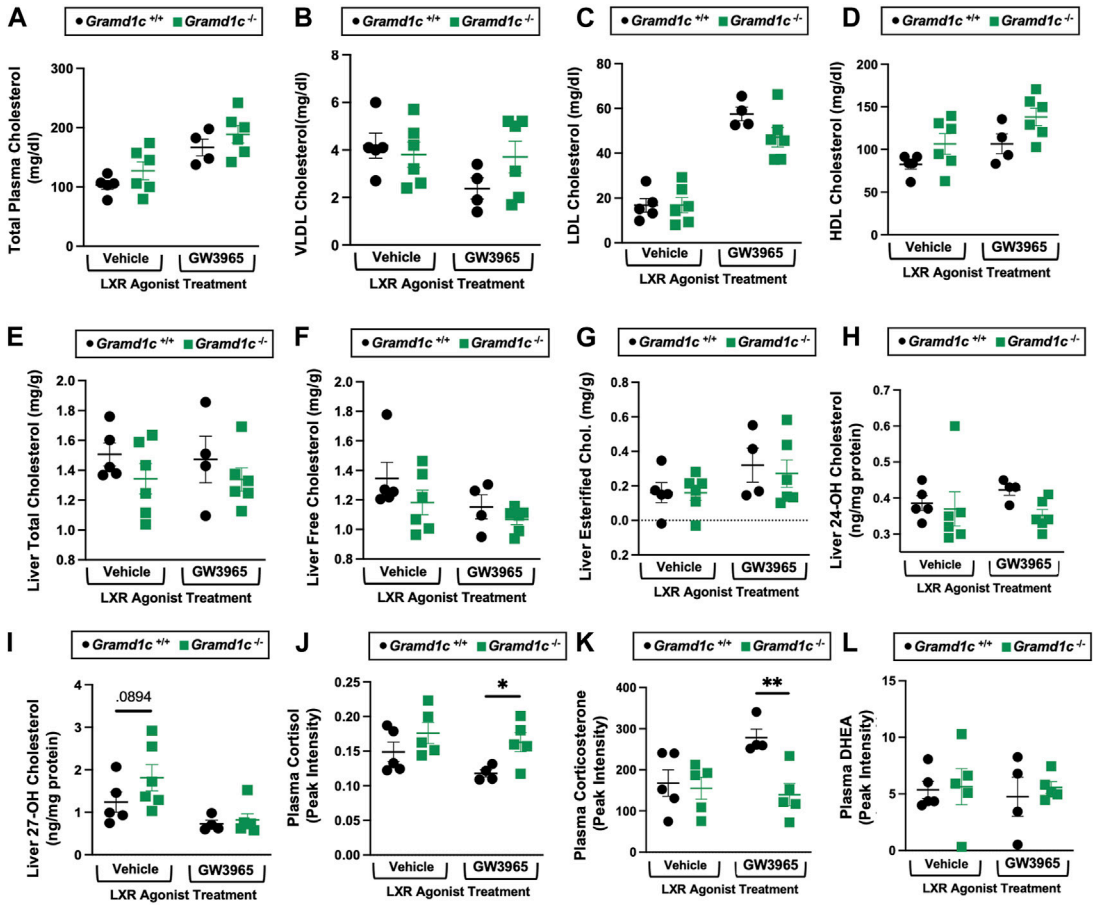

FIGURE 10
Global deletion of *Gramd1c* does not significantly alter circulating or hepatic cholesterol levels in male mice. At 8 weeks of age, male wild type (*Gramd1c*$^{+/+}$) or *Gramd1c* knockout mice (*Gramd1c*$^{-/-}$) were maintained on a standard chow diet in the absence (vehicle) or presence of the LXR agonist GW3965 (40 mg/kg per day) for 7 consecutive days. **(A)** Total plasma cholesterol levels were measure by gas chromatography-tandem mass spectrometry (GC-MS/MS). **(B–D)** Plasma was subjected to size exclusion chromatography to examine total cholesterol distribution across very low density (VLDL), low density (LDL), or high density (HDL) lipoprotein fractions. In addition, a variety of hepatic lipids were quantified by targeted mass spectrometry assays including **(E)** liver total cholesterol, **(F)** liver free cholesterol, **(G)** liver esterified cholesterol, **(H)** 24-hydoxycholesterol (24-OH Chol.), and **(I)** 27-hydroxycholesterol (27-OH Chol.) The plasma levels of various steroid hormones including **(J)** cortisol, **(L)** corticosterone, and **(L)** dehydroepiandrosterone (DHEA) were measured semi-quantitatively by liquid chromatography-tandem mass spectrometry (LC-MS/MS). Data are presented as mean ± SEM from n = four to six mice per group. *($p \leq 0.05$), **($p \leq 0.01$) = significantly different when comparing *Gramd1c*$^{+/+}$ and *Gramd1c*$^{-/-}$ mice within each drug treatment group.

Lipoprotein cholesterol distribution by size-exclusion chromatography

Plasma (40–50 mL) was diluted to a total volume of 500 mL in PBS and loaded into an Akta Pure 25L liquid chromatography system. Samples were passed through a Superose 6 Increase column (Cytiva) at a flow rate of 0.75 mL/min in PBS. Fractions were collected (0.5 mL/fraction) and assayed for total cholesterol content by enzymatic assay (Fujifilm; catalog # 999–02601). Independent runs were performed for each mouse, and cholesterol distribution in very low density (VLDL), low density (LDL), and high density (HDL) lipoproteins was calculated based on the percent distribution in each fraction compared to the total plasma cholesterol measured by GC-MS/MS.

Real-Time PCR and bulk RNA sequencing analysis of gene expression

Tissue RNA extraction and quantitative polymerase chain reaction (qPCR) analyses of relative mRNA abundance were conducted as previously described (Helsley et al., 2019; Pathak et al., 2020). mRNA expression levels were calculated based on the ΔΔ-CT method using Cyclophilin A as a housekeeping gene. qPCR was conducted using SYBR Fast reagents (AB#4385612) on the Applied Biosystems 7,500 Real-Time PCR System. Primers used for qPCR are *CycloA* F - GCGGCAGGTCCATCTACG, *CycloA* R - GCCATC CAGCCATTCAGTC, *Gramd1a* F - CATGCACACCTCAGGTTC CC, *Gramd1a* R - ACGATGAGGACAATGCTGATG, *Gramd1b* F - GCTGGTTATCAGCTGTGTTCTG, *Gramd1b* R - GTGAGGGTC TGGGTGGTGTA, *Gramd1c* F -CAGTTATGACACCGCCCTTAT

Gramd1c R - CTGGGTAGCGTGTTCTATCTTT. RNA extraction, library preparation, sequencing and analysis was conducted at Azenta Life Sciences (South Plainfield, NJ, United States) as follows: Extraction: Total RNA was extracted using Qiagen Rneasy Plus Universal Mini kit following manufacturer's instructions (Qiagen, Hilden, Germany). Library Preparation with PolyA selection and Illumina Sequencing: RNA samples were quantified using Qubit 2.0 Fluorometer (Life Technologies, Carlsbad, CA, United States) and RNA integrity was checked using Agilent TapeStation 4,200 (Agilent Technologies, Palo Alto, CA, United States). RNA sequencing libraries were prepared using the NEBNext Ultra RNA Library Prep Kit for Illumina using manufacturer's instructions (NEB, Ipswich, MA, United States). Briefly, mRNAs were initially enriched with Oligod(T) beads. Enriched mRNAs were fragmented for 15 min at 94°C. First strand and second strand cDNA were subsequently synthesized. cDNA fragments were end repaired and adenylated at 3′ends, and universal adapters were ligated to cDNA fragments, followed by index addition and library enrichment by PCR with limited cycles. The sequencing library was validated on the Agilent TapeStation (Agilent Technologies, Palo Alto, CA, United States), and quantified by using Qubit 2.0 Fluorometer (Invitrogen, Carlsbad, CA) as well as by quantitative PCR (KAPA Biosystems, Wilmington, MA, United States). The sequencing libraries were multiplexed and clustered onto a flowcell on the Illumina NovaSeq instrument according to manufacturer's instructions. The samples were sequenced using a 2 × 150 bp Paired End (PE) configuration. Image analysis and base calling were conducted by the NovaSeq Control Software (NCS). Raw sequence data (.bcl files) generated from Illumina NovaSeq was converted into fastq files and de-multiplexed using Illumina bcl2fastq 2.20 software. One mismatch was allowed for index sequence identification. Transcript per million (TPM) values for each differentially expressed gene were plotted using Prism Software and the statistical analysis was done using JMP software.

Immunoblotting

Whole liver homogenates were made from tissues in a modified RIPA buffer (Abcam #156034) as previously described (Helsley et al., 2019; Pathak et al., 2020), and protein was quantified using the bicinchoninic (BCA) assay (Pierce). Proteins were separated by 4%–12% SDS-PAGE, transferred to polyvinylidene difluoride (PVDF) membranes (ThermoSci #88518), and proteins were detected after incubation with an antibody recognizing mouse ASTER-C (generated here) or β-actin (Cell Signaling Technologies product # 4970S). Given the paucity of available antibodies, a custom rabbit polyclonal antibody was generated in collaboration with Thermofisher. The antigen used was the N-terminus 34 kDa mouse Aster-C protein (Uniprot Q8CI52; amino acids 1–300). A 72 days injection protocol with a primary immunization and three subsequent boosters was followed, and the terminal 72 days crude anti-sera sample (50 mL) was affinity purified (expressed protein conjugated to the affinity column) by ThermoFisher. Affinity-purified antibodies were eluted using a step-wise pH gradient and collected in neutralizing buffer. Purified antibodies were then concentrated and final concentration is measured by BCA. Membrane was blocked with 5% milk in Tris buffered saline containing 0.2% Tween 20.1:500 dilution of this Gramd1c antibody in Blocking buffer was used for Western blotting and the bands were detected using an anti-rabbit-HRP conjugated secondary antibody.

Cell culture and generation of *Gramd1c*-Deficient RAW264.7 cells

Mycoplasma-tested RAW264.7 macrophage cells were cultured under standard conditions in Dulbecco-modified Eagle's minimum essential medium (D-MEM) (GIBCO, Life Technologies, Carlsbad, CA) supplemented with 10% fetal bovine serum (FBS, GIBCO), 1% l-glutamine, 1% penicillin-streptomycin and 1% nonessential amino acids in a 5% CO2-humidified chamber at 37°C.

CRISPR-Cas9 genome editing was accomplished using methods previously described (Ran et al., 2013). Gramd1c sgRNAs were designed by an online tool (https://www.benchling.com/) and cloned into the Lenti-CRISPER v2 vector (Addgene (Ran et al., 2013) with D10A nickase version of Cas9 (Cas9n)). *Gramd1c KO* cell lines were generated following lentiviral transduction of the Lenti-CRISPER v2-Cas9 D10A- Gramd1c sgRNA in RAW264.7cells. *Gramd1c KO* cells were validated by analyzing the expression of GRAMD1c by Western blot. Primers used for gene editing were: *GRAMD1c*-E5-Nick-5F: 5′-CACCGCAGAGCACCCTCCAAG TCAC-3′, *GRAMD1c*-E5-Nick-5R: 5′-AAACGTGACTTGGAG GGTGCTCTGC-3′, *GRAMD1c*-E5-Nick-3F: 5′- CACCGCTCT TTTCTGAAGCTAGCGA-3′, and *GRAMD1c*-E5-Nick-3R: 5′-AAACTCGCTAGCTTCAGAAAAGAGC-3'.

cDNA cloning and expression of GRAMD1c

Gramd1C construct was cloned by double-stranded gene fragment synthesis (IDT, Coralville, IA) and assembled using NEBuilder® HiFi DNA Assembly (NEB, Ipswich, MA). The double-stranded gene fragment was assembled in a pLENTI-EF1alpha-3XFLAG vector backbone. pLENTI-EF1alpha-3XFLAG-Gramd1c was expressed in RAW264.7 cells by transient transfection using Lipofectamine 3,000. Cells were harvested 72 h after transfection in RIPA lysis buffer supplemented with complete protease inhibitors (Roche Applied Science). Lysates were cleared by centrifugation at 16,000 × *g* for 20 min, and Western blots were performed as described above as well as in the online data supplement.

Statistical analysis

All data were analyzed using one-way analysis of variance (ANOVA) where appropriate, followed by either a Tukey's or Student's t tests for *post hoc* analysis. Differences were considered significant at $p < 0.05$. All mouse data analyses were performed using Graphpad Prism 6 (La Jolla, CA, United States) software or JMP version 17 (SAS Institute, Cary, NC, United States) software.

Results

Global deletion of *Gramd1c* does not alter circulating sterol levels

To examine whether Aster-C can alter systemic cholesterol metabolism under normal physiologic conditions, we fed young wild type (*Gramd1c*$^{+/+}$) or global *Gramd1c* knockout mice (*Gramd1c*$^{-/-}$) one of two experimental diets containing low (0.02%, wt/wt) or high (0.2%, wt/wt) levels of dietary cholesterol for a period up to 4 weeks. Deletion of *Gramd1c* was confirmed in the liver, where both messenger RNA (Figure 1A) and protein (Figure 1B) were significantly reduced in *Gramd1c*$^{-/-}$ mice compared to littermate controls (*Gramd1c*$^{+/+}$). *Gramd1c*$^{-/-}$ mice were born at normal Mendelian ratios and were indistinguishable from wild type littermates. Irrespective of dietary cholesterol level, *Gramd1c*$^{-/-}$ mice maintained similar body weights compared to wild type mice throughout the study (Figure 1C). When we examined either the total, unesterified (free), or esterified levels of cholesterol in the plasma, *Gramd1c*$^{-/-}$ mice were not significantly different when compared to wild type controls (Figures 2B–D). Likewise, the cholesterol levels in very low-density (VLDL), low-density (LDL), or high-density lipoproteins (HDL) were similar when comparing *Gramd1c*$^{+/+}$ to *Gramd1c*$^{-/-}$ mice (Figures 2A,E,G). Given plasma cholesterol levels were unchanged in *Gramd1c*$^{-/-}$ mice (Figure 2), we wanted to look more broadly at other potential sterol substrates including several phytosterols and biosynthetic intermediates generated during the *de novo* synthesis of cholesterol. It is important to note that *Gramd1c*$^{-/-}$ mice had normal circulating levels of 7-dehydrocholesterol, desmosterol, lanosterol, lathosterol, β-sitosterol, campesterol, brassicasterol, and stigmasterol (Figure 3). These data show that Aster-C alone does not play a quantitatively important role in determining the circulating levels of cholesterol or other diverse sterols of plant or mammalian origin under conditions of low and excess dietary cholesterol.

Aster-C modestly shapes the hepatic lipidome

We next turned our attention to test whether Aster-C plays a role in sterol homeostasis in the liver, given the central role the liver plays in whole body cholesterol balance. Here, we applied several complimentary and broad targeted lipidomic methods to quantify diverse sterols, but also major classes of glycerophospholipids and neutral lipids. Similar to findings in plasma (Figure 2), compared to wild type mice, *Gramd1c*$^{-/-}$ mice have unaltered levels of total, free, and esterified cholesterol in the liver (Figures 4A–C). *Gramd1c*$^{+/+}$ and *Gramd1c*$^{-/-}$ mice also had similar hepatic levels of 7-dehydrocholesterol, desmosterol, lanosterol, lathosterol, β-sitosterol, campesterol, brassicasterol, and stigmasterol (Figure 5). We next examined the hepatic levels of the major oxysterol species that are generated from cholesterol substrate (24-hydroxycholesterol and 27-hydroxycholesterol), and found similar levels in *Gramd1c*$^{+/+}$ and *Gramd1c*$^{-/-}$ mice (Figures 4D,E). Finally, we performed a broad lipidomic approach to examine a variety of glycerophospholipid and neutral lipids in the liver. *Gramd1c*$^{+/+}$ and *Gramd1c*$^{-/-}$ mice had similar levels of all molecular species of glycerophospholipids detected (data not shown). However, this broader method was able to uncover a modest increase in cholesterol esters containing a 17:2 fatty acyl chain in high cholesterol diet-fed mice (Figure 4F). Yet, all other molecular species of cholesteryl esters were unchanged in *Gramd1c*$^{-/-}$ mice (Figure 4G). Furthermore, under low dietary cholesterol conditions, one specific molecular species of triacylglycerol (TG 58:8) was increased in *Gramd1c*$^{-/-}$ mice (Figure 4H), but all other detected species of triacylglycerol were similar to wild to mice (Figures 4I,J).

Aster-C shapes bile acid homeostasis but does not impact fecal sterol loss

A recent report by Xiao and colleagues reported that mice lacking both Aster-A and Aster-C selectively in hepatocytes have impaired reverse cholesterol transport (RCT) (Xiao et al., 2023). This important work showed that Aster-A/Aster-C double knockout mice have reduced movement of cholesterol radiotracer (^{14}C-cholesterol) into the feces when either derived from LDL or HDL sources (Xiao et al., 2023). However, they did not test whether Aster-C alone can impact the mass amount of cholesterol excreted in the feces. When we examined the quantitative fecal excretion of cholesterol in global *Gramd1c*$^{-/-}$ mice fed low or high cholesterol, there was no significant difference when compared to wild type littermates (Figure 6). Likewise, the fecal excretion of other phytosterols and sterol intermediates such as 7-dehydrocholesterol, desmosterol, lanosterol, lathosterol, β-sitosterol, campesterol, brassicasterol, and stigmasterol were similar in *Gramd1c*$^{+/+}$ and *Gramd1c*$^{-/-}$ mice (Figure 6). Another way the liver can facilitate RCT is via the enzymatic conversion of cholesterol into bile acids, which can further contribute to removal of cholesterol from the body. Although the majority of plasma bile acid species were unchanged in *Gramd1c*$^{-/-}$ mice, levels of deoxycholic acid were significantly reduced in *Gramd1c*$^{-/-}$ mice fed a low cholesterol diet (Figure 7). Given the clear role that Aster-B plays in adrenal gland cholesterol homeostasis (Sandhu et al., 2018), we also wanted to understand whether Aster-C may play a role in cholesterol-derived hormone production. Only under low dietary cholesterol conditions, *Gramd1c*$^{-/-}$ mice have elevated plasma cortisol compared to wild type controls (Figure 8A). However, all other steroid hormones measured including corticosterone, progesterone, 17-α-hydroxyprogesterone, allo-pregnanolone, β-pregnanolone, dehydroepiandrosterone (DHEA) sulfate, cortexolone, androstenedione, free DHEA, dihydrotestosterone, and aldosterone were unaltered in *Gramd1c*–/– mice (Figures 8B–L).

Gramd1c-deficient mice show diet-dependent alterations in hepatic gene expression

We next performed bulk RNA sequencing to understand the effects of *Gramd1c* deletion on global gene expression in the liver (Figure 9). The most differentially expressed gene was *Gramd1c*, which was markedly reduced in *Gramd1c*$^{-/-}$ mice compared to wild

type *Gramd1c*$^{+/+}$ controls in both low and high cholesterol diet conditions (Figure 9). It is important to note that several sterol-responsive genes including proprotein convertase subtilisin/kexin type 9 (*Pcsk9*), squalene epoxidase (*Sqle*), low density lipoprotein receptor (*Ldlr*), 3-hydroxy-3-methylglutaryl-CoA synthase 1 (*Hmgcs1*), and 7-dehydrocholesterol reductase (*Dhcr7*) were significantly repressed under high dietary cholesterol conditions, but the dietary cholesterol-driven suppression of these genes was similar in both *Gramd1c*$^{+/+}$ and *Gramd1c*$^{-/-}$ mice (Figure 9). Unexpectedly, the expression of two mitochondrially-encoded genes, mitochondria encoded tRNA-Ile (AUU/C) (*Mt-Ti*) and mitochondrially-encoded tRNA-Gln (CAA/G) (*Mt-Tq*), were elevated in *Gramd1c*$^{-/-}$ mice only under low dietary cholesterol conditions (Figure 9). In parallel, only under low dietary cholesterol conditions, the expression of several members of the cytochrome P450 family 3 subfamily A genes (*Cyp3a41a*, *Cyp3a41b*, *Cyp3a44*, and *Cyp3a16*) were significantly lower in *Gramd1c*$^{-/-}$ mice when compared to *Gramd1c*$^{+/+}$mice (Figure 9). Also, the hepatic expression of several genes encoding major urinary proteins (*Mup7*, *Mup11*, *Mup12*, and *Mup20*) were elevated in *Gramd1c*$^{-/-}$ mice, only under low dietary cholesterol conditions (Figure 9). Other genes altered in low cholesterol-fed *Gramd1c*$^{-/-}$ mice includes solute transport genes (*Slc22a28* and *Slc41a2*), sulfotransferase family 3A, member 2 (*Sult3a2*), and sushi domain-containing 4 (*Susd4*). These data show that, particularly under low dietary cholesterol conditions, *Gramd1c* deficiency is associated with reduced expression of several genes involved in xenobiotic metabolism (*Cyp3a41a*, *Cyp3a41b*, *Cyp3a44*, *Cyp3a16, and Sult3a2*) as well as increased expression of major urinary protein genes (*Mup7*, *Mup11*, *Mup12*, and *Mup20*) that encode lipid-binding proteins within the lipocalin family.

Gramd1c-null male mice also have modest alterations in whole body sterol balance

Given previous reports (Sandhu et al., 2018) have shown that *Gramd1b* can be a direct transcriptional target of the nuclear hormone receptor liver X receptor (LXR), we next treated male *Gramd1c*$^{+/+}$ and *Gramd1c*$^{-/-}$ mice with a pharmacologic LXR agonist (Figure 10). Much like in female mice (Figures 1–9), males lacking *Gramd1c*$^{-/-}$ had normal plasma and liver cholesterol levels both under vehicle and GW3965-treated conditions (Figures 10A–G). Although there were some modest trends, *Gramd1c*$^{-/-}$ mice also did not have statistically significant differences in hepatic oxysterol levels (Figures 10H,I). Although *Gramd1c*$^{-/-}$ mice did not have altered steroid hormone levels under vehicle-treated conditions (Figures 10J–L), upon LXR agonist treatment *Gramd1c*$^{-/-}$ mice had slightly elevated plasma cortisol levels and reduced levels of corticosterone (Figure 10K) compared to *Gramd1c*$^{+/+}$ mice. All other steroid hormones measured were not altered in *Gramd1c*$^{-/-}$ mice (Figure 10L).

Discussion

It has been nearly 5 years since the original discovery of the Aster protein family as novel regulators of non-vesicular transport of PM cholesterol to the ER (Sandhu et al., 2018). This seminal report unequivocally established that Aster-B plays an essential roles in cholesterol balance and steroid hormone production, given that *Gramd1b*$^{-/-}$ mice have very low levels of cholesteryl ester storage in the adrenal gland (Sandhu et al., 2018). However, the cell autonomous and systemic roles of Aster-A and Aster-C in cholesterol uptake and metabolism have been more elusive. Given the tissue-specific expression patterns of Aster proteins, and unique nuclear hormone receptor-driven transcriptional control (i.e., LXR-driven transcription of *Gramd1b* and FXR-driven transcription of *Gramd1c*) (Sandhu et al., 2018; Xiao et al., 2023; Ferrari et al., 2023), it is logical to assume that each Aster protein may play unique roles in cholesterol homeostasis. Here, we have specifically addressed the role of Aster-C in tissue and systemic balance. The main findings of this work are: 1) Aster-C does not play a quantitatively important role in determining plasma, liver, or fecal levels of cholesterol itself, cholesterol synthetic intermediates, oxysterols, or phytosterols, 2) Global deletion of *Gramd1c* is associated with reduced deoxycholic acid and increased plasma cortisol, but only in low cholesterol diet-fed settings, 3) *Gramd1c*$^{-/-}$ mice did not show alterations in sterol-sensitive genes in the liver, but instead showed altered expression of genes in major urinary protein (MUP) and cytochrome P450 (CYP) families only under low dietary cholesterol conditions. Collectively, our results show that Aster-C plays a relatively minor role in whole body sterol balance under conditions where dietary cholesterol is limited or in excess.

Although global *Gramd1c*$^{-/-}$ mice show a relatively minor phenotype, when compared to the striking adrenal phenotype in *Gramd1b*$^{-/-}$ mice (Sandhu et al., 2018), a plausible explanation is the potential for functional redundancy of Aster proteins in tissues where several are co-expressed together. For instance, the adrenal gland has relatively high expression of Aster-B compared to Aster-A and Aster-C, and therefore deletion of *Gramd1b* has a profound impact on adrenal cholesterol ester storage (Sandhu et al., 2018). In contrast, the liver expresses all three Gramd1 genes, and there is emerging evidence of functional redundancy. In support of this, findings here show that global deletion of Gramd1c does not alter hepatic sterol homeostasis. However, a recent study by the Tontonoz group (Xiao et al., 2023) demonstrated that hepatocyte-specific deletion of both *Gramd1a* and *Gramd1c* (i.e., hepatocyte-specific *Gramd1a* and *Gramd1c* double knockout) have impaired movement of lipoprotein-derived free cholesterol out of the body via RCT. In further support of functional redundancy, only double knockout of both *Gramd1b* and *Gramd1c* in intestinal enterocytes, but not single deficiency, can reduce intestinal cholesterol absorption (Ferrari et al., 2023). Also, the ability of Chinese hamster ovary (CHO-K1) cells to esterify LDL-derived cholesterol depends on the deletion of all three Aster proteins (A, B, and C), whereas single deletion had modest to no effect (Trinh et al., 2021). Given there is some interest in potentially drugging the Aster proteins for disease of cholesterol imbalance like atherosclerosis and some cancers (Xiao et al., 2021), it will be imperative to understand where functional redundancy exists and those situations where one family member can be selectively targeted for therapeutic benefit.

Although there is mounting evidence of functional redundancy for Asters, further studies are needed to understand where certain family members predominate. For example, it is clear that

LXR-driven expression of Aster-B is essential for the esterification and storage of cholesterol esters in the adrenal gland, and that Aster-A and -C cannot combine to overcome the loss of Aster-B (Sandhu et al., 2018). Here we show that under conditions of global Aster-C deficiency, there is clearly significant reduction in the major bile acid species deoxycholic acid (Figure 7A). Given recent reports showing that *Gramd1c* is a direct transcriptional target of the bile acid sensing nuclear receptor FXR (Xiao et al., 2023), additional studies are needed to further understand whether Aster-C-driven modulation of bile acid homeostasis may hold therapeutic potential in liver disease (Wang et al., 2020). In addition to cholesterol transport, Aster proteins have also been shown to transport carotenoids in the retina (Bandara et al., 2022). It is interesting to speculate whether diverse Aster proteins including Aster-C may play a broader role in lipid transport and metabolism beyond sterols and carotenoids. Of potential interest in this study, the clear upregulation of the hepatic major urinary protein (MUP) genes (*Mup7*, *Mup11*, *Mup12*, and *Mup20*) may be worth further exploration. MUP proteins are lipid-binding proteins within the lipocalin family, and are known to carry diverse lipid cargos in the bloodstream and urine for the purpose of chemical signaling (Zhou and Rui, 2010). Additional work is clearly needed to fully understand the specific role of Aster-C in lipid transport and metabolism. In conclusion, this work shows that Aster-C plays a minor role in whole body sterol homeostasis. However, additional work is needed to determine whether this is simply due to functional redundancy of other Aster proteins or indicative of other elusive functions of Aster-C in lipid trafficking. Naito et al., 2023.

Data availability statement

The datasets presented in this study can be found in online repositories. The names of the repository/repositories and accession number(s) can be found below: https://www.ncbi.nlm.nih.gov/genbank/, GSE250230.

Ethics statement

The animal study was approved by Cleveland Clinic Institutional Animal Care and Use Committee. The study was conducted in accordance with the local legislation and institutional requirements.

Author contributions

RB: Data curation, Formal Analysis, Investigation, Methodology, Writing–original draft, Writing–review and editing. RH: Data curation, Investigation, Methodology, Writing–review and editing. SC: Data curation, Investigation, Methodology, Writing–review and editing. BJ: Data curation, Formal Analysis, Investigation, Methodology, Software, Writing–review and editing. AH: Data curation, Investigation, Methodology, Writing–review and editing. WM: Data curation, Formal Analysis, Investigation, Methodology, Software, Writing–review and editing. VV: Data curation, Formal Analysis, Investigation, Methodology, Software, Writing–review and editing. NZ: Data curation, Formal Analysis, Investigation, Methodology, Software, Writing–review and editing. AB: Data curation, Investigation, Methodology, Project administration, Software, Writing–review and editing. SD: Data curation, Formal Analysis, Investigation, Methodology, Software, Writing–review and editing. MG: Data curation, Formal Analysis, Investigation, Methodology, Software, Writing–review and editing. KM: Investigation, Methodology, Formal Analysis, Software, Writing–review and editing. AC: Data curation, Formal Analysis, Investigation, Methodology, Software, Writing–review and editing. RH: Data curation, Formal Analysis, Investigation, Methodology, Software, Writing–review and editing. SG: Data curation, Formal Analysis, Investigation, Methodology, Software, Writing–review and editing. CS: Data curation, Formal Analysis, Investigation, Methodology, Software, Writing–review and editing. Belinda Belle BW: Data curation, Formal Analysis, Investigation, Methodology, Software, Writing–review and editing. CG: Data curation, Formal Analysis, Investigation, Methodology, Writing–review and editing. VG: Data curation, Formal Analysis, Investigation, Methodology, Software, Writing–review and editing. MP: Data curation, Formal Analysis, Investigation, Software, Writing–review and editing. PP: Data curation, Formal Analysis, Investigation, Methodology, Software, Writing–review and editing. JB: Conceptualization, Data curation, Formal Analysis, Funding acquisition, Investigation, Methodology, Project administration, Resources, Software, Supervision, Validation, Visualization, Writing–original draft, Writing–review and editing.

Funding

The author(s) declare financial support was received for the research, authorship, and/or publication of this article. This work was supported in part by National Institutes of Health grants R01 DK120679 (JB), P01 HL147823 (JB), P50 AA024333 (J.M.B.), R01 DK130227 (JB), and RF1 NS133812 (JB). Some of the metabolomic data (steroid hormones) were acquired at the University of California - Davis West Coast Metabolomics Center which is funded in part by U2CES030158.

Conflict of interest

The authors declare that the research was conducted in the absence of any commercial or financial relationships that could be construed as a potential conflict of interest.

Publisher's note

References

Bandara, S., Ramkumar, S., Imanishi, S., Thomas, L. D., Sawant, O. B., Imanishi, Y., et al. (2022). Aster proteins mediate carotenoid transport in mammalian cells. *Proc. Natl. Acad. Sci. U.S.A.* 119 (15), e2200068119. doi:10.1073/pnas.2200068119

Charsou, C., Ng, M. Y. W., and Simonsen, A. (2022). Regulation of autophagosome biogenesis and mitochondrial bioenergetics by the cholesterol transport protein GRAMD1c. *Autophagy* 19 (7), 2159–2161. doi:10.1080/15548627.2022.2155020

Choucair, I., Nemet, I., Li, L., Cole, M. A., Skye, S. M., Kirsop, J. D., et al. (2020). Quantification of bile acids: a mass spectrometry platform for studying gut microbe connection to metabolic diseases. *J. Lipid Res.* 61 (2), 159–177. doi:10.1194/jlr.RA119000311

Dzeletovic, S., Breuer, O., Lund, E., and Diczfalusy, U. (1995). Determination of cholesterol oxidation products in human plasma by isotope dilution-mass spectrometry. *Anal. Biochem.* 225 (1), 73–80. doi:10.1006/abio.1995.1110

Fan, X., Song, Z., Qin, W., Yu, T., Peng, B., and Shen, Y. (2023). Potential common molecular mechanisms between periodontitis and hepatocellular carcinoma: a bioinformatic analysis and validation. *Cancer Genomics Proteomics* 20 (6), 602–616. doi:10.21873/cgp.20409

Ferrari, A., He, C., Kennelly, J. P., Sandhu, J., Xiao, X., Chi, X., et al. (2020). Aster proteins regulate the accessible cholesterol pool in the plasma membrane. *Mol. Cell Biol.* 40 (19), 002555–e320. doi:10.1128/MCB.00255-20

Ferrari, A., Whang, E., Xiao, X., Kennelly, J. P., Romartinez-Alonso, B., Mack, J. J., et al. (2023). Aster-dependent nonvesicular transport facilitates dietary cholesterol uptake. *Science* 382 (6671), eadf0966. doi:10.1126/science.adf0966

Gong, J., Yu, R., Hu, X., Luo, H., Gao, Q., Li, Y., et al. (2023). Development and validation of a novel prognosis model based on a panel of three immunogenic cell death-related genes for non-cirrhotic hepatocellular carcinoma. *J. Hepatocell. Carcinoma* 10, 1609–1628. doi:10.2147/JHC.S424545

Hao, H., Wang, Z., Ren, S., Shen, H., Xian, H., Ge, W., et al. (2019). Reduced GRAMD1C expression correlates to poor prognosis and immune infiltrates in kidney renal clear cell carcinoma. *PeerJ* 20 (7), e8205. doi:10.7717/peerj.8205

Helsley, R. N., Varadharajan, V., Brown, A. L., Gromovsky, A. D., Schugar, R. C., Ramachandiran, I., et al. (2019). Obesity-linked suppression of membrane-bound O-acyltransferase 7 (MBOAT7) drives non-alcoholic fatty liver disease. *Elife* 8, e49882. doi:10.7554/eLife.49882

Li, X., Zhou, C., Qiu, C., Li, W., Yu, Q., Huang, H., et al. (2022). A cholesterogenic gene signature for predicting the prognosis of young breast cancer patients. *PeerJ* 10, e13922. doi:10.7717/peerj.13922

Naito, T., Ercan, B., Krshnan, L., Triebl, A., Koh, D. H. Z., Wei, F. Y., et al. (2019). Movement of accessible plasma membrane cholesterol by the GRAMD1 lipid transfer protein complex. *Elife* 8, e51401. doi:10.7554/eLife.51401

Naito, T., Yang, H., Koh, D. H. Z., Mahajan, D., Lu, L., and Saheki, Y. (2023). Regulation of cellular cholesterol distribution via non-vesicular lipid transport at ER-Golgi contact sites. *Nat. Commun.* 14 (1), 5867. doi:10.1038/s41467-023-41213-w

Ng, M. Y. W., Charsou, C., Lapao, A., Singh, S., Trachsel-Moncho, L., Schultz, S. W., et al. (2022). The cholesterol transport protein GRAMD1C regulates autophagy initiation and mitochondrial bioenergetics. *Nat. Commun.* 13 (1), 6283. doi:10.1038/s41467-022-33933-2

Osborn, L. J., Orabi, D., Goudzari, M., Sangwan, N., Banerjee, R., Brown, A. L., et al. (2021). A single human-relevant Fast food meal rapidly reorganizes metabolomic and transcriptomic signatures in a gut microbiota-dependent manner. *Immunometabolism* 3 (4), e210029. doi:10.20900/immunometab20210029

Pathak, P., Helsley, R. N., Brown, A. L., Buffa, J. A., Choucair, I., Nemet, I., et al. (2020). Small molecule inhibition of gut microbial choline trimethylamine lyase activity alters host cholesterol and bile acid metabolism. *Am. J. Physiol. Heart Circ. Physiol.* 318 (6), H1474–H1486. doi:10.1152/ajpheart.00584.2019

Pedersen, T. L., and Newman, J. W. (2018). "Clinical metabolomics," in *Methods molec. Biol.* Editor M. Giera (New York, NY, USA: Humana Press), 1730, 175–212.

Ran, F. A., Hsu, P. D., Wright, J., Agarwala, V., Scott, D. A., and Zhang, F. (2013). Genome engineering using the CRISPR-Cas9 system. *Nat. Protoc.* 8, 2281–2308. doi:10.1038/nprot.2013.143

Sandhu, J., Li, S., Fairall, L., Pfisterer, S. G., Gurnett, J. E., Xiao, X., et al. (2018). Aster proteins facilitate nonvesicular plasma membrane to ER cholesterol transport in mammalian cells. *Cell* 175 (2), 514–529. doi:10.1016/j.cell.2018.08.033

Trinh, M. N., Brown, M. S., Seemann, J., Vale, G., McDonald, J. G., Goldstein, J. L., et al. (2022). Interplay between Asters/GRAMD1s and phosphatidylserine in intermembrane transport of LDL cholesterol. *Proc. Natl. Acad. Sci. U.S.A.* 119 (2), e2120411119. doi:10.1073/pnas.2120411119

Wang, X., Cai, B., Yang, X., Sonubi, O. O., Zheng, Z., Ramakrishnan, R., et al. (2020). Cholesterol stabilizes TAZ in hepatocytes to promote experimental non-alcoholic steatohepatitis. *Cell Metab.* 31 (5), 969–986. doi:10.1016/j.cmet.2020.03.010

Xiao, X., Kennelly, J. P., Ferrari, A., Clifford, B. L., Whang, E., Gao, Y., et al. (2023). Hepatic nonvesicular cholesterol transport is critical for systemic lipid homeostasis. *Nat. Metab.* 5 (1), 165–181. doi:10.1038/s42255-022-00722-6

Xiao, X., Kim, Y., Romartinez-Alonso, B., Sirvydis, K., Ory, D. S., Schwabe, J. W. R., et al. (2021). Selective Aster inhibitors distinguish vesicular and nonvesicular sterol transport mechanisms. *Proc. Natl. Acad. Sci. U.S.A.* 118 (2), e2024149118. doi:10.1073/pnas.2024149118

Zhang, J., Andersen, J. P., Sun, H., Liu, X., Sonenberg, N., Nie, J., et al. (2020). Aster-C coordinates with COP I vesicles to regulate lysosomal trafficking and activation of mTORC1. *EMBO Rep.* 21 (9), e49898. doi:10.15252/embr.201949898

Zhou, Y., and Rui, L. (2010). Major urinary protein regulation of chemical communication and nutrient metabolism. *Vitam. Horm.* 83, 151–163. doi:10.1016/S0083-6729(10)83006-7

frontiers | Frontiers in Endocrinology

TYPE Review
PUBLISHED 10 May 2024
DOI 10.3389/fendo.2024.1393253

OPEN ACCESS

EDITED BY
Lin Zhu,
Vanderbilt University Medical Center,
United States

REVIEWED BY
Carolina Dalmasso,
University of Kentucky, United States
Kazuki Harada,
The University of Tokyo, Japan

*CORRESPONDENCE
Yue Rensong
songrenyue@cdutcm.edu.cn

†These authors have contributed equally to this work and share first authorship

RECEIVED 28 February 2024
ACCEPTED 25 April 2024
PUBLISHED 10 May 2024

CITATION
Li Z, Jiang Y, Long C, Peng X, Tao J, Pu Y and Yue R (2024) Bridging metabolic syndrome and cognitive dysfunction: role of astrocytes. *Front. Endocrinol.* 15:1393253. doi: 10.3389/fendo.2024.1393253

Bridging metabolic syndrome and cognitive dysfunction: role of astrocytes

Zihan Li[1,2†], Ya-yi Jiang[1,2†], Caiyi Long[1,2], Xi Peng[1,2], Jiajing Tao[1,2], Yueheng Pu[1,2] and Rensong Yue[1,2*]

[1]Department of Endocrinology, Hospital of Chengdu University of Traditional Chinese Medicine, Chengdu, China, [2]Clinical Medical School, Chengdu University of Traditional Chinese Medicine, Chengdu, China

Metabolic syndrome (MetS) and cognitive dysfunction pose significant challenges to global health and the economy. Systemic inflammation, endocrine disruption, and autoregulatory impairment drive neurodegeneration and microcirculatory damage in MetS. Due to their unique anatomy and function, astrocytes sense and integrate multiple metabolic signals, including peripheral endocrine hormones and nutrients. Astrocytes and synapses engage in a complex dialogue of energetic and immunological interactions. Astrocytes act as a bridge between MetS and cognitive dysfunction, undergoing diverse activation in response to metabolic dysfunction. This article summarizes the alterations in astrocyte phenotypic characteristics across multiple pathological factors in MetS. It also discusses the clinical value of astrocytes as a critical pathologic diagnostic marker and potential therapeutic target for MetS-associated cognitive dysfunction.

KEYWORDS

metabolic syndrome, cognitive dysfunction, astrocytes, immunometabolism, neurodegeneration

1 Introduction

MetS is a syndrome of multiple metabolic disorders that seriously jeopardize cardiovascular health. MetS leads to myocardial metabolic, hemodynamic, and microcirculatory dysfunction by activating the sympathetic nervous system, the renin-angiotensin system, and pro-inflammatory adipokines (1, 2). Combining several recognized diagnostic criteria, the main diagnostic features of MetS include abdominal obesity, dyslipidemia, hyperglycemia, insulin resistance (IR), and elevated blood pressure (3–10). The multivessel risk factors of MetS jeopardize the cerebral vasculature and reduce cerebral perfusion while accelerating neuronal cell senescence and degeneration (11, 12). Evidence from diverse studies supports the association of MetS with vascular dementia and Alzheimer's disease dementia (13). Various components of MetS have been found in cross-sectional and longitudinal studies to cause decreases in learning memory, attention,

visuospatial and executive functions, and processing speed (14, 15). A 15-year follow-up analysis of 176,000 non-demented participants found that MetS led to a 12% increased risk of developing all-cause dementia (16).

Astrocytes are the primary glial cells and are essential for maintaining brain homeostasis. Astrocytes endfeet envelop neurons and the cerebral vasculature, linking cerebrovascular nutrient uptake transport to high oxygen- and sugar-dependent synaptic activity. Astrocytes shape synapses and their surrounding microenvironment, regulate cerebrovascular structure and perfusion, and influence neuroinflammation. Astrocytes become "reactive astrocytes" when stimulated by metabolic changes (e.g., glucose and lipid metabolism) (17). Reactive astrocytes are traditionally thought to have a double-edged role in cytotoxicity and neuroprotection (18). Cytotoxicity of astrocytes is defined as driving pathologic progression through the release of toxic factors such as inflammatory cytokines. Neuroprotective effects are usually heavy in ischemic injury, and reactive astrocytes promote vascular repair and remodeling. Escartin et al. (19) have pointed out the shortcomings of this binary division in recent years based on transcriptomic studies, suggesting that heterogeneity of reactive astrocytes should be emphasized.

Chronic low-level inflammatory states, peripherally and centrally, and systemic IR, are critical in the MetS, leading to cognitive dysfunction (20). A more detailed understanding of the underlying molecular mechanisms of MetS-related cognitive dysfunction will facilitate the development of new approaches to prevention and treatment. MetS-related nutritional and hormonal changes can significantly alter blood metabolic signaling, thereby regulating astrocytes' responsive activation and specific genomic programs and functional transitions (17). Astrocyte activation is often considered an adaptive mechanism for metabolic adaptation and relief of neuronal stress, but it can also have multifaceted effects on cognitive function and metabolic homeostasis (21). However, persistent astrocyte proliferation and neurotoxic phenotype are essential causes of neuroinflammatory spread and chronicity (18, 22). Identifying the activation state of these astrocytes and the associated molecular mechanisms may provide new targets for treating MetS-related cognitive dysfunction (23).

In this review, we overview the multifaceted role of astrocytes in MetS-related cognitive impairment. Recent discoveries on astrocyte subpopulations and their regulation of cognitive and metabolic functions are highlighted.

2 MetS and cognitive dysfunction

Neuroimaging changes associated with MetS have been observed in clinical studies, including reduced gray matter volume, cerebral white matter microstructural changes, cerebral atrophy, and lacunar cerebral infarcts (24, 25). Reduced resting-state functional connectivity between MetS-related vascular risk factors and multiple higher-order cognitive function-related neural networks (26). MetS leads to cerebrovascular injury and neurodegenerative lesions through complex mechanisms that ultimately produce altered cognitive function (27) (Figure 1).

MetS components such as low-density lipoprotein (LDL), high-density lipoprotein (HDL), hypertension, and advanced glycation end products (AGEs) accumulation all contribute to cerebral atherosclerosis, accelerating white matter damage, lacunar microinfarcts, and microhemorrhages (28, 29). The cerebral circulatory system has the capacity for adaptive regulation to

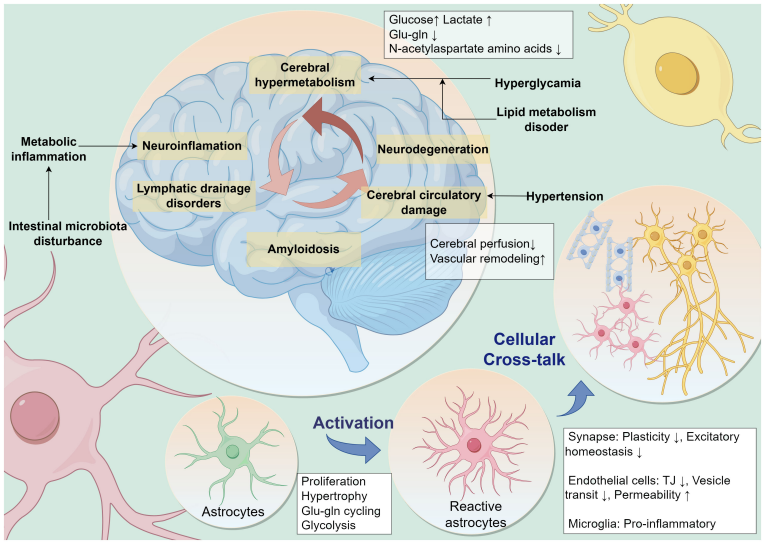

FIGURE 1
MetS leads to cognitive dysfunction through multiple pathologic factors. Multiple peripheral metabolic disorders in MetS, such as persistent hyperglycemic states, disorders of lipid metabolism, hypertension, metabolic inflammation, and disturbances in intestinal microbiota, are contributing to neurocognitive decline. Neuropathology in the brain leads to a vicious cycle of cognitive decline caused by neuroinflammation, cerebral microcirculatory dysfunction, impaired glial lymphatic system drainage, and accumulation of pathologic proteins. Astrocytes are potentially central to this vicious cycle. Metabolic stress pressure drives reactive activation of astrocytes and influences their interactive dialog with surrounding cells. Glu-gln, glutamate-glutamine; TJ, Tight Junction.

maintain cerebral perfusion in fluctuating arterial blood pressure. MetS contributes to decreased cerebral microvascular density and blood flow, impairing cerebrovascular responsive autoregulation and blood flow reserve functions (30, 31). Excessive or unstable arterial blood pressure levels reduce cerebrovascular autoregulation, leading to cerebral hypoperfusion and neurodegenerative pathologies (32) and amyloid-β (Aβ) protein deposition by mechanical stretch (33). Stimulation by high blood pressure arterial wall shear stress increases vascular smooth muscle cell hypertrophy and proliferation, leading to vascular remodeling (34, 35). High-fat diet(HFD) rats were more sensitive to ischemia-reperfusion injury. Compared to normal diet rats, they exhibited more significant decreases in cerebral blood flow (CBF) and elevated levels of oxidative stress (36).

Oxidative stress and mitochondrial malfunction in MetS also promote neuroinflammation and neurodegeneration (37). High levels of circulating inflammatory markers are a common feature of MetS and cognitive dysfunction (38, 39). Ectopic fat accumulation, fatty inflammation (40), and disruption of intestinal flora (41) during the MetS disease process lead to a chronic low-grade inflammatory state. High levels of circulating pro-inflammatory cytokines in MetS disrupt and cross the blood-brain barrier (BBB) into the brain, thereby activating astrocytes and microglia to trigger a neuroinflammatory response, leading to a critical mechanism of MetS-related cognitive dysfunction (42, 43). Peripheral inflammation leads to neuroinflammation and oxidative stress, impairing energy supply to synaptic mitochondria (44).

3 Neurocognitive perspectives of astrocytes

Astrocytes serve as a communication bridge between the central and peripheral nervous systems. They are essential components of the neurovascular unit and communicate extensively with neurons, endothelial cells, and glia via dendritic structures (45). The complex and diverse dynamic network of astrocytes is the anatomical basis for their maintenance of metabolic and immune homeostasis of the brain. The astrocyte network integrates nutrient metabolic signals and interacts with hypothalamic functional neurons to exert central feedback regulation of appetite regulation, glucose sensing, and other systemic metabolism (46–48).

3.1 Astrocyte participate in neurosynaptic activity

Synaptic plasticity and presynaptic vesicle release in neurons are the mechanisms underlying working memory. Astrocytes are a new target for improving cognitive function, forming glial isolates that wrap 50-60% of brain synapses and regulate synaptic plasticity through glycolytic energy supply and release of multiple neuroactive substances (e.g., glutamate, ATP, adenosine, and D-serine) (49). Astrocytes regulate the neurosynaptic microenvironment with their unique glial-isolated structure and immunometabolic properties (50, 51). Perisynaptic astrocyte processes (PAPs) constitute the glial segregation of the synaptic gap. Astrocytes regulate glutamate concentration through glutamate transporter subtype 1(GLT-1) and deliver lactate through monocarboxylate transporters1 and 4 (MCT1, MCT4). Aging and atrophy of PAPs are accompanied by a decline in glutamate clearance and a decrease in Ca^{2+} events, and excess glutamic acid spillage in the synaptic gap will activate N-methyl-D-aspartic acid (NMDA) receptors to reduce the amplitude of the neuron's long-term potentiation (LTP) (52). Furthermore, astrocytes control synaptic plasticity by producing neurotrophic factors, releasing and clearing neurotransmitters, and regulating ion levels in the extracellular environment (53).

In addition to regulating synapses, astrocytes regulate the electrical activity of neuronal networks by releasing gliotransmitters such as ATP, glutamate, and Ca^{2+} wave oscillations (54). Computational model studies of working memory suggest that astrocytes can store traces of neuronal activation in information processing (55). In contrast, memory extraction depends on astrocytes' modulation of spiking neuron network connections (56). Astrocytes influence memory performance through states of conscious vigilance and basal arousal. Sustained neuronal firing in the hippocampus induces astrocytic γ-aminobutyric acid G protein-coupled receptor signals that control the oscillatory activity of the θ and γ oscillations of the hippocampal neuronal network (57).

Astrocytes coordinate interneuronal network projections between the hippocampus and cortex, thus participating in memory consolidation and storage. Astrocytes modulate communication between hippocampal CA1 and cingulate cortex to promote memory consolidation and retention (58). Dysfunctional cell division in astrocytes impairs hippocampal-prefrontal theta synchronization (59).

3.2 Astrocyte maintain brain energy metabolism

The neural axons and telopods of astrocytes wrap around the cerebral vascular system to detect nutrients and metabolic hormones in the arterial blood that enters the brain (60). Astrocytes form an intercellular communication network with each other through connexins, bridging the intravascular nutrient supply with the energy demand of neuronal activity. The astrocyte network enables the propagation and sharing of small molecule nutrient metabolic signals at the cellular network level (61). Astrocytes are the primary cells for glycogen storage and glycolysis in the brain. They shape the fundamental pattern of brain energy metabolism by coupling with neuronal oxidative phosphorylation (62, 63). Astrocytes can bridge the transient energy demands of neurosynaptic activity with the supply of circulating fuel (64).

Astrocytes store lipid droplets (LDs) by taking up excess fatty acids (FAs) from neurons via rich acid transport protein and lipid transport protein, making them critical sites for fatty acid oxidation.

Astrocytes take up FAs produced by neuronal metabolism and help highly active neurons relieve lipid oxidative stress through astrocyte consumption of LDs for ATP production via NMDA receptor-mediated mitochondrial β-oxidation (65).

Recent studies have shown that astrocyte function is equally dependent on mitochondria and oxidative phosphorylation (66). Mitochondrial disorders in astrocytes affect brain oxidative phosphorylation metabolism and contribute to forming metabolic stresses such as reactive oxygen species (ROS) (67). Astrocytes can exert neuroprotective effects by delivering mitochondria to neurons. Peroxisome proliferator-activated receptor gamma coactivator-1 alpha (PGC-1α) and mGluR5(metabotropic glutamate receptor 5) modulate the mitochondrial network of astrocyte cells and produce positive Ca^{2+} signaling ion conductance to synapses (68). Restoring mitochondrial biogenesis in astrocytes may be a therapeutic target for neuropsychiatric disorders with impaired synapse formation.

3.3 Astrocyte control of the cerebrovasculature

The endfoot of astrocytes envelop the endothelium of the cerebral microcirculation. Astrocytes rapidly regulate CBF to meet neurocognitive energy demands, ensuring nutrient and oxygen delivery (69). Arachidonic acid, prostaglandin E2, and nitric oxide produced by astrocytes connect directly with small smooth muscle cells in the arteries (70). Additionally, astrocytes monitor cerebral perfusion pressure and regulate blood flow by modulating the diameter of cerebral arteries through their unique anatomical location and pressure-sensitive membrane structures (71). The end-foot of astrocytes abutting endothelial cells expresses the transient potential receptor vanilloid 4 (TRPV4) and is influenced by transmural pressure in penetrating arterioles and blood flow levels (72).

The endfoot of astrocytes with tight junction (TJ) proteins are the basic structures that comprise the BBB (73). Ablating astrocytes increases BBB permeability and impairs repair (74). Astrocytes regulate the TJ structure through the vascular permeability factor, matrix metalloproteinase (75). Astrocyte endfoot around blood vessels are tightly connected by connexins 30 (Cx30) and connexins 43 (Cx43), which allow ion exchange in the peri-endothelial astrocyte network. Deletion of these connexins weakens the BBB, leading to its opening under increased hydrostatic vascular pressure (76). Physiologically, astrocytes Cx30 and Cx43 are involved in memory formation (77). Astrocyte Cx43 controls the rate of synaptic vesicle release to regulate presynaptic function, controls glutamate levels and allows glutamine release to maintain synaptic transmission (78). Astrocyte-specific Cx30 and Cx43 double knockouts lead to widespread activation of astrocytes and microglia, significant suppression of neuronal excitability, excitatory synaptic transmission in hippocampal CA1 region, and decrease of spatial learning and memory (79). In addition, astrocytes secrete a variety of vasoactive substances, among which angiopoietin-1 (ANG-1), sonic hedgehog (SHH), and insulin-like growth factor-1 (IGF-1) protect the BBB. In contrast, vascular endothelial growth factors (VEGF), matrix metalloproteinases (MMP), nitric oxide, glutamate, and endothelin-1 lead to structural damage of the BBB (80). Damage to astrocyte structures reduces BBB permeability, thus allowing pathogens and toxins to enter the central nervous system (81). Peripheral inflammatory factor across BBB and drives the pro-inflammatory phenotype of glial cells. This is a crucial pathway by which systemic inflammation triggers neuroinflammation (82).

4 MetS alters astrocyte phenotype

Astrocytes undergo adaptive activation both anatomically morphologically and functionally as they respond to and maintain homeostasis in the brain's internal environment. Both clinical and animal studies have found that disorders of glucolipid metabolism and hypertension can induce reactive activation of brain astrocytes and overexpression of glial fibrillary acidic protein (GFAP) (83). Astrocytes, as reactive cells, are regulated by complex factors of circulating origin. Different types of stimuli induce specific reactive changes. In addition, sex was an essential variable in the analysis of MetS and cognitive dysfunction, and there was sex- and age-related heterogeneity in the altered responsiveness of astrocytes (84). The prevalence of MetS and related complications is higher in men than in women at ages younger than 50 years. The risk of MetS and associated complications in women exceeds that of men, with a decline in estrogen levels after menopause (85, 86). Recent reports suggest that astrocyte numbers, differentiation, and function differ between the sexes. Sex differences in reactive astrocytes are responsible for the emergence of sex differences in neuroendocrine regulation and cognitive function. Astrocytes isolated from female rats were more resistant to cell death induced by hypoxia, palmitic acid (PA), and lipopolysaccharide (LPS) than male astrocytes (87–89).

4.1 Hypertension

Increased numbers and morphological hypertrophy of reactive astrocytes in the brain have been observed in several animal models of hypertension (Table 1). 26-week-old SHR showed increased numbers and areas of immunoreactive positive astrocytes in the prefrontal cortex, occipital cortex and significantly higher numbers of GFAP immunoreactive positive astrocytes in the hippocampal region, compared to the same-week-old WKY rats (94). In the chronic hypertension model induced by 8 weeks of AngII infusion, a linear positive correlation between astrocyte morphology and elevated arterial blood pressure proliferated in cerebral white matter (95). Astrocyte endfoot are in contact with cerebral blood vessels, directly sensing circulating hemodynamic changes and releasing vasoactive substances to modulate slight arterial tone to maintain CBF independent of blood pressure fluctuations (96). Astrocyte reactive activation accompanied by transient potential receptor vanilloid 4 (TRPV4) activation was observed in the hippocampus of an AngII 28-day injection-induced mouse model of chronic hypertension. In this study, astrocyte TRPV4 mediated an increase in spontaneous Ca^{2+} events within microdomains, which enhanced parenchymal arteriole tone and decreased cognitive function (90).

TABLE 1 Effects of hypertension on astrocyte pathology and cognitive functions.

Experimental animal			Brain region	Astrocyte Phenotypes		Potential/associated impacts		Molecular mechanisms	Reference
Animal	Model	Control		Activation	Dysfunctions	Neuropathology	Behavioral		
C57BL6 (male), 8 weeks/ NM	Ang II for 14 or 28 days (pump in,600 ng/kg/min)	NM	Cortex	GFAP↑ Number of cells↑	Ca2+ activity↑	PA tone↑ Myogenic responses↑	NM	TRPV4 channel	Ramiro et al., 2019 (90)
SD rats (male), 8 weeks/ 200-230 g	Partial occlusion of left renal artery	Renal artery was only exposed but not occluded	Cortex Hippocampus	GFAP↑	TRAF6↑ IκB-α↓ pP38↓ pERK1/2↓	NM	NM	CD40L	Ali et al., 2017 (91)
SHRs (male) 32 and 64 weeks/NM		WKY rats (male) 32 and 64 weeks/NM	Hippocampus	Cell body↑ Branches↑	PPARγ↓	Bax↑ Bcl-2↑ Caspase-3↑ INOS↓ Gp47phox↓	NM	NM	Yali et al., 2016 (92)
SD rats (male), 8 weeks/ NM	Partial occlusion of left renal artery	Renal artery exposed	Cortex Hippocampus	GFAP↑ Processes↑ Cell body↑	NM	NM	NM	NM	Shahnawaz Ali et al., 2018 (93)

Bax, Bcl-2-associated X protein; Bcl-2, B-cell lymphoma 2; CD40L, CD40 Ligand; GFAP, Glial fibrillary acidic protein; pERK, Phospho extracellular regulated protein kinases; SD rat, Sprague dawley rat; SHR, Spontaneously hypertensive rats; TRAF6, TNF receptor associated factor; TRPV4, Transient receptor potential vanilloid 4; PPARγ, Peroxisome proliferator-activated receptor γ; iNOS, Inducible nitric oxide synthase; NM, Not mentioned.
↑, Increase; ↓, Decrease.

Studies in hypertensive humans and hypertensive rat models have shown that an overactive brain renin-angiotensin system (RAS), which leads to oxidative stress and neuroinflammation in several brain regions, including the brainstem cardiovascular centers and the hippocampus (97, 98). The overactive brain RAS in hypertension also contributes to cognitive dysfunction and exacerbates hypertension through sympathetic excitation. In several experimental and genetic models of hypertension, including spontaneously hypertensive rats (SHR) (99, 100) and desoxycorticosterone acetate salt hypertensive rats (101), hyperactivity of the central RAS was observed, especially increased levels of angiotensin II (AngII), angiotensin III (AngIII) and angiotensin II receptor type 1 (AT1R). *In vitro* studies have shown the expression of AT1R and AT2R on human astrocytoma cell lines (102)and primary cerebral cortex astrocytes (103). Therefore, it has been suggested that astrocytes may play a role in neuroinflammation and oxidative stress caused by AngII and AngIII in the brain RAS (102). Studies conducted on primary astrocytes isolated from SHR have shown that AngII causes the secretion of IL-6 from astrocytes through the activation of NF-κB/ROS and overexpressing cyclooxygenase 2 via astrocyte AT1R (104, 105). In primary rat astrocytes derived from SD rats, AngIII targets AT1R to activate extracellular regulated protein kinases (ERK)1/2 MAP kinases and c-Jun N-terminal kinase (JNK) phosphorylation to promote astrocyte proliferation (106).

4.2 Lipid metabolism disorders

Astrocyte activation and proliferation in the hippocampus and hypothalamus have been observed in HFD-induced obese rat models (Table 2) (114–117).

HFD-induced obesity also affects astrocyte lipid oxidation and mitochondrial metabolism. Fatty acid β-oxidation (FAO) in the brain occurs mainly in astrocytes. Astrocytes store overloaded free fatty acids as LDs, which are used via FAO to energize neurons and protect them from lipotoxic damage. Obesity leads to the accumulation of astrocyte misfolded proteins, induced endoplasmic reticulum stress, and thus crosstalk with neurodegenerative (21). Obesity decreases fatty acid oxidation in hypothalamic astrocytes, leading to disturbed mitochondrial dynamics (118). In the hippocampus of mice raised on a HFD for 1 month, astrocytes' lipid and cholesterol content was elevated, accompanied by an increase in the number of secondary branches and lobules of neural protrusions (119). *In vitro* studies have found that saturated and unsaturated fatty acids have opposite regulatory effects on astrocyte lipoprotein lipase (LPL). TGs and palmitic acid decrease LPL expression and oleic acid elevate LPL. HFD-induced elevation of LPL in hypothalamic astrocytes of obese rats increases the accumulation of LDs. It impairs glycolytic metabolism, impairing glucose tolerance, increases food intake, and aggravates obesity (120).

In addition, obesity and pathologic fat accumulation lead to decreased function of astrocyte-neuron crosstalk, in which high serum levels of leptin inhibit astrocyte excitatory amino acid transporter protein (EAAT) expression and promote sympathetic overactivation (121). Obesity impairs glutamate clearance from the synaptic gap by astrocytes and attenuates the endogenous cannabinoid pathway and the synaptic plasticity it mediates in vertebral neurons in the orbitofrontal cortex (111). Astrocytes present a compensatory neuroprotective effect in the early stages of lipid metabolism disorders and are progressively bettered by chronic stressful pressures. It was found that 8 weeks of HFD induced astrocyte proliferation and limited neuronal damage by releasing heat shock protein 70 (HSP70) and ciliary neurotrophic

TABLE 2 Effects of hyperlipidemia and obesity on astrocyte pathology and cognitive functions.

Experimental animal			Brain region	Astrocyte Phenotypes		Potential/associated impacts		Molecular mechanisms	Reference
Animal	Model	Control		Activation	Dysfunctions	Neuropathology	Behavioral		
C57BL/6N mice (male),8 weeks/NM	HFD for 12 weeks	CD for 12 weeks	VAc	NM	GLAST↓ GLT-1↓	Glutamatergic inputs↑	Depression (SPT, FST)	NM	Tsai et al., 2022 (107)
C57BL/6 mice (male),7-8 weeks/20 g	HFD for 1 month	CD for 1 month	Hippocampus	GFAP↑	NM	BDNF↓ NLRP3↑ ASC↑ IL-1β↑ TNF-α↑	Depression and anxiety (OFT, EPM, SPT, FST)	NM	Li et al., 2022 (108)
C57BL/6 mice (male), NM/NM	HFD for 8 weeks + CSDS	CD for 8 weeks + CSDS	mPFC	Spreading area↑	D-serine↑, Glutamate↑	sIPSCs↓ sEPSCs↓	Depression (SPT, TST)	JNK–STAT3	Yu et al., 2022 (109)
C57BL/6J mice (male),6 weeks,NM	HFD for 12 weeks	LFD for 12 weeks		GFAP↑	AQP4↓	GS functions↓ CBF↓ Neuropathological alterations	Cognitive dysfunction (MWM)	NM	Zhan et al., 2024 (110)
Long-Evans rats (male), NM/NM	Cafeteria diet for 40 days	CD for 40 days	OFC	GFAP↑ Astrocyte hypertrophy↑	GLT-1 function↓	LTD of GABA transmission↓	NM	NM	Lau et al., 2021 (111)
SD rats (male), NM/250-270g	HFFD for 7 days	CD for 7 days	Hippocampus	GFAP+ cell number↑ GFAP area↑	NM	NM	NM	NM	Erika et al, 2014 (112)
WKY rat (male),6 weeks/NM	HFrD for 12 weeks	CD for 12 weeks	Hippocampus	GFAP↑	NM	NM	NM	NM	Liu et al., 2018 (113)

AQP4, Aquaporin 4; BDNF, Brain-derived neurotrophic factor; CBF, Cerebral blood flow; CD, Control diet; CSDS, Chronic social defeat stress; EPM, Elevated plus maze; FST, Forced swim test; GFAP, Glial fibrillary acidic protein; GLAST, Glutamate aspartate transporter; GLT-1, Glutamate transporter-1; GS, Glutamine synthetase; HFD, High-fat diet; HFFD, High-fat and High-fructose diet; HFrD, High-fructose diet; IL-1β, Interleukin-1 beta; JNK, c-Jun N-terminal kinase; STAT3, Signal transducer and activator of transcription 3; LTD, Long-term depression; LFD, Low-fat diet; MWM, Morris water maze; MyD88, Myeloid differentiation primary response 88; NLRP3, NOD-like receptor thermal protein domain associated protein; NM, Not mentioned; OFT, Open field test; POMC, Pro-opiomelanocortin; SPT, Sucrose preference test; TST, Tail suspension test; TNF-α, Tumor necrosis factor alpha; VAc, Ventral hippocampus; sEPSCs, Spontaneous excitatory postsynaptic currents; sIPSCs, Spontaneous inhibitory postsynaptic currents.
↑, Increase; ↓, Decrease.

factor (CNTF). In contrast, the compensatory neuroprotective effect of astrocytes was depleted after 20 consecutive weeks of HFD (122).

4.3 Glycemic derangement

High blood glucose levels in both *in vivo* and *ex vivo* studies resulted in reactive activation of astrocytes accompanied by changes in metabolic processes (Table 3). The astrocyte glycolytic effect is two-sided, with increased glycolytic flux supplying neurons with energy and antioxidants (133), while glycolysis also provides energetic support for inflammatory responses (134). A comprehensive review of astrocyte glycolysis in cellular metabolic immunity is lacking, but some studies have suggested that it undergoes the same progression from compensation to decompensation as immune cells (135). Multiple *in vitro* studies have found increased glycogen content and glycolytic activity in astrocytes chronically exposed to high glucose (136). In a ^{1}H NMR-based metabonomic approach study, an increase in glucose uptake, glycolytic activity lactate release, and downregulation of TCA cycling activity were found in astrocytes after 72 hours of high-glucose exposure (137). High glucose promotes glucose uptake and glycogen storage in primary astrocytes but reduces maximal respiratory and glycolytic reserve capacity (138). It is suggested that high glucose leads to an increase in astrocyte glucose metabolic flux, but the efficiency of cellular energy utilization is reduced, making it more vulnerable to stressful pressures.

Astrocyte metabolic plasticity has a double-edged role, feeding the inflammatory immune response process and acting as a buffer against metabolic stress. The astrocyte pentose phosphate pathway and glutathione levels increase with blood glucose, reduce ROS production, and protect neurons from oxidative stress damage (139). *In vitro* metabolomics studies have found that astrocytes produce and transport more lactate in high-sugar environments, which may work to enhance astrocyte-neuron lactate shuttling (137).

High glucose leads to increased secretion of multiple pro-inflammatory factors by astrocytes, leading to neuroinflammation (140). High glucose increases the expression and secretion of pro-inflammatory cytokines IL-6 and IL-8 in human primary astrocytes and U-118MG astrocytoma cells via STAT-3 (141). Hyperglycemia induces enlargement of astrocytes in the hippocampus and is linked to peripheral recruitment of leukocytes to the cerebrovascular system (142). High glucose exacerbates neuroinflammation via ROS/mitogen-activated protein kinase (MAPK)/NF-κB, ERK, and JNK pathways by upregulating matrix metalloproteinase-9 expression in rat brain astrocytes (143, 144). The toll-like receptor (TLR) of

TABLE 3 Effects of hyperglycemia on astrocyte pathology and cognitive functions.

Experimental animal			Brain region	Astrocyte Phenotypes		Potential/associated impacts		Molecular mechanisms	Reference
Animal	Model	Control		Activation	Dysfunctions	Neuropathology	Behavioral		
C57BL/6J mice (male), 8 weeks/NM	HFFD for 9 weeks	CD for 9 weeks	Hypothalamic	GFAP↑ Vimentin ↑	HMG20A↑	NM	NM	HMG20A	Petra I et al., 2021 (123)
C57BL/6N mice (male), 8 weeks/NM	HFD for 4 weeks (from 20 to 24 weeks old)	CD for 4 weeks	Ventral hippocampal	Process lengths, branch points, intersections↓ GFAP↑	NM	NM	Depression (OFT, EPM) Cognitive dysfunction (ORT)-	NM	Ying-Yiu et al., 2021 (124)
Wistar rats (male), 6 weeks/NM	HFD for 50 days + STZ (35mg/kg bw i.p)	CD for 50 days+ sodium citrate buffer i.p	Hippocampus	GFAP↑	NM	NM	NM	NM	Velia et al., 2022 (125)
C57Bl/6J mice (male), 4 weeks/NM	HFD for 17 weeks	CD for 17 weeks	Hippocampus CA1 DG	GFAP↑	NM	NM	NM	NM	Saieva et al., 2022 (126)
			POCTX	GFAP↑					
			FCTX	GFAP-					
SD rats (male), 8 weeks/200-230 g	HFD for 16 weeks + STZ (40mg/kg on 5 consecutive days i.p)	CD for 16 weeks	ARC of hypothalamus	GFAP↑	PDK2 p-PDH↑	Tnf-α↑ Il-1β↑ Il-6↑ NPY/AgRP neurons↑	Feeding behavior dysregulation	PDK2-lactic acid axis	Rahman et al., 2020 (127)
C57BL/6 mice (male), 6 weeks/NM	MLDS STZ (40mg/kg on 5 consecutive days i.p)	Sodium citrate buffer i.p	Hippocampus	GFAP↑ Hypertrophic morphology	NM	Tnf-α↑ Il-6↑	Cognitive dysfunction (NOR, Y maze)	LCN2 ↑	Anup et al., 2019 (128)
Obese Zucker rats(male), 12 weeks/NM		LZRs, 12 weeks/NM	Hippocampus	GFAP↑	NM	NM	NM	NM	Daniele et al., 2013 (129)
KK-Ay mice(male), 5 months/NM +HFD for 3 months		C57BL/6J mice male), 5 months/NM + CD for 3 months	Hippocampal	Cell body↓ Branches↓	vGLUT1↑ GLUT1↓ EAAT2- GDNF↓	IL-1β↑ TNF-α↑ BDNF↓	Cognitive dysfunction (MWM)	NM	Si et al., 2020 (130)
db/db(male), 15 weeks/NM		C57BLKS/J (male), 15 weeks/NM	Hippocampal	GFAP↑	Glu-gln cycle↑ GAD↑ GLS↑ GS↑ Lactate↑ Taurine↑ Pyruvate↓ Succinate↓ Citrate↓	TUNEL↑	Cognitive dysfunction (MWM)	NM	Yongquan et al., 2016 (131)
db/db(male), 8 weeks/NM		C57BLKS/J (male), 8 weeks/NM	Hippocampal	GFAP↑	C3↑ S100A10↓	IL-6↑ IL-1β↑ TNF-α↑ IL-18↑ TfR1↑ DMT1↑ FPN1↓	Cognitive dysfunction (MWM)	NM	Ji-Ren et al., 2023 (132)

(Continued)

TABLE 3 Continued

Experimental animal			Brain region	Astrocyte Phenotypes		Potential/associated impacts		Molecular mechanisms	Reference
Animal	Model	Control		Activation	Dysfunctions	Neuropathology	Behavioral		
						MDA↑ SOD↓ GSH↓ ROS↑			

AgRP, Agouti-related peptide; ARC, Arcuate nucleus; BDNF, Brain-derived neurotrophic factor; CD, Control diet; C3, Complement component 3; DMT1, Divalent metal transporter 1; db/db, Diabetic (leptin receptor deficient) mice; EPM, Elevated plus maze; EAAT2, Excitatory amino acid transporter 2; FCTX, Frontal cortex; FPN1, Ferroportin 1; GAD, Glutamate decarboxylase; GDNF, Glial cell-derived Neurotrophic Factor; GFAP, Glial fibrillary acidic protein; GLS, Glutaminase; GLUT1, Glucose transporter 1; GSH, Glutathione; HFD, High-fat diet; HFFD, High-fat and high-fructose diet; HMG20A, High Mobility Group 20A; Il-1β, Interleukin 1 Beta; IL-6, Interleukin 6; IL-18, Interleukin 18; LCN2, Lipocalin-2; MDA, Malondialdehyde; MWM, Morris water maze; NPY, Neuropeptide Y; NM, Not mentioned; NOR, Novel object recognition test; OFT, Open field test; ORT, Object recognition test; PDK2, Pyruvate dehydrogenase kinase 2; POCTX, Posterior cortex; p-PDH, Phosphorylated pyruvate dehydrogenase; ROS, Reactive oxygen species; S100A, S100 protein; SOD, Superoxide dismutase; STZ, Streptozotocin; TfR1, Transferrin receptor 1; Tnf-α, Tumor necrosis factor alpha; TUNEL, Terminal deoxynucleotidyl transferase dUTP nick end labeling; vGLUT1, Vesicular glutamate transporter 1; Y maze, Y-shaped maze task.
↑, Increase; ↓, Decrease.

astrocytes serves as an essential target of the innate immune system, and high glucose promotes neuroinflammation and altered cellular metabolism via the TLR/MAPK/PPARs pathway (145).

Astrocyte responsiveness to high glucose affects microcirculatory endothelial barrier structure. Hyperglycemia induces increased secretion of VEGF protein in astrocytes, impairment of gap junctional Cx43 and Cx30 proteins, and reduced transendothelial cell electrical resistance (TEER), which are critical factors for reduced BBB permeability (146, 147). Sustained hyperglycemia induces the non-enzymatic glycosylation of various proteins and the resulting formation of advanced glycation endproducts (AGEs), which mediate the development of diabetic complications by targeting the receptor of advanced glycation endproducts (RAGE). Primary astrocytes from mice cultured with high glucose showed increased expression of immune complement C3 and decreased synaptic number, suggesting that high glucose promotes synaptic phagocytosis of the complement pathway in astrocytes. In this study, the RAGE-p38MAPK-NF-κB pathway was a vital upstream of the synaptic phagocytosis promoted by high glucose in astrocytes (148).

5 MetS leading to cognitivedysfunction via astrocyte pathology

The hippocampus is a major brain region involved in memory functions, and its synaptic plasticity activities of vesicular and ionic channel activity depend on continuous energy support and are susceptible to nutrient metabolism (149). The release of gliotransmitters in astrocytes modulates neural theta oscillations between the dorsal hippocampus and prefrontal cortex, which are involved in memory formation and storage (59). Morphologic, immunologic, and metabolic alterations in astrocytes mediate the contribution of multiple factors to the development of cognitive dysfunction in MetS (Figure 2).

5.1 Astrocyte morphologic alteration

In MetS, astrocytes undergo reactive changes in cell morphology, as demonstrated by increased cell proliferation and hypertrophy, neural protrusion density and axon length. It was found that glial segregation and TJ barrier structures constituted by astrocytes proliferating their endfoot can limit neuroinflammatory damage (73). The morphologic plasticity of astrocytes is compatible with their functional transformation to limit the spread of inflammation and support nerve regeneration (150).

The altered morphology of astrocytes leads to impaired communication with other cells in the neural vascular unit, which in turn impairs the barrier immunity and energy substance uptake function of the BBB (151). Both *in vivo* and *ex vivo* studies have shown that a hyperglycemic state impairs gap junction communication in astrocytes, inducing swelling of the astrocyte endfoot and detachment from the endothelial cell basement membrane (146). Astrocyte endfoot processes (ACfp) from the neurovascular unit (NVU) were observed in the prefrontal cortex of female diabetic db/db mice. Loss of ACfp/NVU adhesion has been suggested as a potential mechanism contributing to impaired cognitive function in diabetes (152). Obesity induces reactive proliferation of astrocytes, which in turn induces structural remodeling of the neuroglial interface in multiple brain regions and alters the immune and transport functions of the BBB (153, 154). HFD-induced glial proliferation of astrocytes affects the BBB structure in the arcuate nucleus region. It makes it more difficult for neuropeptide Y (NPY) and proopiomelanocortin (POMC) neuronal cytosomes and dendrites in this region to reach the vasculature (155). Obesity is accompanied by increased serum leptin levels, which activate hypoxia-inducible factor 1-alpha (HIF-1α)-VEGF signaling in hypothalamic astrocytes, thereby inducing structural remodeling of the glial interface (156). Astrocytes isolated from stroke-prone spontaneously hypertensive rats (SHRSP) cause TJ damage and high resistance in endothelial cells by secreting large amounts of lactate (157).

Several studies have found that the overall neural processes of astrocytes are shortened in states of metabolic dysregulation, diminishing their modulation of synapses. A HFD for 12 weeks induced an increase in GFAP expression in the rat hippocampus but in turn impaired the length of neural protrusions in astrocytes, as well as the expression of the proteins glutamate aspartate transporter (GLAST), GLT-1, and Cx43, which are associated with synaptic plasticity (124, 158, 159). Chronic overnutrition leads to the shortening of the central neural protrusions of astrocytes through upregulation of the IκB kinase β (IKKβ)/

10.3389/fendo.2024.1393253

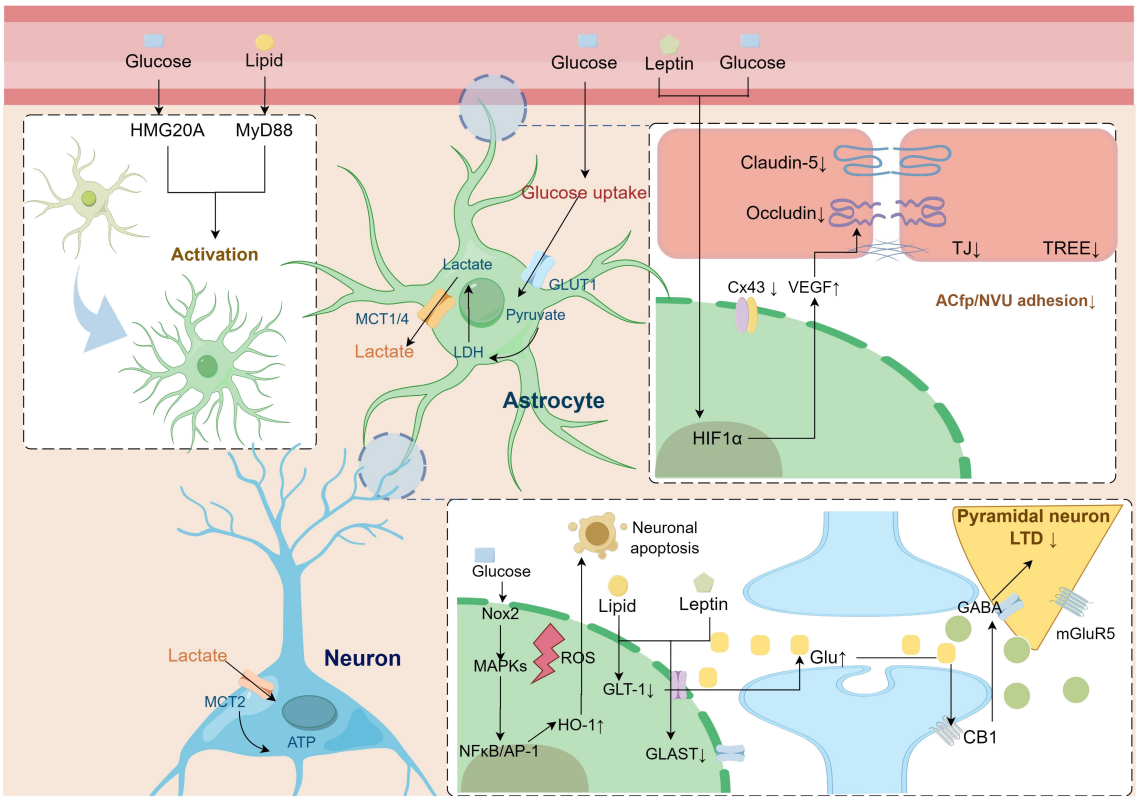

FIGURE 2
Pathologic alterations of astrocytes in metabolic syndrome leading to cognitive dysfunction. Astrocytes undergo reactive activation driven by a disturbed metabolic state. Activation of the astrocyte HIF-1α pathway secretes multiple factors, including VEGF, that impair BBB-linked proteins, leading to increased blood-brain barrier permeability. At the same time, the lipid, glucose, and amino acid metabolism coupling pathway between astrocytes and neurons is impaired, leading to an imbalance in neuronal excitability and decreased synaptic plasticity. AP-1, activator protein-1; CB1, cannabinoid 1; Cx43, connexin 43; GABA, γ-aminobutyric acid; GLAST, glutamate aspartate transporter; Glu, glutamate; GLUT1, glucose transporter type 1; GLT-1, glutamate transporter subtype I; HIF1-α, hypoxia-inducible factor1-α; HMG20A, high mobility group domain protein 20A; HO-1, heme oxygenase-1; LDH, lactate dehydrogenase; LTD, long-term depression; MAPK, mitogen-activated protein kinase; MCT, monocarboxylate transporter; mGluR5, metabotropic glutamate receptor 5; MyD88, myeloid differentiation primary response 88; NFκB, nuclear Factor-κB; NOX, nicotinamide adenine dinucleotide phosphate oxidase; ROS, reactive oxygen species; TJ, tight Junction; TREE, trans-endothelial/epithelial electrical resistance; VEGF, vascular endothelial growth factor.

nuclear factor-κB (NF-κB) pathway, which in turn affects their glutamate uptake in the synaptic gap and modulation of synaptic excitability (160).

5.2 Astrocyte immunoreactivity

Astrocytes are thought to be critical regulators of neuroinflammation (161). Peripheral immune signaling drives glial cell immune function switching as a potential mechanism for systemic inflammation to trigger neuroinflammation (82). Astrocytes play a vital role in developing and expanding neuroinflammation by interacting with various central nervous system *in situ* immune cells, including microglia and T cells (162, 163). Moreover, astrocytes drive perivascular leukocyte recruitment to the brain by secreting C-C motif chemokine ligand 2 (CCL2) and C-X-C motif chemokine ligand 10 (CXCL10) (163, 164). GFAP, S100 calcium-binding protein B (S100B), monoamine oxidase-B (MAO-B), chitinase-3-like protein 1 (YKL-40), and D-serine were used as biomarkers to assess the reactivity and proliferation intensity of astrocytes in tissues, cerebrospinal fluid, and blood (165, 166). High glucose activation of the complement 3 (C3) pathway in astrocytes can lead indirectly and directly to synaptic loss. C3 secreted by astrocytes is able to interact with microglial component 3a (C3a) receptors to modulate synaptic phagocytosis in microglia (167). Reduced secretion of complement factor C3/C3a in high glucose-treated primary astrocytes leads to synaptic protein damage and cognitive dysfunction (168).

As previously described, multiple factors in MetS, such as peripheral metabolic glucolipid metabolism disorders and metabolic inflammation, can drive astrocyte reactive activation. Several studies have demonstrated that enhanced GFAP immunoblotting is observed for T2DM disease states lasting 2-4 weeks, whereas GFAP expression is significantly reduced in more extended weekly studies (169, 170). HFD induces increased hippocampal GFAP expression in rats, which is associated with neuroinflammation, microvascular damage, and subsequent cognitive dysfunction (171, 172). The IKKβ/NF-κB of astrocytes is an essential pathway for HFD-induced hypothalamic inflammation. Knockdown of IKKβ in astrocytes can improve

HFD-induced hypothalamic neuroinflammation, insulin resistance status, and glucolipid metabolism (173). HFD induces upregulation of hypothalamic potassium inwardly rectifying channel subfamily J member 2 Gene (*Kcnj2*), Complement 4b (*C4b*) and discoidin domain receptor 1 (*Ddr1*) and co-localizes with GFAP, and is therefore considered an early marker of obesity and diabetes-related cognitive dysfunction (174). Secretion of inflammatory factors by astrocytes is associated with synaptic loss. In neuron-astrocyte co-culture cell studies, LPS increased astrocyte secretion of inflammatory factors and correlated with decreased neuronal synaptophysin (SYN) (175).

MetS leads to the activation of astrocytes, thereby affecting their regulatory role in cognition and behavior. Reactive astrocytes are a potential therapeutic target for ameliorating vascular and neurodegeneration-related cognitive dysfunction (176, 177). Targeting the neurotoxic phenotype of reactive astrocytes alleviates cognitive-behavioral alterations induced by MetS-related factors (169).

5.3 Astrocyte immunometabolic disorders

Reactive astrocytes respond to metabolic stress by reprogramming metabolic processes and exerting various adaptive compensatory effects to maintain neuronal energy supply (178, 179). Various components of MetS can act directly on metabolic processes such as glycolysis and mitochondrial metabolism in astrocytes. Astrocyte metabolism progresses towards dysregulation under metabolic stress, with mitochondrial malfunction, energy failure, and oxidative stress, which can affect the energy supply of neurosynapses and impaired lymphatic efflux of Aβ proteins (180). Astrocyte glycolysis, gluconeogenesis, and lipid metabolism are plastic to undergo reprogramming during MetS metabolic stress to maintain neuronal energy homeostasis (181). Excessive chronic stressful pressure leads to a compensatory decrease in astrocyte energy metabolism, which may be impaired by promoting cerebral insulin resistance, decreased glucose uptake, and oxidative stress (66).

Central leptin signaling activation in HFD rats reduces astrocytic ghrelin transporter protein and EAAT1 and EAAT2 in the arcuate nucleus of the hypothalamus, resulting in decreased ghrelin uptake and reduced glutamine synthesis (121). Chronic lipid exposure-induced ectopic lipid loading in astrocytes leads to reduced insulin-induced protein kinase B (AKT) phosphorylation and dysregulated glycogen metabolism (182). The metabolomic study showed that selenium amino acid metabolism, urea cycle, and glutamate metabolism were up-regulated in human astrocytes in a palmitic acid-induced lipotoxic environment for several amino acid metabolic pathways (183). Several tricarboxylic acid cycle intermediates, such as succinate and citrate were reduced, glutamine synthetase was increased, and glutaminase and glutamic acid decarboxylase decreased in the hippocampal region of db/db mice (131). During physiological states, lipid synthesis and metabolism in astrocytes regulate hippocampal synapse development and function. Diminishing of sterol regulatory element-binding protein 2 (SREBP2) cleavage-activating protein (SCAP) resulted in lower levels of the synaptosome associated protein 25(SNAP-25) and reduced numbers of synaptic vesicles in the hippocampus of mice (184). Diabetes mellitus leads to impaired brain cholesterol synthesis and reduced synapse number by reducing the transcription factor SREBP2 (185).

Metabolic reprogramming of astrocytes is also thought to be an adaptive change in response to central insulin resistance (186). Astrocytes express insulin receptor and insulin-like growth factor 1 (IGF1), which regulate glucose transporter type 1 (GLUT1) expression to take up circulating glucose (187). In another study, IR knockdown in astrocytes was found to impair tyrosine phosphorylation of Munc18c, reduce ATP cytokinesis, and subsequently lead to reduced neuronal dopamine release and depressive-like behavior (188).

The process of reactive activation of astrocytes is accompanied by a metabolic paradigm shift (189). Activation and maintenance of reactive astrocytes depend on a continuous supply of energy from glycolytic metabolism. The downright inflammatory response of astrocytes to LPS is accompanied by elevated glycolytic flux and elevated activity of critical metabolic enzymes, such as 6-phosphofructose-2-kinase/fructose-2,6-bisphosphatase isoform 3 (PFKFB3) (190). 2-DG glycolysis inhibitor and glycogen phosphorylase inhibitor intervened to regulate the astrocyte glycolysis process and significantly attenuated LPS-induced cytokine release and NF-κB phosphorylation (134). Inhibition of pyruvate dehydrogenase kinase-2(PDK2) in hypothalamic astrocytes of diabetic rats inhibited cellular glycolysis and its inflammatory activation, thus reducing hypothalamic inflammation as well as lactate levels and reversing the increase in food intake (127). The peroxisome proliferator-activated receptor (PPAR) pathway is one of the critical pathways of astrocyte immunometabolism, among which PPARγ stimulates glucose and glutamate uptake and lactate release from astrocytes. At the same time, PPARα induces fatty acid β-oxidation in the presence of impaired glucose metabolism (191). Regulators of aerobic glycolysis, such as HIF-1α and AMPK in astrocytes, are affected by inflammation (192). Nicotinamide phosphoribosyltransferase (NAMPT)-dependent nicotinamide adenine dinucleotide (NAD^+) upregulation in astrocytes provides energy for cellular activation and drives transcriptional inflammatory program rearrangements, and inhibition of endogenous NAD^+ synthesis impairs astrocyte transcriptional responses to LPS/Interferon-γ(IFNγ) stimulation and attenuates activation-associated neuroinflammation (193).

6 Clinical practice of astrocyte in MetS-related cognitive dysfunction

In summary, it has been elaborated that astrocytes are susceptible to morphologically and functionally responsive changes in metabolically disturbed environments. Reactive astrocytes are involved in pathological processes such as neuroinflammation, energy metabolic homeostasis, and cross-barrier transport of nutrients and amyloid in MetS-associated cognitive dysfunction (165, 194).

6.1 Diagnostic markers

Astrocytes express and secrete a variety of specific molecular substances during pathological processes, which are considered promising targets for the development of early screening with humoral or imaging biomarkers (195). Several studies and meta-analyses have found a strong association between astrocyte biomarkers and cognitive decline (166). In a clinical study of 121 older adults, cerebrospinal fluid and plasma levels of GFAP and YKL-40 were shown to relate to Aβ and tau pathology and to mediate hippocampal volume atrophy (196).

Proteomic studies have identified increased levels of the metabolism-related proteins lactate dehydrogenase B-chain (LDHB), pyruvate kinase (PKM), and glyceraldehyde 3-phosphate dehydrogenase (GAPDH) in M4 Astrocyte in cerebrospinal fluid, which can be used as a biomarker for the early diagnosis of cognitive impairment (197). In addition, at the level of genetic material, astrocyte-derived extracellular vesicles (EVs) and a variety of miRNAs therein are thought to potentially become biomarkers for neurodegenerative diseases (198). Increased secretion of miR-141-3p and miR-30d is detected in primary human astrocytes activated by stimulation with the neuroinflammatory factor IL-1β (199). Regarding imaging, astrocyte metabolic levels and associated metabolites are visualized and analyzed by PET/CT imaging with 11C-acetate and 18F-fluorodeoxyglucose (18F-FDG). In a study, astrocyte acetate hypermetabolism and neuronal glucose hypometabolism were used as a visual diagnostic strategy for early diagnosis of Alzheimer's disease (200). In addition, machine learning research is an emerging tool for constructing diagnostic models. In a study, automata theory was used to build a diagnostic computational model to monitor the astrocyte metabolic end-product lactate, thereby characterizing the level of glycogen metabolism in the brain (201).

Astrocytes have been progressively recognized as potential biomarkers for the development of cognitive impairment. At the same time, these markers are highly expressed in MetS and its related components. A joint examination of astrocytes in both diseases is still lacking. However, as reactive cells, their immunometabolic flexibility and sensitivity make them valuable as potential diagnostic markers of MetS-associated cognitive disorders.

6.2 Therapeutic strategies

Conventional treatments have focused on neuron-focused mechanistic interventions, but drug development and clinical translation have been limited. It is currently considered effective in improving the homeostasis of synapses and their adjacent microenvironments through systems biology and multi-targeted therapeutic approaches. The supportive role and pathologic criticality of neuroglia for neuronal function are gradually being demonstrated. Astrocytes have been proposed at multiple levels as potential targets for drug development to ameliorate central neuropathy and restore cognitive function (202, 203). Based on the altered functional and molecular pathways in astrocytes in MetS, targeting their biological processes may have therapeutic value.

Astrocytes have a central role in neuroinflammation (204). Several studies have targeted toll-like receptor proteins (TLRs) (205), NF-κB, and the transcription factor NF-E2-related factor 2 (Nrf2) (206) in astrocytes, thereby limiting their cell proliferation and neurotoxicity (207). In addition, the repair of astrocyte TJ protein structures resulted in the amelioration of BBB permeability damage. *In vitro* and *in vivo* studies showed that inhibition of astrocyte Cx43 hemichannel opening prevented astrocyte proliferation (astrogliosis) and improved BBB permeability (208). Clomipramine is a classical tricyclic antidepressant. Epoxomicin is a natural selective proteasome inhibitor and has an anti-inflammatory effect. Both drugs have been attempted as inhibitors of intermediate filament proteins and vimentin associated with astrogliosis, thereby facilitating the limitations on nerve regeneration imposed by persistent, excessive glial proliferation (209).

Astrocytic metabolic plasticity allows astrocytes to act as critical cells in maintaining homeostasis (210), with their glycolytic metabolism and derived metabolites, such as lactate and serine, providing energy support to synapses and maintaining homeostasis of neural excitability (211). Therefore, regulation of astrocyte metabolism has also been recognized as a potential therapeutic target (212). The astrocyte glycolytic metabolite L-lactate and secreted vesicles have also been identified as potential targets in neurological disorders (213). Antidiabetic drugs have been found to improve brain glucose uptake by targeting astrocytes. Metformin, which crosses the BBB, increases glucose consumption and lactate release in astrocytes (214). Metformin treatment normalized GLUT-1 expression in STZ-induced diabetic rats and partially restored hippocampal glucose uptake and transport (215). Notably, glucagon-like peptide-1 (GLP-1) receptor agonists have been shown preclinically in small pilot trials to improve cerebral glucose metabolism and functional connectivity (216, 217). Liraglutide (an analog of GLP-1) improves cognitive function by enhancing astrocyte-promoted aerobic glycolysis and alleviating OXPHOS activation to maintain neuronal support (133).

In addition, promoting the transformation of astrocytes into neurons or other glial cells is a potential but controversial therapeutic modality. Several drug tools for astrocyte-specific delivery have been developed, including pluripotent stem cell therapies (218) and effective viral vectors (219) to control astrocyte-specific gene expression. Some studies have used lineage-tracing strategies to target astrocytes *in vivo* for transformation into neurons (220). Other studies have attempted to reprogram astrocyte lineage cells into oligodendrocyte cells by targeting Sox2 and Sox10. This method could relieve astrocyte glial scarring and promote myelin regeneration of neural axons (221–223).

7 Conclusions and future perspectives

MetS causes multiple disorders that worsen in the peripheral circulation and affect the brain, which is considered its target organ for generating metabolic stress damage. As a result, MetS accelerates cognitive decline through the acceleration of neurodegeneration

and cerebral circulatory disturbances. Astrocytes change their metabolic and immune phenotypes in response to peripheral metabolic stressors, leading to early compensatory regulation of local neurological microenvironmental homeostasis. However, this compensation is lost when the stressors become too much, leading to worsened neuroinflammation. Astrocytes interact with a wide range of cells in the vascular, neural unit to influence BBB permeability and glial lymphatic system drainage functions and also form structures with neural synapses known as tripartite synapses, which play diverse and complex regulatory roles in neural circuit modulation.

The sensitive metabolic and functional plasticity of astrocytes makes them potential targets for improving the maintenance of brain energy metabolism and sustaining synaptic energy support. Also their cellular markers with specific functional proteins are also being developed as diagnostic markers for cognitive disorders. However, the complex and challenging nature of targeting astrocytes by transgenic techniques still poses a challenge due to the rich diversity of astrocytes and their overlap with other CNS cell genetic lineages (224). Contradictory findings in basic research cast doubt on the transdifferentiation capacity of astrocytes (225, 226). Additionally, there is still caution in clinical development regarding immunogenicity mapping in viral manipulation and the potential off-target risk of transgenic manipulation. Nevertheless, this cell implantation strategy could potentially enable endogenous neuronal regeneration in the future.

Author contributions

LZ: Writing – original draft, Writing – review & editing. JY-Y: Writing – original draft, Writing – review & editing. LC: Formal Analysis, Investigation, Validation, Writing – review & editing. XP: Data curation, Formal Analysis, Funding acquisition, Methodology, Writing – review & editing. TJ: Funding acquisition, Resources, Validation, Visualization, Writing – review & editing. PY: Software, Writing – review & editing. YR: Funding acquisition, Resources, Software, Visualization, Writing – review & editing. PQ:.

Funding

The author(s) declare financial support was received for the research, authorship, and/or publication of this article. The authors' work in this area is supported by the Natural Science Foundation of China (82274486); Science and Technology Research Special project of Sichuan Provincial; Department (2022YFS0382); YR's TCM studio.

Acknowledgments

Figures were created with Figdraw.com.

Conflict of interest

The authors declare that the research was conducted in the absence of any commercial or financial relationships that could be construed as a potential conflict of interest.

Publisher's note

References

1. Lambert GW, Straznicky NE, Lambert EA, Dixon JB, Schlaich MP. Sympathetic nervous activation in obesity and the metabolic syndrome–causes, consequences and therapeutic implications. *Pharmacol Ther*. (2010) 126:159–72. doi: 10.1016/j.pharmthera.2010.02.002

2. Tune JD, Goodwill AG, Sassoon DJ, Mather KJ. Cardiovascular consequences of metabolic syndrome. *Transl Res*. (2017) 183:57–70. doi: 10.1016/j.trsl.2017.01.001

3. Lemieux I, Després JP. Metabolic syndrome: past, present and future. *Nutrients*. (2020) 12:3501. doi: 10.3390/nu12113501

4. Saklayen MG. The global epidemic of the metabolic syndrome. *Curr Hypertens Rep*. (2018) 20:12. doi: 10.1007/s11906-018-0812-z

5. World Health O. *Definition, Diagnosis and Classification of Diabetes Mellitus and Its Complications: Report of a Who Consultation. Part 1, Diagnosis and Classification of Diabetes Mellitus*. Geneva: World Health Organization (1999).

6. Third report of the national cholesterol education program (Ncep) expert panel on detection, evaluation, and treatment of high blood cholesterol in adults (Adult treatment panel iii) final report. *Circulation*. (2002) 106:3143–421. doi: 10.1161/circ.106.25.3143

7. Einhorn D, Reaven GM, Cobin RH, Ford E, Ganda OP, Handelsman Y, et al. American college of endocrinology position statement on the insulin resistance syndrome. *Endocr Pract*. (2003) 9:237–52. doi: 10.4158/EP.9.S2.5

8. Alberti KG, Zimmet P, Shaw J. The metabolic syndrome–a new worldwide definition. *Lancet*. (2005) 366:1059–62. doi: 10.1016/s0140-6736(05)67402-8

9. Lone S, Lone K, Khan S, Pampori RA. Assessment of metabolic syndrome in kashmiri population with type 2 diabetes employing the standard criteria's given by who, ncepatp iii and idf. *J Epidemiol Glob Health*. (2017) 7:235–9. doi: 10.1016/j.jegh.2017.07.004

10. Alberti KG, Eckel RH, Grundy SM, Zimmet PZ, Cleeman JI, Donato KA, et al. Harmonizing the metabolic syndrome: A joint interim statement of the international diabetes federation task force on epidemiology and prevention; national heart, lung, and blood institute; american heart association; world heart federation; international atherosclerosis society; and international association for the study of obesity. *Circulation*. (2009) 120:1640–5. doi: 10.1161/circulationaha.109.192644

11. Fakih W, Zeitoun R, AlZaim I, Eid AH, Kobeissy F, Abd-Elrahman KS, et al. Early metabolic impairment as a contributor to neurodegenerative disease: mechanisms and potential pharmacological intervention. *Obes (Silver Spring)*. (2022) 30:982–93. doi: 10.1002/oby.23400

12. Livingston JM, McDonald MW, Gagnon T, Jeffers MS, Gomez-Smith M, Antonescu S, et al. Influence of metabolic syndrome on cerebral perfusion and cognition. *Neurobiol Dis*. (2020) 137:104756. doi: 10.1016/j.nbd.2020.104756

13. Kim YJ. Different effects of metabolic syndrome according to dementia type. *Alzheimer's Dementia*. (2020) 16:e042370. doi: 10.1002/alz.042370

14. Yaffe K, Kanaya A, Lindquist K, Simonsick EM, Harris T, Shorr RI, et al. The metabolic syndrome, inflammation, and risk of cognitive decline. *Jama*. (2004) 292:2237–42. doi: 10.1001/jama.292.18.2237

15. Kazlauskaite R, Janssen I, Wilson RS, Appelhans BM, Evans DA, Arvanitakis Z, et al. Is midlife metabolic syndrome associated with cognitive function change? The study of women's health across the nation. *J Clin Endocrinol Metab*. (2020) 105:e1093–105. doi: 10.1210/clinem/dgaa067

16. Qureshi D, Collister J, Allen NE, Kuźma E, Littlejohns T. Association between metabolic syndrome and risk of incident dementia in uk biobank. *Alzheimers Dement*. (2024) 20:447–58. doi: 10.1002/alz.13439

17. Xiong X-Y, Tang Y, Yang Q-W. Metabolic changes favor the activity and heterogeneity of reactive astrocytes. *Trends Endocrinol Metab*. (2022) 33:390–400. doi: 10.1016/j.tem.2022.03.001

18. Ding ZB, Song LJ, Wang Q, Kumar G, Yan YQ, Ma CG. Astrocytes: A double-edged sword in neurodegenerative diseases. *Neural Regener Res*. (2021) 16:1702–10. doi: 10.4103/1673-5374.306064

19. Escartin C, Galea E, Lakatos A, O'Callaghan JP, Petzold GC, Serrano-Pozo A, et al. Reactive astrocyte nomenclature, definitions, and future directions. *Nat Neurosci*. (2021) 24:312–25. doi: 10.1038/s41593-020-00783-4

20. Arnoriaga-Rodríguez M, Fernández-Real JM. Microbiota impacts on chronic inflammation and metabolic syndrome - related cognitive dysfunction. *Rev Endocr Metab Disord*. (2019) 20:473–80. doi: 10.1007/s11154-019-09537-5

21. Martin-Jiménez CA, García-Vega Á, Cabezas R, Aliev G, Echeverria V, González J, et al. Astrocytes and endoplasmic reticulum stress: A bridge between obesity and neurodegenerative diseases. *Prog Neurobiol*. (2017) 158:45–68. doi: 10.1016/j.pneurobio.2017.08.001

22. Uddin MS, Lim LW. Glial cells in Alzheimer's disease: from neuropathological changes to therapeutic implications. *Ageing Res Rev*. (2022) 78:101622. doi: 10.1016/j.arr.2022.101622

23. Giovannoni F, Quintana FJ. The role of astrocytes in cns inflammation. *Trends Immunol*. (2020) 41:805–19. doi: 10.1016/j.it.2020.07.007

24. Alfaro FJ, Gavrieli A, Saade-Lemus P, Lioutas VA, Upadhyay J, Novak V. White matter microstructure and cognitive decline in metabolic syndrome: A review of diffusion tensor imaging. *Metabolism*. (2018) 78:52–68. doi: 10.1016/j.metabol.2017.08.009

25. Kotkowski E, Price LR, Franklin C, Salazar M, Woolsey M, DeFronzo RA, et al. A neural signature of metabolic syndrome. *Hum Brain Mapp*. (2019) 40:3575–88. doi: 10.1002/hbm.24617

26. Rashid B, Poole VN, Fortenbaugh FC, Esterman M, Milberg WP, McGlinchey RE, et al. Association between metabolic syndrome and resting-state functional brain connectivity. *Neurobiol Aging*. (2021) 104:1–9. doi: 10.1016/j.neurobiolaging.2021.03.012

27. Kouvari M, D'Cunha NM, Travica N, Sergi D, Zec M, Marx W, et al. Metabolic syndrome, cognitive impairment and the role of diet: A narrative review. *Nutrients*. (2022) 14:333. doi: 10.3390/nu14020333

28. van Sloten TT, Sedaghat S, Carnethon MR, Launer LJ, Stehouwer CDA. Cerebral microvascular complications of type 2 diabetes: stroke, cognitive dysfunction, and depression. *Lancet Diabetes Endocrinol*. (2020) 8:325–36. doi: 10.1016/S2213-8587(19)30405-X

29. Borshchev YY, Uspensky YP, Galagudza MM. Pathogenetic pathways of cognitive dysfunction and dementia in metabolic syndrome. *Life Sci*. (2019) 237:116932. doi: 10.1016/j.lfs.2019.116932

30. Bendlin B, Willette A, Carlsson C, Johnson S, Davenport N, Birdsill A, et al. O3-06-06: metabolic syndrome in middle-aged adults is associated with brain perfusion deficits. *Alzheimer's Dementia*. (2012) 8:P442–P. doi: 10.1016/j.jalz.2012.05.1176

31. Efimova I, Efimova N, Lishmanov Y. Cerebral blood flow and cognitive function in patients with metabolic syndrome: effect of antihypertensive therapy. *J Clin Hypertension*. (2014) 16:900–6. doi: 10.1111/jch.12435

32. Hughes TM, Lockhart SN, Suerken CK, Jung Y, Whitlow CT, Bateman JR, et al. Hypertensive aspects of cardiometabolic disorders are associated with lower brain microstructure, perfusion, and cognition. *J Alzheimers Dis*. (2022) 90:1589–99. doi: 10.3233/jad-220646

33. Avolio A, Kim MO, Adji A, Gangoda S, Avadhanam B, Tan I, et al. Cerebral haemodynamics: effects of systemic arterial pulsatile function and hypertension. *Curr Hypertens Rep*. (2018) 20:20. doi: 10.1007/s11906-018-0822-x

34. Schiffrin EL. How structure, mechanics, and function of the vasculature contribute to blood pressure elevation in hypertension. *Can J Cardiol*. (2020) 36:648–58. doi: 10.1016/j.cjca.2020.02.003

35. Wang M, Yang H, Zheng LY, Zhang Z, Tang YB, Wang GL, et al. Downregulation of tmem16a calcium-activated chloride channel contributes to cerebrovascular remodeling during hypertension by promoting basilar smooth muscle cell proliferation. *Circulation*. (2012) 125:697–707. doi: 10.1161/circulationaha.111.041806

36. Obadia N, Lessa MA, Daliry A, Silvares RR, Gomes F, Tibiriçá E, et al. Cerebral microvascular dysfunction in metabolic syndrome is exacerbated by ischemia-reperfusion injury. *BMC Neurosci*. (2017) 18:67. doi: 10.1186/s12868-017-0384-x

37. Jha SK, Jha NK, Kumar D, Ambasta RK, Kumar P. Linking mitochondrial dysfunction, metabolic syndrome and stress signaling in neurodegeneration. *Biochim Biophys Acta Mol Basis Dis*. (2017) 1863:1132–46. doi: 10.1016/j.bbadis.2016.06.015

38. Kipinoinen T, Toppala S, Rinne JO, Viitanen MH, Jula AM, Ekblad LL. Association of midlife inflammatory markers with cognitive performance at 10-year follow-up. *Neurology*. (2022) 99:e2294–e302. doi: 10.1212/wnl.0000000000201116

39. Pedersen KM, Cordua S, Hasselbalch HC, Ellervik C. The association between circulating inflammatory markers and metabolic syndrome: A general population study. *Blood*. (2018) 132:4305. doi: 10.1182/blood-2018-99-120356

40. Caprio S, Perry R, Kursawe R. Adolescent obesity and insulin resistance: roles of ectopic fat accumulation and adipose inflammation. *Gastroenterology*. (2017) 152:1638–46. doi: 10.1053/j.gastro.2016.12.051

41. Boulangé CL, Neves AL, Chilloux J, Nicholson JK, Dumas ME. Impact of the gut microbiota on inflammation, obesity, and metabolic disease. *Genome Med*. (2016) 8:42. doi: 10.1186/s13073-016-0303-2

42. Więckowska-Gacek A, Mietelska-Porowska A, Wydrych M, Wojda U. Western diet as a trigger of Alzheimer's disease: from metabolic syndrome and systemic inflammation to neuroinflammation and neurodegeneration. *Ageing Res Rev*. (2021) 70:101397. doi: 10.1016/j.arr.2021.101397

43. Khan MSH, Hegde V. Obesity and diabetes mediated chronic inflammation: A potential biomarker in Alzheimer's disease. *J Pers Med*. (2020) 10:42. doi: 10.3390/jpm10020042

44. Crispino M, Trinchese G, Penna E, Cimmino F, Catapano A, Villano I, et al. Interplay between peripheral and central inflammation in obesity-promoted disorders: the impact on synaptic mitochondrial functions. *Int J Mol Sci*. (2020) 21:5964. doi: 10.3390/ijms21175964

45. Aten S, Kiyoshi CM, Arzola EP, Patterson JA, Taylor AT, Du Y, et al. Ultrastructural view of astrocyte arborization, astrocyte-astrocyte and astrocyte-synapse contacts, intracellular vesicle-like structures, and mitochondrial network. *Prog Neurobiol*. (2022) 213:102264. doi: 10.1016/j.pneurobio.2022.102264

46. Nampoothiri S, Nogueiras R, Schwaninger M, Prevot V. Glial cells as integrators of peripheral and central signals in the regulation of energy homeostasis. *Nat Metab*. (2022) 4:813–25. doi: 10.1038/s42255-022-00610-z

47. García-Cáceres C, Balland E, Prevot V, Luquet S, Woods SC, Koch M, et al. Role of astrocytes, microglia, and tanycytes in brain control of systemic metabolism. *Nat Neurosci*. (2019) 22:7–14. doi: 10.1038/s41593-018-0286-y

48. Kim JG, Suyama S, Koch M, Jin S, Argente-Arizon P, Argente J, et al. Leptin signaling in astrocytes regulates hypothalamic neuronal circuits and feeding. *Nat Neurosci*. (2014) 17:908–10. doi: 10.1038/nn.3725

49. Dallérac G, Rouach N. Astrocytes as new targets to improve cognitive functions. *Prog Neurobiol*. (2016) 144:48–67. doi: 10.1016/j.pneurobio.2016.01.003

50. Kaur D, Sharma V, Deshmukh R. Activation of microglia and astrocytes: A roadway to neuroinflammation and Alzheimer's disease. *Inflammopharmacology*. (2019) 27:663–77. doi: 10.1007/s10787-019-00580-x

51. Zhang H, Zheng Q, Guo T, Zhang S, Zheng S, Wang R, et al. Metabolic reprogramming in astrocytes results in neuronal dysfunction in intellectual disability. *Mol Psychiatry*. (2022). doi: 10.1038/s41380-022-01521-x

52. Popov A, Brazhe A, Denisov P, Sutyagina O, Li L, Lazareva N, et al. Astrocyte dystrophy in ageing brain parallels impaired synaptic plasticity. *Aging Cell*. (2021) 20:e13334. doi: 10.1111/acel.13334

53. Santello M, Toni N, Volterra A. Astrocyte function from information processing to cognition and cognitive impairment. *Nat Neurosci*. (2019) 22:154–66. doi: 10.1038/s41593-018-0325-8

54. Wade JJ, McDaid LJ, Harkin J, Crunelli V, Kelso JA. Bidirectional coupling between astrocytes and neurons mediates learning and dynamic coordination in the brain: A multiple modeling approach. *PloS One*. (2011) 6:e29445. doi: 10.1371/journal.pone.0029445

55. Tsybina Y, Kastalskiy I, Krivonosov M, Zaikin A, Kazantsev V, Gorban AN, et al. Astrocytes mediate analogous memory in a multi-layer neuron–astrocyte network. *Neural Comput Appl*. (2022) 34:9147–60. doi: 10.1007/s00521-022-06936-9

56. Gordleeva SY, Tsybina YA, Krivonosov MI, Ivanchenko MV, Zaikin AA, Kazantsev VB, et al. Modeling working memory in a spiking neuron network accompanied by astrocytes. *Front Cell Neurosci*. (2021) 15:631485. doi: 10.3389/fncel.2021.631485

57. Perea G, Gómez R, Mederos S, Covelo A, Ballesteros JJ, Schlosser L, et al. Activity-dependent switch of gabaergic inhibition into glutamatergic excitation in astrocyte-neuron networks. *Elife*. (2016) 5:e20362. doi: 10.7554/eLife.20362

58. Kol A, Adamsky A, Groysman M, Kreisel T, London M, Goshen I. Astrocytes contribute to remote memory formation by modulating hippocampal-cortical communication during learning. *Nat Neurosci*. (2020) 23:1229–39. doi: 10.1038/s41593-020-0679-6

59. Sardinha VM, Guerra-Gomes S, Caetano I, Tavares G, Martins M, Reis JS, et al. Astrocytic signaling supports hippocampal-prefrontal theta synchronization and cognitive function. *Glia*. (2017) 65:1944–60. doi: 10.1002/glia.23205

60. Marina N, Turovsky E, Christie IN, Hosford PS, Hadjihambi A, Korsak A, et al. Brain metabolic sensing and metabolic signaling at the level of an astrocyte. *Glia*. (2018) 66:1185–99. doi: 10.1002/glia.23283

61. Cooper ML, Pasini S, Lambert WS, D'Alessandro KB, Yao V, Risner ML, et al. Redistribution of metabolic resources through astrocyte networks mitigates neurodegenerative stress. *Proc Natl Acad Sci U.S.A*. (2020) 117:18810–21. doi: 10.1073/pnas.2009425117

62. Welcome MO, Mastorakis NE. Emerging concepts in brain glucose metabolic functions: from glucose sensing to how the sweet taste of glucose regulates its own metabolism in astrocytes and neurons. *Neuromol Med*. (2018) 20:281–300. doi: 10.1007/s12017-018-8503-0

63. Bélanger M, Allaman I, Magistretti PJ. Brain energy metabolism: focus on astrocyte-neuron metabolic cooperation. *Cell Metab*. (2011) 14:724–38. doi: 10.1016/j.cmet.2011.08.016

64. Dienel GA. Astrocytic energetics during excitatory neurotransmission: what are contributions of glutamate oxidation and glycolysis? *Neurochem Int*. (2013) 63:244–58. doi: 10.1016/j.neuint.2013.06.015

65. Ioannou MS, Jackson J, Sheu SH, Chang CL, Weigel AV, Liu H, et al. Neuron-astrocyte metabolic coupling protects against activity-induced fatty acid toxicity. *Cell*. (2019) 177:1522–35.e14. doi: 10.1016/j.cell.2019.04.001

66. Shen Z, Li ZY, Yu MT, Tan KL, Chen S. Metabolic perspective of astrocyte dysfunction in Alzheimer's disease and type 2 diabetes brains. *BioMed Pharmacother*. (2023) 158:114206. doi: 10.1016/j.biopha.2022.114206

67. Gollihue JL, Norris CM. Astrocyte mitochondria: central players and potential therapeutic targets for neurodegenerative diseases and injury. *Ageing Res Rev*. (2020) 59:101039. doi: 10.1016/j.arr.2020.101039

68. Zehnder T, Petrelli F, Romanos J, De Oliveira Figueiredo EC, Lewis TL Jr., Déglon N, et al. Mitochondrial biogenesis in developing astrocytes regulates astrocyte maturation and synapse formation. *Cell Rep*. (2021) 35:108952. doi: 10.1016/j.celrep.2021.108952

69. Marina N, Christie IN, Korsak A, Doronin M, Brazhe A, Hosford PS, et al. Astrocytes monitor cerebral perfusion and control systemic circulation to maintain brain blood flow. *Nat Commun*. (2020) 11:131. doi: 10.1038/s41467-019-13956-y

70. Gordon GRJ, Mulligan SJ, MacVicar BA. Astrocyte control of the cerebrovasculature. *Glia*. (2007) 55:1214–21. doi: 10.1002/glia.20543

71. Cohen-Salmon M, Slaoui L, Mazaré N, Gilbert A, Oudart M, Alvear-Perez R, et al. Astrocytes in the regulation of cerebrovascular functions. *Glia*. (2021) 69:817–41. doi: 10.1002/glia.23924

72. Kim KJ, Ramiro Diaz J, Iddings JA, Filosa JA. Vasculo-neuronal coupling: retrograde vascular communication to brain neurons. *J Neurosci*. (2016) 36:12624–39. doi: 10.1523/jneurosci.1300-16.2016

73. Horng S, Therattil A, Moyon S, Gordon A, Kim K, Argaw AT, et al. Astrocytic tight junctions control inflammatory cns lesion pathogenesis. *J Clin Invest*. (2017) 127:3136–51. doi: 10.1172/jci91301

74. Heithoff BP, George KK, Phares AN, Zuidhoek IA, Munoz-Ballester C, Robel S. Astrocytes are necessary for blood-brain barrier maintenance in the adult mouse brain. *Glia*. (2021) 69:436–72. doi: 10.1002/glia.23908

75. Pivoriūnas A, Verkhratsky A. Astrocyte-endotheliocyte axis in the regulation of the blood-brain barrier. *Neurochem Res*. (2021) 46:2538–50. doi: 10.1007/s11064-021-03338-6

76. Ezan P, André P, Cisternino S, Saubaméa B, Boulay AC, Doutremer S, et al. Deletion of astroglial connexins weakens the blood-brain barrier. *J Cereb Blood Flow Metab*. (2012) 32:1457–67. doi: 10.1038/jcbfm.2012.45

77. He JT, Li XY, Yang L, Zhao X. Astroglial connexins and cognition: memory formation or deterioration? *Biosci Rep*. (2020) 40:BSR20193510. doi: 10.1042/bsr20193510

78. Cheung G, Chever O, Rollenhagen A, Quenech'du N, Ezan P, Lübke JHR, et al. Astroglial connexin 43 regulates synaptic vesicle release at hippocampal synapses. *Cells*. (2023) 12:3501. doi: 10.3390/cells12081133

79. Hösli L, Binini N, Ferrari KD, Thieren L, Looser ZJ, Zuend M, et al. Decoupling astrocytes in adult mice impairs synaptic plasticity and spatial learning. *Cell Rep*. (2022) 38:110484. doi: 10.1016/j.celrep.2022.110484

80. MiChinaga S, Koyama Y. Dual roles of astrocyte-derived factors in regulation of blood-brain barrier function after brain damage. *Int J Mol Sci*. (2019) 20:571. doi: 10.3390/ijms20030571

81. Osipova ED, Semyachkina-Glushkovskaya OV, Morgun AV, Pisareva NV, Malinovskaya NA, Boitsova EB, et al. Gliotransmitters and cytokines in the control of blood-brain barrier permeability. *Rev Neurosci*. (2018) 29:567–91. doi: 10.1515/revneuro-2017-0092

82. Hashioka S, Wu Z, Klegeris A. Glia-driven neuroinflammation and systemic inflammation in Alzheimer's disease. *Curr Neuropharmacol*. (2021) 19:908–24. doi: 10.2174/1570159x18666201111104509

83. Treviño S, Díaz A, González-López G, Guevara J. Differential biochemical-inflammatory patterns in the astrocyte-neuron axis of the hippocampus and frontal cortex in wistar rats with metabolic syndrome induced by high fat or carbohydrate diets. *J Chem Neuroanat*. (2022) 126:102186. doi: 10.1016/j.jchemneu.2022.102186

84. Chowen JA, Argente-Arizón P, Freire-Regatillo A, Argente J. Sex differences in the neuroendocrine control of metabolism and the implication of astrocytes. *Front Neuroendocrinol*. (2018) 48:3–12. doi: 10.1016/j.yfrne.2017.05.003

85. Pucci G, Alcidi R, Tap L, Battista F, Mattace-Raso F, Schillaci G. Sex- and gender-related prevalence, cardiovascular risk and therapeutic approach in metabolic syndrome: A review of the literature. *Pharmacol Res*. (2017) 120:34–42. doi: 10.1016/j.phrs.2017.03.008

86. Jaber SM, Bordt EA, Bhatt NM, Lewis DM, Gerecht S, Fiskum G, et al. Sex Differences in the Mitochondrial Bioenergetics of Astrocytes but Not Microglia at a Physiologically Relevant Brain Oxygen Tension. *Neurochem Int*. (2018) 117:82–90. doi: 10.1016/j.neuint.2017.09.003

87. Santos-Galindo M, Acaz-Fonseca E, Bellini MJ, Garcia-Segura LM. Sex differences in the inflammatory response of primary astrocytes to lipopolysaccharide. *Biol Sex Differ*. (2011) 2:7. doi: 10.1186/2042-6410-2-7

88. Chanana V, Tumturk A, Kintner D, Udho E, Ferrazzano P, Cengiz P. Sex differences in mouse hippocampal astrocytes after *in-vitro* ischemia. *J Vis Exp*. (2016) 116:53695. doi: 10.3791/53695

89. Hidalgo-Lanussa O, González Santos J, Barreto GE. Sex-specific vulnerabilities in human astrocytes underpin the differential impact of palmitic acid. *Neurobiol Dis*. (2024) 195:106489. doi: 10.1016/j.nbd.2024.106489

90. Diaz JR, Kim KJ, Brands MW, Filosa JA. Augmented astrocyte microdomain ca (2+) dynamics and parenchymal arteriole tone in angiotensin ii-infused hypertensive mice. *Glia*. (2019) 67:551–65. doi: 10.1002/glia.23564

91. Bhat SA, Goel R, Shukla R, Hanif K. Platelet cd40l induces activation of astrocytes and microglia in hypertension. *Brain Behav Immun*. (2017) 59:173–89. doi: 10.1016/j.bbi.2016.09.021

92. Li Y, Liu J, Gao D, Wei J, Yuan H, Niu X, et al. Age-related changes in hypertensive brain damage in the hippocampi of spontaneously hypertensive rats. *Mol Med Rep*. (2016) 13:2552–60. doi: 10.3892/mmr.2016.4853

93. Bhat SA, Goel R, Shukla S, Shukla R, Hanif K. Angiotensin receptor blockade by inhibiting glial activation promotes hippocampal neurogenesis via activation of wnt/B-catenin signaling in hypertension. *Mol Neurobiol*. (2018) 55:5282–98. doi: 10.1007/s12035-017-0754-5

94. Sabbatini M, Tomassoni D, Amenta F. Hypertensive brain damage: comparative evaluation of protective effect of treatment with dihydropyridine derivatives in spontaneously hypertensive rats. *Mech Ageing Dev*. (2001) 122:2085–105. doi: 10.1016/s0047-6374(01)00318-9

95. Levit A, Cheng S, Hough O, Liu Q, Agca Y, Agca C, et al. Hypertension and pathogenic happ independently induce white matter astrocytosis and cognitive impairment in the rat. *Front Aging Neurosci*. (2020) 12:82. doi: 10.3389/fnagi.2020.00082

96. Turovsky EA, Braga A, Yu Y, Esteras N, Korsak A, Theparambil SM, et al. Mechanosensory signaling in astrocytes. *J Neurosci*. (2020) 40:9364–71. doi: 10.1523/jneurosci.1249-20.2020

97. Su C, Xue J, Ye C, Chen A. Role of the central renin–Angiotensin system in hypertension (Review). *Int J Mol Med*. (2021) 47:95. doi: 10.3892/ijmm.2021.4928

98. Elsaafien K, de Kloet AD, Krause EG, Sumners C. Brain angiotensin type-1 and type-2 receptors in physiological and hypertensive conditions: focus on neuroinflammation. *Curr Hypertens Rep*. (2020) 22:48. doi: 10.1007/s11906-020-01062-0

99. Healy DP, Printz MP. Angiotensinogen levels in the brain and cerebrospinal fluid of the genetically hypertensive rat. *Hypertension*. (1985) 7:752–9. doi: 10.1161/01.hyp.7.5.752

100. Huang BS, Leenen FH. Brain "Ouabain" and angiotensin ii in salt-sensitive hypertension in spontaneously hypertensive rats. *Hypertension*. (1996) 28:1005–12. doi: 10.1161/01.hyp.28.6.1005

101. Xia H, Sriramula S, Chhabra KH, Lazartigues E. Brain angiotensin-converting enzyme type 2 shedding contributes to the development of neurogenic hypertension. *Circ Res*. (2013) 113:1087–96. doi: 10.1161/circresaha.113.301811

102. O'Connor AT, Clark MA. Astrocytes and the renin angiotensin system: relevance in disease pathogenesis. *Neurochem Res*. (2018) 43:1297–307. doi: 10.1007/s11064-018-2557-0

103. Park MH, Kim HN, Lim JS, Ahn JS, Koh JY. Angiotensin ii potentiates zinc-induced cortical neuronal death by acting on angiotensin ii type 2 receptor. *Mol Brain*. (2013) 6:50. doi: 10.1186/1756-6606-6-50

104. O'Connor AT, Clark MA. Angiotensin ii induces cyclooxygenase 2 expression in rat astrocytes via the angiotensin type 1 receptor. *Neuropeptides*. (2019) 77:101958. doi: 10.1016/j.npep.2019.101958

105. Gowrisankar YV, Clark MA. Angiotensin ii induces interleukin-6 expression in astrocytes: role of reactive oxygen species and nf-Kb. *Mol Cell Endocrinol*. (2016) 437:130–41. doi: 10.1016/j.mce.2016.08.013

106. Clark MA, Nguyen C, Tran H. Angiotensin iii induces C-jun N-terminal kinase leading to proliferation of rat astrocytes. *Neurochem Res*. (2012) 37:1475–81. doi: 10.1007/s11064-012-0738-9

107. Tsai SF, Hsu PL, Chen YW, Hossain MS, Chen PC, Tzeng SF, et al. High-fat diet induces depression-like phenotype via astrocyte-mediated hyperactivation of ventral hippocampal glutamatergic afferents to the nucleus accumbens. *Mol Psychiatry*. (2022) 27:4372–84. doi: 10.1038/s41380-022-01787-1

108. Li Y, Cheng Y, Zhou Y, Du H, Zhang C, Zhao Z, et al. High fat diet-induced obesity leads to depressive and anxiety-like behaviors in mice via ampk/mtor-mediated autophagy. *Exp Neurol*. (2022) 348:113949. doi: 10.1016/j.expneurol.2021.113949

109. Yu G, Cao F, Hou T, Cheng Y, Jia B, Yu L, et al. Astrocyte reactivation in medial prefrontal cortex contributes to obesity-promoted depressive-like behaviors. *J Neuroinflamm*. (2022) 19:166. doi: 10.1186/s12974-022-02529-4

110. Zhan M, Liu X, Xia X, Yang Y, Xie Y, Zhang L, et al. Promotion of Neuroinflammation by the Glymphatic System: A New Insight into Ethanol Extracts

from Alisma Orientale in Alleviating Obesity-Associated Cognitive Impairment. *Phytomedicine*. (2024) 122:155147. doi: 10.1016/j.phymed.2023.155147

111. Lau BK, Murphy-Royal C, Kaur M, Qiao M, Bains JS, Gordon GR, et al. Obesity-induced astrocyte dysfunction impairs heterosynaptic plasticity in the orbitofrontal cortex. *Cell Rep*. (2021) 36:109563. doi: 10.1016/j.celrep.2021.109563

112. Calvo-Ochoa E, Hernández-Ortega K, Ferrera P, Morimoto S, Arias C. Short-term high-fat-and-fructose feeding produces insulin signaling alterations accompanied by neurite and synaptic reduction and astroglial activation in the rat hippocampus. *J Cereb Blood Flow Metab*. (2014) 34:1001–8. doi: 10.1038/jcbfm.2014.48

113. Liu WC, Wu CW, Tain YL, Fu MH, Hung CY, Chen IC, et al. Oral pioglitazone ameliorates fructose-induced peripheral insulin resistance and hippocampal gliosis but not restores inhibited hippocampal adult neurogenesis. *Biochim Biophys Acta Mol Basis Dis*. (2018) 1864:274–85. doi: 10.1016/j.bbadis.2017.10.017

114. Kim N, Lee J, Song HS, Oh YJ, Kwon MS, Yun M, et al. Kimchi intake alleviates obesity-induced neuroinflammation by modulating the gut-brain axis. *Food Res Int*. (2022) 158:111533. doi: 10.1016/j.foodres.2022.111533

115. Jin S, Kim KK, Park BS, Kim DH, Jeong B, Kang D, et al. Function of astrocyte myd88 in high-fat-diet-induced hypothalamic inflammation. *J Neuroinflamm*. (2020) 17:195. doi: 10.1186/s12974-020-01846-w

116. Mongin AA. Astrocytes on "Cholesteroids": the size- and function-promoting effects of a high-fat diet on hippocampal astroglia. *Acta Physiol (Oxf)*. (2022) 236: e13859. doi: 10.1111/apha.13859

117. González-García I, García-Cáceres C. Hypothalamic astrocytes as a specialized and responsive cell population in obesity. *Int J Mol Sci*. (2021) 22:6176. doi: 10.3390/ijms22126176

118. Varela L, Kim JG, Fernández-Tussy P, Aryal B, Liu ZW, Fernández-Hernando C, et al. Astrocytic lipid metabolism determines susceptibility to diet-induced obesity. *Sci Adv*. (2021) 7:eabj2814. doi: 10.1126/sciadv.abj2814

119. Popov A, Brazhe N, Fedotova A, Tiaglik A, Bychkov M, Morozova K, et al. A high-fat diet changes astrocytic metabolism to promote synaptic plasticity and behavior. *Acta Physiol (Oxf)*. (2022) 236:e13847. doi: 10.1111/apha.13847

120. Gao Y, Layritz C, Legutko B, Eichmann TO, Laperrousaz E, Moullé VS, et al. Disruption of lipid uptake in astroglia exacerbates diet-induced obesity. *Diabetes*. (2017) 66:2555–63. doi: 10.2337/db16-1278

121. Liu X, Zheng H. Leptin-mediated sympathoexcitation in obese rats: role for neuron-astrocyte crosstalk in the arcuate nucleus. *Front Neurosci*. (2019) 13:1217. doi: 10.3389/fnins.2019.01217

122. Dalvi PS, Chalmers JA, Luo V, Han DY, Wellhauser L, Liu Y, et al. High fat induces acute and chronic inflammation in the hypothalamus: effect of high-fat diet, palmitate and tnf-A on appetite-regulating npy neurons. *Int J Obes (Lond)*. (2017) 41:149–58. doi: 10.1038/ijo.2016.183

123. Lorenzo PI, Martin Vazquez E, López-Noriega L, Fuente-Martín E, Mellado-Gil JM, Franco JM, et al. The metabesity factor hmg20a potentiates astrocyte survival and reactive astrogliosis preserving neuronal integrity. *Theranostics*. (2021) 11:6983–7004. doi: 10.7150/thno.57237

124. Lam YY, Tsai SF, Chen PC, Kuo YM, Chen YW. Pioglitazone rescues high-fat diet-induced depression-like phenotypes and hippocampal astrocytic deficits in mice. *BioMed Pharmacother*. (2021) 140:111734. doi: 10.1016/j.biopha.2021.111734

125. Cassano V, Tallarico M, Armentaro G, De Sarro C, Iannone M, Leo A, et al. Ranolazine attenuates brain inflammation in a rat model of type 2 diabetes. *Int J Mol Sci*. (2022) 23:16160. doi: 10.3390/ijms232416160

126. Saieva S, Taglialatela G. Near-infrared light reduces glia activation and modulates neuroinflammation in the brains of diet-induced obese mice. *Sci Rep*. (2022) 12:10848. doi: 10.1038/s41598-022-14812-8

127. Rahman MH, Bhusal A, Kim JH, Jha MK, Song GJ, Go Y, et al. Astrocytic pyruvate dehydrogenase kinase-2 is involved in hypothalamic inflammation in mouse models of diabetes. *Nat Commun*. (2020) 11:5906. doi: 10.1038/s41467-020-19576-1

128. Bhusal A, Rahman MH, Lee IK, Suk K. Role of hippocampal lipocalin-2 in experimental diabetic encephalopathy. *Front Endocrinol (Lausanne)*. (2019) 10:25. doi: 10.3389/fendo.2019.00025

129. Tomassoni D, Nwankwo IE, Gabrielli MG, Bhatt S, Muhammad AB, Lokhandwala MF, et al. Astrogliosis in the brain of obese zucker rat: A model of metabolic syndrome. *Neurosci Lett*. (2013) 543:136–41. doi: 10.1016/j.neulet.2013.03.025

130. Shi S, Yin HJ, Li J, Wang L, Wang WP, Wang XL. Studies of pathology and pharmacology of diabetic encephalopathy with kk-ay mouse model. *CNS Neurosci Ther*. (2020) 26:332–42. doi: 10.1111/cns.13201

131. Zheng Y, Yang Y, Dong B, Zheng H, Lin X, Du Y, et al. Metabonomic profiles delineate potential role of glutamate-glutamine cycle in db/db mice with diabetes-associated cognitive decline. *Mol Brain*. (2016) 9:40. doi: 10.1186/s13041-016-0223-5

132. An JR, Liu JT, Gao XM, Wang QF, Sun GY, Su JN, et al. Effects of liraglutide on astrocyte polarization and neuroinflammation in db/db mice: focus on iron overload and oxidative stress. *Front Cell Neurosci*. (2023) 17:1136070. doi: 10.3389/fncel.2023.1136070

133. Zheng J, Xie Y, Ren L, Qi L, Wu L, Pan X, et al. Glp-1 improves the supportive ability of astrocytes to neurons by promoting aerobic glycolysis in Alzheimer's disease. *Mol Metab*. (2021) 47:101180. doi: 10.1016/j.molmet.2021.101180

134. Robb JL, Hammad NA, Weightman Potter PG, Chilton JK, Beall C, Ellacott KLJ. The metabolic response to inflammation in astrocytes is regulated by nuclear factor-kappa B signaling. *Glia*. (2020) 68:2246–63. doi: 10.1002/glia.23835

135. Robb JL, Morrissey NA, Weightman Potter PG, Smithers HE, Beall C, Ellacott KLJ. Immunometabolic changes in glia - a potential role in the pathophysiology of obesity and diabetes. *Neuroscience*. (2020) 447:167–81. doi: 10.1016/j.neuroscience.2019.10.021

136. Li W, Roy Choudhury G, Winters A, Prah J, Lin W, Liu R, et al. Hyperglycemia alters astrocyte metabolism and inhibits astrocyte proliferation. *Aging Dis*. (2018) 9:674–84. doi: 10.14336/ad.2017.1208

137. Wang D, Zhao L, Zheng H, Dong M, Pan L, Zhang X, et al. Time-dependent lactate production and amino acid utilization in cultured astrocytes under high glucose exposure. *Mol Neurobiol*. (2018) 55:1112–22. doi: 10.1007/s12035-016-0360-y

138. Staricha K, Meyers N, Garvin J, Liu Q, Rarick K, Harder D, et al. Effect of high glucose condition on glucose metabolism in primary astrocytes. *Brain Res*. (2020) 1732:146702. doi: 10.1016/j.brainres.2020.146702

139. Takahashi S, Izawa Y, Suzuki N. Astroglial pentose phosphate pathway rates in response to high-glucose environments. *ASN Neuro*. (2012) 4:e00078. doi: 10.1042/an20120002

140. Abdyeva A, Kurtova E, Savinkova I, Galkov M, Gorbacheva L. Long-term exposure of cultured astrocytes to high glucose impact on their lps-induced activation. *Int J Mol Sci*. (2024) 25:1122. doi: 10.3390/ijms25021122

141. Bahniwal M, Little JP, Klegeris A. High glucose induces pro-inflammatory phenotype in human astrocytes and enhances neurotoxicity. *FASEB J*. (2013) 27:691. doi: 10.1096/fasebj.27.1_supplement.691.8

142. Wanrooy BJ, Kumar KP, Wen SW, Qin CX, Ritchie RH, Wong CHY. Distinct contributions of hyperglycemia and high-fat feeding in metabolic syndrome-induced neuroinflammation. *J Neuroinflamm*. (2018) 15:293. doi: 10.1186/s12974-018-1329-8

143. Hsieh HL, Wang HH, Wu WB, Chu PJ, Yang CM. Transforming growth factor-B1 induces matrix metalloproteinase-9 and cell migration in astrocytes: roles of ros-dependent erk- and jnk-nf-Kb pathways. *J Neuroinflamm*. (2010) 7:88. doi: 10.1186/1742-2094-7-88

144. Hsieh HL, Lin CC, Hsiao LD, Yang CM. High glucose induces reactive oxygen species-dependent matrix metalloproteinase-9 expression and cell migration in brain astrocytes. *Mol Neurobiol*. (2013) 48:601–14. doi: 10.1007/s12035-013-8442-6

145. Chistyakov DV, Azbukina NV, Astakhova AA, Polozhintsev AI, Sergeeva MG, Reiser G. Toll-like receptors control P38 and jnk mapk signaling pathways in rat astrocytes differently, when cultured in normal or high glucose concentrations. *Neurochem Int*. (2019) 131:104513. doi: 10.1016/j.neuint.2019.104513

146. Gandhi GK, Ball KK, Cruz NF, Dienel GA. Hyperglycaemia and diabetes impair gap junctional communication among astrocytes. *ASN Neuro*. (2010) 2:e00030. doi: 10.1042/an20090048

147. Garvin J, Semenikhina M, Liu Q, Rarick K, Isaeva E, Levchenko V, et al. Astrocytic responses to high glucose impair barrier formation in cerebral microvessel endothelial cells. *Am J Physiol Regul Integr Comp Physiol*. (2022) 322:R571–r80. doi: 10.1152/ajpregu.00315.2020

148. Zhao Y, Luo C, Chen J, Sun Y, Pu D, Lv A, et al. High glucose-induced complement component 3 up-regulation via rage-P38mapk-nf-Kb signalling in astrocytes: *in vivo* and *in vitro* studies. *J Cell Mol Med*. (2018) 22:6087–98. doi: 10.1111/jcmm.13884

149. Kirschen GW, Kéry R, Ge S. The hippocampal neuro-glio-vascular network: metabolic vulnerability and potential neurogenic regeneration in disease. *Brain Plast*. (2018) 3:129–44. doi: 10.3233/bpl-170055

150. Lawal O, Ulloa Severino FP, Eroglu C. The role of astrocyte structural plasticity in regulating neural circuit function and behavior. *Glia*. (2022) 70:1467–83. doi: 10.1002/glia.24191

151. Mills WA 3rd, Woo AM, Jiang S, Martin J, Surendran D, Bergstresser M, et al. Astrocyte plasticity in mice ensures continued endfoot coverage of cerebral blood vessels following injury and declines with age. *Nat Commun*. (2022) 13:1794. doi: 10.1038/s41467-022-29475-2

152. Hayden MR. Hypothesis: astrocyte foot processes detachment from the neurovascular unit in female diabetic mice may impair modulation of information processing-six degrees of separation. *Brain Sci*. (2019) 9:83. doi: 10.3390/brainsci9040083

153. Stranahan AM. Visceral adiposity, inflammation, and hippocampal function in obesity. *Neuropharmacology*. (2022) 205:108920. doi: 10.1016/j.neuropharm.2021.108920

154. de Paula GC, Brunetta HS, Engel DF, Gaspar JM, Velloso LA, Engblom D, et al. Hippocampal function is impaired by a short-term high-fat diet in mice: increased blood-brain barrier permeability and neuroinflammation as triggering events. *Front Neurosci*. (2021) 15:734158. doi: 10.3389/fnins.2021.734158

155. Horvath TL, Sarman B, García-Cáceres C, Enriori PJ, Sotonyi P, Shanabrough M, et al. Synaptic input organization of the melanocortin system predicts diet-induced hypothalamic reactive gliosis and obesity. *Proc Natl Acad Sci U.S.A*. (2010) 107:14875–80. doi: 10.1073/pnas.1004282107

156. Gruber T, Pan C, Contreras RE, Wiedemann T, Morgan DA, Skowronski AA, et al. Obesity-associated hyperleptinemia alters the gliovascular interface of the

hypothalamus to promote hypertension. *Cell Metab*. (2021) 33:1155–70.e10. doi: 10.1016/j.cmet.2021.04.007

157. Yamagata K, Tagami M, Nara Y, Fujino H, Kubota A, Numano F, et al. Faulty induction of blood-brain barrier functions by astrocytes isolated from stroke-prone spontaneously hypertensive rats. *Clin Exp Pharmacol Physiol*. (1997) 24:686–91. doi: 10.1111/j.1440-1681.1997.tb02113.x

158. Tsai SF, Wu HT, Chen PC, Chen YW, Yu M, Wang TF, et al. High-fat diet suppresses the astrocytic process arborization and downregulates the glial glutamate transporters in the hippocampus of mice. *Brain Res*. (2018) 1700:66–77. doi: 10.1016/j.brainres.2018.07.017

159. Cano V, Valladolid-Acebes I, Hernández-Nuño F, Merino B, del Olmo N, Chowen JA, et al. Morphological changes in glial fibrillary acidic protein immunopositive astrocytes in the hippocampus of dietary-induced obese mice. *NeuroReport*. (2014) 25:819–22. doi: 10.1097/WNR.0000000000000180

160. Zhang Y, Reichel JM, Han C, Zuniga-Hertz JP, Cai D. Astrocytic process plasticity and ikkβ/nf-Kb in central control of blood glucose, blood pressure, and body weight. *Cell Metab*. (2017) 25:1091–102.e4. doi: 10.1016/j.cmet.2017.04.002

161. Kwon HS, Koh SH. Neuroinflammation in neurodegenerative disorders: the roles of microglia and astrocytes. *Transl Neurodegener*. (2020) 9:42. doi: 10.1186/s40035-020-00221-2

162. Williams JL, Manivasagam S, Smith BC, Sim J, Vollmer LL, Daniels BP, et al. Astrocyte-T cell crosstalk regulates region-specific neuroinflammation. *Glia*. (2020) 68:1361–74. doi: 10.1002/glia.23783

163. Bhusal A, Afridi R, Lee WH, Suk K. Bidirectional communication between microglia and astrocytes in neuroinflammation. *Curr Neuropharmacol*. (2023) 21:2020–9. doi: 10.2174/1570159x21666221129121715

164. Colombo E, Farina C. Astrocytes: key regulators of neuroinflammation. *Trends Immunol*. (2016) 37:608–20. doi: 10.1016/j.it.2016.06.006

165. Carter SF, Herholz K, Rosa-Neto P, Pellerin L, Nordberg A, Zimmer ER. Astrocyte biomarkers in Alzheimer's disease. *Trends Mol Med*. (2019) 25:77–95. doi: 10.1016/j.molmed.2018.11.006

166. Bruna B, João Pedro F-S, Lucas Uglione da R, Stephen FC, Elena R-V, Agneta N, et al. Astrocyte biomarkers in Alzheimer disease. *Neurology*. (2021) 96:e2944. doi: 10.1212/WNL.0000000000012109

167. Lian H, Litvinchuk A, Chiang AC, Aithmitti N, Jankowsky JL, Zheng H. Astrocyte-microglia cross talk through complement activation modulates amyloid pathology in mouse models of Alzheimer's disease. *J Neurosci*. (2016) 36:577–89. doi: 10.1523/jneurosci.2117-15.2016

168. Du M, Jiang T, He S, Cheng B, Zhang X, Li L, et al. Sigma-1 receptor as a protective factor for diabetes-associated cognitive dysfunction via regulating astrocytic endoplasmic reticulum-mitochondrion contact and endoplasmic reticulum stress. *Cells*. (2023) 12:197. doi: 10.3390/cells12010197

169. Meng F, Fu J, Zhang L, Guo M, Zhuang P, Yin Q, et al. Function and therapeutic value of astrocytes in diabetic cognitive impairment. *Neurochem Int*. (2023) 169:105591. doi: 10.1016/j.neuint.2023.105591

170. Afsari ZH, Renno WM, Abd-El-Basset E. Alteration of glial fibrillary acidic proteins immunoreactivity in astrocytes of the spinal cord diabetic rats. *Anat Rec (Hoboken)*. (2008) 291:390–9. doi: 10.1002/ar.20678

171. Bondan E, Cardoso C, Martins MF, Otton R. Obesity in rats causes hippocampal astrogliosis. *J Comp Pathol*. (2019) 166:148. doi: 10.1016/j.jcpa.2018.10.158

172. Buckman LB, Thompson MM, Moreno HN, Ellacott KL. Regional astrogliosis in the mouse hypothalamus in response to obesity. *J Comp Neurol*. (2013) 521:1322–33. doi: 10.1002/cne.23233

173. Douglass JD, Dorfman MD, Fasnacht R, Shaffer LD, Thaler JP. Astrocyte ikkβ/nf-Kb signaling is required for diet-induced obesity and hypothalamic inflammation. *Mol Metab*. (2017) 6:366–73. doi: 10.1016/j.molmet.2017.01.010

174. Lin L, Basu R, Chatterjee D, Templin AT, Flak JN, Johnson TS. Disease-associated astrocytes and microglia markers are upregulated in mice fed high fat diet. *Sci Rep*. (2023) 13:12919. doi: 10.1038/s41598-023-39890-0

175. Wasilewski D, Villalba-Moreno ND, Stange I, Glatzel M, Sepulveda-Falla D, Krasemann S. Reactive astrocytes contribute to Alzheimer's disease-related neurotoxicity and synaptotoxicity in a neuron-astrocyte co-culture assay. *Front Cell Neurosci*. (2021) 15:739411. doi: 10.3389/fncel.2021.739411

176. Saggu R, Schumacher T, Gerich F, Rakers C, Tai K, Delekate A, et al. Astroglial nf-kb contributes to white matter damage and cognitive impairment in a mouse model of vascular dementia. *Acta Neuropathol Commun*. (2016) 4:76. doi: 10.1186/s40478-016-0350-3

177. Sadick JS, Liddelow SA. Don't forget astrocytes when targeting Alzheimer's disease. *Br J Pharmacol*. (2019) 176:3585–98. doi: 10.1111/bph.14568

178. Henn RE, Noureldein MH, Elzinga SE, Kim B, Savelieff MG, Feldman EL. Glial-neuron crosstalk in health and disease: A focus on metabolism, obesity, and cognitive impairment. *Neurobiol Dis*. (2022) 170:105766. doi: 10.1016/j.nbd.2022.105766

179. Chen Z, Yuan Z, Yang S, Zhu Y, Xue M, Zhang J, et al. Brain energy metabolism: astrocytes in neurodegenerative diseases. *CNS Neurosci Ther*. (2023) 29:24–36. doi: 10.1111/cns.13982

180. Zyśk M, Beretta C, Naia L, Dakhel A, Påvénius L, Brismar H, et al. Amyloid-B Accumulation in human astrocytes induces mitochondrial disruption and changed energy metabolism. *J Neuroinflamm*. (2023) 20:43. doi: 10.1186/s12974-023-02722-z

181. Morita M, Ikeshima-Kataoka H, Kreft M, Vardjan N, Zorec R, Noda M. Metabolic plasticity of astrocytes and aging of the brain. *Int J Mol Sci*. (2019) 20:941. doi: 10.3390/ijms20040941

182. Heni M, Eckstein SS, Schittenhelm J, Böhm A, Hogrefe N, Irmler M, et al. Ectopic fat accumulation in human astrocytes impairs insulin action. *R Soc Open Sci*. (2020) 7:200701. doi: 10.1098/rsos.200701

183. Castellanos DB, Martín-Jiménez CA, Pinzón A, Barreto GE, Padilla-González GF, Aristizábal A, et al. Metabolomic analysis of human astrocytes in lipotoxic condition: potential biomarker identification by machine learning modeling. *Biomolecules*. (2022) 12:986. doi: 10.3390/biom12070986

184. van Deijk AF, Camargo N, Timmerman J, Heistek T, Brouwers JF, Mogavero F, et al. Astrocyte lipid metabolism is critical for synapse development and function *in vivo*. *Glia*. (2017) 65:670–82. doi: 10.1002/glia.23120

185. Ferris HA, Perry RJ, Moreira GV, Shulman GI, Horton JD, Kahn CR. Loss of astrocyte cholesterol synthesis disrupts neuronal function and alters whole-body metabolism. *Proc Natl Acad Sci U.S.A*. (2017) 114:1189–94. doi: 10.1073/pnas.1620506114

186. Cao Y, Wang G, Li Z. The effects of antidiabetic drugs on cerebral metabolism in mice with central insulin resistance. *Diabetes*. (2018) 67:247–LB. doi: 10.2337/db18-247-LB

187. Fernandez AM, Hernandez-Garzón E, Perez-Domper P, Perez-Alvarez A, Mederos S, Matsui T, et al. Insulin regulates astrocytic glucose handling through cooperation with igf-I. *Diabetes*. (2017) 66:64–74. doi: 10.2337/db16-0861

188. Cai W, Xue C, Sakaguchi M, Konishi M, Shirazian A, Ferris HA, et al. Insulin regulates astrocyte gliotransmission and modulates behavior. *J Clin Invest*. (2018) 128:2914–26. doi: 10.1172/jci99366

189. Mitra S, Banik A, Saurabh S, Maulik M, Khatri SN. Neuroimmunometabolism: A new pathological nexus underlying neurodegenerative disorders. *J Neurosci*. (2022) 42:1888–907. doi: 10.1523/jneurosci.0998-21.2022

190. Vizuete AFK, Fróes F, Seady M, Zanotto C, Bobermin LD, Roginski AC, et al. Early effects of lps-induced neuroinflammation on the rat hippocampal glycolytic pathway. *J Neuroinflamm*. (2022) 19:255. doi: 10.1186/s12974-022-02612-w

191. Iglesias J, Morales L, Barreto GE. Metabolic and inflammatory adaptation of reactive astrocytes: role of ppars. *Mol Neurobiol*. (2017) 54:2518–38. doi: 10.1007/s12035-016-9833-2

192. Bolaños JP. Bioenergetics and redox adaptations of astrocytes to neuronal activity. *J Neurochem*. (2016) 139 Suppl 2:115–25. doi: 10.1111/jnc.13486

193. Meyer T, Shimon D, Youssef S, Yankovitz G, Tessler A, Chernobylsky T, et al. Nad(+) metabolism drives astrocyte proinflammatory reprogramming in central nervous system autoimmunity. *Proc Natl Acad Sci U.S.A*. (2022) 119:e2211310119. doi: 10.1073/pnas.2211310119

194. Galea E, Weinstock LD, Larramona-Arcas R, Pybus AF, Giménez-Llort L, Escartin C, et al. Multi-transcriptomic analysis points to early organelle dysfunction in human astrocytes in Alzheimer's disease. *Neurobiol Dis*. (2022) 166:105655. doi: 10.1016/j.nbd.2022.105655

195. Bolsewig K, Hok-A-Hin YS, Sepe FN, Boonkamp L, Jacobs D, Bellomo G, et al. A panel of novel astrocytic and synaptic biomarkers in serum and csf for the differential diagnosis of frontotemporal dementia. *Alzheimer's Dementia*. (2021) 17:e051338. doi: 10.1002/alz.051338

196. Ferrari-Souza JP, Ferreira PCL, Bellaver B, Tissot C, Wang YT, Leffa DT, et al. Astrocyte biomarker signatures of amyloid-B and tau pathologies in Alzheimer's disease. *Mol Psychiatry*. (2022) 27:4781–9. doi: 10.1038/s41380-022-01716-2

197. Johnson ECB, Dammer EB, Duong DM, Ping L, Zhou M, Yin L, et al. Large-scale proteomic analysis of Alzheimer's disease brain and cerebrospinal fluid reveals early changes in energy metabolism associated with microglia and astrocyte activation. *Nat Med*. (2020) 26:769–80. doi: 10.1038/s41591-020-0815-6

198. Wang X, Yang H, Liu C, Liu K. A new diagnostic tool for brain disorders: extracellular vesicles derived from neuron, astrocyte, and oligodendrocyte. *Front Mol Neurosci*. (2023) 16:1194210. doi: 10.3389/fnmol.2023.1194210

199. Gayen M, Bhomia M, Balakathiresan N, Knollmann-Ritschel B. Exosomal micrornas released by activated astrocytes as potential neuroinflammatory biomarkers. *Int J Mol Sci*. (2020) 21:2312. doi: 10.3390/ijms21072312

200. Giannoni P, Arango-Lievano M, Neves ID, Rousset MC, Baranger K, Rivera S, et al. Cerebrovascular pathology during the progression of experimental Alzheimer's disease. *Neurobiol Dis*. (2016) 88:107–17. doi: 10.1016/j.nbd.2016.01.001

201. Selvakumar R, Muhammad MR. Diagnostic computational model for neuronal disorder through glycogen metabolism in astrocytes. *Int J Comput Sci Math*. (2018) 9:232–9. doi: 10.1504/IJCSM.2018.093151

202. Gorshkov K, Aguisanda F, Thorne N, Zheng W. Astrocytes as targets for drug discovery. *Drug Discovery Today*. (2018) 23:673–80. doi: 10.1016/j.drudis.2018.01.011

203. Stogsdill JA, Harwell CC, Goldman SA. Astrocytes as master modulators of neural networks: synaptic functions and disease-associated dysfunction of astrocytes. *Ann N Y Acad Sci*. (2023) 1525:41–60. doi: 10.1111/nyas.15004

204. Linnerbauer M, Wheeler MA, Quintana FJ. Astrocyte crosstalk in cns inflammation. *Neuron*. (2020) 108:608–22. doi: 10.1016/j.neuron.2020.08.012

205. Bowman CC, Rasley A, Tranguch SL, Marriott I. Cultured astrocytes express toll-like receptors for bacterial products. *Glia*. (2003) 43:281–91. doi: 10.1002/glia.10256

206. Nakano-Kobayashi A, Canela A, Yoshihara T, Hagiwara M. Astrocyte-targeting therapy rescues cognitive impairment caused by neuroinflammation via the nrf2 pathway. *Proc Natl Acad Sci U.S.A.* (2023) 120:e2303809120. doi: 10.1073/pnas.2303809120

207. Klegeris A. Targeting neuroprotective functions of astrocytes in neuroimmune diseases. *Expert Opin Ther Targets.* (2021) 25:237–41. doi: 10.1080/14728222.2021.1915993

208. De Bock M, De Smet M, Verwaerde S, Tahiri H, Schumacher S, Van Haver V, et al. Targeting gliovascular connexins prevents inflammatory blood-brain barrier leakage and astrogliosis. *JCI Insight.* (2022) 7:e135263. doi: 10.1172/jci.insight.135263

209. de Pablo Y, Chen M, Möllerström E, Pekna M, Pekny M. Drugs targeting intermediate filaments can improve neurosupportive properties of astrocytes. *Brain Res Bull.* (2018) 136:130–8. doi: 10.1016/j.brainresbull.2017.01.021

210. Barros LF, Schirmeier S, Weber B. The astrocyte: metabolic hub of the brain. *Cold Spring Harb Perspect Biol.* (2024). doi: 10.1101/cshperspect.a041355

211. Beard E, Lengacher S, Dias S, Magistretti PJ, Finsterwald C. Astrocytes as key regulators of brain energy metabolism: new therapeutic perspectives. *Front Physiol.* (2021) 12:825816. doi: 10.3389/fphys.2021.825816

212. Magistretti PJ, Allaman I. Lactate in the brain: from metabolic end-product to signalling molecule. *Nat Rev Neurosci.* (2018) 19:235–49. doi: 10.1038/nrn.2018.19

213. Horvat A, Vardjan N, Zorec R. Targeting astrocytes for treating neurological disorders: carbon monoxide and noradrenaline-induced increase in lactate. *Curr Pharm Des.* (2017) 23:4969–78. doi: 10.2174/1381612823666170622112734

214. Hohnholt MC, Blumrich EM, Waagepetersen HS, Dringen R. The antidiabetic drug metformin decreases mitochondrial respiration and tricarboxylic acid cycle activity in cultured primary rat astrocytes. *J Neurosci Res.* (2017) 95:2307–20. doi: 10.1002/jnr.24050

215. Pilipenko V, Narbute K, Pupure J, Langrate IK, Muceniece R, Kluša V. Neuroprotective potential of antihyperglycemic drug metformin in streptozocin-induced rat model of sporadic Alzheimer's disease. *Eur J Pharmacol.* (2020) 881:173290. doi: 10.1016/j.ejphar.2020.173290

216. Monney M, Jornayvaz FR, Gariani K. Glp-1 receptor agonists effect on cognitive function in patients with and without type 2 diabetes. *Diabetes Metab.* (2023) 49:101470. doi: 10.1016/j.diabet.2023.101470

217. Gejl M, Gjedde A, Egefjord L, Møller A, Hansen SB, Vang K, et al. In Alzheimer's disease, 6-month treatment with glp-1 analog prevents decline of brain glucose metabolism: randomized, placebo-controlled, double-blind clinical trial. *Front Aging Neurosci.* (2016) 8:108. doi: 10.3389/fnagi.2016.00108

218. Takahashi K, Yamanaka S. Induction of pluripotent stem cells from mouse embryonic and adult fibroblast cultures by defined factors. *Cell.* (2006) 126:663–76. doi: 10.1016/j.cell.2006.07.024

219. Colin A, Faideau M, Dufour N, Auregan G, Hassig R, Andrieu T, et al. Engineered lentiviral vector targeting astrocytes *in vivo*. *Glia.* (2009) 57:667–79. doi: 10.1002/glia.20795

220. Wang L-L, Serrano C, Zhong X, Ma S, Zou Y, Zhang C-L. Revisiting astrocyte to neuron conversion with lineage tracing *in vivo*. *Cell.* (2021) 184:5465–81.e16. doi: 10.1016/j.cell.2021.09.005

221. Farhangi S, Dehghan S, Totonchi M, Javan M. *In vivo* conversion of astrocytes to oligodendrocyte lineage cells in adult mice demyelinated brains by sox2. *Mult Scler Relat Disord.* (2019) 28:263–72. doi: 10.1016/j.msard.2018.12.041

222. Liu X, Li C, Li J, Xie L, Hong Z, Zheng K, et al. Egf signaling promotes the lineage conversion of astrocytes into oligodendrocytes. *Mol Med.* (2022) 28:50. doi: 10.1186/s10020-022-00478-5

223. Zare L, Baharvand H, Javan M. *In vivo* conversion of astrocytes to oligodendrocyte lineage cells using chemicals: targeting gliosis for myelin repair. *Regener Med.* (2018) 13:803–19. doi: 10.2217/rme-2017-0155

224. Zhang Y, Barres BA. Astrocyte heterogeneity: an underappreciated topic in neurobiology. *Curr Opin Neurobiol.* (2010) 20:588–94. doi: 10.1016/j.conb.2010.06.005

225. Hoang T, Kim DW, Appel H, Ozawa M, Zheng S, Kim J, et al. Ptbp1 deletion does not induce astrocyte-to-neuron conversion. *Nature.* (2023) 618:E1–e7. doi: 10.1038/s41586-023-06066-9

226. Wang LL, Serrano C, Zhong X, Ma S, Zou Y, Zhang CL. Revisiting astrocyte to neuron conversion with lineage tracing *in vivo*. *Cell.* (2021) 184:5465–81.e16. doi: 10.1016/j.cell.2021.09.005

10.3389/fendo.2024.1393253

Glossary

18F-FDG	18F-fluorodeoxyglucose
AMPK	5'-AMP-activated protein kinase
PFKFB3	6-phosphofructose-2-kinase/fructose-2 6-bisphosphatase isoform 3
AGEs	Advanced glycation end products
AGT	Ang II precursor molecule angiotensinogen
ANG-1	Angiopoietin-1
ANG	Angiotensin
ACfp	Astrocyte end-feet foot processes
ACfp	Astrocyte endfoot processes
BBB	Blood-brain barrier
CCL2	C-C motif chemokine ligand 2
CBF	Cerebral blood flow
YKL-40	Chitinase-3-like protein 1
CNTF	Ciliary neurotrophic factor
C4b	Complement 4b
Cx43	Connexin 43
CXCL10	C-X-C motif chemokine ligand 10
Ddr1	Discoidin domain receptor 1
EAAT	Excitatory amino acid transporter protein
EVs	Extracellular vesicles
FAs	Fatty acids
GFAP	Glial fibrillary acidic protein
GLUT1	Glucose transporter type 1
GLAST	Glutamate aspartate transporter
GLT-1	Glutamate transporter subtype 1
GAPDH	Glyceraldehyde 3-phosphate dehydrogenase
HSP70	Heat shock protein 70
HDL	High density lipoprotein
HFD	High fat diet
HIF-1α	hypoxia-inducible factor 1-alpha
HIF-1α	hypoxia-inducible factor 1-alpha
IKK β	Inhibitor kappa B kinase β
IR	Insulin resistance
IGF-1	Insulin-like growth factor-1
IKK β	IκB kinase β
LDHB	Lactate dehydrogenase B-chain
LDs	Lipid droplets
LPS	Lipopolysaccharide

(Continued)

Continued

LTP	Long-term potentiation
LDL	Low density lipoprotein
MetS	Metabolic syndrome
MCT	Monocarboxylate transporter
mGluR5	Metabotropic glutamate receptor 5
MAO-B	Monoamine oxidase-B
NPY	Neuropeptide Y
NVU	Neurovascular unit
NAD+	Nicotinamide adenine dinucleotide
NAMPT	Nicotinamide phosphoribosyltransferase
NMDA	N-methyl-D-aspartic acid
NF-κB	Nuclear factor-κB
NF-κB	Nuclear transcription factor kappa B
PAPs	Perisynaptic astrocytes processes
PGC-1α	Peroxisome proliferator-activated receptor gamma coactivator-1 alpha
PPAR	Peroxisome proliferator-activated receptor
Kcnj2	Potassium inwardly rectifying channel subfamily J member 2
POMC	Proopiomelanocortin
PTG	Protein targeting glycogen
PKM	Pyruvate kinase
ROS	Reactive oxygen species
RAGEs	Receptors for advanced glycosylation end products
RAS	Renin-angiotensin system
SHH	Sonic hedgehog
Nrf2	Transcription factor NF-E2-related factor 2
TEER	Transendothelial cell electrical resistance
TRPV4	Transient potential receptor vanilloid 4
VEGF	Vascular endothelial growth factor

frontiers | Frontiers in Endocrinology

TYPE Original Research
PUBLISHED 04 June 2024
DOI 10.3389/fendo.2024.1383318

OPEN ACCESS

EDITED BY
Lin Zhu,
Vanderbilt University Medical Center,
United States

REVIEWED BY
David Araujo-Vilar,
University of Santiago de Compostela, Spain
Sun Manyi,
Nankai University, China

*CORRESPONDENCE
Baris Akinci
barisakincimd@gmail.com

RECEIVED 07 February 2024
ACCEPTED 13 May 2024
PUBLISHED 04 June 2024

CITATION
Fourman LT, Lima JG, Simha V, Cappa M, Alyaarubi S, Montenegro Jr. R, Akinci B and Santini F (2024) A rapid action plan to improve diagnosis and management of lipodystrophy syndromes.
Front. Endocrinol. 15:1383318.
doi: 10.3389/fendo.2024.1383318

A rapid action plan to improve diagnosis and management of lipodystrophy syndromes

Lindsay T. Fourman[1], Josivan Gomes Lima[2], Vinaya Simha[3], Marco Cappa[4], Saif Alyaarubi[5], Renan Montenegro Jr.[6], Baris Akinci[7,8]* and Ferruccio Santini[9]

[1]Metabolism Unit, Massachusetts General Hospital and Harvard Medical School, Boston, MA, United States, [2]Hospital Universitário Onofre Lopes, Departamento de Clinica Medica, Universidade Federal do Rio Grande do Norte, Natal, Brazil, [3]Division of Endocrinology, Mayo Clinic, Rochester, MN, United States, [4]Research Area for Innovative Therapies in Endocrinopathies Bambino Gesù Children's Hospital, IRCCS, Rome, Italy, [5]Pediatric Endocrinology, Oman Medical Specialty Board, Muscat, Oman, [6]Brazilian Group for the Study of Inherited and Acquired Lipodystrophies (BRAZLIPO), Clinical Research Unit, Walter Cantidio University Hospital, Federal University of Ceará/Ebserh, Fortaleza, Brazil, [7]Dokuz Eylul University Health Campus Technopark (DEPARK), Dokuz Eylul University, Izmir, Türkiye, [8]Department of Research Programs, Technological Research, Izmir Biomedicine and Genome Center (IBG), Izmir, Türkiye, [9]Obesity and Lipodystrophy Center, Endocrinology Unit, University Hospital of Pisa, Pisa, Italy

Introduction: Lipodystrophy syndromes are rare diseases that can present with a broad range of symptoms. Delays in diagnosis are common, which in turn, may predispose to the development of severe metabolic complications and end-organ damage. Many patients with lipodystrophy syndromes are only diagnosed after significant metabolic abnormalities arise. Prompt action by clinical teams may improve disease outcomes in lipodystrophy syndromes. The aim of the Rapid Action Plan is to serve as a set of recommendations from experts that can support clinicians with limited experience in lipodystrophy syndromes.

Methods: The Rapid Action Plan was developed using insights gathered through a series of advisory meetings with clinical experts in lipodystrophy syndromes. A skeleton template was used to facilitate interviews. A consensus document was developed, reviewed, and approved by all experts.

Results: Lipodystrophy is a clinical diagnosis. The Rapid Action Plan discusses tools that can help diagnose lipodystrophy syndromes. The roles of clinical and family history, physical exam, patient and family member photos, routine blood tests, leptin levels, skinfold measurements, imaging studies, and genetic testing are explored. Additional topics such as communicating the diagnosis to the patients/families and patient referrals are covered. A set of recommendations regarding screening and monitoring for metabolic diseases and end-organ abnormalities is presented. Finally, the treatment of lipodystrophy syndromes is reviewed.

Discussion: The Rapid Action Plan may assist clinical teams with the prompt diagnosis and holistic work-up and management of patients with lipodystrophy syndromes, which may improve outcomes for patients with this rare disease.

KEYWORDS

delay in diagnosis, disease management, lipodystrophy, screening, clinical assessment

1 Introduction

Lipodystrophies are a group of heterogeneous, rare, and irreversible conditions characterized by an absence of subcutaneous fat (1, 2). The pattern of fat loss can either be across the whole body [generalized lipodystrophy (GL)] or in specific areas [partial lipodystrophy (PL)]. Both forms of lipodystrophy syndromes (GL or PL) may be genetic or acquired, leading to four major categories: congenital generalized lipodystrophy (CGL), familial partial lipodystrophy (FPLD), acquired generalized lipodystrophy (AGL), and acquired partial lipodystrophy (APL) (3, 4). Typical characteristics of these four major categories are summarized in Table 1 (5–13). In addition to these classical categories, additional etiologies such as progeroid syndromes, complex genetic syndromes, autoimmune syndromes, and lipodystrophy induced by myeloablative therapy can also manifest with GL or PL.

Patients with lipodystrophy syndromes present with a broad range of symptoms. Clinical characteristics of lipodystrophy syndromes are heterogeneous and may depend on molecular etiology in genetic cases (14). Adipose tissue loss leads to ectopic fat accumulation which, in turn, triggers the development of severe insulin resistance and metabolic disease (15). Reduced leptin secretion contributes to the pathogenesis of lipodystrophy by adversely affecting appetite control, glucose and lipid homeostasis and metabolism (16, 17). In later stages of the disease, symptoms can include severe metabolic abnormalities (e.g., severe insulin resistance and difficult-to-treat diabetes, severe hypertriglyceridemia) and end-organ complications (e.g., non-alcoholic steatohepatitis (NASH), nephropathy, pancreatitis, cardiovascular disorders, neuromuscular system abnormalities) (1, 14, 15, 18–22).

While an international multi-society guideline exists (4) that covers the diagnosis and management of lipodystrophy syndromes, there is still a great amount of variation in the care that patients with lipodystrophy syndromes receive, including the speed with which they receive it. Despite a gradually increasing awareness of lipodystrophy syndromes among clinicians, it is still common for patients to be diagnosed only after they develop severe metabolic abnormalities and organ complications. Delays in diagnosis expose patients to the risk of developing severe metabolic disease and end-organ damage, which have already developed at the time of diagnosis in many cases (19, 23, 24). To address this knowledge gap, we aimed to create a Rapid Action Plan to support clinicians with limited experience in lipodystrophy syndromes by providing expertise from leading clinical teams. The goal of this plan is to reduce the time it takes for patients with lipodystrophy syndromes to receive a comprehensive diagnosis followed by the care and holistic support that they need.

2 Methods

This Rapid Action Plan was developed using insights gathered through a series of advisory meetings with clinical experts in lipodystrophy syndromes. A consensus meeting was held to initiate development of the Rapid Action Plan document at which time a group of international experts in lipodystrophy syndromes (United States, Brazil, Italy, Turkey, and Oman) was invited to discuss the key priorities for clinicians in the first 100 days after seeing a patient with clinical suspicion for the diagnosis. The rationale of the project, its scope and the role of expert contributors were further presented at this meeting. There was broad agreement from experts across this field that additional tools to help clinicians understand key indicators, priority tests and patient follow-up would be valuable. All parties have reviewed and endorsed the steps within this plan. The steps outlined reflect a consensus from experts on what action they would recommend given their experience. It is designed to be a reference tool for clinical teams that can complement national and international guidelines.

TABLE 1 Clinical features of four major subtypes of lipodystrophy syndromes.

Clinical feature	Generalized lipodystrophy (GL)		Partial lipodystrophy (PL)	
	Congenital generalized lipodystrophy (CGL)	Acquired generalized lipodystrophy (AGL)	Familial partial lipodystrophy (FPLD)	Acquired partial lipodystrophy (APL)
Fat loss and distribution pattern	Near total absence of body fat starting at birth or shortly after	Progressive loss of fat leading to near-complete lack of adipose tissue	Partial loss of fat predominantly affecting the limbs	Gradual loss of adipose tissue from head downwards
Family history	Yes, consanguinity (usually AR)	No	Yes (usually AD)	No
Associated diseases and comorbidities	Metabolic abnormalities are severe and usually start early in childhood Subtype specific features can be distinctive*	Low serum complement 3 and 4 (C3 and C4); perilipin 1 autoantibodies Can be associated with autoimmune diseases# Metabolic abnormalities are usually severe	Metabolic abnormalities are common Metabolic abnormalities may start later than CGL but can be as severe as CGL in adulthood	Low serum complement 3 (C3) levels, glomerulonephritis Metabolic abnormalities are less common, but can vary in severity

AD, autosomal dominant; AR, autosomal recessive. *i.e., patients with CGL4 present with myopathy, skeletal abnormalities, pyloric stenosis, gastrointestinal motility problems, and cardiac arrhythmias. #e.g., juvenile dermatomyositis, autoimmune hepatitis, type 1 diabetes, panniculitis. In addition to these classical categories, there is additional etiology including progeroid syndromes, complex genetic syndromes, autoinflammatory syndromes, and myeloablative therapy induced lipodystrophy that can present with GL and PL.

A skeleton template was used to facilitate interviews with experts. The first two sections of the skeleton were developed to review general information on lipodystrophy syndromes such as explaining the main subtypes of lipodystrophy. The next section was about the Rapid Action Plan focusing on diagnosing and supporting a patient with a suspicion of lipodystrophy syndromes. The aim of this section was to generate an action plan for clinical teams that can help reach a diagnosis without delay. This section was developed to answer specific questions such as:

- What physical findings and clinical features should raise suspicion for lipodystrophy syndromes?
- What are the other differential diagnoses that are likely to be considered by peers and experts? What is the list of conditions that need to be included in differential diagnosis?
- How can I confirm the diagnosis and screen for complications and comorbidities?
- How can I educate patients about the diagnosis and available support?

Experts were asked to provide information on tools that can support prompt diagnosis and referral. The role of physical signs and clinical history, skinfolds and radiology, laboratory testing, leptin level, and genetic testing was explored. Treatment strategies for lipodystrophy syndromes following metabolic risk stratification were also discussed.

After all interviews were completed, experts were asked for a second round of meetings to review outputs from initial interviews. Based on feedback from experts, revisions were made. A consensus document was developed, reviewed, and approved by all experts.

3 Results

3.1 Diagnosing lipodystrophy syndromes

3.1.1 Physical and metabolic signs

In patients with GL, the condition may be relatively apparent due to absence of fat in the whole body, prominent veins, and increased muscular appearance. However, parents and patients can easily get accustomed to this physical appearance if GL is not diagnosed at birth, and this may delay diagnosis until the development of potentially severe metabolic abnormalities. Children with GL more frequently present with elevated liver enzymes and severe hypertriglyceridemia compared to their counterparts with PL. Abdominal distension and protrusion of the umbilical scar are common and may help with diagnosis.

PL may be more challenging to identify as fat loss is selective. Phenotype also varies according to sex, with men usually presenting with a less prominent fat distribution abnormality and less severe metabolic profile than women. In certain subtypes of lipodystrophy syndromes, such as FPLD type 2 (Dunnigan variety), abnormal fat accumulation, particularly in the face and neck, can be remarkable. Patients with FPLD may exhibit significant muscularity and phlebomegaly in the limbs, which can be remarkable in lower extremities. In pediatric patients, metabolic abnormalities can be absent so adipose tissue distribution should be carefully considered.

Other associated signs and symptoms include insatiable appetite, skin findings (e.g., acanthosis nigricans, hirsutism in women, eruptive xanthomata), skeletal abnormalities (e.g., bone cysts, scoliosis), other organ abnormalities based on molecular etiology (in genetic cases), and autoimmune features (in acquired cases).

There are several disorders that need to be considered in the differential diagnosis of GL and PL. A list of common entities is listed in Table 2 (11, 25).

- Lack of subcutaneous fat is the most critical manifestation.
- Any person with partial or complete lack of subcutaneous fat should be evaluated for the diagnosis of lipodystrophy syndromes.
- Be wary of features of metabolic syndrome in the absence of increased adiposity or high BMI.
- Lipodystrophy syndromes should be considered when metabolic symptoms are disproportionate to body size, including diabetes with high insulin requirements, hypertriglyceridemia, fatty liver disease, or polycystic ovary syndrome (PCOS).

3.1.2 Clinical and family history

Taking a detailed clinical and family history of the patient can help in diagnosing lipodystrophy syndromes and understanding the type of lipodystrophy a patient may have, especially for genetic forms of the disease. The family history should include questions about body shape as well as a history of known (or suspected) metabolic comorbidities or other clinical characteristics. It is important to remember phenotypic differences between men and women as it can be easy to overlook a male relative with lipodystrophy syndromes. Although no other family member with lipodystrophy can be detected in acquired lipodystrophies, it is important to assess for a history of autoimmunity and radiation and rule out HIV infection.

TABLE 2 Differential diagnosis of GL and PL.

Generalized lipodystrophy (GL)	Partial lipodystrophy (PL)
• Conditions associated with very lean body shape (e.g., malnutrition/ starvation, anorexia nervosa, cachexia caused by various etiology such as cancers, inflammatory disorders, hyperthyroidism, adrenal insufficiency, HIV associated wasting, diencephalic cachexia, etc.) • Constitutional thinness • Severe insulin resistance due to insulin receptor mutations • Acromegaly/pseudoacromegaly	• Truncal obesity • Metabolic syndrome • Type 2 diabetes (especially when poorly controlled and/or associated with hepatic steatosis and high triglycerides) • HIV-associated lipodystrophy • Lipodystrophy-like phenotype • Cushing syndrome

- Collating photos of patients through their lifetime can be very helpful. Sensitively ask for photos of the patient before/after symptoms (and ideally in different states of dress).
- The absence of adipose tissue can be identified at birth or within the first year of life in CGL, while fat loss develops at any time in life in AGL. In FPLD, fat loss can be detected in childhood, but it typically becomes prominent around puberty. Fat loss can start at any time in life in APL (usually in childhood, adolescence, or young adulthood).
- Photos of family members can also be helpful to assess and determine if a suspected lipodystrophy syndrome is genetic.
- Personal or family history of autoimmune diseases can be helpful.

3.1.3 Routine tests

In general, upon initial evaluation of the patient (and at follow-up appointments), routine laboratory tests should be considered to assess diabetes [e.g., fasting glucose levels, glycated hemoglobin (HbA1c)] and lipid abnormalities [fasting serum lipids (especially triglyceride levels)]. Oral glucose tolerance test (OGTT) can be considered on a case-by-case basis. In addition, liver function tests along with hepatic ultrasound and/or liver elastography to identify signs of non-alcoholic fatty liver disease (NAFLD) or hepatic fibrosis are recommended to evaluate hepatic disease. A baseline electrocardiogram (ECG) is recommended. As part of cardiac examination, an echocardiogram can be helpful to detect heart abnormalities (e.g., signs of cardiomyopathy).

- Laboratory tests should be considered to assess for insulin resistance, diabetes, and lipid abnormalities (high triglycerides and low HDL cholesterol are typical findings).
- Liver function tests along with hepatic ultrasound and/or elastography can identify signs of NAFLD and hepatic fibrosis.

3.1.4 Leptin assay

While leptin deficiency is a hallmark in the pathology of lipodystrophy syndromes, consensus among the group was that a given leptin level cannot be used to rule in or out a lipodystrophy diagnosis.

- Low leptin level is supportive but not diagnostic of lipodystrophy syndromes.
- Normal or high leptin levels do not rule out a lipodystrophy diagnosis.

3.1.5 Skinfold measurement

The panel thought that it is important to include objective measures of body composition as part of screening tools to aid in the diagnosis of lipodystrophy syndromes. This is particularly the case in PL where fat loss can be subtle. The panel agreed that skinfold measurement can be useful (particularly alongside other parameters) in the diagnosis of lipodystrophy syndromes, However, it is considered a less precise option when compared to alternative methods for measuring body fat. Where the technology and resources allow, alternatives should be considered before skinfold measurement including dual-energy x-ray absorptiometry (DXA) (see below).

- Mid-thigh skinfold thickness is easy to obtain and can be useful, but it is a rather imprecise option compared with alternatives for measuring body fat. Skin fold thickness values of the anterior thigh <10mm in adult men and <22mm in adult women are supportive information for the diagnosis of GL and FPLD (3).

3.1.6 Radiology

Where available, imaging modalities should be seen as an important objective tool to support the diagnosis of lipodystrophy syndromes. While magnetic resonance imaging (MRI) can be considered a useful tool, the panel noted that it is far less practical and more costly than dual energy X-ray absorptiometry (DXA). If physicians consider it impractical and burdensome to use MRI, it is suggested that this be reserved for research or exceptional circumstances, and that DXA is a suitable, cost-effective and appropriate alternative.

- Where available, imaging modalities should be seen as an important objective tool to support diagnosis of lipodystrophy syndromes.
- DXA is a suitable, cost-effective and appropriate strategy to assess fat quantity and distribution.
- Although clear diagnostic definitions are not established, a very low percentage of body fat may suggest GL, and a Fat Mass Ratio (the ratio between percent of the trunk fat mass and the percent of the lower-limb fat mass) higher than 1.2 in females may suggest FPLD (26).
- MRI is a useful tool to assess body composition but can be less practical and more costly.

3.1.7 Genetic testing

Lipodystrophy in a younger patient or with a positive family history (or consanguinity) may suggest a genetic etiology. Genetic testing in patients with suspected congenital or familial lipodystrophy syndromes can be used to confirm the diagnosis. However, a negative genetic test does not rule out an inherited form of the disease since some genes involved in the pathogenesis of lipodystrophy syndromes have yet to be identified. Furthermore, some forms of genetic lipodystrophy syndromes are polygenic in

origin with affected genes not typically included in standard lipodystrophy panels. In patients suspected of lipodystrophy syndromes in whom genetic testing is negative, acquired forms of lipodystrophy syndromes should additionally be considered.

- Preference of the format of genetic testing continues to vary across localities.
- Among the expert panel reviewing this resource, diagnostic genetic panels were generally preferred over single gene testing.
- As caveats to genetic testing, some genes involved in the pathology of lipodystrophy syndromes are yet to be identified and some forms of genetic lipodystrophy syndromes can be polygenic.
- Whole Exome Sequencing (WES) was typically reserved for patients highly suspected of inherited lipodystrophy syndromes for whom the genetic panel did not yield results.
- As technology continues to improve, WES may become increasingly a viable option for routine use.

A diagnostic checklist is presented in Figure 1.

3.2 Communicating the diagnosis to the patient and families

A diagnosis of lipodystrophy is a life-changing moment and careful consideration must be given as to how best to communicate this to patients and their family members. The following are useful areas to consider on this topic:

• Several discussions may be needed.

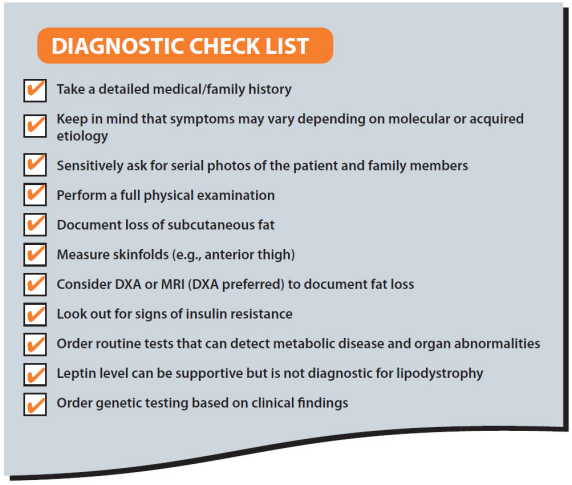

FIGURE 1
Diagnostic check list.

Diagnosis is often a relief for people with lipodystrophy syndromes; however, there is often a lot of information to completely understand and it is likely to take several discussions/consultations before the patient is comfortable with the meaning of the diagnosis.

• Include other members of the multidisciplinary team.

Delivering the diagnosis alongside other specialist(s) from the multidisciplinary team that will likely be involved in the management of the patient can be helpful in some cases.

• Discuss proactive management.

The diagnosis can be framed as an opportunity to be proactive with respect to monitoring and managing risk factors for potential comorbidities.

• Distress over irreversible changes to appearance is common.

It is important that the person with lipodystrophy syndromes understands that it is generally not possible to regain lost fat. This can be very distressing and psychological support should be offered. There are also cosmetic options such as reconstruction surgery and fillers that could be considered.

• Consider genetic counselling in relevant cases.

The diagnosis of a heritable form of lipodystrophy syndromes is accompanied by specific considerations, and genetic counselling should be offered.

3.3 Referrals for patients

Referral to an expert center, where there is a multidisciplinary team with expertise in treating lipodystrophy syndromes, is highly recommended by the expert panel. If a nearby expert center does not exist, efforts should be made to consult with specialists who have experience in treating patients with lipodystrophy syndromes.

• Referral to an expert center is highly recommended.

3.4 Screening and monitoring for metabolic dysfunction and organ abnormalities

3.4.1 Insulin resistance, diabetes mellitus, and associated complications

Once a diagnosis of lipodystrophy syndrome is made, it is important to assess patients for insulin resistance, diabetes mellitus, and associated complications. For most patients, following international/national diabetes treatment guidelines is recommended (4, 27, 28). Even if initial laboratory results appear normal, regular monitoring should be conducted.

- Check fasting glucose (consider ordering fasting insulin alongside) as well as HbA1c at least annually.
- Screen patients for complications of insulin resistance and diabetes.

3.4.2 Lipids and pancreatitis

Dyslipidemia (high triglycerides, low HDL-cholesterol) is a major comorbidity of lipodystrophy syndromes which can lead to development of eruptive xanthomas and episodes of acute pancreatitis and is associated with increased cardiovascular risk (20). Following international/national treatment guidelines for hyperlipidemia is generally recommended (4, 29).

- Monitor fasting lipid panel at least annually and repeat with occurrence of abdominal pain or xanthomata.

3.4.3 Liver disease

Liver disease (severe liver steatosis leading to NASH and eventually liver cirrhosis) remains a major cause of mortality in patients with lipodystrophy syndromes and should be carefully monitored (30).

- Monitor liver enzymes at least annually.
- Consider elastography, liver ultrasound, MRI (with Dixon fat) or magnetic resonance elastography at diagnosis, and then every few years or sooner as clinically indicated.
- Liver biopsy is performed as clinically indicated.

3.4.4 Cardiovascular disease

Several forms of lipodystrophy syndromes are associated with heart disease (e.g., cardiomyopathy, arrhythmias, conduction abnormalities, coronary artery disease) due to frequent and severe metabolic complications and underlying molecular etiology (21, 22, 31–36).

- Blood pressure should be measured at every visit.
- Baseline ECG is recommended and should be repeated as clinically indicated.
- Echocardiogram should be considered as clinically indicated.
- Symptoms of coronary artery disease should be assessed carefully, and further testing should be considered based on clinical findings.
- Consider Holter ECG or ECG with exercise test to evaluate for arrhythmias in select patients.
- Risk of sudden death syndrome should not be overlooked in lipodystrophy syndromes.

3.4.5 Kidney disease

Chronic kidney disease (CKD) is a major cause of mortality in lipodystrophy syndromes. CKD is frequent and has an early onset in patients with lipodystrophy syndromes, and thus vigilance is recommended (37).

- Urine protein/creatinine ratio and serum creatinine levels should be assessed at the time of diagnosis and repeated at least annually.

3.4.6 Reproductive system

Reproductive dysfunction such as PCOS, oligo/amenorrhea, reduced fertility, and hirsutism is commonly detected in women with lipodystrophy syndromes. Also, women with lipodystrophy syndromes are theoretically at increased risk for preeclampsia, miscarriage and macrosomia due to poor metabolic control. Early adrenarche, true precocious puberty, or central hypogonadism also may occur in children with GL (1, 15, 38–40).

- Gonadal steroids, gonadotropins, and pelvic ultrasonography can be helpful in identifying reproductive dysfunction.
- Pubertal staging should be performed annually in children.

3.4.7 Hunger and other additional symptoms

Patients with lipodystrophy syndromes, especially GL, are typically hyperphagic due to leptin deficiency (41–45). However, monitoring hunger can be a challenge. While there was no overall consensus on how best to measure hyperphagia, the panel noted that it may be helpful to consider the use of questionnaires such as the Three-Factor Eating Questionnaire (46).

Comorbidities and other impairments of lipodystrophy syndromes that may affect patient quality of life include, but are not limited to, social anxiety and limitations with symptoms or physical appearance leading to inability to work and a reluctance or inability to socialize, chronic pain that can affect a patient's ability to carry out basic tasks, and fatigue (47, 48).

- Patients with lipodystrophy syndromes, especially GL, typically have hyperphagia due to leptin deficiency which can have implications for patients, family members and caregivers.
- Additional symptoms of lipodystrophy may include anxiety, depression, chronic pain, and fatigue.

3.5 Treating lipodystrophy syndromes

3.5.1 Diet

Generally, patients are advised to follow diets with balanced macronutrient composition (3, 4). Energy-restricted diets improve metabolic abnormalities and may be appropriate in adults. Very-low-fat diets should be used in patients with severe hypertriglyceridemia (triglycerides > 1000 mg/dL). In the absence of severe hypertriglyceridemia, patients should replace refined carbohydrates with unsaturated fat and protein. Alcohol intake should be limited. A dietician should be consulted for specialized dietary needs, especially in infants and young children (3, 4, 49). Overfeeding should be avoided. Medium-chain triglyceride oil formulas can provide energy without raising triglycerides in infants.

- Most patients are recommended to follow a calorically restricted diet with balanced macronutrient composition;

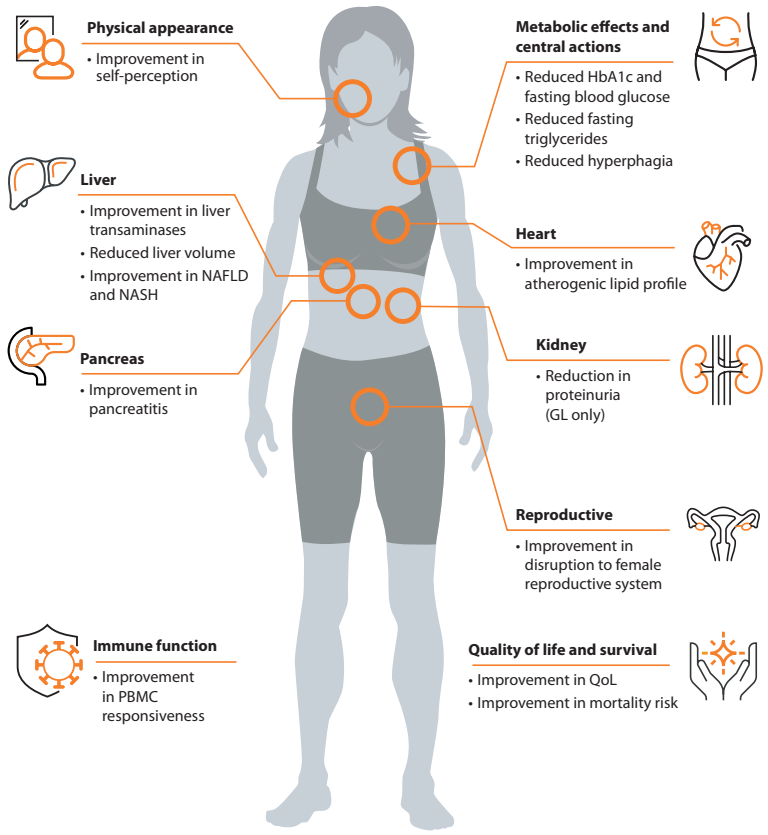

FIGURE 2
Clinical effects of metreleptin in patients with lipodystrophy syndromes.

however, it may be difficult to control hunger in a leptin deficient state.
- Referral to a dietician is strongly recommended.
- Alcohol and smoking should be avoided.

3.5.2 Exercise

Patients with lipodystrophy syndromes should be encouraged to exercise in the absence of specific contraindications. Patients with subtypes of lipodystrophy syndromes predisposed to cardiomyopathy and/or arrhythmias should undergo cardiac evaluation before initiating an exercise regimen. Contact sports should be avoided in patients with severe hepatosplenomegaly and in patients with CGL who have lytic bone lesions. Referral to an exercise specialist may be appropriate.

- Exercise is encouraged in the absence of specific contraindications.

3.5.3 Role of metreleptin

Metreleptin, a recombinant analog of the human hormone leptin, is an orphan drug used to treat complications of leptin deficiency in lipodystrophy syndromes. In the US, metreleptin is approved as an adjunct to diet as replacement therapy to treat the complications of leptin deficiency in patients with CGL or AGL (50). In Europe and Brazil, metreleptin is indicated as an adjunct to diet as a replacement therapy to treat the complications of leptin deficiency in adults and children 2 years of age and above with confirmed CGL or AGL (51, 52). Metreleptin is also approved for this indication in adults and children 12 years of age and above with confirmed FPLD or APL in whom standard treatments have failed to achieve adequate metabolic control (51). The effects of metreleptin treatment are summarized in Figure 2.

- The expert panel concluded that, where available, metreleptin should be used in accordance with local guidelines.

3.5.4 Management of diabetes with standard approaches

In addition to the 2016 multi-society lipodystrophy guideline, international/national diabetes treatment guidelines can be helpful (4, 53). Metformin is the most commonly used agent to improve insulin resistance and glycemic control (3, 4). Thiazolidinediones may improve metabolic complications in PL (4, 54–56) but should be used with caution in GL. While animal data suggest partial reversal of metabolic disturbances in GL mouse models with thiazolidinediones (57), clinical experience in patients with GL is very limited (54, 58, 59). Preliminary data from case reports (60) and a case series indicate sodium-glucose cotransporter 2 (SGLT2) inhibitors can help improve glycemic control among patients with

PL (61). Due to severe insulin resistance, many patients with lipodystrophy syndromes will need large amounts of insulin to control their blood glucose. Concentrated insulins should be considered (4, 62). In patients with PL, reduction of body mass index (BMI) may reduce the risk of metabolic comorbidities (63). Glucagon-like peptide-1 (GLP-1) receptor analogues may improve metabolic levels (64, 65). It is not known whether GLP-1 receptor analogues affect fat distribution in lipodystrophy syndromes. Some experts felt that GLP-1 receptor agonists may help reduce localized fat accumulation (e.g., on the abdominal fat) and may also help manage hyperphagia in some cases, although these effects have not been systematically studied in patients with lipodystrophy syndromes. Prior episodes of acute pancreatitis and severely elevated triglyceride levels can be limiting factors to GLP-1 receptor agonist use (66, 67).

- Treat diabetes per guidelines. Maintain oversight but include referral to an endocrinologist as part of management.

3.5.5 Management of lipid abnormalities with standard approaches

Lifestyle modifications are essential in the management of hypertriglyceridemia (see Diet and Exercise sections above). Statins should be used concomitantly with lifestyle interventions in the setting of hypertriglyceridemia, high low-density lipoprotein cholesterol (LDL-C), or diabetes mellitus for cardiovascular risk reduction. Fibrates are commonly used to treat severely elevated triglycerides though physicians should confer with their local prescribing guidelines regarding use in children. Long-chain omega-3 fatty acid use also may be helpful in treating hypertriglyceridemia. Although no studies are available in patients with lipodystrophies, a previous large-scale clinical study (68) reported cardiovascular benefits in patients with fasting triglyceride levels of 135–499 mg/dL following treatment with icosapent ethyl. However, the use of these agents may be limited in patients with lipodystrophies who are at higher risk of developing arrhythmias, as an increased risk of atrial fibrillation has been reported after the use of omega-3 fatty acids, particularly in high doses (69–71).

- Treat dyslipidemia aggressively using lifestyle modification and statins with or without fibrates.
- Cardiovascular disease risk calculators may not necessarily be accurate in patients with lipodystrophy syndromes.

3.5.6 Management of liver disease with standard approaches

The panel agreed that monitoring for liver disease is critical in patients with lipodystrophy. NAFLD may develop early and progress rapidly to NASH and cirrhosis in this population. Weight loss, exercise, and avoidance of excess alcohol are mainstays of treatment per international/national guidelines (3, 4, 72). However, from a patient perspective, significant weight loss can be an undesired outcome in lipodystrophy syndromes, especially in patients with GL.

- Monitor and treat for liver disease per guidelines.
- Consider referral to a hepatologist as part of management.

3.5.7 Management of cardiovascular disease with standard approaches

The panel considers patients with lipodystrophy syndromes to be at high risk of cardiovascular disease and believes that an aggressive risk mitigation and management strategy is needed. In addition to the 2016 multi-society lipodystrophy guidelines (4), the American Diabetes Association (ADA) guideline can be helpful for cardiovascular risk management and hypertension treatment among patients with diabetes (27, 29). Patients with subtypes of lipodystrophy syndromes predisposed to cardiomyopathy or arrhythmia should undergo more detailed cardiac evaluation (32, 33). This is especially important before initiating an exercise regimen.

- Monitor and treat for cardiovascular disease per guidelines.
- Consider referral to a cardiologist as part of management.
- Strongly advise against smoking and assist with smoking cessation.

3.5.8 Management of kidney disease with standard approaches

CKD has a complex background in lipodystrophy syndromes and can be severe and rapidly progressing (37). Depending on the subtype, the etiology of CKD may vary. Although patients with lipodystrophy syndromes may develop CKD in the absence of diabetes, consensus from the group was to treat many of them in a way similar to patients with CKD caused by diabetes (unless CKD is caused by a specific form of kidney disease such as C3-positive membranoproliferative glomerulonephritis) according to international/local guidelines (despite lack of evidence in patients with lipodystrophy syndromes) (73, 74). Angiotensin-converting enzyme inhibitors (ACEi) or angiotensin receptor blockers (ARB) in addition to sodium-glucose cotransporter 2 (SGLT2) inhibitors can be considered if urine protein is elevated (73).

- Monitor and treat for kidney disease per guidelines.
- Consider referral to nephrologist if patient is hypertensive, has elevated creatinine or low estimate glomerular filtration rate (eGFR), or proteinuria.

3.5.9 Management of reproductive health with standard approaches

In patients with low leptin levels, irregular menses may normalize on leptin replacement therapy (40). In patients who are not candidates for or whose menses do not normalize on leptin

replacement, if a patient is amenorrhoeic due to a low leptin level and does not improve after leptin treatment, or cannot access leptin treatment, consider hormone replacement therapy– an estrogen patch (less harmful than oral estrogens on triglycerides) and oral progesterone, according to international/local guidelines (4, 75). PCOS in lipodystrophy syndromes is generally managed in line with international guidelines (76). Oral estrogens are generally contraindicated in the presence of severe hypertriglyceridemia (4). Patient attempting pregnancy should be referred to a reproductive clinic.

- Maintain oversight but consider referral to a reproductive endocrinologist or gynecologist as indicated.

4 Discussion

As a rare disease, lipodystrophy syndromes often pose a diagnostic and treatment challenge. In this regard, an international chart review study (19) involving five treatment centers in Brazil, Turkey and the United States has illustrated that patients commonly experience delays of several years before receiving a definitive diagnosis of lipodystrophy syndrome. Although fat loss is known to be prominent at birth in CGL and around puberty in FPLD, first symptoms of lipodystrophy were typically identified during childhood (mean age: 9.2 years) among patients with GL and during early adulthood (mean age: 24.7 years) among those with PL. More importantly, from the time symptoms were first noted, it took an average of 3.1 years in GL and 9.0 years in PL for physicians to diagnose them accurately. Delays in diagnosis and intervention predispose patients with lipodystrophy syndromes to irreversible end-organ damage, and as such comprehensive, multi-disciplinary diagnostic and treatment plans are critically needed. We developed the Rapid Action Plan to enable clinical teams to promptly diagnose and holistically manage patients with lipodystrophy syndromes. This set of guidance from experts is intended to enhance outcomes for individuals afflicted by this disease.

It is important to recognize that lipodystrophy syndromes are heterogeneous, resulting in a wide spectrum of clinical presentations. Nonetheless, regional or generalized absence of subcutaneous fat is the sine qua non of lipodystrophy and should be assessed for on physical exam. Clinical history is also important to differentiate this diagnosis from other possibilities, and to distinguish genetic versus acquired etiologies. Basic laboratory testing and imaging are useful adjuncts to the history and physical exam and can help to risk stratify patients for cardiometabolic complications. Insulin resistance, diabetes mellitus, hypertriglyceridemia, ectopic fat accumulation (e.g., hepatic steatosis), and low leptin level are common characteristics of the disease. However, these features may not be present in patients with all forms of lipodystrophy syndromes and are not specific for the condition.

Several tools can help to verify clinical suspicion for lack of subcutaneous fat. Skinfold measurement is an important part of objective assessment that is portable, fast, and affordable. Specifically, mid-thigh skinfolds with a cut-off of less than 10 mm in adult men and less than 22 mm in adult women (corresponding to approximately the 10th percentile of the US population) are useful to support the diagnosis (3). However, skinfold thicknesses are highly operator-dependent, do not give a comprehensive representation of overall fat distribution, and may be prone to error in patients with low body fat. Thus, imaging modalities are preferred, where available, as discussed below.

Among the most important and practical imaging modality noted by this expert panel was the DXA scan (77–79). Where skinfold measurement provides a simple on-the-spot measurement for body fat, DXA allows for the quantification of not only body fat, but also lean mass over time. Also, fat shadow images, which are color-coded representations highlighting only the fat tissue, can be generated from DXA images to facilitate visualization of fat distribution (80). Body composition can alternatively be assessed by computed tomography (CT) and MRI scans. Among the panel, use of MRI was generally recommended to obtain objective ratios of different fat compartments in patients with for PL (81, 82) and to provide information regarding residual mechanical fat in patients with CGL (83, 84). MRI also can determine the lipid content of tissues, solid organs (such as the liver) (85), and bone marrow fat (84) using the Dixon method or spectroscopy.

Despite the need to be mindful of a 'false negative', genetic testing remains an important supportive diagnostic and prognostic tool. A genetic test where the commonly known variants (e.g., *LMNA*) are negative should not rule out familial or congenital forms of lipodystrophy syndromes, which remain clinical diagnoses. On the other hand, positive genetic testing can be confirmatory of the diagnosis and should prompt a clinician to screen for complications directly or indirectly associated with molecular etiology and to offer genetic testing to affected family members.

Given the progressive nature of lipodystrophy syndromes, regular screening for metabolic abnormalities and end-organ complications is imperative. The comprehensive follow-up algorithm encompasses various components, including detection of insulin resistance, diabetes, complications associated with diabetes, lipid abnormalities, pancreatitis, liver disease, cardiovascular disease, kidney disease, reproductive system abnormalities, and other comorbidities driven by molecular or acquired etiologies. Emerging evidence emphasizes the importance of cardiovascular health in patients with lipodystrophy syndromes. Patients with lipodystrophy syndromes are at risk of coronary artery disease as a result of severe insulin resistance and poor metabolic control (22, 86). It should be noted that patients with *LMNA* mutations are more likely to develop cardiac disease than others with FPLD (33). Moreover, certain types of lipodystrophy syndromes (e.g., CGL4) are linked to potentially fatal cardiac rhythm changes and prompt diagnosis is therefore vital to minimize risk of sudden cardiac death (31, 32). It is critical to identify and to treat these arrhythmias before they lead to sudden cardiac death.

The current management strategy for lipodystrophy syndromes primarily focuses on metabolic health. Maintaining a controlled diet

is key for individuals with lipodystrophy syndromes, although this can be challenging for some patients given a lack of fat and insatiable appetite due to leptin deficiency. Standard medications to treat metabolic disease (e.g., diabetes, hyperlipidemia) can be used with limited efficacy (56, 61, 64, 87). Recombinant leptin, metreleptin, is used as an adjunct to diet as a replacement therapy to treat metabolic complications of lipodystrophy syndromes. The clinical development program for metreleptin includes a pivotal study integrating data from two trials (NIH 991265/20010769; Clinical Trials IDs: NCT00005905 and NCT00025883) and a supportive study (FHA101; Clinical Trials ID: NCT00677313). In patients with GL, the NIH 991265/20010769 study showed a mean absolute reduction of 2.2% in HbA1c levels and a mean relative reduction of 32.1% in plasma triglycerides (88). The supportive study FHA101 yielded consistent efficacy results, albeit with a smaller number of patients (89). Discontinuation of insulin, oral antidiabetic medications, and lipid-lowering therapies was observed in a significant percentage of GL patients after starting metreleptin treatment (88). In patients with PL, metreleptin treatment resulted in significant reductions in HbA1c, fasting triglycerides, and liver volume. A subgroup of patients with baseline HbA1c ≥ 6.5% or plasma triglycerides ≥ 500 mg/dL experienced an absolute reduction of 0.9% in HbA1c and a relative reduction of 37.4% in triglycerides (90). Further studies at the NIH and other treatment centers showed that metreleptin decreased hyperphagia (17), improved insulin sensitivity (91, 92), reduced liver steatosis and improved NASH score on biopsy specimens (30, 93). Improvements in reproductive abnormalities in women (40) and reduction in proteinuria in patients with GL (94, 95) were also observed. While limited, real-life studies have supported the robust effectiveness of metreleptin in GL, whereas the impact of treatment has been heterogeneous in patients with PL. Araujo-Vilar et al. (96) reported a decrease from 11.8% to 6.7% in average HbA1c and a 78% reduction in triglycerides in patients with CGL. In a real-world experience analysis of 53 patients (28 GL and 25 PL) from four countries (France, Spain, Italy, and the UK) (97), one year of metreleptin treatment resulted in a mean reduction of 53% in triglycerides and a 1.9% point decrease in HbA1c in subjects with GL. In patients with PL, the mean percentage reduction in triglycerides was 22% and mean decrease in HbA1c was a 0.5%. A recent multicenter retrospective observational cohort study of 47 patients with lipodystrophy (28 GL and 19 PL) who started metreleptin therapy in France between 2009 and 2020 (98) reported significant improvements in HbA1c (from 8.4% to 6.8%) and fasting triglycerides (from 3.6 mmol/L to 2.2 mmol/L) after one year of treatment with metreleptin, with sustained efficacy thereafter. Additionally, a significant decrease was noted in liver enzymes. However, the impact of treatment was heterogeneous in patients with PL, and overall changes in HbA1c within this subgroup were not significant. Among patients with PL, 61% were responders regarding glucose homeostasis, and 61% were responders regarding hypertriglyceridemia at year 1, with those with more severe metabolic disease and lower leptin at baseline, as well as those with preserved β-cell functions, likely being better responders. Metreleptin has a black box warning for the risk of anti-metreleptin antibodies with neutralizing activity and risk of lymphoma in the US and is available only through a restricted program (50). Metreleptin is subject to additional monitoring in Europe (51). Other potential adverse reactions include hypersensitivity reactions, acute pancreatitis associated with discontinuation of metreleptin, hypoglycemia with concomitant use of insulin and other anti-diabetics, T-cell lymphoma, immunogenicity, and serious and severe infections. Also, data from clinical trials do not support safety and efficacy in patients with HIV-related lipodystrophy. A summary of the reported clinical effects of metreleptin in patients with lipodystrophy syndromes are shown in Figure 2.

Lipodystrophy syndromes not only impacts physical health but can also significantly affect mental well-being and quality of life (47, 48). Therefore, it is essential to assess patients' psychological health and, where available, patients should be referred to a psychologist or counselor for support. Given that many patients may experience body dysmorphia, referral to a plastic surgeon or aesthetic specialist may be appropriate to address these concerns.

In a rare disease setting, consultation with dedicated specialized centers hold significant potential to reduce or even prevent lengthy diagnostic and treatment journeys. There are several ways to find the nearest specialist or specialist center for lipodystrophy syndromes. Because lipodystrophy specialists can be found via publications, running a PubMed search may be helpful. In Europe, there are specialist centers listed on the European Lipodystrophy Consortium's (ECLip) website (https://www.eclip-web.org/lipodystrophies/). Also, European Reference Networks (ERN) for rare diseases might be helpful; the endocrinology ERN has a main thematic group on 'genetic disorder of glucose & insulin homeostasis' (MTG3) (https://endo-ern.eu/rare-genetic-disorders-of-glucose-insulin-homeostasis/). In the United States (US), the Endocrine Society website hosts a member-exclusive community to connect with specialists (DocMatter tool) (https://www.endocrine.org/membership/endoforum). In the Middle East, there is growing collaboration around lipodystrophy [Arab Society for Pediatric Endocrinology and Diabetes (ASPED)] (https://asped.net/). In Brazil, BrazLipo (https://brazlipo.org/) exists as a reference point for professionals and the public.

In conclusion, the complexity of lipodystrophy syndromes poses a challenge to clinicians with limited expertise in the field. The Rapid Action Plan may prove helpful for clinical teams seeking to promptly diagnose and holistically manage patients with lipodystrophy syndromes. This information has the potential to enhance outcomes for individuals with this rare disease.

Data availability statement

The original contributions presented in the study are included in the article/supplementary material, further inquiries can be directed to the corresponding author/s.

Author contributions

LF: Writing – original draft, Writing – review & editing. JL: Writing – original draft, Writing – review & editing. VS: Writing – original draft, Writing – review & editing. MC: Writing – original draft, Writing – review & editing. SA: Writing – original draft, Writing – review & editing. RM: Writing – original draft, Writing – review & editing. BA: Writing – original draft, Writing – review & editing. FS: Writing – original draft, Writing – review & editing.

Funding

The author(s) declare that financial support was received for the research, authorship, and/or publication of this article. Amryt Pharmaceuticals provided funding solely for the research and publication costs associated with the manuscript. Amryt Pharmaceuticals did not provide any funding for authorship of the manuscript. Amryt Pharmaceuticals was not involved in data analysis, in the preparation of the abstract/manuscript nor in the decision to submit it for publication. Amryt Pharmaceuticals is a wholly owned subsidiary of Chiesi Farmaceutici S.p.A.

Acknowledgments

The authors extend their appreciation to Akt Health for not only conducting structured interviews but also for diligently preparing a report based on these interviews.

Conflict of interest

LF serves as a consultant for Amryt Pharmaceuticals (wholly owned subsidiary of Chiesi Farmaceutici S.p.A.) and Thera Technologies and receives grant support to her institution from Amryt Pharmaceuticals (wholly owned subsidiary of Chiesi Farmaceutici S.p.A.). JL received a consultancy fee from Amryt Pharmaceuticals (wholly owned subsidiary of Chiesi Farmaceutici S.p.A.), is a speaker to Amryt Pharmaceuticals (wholly owned subsidiary of Chiesi Farmaceutici S.p.A.), Astra Zeneca, NovoNordisk, and Abbott. VS received a consultancy fee from Amryt Pharmaceuticals (wholly owned subsidiary of Chiesi Farmaceutici S.p.A.). MC received a consultancy fee from Amryt Pharmaceuticals (wholly owned subsidiary of Chiesi Farmaceutici S.p.A.). SA received a consultancy fee from Amryt Pharmaceuticals (wholly owned subsidiary of Chiesi Farmaceutici S.p.A.). RM received a consultancy fee from Amryt Pharmaceuticals (wholly owned subsidiary of Chiesi Farmaceutici S.p.A.). BA received a consultancy fee from Amryt Pharmaceuticals (wholly owned subsidiary of Chiesi Farmaceutici S.p.A.), has run projects for and/or served as a consultant, board member, steering committee member, and/or speaker to Amryt Pharmaceuticals (wholly owned subsidiary of Chiesi Farmaceutici S.p.A.), Alnylam, Regeneron, ThirdRock Ventures, Astra Zeneca, Novonordisk, Boehringer Ingelheim, Sanofi, Bilim Ilac, ARIS, and Servier. FS received a consultancy fee from Amryt Pharmaceuticals (wholly owned subsidiary of Chiesi Farmaceutici S.p.A.), has run projects for and/or served as a consultant, board member, steering committee member, and/or speaker to Amryt Pharmaceuticals (wholly owned subsidiary of Chiesi Farmaceutici S.p.A.), Novonordisk, Boehringer Ingelheim, Ely Lilly, Pfizer, Bruno Farmaceutici, and BioItalia.

Publisher's note

References

1. Garg A. Acquired and inherited lipodystrophies. *N Engl J Med*. (2004) 350:1220–34. doi: 10.1056/NEJMra025261

2. Simha V, Garg A. Lipodystrophy: lessons in lipid and energy metabolism. *Curr Opin Lipidol*. (2006) 17:162–9. doi: 10.1097/01.mol.0000217898.52197.18

3. Handelsman Y, Oral EA, Bloomgarden ZT, Brown RJ, Chan JL, Einhorn D, et al. The clinical approach to the detection of lipodystrophy - an aace consensus statement. *Endocr Pract*. (2013) 19:107–16. doi: 10.4158/endp.19.1.v767575m65p5mr06

4. Brown RJ, Araujo-Vilar D, Cheung PT, Dunger D, Garg A, Jack M, et al. The diagnosis and management of lipodystrophy syndromes: A multi-society practice guideline. *J Clin Endocrinol Metab*. (2016) 101:4500–11. doi: 10.1210/jc.2016–2466

5. Patni N, Garg A. Congenital generalized lipodystrophies–new insights into metabolic dysfunction. *Nat Rev Endocrinol*. (2015) 11:522–34. doi: 10.1038/nrendo.2015.123

6. Hussain I, Garg A. Lipodystrophy syndromes. *Endocrinol Metab Clin North Am*. (2016) 45:783–97. doi: 10.1016/j.ecl.2016.06.012

7. Misra A, Garg A. Clinical features and metabolic derangements in acquired generalized lipodystrophy: case reports and review of the literature. *Med (Baltimore)*. (2003) 82:129–46. doi: 10.1097/00005792–200303000–00007

8. Misra A, Peethambaram A, Garg A. Clinical features and metabolic and autoimmune derangements in acquired partial lipodystrophy: report of 35 cases and review of the literature. *Med (Baltimore)*. (2004) 83:18–34. doi: 10.1097/01.md.0000111061.69212.59

9. Fernandez-Pombo A, Sanchez-Iglesias S, Cobelo-Gomez S, Hermida-Ameijeiras A, Araujo-Vilar D. Familial partial lipodystrophy syndromes. *Presse Med*. (2021) 50:104071. doi: 10.1016/j.lpm.2021.104071

10. Hegele RA. Familial partial lipodystrophy: A monogenic form of the insulin resistance syndrome. *Mol Genet Metab*. (2000) 71:539–44. doi: 10.1006/mgme.2000.3092

11. Vantyghem MC, Balavoine AS, Douillard C, DeFrance F, Dieudonne L, Mouton F, et al. How to diagnose a lipodystrophy syndrome. *Ann Endocrinol (Paris)*. (2012) 73:170–89. doi: 10.1016/j.ando.2012.04.010

12. Corvillo F, Abel BS, Lopez-Lera A, Ceccarini G, Magno S, Santini F, et al. Characterization and clinical association of autoantibodies against perilipin 1 in patients with acquired generalized lipodystrophy. *Diabetes*. (2023) 72:71–84. doi: 10.2337/db21–1086

13. Ceccarini G, Magno S, Gilio D, Pelosini C, Santini F. Autoimmunity in lipodystrophy syndromes. *Presse Med*. (2021) 50:104073. doi: 10.1016/j.lpm.2021.104073

14. Akinci B, Meral R, Oral EA. Phenotypic and genetic characteristics of lipodystrophy: pathophysiology, metabolic abnormalities, and comorbidities. *Curr Diabetes Rep*. (2018) 18:143. doi: 10.1007/s11892–018–1099–9

15. Akinci B, Sahinoz M, Oral E. *Lipodystrophy Syndromes: Presentation and Treatment*. Feingold KR, Anawalt B, Blackman MR, Boyce A, Chrousos G, Corpas E, et al, editors. South Dartmouth (MA: Endotext (2000).

16. Papathanasiou AE, Nolen-Doerr E, Farr OM, Mantzoros CS. Geoffrey harris prize lecture 2018: novel pathways regulating neuroendocrine function, energy homeostasis and metabolism in humans. *Eur J Endocrinol*. (2019) 180:R59–71. doi: 10.1530/EJE-18–0847

17. McDuffie JR, Riggs PA, Calis KA, Freedman RJ, Oral EA, DePaoli AM, et al. Effects of exogenous leptin on satiety and satiation in patients with lipodystrophy and leptin insufficiency. *J Clin Endocrinol Metab*. (2004) 89:4258–63. doi: 10.1210/jc.2003–031868

18. Pedicelli S, de Palma L, Pelosini C, Cappa M. Metreleptin for the treatment of progressive encephalopathy with/without lipodystrophy (Peld) in a child with progressive myoclonic epilepsy: A case report. *Ital J Pediatr*. (2020) 46:158. doi: 10.1186/s13052–020-00916–2

19. Akinci B, Oral EA, Neidert A, Rus D, Cheng WY, Thompson-Leduc P, et al. Comorbidities and survival in patients with lipodystrophy: an international chart review study. *J Clin Endocrinol Metab*. (2019) 104:5120–35. doi: 10.1210/jc.2018–02730

20. Simha V, Garg A. Inherited lipodystrophies and hypertriglyceridemia. *Curr Opin Lipidol*. (2009) 20:300–8. doi: 10.1097/MOL.0b013e32832d4a33

21. Hegele RA. Premature atherosclerosis associated with monogenic insulin resistance. *Circulation*. (2001) 103:2225–9. doi: 10.1161/01.cir.103.18.2225

22. Hussain I, Patni N, Garg A. Lipodystrophies, dyslipidaemias and atherosclerotic cardiovascular disease. *Pathology*. (2019) 51:202–12. doi: 10.1016/j.pathol.2018.11.004

23. Araujo-Vilar D, Santini F. Diagnosis and treatment of lipodystrophy: A step-by-step approach. *J Endocrinol Invest*. (2019) 42:61–73. doi: 10.1007/s40618-018-0887-z

24. Fourman LT, Grinspoon SK. Approach to the patient with lipodystrophy. *J Clin Endocrinol Metab*. (2022) 107:1714–26. doi: 10.1210/clinem/dgac079

25. Foss-Freitas MC, Akinci B, Luo Y, Stratton A, Oral EA. Diagnostic strategies and clinical management of lipodystrophy. *Expert Rev Endocrinol Metab*. (2020) 15:95–114. doi: 10.1080/17446651.2020.1735360

26. Valerio CM, Zajdenverg L, de Oliveira JE, Mory PB, Moyses RS, Godoy-Matos AF. Body composition study by dual-energy X-ray absorptiometry in familial partial lipodystrophy: finding new tools for an objective evaluation. *Diabetol Metab Syndr*. (2012) 4:40. doi: 10.1186/1758–5996-4–40

27. American Diabetes Association Professional Practice C. 4. Comprehensive medical evaluation and assessment of comorbidities: standards of care in diabetes-2024. *Diabetes Care*. (2024) 47:S52–76. doi: 10.2337/dc24-S004

28. American Diabetes Association Professional Practice C. 6. Glycemic goals and hypoglycemia: standards of care in diabetes-2024. *Diabetes Care*. (2024) 47:S111–S25. doi: 10.2337/dc24-S006

29. American Diabetes Association Professional Practice C. 10. Cardiovascular disease and risk management: standards of care in diabetes-2024. *Diabetes Care*. (2024) 47:S179–218. doi: 10.2337/dc24-S010

30. Javor ED, Ghany MG, Cochran EK, Oral EA, DePaoli AM, Premkumar A, et al. Leptin reverses nonalcoholic steatohepatitis in patients with severe lipodystrophy. *Hepatology*. (2005) 41:753–60. doi: 10.1002/hep.20672

31. Rajab A, Straub V, McCann LJ, Seelow D, Varon R, Barresi R, et al. Fatal cardiac arrhythmia and long-qt syndrome in a new form of congenital generalized lipodystrophy with muscle rippling (Cgl4) due to ptrf-cavin mutations. *PloS Genet*. (2010) 6:e1000874. doi: 10.1371/journal.pgen.1000874

32. Akinci G, Alyaarubi S, Patni N, Alhashmi N, Al-Shidhani A, Prodam F, et al. Metabolic and other morbid complications in congenital generalized lipodystrophy type 4. *Am J Med Genet A*. (2024) 194(6):e63533. doi: 10.1002/ajmg.a.63533

33. Eldin AJ, Akinci B, da Rocha AM, Meral R, Simsir IY, Adiyaman SC, et al. Cardiac phenotype in familial partial lipodystrophy. *Clin Endocrinol (Oxf)*. (2021) 94:1043–53. doi: 10.1111/cen.14426

34. Haque WA, Vuitch F, Garg A. Post-mortem findings in familial partial lipodystrophy, dunnigan variety. *Diabetes Med*. (2002) 19:1022–5. doi: 10.1046/j.1464-5491.2002.00796.x

35. Yildirim Simsir I, Tuysuz B, Ozbek MN, Tanrikulu S, Celik Guler M, Karhan AN, et al. Clinical features of generalized lipodystrophy in Turkey: A cohort analysis. *Diabetes Obes Metab*. (2023) 25:1950–63. doi: 10.1111/dom.15061

36. Sanon VP, Handelsman Y, Pham SV, Chilton R. Cardiac manifestations of congenital generalized lipodystrophy. *Clin Diabetes*. (2016) 34:181–6. doi: 10.2337/cd16–0002

37. Akinci B, Unlu SM, Celik A, Simsir IY, Sen S, Nur B, et al. Renal complications of lipodystrophy: A closer look at the natural history of kidney disease. *Clin Endocrinol (Oxf)*. (2018) 89:65–75. doi: 10.1111/cen.13732

38. Huseman CA, Johanson AJ, Varma MM, Blizzard RM. Congenital lipodystrophy. Ii. Association with polycystic ovarian disease. *J Pediatr*. (1979) 95:72–4. doi: 10.1016/s0022–3476(79)80087–6

39. Blackwell VC, Salis P, Groves RW, Baldeweg SE, Conway GS. Unwin RJ. Partial lipodystrophy, polycystic ovary syndrome and proteinuria: A common link to insulin resistance? *J R Soc Med*. (2001) 94:238–40. doi: 10.1177/014107680109400510

40. Oral EA, Ruiz E, Andewelt A, Sebring N, Wagner AJ, Depaoli AM, et al. Effect of leptin replacement on pituitary hormone regulation in patients with severe lipodystrophy. *J Clin Endocrinol Metab*. (2002) 87:3110–7. doi: 10.1210/jcem.87.7.8591

41. Unger RH. Longevity, lipotoxicity and leptin: the adipocyte defense against feasting and famine. *Biochimie*. (2005) 87:57–64. doi: 10.1016/j.biochi.2004.11.014

42. Javor ED, Cochran EK, Musso C, Young JR, Depaoli AM, Gorden P. Long-term efficacy of leptin replacement in patients with generalized lipodystrophy. *Diabetes*. (2005) 54:1994–2002. doi: 10.2337/diabetes.54.7.1994

43. Ebihara K, Nakao K. Translational Research of Leptin in Lipodystrophy and Its Related Diseases. In: Nakao K, Minato N, Uemoto S, editors. *Innovative Medicine: Basic Research and Development*. Tokyo: Springer. (2015). p. 165–75.

44. Aotani D, Ebihara K, Sawamoto N, Kusakabe T, Aizawa-Abe M, Kataoka S, et al. Functional magnetic resonance imaging analysis of food-related brain activity in patients with lipodystrophy undergoing leptin replacement therapy. *J Clin Endocrinol Metab*. (2012) 97:3663–71. doi: 10.1210/jc.2012–1872

45. Ahima R, Osei SY. Leptin and appetite control in lipodystrophy. *J Clin Endocrinol Metab*. (2004) 89:4254–7. doi: 10.1210/jc.2004–1232

46. Karlsson J, Persson LO, Sjostrom L, Sullivan M. Psychometric properties and factor structure of the three-factor eating questionnaire (Tfeq) in obese men and women. Results from the swedish obese subjects (Sos) study. *Int J Obes Relat Metab Disord*. (2000) 24:1715–25. doi: 10.1038/sj.ijo.0801442

47. Calabro PF, Ceccarini G, Calderone A, Lippi C, Piaggi P, Ferrari F, et al. Psychopathological and psychiatric evaluation of patients affected by lipodystrophy. *Eat Weight Disord*. (2020) 25:991–8. doi: 10.1007/s40519–019-00716–6

48. Demir T, Simsir IY, Tuncel OK, Ozbaran B, Yildirim I, Pirildar S, et al. Impact of lipodystrophy on health-related quality of life: the qualip study. *Orphanet J Rare Dis*. (2024) 19:10. doi: 10.1186/s13023-023-03004-w

49. Cecchetti C, Belardinelli E, Dionese P, Teglia R, Fazzeri R, MR DA, et al. Is it possible to achieve an acceptable disease control by dietary therapy alone in berardinelli seip type 1? Experience from a case report. *Front Endocrinol (Lausanne)*. (2023) 14:1190363. doi: 10.3389/fendo.2023.1190363

50. Available online at: https://www.accessdata.fda.gov/drugsatfda_docs/label/2022/125390s024lbl.pdf.

51. Available online at: https://www.ema.europa.eu/en/medicines/human/EPAR/Myalepta.

52. Available online at: https://consultas.anvisa.gov.br/#/bulario/q/?numeroRegistro=175040002.

53. American Diabetes Association Professional Practice C. 9. Pharmacologic approaches to glycemic treatment: standards of care in diabetes-2024. *Diabetes Care*. (2024) 47:S158–S78. doi: 10.2337/dc24-S009

54. Arioglu E, Duncan-Morin J, Sebring N, Rother KI, Gottlieb N, Lieberman J, et al. Efficacy and safety of troglitazone in the treatment of lipodystrophy syndromes. *Ann Intern Med*. (2000) 133:263–74. doi: 10.7326/0003–4819-133–4-200008150–00009

55. Agostini M, Schoenmakers E, Beig J, Fairall L, Szatmari I, Rajanayagam O, et al. A pharmacogenetic approach to the treatment of patients with pparg mutations. *Diabetes*. (2018) 67:1086–92. doi: 10.2337/db17–1236

56. Collet-Gaudillat C, Billon-Bancel A, Beressi JP. Long-term improvement of metabolic control with pioglitazone in a woman with diabetes mellitus related to dunnigan syndrome: A case report. *Diabetes Metab*. (2009) 35:151–4. doi: 10.1016/j.diabet.2009.01.001

57. Prieur X, Dollet L, Takahashi M, Nemani M, Pillot B, Le May C, et al. Thiazolidinediones partially reverse the metabolic disturbances observed in bscl2/seipin-deficient mice. *Diabetologia*. (2013) 56:1813–25. doi: 10.1007/s00125–013-2926–9

58. Kumar R, Pilania RK, Bhatia A, Dayal D. Acquired generalised lipodystrophy and type 1 diabetes mellitus in a child: A rare and implacable association. *BMJ Case Rep*. (2018) 2018:bcr2018225553. doi: 10.1136/bcr-2018–225553

59. Bhatia R, Chennupathi P, Rosenstein ED, Advani S. Spontaneous remission of acquired generalized lipodystrophy presenting in the postpartum period. *JCEM Case Rep*. (2024) 2:luae009. doi: 10.1210/jcemcr/luae009

60. Nagayama A, Ashida K, Watanabe M, Moritaka K, Sonezaki A, Kitajima Y, et al. Case report: metreleptin and sglt2 inhibitor combination therapy is effective for acquired incomplete lipodystrophy. *Front Endocrinol (Lausanne)*. (2021) 12:690996. doi: 10.3389/fendo.2021.690996

61. Bansal R, Cochran E, Startzell M, Brown RJ. Clinical effects of sodium-glucose transporter type 2 inhibitors in patients with partial lipodystrophy. *Endocr Pract*. (2022) 28:610–4. doi: 10.1016/j.eprac.2022.03.006

62. Cochran E, Musso C, Gorden P. The use of U-500 in patients with extreme insulin resistance. *Diabetes Care*. (2005) 28:1240–4. doi: 10.2337/diacare.28.5.1240

63. Koo E, Foss-Freitas MC, Meral R, Ozer M, Eldin AJ, Akinci B, et al. The metabolic equivalent bmi in patients with familial partial lipodystrophy (Fpld) compared with those with severe obesity. *Obes (Silver Spring)*. (2021) 29:274–8. doi: 10.1002/oby.23049

64. Banning F, Rottenkolber M, Freibothe I, Seissler J, Lechner A. Insulin secretory defect in familial partial lipodystrophy type 2 and successful long-term treatment with a glucagon-like peptide 1 receptor agonist. *Diabetes Med*. (2017) 34:1792–4. doi: 10.1111/dme.13527

65. Oliveira J, Lau E, Carvalho D, Freitas P. Glucagon-like peptide-1 analogues - an efficient therapeutic option for the severe insulin resistance of lipodystrophic syndromes: two case reports. *J Med Case Rep*. (2017) 11:12. doi: 10.1186/s13256–016-1175–1

66. Cao C, Yang S, Zhou Z. Glp-1 receptor agonists and pancreatic safety concerns in type 2 diabetic patients: data from cardiovascular outcome trials. *Endocrine*. (2020) 68:518–25. doi: 10.1007/s12020–020-02223–6

67. Sodhi M, Rezaeianzadeh R, Kezouh A, Etminan M. Risk of gastrointestinal adverse events associated with glucagon-like peptide-1 receptor agonists for weight loss. *JAMA*. (2023) 330:1795–7. doi: 10.1001/jama.2023.19574

68. Bhatt DL, Steg PG, Miller M, Brinton EA, Jacobson TA, Ketchum SB, et al. Cardiovascular risk reduction with icosapent ethyl for hypertriglyceridemia. *N Engl J Med*. (2019) 380:11–22. doi: 10.1056/NEJMoa1812792

69. Nicholls SJ, Lincoff AM, Garcia M, Bash D, Ballantyne CM, Barter PJ, et al. Effect of high-dose omega-3 fatty acids vs corn oil on major adverse cardiovascular events in patients at high cardiovascular risk: the strength randomized clinical trial. *JAMA*. (2020) 324:2268–80. doi: 10.1001/jama.2020.22258

70. Curfman G. Omega-3 fatty acids and atrial fibrillation. *JAMA*. (2021) 325:1063. doi: 10.1001/jama.2021.2909

71. Bork CS, Myhre PL, Schmidt EB. Do omega-3 fatty acids increase risk of atrial fibrillation? *Curr Opin Clin Nutr Metab Care*. (2023) 26:78–82. doi: 10.1097/MCO.0000000000000907

72. Cusi K, Isaacs S, Barb D, Basu R, Caprio S, Garvey WT, et al. American association of clinical endocrinology clinical practice guideline for the diagnosis and management of nonalcoholic fatty liver disease in primary care and endocrinology clinical settings: co-sponsored by the american association for the study of liver diseases (Aasld). *Endocr Pract*. (2022) 28:528–62. doi: 10.1016/j.eprac.2022.03.010

73. American Diabetes Association Professional Practice C. 11. Chronic kidney disease and risk management: standards of care in diabetes-2024. *Diabetes Care*. (2024) 47:S219–S30. doi: 10.2337/dc24-S011

74. Slinin Y, Ishani A, Rector T, Fitzgerald P, MacDonald R, Tacklind J, et al. Management of hyperglycemia, dyslipidemia, and albuminuria in patients with diabetes and ckd: A systematic review for a kdoqi clinical practice guideline. *Am J Kidney Dis*. (2012) 60:747–69. doi: 10.1053/j.ajkd.2012.07.017

75. The Hormone Therapy Position Statement of The North American Menopause Society" Advisory P. The 2022 hormone therapy position statement of the north american menopause society. *Menopause*. (2022) 29:767–94. doi: 10.1097/GME.0000000000002028

76. Teede HJ, Tay CT, Laven JJE, Dokras A, Moran LJ, Piltonen TT, et al. Recommendations from the 2023 international evidence-based guideline for the assessment and management of polycystic ovary syndrome. *J Clin Endocrinol Metab*. (2023) 108:2447–69. doi: 10.1210/clinem/dgad463

77. Valerio CM, Godoy-Matos A, Moreira RO, Carraro L, Guedes EP, Moises RS, et al. Dual-energy X-ray absorptiometry study of body composition in patients with lipodystrophy. *Diabetes Care*. (2007) 30:1857–9. doi: 10.2337/dc07–0025

78. Vasandani C, Li X, Sekizkardes H, Adams-Huet B, Brown RJ, Garg A. Diagnostic value of anthropometric measurements for familial partial lipodystrophy, dunnigan variety. *J Clin Endocrinol Metab*. (2020) 105:2132–41. doi: 10.1210/clinem/dgaa137

79. Ajluni N, Meral R, Neidert AH, Brady GF, Buras E, McKenna B, et al. Spectrum of disease associated with partial lipodystrophy: lessons from a trial cohort. *Clin Endocrinol (Oxf)*. (2017) 86:698–707. doi: 10.1111/cen.13311

80. Meral R, Ryan BJ, Malandrino N, Jalal A, Neidert AH, Muniyappa R, et al. "Fat shadows" from dxa for the qualitative assessment of lipodystrophy: when a picture is worth a thousand numbers. *Diabetes Care*. (2018) 41:2255–8. doi: 10.2337/dc18–0978

81. Lim K, Haider A, Adams C, Sleigh A, Savage DB. Lipodistrophy: A paradigm for understanding the consequences of "Overloading" Adipose tissue. *Physiol Rev*. (2021) 101:907–93. doi: 10.1152/physrev.00032.2020

82. Adiyaman SC, Altay C, Kamisli BY, Avci ER, Basara I, Simsir IY, et al. Pelvis magnetic resonance imaging to diagnose familial partial lipodystrophy. *J Clin Endocrinol Metab*. (2023) 108:e512–e20. doi: 10.1210/clinem/dgad063

83. Simha V, Garg A. Phenotypic heterogeneity in body fat distribution in patients with congenital generalized lipodystrophy caused by mutations in the agpat2 or seipin genes. *J Clin Endocrinol Metab*. (2003) 88:5433–7. doi: 10.1210/jc.2003–030835

84. Altay C, Secil M, Demir T, Atik T, Akinci G, Ozdemir Kutbay N, et al. Determining residual adipose tissue characteristics with mri in patients with various subtypes of lipodystrophy. *Diagn Interv Radiol*. (2017) 23:428–34. doi: 10.5152/dir.2017.17019

85. Reeder SB, Sirlin CB. Quantification of liver fat with magnetic resonance imaging. *Magn Reson Imaging Clin N Am*. (2010) 18:337–57, ix. doi: 10.1016/j.mric.2010.08.013

86. Kinzer AB, Shamburek RD, Lightbourne M, Muniyappa R, Brown RJ. Advanced lipoprotein analysis shows atherogenic lipid profile that improves after metreleptin in patients with lipodystrophy. *J Endocr Soc*. (2019) 3:1503–17. doi: 10.1210/js.2019–00103

87. Shamsudeen I, Hegele RA. Advances in the care of lipodystrophies. *Curr Opin Endocrinol Diabetes Obes*. (2022) 29:152–60. doi: 10.1097/MED.0000000000000695

88. Brown RJ, Oral EA, Cochran E, Araujo-Vilar D, Savage DB, Long A, et al. Long-term effectiveness and safety of metreleptin in the treatment of patients with generalized lipodystrophy. *Endocrine*. (2018) 60:479–89. doi: 10.1007/s12020–018-1589–1

89. Ajluni N, Dar M, Xu J, Neidert AH, Oral EA. Efficacy and safety of metreleptin in patients with partial lipodystrophy: lessons from an expanded access program. *J Diabetes Metab*. (2016) 7(3):659. doi: 10.4172/2155–6156.1000659

90. Oral EA, Gorden P, Cochran E, Araujo-Vilar D, Savage DB, Long A, et al. Long-term effectiveness and safety of metreleptin in the treatment of patients with partial lipodystrophy. *Endocrine*. (2019) 64:500–11. doi: 10.1007/s12020–019-01862–8

91. Oral EA, Simha V, Ruiz E, Andewelt A, Premkumar A, Snell P, et al. Leptin-replacement therapy for lipodystrophy. *N Engl J Med*. (2002) 346:570–8. doi: 10.1056/NEJMoa012437

92. Petersen KF, Oral EA, Dufour S, Befroy D, Ariyan C, Yu C, et al. Leptin reverses insulin resistance and hepatic steatosis in patients with severe lipodystrophy. *J Clin Invest*. (2002) 109:1345–50. doi: 10.1172/JCI15001

93. Safar Zadeh E, Lungu AO, Cochran EK, Brown RJ, Ghany MG, Heller T, et al. The liver diseases of lipodystrophy: the long-term effect of leptin treatment. *J Hepatol*. (2013) 59:131–7. doi: 10.1016/j.jhep.2013.02.007

94. Javor ED, Moran SA, Young JR, Cochran EK, DePaoli AM, Oral EA, et al. Proteinuric nephropathy in acquired and congenital generalized lipodystrophy: baseline characteristics and course during recombinant leptin therapy. *J Clin Endocrinol Metab*. (2004) 89:3199–207. doi: 10.1210/jc.2003–032140

95. Lee HL, Waldman MA, Auh S, Balow JE, Cochran EK, Gorden P, et al. Effects of metreleptin on proteinuria in patients with lipodystrophy. *J Clin Endocrinol Metab*. (2019) 104:4169–77. doi: 10.1210/jc.2019–00200

96. Araujo-Vilar D, Sanchez-Iglesias S, Guillin-Amarelle C, Castro A, Lage M, Pazos M, et al. Recombinant human leptin treatment in genetic lipodystrophic syndromes: the long-term spanish experience. *Endocrine*. (2015) 49:139–47. doi: 10.1007/s12020–014-0450–4

97. Cook K, Stears A, Araujo VD, Santini F, O'Rahilly S, Ceccarini G, et al. Savage DB real-world experience of generalized and partial lipodystrophy patients enrolled in the metreleptin early access program. *Endocrine Abstracts*. (2019) 63:586. doi: 10.1530/endoabs.63.P586

98. Mosbah H, Vantyghem MC, Nobecourt E, Andreelli F, Archambeaud F, Bismuth E, et al. Therapeutic indications and metabolic effects of metreleptin in patients with lipodystrophy syndromes: real-life experience from a national reference network. *Diabetes Obes Metab*. (2022) 24:1565–77. doi: 10.1111/dom.14726

frontiers | Frontiers in Endocrinology

TYPE General Commentary
PUBLISHED 10 September 2024
DOI 10.3389/fendo.2024.1445226

OPEN ACCESS

EDITED BY
Habib Yaribeygi,
Semnan University of Medical Sciences, Iran

REVIEWED BY
Flavia Prodam,
University of Eastern Piedmont, Italy
Phiwayinkosi V. Dludla,
South African Medical Research Council, South Africa

*CORRESPONDENCE
William J. Massey
masseyw2@ccf.org
Lin Zhu
lin.zhu@vumc.org

RECEIVED 07 June 2024
ACCEPTED 26 August 2024
PUBLISHED 10 September 2024

CITATION
Massey WJ and Zhu L (2024) Commentary: A rapid action plan to improve diagnosis and management of lipodystrophy syndromes. *Front. Endocrinol.* 15:1445226. doi: 10.3389/fendo.2024.1445226

Commentary: A rapid action plan to improve diagnosis and management of lipodystrophy syndromes

William J. Massey[1,2*] and Lin Zhu[3*]

[1]Department of Inflammation and Immunity, Lerner Research Institute, Cleveland Clinic, Cleveland, OH, United States, [2]Center for Microbiome and Human Health, Lerner Research Institute, Cleveland Clinic, Cleveland, OH, United States, [3]Department of Medicine, Division of Diabetes, Endocrinology and Metabolism, Vanderbilt University Medical Center, Nashville, TN, United States

KEYWORDS

lipodystrophy syndromes, adipose tissue, concomitant disease, rare endocrine disorders, metabolic disease, diabetic obesity

A commentary on

A rapid action plan to improve diagnosis and management of lipodystrophy syndromes

By Fourman LT, Lima JG, Simha V, Cappa M, Alyaarubi S, Montenegro Jr. R, Akinci B and Santini F (2024). *Front. Endocrinol.* 15:1383318. doi: 10.3389/fendo.2024.1383318

1 Introduction

Fourman et al. have recently published a clinically-oriented rapid action plan for the diagnosis and management of lipodystrophy syndromes (1). Lipodystrophy syndromes may be characterized by two factors: the pattern of fat loss which may occur across the whole body (generalized) or in specific body parts (partial) and whether the condition is genetic (congenital/familial) or acquired (2, 3). Unlike their clinical antithesis, obesity, lipodystrophy syndromes are rare, has heterogeneous clinical presentation, and are challenging to diagnose, yet the metabolic complications and end-organ damage that result from these two conditions can be similar. It took an average of 3.1 years in generalized lipodystrophy and 9.0 years in partial lipodystrophy for physicians to diagnose them accurately (4). Fourman et al. developed the quick action plan based on a large-scale study of comprehensive and long-term data across multiple countries (1, 4). An international panel of clinical experts were invited to discuss the key priorities for clinicians in the first 100 days after seeing a patient with clinical suspicion for the diagnosis (1). In comparison to the previous version of "step-by-step approach to diagnosis and treatment of lipodystrophy" (5), the rapid action plan has been updated with more detailed guidance for early diagnosis including the criteria for the skin thickness in men and women, which is considered important for early screening and can be precisely measured with dual-energy x-ray absorptiometry (1). Although the lack of adipose tissue is required for diagnosis of a lipodystrophy syndrome, common indicators that healthcare providers should watch for in their routine assessment of patients include features of metabolic syndrome such as insulin

resistance, hypertriglyceridemia, fatty liver disease, and polycystic ovarian syndrome (PCOS) that is disproportionate to body size (i.e., in the absence of increased adiposity).

Treatment of lipodystrophies generally includes addressing the body's inability to properly store lipid by limiting dietary fat, supplementation of adipokines, and common treatments for affected organs. The ultimate goal of the rapid action plan proposed by Fourman et al. is to improve the diagnosis for lipodystrophy syndromes to enable earlier and more consistent treatment for patients.

A prompt action in diagnosis and treatment for lipodystrophy can provide clinical data of the disease in its early stages, which is currently scarce due to its rarity and heterogeneity. Clinical data for lipodystrophy at its early stages are important to explore therapeutic strategies not only for lipodystrophy syndromes but also for diabetic obesity. The metabolic reflection of the lack of adipose tissue is similar in diabetic obesity, in line with the concept that the functional capacity of adipose tissue in diabetic obesity has been overwhelmed by nutrition. Lipodystrophies and diabetic obesity together highlight the critical roles of adipose tissue in metabolism. Research in lipodystrophy syndromes may provide critical information to explore novel therapeutic strategies for diabetic obesity. For example, metabolic disorders are reduced by leptin replacement therapy in generalized lipodystrophy patients (6, 7), which makes strategies of increasing signaling sensitivity to adipokines appealing to improve metabolic complications in diabetic obesity because adipokine levels are generally high in those patients.

2 Relevance to other concomitant diseases

While the Fourman et al. rapid action plan focuses on the clinical diagnosis and management of the metabolic consequences of lipodystrophy syndromes, it is important to note that other concomitant disease states may also contribute to lipodystrophy. These states include neurological diseases, autoimmune disorders, and inflammatory bowel diseases (IBD). Given the numerous insights lipodystrophy syndromes have provided in the metabolic disease space, further consideration should be given to lipodystrophies' mechanistic relationships to other disease processes.

There have been reports of concomitant neurological diseases with lipodystrophy syndromes including a case report where a patient with congenital partial lipodystrophy and cataracts presented with paresthesia in the lower limbs and abnormal gait (8). Upon further investigation, the authors concluded that based on family history, the syndrome was likely autosomal dominant, but could not identify the underlying genetics. Subsequently, a study of six children carrying the c.985C>T mutation in the *BSCL2* (*Seipin*) gene lead to the association of the mutation with fatal neurodegeneration in homozygous carriers and this mutation was linked to exon 7-skipping transcripts of this gene (9). Most recently, a case series describing patients with a form of congenital generalized lipodystrophy presented with progressive myoclonus epilepsy was reported and attributed to novel mutations in the *BSCL2* (*Seipin*) gene (10). Importantly, none of these reports sought to understand the mechanistic basis of these neurological conditions with the lipodystrophy syndrome.

With respect to autoimmunity, it has been described that acquired generalized lipodystrophy can co-occur with type 1 diabetes. In a report of two such cases, the patients developed both conditions in prepubescence and exhibited poor glycemic control on insulin alone; however following a year of metreleptin treatment, both children had marked improvements in glycemic control with lower insulin requirements (7). Generalized lipodystrophy has also been acquired in pediatric patients with Hashimoto's thyroiditis, rheumatoid arthritis, hemolytic anemia, and chronic hepatitis (6). In these cases, metreleptin therapy improved metabolic parameters, but did not affect the clinical course of the autoimmune conditions. The best described relationship between autoimmunity and lipodystrophies involves the C3 nephritic factor and acquired partial lipodystrophy. In these cases it was observed that autoimmune conditions such as systemic lupus erythematosus, dermatomyositis, and membranoproliferative glomerulonephritis consequently occurred with upper body partial lipodystrophy (11, 12). In three cases of chronic hepatitis with features of autoimmunity where patients developed generalized lipodystrophy, the mechanism of the observed low C4 complement factor levels was investigated. These studies showed that while the few patients had differing etiologies of autoimmunity constitutive activation of the alternative complement pathway appeared to be common between these cases (13). Collectively these reports indicate that both partial and general lipodystrophy syndromes do co-occur with numerous autoimmune conditions and therefore may influence one another.

There is a known relationship between adipose tissue and Crohn's disease, one of the two main types of IBD. In Crohn's disease there is an expansion of mesenteric adipose tissue that wraps around the diseased bowel wall, termed "creeping fat" (14, 15). Notably, there were two case reports in 2019 related to generalized lipodystrophy syndromes and Crohn's disease. In the first case a pediatric patient with congenital generalized lipodystrophy experienced bowel perforation, which was associated with smooth muscle hypertrophy (16). The other report discussed a patient that experienced TNFα-dependent inflammation as a result of recombinant leptin therapy (17). Given the studies that have shown the contribution of adipose tissue to Crohn's disease further work is warranted to clarify the molecular basis underpinning the role of lipodystrophy in Crohn's disease pathology.

3 Conclusions

While Fourman et al. provide an up-to-date action plan for the clinical diagnosis and management of lipodystrophy syndromes' numerous adverse metabolic consequences, there remains little work done in basic and translational research to understand the

relationship between lipodystrophy syndromes and other concomitant conditions. Given the burden described in the studies cited above, especially in pediatric patients, and the tremendous insights that lipodystrophy syndromes have provided in the context of metabolic disease as well as adipose and lipid biology, greater consideration should be given to the role of adipose tissue cross talk with other organs involved in these concomitant conditions. Importantly, there are animal models available for lipodystrophies (18–20), which can facilitate such studies.

Author contributions

WM: Conceptualization, Visualization, Writing – original draft, Writing – review & editing. LZ: Conceptualization, Funding acquisition, Visualization, Writing – review & editing.

Funding

The author(s) declare financial support was received for the research, authorship, and/or publication of this article. WM is supported by a Cleveland Clinic Global Center for Pathogen and Human Health Research Postdoctoral Fellowship. LZ is supported by NIA (K01AG077038).

Conflict of interest

The authors declare that the research was conducted in the absence of any commercial or financial relationships that could be construed as a potential conflict of interest.

Publisher's note

References

1. Fourman LT, Lima JG, Simha V, Cappa M, Alyaarubi S, Montenegro RJr., et al. A rapid action plan to improve diagnosis and management of lipodystrophy syndromes. *Front Endocrinol (Lausanne)*. (2024) 15:1383318. doi: 10.3389/fendo.2024.1383318

2. Garg A. Acquired and inherited lipodystrophies. *New Engl J Med*. (2004) 350:1220–34. doi: 10.1056/NEJMra025261

3. Simha V, Garg A. Lipodystrophy: lessons in lipid and energy metabolism. *Curr Opin Lipidol*. (2006) 17:162–9. doi: 10.1097/01.mol.0000217898.52197.18

4. Akinci B, Oral EA, Neidert A, Rus D, Cheng WY, Thompson-Leduc P, et al. Comorbidities and survival in patients with lipodystrophy: an international chart review study. *J Clin Endocrinol Metab*. (2019) 104:5120–35. doi: 10.1210/jc.2018-02730

5. Araújo-Vilar D, Santini F. Diagnosis and treatment of lipodystrophy: a step-by-step approach. *J Endocrinol Invest*. (2019) 42:61–73. doi: 10.1007/s40618-018-0887-z

6. Lebastchi J, Ajluni N, Neidert A, Oral EA. A report of three cases with acquired generalized lipodystrophy with distinct autoimmune conditions treated with metreleptin. *J Clin Endocrinol Metab*. (2015) 100:3967–70. doi: 10.1210/jc.2015-2589

7. Park JY, Chong AY, Cochran EK, Kleiner DE, Haller MJ, Schatz DA, et al. Type 1 diabetes associated with acquired generalized lipodystrophy and insulin resistance: the effect of long-term leptin therapy. *J Clin Endocrinol Metab*. (2008) 93:26–31. doi: 10.1210/jc.2007-1856

8. Berger JR, Arioglu Oral E, Taylor SI. Familial lipodystrophy associated with neurodegeneration and congenital cataracts. *Neurology*. (2002) 58:43–7. doi: 10.1212/WNL.58.1.43

9. Guillén-Navarro E, Sánchez-Iglesias S, Domingo-Jiménez R, Victoria B, Ruiz-Riquelme A, Rábano A, et al. A new seipin-associated neurodegenerative syndrome. *J Med Genet*. (2013) 50:401–9. doi: 10.1136/jmedgenet-2013-101525

10. Opri R, Fabrizi GM, Cantalupo G, Ferrarini M, Simonati A, Dalla Bernardina B, et al. Progressive Myoclonus Epilepsy in Congenital Generalized Lipodystrophy type 2: Report of 3 cases and literature review. *Seizure*. (2016) 42:1–6. doi: 10.1016/j.seizure.2016.08.008

11. Misra A, Peethambaram A, Garg A. Clinical features and metabolic and autoimmune derangements in acquired partial lipodystrophy: report of 35 cases and review of the literature. *Medicine*. (2004) 83:18–34. doi: 10.1097/01.md.0000111061.69212.59

12. Sissons JGP, West RJ, Fallows J, Williams DG, Boucher BJ, Amos N, et al. The complement abnormalities of lipodystrophy. *New Engl J Med*. (1976) 294:461–5. doi: 10.1056/NEJM197602262940902

13. Savage DB, Semple RK, Clatworthy MR, Lyons PA, Morgan BP, Cochran EK, et al. Complement abnormalities in acquired lipodystrophy revisited. *J Clin Endocrinol Metab*. (2009) 94:10–6. doi: 10.1210/jc.2008-1703

14. Kredel LI, Siegmund B. Adipose-tissue and intestinal inflammation – visceral obesity and creeping fat. *Front Immunol*. (2014) 5:462. doi: 10.3389/fimmu.2014.00462

15. Sheehan AL, Warren BF, Gear MWL, Shepherd NA. Fat-wrapping in Crohn's disease: Pathological basis and relevance to surgical practice. *Br J Surg*. (2005) 79:955–8. doi: 10.1002/bjs.1800790934

16. Muñoz A, Radulescu A, Baerg J, Mendez Y, Khan FA. Bowel perforation in a pediatric patient with congenital generalized lipodystrophy type 4. *J Pediatr Surg Case Rep*. (2019) 48:101257. doi: 10.1016/j.epsc.2019.101257

17. Ziegler JF, Böttcher C, Letizia M, Yerinde C, Wu H, Freise I, et al. Leptin induces TNFα-dependent inflammation in acquired generalized lipodystrophy and combined Crohn's disease. *Nat Commun*. (2019) 10:5629. doi: 10.1038/s41467-019-13559-7

18. Kim S, Huang L-W, Snow KJ, Ablamunits V, Hasham MG, Young TH, et al. A mouse model of conditional lipodystrophy. *Proc Natl Acad Sci*. (2007) 104:16627–32. doi: 10.1073/pnas.0707797104

19. Le Lay S, Magré J, Prieur X. Not enough fat: mouse models of inherited lipodystrophy. *Front Endocrinol*. (2022) 13:785819. doi: 10.3389/fendo.2022.785819

20. Pajvani UB, Trujillo ME, Combs TP, Iyengar P, Jelicks L, Roth KA, et al. Fat apoptosis through targeted activation of caspase 8: a new mouse model of inducible and reversible lipoatrophy. *Nat Med*. (2005) 11:797–803. doi: 10.1038/nm1262

frontiers | Frontiers in Pharmacology

TYPE Review
PUBLISHED 11 June 2024
DOI 10.3389/fphar.2024.1410479

OPEN ACCESS

EDITED BY
Lin Zhu,
Vanderbilt University Medical Center,
United States

REVIEWED BY
Feng Liu,
Soochow University Medical College, China
Kenneth Maiese,
National Institutes of Health (NIH), United States

*CORRESPONDENCE
Jiang-Hua Li,
lijianghua8@sina.com

RECEIVED 01 April 2024
ACCEPTED 21 May 2024
PUBLISHED 11 June 2024

CITATION
Sun W-D, Zhu X-J, Li J-J, Mei Y-Z, Li W-S and Li J-H (2024), Nicotinamide N-methyltransferase (NNMT): a novel therapeutic target for metabolic syndrome. *Front. Pharmacol.* 15:1410479. doi: 10.3389/fphar.2024.1410479

Nicotinamide N-methyltransferase (NNMT): a novel therapeutic target for metabolic syndrome

Wei-Dong Sun, Xiao-Juan Zhu, Jing-Jing Li, Ya-Zhong Mei, Wen-Song Li and Jiang-Hua Li*

Key Lab of Aquatic Training Monitoring and Intervention of General Administration of Sport of China, Physical Education College, Jiangxi Normal University, Nanchang, China

Metabolic syndrome (MetS) represents a constellation of metabolic abnormalities, typified by obesity, hypertension, hyperglycemia, and hyperlipidemia. It stems from intricate dysregulations in metabolic pathways governing energy and substrate metabolism. While comprehending the precise etiological mechanisms of MetS remains challenging, evidence underscores the pivotal roles of aberrations in lipid metabolism and insulin resistance (IR) in its pathogenesis. Notably, nicotinamide N-methyltransferase (NNMT) has recently surfaced as a promising therapeutic target for addressing MetS. Single nucleotide variants in the NNMT gene are significantly correlated with disturbances in energy metabolism, obesity, type 2 diabetes (T2D), hyperlipidemia, and hypertension. Elevated NNMT gene expression is notably observed in the liver and white adipose tissue (WAT) of individuals with diabetic mice, obesity, and rats afflicted with MetS. Knockdown of NNMT elicits heightened energy expenditure in adipose and hepatic tissues, mitigates lipid accumulation, and enhances insulin sensitivity. NNMT catalyzes the methylation of nicotinamide (NAM) using S-adenosyl-methionine (SAM) as the donor methyl group, resulting in the formation of S-adenosyl-l-homocysteine (SAH) and methylnicotinamide (MNAM). This enzymatic process results in the depletion of NAM, a precursor of nicotinamide adenine dinucleotide (NAD^+), and the generation of SAH, a precursor of homocysteine (Hcy). Consequently, this cascade leads to reduced NAD^+ levels and elevated Hcy levels, implicating NNMT in the pathogenesis of MetS. Moreover, experimental studies employing RNA interference (RNAi) strategies and small molecule inhibitors targeting NNMT have underscored its potential as a therapeutic target for preventing or treating MetS-related diseases. Nonetheless, the precise mechanistic underpinnings remain elusive, and as of yet, clinical trials focusing on NNMT have not been documented. Therefore, further investigations are warranted to elucidate the intricate roles of NNMT in MetS and to develop targeted therapeutic interventions.

KEYWORDS

nicotinamide N-methyltransferase (NNMT), metabolic syndrome (MetS), nicotinamide adenine dinucleotide (NAD^+), homocysteine (Hcy), obesity, diabetes, hyperlipidemia, hypertension

1 Introduction

Metabolic syndrome (MetS) constitutes a multifaceted array of metabolic disorders, manifesting as disturbances in the body's handling of energy substrates, including proteins, fats, and carbohydrates. As per the latest diagnostic criteria, MetS necessitates the presence of any three out of the following five conditions: elevated fasting glucose or type 2 diabetes (T2D), hypertriglyceridemia, lowered high-density lipoprotein (HDL) cholesterol levels, central obesity, or hypertension (Alberti et al., 2009). Furthermore, these conditions can also result in the prothrombotic state, proinflammatory state, nonalcoholic fatty liver disease, and reproductive disorders (Cornier et al., 2008). It is evident that MetS embodies not a singular malady but rather a confluence of ailments typified by obesity, hypertension, diabetes, and hyperlipidemia (Kane and Sinclair, 2018; Tilg et al., 2020).

The etiology and pathogenesis of MetS remain incompletely elucidated. However, obesity and insulin resistance (IR) are presently acknowledged as significant causative factors in MetS. Nicotinamide N-methyltransferase (NNMT) is a cytoplasmic enzyme that catalyzes the methylation of nicotinamide (NAM) with the methyl donor S-adenosyl-methionine (SAM) to form methylnicotinamide (MNAM) and S-adenosyl-l-homocysteine (SAH) (Alston and Abeles, 1988; Van Haren et al., 2016). NNMT predominantly localizes in adipose tissue and liver (Aksoy et al., 1994). Previous investigations have highlighted elevated NNMT expression in the liver and white adipose tissue (WAT) of diabetic mice and obese, with evidence suggesting that downregulating NNMT expression can mitigate diet-induced IR and obesity (Kraus et al., 2014; Pissios, 2017). Our prior research identified a positive correlation between body mass index (BMI) and urinary MNAM levels (Li and Wang, 2011). Additionally, significant associations were observed between single nucleotide variants in the NNMT gene and energy metabolism, obesity, T2D, hyperlipidemia, and hypertension (Zhu et al., 2016; Zhou et al., 2017; Li et al., 2018; Guan et al., 2021; Liu et al., 2021). Giuliante et al. (Giuliante et al., 2015) reported pronounced elevation of NNMT protein expression, gene expression, and enzyme activity in the adipose tissue of rats afflicted with MetS. Collectively, These results suggest a central position of NNMT in the development of MetS. This review delineates potential mechanisms underlying the NNMT-MetS association and provides insights into the progress of NNMT research within the domain of MetS-related diseases.

2 Potential mechanisms linking NNMT to MetS

As shown in Figure 1, NNMT utilizes SAM as a methyl donor to methylate NAM, yielding SAH and MNAM. This enzymatic process has the potential to deplete NAM, a precursor for nicotinamide adenine dinucleotide (NAD^+), while generating SAH, a precursor for Hcy. Consequently, this reaction could lead to a decline in NAD^+ levels and an elevation in Hcy levels. Numerous studies have substantiated the significance of reduced NAD^+ levels and heightened Hcy levels in the pathogenesis of MetS. In subsequent sections, we will delve into the mechanisms through which NNMT activity contributes to diminished NAD^+ levels and augmented Hcy levels, respectively, and their implications in the context of MetS.

2.1 Decreased NAD^+ levels and MetS

NAD^+ serves as a critical coenzyme in the conversion of carbohydrates into lipids and fuel oxidation (Belenky et al., 2007). The reduction of NAD^+ levels potentially represents a pivotal mechanism underlying NNMT's implication in MetS development. The competitive relationship between NAM methylation and NAD^+ recycling suggests that NNMT could impede energy expenditure while promoting lipid accumulation. This is attributed to the heightened levels of NNMT potentially rendering NAM irretrievable, thereby constraining NAD^+-dependent processes (Trammell and Brenner, 2015).

Figure 1 shows the three primary synthetic pathways for NAD^+: the *de novo* pathway, the Preiss Handler pathway, and the salvage pathway. Among these pathways, the salvage pathway predominates as the principal route for NAD^+ biosynthesis in mammals (Collins and Chaykin, 1972; Revollo et al., 2007; Mori et al., 2014), contributing to more than 85% of NAD^+ synthesis (Frederick et al., 2016). Conversely, the *de novo* pathway and Preiss Handler pathway synthesize NAD^+ using nicotinic acid (NA) and tryptophan

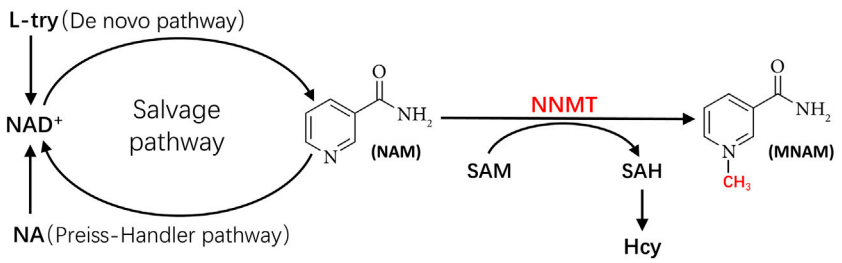

FIGURE 1
The metabolic pathways linking NNMT to NAD^+ and to Hcy. Hcy, homocysteine; L-try, L-Tryptophan; MNAM, methylnicotinamide; NA, nicotinic acid; NAD^+, nicotinamide adenine dinucleotide; NAM, nicotinamide; NNMT, nicotinamide N-methyl transferase; SAH, S-adenosyl-l-homocysteine; SAM, S-adenosyl-methionine.

as substrates, respectively, albeit in smaller quantities. Notably, NAM serves as the substrate for NAD^+ synthesis in the salvage pathway (Pissios, 2017). However, NNMT can methylate NAM, converting it to MNAM. Once NAM undergoes methylation by NNMT, it becomes unavailable for NAD^+ generation via the salvage pathway. Consequently, NNMT activity can directly influence the primary pathway of NAD^+ production (i.e., the salvage pathway), culminating in diminished NAD^+ levels.

Studies have consistently reported that inhibiting NNMT activity or downregulating NNMT expression leads to significant increases in NAD^+ levels in mouse adipocytes (Kraus et al., 2014; Neelakantan et al., 2018) and hepatocytes (Song et al., 2020). In contrast, it has been demonstrated that overexpression of NNMT in mouse liver leads to a decrease in NAD^+ levels (Komatsu et al., 2018). Regulation of NNMT may affect cancer-related pathways, Huang et al. (Huang et al., 2024) found through *in vitro* experiments that NNMT promotes the migration and invasive ability of esophageal squamous cell carcinoma (ESCC), and NNMT also promotes the process of epithelial mesenchymal transition (EMT) by affecting the post-transcriptional modification of E-calmodulin. Numakura et al. (Numakura and Uozaki, 2024) found that NNMT-positive gastric cancer stromal cells, especially fibroblasts, may promote tumor growth and progression by altering their surrounding epigenetic environment. In human colon cancer cells, silencing NNMT resulted in approximately a 30% increase in NAD^+ levels (Xie et al., 2014), whereas NNMT overexpression decreased NAD^+ levels by 30% (Xie et al., 2014). Moreover, Eckert *et al.* (Eckert et al., 2019) reported that the suppression of NNMT resulted in increased NAD^+ levels in cancer-associated fibroblasts (CAFs). In a study of a mouse unilateral ureteral obstruction (UUO) model, Takahashi *et al.* (Takahashi et al., 2022) observed an elevation in renal NNMT expression and a reduction in NAD^+ levels. Additionally, Sun et al. (Sun et al., 2022) illustrated that NNMT knockdown in a low-glucose environment enhanced the NAD^+/NADH ratio in U251 glioma cells.

2.1.1 Association between decreased levels of NAD^+ and MetS

NAD^+ functions as a crucial coenzyme in cellular energy metabolism. Loss of NAD^+ levels results in impairment of mitochondria function, which leads to failure of essential metabolic processes (Klimova and Kristian, 2019; Guimera et al., 2022). This may lead to a less efficient oxidative phosphorylation process, resulting in the production of more free radicals and reactive oxygen species (ROS) (Reid et al., 2018). ROS are a hallmark of oxidative stress and they can damage intracellular proteins, lipids, and DNA, leading to impairment of cellular function and structure, which has been implicated in the development of a variety of diseases including aging, diabetes mellitus, vascular endothelial cell injury, neurodegenerative diseases, and the onset of cellular senescence, strategies to replenish depleted NAD^+ pools can offer significant improvements of pathologic states (Klimova and Kristian, 2019; Maiese, 2023). A decrease in NAD^+ levels directly affects the metabolism of the body's three major energy substances: sugar, fat, and protein, inducing MetS (Covarrubias et al., 2021). Numerous studies have documented a reduction in NAD^+ levels across various mouse tissues, including adipose (Yoshino et al., 2011), skeletal muscle (Frederick et al., 2015), liver (Trammell et al., 2016), and hypothalamus (Sasaki et al., 2014), concomitant with the development of obesity. Nagahisa *et al.* (Nagahisa et al., 2022) observed that impaired NAD^+ biosynthesis correlates with the emergence of obesity-associated postprandial hyperglycemia. Specifically, diet-induced obese (DIO) mice exhibited diminished NAD^+ levels and impaired postprandial glucose metabolism compared to their lean counterparts. Conversely, pharmacological interventions aimed at augmenting NAD^+ biosynthesis have demonstrated significant improvements in IR and glucose homeostasis (Stromsdorfer et al., 2016; Poddar et al., 2019). Bruckbauer et al. (Bruckbauer et al., 2017) investigated the effects of NAM (a precursor of NAD^+) administration on lipid metabolism in cells and mice. They found that NAM supplementation elevated NAD^+ levels, thereby ameliorating lipid metabolism and hyperlipidemia. Similarly, Mills *et al.* (Mills et al., 2016) found nicotinamide mononucleotide (NMN) supplemented in mice decreased body weight and increased insulin sensitivity as well as improved plasma lipid profile. Furthermore, Qiu *et al.* (Qiu et al., 2023) reported low levels of NAD^+ in the aorta from hypertensive patients showing that supplementation with NAD^+ precursors effectively lowered blood pressure and improved impaired vascular function in both hypertensive patients and mice.

2.1.2 Mechanisms linking decreased NAD^+ levels to MetS

Decreased NAD^+ levels are associated with obesity, with studies demonstrating reduced NAD^+ levels in obese individuals. Elevating NAD^+ levels can increase lipolysis and reduce body weight. Picard et al. (Picard et al., 2004) observed that overweight and obese patients could activate Sirtuin 1 (SIRT1) and Peroxisome proliferator-activated receptors (PPAR) through NAD^+ supplementation, resulting in weakened adipogenesis. Barbagallo et al. (Barbagallo et al., 2022) demonstrated that NAD^+ supplementation activates Sirtuin 2 (SIRT2), enhancing the reciprocal inhibition of forkhead box O1 (FOXO1) and PPAR-γ to inhibit adipocyte differentiation and induce fat loss. Uddin et al. (Uddin et al., 2017) reported that NAD^+ supplementation upregulates mitochondrial function, enhancing metabolism and promoting weight loss. Yamaguchi et al. (Yamaguchi et al., 2019) created the ANKO (adipocyte-specific nicotinamide phosphoribosyl transferase (Nampt) knockout) mice to elucidate the role of NAD^+ in the regulation of adaptive thermogenesis and lipolysis. NAMPT serves as the rate-limiting enzyme in NAD^+ biosynthesis. The study found that ANKO mice, which lack NAMPT in both brown adipose tissue (BAT) and WAT, showed disturbed gene programs involving thermogenesis and mitochondrial function in BAT, resulting in a dampened thermal response. Furthermore, the absence of NAMPT in WAT resulted in a significant reduction in adrenergic-induced lipolysis. These results underscore the critical role of adipose NAD^+ in modulating adaptive thermogenesis, lipolysis, and overall energy metabolism.

Decreased NAD^+ levels have been associated with hyperglycemia. NAD^+ plays a pivotal role in regulating the insulin signaling pathway and enhancing mitochondrial function, thereby contributing to the regulation of blood glucose levels. However, a decline in NAD^+ levels can precipitate a NAD^+/NADH redox imbalance, resulting in an accumulation of excess NADH. This surplus of electron donors in the mitochondrial electron transport chain can overwhelm and impair

mitochondrial complex I (Yan et al., 2016). Furthermore, excessive accumulation of NADH in conjunction with reduced NAD^+ availability can inhibit glyceraldehyde-3-phosphate dehydrogenase (GAPDH) activity in the glycolytic pathway, leading to glucose shunting to the glycolytic branch pathway (Yan et al., 2016; Song et al., 2019). This diversion activates the polyol pathway while diminishing cytoplasmic NAD^+ levels (Luo et al., 2015). The hexosamine pathway can be activated to enhance O-GlcNAc acylation, potentially leading to IR (Chen Y. et al., 2019). Additionally, Protein kinase C (PKC) pathway activation can induce insulin receptor substrate 1 (IRS-1) phosphorylation, inhibiting insulin signaling through downstream effectors such as Akt, phosphoinositide 3-kinase (PI3K), and glucose transporter 4 (GLUT-4) (Ritter et al., 2015; Kolczynska et al., 2020). Furthermore, the formation of advanced glycosylation end products can exacerbate IR, pancreatic β-cell dysfunction, and cellular apoptosis (Nowotny et al., 2015).

Decreased levels of NAD^+ have been implicated in hypertension. NAD^+ exhibits vasorelaxant effects and diminishes oxidative stress, potentially contributing to the regulation of blood pressure. It is imperative to note that while these effects suggest a potential benefit, further research is needed to clarify the relationship between NAD^+ and hypertension. Investigations conducted on rat thoracic aorta and porcine coronary arteries have demonstrated that elevated levels of NAD^+ induce concentration-dependent vasorelaxation in endothelial cells (ECs) across various arterial beds. This vasorelaxation is mediated through actions on purinergic receptors, specifically adenosine receptors (Alefishat et al., 2015). Moreover, NAD^+ regulates the activity of NADPH oxidase, a significant ROS source in vascular cells, thereby playing a key role in the modulation of vascular tone (Reid et al., 2018). Elevated oxidative stress fosters the proliferation and hypertrophy of vascular smooth muscle cells, as well as collagen deposition, culminating in vascular medial thickening and constriction. Enhanced oxidative stress may also impair endothelial function, leading to diminished endothelium-dependent vasorelaxation and heightened vascular contractility. These observations underscore the potential link between heightened oxidative stress and the pathogenesis of hypertension (Grossman, 2008). Consequently, by mitigating oxidative stress and enhancing vascular function, NAD^+ holds promise as a therapeutic target for blood pressure regulation.

Decreased levels of NAD^+ have been associated with dyslipidemia. While direct evidence of NAD^+'s impact on lipid levels is limited, several studies have indicated that supplementation with NAD^+ precursors can ameliorate lipid profiles. Meta-analyses have shown that supplementation with NAD^+ precursors, including NMN, nicotinamide riboside (NR), NA, and NAM, significantly reduces levels of triglycerides (TG), total cholesterol (TC), and low-density lipoprotein (LDL), while concurrently increasing high-density lipoprotein levels (Zhong et al., 2022). Imi et al (Imi et al., 2023). Demonstrated that administration of NMN, an NAD^+ precursor, markedly reduced subcutaneous fat mass in mice fed a high-fat diet (HFD). The study showed a decrease in the size of adipocytes in subcutaneous adipose tissue after NMN treatment. Furthermore, the treatment with NMN resulted in a significant upregulation of adipose triglyceride lipase (ATGL) expression in subcutaneous fat, which is in line with the observed alterations in fat mass and adipocyte size (Imi et al., 2023). These findings suggest that NAD^+ may exert beneficial effects on lipid profiles by modulating the expression of lipid-metabolizing enzymes.

2.2 Increased Hcy levels and MetS

Hyperhomocysteinemia (HHcy) stands as a well-established independent risk factor for cardiovascular and cerebrovascular diseases (Dubchenko et al., 2019). Hence, understanding the potential pathophysiological interplay between Hcy levels and MetS is of paramount' importance. Moreover, there exists evidence linking elevated Hcy levels to an increased risk of MetS (Sreckovic et al., 2017). Esteghamati et al. (Esteghamati et al., 2014) documented a significantly relationship among elevated Hcy levels and major manifestations of MetS, including impaired glucose tolerance (IGT), abdominal obesity, elevated blood pressure, and hypertriglyceridemia. Consequently, the elevation in Hcy levels induced during NAM methylation emerges as another crucial mechanism underlying the involvement of NNMT in MetS development. Figure 1 illustrates NNMT utilizing SAM as a methyl donor to methylate NAM, yielding MNAM and SAH. Subsequently, SAH is converted to Hcy by SAH hydrolase (SAHase) (Aksoy et al., 1994; Okamoto et al., 2003; Souto et al., 2005). Therefore, heightened NNMT activity leads to elevated blood Hcy levels. A genome-wide scanning study conducted by Souto et al. (Souto et al., 2005) on Spanish families corroborated NNMT as the principal genetic determinant of plasma Hcy levels.

2.2.1 Association between increased Hcy levels and MetS

While the precise mechanism underlying how HHcy contributes to MetS remains incompletely understood, substantial evidence supports HHcy as a major risk factor for MetS development. Lee et al. (Lee et al., 2021) conducted comprehensive analyses utilizing datasets such as the Korean Association Resource (KARE), Health Examinees (HEXA), and Cardiovascular Disease Association Study (CAVAS), employing both one-sample Mendelian Randomization (MR) and two-sample MR methods. Their findings consistently demonstrated a significant association between HHcy and increased risk of MetS. Similarly, Ulloque-Badaracco et al. (Ulloque-Badaracco et al., 2023) identified a significant correlation between elevated Hcy levels and MetS. You et al. (You et al., 2023) observed a substantial correlation between HHcy and MetS prevalence among Chinese older adults. Liu et al. (Liu et al., 2022) conducted a longitudinal study involving Chinese community residents aged ≥65 years, revealing that HHcy escalates the risk of MetS, particularly among individuals with abdominal obesity. Piazzolla et al. (Piazzolla et al., 2019) conducted a cross-sectional analysis of MetS patients, noting elevated Hcy levels in a considerable proportion of cases. Butkowski et al. (Butkowski et al., 2017) investigated the interplay among Hcy, oxidative stress processes, and MetS, elucidating a positive association between Hcy levels and the presence of MetS factors. Yakub et al. (Yakub et al., 2014) evaluated a cohort of rural Nepalese children aged 6–8 years, discovering an elevated risk of MetS associated with increased Hcy levels. These collective findings underscore the significant role of HHcy in the pathogenesis of MetS across diverse populations and age groups.

2.2.2 Mechanisms linking increased Hcy levels to MetS

Elevated Hcy levels exert inhibitory effects on the insulin signaling pathway, primarily by inducing IR through the cysteine-homocysteinylation of the pro-insulin receptor. Hcy interacts with cysteine-825 residues situated on the pro-insulin receptor within the endoplasmic reticulum (ER), thereby disrupting the formation of initial disulfide bonds. This cysteine-homocysteinylation event perturbs the pro-insulin receptor and furin protease interaction within the Golgi apparatus, consequently inhibiting the cleavage of the pro-insulin receptor. Elevated Hcy levels in mice result in diminished levels of mature insulin receptors across various tissues, culminating in IR and the onset of T2D (Zhang et al., 2021).

1Increased Hcy levels promote oxidative stress. Elevated Hcy leads to an increase in the generation of mitochondrial ROS, resulting in oxidative damage at the cellular and molecular levels, and suppression of antioxidant enzyme systems (Kaplan et al., 2020). Hcy triggers oxidative stress by multiple means, such as generating ROS directly through auto-oxidation with transition metals, activating oxidative pathways, and blocking antioxidant pathways (Perna et al., 2003; Esse et al., 2019; Ostrakhovitch and Tabibzadeh, 2019). This leads to damage to tissue cells, including vascular ECs (Incalza et al., 2018), adipocytes (Furukawa et al., 2004), and pancreatic β-cells (Gerber and Rutter, 2017). Ultimately, this results in the development of MetS.

Elevated Hcy levels have been implicated in perturbing fat metabolism, presenting a potential link between Hcy and adipose tissue dysfunction, which further contributes to cardiovascular disease risk. Recent research indicates that Hcy disrupts the breakdown of fats in fat cells by activation of the AMP-activated protein kinase (AMPK) pathway (Wang et al., 2011). Exposure to Hcy leads to a decrease in glycerol and free fatty acid (FFA) release in fully differentiating 3T3-L1 and primary adipose cells in a dose-dependent manner. Notably, the inhibitory effects of Hcy on lipolysis are mediated through AMPK activation in adipocytes, underscoring the significance of AMPK in mitigating the impacts of Hcy on fat metabolism (Wang et al., 2011). Furthermore, elevated plasma Hcy levels have been associated with decreased levels of HDL-cholesterol and disturbances in plasma lipid profiles, potentially leading to fatty liver accumulation (Obeid and Herrmann, 2009). Hypomethylation induced by HHcy appears to contribute to lipid deposition in tissues. Investigating mechanisms underlying dysregulated lipid metabolism, Visram et al. (Visram et al., 2018) established a model of HHcy in yeast and showed that Hcy supplementation resulted in increased cellular levels of fatty acids and triacylglycerols. Furthermore, the model demonstrated increased resistance to cerulenin, a fatty acid synthase inhibitor, and lower levels of condensing enzymes linked to the synthesis of very long-chain fatty acids (Visram et al., 2018). These findings underscore the intricate relationship between Hcy and lipid metabolism dysregulation, shedding light on potential mechanisms underlying adipose tissue dysfunction and its implications for cardiovascular health.

Increased Hcy levels activate inflammatory response. HHcy activates the release of inflammatory factors, induces leukocyte chemotaxis and activation, and causes ER stress. This results in an increased inflammatory response, which damages tissue cells, such as vascular ECs and pancreatic β-cells, ultimately leading to Mets. High levels of Hcy can activate the expression and release of inflammatory factors, leading to vascular endothelial dysfunction (Balint et al., 2020). Numerous *in vitro* studies have corroborated the ability of Hcy to induce the release of inflammatory cytokines from ECs, including interleukin-6, interleukin-8, and tumor necrosis factor-α (Kamat et al., 2013; Han et al., 2015; Li et al., 2016). This inflammatory response within the vasculature may stem from the activation of Nuclear Factor-kappa β (NFkβ) (Zhao et al., 2017). Animal models of HHcy corroborate these findings. For instance, in a murine model, Hofmann *et al.* (Hofmann et al., 2001) reported that HHcy exacerbates vascular inflammation and accelerates atherosclerosis. Additionally, Wu et al. (Wu et al., 2019) demonstrated in human umbilical vein ECs and arteries of HHcy mice that Hcy triggers the expression of ER oxidoreductin-1α (Ero1α), leading to ER stress and subsequent inflammation. Notably, Ero1α knockdown has been found to mitigate HHcy-induced ER oxidative stress and inflammation.

3 Study progress of NNMT in MetS-related diseases

Metabolic Syndrome (MetS) represents a constellation of metabolic disorders arising from intricate interplays between genetic predisposition and environmental influences. While the precise etiology remains incompletely understood, central obesity and insulin resistance (IR) stand prominently as pivotal contributors to MetS onset. Additionally, dyslipidemia, hypertension, and other factors are recognized as potential drivers of MetS pathogenesis (Kane and Sinclair, 2018; Tilg et al., 2020). The ensuing sections will delineate the advancements in NNMT research pertaining to obesity, diabetes, hyperlipidemia, and hypertension.

3.1 NNMT and obesity

Obesity stands as a pathological state characterized by the excessive accumulation of body fat and constitutes a significant contributor to MetS. Emerging evidence suggests a pivotal role of NNMT in the context of obesity. Initial metabolomics investigations unveiled a noteworthy correlation between urinary MNAM levels and BMI (Salek et al., 2007; Li and Wang, 2011). Subsequent studies by Liu *et al.* (Liu et al., 2015) extended these findings, revealing a positive association between serum MNAM levels and obesity. These observations hint at a potential linkage between obesity and augmented NNMT activity, given MNAM's production during NNMT enzymatic reactions. This notion gains further support from recent experimental endeavors. Multiple studies have reported a conspicuous upregulation of NNMT expression in WAT among mice prone to obesity compared to their obesity-resistant counterparts (Alexander et al., 2006; Svenson et al., 2007; Wu et al., 2009). Notably, Lee et al. (Lee et al., 2005) documented significantly elevated NNMT expression in abdominal subcutaneous adipocytes of obese Pima Indians relative to non-obese counterparts. Furthermore, Kraus et al. (Kraus et al., 2014) elucidated that NNMT silencing significantly reduced relative adiposity in mice by approximately 47%. They proposed that heightened NNMT expression in WATs and/or liver could potentially serve as a

contributory factor to obesity. Additionally, it has been documented that NNMT knockdown significantly mitigated both body weight and adiposity in female mice subjected to a Western diet, characterized by a composition of 47% kcal of fat and 34% kcal of carbohydrate (Brachs et al., 2019). Moreover, Roberti et al. (Roberti et al., 2023) highlighted the preventive effects of NNMT blockade during the initial phases of adipogenesis, which inhibited preadipocyte differentiation into adipocytes in response to glucocorticoids. Furthermore, NNMT gene knockout resulted in a significant reduction in adipogenesis. Dong et al. demonstrated that knockdown of the Nmnat1 gene in hepatic cells leads to depletion of nuclear NAD^+, thereby causing mitochondrial dysfunction (Dong et al., 2024). NMNAT is an essential key enzyme in the NAD^+ salvage pathway. Its deficiency results in reduced NAD^+ synthesis and accumulation of its substrate, NAM, leading to increased NNMT activity and further decline in NAD^+ levels. NAD^+ plays a crucial role in maintaining mitochondrial function and energy metabolism. Decreased NAD^+ levels can impair the efficiency of the mitochondrial respiratory chain, resulting in reduced energy production, which may exacerbate obesity and related metabolic disorders (Amjad et al., 2021). Our previous research investigated the association between NNMT gene sequence variants and obesity, revealing significant findings. Specifically, investigations on the Chinese Han population identified the rs10891644 variant as significantly associated with obesity susceptibility, with heterozygous individuals (GT type) exhibiting heightened vulnerability (Zhou et al., 2017). Analogously, Bañales-Luna *et al* (Bañales-Luna et al., 2020). Reported a significantly correlation of the variant rs694539 of the NNMT gene sequence with BMI values in the Mexican population, with carriers of the GG and AG genotypes having an increased susceptibility to obesity.

Obesity arises from an imbalance in energy metabolism, wherein energy intake surpasses energy expenditure. As shown in Figure 2, NNMT's influence on obesity predominantly stems from its regulatory role in energy metabolism, particularly through NAM methylation, which significantly impacts energy modulation. Upon methylation, NAM becomes irretrievable for NAD^+ synthesis (Trammell and Brenner, 2015). NAD^+ is a vital coenzyme in fuel metabolism and the transformation of carbohydrate into lipid (Houtkooper et al., 2010). The relationship between NAM metabolism and NAD^+ utilization indicates that elevated NNMT expression may inhibit energy expenditure and promote fat deposition by limiting NAD^+-dependent processes (Trammell and Brenner, 2015). Our prior investigations have unveiled substantial correlations between NNMT genetic variants and resting energy expenditure (Zhu et al., 2016), as well as maximal oxygen uptake (Teperino et al., 2010) in the Chinese populace. Bañales-Luna et al. (Bañales-Luna et al., 2020) recently corroborated these findings, discovering a significant link between NNMT genetic variants and resting energy expenditure in Mexican individuals. Additionally, Kraus *et al.* (Kraus et al., 2014) shed light on NNMT's regulation of energy metabolism and associated mechanisms through laboratory experiments. *In vitro* studies revealed that diminishing NNMT expression via RNA interference (RNAi) and inhibiting NNMT with MNAM substantially augmented oxygen consumption (OC) in adipocytes. Conversely, adipocytes exhibited a considerable decrease in oxygen consumption upon NNMT overexpression (Kraus et al., 2014). In animal models, mice with decreased NNMT levels exhibited heightened energy expenditures compared to control mice of similar weights (Kraus et al., 2014). NNMT modulates energy expenditure by regulating SAM and NAD^+ during NAM methylation. SAM and NAD^+ serve as critical cofactors in cellular energy metabolism and redox states (Jell et al., 2007). SAM facilitates polyamine synthesis by providing propylamine and adding a methyl group for histone methylation (Doench et al., 2003). Enhanced polyamine flux activation leads to elevated energy expenditure via polyamine acetylation, utilizing Acetyl-coenzyme A (acetyl-CoA) to generate acetylpolyamines (Jackson et al., 2003). Inhibition of NNMT augments SAM and NAD^+ levels, resulting in the upregulation of polyamine flux activation and increased energy expenditure (Kraus et al., 2014).

3.2 NNMT and diabetes

Diabetes is caused by a fundamental disturbance in the metabolism of glucose and is characterised by IGT, elevated fasting blood glucose, and inadequate insulin secretion or IR (Tripathi and Srivastava, 2006; Goldberg and Mather, 2012). MetS is a multifaceted condition that is defined as IR, IGT, T2D, or impaired fasting glucose (IFG) along with the existence of two or more of the followings: hypertension, microalbuminuria, hyperlipidemia, and obesity (Giuliante et al., 2015). It is evident that disorders of glucose metabolism in the form of diabetes and IR are the core elements of the MetS.

Multiple trials have robustly shown a strong association of NNMT with IR and T2D (Kraus et al., 2014; Kannt et al., 2015; Liu et al., 2015). Our previous study also identified a significant association between the NNMT genetic variant at rs1941404 and T2D in the Chinese Han population (Li et al., 2018). Additionally, NNMT has been shown to play a causal role in the development of

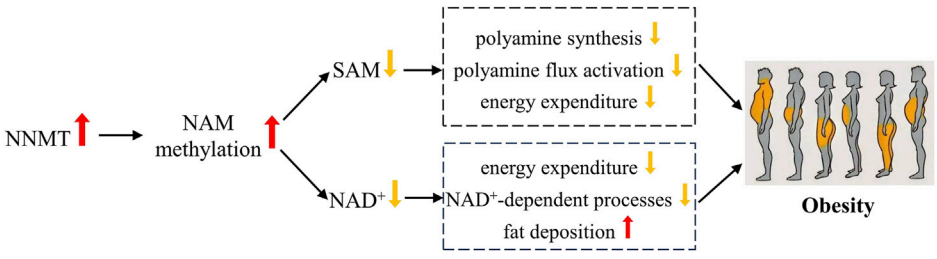

FIGURE 2
Possible mechanisms of NNMT associated with obesity.

T2D through quantitative trait locus mapping in mice (Yaguchi et al., 2005). Elevated levels of MNAM were detected in the urine (Li et al., 2018) and serum (Kannt et al., 2015) of individuals with T2D, suggesting an increase in NNMT activity during T2D development. Further direct evidence supporting this relationship is primarily derived from the reports outlined below. Kannt et al. (Souto et al., 2005) demonstrated an upregulation of NNMT expression in the WAT of individuals with IR or T2D. Additionally, a noteworthy correlation was found among plasma levels of MNAM and both the degree of IR and the expression levels of NNMT in WAT. Kraus *et al.* (Kraus et al., 2014) reported an increase in NNMT expression levels in the livers and WATs of T2D mice. They also found that knockdown of NNMT improved insulin sensitivity and glucose tolerance in the T2D mice. The role of NNMT in the development of T2D was further confirmed by Hong et al. (Hong et al., 2015). Their study revealed that hepatocyte glucose output decreased by 50% with NNMT knockdown, while NNMT overexpression increased it by 1.4-fold. Meanwhile, they observed a significantly lower overnight fasted glucose level in the livers of C57BL6/J mice with NNMT knockdown (Hong et al., 2015).

The potential mechanisms underlying NNMT's regulation of glucose metabolism are primarily derived from two key reports. Kraus *et al.* (Kraus et al., 2014) demonstrated that reduced NNMT expression enhances glucose tolerance and improves insulin sensitivity in DIO mice. The role of NNMT in gluconeogenesis was further elucidated by Hong et al. (Hong et al., 2015). Their results revealed that decreasing NNMT expression in primary hepatocytes led to a reduction in the expression of phosphoenolpyruvate carboxykinase 1 (Pck1) and glucose-6-phosphatase (G6pc), resulting in decreased glucose output. Conversely, increasing NNMT expression in primary hepatocytes resulted in elevated glucose output and increased expression of Pck1 and G6pc. Furthermore, Hong *et al.* (Hong et al., 2015) observed that mice subjected to NNMT knockdown exhibited reduced fasting glucose levels and diminished conversion of pyruvate to glucose. Such observations indicate that NNMT plays a beneficial role in regulating gluconeogenesis in hepatocytes.

As shown in Figure 3, in elucidating the regulatory mechanism of NNMT on glucose metabolism, Hong *et al.* (Hong et al., 2015) proposed that NNMT's product, MNAM, mediates its regulatory impact, with Sirt1 playing a pivotal role in this process. Their findings revealed a significant reduction in glucose production and expression of both G6pc and Pck1 in hepatocytes with NNMT overexpression and concurrent Sirt1 inhibition, compared to hepatocytes with NNMT overexpression alone. Furthermore, the downregulation of G6pc and Pck1 expressed by NNMT knockdown was reversed by the upregulation of Sirt1. These observations underscore the essential role of Sirt1 in mediating NNMT's regulatory effect on glucose metabolism. Additionally, a significant correlation between Sirt1 protein expression and NNMT expression was noted in hepatocytes. *In vitro* experiments demonstrated that NNMT overexpression significantly increased Sirt1 protein expression in primary hepatocytes, while NNMT knockdown led to a notable decrease in Sirt1 protein expression. Consistent with these findings, *in vivo* experiments revealed a significant reduction in Sirt1 protein expression in the livers of mice upon NNMT knockdown. Furthermore, MNAM, a product of NNMT, was found to playing a key part in this process. Similar to the effects of NNMT overexpression, hepatocytes treated with MNAM exhibited significant increases in glucose production and expression of Sirt1, G6pc, and Pck1. Notably, the alterations induced by MNAM treatment were abrogated upon Sirt1 knockdown. These results collectively indicate that Sirt1 is indispensable for NNMT-mediated regulation of glucose metabolism, and both NNMT and MNAM have the ability to upregulate Sirt1 expression.

3.3 NNMT and hyperlipidemia

Hyperlipidemia is a medical condition characterized by elevated levels of one or more plasma lipids, including TG, cholesterol, cholesteryl esters, phospholipids, and LDL, coupled with a reduction in HDL levels (P et al., 2021). It represents one of the complications associated with MetS. Despite limited research

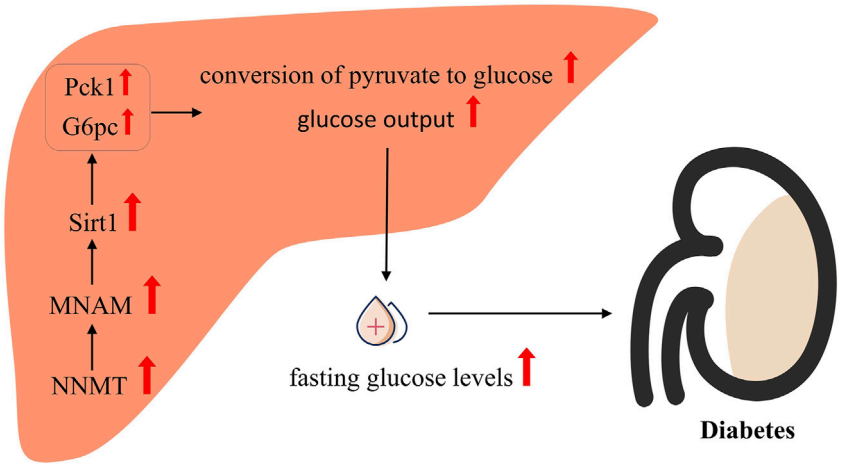

FIGURE 3
Possible mechanisms of NNMT associated with diabetes.

on the association between NNMT and hyperlipidemia, compelling evidence suggests its potential role in lipid metabolism. Notably, studies have shown that knocking down NNMT in adipose tissues and livers of mice fed a high-fat diet resulted in decreased serum TG and FFA levels (Kraus et al., 2014). Furthermore, our previous analysis of 19 tagSNPs in the NNMT gene sequences of Chinese Han patients revealed a significant association between the variant at rs1941404 and hyperlipidemia. Specifically, individuals carrying the CC genotype at this locus were identified as the susceptible population. The regulatory effect of the rs1941404 variant on resting energy expenditure offers a plausible explanation for the observed association between NNMT and hyperlipidemia. These findings underscore the potential involvement of NNMT in lipid metabolism regulation and its relevance to the development of hyperlipidemia, a key component of MetS (Zhu et al., 2016).

The etiology of hyperlipidemia remains incompletely elucidated; however, it is widely believed to be linked to aberrations in both sugar and fat metabolism. Epidemiological investigations have underscored a significant correlation between hyperlipidemia and conditions such as obesity or disruptions in energy metabolism (Zhu et al., 2016). Numerous studies have underscored a robust association between obesity and dyslipidemia (Vekic et al., 2019). As shown in Figure 4, Evidence suggests that dyslipidemia predominantly stems from IR and the influence of pro-inflammatory adipokines (Klop et al., 2013). Consequently, it is plausible that NNMT's involvement in hyperlipidemia is mediated through its impact on both sugar and fat metabolism. Moreover, NNMT might contribute to hyperlipidemia by influencing plasma Hcy levels. Multiple studies have highlighted a pronounced link between plasma Hcy levels and hyperlipidemia (Sreckovic et al., 2017; Hasan et al., 2019). Additionally, Mondal *et al.* (Mondal et al., 2018) demonstrated that elevated homocysteine levels can directly modulate lipid metabolism and induce hyperlipidemia in rats through Hcy administration (50 mg/kg/d).

3.4 NNMT and hypertension

Hypertension is another common complication of MetS. Although there are limited reports regarding the association between NNMT and hypertension, our research has identified a significant association between a SNP in the NNMT gene (rs1941404) and hypertension within the Chinese Han population (Guan et al., 2021).

While direct evidence linking NNMT activity to hypertension is currently lacking, numerous studies have established a strong association between NNMT activity and various metabolic disorders, including cardiovascular diseases (Li et al., 2006; Williams et al., 2012). For instance, Liu et al. (Liu et al., 2017) demonstrated a significant association between serum MNAM levels and coronary artery disease, as well as left ventricular systolic dysfunction in Chinese patients (Liu M. et al., 2018). Additionally, Bubenek *et al.* (Bubenek et al., 2012) reported a robust association between NNMT expression, serum MNAM levels, and the onset and progression of peripheral arterial occlusive disease. Notably, NNMT expression has been found to be positively correlated with LDL levels and negatively correlated with HDL levels, both of which are relevant factors in cardiovascular diseases (Herfindal et al., 2020; Kornev et al., 2023; Rus et al., 2023). As shown in Figure 5, left ventricular contractile dysfunction and arterial

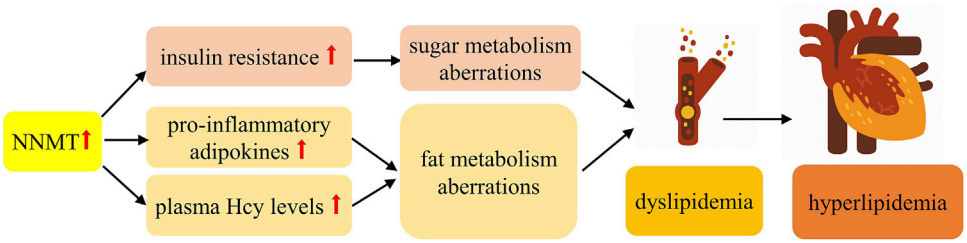

FIGURE 4
Possible Mechanisms of NNMT associated with hyperlipidemia.

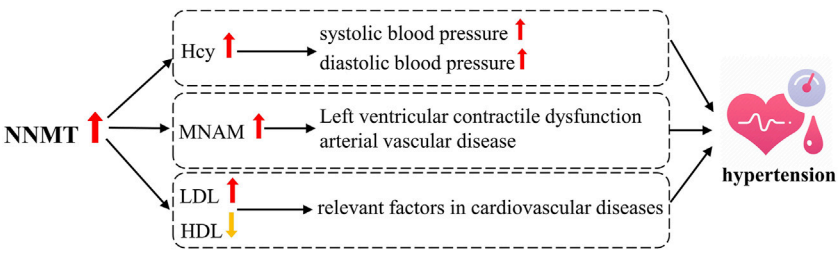

FIGURE 5
Possible Mechanisms of NNMT associated with hypertension.

vascular disease are significant contributors to the development of hypertension, suggesting a potential pathway through which NNMT may influence hypertension. Moreover, elevated plasma Hcy levels have been significantly associated with hypertension (Van Guldener et al., 2003), particularly with systolic blood pressure (SBP) (Esteghamati et al., 2014). Junedi et al. (Junedi et al., 2022) reported higher Hcy levels in hypertensive cases compared to controls. Moreover, increased plasma Hcy levels were associated with elevated SBP, diastolic blood pressure (DBP), and a higher prevalence of hypertension among middle-aged and elderly individuals of Chinese descen (Hidru et al., 2019). Notably, patients with HHcy exhibit significantly higher blood pressure compared to those without HHcy, and serum Hcy levels have been positively correlated with blood pressure in Wistar rats (Shi et al., 2019). Thus, influencing Hcy levels may represent another important pathway through which NNMT is implicated in the development of hypertension.

4 NNMT as a therapeutic target for MetS

4.1 RNAi drugs

As previously stated, NNMT activity results in reduced NAD^+ production and increased Hcy production. Studies have shown that knocking down the NNMT gene leads to increased expenditure of energy in adipocytes (Kraus et al., 2014) and decreased output of glucose from hepatocytes (Hong et al., 2015). Additionally, in animal models, NNMT gene knockdown has been found to improve insulin sensitivity (IS), glucose tolerance (GT), and overnight fasting glucose (OFG) levels, while also reducing lipid accumulation and triglyceride content (Kraus et al., 2014; Hong et al., 2015; Xu et al., 2022). These findings suggest that NNMT may represent a promising therapeutic target for the development of RNAi drugs aimed at preventing or treating MetS (Iyamu and Huang, 2020; Van Haren et al., 2021; Harikrishna and Venkitasamy, 2023). Some studies have used endogenous small interfering RNAs (miRNAs) to inhibit NNMT and competitive endogenous RNAs (ceRNAs) as "sponges" of miRNAs to reduce the inhibitory effect of miRNAs on target genes. MiRNAs are small noncoding RNAs that regulate gene expression via recognition of cognate sequences and interference of transcriptional, translational or epigenetic processes (Chen L. et al., 2019), miRNAs control mRNA expression, miRNAs are also capable of targeting non-coding RNAs, including long non-coding RNAs and miRNAs (Hill and Tran, 2021). Recently Yu et al. (Yu et al., 2021) and Wang et al. (Wang et al., 2021) identified miR-29b-3p and miR-378g as potential miRNAs upstream of NNMT by bioinformatics analysis. It was confirmed by dual luciferase reporter assay that miR-29b-3p and miR-378g directly target the 3′UTR of NNMT and negatively regulate NNMT expression. In osteoporosis, both miR-29b-3p and miR-378g regulate osteogenic differentiation of BMSCs by targeting NNMT. Inhibition of miR-29b-3p or miR-378g upregulates NNMT expression and promotes osteogenic differentiation of bone marrow mesenchymal stem cells (BMSCs), whereas overexpression of miR-29b-3p or miR-378g downregulates NNMT expression and inhibits osteogenic differentiation of BMSCs. Competitive endogenous RNAs (ceRNAs) act as "sponges" for miRNAs, ceRNAs can bind to miRNAs and reduce the abundance of miRNAs in the cell, thus reducing the inhibitory effect of miRNAs on target genes. Yu et al. (Yu et al., 2021) and Wang et al. (Wang et al., 2021) found that XIST and HOTAIR are long non-coding RNAs (lncRNAs) with significantly elevated expression in the serum of patients with osteoporosis, and that XIST and HOTAIR acted as ceRNAs (competing endogenous RNAs) to upregulate NNMT expression by adsorbing miR-29b-respectively. 3p and miR-378g, respectively, to upregulate the expression of NNMT, thereby inhibiting the osteogenic differentiation of BMSCs.

However, RNAi therapeutics still face technical obstacles, such as achieving efficient delivery of RNAi drugs targeting organs or tissues and overcoming the off-target interactions (Doench et al., 2003; Jackson et al., 2003; Persengiev et al., 2004; Scacheri et al., 2004), as well as addressing the issues of sequence-dependent and chemical-dependent toxicity (Grimm et al., 2006; Jackson et al., 2006). While certain RNAi drugs aimed at NNMT have shown efficacy *in vitro* and animal studies, there are no reports of such products being utilized in clinical trials thus far. It is worth noting, however, that the Food and Drug Administration (FDA) of the U.S. has approved over 10 RNAi drugs (Roberts et al., 2020). The technical barriers to RNAi therapies are gradually being resolved, implying that developing RNAi drugs that target NNMT remains a viable approach to prevent or treat MetS.

4.2 Small molecule inhibitors targeting NNMT

In addition to RNAi drugs, the development of small molecule inhibitors targeting NNMT represents a current research focus for the treatment of MetS-related diseases. As shown in Table 1 and Figure 6, the small molecule inhibitors targeting NNMT can be categorized into SAM-competitive inhibitors, NAM-competitive inhibitors, Dual-substrate-competitive inhibitors and isomerization inhibitors.

4.2.1 SAM-competitive inhibitors

SAM-competitive inhibitors compete with the substrate SAM for the binding site in NNMT. There are two main types of such inhibitors, SAH (Gao et al., 2021) and sinefungin (Zweygarth et al., 1986) (Table 1; Figure 6), but they are non-selective and inhibit all methyltransferases (Van Haren et al., 2016). However, SAH demonstrates activity solely in enzyme-based biochemical assays; its activity is diminished in cellular assays owing to its swift degradation to adenosine and Hcy by SAH hydrolase (Gao et al., 2021). Sinefungin, a naturally occurring compound derived from *Streptomyces*, serves as a SAM-mimicking methyltransferase inhibitor. However, it exhibits low cell membrane permeability and demonstrates substantial toxicity in animal models, thereby constraining its potential application as a therapeutic agent (Zweygarth et al., 1986).

4.2.2 NAM-competitive inhibitors

NAM-competitive inhibitors are substances that can compete with the substrate NAM for the binding site in NNMT. Table 1 and

TABLE 1 Overview of the small molecule inhibitors targeting NNMT.

NNMT inhibitor type	Compound
SAM-competitive inhibitors	SAH (Gao et al., 2021), sinefungin[a] (Zweygarth et al., 1986)
NAM-competitive inhibitors	MNAM (Kraus et al., 2014; Hong et al., 2015), 5-amino-1MQ (NNMTi) (Neelakantan et al., 2017; Neelakantan et al., 2018; Neelakantan et al., 2019), **JBSNF-000088** (Kannt et al., 2018), **JBSNF-000265** (Ruf et al., 2018), **JBSNF-000028** (Ruf et al., 2022), **RS004** (Horning et al., 2016), 4-chloro-3-ethynylpyridine (Sen et al., 2019)
Dual-substrate-competitive inhibitors	MvH45 (Van Haren et al., 2017), **AK-12** (Ruf et al., 2022), **MS2756** (Babault et al., 2018), **MS2734** (Babault et al., 2018), **GYZ-78** (Gao et al., 2019), **NS1** (Kuzmi et al., 2021), **LL320** (Chen et al., 2019a), Yuanhuadine[a] (Bach et al., 2018), **CC-410** (Roberti et al., 2023)
Allosteric inhibitors	Macrocyclic peptides (Van Haren et al., 2021)

[a]A natural inhibitor.

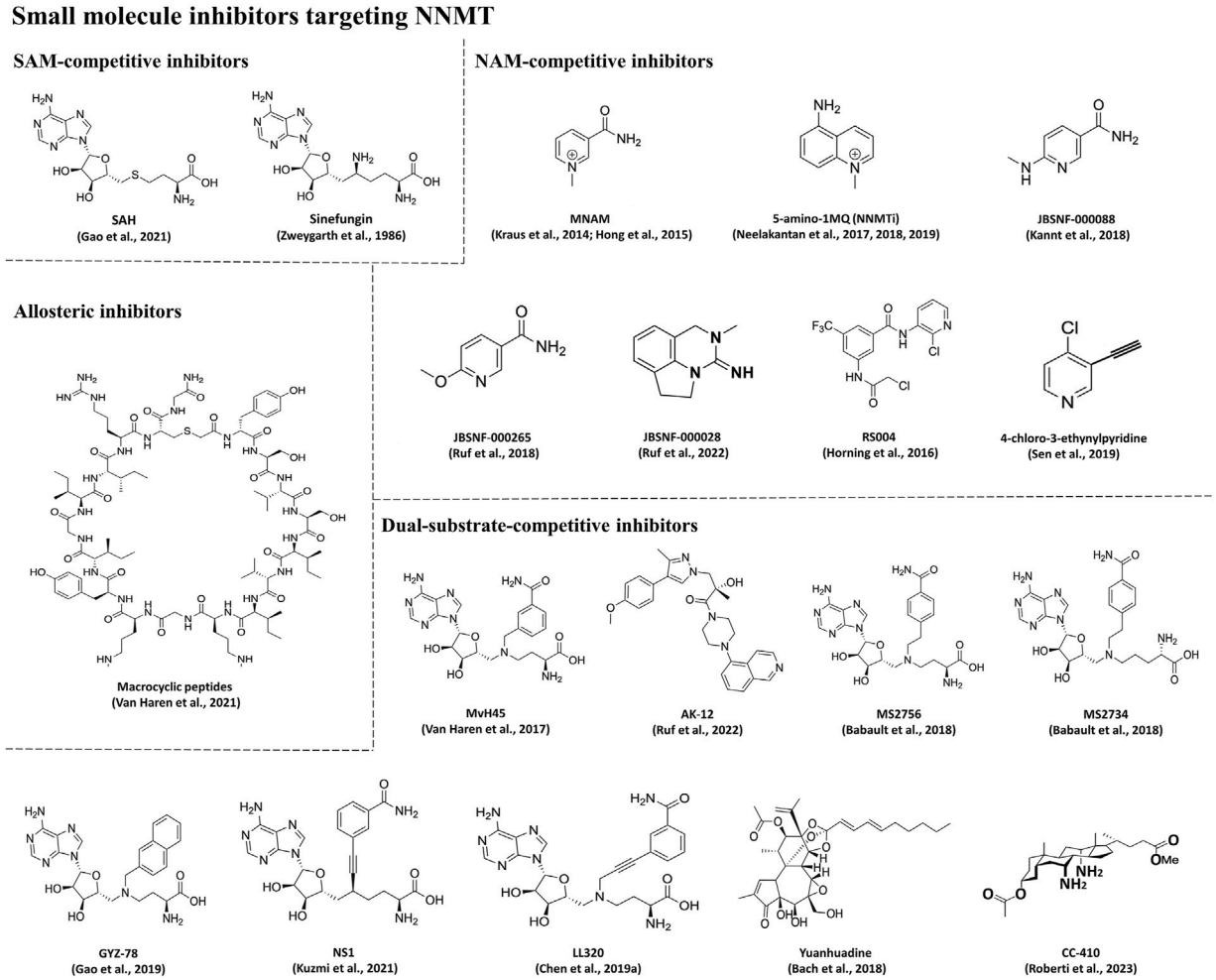

FIGURE 6
Chemical structures of small molecule inhibitors targeting NNMT.

Figure 6 lists several inhibitors in this category, but the most frequently reported ones are MNAM and 5-amino-1MQ (NNMTi).

MNAM, a natural inhibitor of NNMT, is generated through the enzymatic reaction catalyzed by NNMT (Gao et al., 2021). In a study conducted by Swaminathan et al. (Swaminathan et al., 2017), the X-ray crystal structure of a ternary complex of NNMT bound with MNAM was elucidated, revealing that MNAM binds to the active site of NNMT, thereby impeding NAM binding and suppressing NNMT's enzymatic activity. MNAM has been shown *in vitro* to be a significant enhancer of energy expenditure as well as a regulator of glucose metabolism. Kraus *et al.* (Kraus et al., 2014) used MNAM to inhibit NNMT activity in adipocytes and found that it induced an

increase in oxygen consumption. However, its effectiveness inside the body is controversial. Hong *et al.* (Hong et al., 2015) demonstrated that MNAM administration prevents changes in fasting blood glucose levels and insulin sensitivity in mice fed a HFD. Moreover, MNAM inhibits the biosynthesis of fatty acids and cholesterol, along with suppressing the expression of lipogenic and cholesterol-synthesizing genes, leading to significant reductions in liver cholesterol and TC levels. However, Przyborowski et al. (Przyborowski et al., 2015) reported that administering MNAM (100 mg/kg) to diabetic db/db mice for 4 weeks did not result in significant differences in fasting blood glucose and Glycated Hemoglobin A1c (HbA1c) levels between MNAM-treated and untreated diabetic db/db mice. Additionally, there was no decrease in body weight observed in the MNAM-treated diabetic db/db mice; rather, there was a tendency for weight gain compared to the untreated diabetic db/db mice. It was also noted by Hong *et al.* (Hong et al., 2015) that MNAM supplementation did not prevent weight gain. The reason why MNAM is not as effective in controlling fasting glucose, HbA1c, and body weight *in vivo* can be explained by two factors. Firstly, MNAM is unstable *in vivo*. It can be quickly excreted through urine in the form of MNAM or MNAM oxides (Shibata et al., 1987; Shibata et al., 1988; Menon et al., 2007). Additionally, MNAM has a low permeability to the membrane, which is crucial for achieving the desired therapeutic effect of the drug (Neelakantan et al., 2018). These findings may partially explain the limited effectiveness of MNAM in controlling body weight and glucose homeostasis.

NNMTi is a NAM analog that inhibits NNMT activity by competing with NAM (Parsons and Facey, 2021). Evidence suggests that it can reverse HFD-induced obesity in mice (Neelakantan et al., 2018; Sampson et al., 2021). Neelakantan et al. (Neelakantan et al., 2018) observed that systemic administration of NNMTi to mice with diet-induced obesity markedly attenuated WAT mass and body weight, diminished adipocyte volume, and reduced plasma TC levels. NNMTi was shown to have high permeability to the membrane in a bidirectional permeation assay in Caco-2 cells. Importantly, NNMTi is highly selective and has no inhibitory effect on other SAM-dependent methyltransferases or NAD^+ salvage pathway enzymes. *In vitro*, NNMTi significantly decreased the intracellular production of MNAM, increased the intracellular levels of NAD^+, and inhibited adipogenesis. *In vitro*, mice treated with NNMTi exhibited a notable decrease in body weight, white fat mass, and adipocyte volume. Notably, NNMTi did not affect food intake or cause any observed side effects. The findings indicate that NNMTi is a promising inhibitor that targets NNMT and can reverse the obesity induced by diet and prevent the associated T2D. (Neelakantan et al., 2018). Similar to the NNMT knockdown experiments, NNMT inhibitors reversed obesity by modulating NAD^+ rescue and the pathways mediated by SAM. These findings suggest that the combination of small molecule NNMT inhibitors with other nutritional supplements, such as the precursors of NAD^+, may have the potential to enhance the efficacy of treatment for MetS and minimize the side effects caused by high pharmacological dosages (Roberti et al., 2021).

In addition to MNAM and NNMTi, three new NAM analog inhibitors were reported for the treatment of MetS-related disorders in animal models: **JBSNF-000088** (Kannt et al., 2018), **JBSNF-000265** (Ruf et al., 2018), and **JBSNF-000028** (Ruf et al., 2022). **JBSNF-000088** binds to the active site on NNMT and leads to the demethylation of SAM to SAH (Kannt et al., 2018). This inhibits NNMT-catalyzed methylation of NAM and reduces the production of MNAM. In animal models of metabolic diseases, **JBSNF-000028** (Ruf et al., 2022) and **JBSNF-000088** (Kannt et al., 2018) were identified to inhibit human and mouse NNMT activity. These compounds effectively reduced MNAM levels in adipose tissue, liver, and plasma, leading to improved insulin sensitivity and decreased body weight. Moreover, in a mouse model of diet-induced obesity and diabetes, they restored normal glucose tolerance. **JBSNF-000265** was discovered through Structure-Activity Relationship (SAR) studies (Ruf et al., 2018) as a compound that binds to NNMT in a manner similar to that of NAM. It has an improved ability to inhibit the enzymatic activity of NNMT and drastically reduces the formation of MNAM. When mice were orally administered 50 mg/kg of this compound, MNAM production decreased by approximately 80% within 2 h. Moreover, **RS004** (Horning et al., 2016) and 4-chloro-3-ethynylpyridine (Sen et al., 2019) were also reported to compete with NAM for binding by covalently linking to Cys165 and Cys159 in the active site of NNMT. However, their efficacy *in vivo* models has not been reported yet.

4.2.3 Dual-substrate-competitive inhibitors

Dual-substrate-competitive inhibitors compete with the both substrates (SAM and NAM) for the binding sites in NNMT, thereby increasing inhibitors' activity and selectivity (Gao et al., 2021). As shown in Table 1 and Figure 6, such inhibitors mainly include MvH45 (Van Haren et al., 2017), **AK-12** (Ruf et al., 2022), **MS2756** (Babault et al., 2018), **MS2734** (Babault et al., 2018), **GYZ-78** (Gao et al., 2019), **NS1** (Kuzmi et al., 2021), **LL320** (Chen D. et al., 2019), Yuanhuadine (Bach et al., 2018), and **CC-410** (Roberti et al., 2023). This class of inhibitors has been recently developed, thus there is a scarcity of reported cellular or *in vivo* data concerning these compounds. However, it will be intriguing to investigate whether this class of inhibitors targeting NNMT exhibits improved efficacy in this context. One notable dual-substrate NNMT inhibitor is Yuanhuadine, which is isolated from the flower buds of the traditional Chinese medicine Daphne genkwa. Some studies have reported that Yuanhuadine demonstrates a favorable inhibitory effect on the growth of various tumor cell lines (He, 2002; Zhang et al., 2006; Hong et al., 2011). Additionally, Roberti *et al.* (Roberti et al., 2023) reported a novel dual-substrate NNMT inhibitor, **CC-410**, which stably binds to and exhibits high specificity in inhibiting NNMT.

4.2.4 Allosteric inhibitors

Allosteric inhibitors represent a class of inhibitors that do not compete for the SAM or NAM binding sites on NNMT. Instead, they bind to an allosteric site, thereby inhibiting NNMT activity. As previously mentioned, inhibitors targeting NNMT often bear structural resemblance to one or both of its substrates. As shown in Table 1 and Figure 6, in the pursuit of structurally diverse NNMT inhibitors, researchers have identified certain macrocyclic peptides that bind to NNMT, displaying potent inhibition with Half-maximal inhibitory concentration (IC_{50}) values as low as 229 nM (Van Haren et al., 2021). Moreover, these macrocyclic peptides have been

observed to downregulate MNAM production in cellular assays. Notably, these macrocyclic peptides exhibit noncompetitive behavior with either SAM or NAM, suggesting that they may function as allosteric inhibitors targeting NNMT (Van Haren et al., 2021).

5 Implications and recommendations for future research

As delineated in the text, NNMT is a crucial factor in MetS and has become a promising target for preventing or treating MetS-related diseases. However, despite the encouraging evidence, gaps in our knowledge remain to be filled in order to fully understand the mechanisms connecting NNMT with MetS-related disorders and to develop clinical agents against NNMT. The roles of NNMT in adipose tissues and livers appear to exhibit some contrasting effects. NNMT emerges as a novel regulator of adipose tissue function and energy expenditure. While NNMT influences energy metabolism in both adipose tissue and liver, its expression suppresses NAD^+ levels specifically in adipose tissue. However, it is noteworthy that knockdown of NNMT does not seem to affect NAD^+ levels in the liver, indicating potential divergent regulatory mechanisms of NNMT in these tissues and suggesting the existence of redundant pathways in NAD^+ metabolism regulation (Kraus et al., 2014). Nonetheless, additional research is necessary to clarify the exact mechanisms behind NNMT's actions in adipose tissues and liver. Specifically, it is necessary to determine how NNMT promotes fat accumulation in adipose tissues while managing fat accumulation in livers caused by nutrient overload (Trammell and Brenner, 2015). Further study also is needed to understand how NNMT inhibits the formation of NAD^+ in adipose tissues and why there are redundant regulatory pathways for the metabolism of NAD^+ in livers. This could provide insight into the functional differences of NNMT in different tissues.

Is NAD^+ necessary for NNMT to regulate energy metabolism processes? The competition between NAD^+ salvage and the methylation of NAM suggests that NNMT may reduce the oxidation of fuel and increase the storage of fat by regulating the formation of NAD^+ (Trammell and Brenner, 2015). However, experiments have not demonstrated direct effects of NNMT on the intracellular levels of NAM and NAD^+. In murine models, NNMT knockdown did not induce the accumulation of NAM in livers and adipose tissues, nor did it cause significant alterations in the intracellular levels of NAD^+ in hepatocytes (Kraus et al., 2014; Hong et al., 2015). Therefore, it is possible that NNMT may regulate energy metabolism through other mechanisms, and that NAD^+ is not necessary for this regulatory process.

Effects of NNMT on anaerobic energy metabolism remain unknown. Numerous studies have reported that NNMT has an inhibitory effect on the aerobic metabolism of sugars and fats, and NNMT Knockdown can increase oxygen consumption, promote sugar consumption and reduce fat synthesis, but the effects of NNMT on anaerobic energy metabolism have not been reported. Our previous study (Li et al., 2017) revealed higher expression levels of NNMT in the toe extensor muscle, typically reliant on anaerobic energy metabolism for power generation, compared to the soleus muscle, typically reliant on aerobic energy metabolism. Additionally, inhibition of NNMT using MNAM resulted in a decline in performance during anaerobic endurance exercise in rats (Zhou et al., 2018). These results suggest that NNMT may also contribute to the regulation of anaerobic energy metabolism.

Additional investigations are warranted to ascertain the suitability of NNMT as a therapeutic target for MetS. The development of RNAi drugs and small molecule inhibitors targeting NNMT is facing several challenges. For RNAi drugs, challenges include safety, efficacy, and delivery issues. To address these challenges, various delivery methods have been investigated, including viral vectors, non-viral vectors, and rational design strategies such as chemical modifications, cationic liposomes, polymers, nanocarriers, and biocoupled siRNAs, aimed at enhancing stability and intracellular delivery (Liu F. et al., 2018). Several RNAi drugs, including aptamers like pegaptanib targeting protein targets, and micro interfering RNAs like givosiran and patisiran, as well as antisense oligonucleotides like golodirsen and inotersen that interfere directly with RNA targets, have received FDA approval for medical use (Yu et al., 2020). Despite significant progress in clinical RNAi drug development, there remains considerable room for improvement in pharmacokinetics, pharmacodynamics, and strategies to mitigate toxicity (Setten et al., 2019). Regarding small molecule inhibitors targeting NNMT, challenges include the identification of efficient and selective inhibitors with robust *in vivo* activity (Barrows et al., 2022). Presently, NNMTi, a small molecule inhibitor of NNMT, has been widely employed to investigate the pharmacological effects of NNMT. However, the efficacy of small molecule inhibitors targeting NNMT remains uncertain due to their lack of selectivity and low metabolic stability (Iyamu and Huang, 2021).

6 Conclusion

NNMT is considered to play a significant role in MetS-related diseases. Inhibiting NNMT has been shown to increase energy expenditure, reduce fat accumulation, improve insulin sensitivity, and normalize glucose tolerance and fasting glucose levels. However, the precise mechanisms responsible for these effects are still unclear. Experiments utilizing various RNAi drugs and small molecule inhibitors targeting NNMT have highlighted its potential as a therapeutic target for preventing and treating diseases associated with MetS. Nevertheless, there have been no documented clinical trials focusing on NNMT to date. Further research is needed to elucidate the mechanisms by which NNMT operates in MetS and to develop therapeutic strategies targeting NNMT.

Author contributions

W-DS: Resources, Writing–original draft, Writing–review and editing. X-JZ: Formal Analysis, Resources, Writing–review and editing. J-JL: Formal Analysis, Resources, Writing–review and editing. Y-ZM: Formal Analysis, Resources, Writing–review and

editing. W-SL: Formal Analysis, Resources, Writing–review and editing. J-HL: Data curation, Funding acquisition, Methodology, Project administration, Supervision, Validation, Writing–review and editing.

Funding

The author(s) declare that financial support was received for the research, authorship, and/or publication of this article. Supported by the National Natural Science Foundation of China (NSFC 21365013), Social Science Planning Project of Jiangxi Province (19WT94) and the Key Lab of Aquatic Training Monitoring and Intervention of General Administration of Sport of China (No. 201901).

Conflict of interest

The authors declare that the research was conducted in the absence of any commercial or financial relationships that could be construed as a potential conflict of interest.

Publisher's note

References

Aksoy, S., Szumlanski, C. L., and Weinshilboum, R. M. (1994). Human liver nicotinamide N-methyltransferase. cDNA cloning, expression, and biochemical characterization. *J. Biol. Chem.* 269, 14835–14840. doi:10.1016/s0021-9258(17)36700-5

Alberti, K. G. M. M., Eckel, R. H., Grundy, S. M., Zimmet, P. Z., Cleeman, J. I., Donato, K. A., et al. (2009). Harmonizing the metabolic syndrome: a joint interim statement of the international diabetes federation task force on epidemiology and prevention; national heart, lung, and blood institute; American heart association; world heart federation; international atherosclerosis society; and international association for the study of obesity. *Circulation* 120, 1640–1645. doi:10.1161/CIRCULATIONAHA.109.192644

Alefishat, E., Alexander, S. P. H., and Ralevic, V. (2015). Effects of NAD at purine receptors in isolated blood vessels. *Purinergic Signal.* 11, 47–57. doi:10.1007/s11302-014-9428-1

Alexander, J., Chang, G. Q., Dourmashkin, J. T., and Leibowitz, S. F. (2006). Distinct phenotypes of obesity-prone AKR/J, DBA2J and C57BL/6J mice compared to control strains. *Int. J. Obes.* 30, 50–59. doi:10.1038/sj.ijo.0803110

Alston, T. A., and Abeles, R. H. (1988). Substrate specificity of nicotinamide methyltransferase isolated from porcine liver. *Archives Biochem. Biophysics* 260, 601–608. doi:10.1016/0003-9861(88)90487-0

Amjad, S., Nisar, S., Bhat, A. A., Shah, A. R., Frenneaux, M. P., Fakhro, K., et al. (2021). Role of NAD+ in regulating cellular and metabolic signaling pathways. *Mol. Metab.* 49, 101195. doi:10.1016/j.molmet.2021.101195

Babault, N., Allali-Hassani, A., Li, F., Fan, J., Yue, A., Ju, K., et al. (2018). Discovery of bisubstrate inhibitors of nicotinamide N -methyltransferase (NNMT). *J. Med. Chem.* 61, 1541–1551. doi:10.1021/acs.jmedchem.7b01422

Bach, D.-H., Kim, D., Bae, S. Y., Kim, W. K., Hong, J.-Y., Lee, H.-J., et al. (2018). Targeting nicotinamide N-methyltransferase and miR-449a in EGFR-TKI-resistant non-small-cell lung cancer cells. *Mol. Ther. - Nucleic Acids* 11, 455–467. doi:10.1016/j.omtn.2018.03.011

Balint, B., Jepchumba, V. K., Guéant, J.-L., and Guéant-Rodriguez, R.-M. (2020). Mechanisms of homocysteine-induced damage to the endothelial, medial and adventitial layers of the arterial wall. *Biochimie* 173, 100–106. doi:10.1016/j.biochi.2020.02.012

Bañales-Luna, M., Figueroa-Vega, N., Marín-Aragón, C. I., Perez-Luque, E., Ibarra-Reynoso, L., Gallardo-Blanco, H. L., et al. (2020). Associations of nicotidamide-N-methyltransferase, FTO, and IRX3 genetic variants with body mass index and resting energy expenditure in Mexican subjects. *Sci. Rep.* 10, 11478. doi:10.1038/s41598-020-67832-7

Barbagallo, F., La Vignera, S., Cannarella, R., Mongioì, L. M., Garofalo, V., Leanza, C., et al. (2022). Obesity and male reproduction: do sirtuins play a role? *IJMS* 23, 973. doi:10.3390/ijms23020973

Barrows, R. D., Jeffries, D. E., Vishe, M., Tukachinsky, H., Zheng, S.-L., Li, F., et al. (2022). Potent uncompetitive inhibitors of nicotinamide N -methyltransferase (NNMT) as *in vivo* chemical probes. *J. Med. Chem.* 65, 14642–14654. doi:10.1021/acs.jmedchem.2c01166

Belenky, P., Bogan, K. L., and Brenner, C. (2007). NAD+ metabolism in health and disease. *Trends Biochem. Sci.* 32, 12–19. doi:10.1016/j.tibs.2006.11.006

Brachs, S., Polack, J., Brachs, M., Jahn-Hofmann, K., Elvert, R., Pfenninger, A., et al. (2019). Genetic nicotinamide N-methyltransferase (nnmt) deficiency in male mice improves insulin sensitivity in diet-induced obesity but does not affect glucose tolerance. *Diabetes* 68, 527–542. doi:10.2337/db18-0780

Bruckbauer, A., Banerjee, J., Cao, Q., Cui, X., Jing, J., Zha, L., et al. (2017). Leucine-nicotinic acid synergy stimulates AMPK/Sirt1 signaling and regulates lipid metabolism and lifespan in *Caenorhabditis elegans*, and hyperlipidemia and atherosclerosis in mice. *Am. J. Cardiovasc Dis.* 7, 33–47.

Bubenek, S., Nastase, A., Niculescu, A. M., Baila, S., Herlea, V., Lazar, V., et al. (2012). Assessment of gene expression profiles in peripheral occlusive arterial disease. *Can. J. Cardiol.* 28, 712–720. doi:10.1016/j.cjca.2012.03.013

Butkowski, E. G., Al-Aubaidy, H. A., and Jelinek, H. F. (2017). Interaction of homocysteine, glutathione and 8-hydroxy-2′-deoxyguanosine in metabolic syndrome progression. *Clin. Biochem.* 50, 116–120. doi:10.1016/j.clinbiochem.2016.10.006

Chen, D., Li, L., Diaz, K., Iyamu, I. D., Yadav, R., Noinaj, N., et al. (2019a). Novel propargyl-linked bisubstrate analogues as tight-binding inhibitors for nicotinamide N -methyltransferase. *J. Med. Chem.* 62, 10783–10797. doi:10.1021/acs.jmedchem.9b01255

Chen, L., Heikkinen, L., Wang, C., Yang, Y., Sun, H., and Wong, G. (2019b). Trends in the development of miRNA bioinformatics tools. *Brief. Bioinform* 20, 1836–1852. doi:10.1093/bib/bby054

Chen, Y., Zhao, X., and Wu, H. (2019c). Metabolic stress and cardiovascular disease in diabetes mellitus: the role of protein O-GlcNAc modification. *Arterioscler. Thromb. Vasc. Biol.* 39, 1911–1924. doi:10.1161/ATVBAHA.119.312192

Collins, P. B., and Chaykin, S. (1972). The management of nicotinamide and nicotinic acid in the mouse. *J. Biol. Chem.* 247, 778–783. doi:10.1016/S0021-9258(19)45675-5

Cornier, M.-A., Dabelea, D., Hernandez, T. L., Lindstrom, R. C., Steig, A. J., Stob, N. R., et al. (2008). The metabolic syndrome. *Endocr. Rev.* 29, 777–822. doi:10.1210/er.2008-0024

Covarrubias, A. J., Perrone, R., Grozio, A., and Verdin, E. (2021). NAD+ metabolism and its roles in cellular processes during ageing. *Nat. Rev. Mol. Cell Biol.* 22, 119–141. doi:10.1038/s41580-020-00313-x

Doench, J. G., Petersen, C. P., and Sharp, P. A. (2003). siRNAs can function as miRNAs. *Genes Dev.* 17, 438–442. doi:10.1101/gad.1064703

Dong, H., Guo, W., Yue, R., Sun, X., and Zhou, Z. (2024). Nuclear nicotinamide adenine dinucleotide deficiency by Nmnat1 deletion impaired hepatic insulin signaling, mitochondrial function, and hepatokine expression in mice fed a high-fat diet. *Lab. Investig.* 104, 100329. doi:10.1016/j.labinv.2024.100329

Dubchenko, E. A., Ivanov, A. V., Boiko, A. N., Spirina, N. N., Gusev, E. I., and Kubatiev, A. A. (2019). Hyperhomocysteinemia and endothelial dysfunction in patients with cerebral vascular and autoimmune diseases. *Z. Nevrol. Psikhiatr. Im. S.S. Korsakova* 119, 133–138. doi:10.17116/jnevro20191191111133

Eckert, M. A., Coscia, F., Chryplewicz, A., Chang, J. W., Hernandez, K. M., Pan, S., et al. (2019). Proteomics reveals NNMT as a master metabolic regulator of cancer-associated fibroblasts. *Nature* 569, 723–728. doi:10.1038/s41586-019-1173-8

Esse, R., Barroso, M., Tavares De Almeida, I., and Castro, R. (2019). The contribution of homocysteine metabolism disruption to endothelial dysfunction: state-of-the-art. *IJMS* 20, 867. doi:10.3390/ijms20040867

Esteghamati, A., Hafezi-Nejad, N., Zandieh, A., Sheikhbahaei, S., Ebadi, M., and Nakhjavani, M. (2014). Homocysteine and metabolic syndrome: from clustering to additional utility in prediction of coronary heart disease. *J. Cardiol.* 64, 290–296. doi:10.1016/j.jjcc.2014.02.001

Frederick, D. W., Davis, J. G., Dávila, A., Agarwal, B., Michan, S., Puchowicz, M. A., et al. (2015). Increasing NAD synthesis in muscle via nicotinamide

phosphoribosyltransferase is not sufficient to promote oxidative metabolism. *J. Biol. Chem.* 290, 1546–1558. doi:10.1074/jbc.M114.579565

Frederick, D. W., Loro, E., Liu, L., Davila, A., Chellappa, K., Silverman, I. M., et al. (2016). Loss of NAD homeostasis leads to progressive and reversible degeneration of skeletal muscle. *Cell Metab.* 24, 269–282. doi:10.1016/j.cmet.2016.07.005

Furukawa, S., Fujita, T., Shimabukuro, M., Iwaki, M., Yamada, Y., Nakajima, Y., et al. (2004). Increased oxidative stress in obesity and its impact on metabolic syndrome. *J. Clin. Invest.* 114, 1752–1761. doi:10.1172/JCI21625

Gao, Y., Martin, N. I., and Van Haren, M. J. (2021). Nicotinamide N-methyl transferase (NNMT): an emerging therapeutic target. *Drug Discov. Today* 26, 2699–2706. doi:10.1016/j.drudis.2021.05.011

Gao, Y., Van Haren, M. J., Moret, E. E., Rood, J. J. M., Sartini, D., Salvucci, A., et al. (2019). Bisubstrate inhibitors of nicotinamide N -methyltransferase (NNMT) with enhanced activity. *J. Med. Chem.* 62, 6597–6614. doi:10.1021/acs.jmedchem.9b00413

Gerber, P. A., and Rutter, G. A. (2017). The role of oxidative stress and hypoxia in pancreatic beta-cell dysfunction in diabetes mellitus. *Antioxidants Redox Signal.* 26, 501–518. doi:10.1089/ars.2016.6755

Giuliante, R., Sartini, D., Bacchetti, T., Rocchetti, R., Klöting, I., Polidori, C., et al. (2015). Potential involvement of nicotinamide N -methyltransferase in the pathogenesis of metabolic syndrome. *Metabolic Syndrome Relat. Disord.* 13, 165–170. doi:10.1089/met.2014.0134

Goldberg, R. B., and Mather, K. (2012). Targeting the consequences of the metabolic syndrome in the diabetes prevention program. *ATVB* 32, 2077–2090. doi:10.1161/ATVBAHA.111.241893

Grimm, D., Streetz, K. L., Jopling, C. L., Storm, T. A., Pandey, K., Davis, C. R., et al. (2006). Fatality in mice due to oversaturation of cellular microRNA/short hairpin RNA pathways. *Nature* 441, 537–541. doi:10.1038/nature04791

Grossman, E. (2008). Does increased oxidative stress cause hypertension? *Diabetes Care* 31, S185–S189. doi:10.2337/dc08-s246

Guan, X.-X., Zhu, X.-J., Deng, Z.-H., Zeng, Y.-R., Liu, J.-R., Li, J.-H., et al. (2021). The association between nicotinamide N-methyltransferase gene polymorphisms and primary hypertension in Chinese Han Population. *AIMS Bioeng.* 8, 130–139. doi:10.3934/bioeng.2021012

Guimera, A. M., Clark, P., Wordsworth, J., Anugula, S., Rasmussen, L. J., and Shanley, D. P. (2022). Systems modelling predicts chronic inflammation and genomic instability prevent effective mitochondrial regulation during biological ageing. *Exp. Gerontol.* 166, 111889. doi:10.1016/j.exger.2022.111889

Han, S., Wu, H., Li, W., and Gao, P. (2015). Protective effects of genistein in homocysteine-induced endothelial cell inflammatory injury. *Mol. Cell Biochem.* 403, 43–49. doi:10.1007/s11010-015-2335-0

Harikrishna, A. S., and Venkitasamy, K. (2023). Identification of novel human nicotinamide N-methyltransferase inhibitors: a structure-based pharmacophore modeling and molecular dynamics approach. *J. Biomol. Struct. Dyn.* 41, 14638–14650. doi:10.1080/07391102.2023.2183714

Hasan, T., Arora, R., Bansal, A. K., Bhattacharya, R., Sharma, G. S., and Singh, L. R. (2019). Disturbed homocysteine metabolism is associated with cancer. *Exp. Mol. Med.* 51, 1–13. doi:10.1038/s12276-019-0216-4

He, W., Cik, M., Van Puyvelde, L., Van Dun, J., Appendino, G., Lesage, A., et al. (2002). Neurotrophic and antileukemic daphnane diterpenoids from Synaptolepis kirkii. *Bioorg. Med. Chem.* 10, 3245–3255. doi:10.1016/S0968-0896(02)00163-3

Herfindal, B., Gerdts, E., Kringeland, E. A., Saeed, S., Midtbø, H., and Halland, H. (2020). Concomitant hypertension is associated with abnormal left ventricular geometry and lower systolic myocardial function in overweight participants: the FAT associated CardiOvasculaR dysfunction study. *J. Hypertens.* 38, 1158–1164. doi:10.1097/HJH.0000000000002397

Hidru, T. H., Yang, X., Xia, Y., Ma, L., and Li, H.-H. (2019). The relationship between plasma markers and essential hypertension in middle-aged and elderly Chinese population: a community based cross-sectional study. *Sci. Rep.* 9, 6813. doi:10.1038/s41598-019-43278-4

Hill, M., and Tran, N. (2021). miRNA interplay: mechanisms and consequences in cancer. *Dis. Models Mech.* 14, dmm047662. doi:10.1242/dmm.047662

Hofmann, M. A., Lalla, E., Lu, Y., Gleason, M. R., Wolf, B. M., Tanji, N., et al. (2001). Hyperhomocysteinemia enhances vascular inflammation and accelerates atherosclerosis in a murine model. *J. Clin. Invest.* 107, 675–683. doi:10.1172/JCI10588

Hong, J.-Y., Chung, H.-J., Lee, H.-J., Park, H. J., and Lee, S. K. (2011). Growth inhibition of human lung cancer cells via down-regulation of epidermal growth factor receptor signaling by yuanhuadine, a daphnane diterpene from daphne genkwa. *J. Nat. Prod.* 74, 2102–2108. doi:10.1021/np2003512

Hong, S., Moreno-Navarrete, J. M., Wei, X., Kikukawa, Y., Tzameli, I., Prasad, D., et al. (2015). Nicotinamide N-methyltransferase regulates hepatic nutrient metabolism through Sirt1 protein stabilization. *Nat. Med.* 21, 887–894. doi:10.1038/nm.3882

Horning, B. D., Suciu, R. M., Ghadiri, D. A., Ulanovskaya, O. A., Matthews, M. L., Lum, K. M., et al. (2016). Chemical proteomic profiling of human methyltransferases. *J. Am. Chem. Soc.* 138, 13335–13343. doi:10.1021/jacs.6b07830

Houtkooper, R. H., Cantó, C., Wanders, R. J., and Auwerx, J. (2010). The secret life of NAD+: an old metabolite controlling new metabolic signaling pathways. *Endocr. Rev.* 31, 194–223. doi:10.1210/er.2009-0026

Huang, Q., Chen, H., Yin, D., Wang, J., Wang, S., Yang, F., et al. (2024). Multi-omics analysis reveals NNMT as a master metabolic regulator of metastasis in esophageal squamous cell carcinoma. *npj Precis. Onc.* 8, 24. doi:10.1038/s41698-024-00509-w

Imi, Y., Amano, R., Kasahara, N., Obana, Y., and Hosooka, T. (2023). Nicotinamide mononucleotide induces lipolysis by regulating ATGL expression via the SIRT1-AMPK axis in adipocytes. *Biochem. Biophysics Rep.* 34, 101476. doi:10.1016/j.bbrep.2023.101476

Incalza, M. A., D'Oria, R., Natalicchio, A., Perrini, S., Laviola, L., and Giorgino, F. (2018). Oxidative stress and reactive oxygen species in endothelial dysfunction associated with cardiovascular and metabolic diseases. *Vasc. Pharmacol.* 100, 1–19. doi:10.1016/j.vph.2017.05.005

Iyamu, I. D., and Huang, R. (2020). Development of fluorescence polarization-based competition assay for nicotinamide N-methyltransferase. *Anal. Biochem.* 604, 113833. doi:10.1016/j.ab.2020.113833

Iyamu, I. D., and Huang, R. (2021). Mechanisms and inhibitors of nicotinamide N-methyltransferase. *RSC Med. Chem.* 12, 1254–1261. doi:10.1039/D1MD00016K

Jackson, A. L., Bartz, S. R., Schelter, J., Kobayashi, S. V., Burchard, J., Mao, M., et al. (2003). Expression profiling reveals off-target gene regulation by RNAi. *Nat. Biotechnol.* 21, 635–637. doi:10.1038/nbt831

Jackson, A. L., Burchard, J., Schelter, J., Chau, B. N., Cleary, M., Lim, L., et al. (2006). Widespread siRNA "off-target" transcript silencing mediated by seed region sequence complementarity. *RNA* 12, 1179–1187. doi:10.1261/rna.25706

Jell, J., Merali, S., Hensen, M. L., Mazurchuk, R., Spernyak, J. A., Diegelman, P., et al. (2007). Genetically altered expression of spermidine/spermine N1-acetyltransferase affects fat metabolism in mice via acetyl-CoA. *J. Biol. Chem.* 282, 8404–8413. doi:10.1074/jbc.M610265200

Junedi, M., Junaidi, A., and Yadagir, R. (2022). Association of high blood pressure with raised homocysteine level among urban population- A case control study. *Perspect. Med. Res.* 10, 72–76. doi:10.47799/pimr.1003.13

Kamat, P. K., Kalani, A., Givvimani, S., Sathnur, P. B., Tyagi, S. C., and Tyagi, N. (2013). Hydrogen sulfide attenuates neurodegeneration and neurovascular dysfunction induced by intracerebral-administered homocysteine in mice. *Neuroscience* 252, 302–319. doi:10.1016/j.neuroscience.2013.07.051

Kane, A. E., and Sinclair, D. A. (2018). Sirtuins and NAD + in the development and treatment of metabolic and cardiovascular diseases. *Circ. Res.* 123, 868–885. doi:10.1161/CIRCRESAHA.118.312498

Kannt, A., Pfenninger, A., Teichert, L., Tönjes, A., Dietrich, A., Schön, M. R., et al. (2015). Association of nicotinamide-N-methyltransferase mRNA expression in human adipose tissue and the plasma concentration of its product, 1-methylnicotinamide, with insulin resistance. *Diabetologia* 58, 799–808. doi:10.1007/s00125-014-3490-7

Kannt, A., Rajagopal, S., Kadnur, S. V., Suresh, J., Bhamidipati, R. K., Swaminathan, S., et al. (2018). A small molecule inhibitor of Nicotinamide N-methyltransferase for the treatment of metabolic disorders. *Sci. Rep.* 8, 3660. doi:10.1038/s41598-018-22081-7

Kaplan, P., Tatarkova, Z., Sivonova, M. K., Racay, P., and Lehotsky, J. (2020). Homocysteine and mitochondria in cardiovascular and cerebrovascular systems. *IJMS* 21, 7698. doi:10.3390/ijms21207698

Klimova, N., and Kristian, T. (2019). Multi-targeted effect of nicotinamide mononucleotide on brain bioenergetic metabolism. *Neurochem. Res.* 44, 2280–2287. doi:10.1007/s11064-019-02729-0

Klop, B., Elte, J., and Cabezas, M. (2013). Dyslipidemia in obesity: mechanisms and potential targets. *Nutrients* 5, 1218–1240. doi:10.3390/nu5041218

Kolczynska, K., Loza-Valdes, A., Hawro, I., and Sumara, G. (2020). Diacylglycerol-evoked activation of PKC and PKD isoforms in regulation of glucose and lipid metabolism: a review. *Lipids Health Dis.* 19, 113. doi:10.1186/s12944-020-01286-8

Komatsu, M., Kanda, T., Urai, H., Kurokochi, A., Kitahama, R., Shigaki, S., et al. (2018). NNMT activation can contribute to the development of fatty liver disease by modulating the NAD + metabolism. *Sci. Rep.* 8, 8637. doi:10.1038/s41598-018-26882-8

Kornev, M., Caglayan, H. A., Kudryavtsev, A. V., Malyutina, S., Ryabikov, A., Schirmer, H., et al. (2023). Influence of hypertension on systolic and diastolic left ventricular function including segmental strain and strain rate. *Echocardiography* 40, 623–633. doi:10.1111/echo.15625

Kraus, D., Yang, Q., Kong, D., Banks, A. S., Zhang, L., Rodgers, J. T., et al. (2014). Nicotinamide N-methyltransferase knockdown protects against diet-induced obesity. *Nature* 508, 258–262. doi:10.1038/nature13198

Kuzmi, E., Leontiev, V., Petrov, R., Bichurin, M., Petrova, A., Nemtsev, L., et al. (2021). "Magnetoelectric structure for energy harvesting," in *2021 17th conference on electrical machines, drives and power systems (ELMA)* (Sofia, Bulgaria: IEEE), 1–3. doi:10.1109/ELMA52514.2021.9503031

Lee, H.-S., In, S., and Park, T. (2021). The homocysteine and metabolic syndrome: a mendelian randomization study. *Nutrients* 13, 2440. doi:10.3390/nu13072440

Lee, Y. H., Nair, S., Rousseau, E., Allison, D. B., Page, G. P., Tataranni, P. A., et al. (2005). Microarray profiling of isolated abdominal subcutaneous adipocytes from obese

vs non-obese Pima Indians: increased expression of inflammation-related genes. *Diabetologia* 48, 1776–1783. doi:10.1007/s00125-005-1867-3

Li, F., Chong, Z., and Maiese, K. (2006). Cell life versus cell longevity: the mysteries surrounding the NAD+ precursor nicotinamide. *CMC* 13, 883–895. doi:10.2174/092986706776361058

Li, J., Luo, M., Xie, N., Wang, J., and Chen, L. (2016). Curcumin protects endothelial cells against homocysteine induced injury through inhibiting inflammation. *Am. J. Transl. Res.* 8, 4598–4604.

Li, J.-H., Qiu, L.-Q., Zhu, X.-J., and Cai, C.-X. (2017). Influence of exercises using different energy metabolism systems on NNMT expression in different types of skeletal muscle fibers. *Sci. Sports* 32, 27–32. doi:10.1016/j.scispo.2016.06.004

Li, J.-H., Wang, Y.-H., Zhu, X.-J., Zhou, Q., Xie, Z.-H., and Yao, T.-F. (2018). Metabolomics study on the association between nicotinamide N-methyltransferase gene polymorphisms and type 2 diabetes. *Int. J. Diabetes Dev. Ctries.* 38, 409–416. doi:10.1007/s13410-017-0601-2

Li, J. H., and Wang, Z. H. (2011). Association between urinary low-molecular-weight metabolites and body mass index. *Int. J. Obes.* 35, S54.

Liu, C., Liu, L., Wang, Y., Chen, X., Liu, J., Peng, S., et al. (2022). Hyperhomocysteinemia increases risk of metabolic syndrome and cardiovascular death in an elderly Chinese community population of a 7-year follow-up study. *Front. Cardiovasc. Med.* 8, 811670. doi:10.3389/fcvm.2021.811670

Liu, F., Wang, C., Gao, Y., Li, X., Tian, F., Zhang, Y., et al. (2018a). Current transport systems and clinical applications for small interfering RNA (siRNA) drugs. *Mol. Diagn Ther.* 22, 551–569. doi:10.1007/s40291-018-0338-8

Liu, J.-R., Deng, Z.-H., Zhu, X.-J., Zeng, Y.-R., Guan, X.-X., and Li, J.-H. (2021). Roles of nicotinamide N-methyltransferase in obesity and type 2 diabetes. *Biomed. Res. Int.* 2021, 9924314–9924318. doi:10.1155/2021/9924314

Liu, M., Chu, J., Gu, Y., Shi, H., Zhang, R., Wang, L., et al. (2017). Serum N 1 -methylnicotinamide is associated with coronary artery disease in Chinese patients. *JAHA* 6, e004328. doi:10.1161/JAHA.116.004328

Liu, M., He, A., Chu, J., Chen, C., Zhang, S., He, Y., et al. (2018b). Serum N1-methylnicotinamide is associated with left ventricular systolic dysfunction in Chinese. *Sci. Rep.* 8, 8581. doi:10.1038/s41598-018-26956-7

Liu, M., Li, L., Chu, J., Zhu, B., Zhang, Q., Yin, X., et al. (2015). Serum N 1 -methylnicotinamide is associated with obesity and diabetes in Chinese. *J. Clin. Endocrinol. Metabolism* 100, 3112–3117. doi:10.1210/jc.2015-1732

Luo, X., Li, R., and Yan, L.-J. (2015). Roles of pyruvate, NADH, and mitochondrial complex I in redox balance and imbalance in β cell function and dysfunction. *J. Diabetes Res.* 2015, 512618–512712. doi:10.1155/2015/512618

Maiese, K. (2023). The impact of aging and oxidative stress in metabolic and nervous system disorders: programmed cell death and molecular signal transduction crosstalk. *Front. Immunol.* 14, 1273570. doi:10.3389/fimmu.2023.1273570

Menon, R. M., González, M. A., Adams, M. H., Tolbert, D. S., Leu, J. H., and Cefali, E. A. (2007). Effect of the rate of niacin administration on the plasma and urine pharmacokinetics of niacin and its metabolites. *J. Clin. Pharma* 47, 681–688. doi:10.1177/0091270007300264

Mills, K. F., Yoshida, S., Stein, L. R., Grozio, A., Kubota, S., Sasaki, Y., et al. (2016). Long-term administration of nicotinamide mononucleotide mitigates age-associated physiological decline in mice. *Cell Metab.* 24, 795–806. doi:10.1016/j.cmet.2016.09.013

Mondal, K., Chakraborty, P., and Kabir, S. N. (2018). Hyperhomocysteinemia and hyperandrogenemia share PCSK9-LDLR pathway to disrupt lipid homeostasis in PCOS. *Biochem. Biophysical Res. Commun.* 503, 8–13. doi:10.1016/j.bbrc.2018.04.078

Mori, V., Amici, A., Mazzola, F., Di Stefano, M., Conforti, L., Magni, G., et al. (2014). Metabolic profiling of alternative NAD biosynthetic routes in mouse tissues. *PLoS ONE* 9, e113939. doi:10.1371/journal.pone.0113939

Nagahisa, T., Yamaguchi, S., Kosugi, S., Homma, K., Miyashita, K., Irie, J., et al. (2022). Intestinal epithelial NAD+ biosynthesis regulates GLP-1 production and postprandial glucose metabolism in mice. *Endocrinology* 163, bqac023. doi:10.1210/endocr/bqac023

Neelakantan, H., Brightwell, C. R., Graber, T. G., Maroto, R., Wang, H.-Y. L., McHardy, S. F., et al. (2019). Small molecule nicotinamide N-methyltransferase inhibitor activates senescent muscle stem cells and improves regenerative capacity of aged skeletal muscle. *Biochem. Pharmacol.* 163, 481–492. doi:10.1016/j.bcp.2019.02.008

Neelakantan, H., Vance, V., Wetzel, M. D., Wang, H.-Y. L., McHardy, S. F., Finnerty, C. C., et al. (2018). Selective and membrane-permeable small molecule inhibitors of nicotinamide N-methyltransferase reverse high fat diet-induced obesity in mice. *Biochem. Pharmacol.* 147, 141–152. doi:10.1016/j.bcp.2017.11.007

Neelakantan, H., Wang, H.-Y., Vance, V., Hommel, J. D., McHardy, S. F., and Watowich, S. J. (2017). Structure–activity relationship for small molecule inhibitors of nicotinamide N -methyltransferase. *J. Med. Chem.* 60, 5015–5028. doi:10.1021/acs.jmedchem.7b00389

Nowotny, K., Jung, T., Höhn, A., Weber, D., and Grune, T. (2015). Advanced glycation end products and oxidative stress in type 2 diabetes mellitus. *Biomolecules* 5, 194–222. doi:10.3390/biom5010194

Numakura, S., and Uozaki, H. (2024). Gastric cancer with the increased nicotinamide N-methyltransferase-positive stromal cells includes unfavorable prognosis-related cancer-associated fibroblasts. *Anticancer Res.* 44, 1653–1660. doi:10.21873/anticanres.16964

Obeid, R., and Herrmann, W. (2009). Homocysteine and lipids: S-Adenosyl methionine as a key intermediate. *FEBS Lett.* 583, 1215–1225. doi:10.1016/j.febslet.2009.03.038

Okamoto, H., Ishikawa, A., Yoshitake, Y., Kodama, N., Nishimuta, M., Fukuwatari, T., et al. (2003). Diurnal variations in human urinary excretion of nicotinamide catabolites: effects of stress on the metabolism of nicotinamide. *Am. J. Clin. Nutr.* 77, 406–410. doi:10.1093/ajcn/77.2.406

Ostrakhovitch, E. A., and Tabibzadeh, S. (2019). Homocysteine and age-associated disorders. *Ageing Res. Rev.* 49, 144–164. doi:10.1016/j.arr.2018.10.010

Parsons, R. B., and Facey, P. D. (2021). Nicotinamide N-methyltransferase: an emerging protagonist in cancer macro(r)evolution. *Biomolecules* 11, 1418. doi:10.3390/biom11101418

Perna, A. F., Ingrosso, D., Lombardi, C., Acanfora, F., Satta, E., Cesare, C. M., et al. (2003). Possible mechanisms of homocysteine toxicity. *Kidney Int.* 63, S137–S140. doi:10.1046/j.1523-1755.63.s84.33.x

Persengiev, S. P., Zhu, X., and Green, M. R. (2004). Nonspecific, concentration-dependent stimulation and repression of mammalian gene expression by small interfering RNAs (siRNAs). *RNA* 10, 12–18. doi:10.1261/rna5160904

Piazzolla, G., Candigliota, M., Fanelli, M., Castrovilli, A., Berardi, E., Antonica, G., et al. (2019). Hyperhomocysteinemia is an independent risk factor of atherosclerosis in patients with metabolic syndrome. *Diabetol. Metab. Syndr.* 11, 87. doi:10.1186/s13098-019-0484-0

Picard, F., Kurtev, M., Chung, N., Topark-Ngarm, A., Senawong, T., Machado De Oliveira, R., et al. (2004). Sirt1 promotes fat mobilization in white adipocytes by repressing PPAR-gamma. *Nature* 429, 771–776. doi:10.1038/nature02583

Pissios, P. (2017). Nicotinamide N -methyltransferase: more than a vitamin B3 clearance enzyme. *Trends Endocrinol. Metabolism* 28, 340–353. doi:10.1016/j.tem.2017.02.004

Poddar, S. K., Sifat, A. E., Haque, S., Nahid, N. A., Chowdhury, S., and Mehedi, I. (2019). Nicotinamide mononucleotide: exploration of diverse therapeutic applications of a potential molecule. *Biomolecules* 9, 34. doi:10.3390/biom9010034

Przyborowski, K., Wojewoda, M., Sitek, B., Zakrzewska, A., Kij, A., Wandzel, K., et al. (2015). Effects of 1-methylnicotinamide (MNA) on exercise capacity and endothelial response in diabetic mice. *PLoS ONE* 10, e0130908. doi:10.1371/journal.pone.0130908

Qiu, Y., Xu, S., Chen, X., Wu, X., Zhou, Z., Zhang, J., et al. (2023). NAD+ exhaustion by CD38 upregulation contributes to blood pressure elevation and vascular damage in hypertension. *Sig Transduct. Target Ther.* 8, 353. doi:10.1038/s41392-023-01577-3

Reid, M., Spence, J., Nwokocha, M., Palacios, J., and Nwokocha, C. R. (2018). "The role of NADP(H) oxidase inhibition and its implications in cardiovascular disease management using natural plant products," in *Studies in natural products chemistry* (Elsevier), 43–59. doi:10.1016/B978-0-444-64056-7.00002-7

Revollo, J. R., Grimm, A. A., and Imai, S. (2007). The regulation of nicotinamide adenine dinucleotide biosynthesis by Nampt/PBEF/visfatin in mammals. *Curr. Opin. Gastroenterology* 23, 164–170. doi:10.1097/MOG.0b013e32801b3c8f

Ritter, O., Jelenik, T., and Roden, M. (2015). Lipid-mediated muscle insulin resistance: different fat, different pathways? *J. Mol. Med.* 93, 831–843. doi:10.1007/s00109-015-1310-2

Roberti, A., Fernández, A. F., and Fraga, M. F. (2021). Nicotinamide N-methyltransferase: at the crossroads between cellular metabolism and epigenetic regulation. *Mol. Metab.* 45, 101165. doi:10.1016/j.molmet.2021.101165

Roberti, A., Tejedor, J. R., Díaz-Moreno, I., López, V., Santamarina-Ojeda, P., Pérez, R. F., et al. (2023). Nicotinamide N-methyltransferase (NNMT) regulates the glucocorticoid signaling pathway during the early phase of adipogenesis. *Sci. Rep.* 13, 8293. doi:10.1038/s41598-023-34916-z

Roberts, T. C., Langer, R., and Wood, M. J. A. (2020). Advances in oligonucleotide drug delivery. *Nat. Rev. Drug Discov.* 19, 673–694. doi:10.1038/s41573-020-0075-7

Ruf, S., Hallur, M. S., Anchan, N. K., Swamy, I. N., Murugesan, K. R., Sarkar, S., et al. (2018). Novel nicotinamide analog as inhibitor of nicotinamide N-methyltransferase. *Bioorg. Med. Chem. Lett.* 28, 922–925. doi:10.1016/j.bmcl.2018.01.058

Ruf, S., Rajagopal, S., Kadnur, S. V., Hallur, M. S., Rani, S., Kristam, R., et al. (2022). Novel tricyclic small molecule inhibitors of Nicotinamide N-methyltransferase for the treatment of metabolic disorders. *Sci. Rep.* 12, 15440. doi:10.1038/s41598-022-19634-2

Rus, R. R., Pac, M., Obrycki, Ł., Sağsak, E., Azukaitis, K., Sinha, M. D., et al. (2023). Systolic and diastolic left ventricular function in children with primary hypertension: a systematic review and meta-analysis. *J. Hypertens.* 41, 51–62. doi:10.1097/HJH.0000000000003298

Salek, R. M., Maguire, M. L., Bentley, E., Rubtsov, D. V., Hough, T., Cheeseman, M., et al. (2007). A metabolomic comparison of urinary changes in type 2 diabetes in mouse, rat, and human. *Physiol. Genomics* 29, 99–108. doi:10.1152/physiolgenomics.00194.2006

Sampson, C. M., Dimet, A. L., Neelakantan, H., Ogunseye, K. O., Stevenson, H. L., Hommel, J. D., et al. (2021). Combined nicotinamide N-methyltransferase inhibition and reduced-calorie diet normalizes body composition and enhances metabolic benefits in obese mice. *Sci. Rep.* 11, 5637. doi:10.1038/s41598-021-85051-6

Sasaki, T., Kikuchi, O., Shimpuku, M., Susanti, V. Y., Yokota-Hashimoto, H., Taguchi, R., et al. (2014). Hypothalamic SIRT1 prevents age-associated weight gain by improving leptin sensitivity in mice. *Diabetologia* 57, 819–831. doi:10.1007/s00125-013-3140-5

Scacheri, P. C., Rozenblatt-Rosen, O., Caplen, N. J., Wolfsberg, T. G., Umayam, L., Lee, J. C., et al. (2004). Short interfering RNAs can induce unexpected and divergent changes in the levels of untargeted proteins in mammalian cells. *Proc. Natl. Acad. Sci. U.S.A.* 101, 1892–1897. doi:10.1073/pnas.0308698100

Sen, S., Mondal, S., Zheng, L., Salinger, A. J., Fast, W., Weerapana, E., et al. (2019). Development of a suicide inhibition-based protein labeling strategy for nicotinamide N -methyltransferase. *ACS Chem. Biol.* 14, 613–618. doi:10.1021/acschembio.9b00211

Setten, R. L., Rossi, J. J., and Han, S. (2019). The current state and future directions of RNAi-based therapeutics. *Nat. Rev. Drug Discov.* 18, 421–446. doi:10.1038/s41573-019-0017-4

Shi, L., Liu, X.-Y., Huang, Z.-G., Ma, Z.-Y., Xi, Y., Wang, L.-Y., et al. (2019). Endogenous hydrogen sulfide and ERK1/2-STAT3 signaling pathway may participate in the association between homocysteine and hypertension. *J. Geriatr. Cardiol.* 16, 822–834. doi:10.11909/j.issn.1671-5411.2019.11.007

Shibata, K., Kawada, T., and Iwai, K. (1987). Microdetermination of N1-methyl-2-pyridone-5-carboxamide, a major metabolite of nicotinic acid and nicotinamide, in urine by high-performance liquid chromatography. *J. Chromatogr. B Biomed. Sci. Appl.* 417, 173–177. doi:10.1016/0378-4347(87)80104-4

Shibata, K., Kawada, T., and Iwai, K. (1988). Simultaneous micro-determination of nicotinamide and its major metabolites, N1-methyl-2-pyridone-5-carboxamide and N1-methyl-4-pyridone-3-carboxamide, by high-performance liquid chromatography. *J. Chromatogr. B Biomed. Sci. Appl.* 424, 23–28. doi:10.1016/S0378-4347(00)81072-5

Song, J., Yang, X., and Yan, L.-J. (2019). Role of pseudohypoxia in the pathogenesis of type 2 diabetes. *HP* 7, 33–40. doi:10.2147/HP.S202775

Song, Q., Chen, Y., Wang, J., Hao, L., Huang, C., Griffiths, A., et al. (2020). ER stress-induced upregulation of NNMT contributes to alcohol-related fatty liver development. *J. Hepatology* 73, 783–793. doi:10.1016/j.jhep.2020.04.038

Souto, J. C., Blanco-Vaca, F., Soria, J. M., Buil, A., Almasy, L., Ordoñez-Llanos, J., et al. (2005). A genomewide exploration suggests a new candidate gene at chromosome 11q23 as the major determinant of plasma homocysteine levels: results from the GAIT Project. *Am. J. Hum. Genet.* 76, 925–933. doi:10.1086/430409

Sreckovic, B., Sreckovic, V. D., Soldatovic, I., Colak, E., Sumarac-Dumanovic, M., Janeski, H., et al. (2017). Homocysteine is a marker for metabolic syndrome and atherosclerosis. *Diabetes and Metabolic Syndrome Clin. Res. Rev.* 11, 179–182. doi:10.1016/j.dsx.2016.08.026

Stromsdorfer, K. L., Yamaguchi, S., Yoon, M. J., Moseley, A. C., Franczyk, M. P., Kelly, S. C., et al. (2016). NAMPT-mediated NAD + biosynthesis in adipocytes regulates adipose tissue function and multi-organ insulin sensitivity in mice. *Cell Rep.* 16, 1851–1860. doi:10.1016/j.celrep.2016.07.027

Sun, W., Zou, Y., Cai, Z., Huang, J., Hong, X., Liang, Q., et al. (2022). Overexpression of NNMT in glioma aggravates tumor cell progression: an emerging therapeutic target. *Cancers* 14, 3538. doi:10.3390/cancers14143538

Svenson, K. L., Von Smith, R., Magnani, P. A., Suetin, H. R., Paigen, B., Naggert, J. K., et al. (2007). Multiple trait measurements in 43 inbred mouse strains capture the phenotypic diversity characteristic of human populations. *J. Appl. Physiology* 102, 2369–2378. doi:10.1152/japplphysiol.01077.2006

Swaminathan, S., Birudukota, S., Thakur, M. K., Parveen, R., Kandan, S., Juluri, S., et al. (2017). Crystal structures of monkey and mouse nicotinamide N-methyltransferase (NNMT) bound with end product, 1-methyl nicotinamide. *Biochem. Biophysical Res. Commun.* 491, 416–422. doi:10.1016/j.bbrc.2017.07.087

Takahashi, R., Kanda, T., Komatsu, M., Itoh, T., Minakuchi, H., Urai, H., et al. (2022). The significance of NAD + metabolites and nicotinamide N-methyltransferase in chronic kidney disease. *Sci. Rep.* 12, 6398. doi:10.1038/s41598-022-10476-6

Teperino, R., Schoonjans, K., and Auwerx, J. (2010). Histone methyl transferases and demethylases; can they link metabolism and transcription? *Cell Metab.* 12, 321–327. doi:10.1016/j.cmet.2010.09.004

Tilg, H., Zmora, N., Adolph, T. E., and Elinav, E. (2020). The intestinal microbiota fuelling metabolic inflammation. *Nat. Rev. Immunol.* 20, 40–54. doi:10.1038/s41577-019-0198-4

Trammell, S. A. J., and Brenner, C. (2015). NNMT: a bad actor in fat makes good in liver. *Cell Metab.* 22, 200–201. doi:10.1016/j.cmet.2015.07.017

Trammell, S. A. J., Weidemann, B. J., Chadda, A., Yorek, M. S., Holmes, A., Coppey, L. J., et al. (2016). Nicotinamide riboside opposes type 2 diabetes and neuropathy in mice. *Sci. Rep.* 6, 26933. doi:10.1038/srep26933

Tripathi, B. K., and Srivastava, A. K. (2006). Diabetes mellitus: complications and therapeutics. *Med. Sci. Monit.* 12, RA130–147.

Uddin, G. M., Youngson, N. A., Doyle, B. M., Sinclair, D. A., and Morris, M. J. (2017). Nicotinamide mononucleotide (NMN) supplementation ameliorates the impact of maternal obesity in mice: comparison with exercise. *Sci. Rep.* 7, 15063. doi:10.1038/s41598-017-14866-z

Ulloque-Badaracco, J. R., Hernandez-Bustamante, E. A., Alarcon-Braga, E. A., Al-kassab-Córdova, A., Cabrera-Guzmán, J. C., Herrera-Añazco, P., et al. (2023). Vitamin B12, folate, and homocysteine in metabolic syndrome: a systematic review and meta-analysis. *Front. Endocrinol.* 14, 1221259. doi:10.3389/fendo.2023.1221259

Van Guldener, C., Nanayakkara, P. W. B., and Stehouwer, C. D. A. (2003). Homocysteine and blood pressure. *Curr. Sci. Inc* 5, 26–31. doi:10.1007/s11906-003-0007-z

Van Haren, M. J., Sastre Toraño, J., Sartini, D., Emanuelli, M., Parsons, R. B., and Martin, N. I. (2016). A rapid and efficient assay for the characterization of substrates and inhibitors of nicotinamide N -methyltransferase. *Biochemistry* 55, 5307–5315. doi:10.1021/acs.biochem.6b00733

Van Haren, M. J., Taig, R., Kuppens, J., Sastre Toraño, J., Moret, E. E., Parsons, R. B., et al. (2017). Inhibitors of nicotinamide N-methyltransferase designed to mimic the methylation reaction transition state. *Org. Biomol. Chem.* 15, 6656–6667. doi:10.1039/C7OB01357D

Van Haren, M. J., Zhang, Y., Thijssen, V., Buijs, N., Gao, Y., Mateuszuk, L., et al. (2021). Macrocyclic peptides as allosteric inhibitors of nicotinamide N -methyltransferase (NNMT). *RSC Chem. Biol.* 2, 1546–1555. doi:10.1039/D1CB00134E

Vekic, J., Zeljkovic, A., Stefanovic, A., Jelic-Ivanovic, Z., and Spasojevic-Kalimanovska, V. (2019). Obesity and dyslipidemia. *Metabolism* 92, 71–81. doi:10.1016/j.metabol.2018.11.005

Visram, M., Radulovic, M., Steiner, S., Malanovic, N., Eichmann, T. O., Wolinski, H., et al. (2018). Homocysteine regulates fatty acid and lipid metabolism in yeast. *J. Biol. Chem.* 293, 5544–5555. doi:10.1074/jbc.M117.809236

Wang, W., Li, T., and Feng, S. (2021). Knockdown of long non-coding RNA HOTAIR promotes bone marrow mesenchymal stem cell differentiation by sponging microRNA miR-378g that inhibits nicotinamide N-methyltransferase. *Bioengineered* 12, 12482–12497. doi:10.1080/21655979.2021.2006863

Wang, Z., Pini, M., Yao, T., Zhou, Z., Sun, C., Fantuzzi, G., et al. (2011). Homocysteine suppresses lipolysis in adipocytes by activating the AMPK pathway. *Am. J. Physiology-Endocrinology Metabolism* 301, E703–E712. doi:10.1152/ajpendo.00050.2011

Williams, A. C., Hill, L. J., and Ramsden, D. B. (2012). Nicotinamide, NAD(P)(H), and methyl-group homeostasis evolved and became a determinant of ageing diseases: hypotheses and lessons from pellagra. *Curr. Gerontology Geriatrics Res.* 2012, 302875–302924. doi:10.1155/2012/302875

Wu, C., Orozco, C., Boyer, J., Leglise, M., Goodale, J., Batalov, S., et al. (2009). BioGPS: an extensible and customizable portal for querying and organizing gene annotation resources. *Genome Biol.* 10, R130. doi:10.1186/gb-2009-10-11-r130

Wu, X., Zhang, L., Miao, Y., Yang, J., Wang, X., Wang, C., et al. (2019). Homocysteine causes vascular endothelial dysfunction by disrupting endoplasmic reticulum redox homeostasis. *Redox Biol.* 20, 46–59. doi:10.1016/j.redox.2018.09.021

Xie, X., Yu, H., Wang, Y., Zhou, Y., Li, G., Ruan, Z., et al. (2014). Nicotinamide N-methyltransferase enhances the capacity of tumorigenesis associated with the promotion of cell cycle progression in human colorectal cancer cells. *Archives Biochem. Biophysics* 564, 52–66. doi:10.1016/j.abb.2014.08.017

Xu, W., Hou, L., Li, P., and Li, L. (2022). Effect of nicotinamide N-methyltransferase on lipid accumulation in 3T3-L1 adipocytes. *Bioengineered* 13, 12421–12434. doi:10.1080/21655979.2022.2074768

Yaguchi, H., Togawa, K., Moritani, M., and Itakura, M. (2005). Identification of candidate genes in the type 2 diabetes modifier locus using expression QTL. *Genomics* 85, 591–599. doi:10.1016/j.ygeno.2005.01.006

Yakub, M., Schulze, K., Khatry, S., Stewart, C., Christian, P., and West, K. (2014). High plasma homocysteine increases risk of metabolic syndrome in 6 to 8 Year old children in rural Nepal. *Nutrients* 6, 1649–1661. doi:10.3390/nu6041649

Yamaguchi, S., Franczyk, M. P., Chondronikola, M., Qi, N., Gunawardana, S. C., Stromsdorfer, K. L., et al. (2019). Adipose tissue NAD + biosynthesis is required for regulating adaptive thermogenesis and whole-body energy homeostasis in mice. *Proc. Natl. Acad. Sci. U.S.A.* 116, 23822–23828. doi:10.1073/pnas.1909917116

Yan, L.-J., Wu, J., Jin, Z., and Zheng, H. (2016). Sources and implications of NADH/NAD+ redox imbalance in diabetes and its complications. *DMSO* 145, 145–153. doi:10.2147/DMSO.S106087

Yoshino, J., Mills, K. F., Yoon, M. J., and Imai, S. (2011). Nicotinamide mononucleotide, a key NAD+ intermediate, treats the pathophysiology of diet- and age-induced diabetes in mice. *Cell Metab.* 14, 528–536. doi:10.1016/j.cmet.2011.08.014

You, A., Li, Y., Shen, C., Fan, H., He, J., Liu, Z., et al. (2023). Associations of non-traditional cardiovascular risk factors and body mass index with metabolic syndrome in the Chinese elderly population. *Diabetol. Metab. Syndr.* 15, 129. doi:10.1186/s13098-023-01047-4

Yu, A.-M., Choi, Y. H., and Tu, M.-J. (2020). RNA drugs and RNA targets for small molecules: principles, progress, and challenges. *Pharmacol. Rev.* 72, 862–898. doi:10.1124/pr.120.019554

Yu, J., Xiao, M., and Ren, G. (2021). Long non-coding RNA XIST promotes osteoporosis by inhibiting the differentiation of bone marrow mesenchymal stem cell by sponging miR-29b-3p that suppresses nicotinamide N-methyltransferase. *Bioengineered* 12, 6057–6069. doi:10.1080/21655979.2021.1967711

Zhang, S., Li, X., Zhang, F., Yang, P., Gao, X., and Song, Q. (2006). Preparation of yuanhuacine and relative daphne diterpene esters from Daphne genkwa and structure–activity relationship of potent inhibitory activity against DNA topoisomerase I. *Bioorg. Med. Chem.* 14, 3888–3895. doi:10.1016/j.bmc.2006.01.055

Zhang, X., Qu, Y.-Y., Liu, L., Qiao, Y.-N., Geng, H.-R., Lin, Y., et al. (2021). Homocysteine inhibits pro-insulin receptor cleavage and causes insulin resistance via protein cysteine-homocysteinylation. *Cell Rep.* 37, 109821. doi:10.1016/j.celrep.2021.109821

Zhao, J., Chen, H., Liu, N., Chen, J., Gu, Y., Chen, J., et al. (2017). Role of hyperhomocysteinemia and hyperuricemia in pathogenesis of atherosclerosis. *J. Stroke Cerebrovasc. Dis.* 26, 2695–2699. doi:10.1016/j.jstrokecerebrovasdis.2016.10.012

Zhong, O., Wang, J., Tan, Y., Lei, X., and Tang, Z. (2022). Effects of NAD+ precursor supplementation on glucose and lipid metabolism in humans: a meta-analysis. *Nutr. Metab. (Lond)* 19, 20. doi:10.1186/s12986-022-00653-9

Zhou, Q., Huang, Z.-G., Zhu, X.-J., Xie, Z.-H., Yao, T.-F., Wang, Y.-H., et al. (2018). Effects of nicotinamide N-methyltransferase (NNMT) inhibition on the aerobic and the anaerobic endurance exercise capacity. *Sci. Sports* 33, e159–e165. doi:10.1016/j.scispo.2018.02.006

Zhou, Q., Zhu, X.-J., and Li, J.-H. (2017). Association between nicotinamide N-methyltransferase gene polymorphisms and obesity in Chinese han male College students. *BioMed. Res. Int.* 2017, 2984826–6. doi:10.1155/2017/2984826

Zhu, X.-J., Lin, Y.-J., Chen, W., Wang, Y.-H., Qiu, L.-Q., Cai, C.-X., et al. (2016). Physiological study on association between nicotinamide N-methyltransferase gene polymorphisms and hyperlipidemia. *BioMed Res. Int.* 2016, 7521942–7521948. doi:10.1155/2016/7521942

Zweygarth, E., Schillinger, D., Kaufmann, W., and Röttcher, D. (1986). Evaluation of sinefungin for the treatment of Trypanosoma (Nannomonas) congolense infections in goats. *Trop. Med. Parasitol.* 37, 255–257.

frontiers | Frontiers in Endocrinology

TYPE Original Research
PUBLISHED 18 June 2024
DOI 10.3389/fendo.2024.1388245

OPEN ACCESS

EDITED BY
Lin Zhu,
Vanderbilt University Medical Center,
United States

REVIEWED BY
Weilin Wang,
Tianjin Medical University, China
Xiaoli Yu,
Tianjin Children Hospital, China

*CORRESPONDENCE
Gordana Bukara-Radujkovic
gocabr@inecco.net

RECEIVED 19 February 2024
ACCEPTED 04 June 2024
PUBLISHED 18 June 2024

CITATION
Bukara-Radujkovic G and Miljkovic V (2024) Glycemic variability through the perspective of the glycemia risk index and time in range and their association with glycated hemoglobin A1c in pediatric patients on sensor-augmented pump therapy. *Front. Endocrinol.* 15:1388245. doi: 10.3389/fendo.2024.1388245

Glycemic variability through the perspective of the glycemia risk index and time in range and their association with glycated hemoglobin A1c in pediatric patients on sensor-augmented pump therapy

Gordana Bukara-Radujkovic[1,2]* and Vesna Miljkovic[1]

[1]Pediatric Clinic, University Clinical Center of the Republic of Srpska, Banja Luka, Bosnia and Herzegovina, [2]Pediatric Department, Faculty of Medicine, University of Banja Luka, Banja Luka, Bosnia and Herzegovina

Introduction: From the introduction of continuous glucose monitoring (CGM) in treatments of type 1 diabetes, particularly its integration with insulin pumps, there has been a quest for new parameters that describe optimal glycemic control. As of the consensus reached in 2019, the ambulatory glucose profile (AGP) has become the standard, with time in range (TIR) emerging as a fundamental parameter for metabolic control assessment. However, with technological advancements, new parameters, such as the glycemia risk index (GRI), have been introduced and clinically utilized. Therefore, exploring the relationships between traditional and novel parameters to understand metabolic control comprehensively is imperative.

Materials and methods: This study was conducted at the Pediatric Clinic of the University Hospital of the Republic of Srpska Banja Luka between January and July 2023. The participants were randomly selected, with the inclusion criteria specifying an age greater than eight years and a diabetes type 1 duration exceeding two years. All participants were required to use a sensor-augmented insulin pump for the next three months (90 days), irrespective of prior use, with the suspend-before-low option activated.

Results: Of the 35 participants, 30 completed the study, 14 (46.7%) of whom were male. The mean age of the subjects was 14.90 $\pm$ 2.88 years, and the mean duration of diabetes was 7.83 $\pm$ 4.76 years. Over the 90-day period, HbA1c increased to an average of 7.31%. The analysis revealed significant effects of TIR (β=-0.771) and GRI (β=0.651) on HbA1c. Furthermore, GRI and TIR strongly correlated (β=-0.953).

Discussion and conclusion: New parameters generated from the ambulatory glucose profile (AGP) can help clinicians create a complete picture of a patient's metabolic control in relation to HbA1c levels. Additionally, the GRI is a mathematically tailored parameter that incorporates all components of the

ambulatory glucose profile and demonstrates strong correlations with laboratory-measured HbA1c and TIR. The GRI potentially can become a valuable statistical parameter for evaluating and managing patients in routine clinical practice.

KEYWORDS

glycemia risk index, glycemic variability, continuous glucose monitoring, pediatric diabetes, time in range

1 Introduction

Since 2019, after the recommendations of the international consensus on time in range (1) were announced and utilized, the management of diabetes in children and adolescents has encountered significant challenges. Although we are constantly discussing the increased penetration of continuous glucose monitoring technology (CGM), particularly among pediatric populations, glycated hemoglobin A1c (HbA1c) remains the primary parameter for assessing metabolic control in many resource-limited settings and among patients who decline or struggle with CGM technology (2). Global data indicate that only 37% of individuals with type 1 diabetes achieve an HbA1c below 7.50%, with a mere 21% reaching or maintaining levels at or below 7.00%, as recommended by consensus guidelines (3).

The utilization of CGM can mitigate the limitations associated with HbA1c, which include variability in laboratory measurements influenced by various pathological (e.g., anemia, uremia, hemoglobinopathies) and physiological (e.g., pregnancy) factors, as well as the inability to capture daily glycemic fluctuations (3). CGM, particularly when focusing on the time in range (TIR) parameter (i.e., time spent within the target range of 3.9–10 mmol/L or 70–180 mg/dL), is becoming the standard of use in clinical practice, due to its ability to bypass the shortcomings of HbA1c and effectively depict daily glucose fluctuations, thereby reducing glycemic variability—a significant contributor to oxidative stress, particularly in children (4). Recently, TIR has been endorsed as a key parameter for clinical trials (5, 6). However, in addition to TIR, other parameters derived from ambulatory glucose profile (AGP), such as time below range (TBR), time above range (TAR), and coefficient of variation (CV), provide clinicians with valuable insights into glycemic variability beyond the confines of TIR and HbA1c (7, 8).

Because of the multitude of parameters derived from AGP essential for comprehensive glycemic assessment, researchers have recently proposed that the parameters of time above and below the target range should be integrated into a new parameter, the glycemia risk index (GRI). This parameter was generated mathematically from the TBR and TAR values, as already stated in the ambulatory glucose profile. It contains a hypoglycemic component (CHypo) that is twice as significant as the hyperglycemic component (CHyper). Theoretically, lower GRI values, ranging from 0 to 100, correlate with reduced risk of hypoglycemia and hyperglycemia. Contrastingly, the lower the GRI, the higher the TIR (9).

The well-established correlation between HbA1c and TIR (10, 11) prompts further investigation of the relationship between these parameters and GRI across different therapeutic modalities. Therefore, our goal with this study is to explore the interdependence of HbA1c levels and variability parameters derived from ambulatory glucose profile including GRI components, in a pediatric population undergoing sensor-augmented pump therapy.

2 Materials and methods

This study was conducted at the Pediatric Clinic of the University Hospital of the Republic of Srpska, Banja Luka, between January and July 2023. Participants were randomly selected, with every fifth eligible patient attending regular clinic visits being invited to participate. The inclusion criteria were age > 8 years and diabetes type 1 duration exceeding two years. Exclusion criteria included diabetes type 1 duration less than two years. Informed consent was obtained from all participants or their legal guardians. Participants were required to utilize a sensor-augmented insulin pump for the next 3 months from the baseline, no matter of prior use of insulin pump or the CGM, with the suspend before low feature enabled, and attend regular check-ups. The low threshold set was 4.0 mmol/L for all participants, as it is presented in Figure 1. Diagnostic analyses were conducted in accordance with the Declaration of Helsinki, with HbA1c and anthropometric measurements recorded at baseline and after 3 months.

Abbreviations: AGP, Ambulatory Glucose Profile; CGM, Continiouse Glucose Monitoring; CHyper, Hyperglycemic component of GRI; CHypo, Hypoglycemic component of GRI; CV, Coefficient of Variation; GMI, Glucose Management Indicator; GRI, Glycemia Risk Index; HbA1c, Glycated hemoglobin A1c; SG, Sensor Glucose value; TAR, Time Above Range; TBR, Time Below Range; TDD, Total Daily Dose; TIR, Time In Range.

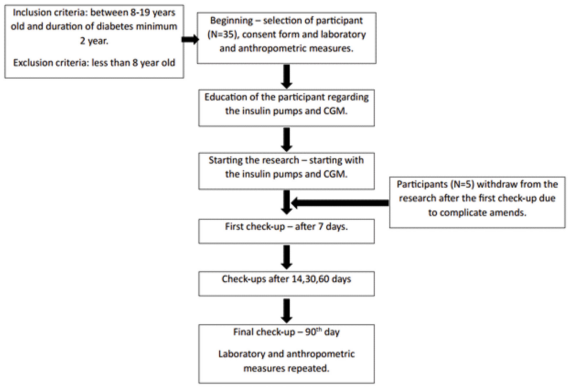

FIGURE 1
Research scheme.

2.1 Statistical analysis

Numerical variables were described using measures of central tendency, mean value, standard deviation, or minimum and maximum values. Categorical variables are described as frequencies (%) of the total sample. The IBM SPSS 22 statistical program was used for statistical analysis. Pearson's correlation coefficient was used to measure the dependence between the numerical variables. The dependence of the numerical variables on time was determined using a t-test for paired samples. A linear regression model was set where the dependent variable was HbA1c at the end of the study, and the independent variables were parameters from AGP or derived from it such as GRI. Statistical significance was set at $p < 0.05$. GRI was calculated using the mathematical formula, and the component of GRI was also considered a significant variable in the statistical analysis, replacing the TBR, levels 1 and 2, and TAR, levels 1 and 2 (9). Other AGP parameters were used in the analysis, and recommendations from the consensus regarding parameter targets in clinical care were used (1).

3 Results

Thirty of the 35 initially enrolled participants successfully completed the study, with 46.7% male participants. The mean age was 14.90 ± 2.88 years, and the mean duration of diabetes was 7.83 ± 4.76 years. Within this cohort, only two participants (6.7%) were diagnosed with celiac disease in addition to type 1 diabetes mellitus. Laboratory analyses and anthropometric measurements were conducted at baseline and after a 90-day period.

No statistically significant changes were observed in BMI (from 20.80 ± 3.76 BMI to 20.94 ± 3.30) after three months of utilizing sensor-augmented pump therapy. However, there was an increase in the average value of laboratory-measured HbA1c levels compared with the baseline measurement. HbA1c levels increased from 7.17 ± 0.92% to 7.31 ± 0.74%. These two parameters exhibited a positive correlation, with a Pearson's correlation coefficient of 0.542 ($p<0.05$). The paired-sample t-test for this variable did not yield statistically significant results (t=-0.945, p=0.352).

Further analysis involved dividing the subjects into two groups based on their initial HbA1c values: those with HbA1c values equal to or less than 7.00% and those with initial HbA1c values higher than 7.00%. Fourteen participants had HbA1c values less than or equal to 7.00%, and a t-test comparison within this group demonstrated a statistical significance (correlation = 0.847, p=0.0001; paired sample t-test: t=-5.090, p=0.0002). In this group, HbA1c increased by an average of 0.59 ± 0.44%. Conversely, no statistically significant reduction was observed in the group where HbA1c was over 7.00%, despite an initial average HbA1c of 7.78 ± 0.76% decreasing to 7.53 ± 0.68%. The correlation between the variables within this group was not significant (correlation = 0.274, p=0.305; t-test: t=1.184, p=0.255). Therefore, the overall correlation between HbA1c levels at the beginning and end of the study was primarily influenced by a statistically significant increase in the group with initial HbA1c values of less than 7.00%.

The variables obtained from the ambulatory glucose profile (AGP) are presented in Table 1, including the hypoglycemic and hyperglycemic components necessary for calculating the Glycemia Risk Index (GRI). Established formula was used to calculate the GRI, and its components (9). The results are provided by month to observe changes, as well as an average for the entire 90-day period.

Analysis of these parameters revealed that they approached the clinical targets by the third month, as set by consensus. The correlations between these parameters and laboratory-measured HbA1c levels at the end of the research period were examined and are presented in Table 2. Most parameters obtained from the AGP and GRI, along with their components, demonstrated high correlations (>0.65 and $p<0.001$), except for the hypoglycemic component of the GRI, coefficient of variation (CV), and total daily dose (TDD), which had p values greater than 0.05.

Average glycemia and GMI, although highly correlated with HbA1c, were not considered predictor variables in the linear

TABLE 1 Values of variables obtained from ambulatory glucose profile and GRI.

Variable	1st month	2nd month	3rd month	Average for 90 days
TIR	68.43 ± 10.70	69.13 ± 10.88	71.40 ± 8.59	69.66 ± 8.96
CHypo	2.05 ± 1.74	1.95 ± 1.39	2.20 ± 1.71	2.07 ± 1.44
CHyper	17.75 ± 7.06	17.45 ± 7.64	15.62 ± 5.88	16.94 ± 6.10
GRI	34.56 ± 13.05	33.78 ± 11.91	31.59 ± 11.15	33.31 ± 10.71
CV	34.28 ± 4.63	34.00 ± 3.13	34.02 ± 4.11	34.10 ± 3.65
GMI	7.04 ± 0.32	7.02 ± 0.37	6.94 ± 0.28	7.00 ± 0.28
MEAN SG	8.66 ± 0.79	8.60 ± 0.86	8.43 ± 0.66	8.56 ± 0.68
TDD	44.45 ± 19.18	45.27 ± 19.76	45.77 ± 18.97	45.16 ± 19.21

Values are presented as mean ± standard deviation. TIR, Time In Range (from ambulatory glucose profile); CHypo, Hypoglycemic component of GRI (mathematically calculated) (9); CHyper, Hyperglycemic component of GRI (mathematically calculated) (9); GRI, Glycemia Risk Index (mathematically calculated) (9); CV, Coefficient of Variation (from ambulatory glucose profile); GMI, Glucose Management Indicator (from ambulatory glucose profile); SG, Sensor Glucose Value; TDD, Total Daily Dose of insulin.

TABLE 2 Pearson correlation between HbA1c and parameters derived from AGP.

Variable	HbA1c after 90 days	
	Pearson correlation coefficient	p-value
TIR	-0.771	p<0.001
Chypo	-0.124	p=0.515
Chyper	0.770	p<0.001
GRI	0.651	p<0.001
CV	0.113	p=0.552
GMI	0.810	p<0.001
Mean SG	0.782	p<0.001
TDD	0.040	p=0.835

AMP, Ambulatory Glucose profile1; HbA1c, Glycated hemoglobin A1c; TIR, Time In Range (from ambulatory glucose profile); CHypo, Hypoglycemic component of GRI (mathematically calculated) (9); CHyper, Hyperglycemic component of GRI (mathematically calculated) (9); GRI, Glycemia Risk Index (mathematically calculated) (9); CV, Coefficient of Variation (from ambulatory glucose profile); GMI, Glucose Management Indicator (from ambulatory glucose profile); SG, Sensor Glucose Value; TDD, Total Daily Dose of insulin.

regression analysis. Our analysis focused on the relationship between the GRI and its components and TIR and HbA1c levels. The results of this linear regression analysis were R=0.822, R^2 = 0.676, and adjusted R^2 = 0.639, indicating that 63.9% of the HbA1c distribution could be explained by these variables (F=18.092, p<0.001). The coefficients of the TIR (t=-2.290, p<0.05) and GRI (t=-2.468, p<0.05) were statistically significant.

In further analysis, we wanted to examine the individual influence of the GRI and TIR on HbA1c; therefore, we performed a single linear regression of these variables with HbA1c as dependent variable. In this regression, the GRI was statistically significant R=0.651, R^2 = 0.423, and adjusted R^2 = 0.403 (F=20.563, t=16.671, p<0.001). Standardized coefficient β=0.651, i.e., if GRI increases by 1 standard deviation, HbA1c increases by 0.651 standard deviations. Also, TIR shows statistical significance R=0.771, R^2 = 0.594, and adjusted R^2 = 0.580 (F=41.028, t=16.677, p<0.001) and standardized coefficient β=-0.771, which means if TIR increases by 1 standard deviation, HbA1c decreases by 0.771 standard deviation. The Figure 2 shows that with an increase in HbA1c, the TIR decreased, and the GRI increased.

We examined the relationship between the parameters obtained from the AGP and the GRI. The correlations of the GRI components with the variability parameters from AGP is presented in Table 3. There is a negative correlation between GRI, CHyper, and TIR, which is logical because a higher TIR indicates a lower GRI and less hyperglycemic component of the GRI. There was no correlation between the TIR and hypoglycemic components. Multivariate linear regression was performed with the GRI as the dependent variable to examine which variability parameters had the greatest influence on the GRI. The model showed a high statistical significance, R=0.991, R^2 = 0.983, and adjusted R^2 = 0.979, F=271.162, p<0.001. This means that 98.3% of the GRI distribution can be explained by TIR, CV, GMI, average SG, and TDD. The coefficients for the variables TIR, CV, and TDD show statistical significance in the model, so their standardized values and t-test values are as follows: β=-0.969, t=-8.162, p<0.001 for TIR, β=0.193, t=4.178, p< 0.001 for CV and β=0.107, t=2.986, p<0.006 for TDD. Because the values for TIR were the highest, a single linear regression analysis of the dependence of the GRI on TIR was performed. The obtained results of R=0.953, R^2 = 0.909, and adjusted R^2 = 0.906, F=280.002, t=-16.733, and standardized β=-0.953 at the significance level p<0.001 tell us that an increase in TIR by 1 standard deviation leads to a decrease in GRI for 0.953 standard deviation in our cohort. It is observed that with the increase in GRI comes the reduction of TIR and vice versa, as it can been seen in Figure 3. In our examined group, the highest GRI is close to 60, and the respondent TIR is approximately 50.

4 Discussion

The sensor-augmented pump, which uses an algorithm that predicts and automatically suspends insulin delivery before reaching a low threshold, set in our study on 4.0 mmol/L, has

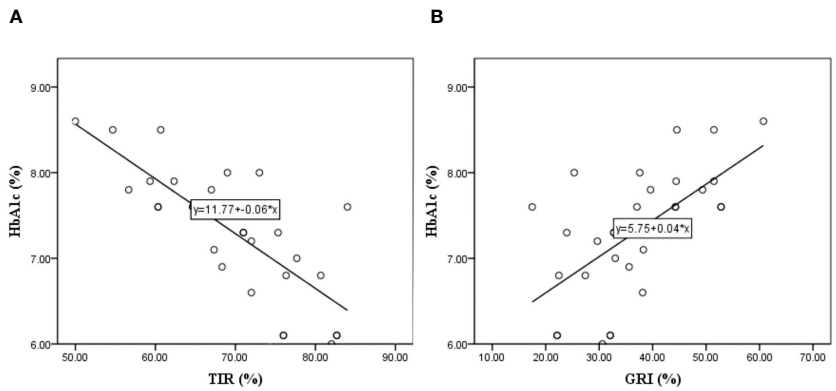

FIGURE 2
Linear regression model where the HbA1c is dependent variable and the Time In Range – TIR **(A)**, and Glycemia Risk Index – GRI **(B)** are independent variable.

TABLE 3 Correlation of variability parameters from AGP and GRI and its components.

Variable	GRI		Chyper		Chypo	
	Pearson correlation coefficient	p-value	Pearson correlation coefficient	p-value	Pearson correlation coefficient	p-value
TIR	-0.953	p<0.001	-0.977	p<0.001	-0.158	p=0.405
CV	0.687	p<0.001	0.446	p<0.05	0.686	p<0.001
GMI	0.774	p<0.001	0.949	p<0.001	-0.224	p=0.233
Mean SG	0.800	p<0.001	0.961	p<0.001	-0.186	p=0.325
TDD	0.404	P<0.05	0.183	P=0.334	-0.589	p<0.001

AMP, Ambulatory Glucose profile1; GRI , Glycemia Risk Index (mathematically calculated) (9); CHypo , Hypoglycemic component of GRI (mathematically calculated) (9); CHyper , Hyperglycemic component of GRI (mathematically calculated) (9); TIR , Time In Range (from ambulatory glucose profile); CV , Coefficient of Variation (from ambulatory glucose profile); GMI , Glucose Management Indicator (from ambulatory glucose profile); SG , Sensor Glucose Value; TDD , Total Daily Dose of insulin.

shown significant benefits over its period of use (12). In our study group, the utilization of this system led to an increase in the parameters derived from the ambulatory glucose profile, culminating in the achievement of consensus-recommended values by the third month (1). Interestingly, in the third month, in addition to the increase in TIR and decrease in CHyper, there was also an increase in CHypo. This can be explained by the fact that the participants began to trust the system and allowed the prediction algorithm to execute fully (13), not correcting the hypoglycemia with carbs on values higher than 4.0 mmol/L. The sensor augmented pump system, designed to suspend insulin delivery 30 minutes before reaching a low threshold of 4.0 mmol/L, allowed users to intervene promptly and prevent hypoglycemic events. As participants familiarized themselves with the system's functionality, there was a noticeable decrease in hypoglycemic incidents during the initial month, followed by a subsequent increase by the third month as users gained confidence in the system's reliability. Over time, the diminishing fear of hypoglycemia, a pivotal psychological component in diabetes management (14), leads to a decreased tendency to react promptly to and correct hypoglycemic episodes upon activation of the algorithm. This behavior typically results in reactive hyperglycemia prior to the adoption of this system (15). Notably, this system effectively mitigated hypoglycemia, as evidenced by the absence of statistical significance in variables describing hypoglycemia (CHypo) in the ambulatory glucose profile and Glycemia Risk Index (GRI) and their lack of association with other examined variables or HbA1c.

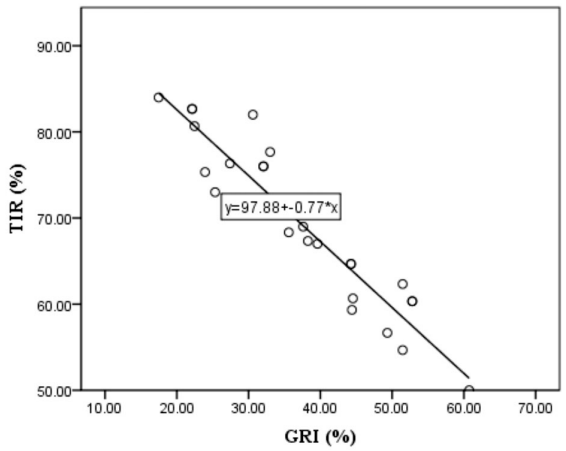

FIGURE 3
Linear regression model of Time In Range - TIR as dependent and Glycemia Risk Index - GRI as independent variable.

Although the HbA1c levels showed a nominal increase across the entire group, this increase was not statistically significant. However, participants with initial HbA1c levels of < 7.00% at baseline displayed a statistically significant increase, whereas the other groups exhibited a non-significant decrease. The observed elevation in HbA1c among participants with initially lower HbA1c levels can be attributed to the aforementioned system and the reduction of hypoglycemic components, suggesting that the initially lower HbA1c levels in this group may have been due to the prior hypoglycemia (16). Given the absence of prior continuous glucose monitoring data, the direct causation of the lower baseline HbA1c cannot be definitively established. However, increasing the HbA1c, especially in the group where baseline values were lower than 7.0, suggested a potential association.

HbA1c demonstrated the highest correlation with the average mean sensor glucose value (17), consistent with previous studies. Surprisingly, the coefficient of variation (CV) did not significantly correlate with HbA1c (18), indicating that this parameter, which characterizes daily glycemic variability, has no notable effect on HbA1c, a long-term prognostic indicator of glycemic control. Our analysis primarily aimed to ascertain whether TIR and GRI, incorporating a hyperglycemic component, could adequately substitute for HbA1c in the long-term prognosis of glycemic control (19) and to elucidate the relationship between these parameters in our cohort. Our findings indicate that a 0.65 standard deviation increase in the GRI corresponds to a one standard deviation increase in HbA1c. This direct proportional relationship is dictated by the hyperglycemic component of the GRI, with the hypoglycemic component exerting no influence. Since the hypoglycemic component has no influence, we can say that the dependence on GRI and HbA1c dictates the hyperglycemic component, and it is logical that an increase in GRI leads to an increase in HbA1c.

In contrast to the GRI, the TIR is inversely proportional to HbA1c levels (20). A decrease in TIR by 0.771 standard deviations corresponded to a 1.00 standard deviation increase in HbA1c. Considering the recommendation that a TIR of 70% approximately corresponds to an HbA1c of 7.00% (10), in our study, where the TIR after 90 days was 69.66% and the HbA1c was 7.31%, a 0.36% decrease in TIR would theoretically result in a 0.47% increase in HbA1c levels. However, this discrepancy does not align with laboratory measurements of HbA1c, underscoring the inadequacy of TIR alone as a variable for forecasting long-term consequences, similar to HbA1c (21). Consequently, to evaluate metabolic control comprehensively, all variables, including TIR and GRI, must be considered, prompting us to investigate the extent of their mutual dependence in our cohort.

Our results revealed a strong correlation: a decrease in TIR by 0.953 standard deviations corresponded to a 1.00 standard deviation increase in GRI. Intriguingly, the GRI exhibited correlations with all parameters from the ambulatory glucose profile (22), as well as with CV. CV, traditionally regarded as a parameter describing glucose variability (23), did not exhibit a statistical significance with the laboratory-measured parameters in our study. Introducing the GRI as a new variability parameter is promising for overcoming this limitation (24). Furthermore, in addition to CV and TIR, the GRI demonstrated a dependence on the total daily insulin dose in our study, indicating its correlation with and dependence on the values derived from all parameters of the ambulatory glucose profile.

As the latest parameter derived from ambulatory glucose profiles, the Glycemia Risk Index (GRI) has yet to find widespread use in daily clinical practice. Studies such as this one, which integrate traditional metrics like HbA1c with modern indicators such as TIR, CV, and other AGP-derived parameters, along with potential future additions like the GRI, play a vital role in advocating for the incorporation of GRI into routine clinical assessments. This article's significance lies in its contribution towards bridging the gap between research findings and practical implementation, thereby enhancing the clinical utility of GRI. Although limited by its small sample size, our study yielded statistically significant results. The primary limitation of our study was the financial constraints, which restricted the number of participants. Nevertheless, the statistical dependencies obtained serve as a solid foundation for future research on potentially larger scales, increasing the sample size, which can yield the statistically stronger conclusions.

5 Conclusion

The GRI is a mathematically tailored variable that, in our research, demonstrated statistical correlations with all AGP parameters and was highly correlated with laboratory-measured HbA1c. The GRI could potentially become a valuable statistical parameter for assessing and managing patients in routine clinical practice. Glycemic variability is a complex phenomenon with significant implications for metabolic control in the short and long term (25). This concept often remains unclear to patients, and since 2019, the dominant parameter describing it, the CV, has caused more confusion than clarity. Therefore, introducing new variables, such as the GRI, that can simplify glycemic variability for clinicians and patients may help alleviate this issue and enhance metabolic control, which is the primary objective. A comprehensive review and evaluation of all parameters, including TIR, along with other elements of AGP and GRI, can provide an accurate and complete understanding of the patient's metabolic control.

Data availability statement

The raw data supporting the conclusions of this article will be made available by the authors, without undue reservation.

Ethics statement

The studies involving humans were approved by Ethics Committee of University Clinical Center of the Republic of Srpska (protocol number: 01-19-82-2/23 from March 22, 2023). The studies were conducted in accordance with the local legislation and institutional requirements. Written informed consent for participation in this study was provided by the participants' legal guardians/next of kin.

Author contributions

GB-R: Conceptualization, Data curation, Formal analysis, Funding acquisition, Investigation, Methodology, Project administration, Resources, Software, Supervision, Validation, Visualization, Writing – original draft, Writing – review & editing. VM: Investigation, Project administration, Writing – review & editing.

Funding

The author(s) declare that no financial support was received for the research, authorship, and/or publication of this article.

Conflict of interest

The authors declare that the research was conducted in the absence of any commercial or financial relationships that could be construed as a potential conflict of interest.

Publisher's note

References

1. Battelino T, Danne T, Bergenstal RM, Amiel SA, Beck R, Biester T, et al. Clinical targets for continuous glucose monitoring data interpretation: Recommendations from the international consensus on time in range. *Diabetes Care*. (2019) 42:1593–603. doi: 10.2337/dci19–0028

2. Lal RA, Maahs DM. Clinical use of continuous glucose monitoring in pediatrics. *Diabetes Technol Ther*. (2017) 19:S37–43. doi: 10.1089/dia.2017.0013

3. Gerhardsson P, Schwandt A, Witsch M, Kordonouri O, Svensson J, Forsander G, et al. The SWEET Project 10-year benchmarking in 19 countries worldwide is associated with improved HbA1c and increased use of diabetes technology in youth with Type 1 diabetes. *Diabetes Technol Ther*. (2021) 23:491–9. doi: 10.1089/dia.2020.0618

4. Pease A, Lo C, Earnest A, Kiriakova V, Liew D, Zoungas S. Time in range for multiple technologies in Type 1 diabetes: A systematic review and network meta-analysis. *Diabetes Care*. (2020) 43:1967–75. doi: 10.2337/dc19–1785

5. Beck RW, Bergenstal RM, Riddlesworth TD, Kollman C, Zhaomian Li, AS B, et al. Validation of time in range as an outcome measure for diabetes clinical trials. *Diabetes Care*. (2019) 42:400–5. doi: 10.2337/dc18–1444

6. Battelino T, Alexander CM, Amiel SA, Arreaza-Rubin G, Beck RW, Bergenstal RM, et al. Continuous glucose monitoring and metrics for clinical trials: An international consensus statement. *Lancet Diabetes Endocrinol*. (2023) 11:42–57. doi: 10.1016/S2213–8587(22)00319–9

7. American Diabetes Association. Standards of care in diabetes—2023 abridged for primary care providers. *Clin Diabetes*. (2022) 41:4–31. doi: 10.2337/cd23-as01

8. Naranjo K, Arbelaez D, Arbelaez AM, Mbogo J, Ganesh J, Timothy J, et al. ISPAD Clinical Practice Consensus Guidelines 2022: Assessment and management of hypoglycemia in children and adolescents with diabetes. *ISPAD Clin Pract Consensus Guidelines. Pediatr Diabetes*. (2022) 23:1322–40. doi: 10.1111/pedi.13443

9. Klonoff DC, Wang J, Rodbard D, Kohn MA, Li C, Liepmann D, et al. A Glycemia Risk Index (GRI) of hypoglycemia and hyperglycemia for continuous glucose monitoring validated by clinician ratings. *J Diabetes Sci Technol*. (2023) 17:1226–42. doi: 10.1177/19322968221085273

10. Vigersky RA, McMahon C. The relationship of hemoglobin A1C to time-in-range in patients with diabetes. *Diabetes Technol Ther*. (2019) 21:81–5. doi: 10.1089/dia.2018.0310

11. Kurozumi A, Okada Y, Mita T, Wakasugi S, Katakami N, Yoshii H, et al. Associations between continuous glucose monitoring-derived metrics and HbA1c in patients with type 2 diabetes mellitus. *Diabetes Res Clin Pract*. (2022) 186:109836. doi: 10.1016/j.diabres.2022.109836

12. Forlenza GP, Li Z, Buckingham BA, Pinsker JE, Cengiz E, Wadwa RP, et al. Predictive low-glucose suspend reduces hypoglycemia in adults, adolescents, and children with Type 1 diabetes in an at-home randomized crossover study: Results of the PROLOG trial. *Diabetes Care*. (2018) 41:2155–61. doi: 10.2337/dc18–0771

13. Biester T, Kordonouri O, Holder M, Remus K, Kieninger-Baum D, Wadien T, et al. 'Let the Algorithm Do the Work': Reduction of hypoglycemia using sensor-augmented pump therapy with predictive insulin suspension (SmartGuard) in pediatric Type 1 diabetes patients. *Diabetes Technol Ther*. (2017) 19:173–82. doi: 10.1089/dia.2016.0349

14. Przezak A, Bielka W, Molęda P. Fear of hypoglycemia-An underestimated problem. *Brain Behav*. (2022) 12:e2633. doi: 10.1002/brb3.2633

15. Acciaroli G, Welsh JB, Akturk HK. Mitigation of rebound hyperglycemia with real-time continuous glucose monitoring data and predictive alerts. *J Diabetes Sci Technol*. (2022) 16:677–82. doi: 10.1177/1932296820982584

16. Seyed Ahmadi S, Westman K, Pivodic A, Ólafsdóttir AF, Dahlqvist S, Hirsch IB, et al. The association between HbA1c and time in hypoglycemia during CGM and self-monitoring of blood glucose in people with Type 1 diabetes and multiple daily insulin injections: A randomized clinical trial (GOLD-4). *Diabetes Care*. (2020) 43:2017–24. doi: 10.2337/dc19–2606

17. Garg P, Pethusamy K, Ranjan R. Correlation between estimated average glucose levels calculated from HbA1c values and random blood glucose levels in a cohort of subjects. *J Lab Phys*. (2023) 15:217–23. doi: 10.1055/s-0042–1757719

18. Lou G, Larramona G, Montaner T, Barbed S. The HbA1c, coefficient of variation of glucose levels and hypoglycaemia in a pediatric sample when using continuous glucose monitoring. *J Pharm Health Serv Res*. (2020) 11:189–91. doi: 10.1111/jphs.12350

19. Pérez-López P, Férnandez-Velasco P, Bahillo-Curieses P, de Luis D, Díaz-Soto G. Impact of glucose variability on the assessment of the glycemia risk index (GRI) and classic glycemic metrics. *Endocrine*. (2023) 82:560–8. doi: 10.1007/s12020–023-03511–7

20. Beck RW, Bergenstal RM, Cheng P, Kollman C, Carlson AL, Johnson ML, et al. The relationships between time in range, hyperglycemia metrics, and HbA1c. *J Diabetes Sci Technol*. (2019) 13:614–26. doi: 10.1177/1932296818822496

21. Nomura S, Sakamoto H, Rauniyar SK, Shimada K, Yamamoto H, Kohsaka S, et al. Analysis of the relationship between the HbA1c screening results and the development and worsening of diabetes among adults aged over 40 years: A 4-year follow-up study of 140,000 people in Japan – The Shizuoka study. *BMC Public Health*. (2021) 21:1880. doi: 10.1186/s12889–021-11933-z

22. Šumnik Z, Pavliková M, Neuman V, Petruželková L, Konečná P, Venháčová P, et al. Glycemic control by treatment modalities: National registry-based population data in children and adolescents with Type 1 diabetes. *Horm Res Paediatr*. (2024) 97:70–9. doi: 10.1159/000530833

23. Castañeda J, Arrieta A, van den Heuvel T, Cohen O. The significance of coefficient of variation as a measure of hypoglycaemia risk and glycaemic control in real world users of the automated insulin delivery MiniMed 780G system. *Diabetes Obes Metab*. (2023) 25:2545–52. doi: 10.1111/dom.15139

24. Díaz-Soto G, Pérez-López P, Férnandez-Velasco P, Nieto de la Marca MO, Delgado E, Del Amo S, et al. Glycemia risk index assessment in a pediatric and adult patient cohort with type 1 diabetes mellitus. *J Diabetes Sci Technol*. (2023), 19322968231154561. doi: 10.1177/19322968231154561

25. Zhou Z, Sun B, Huang S, Zhu C, Bian M. Glycemic variability: Adverse clinical outcomes and how to improve it? *Cardiovasc Diabetol*. (2020) 19:102. doi: 10.1186/s12933–020-01085–6

frontiers | Frontiers in Endocrinology

TYPE Original Research
PUBLISHED 08 July 2024
DOI 10.3389/fendo.2024.1401131

OPEN ACCESS

EDITED BY
Åke Sjöholm,
Gävle Hospital, Sweden

REVIEWED BY
Ying Wu,
Tennessee State University, United States
Suqin Shao,
Agriculture and Agri-Food Canada (AAFC), Canada

*CORRESPONDENCE
Hongliang Zhang
zhanghongliang@csu.edu.cn

†These authors have contributed equally to this work and share first authorship

RECEIVED 14 March 2024
ACCEPTED 11 June 2024
PUBLISHED 08 July 2024

CITATION
Chen T, He H, Tang W, Liu Z and Zhang H (2024) Association of blood trihalomethane concentrations with diabetes mellitus in older adults in the US: a cross-sectional study of NHANES 2013–2018.
Front. Endocrinol. 15:1401131.
doi: 10.3389/fendo.2024.1401131

Association of blood trihalomethane concentrations with diabetes mellitus in older adults in the US: a cross-sectional study of NHANES 2013–2018

Tuotuo Chen[1,2†], Haiqing He[1,3†], Wei Tang[4], Ziyi Liu[1,2] and Hongliang Zhang[1,2*]

[1]Department of Emergency Medicine, The Second Xiangya Hospital, Central South University, Changsha, Hunan, China, [2]Emergency and Difficult Diseases Institute of Central South University, Changsha, Hunan, China, [3]Department of Urology, The Second Xiangya Hospital, Central South University, Changsha, Hunan, China, [4]Department of Nephrology, The Second Xiangya Hospital, Central South University, Changsha, Hunan, China

Background: Previous studies have demonstrated that there is a correlation between trihalomethanes and disease progression, such as allergic diseases. As we know, only few studies focused on the relationship between trihalomethanes and metabolic diseases, such as diabetes mellitus.

Objective: The aim of this study was to further explore the associations between blood trihalomethane concentrations and diabetes mellitus in older adults in the US.

Methods: Data were collected from the National Health and Nutrition Examination Study (NHANES) database in the survey cycle during 2013 to 2018, including 2,511 older adults in the US whose blood trihalomethane concentrations were measured, involving chloroform (TCM) and brominated trihalomethanes (Br-THMs). Br-THMs include bromodichloromethane (BDCM), dibromochloromethane (DBCM), and bromoform (TBM). Meanwhile, the concentration of total trihalomethanes (TTHMs) was also measured later. A multivariate logistic regression and restricted cubic spline were used to examine the relationship between blood THMs and diabetes mellitus. Meanwhile, we performed a subgroup analysis, which aims to explore the stability of this relationship in different subgroups. In order to further consider the impact of various disinfection by-products on diabetes, we also used weighted quantile sum (WQS). To explore the correlation in trihalomethanes, we plot a correlation heatmap.

Results: Adjusting for potential confounders, we found that there was a significant negative association between chloroform and diabetes mellitus [Model 1 (adjusted for covariates including age, sex, and race, OR = 0.71; 95% CI: 0.50–1.02; p = 0.068; p for trend = 0.094); Model 2 (adjusted for all covariates, OR = 0.68; 95% CI: 0.48–0.96; p = 0.029; p for trend = 0.061)].

In the bromodichloromethane, we reached a conclusion that is similar to TCM [Model 1 (adjusted for covariates including age, sex, and race, OR = 0.54; 95% CI: 0.35–0.82; p = 0.005; p for trend = 0.002); Model 2 (adjusted for all covariates, OR = 0.54; 95% CI: 0.35–0.82; p = 0.003; p for trend = 0.002)]. Meanwhile, the restricted cubic spline curve also further confirms this result (p overall = 0.0027; p overall< 0.001). Based on the analysis in the subgroups, we found that the value p for interaction in the majority of subgroups is higher than 0.1. Trihalomethanes and diabetes were inversely associated, and in the WQS, chloroform and bromodichloromethane were found to be the major contributors to this relationship. In the correlation analysis, we found that most trihalomethanes have a weak correlation, except for TBM and TCM with a strong correlation.

Conclusion: Our results in this study showed that blood chloroform, bromodichloromethane concentrations, and diabetes mellitus in older adults in the US are negatively correlated, suggesting that chloroform and bromodichloromethane can be protective factors for diabetes.

KEYWORDS

trihalomethanes, diabetes mellitus, disinfection by-products, NHANES, older adults in the US

1 Introduction

Diabetes mellitus is a systemic disease, whose clinical manifestations usually include polydipsia, polyuria, overeating, and weight loss. Although the etiology of diabetes mellitus is quite complicated, some studies indicated that it can be attributed to lack of insulin secretion or insulin resistance or both (1). Long-term hyperglycemia can lead to damage to the function of our systemic organs, particularly the eyes, kidneys, nerves, heart, and blood vessels (2–7). Some studies showed that the population of patients with diabetes in recent years is increasing gradually (8). As the global population ages, the prevalence of diabetes is evidently increasing in older adults (9). It is expected that the economic burden of diabetes will increase in the next few decades. Therefore, it is necessary to focus on the causative and protective factors of diabetes in the older adult population.

Chlorine disinfection of public water supplies remains one of the main means to control the microbial contamination around the world. When disinfectants (such as hypochlorous acid and calcium hypochlorite) react with substances in the water, more than hundreds of water disinfection by-products (DBPs) are produced (10). Humans are exposed to DBPs when people use water for some daily activities (e.g., swimming, drinking, and bathing). Therefore, residual contaminants formed during water disinfection may have adverse health effects (11). Trihalomethanes are one of the most common DBPs and the humans are most easily exposed to this DBP. Several studies have linked trihalomethanes to some allergic diseases, such as asthma (12, 13). In addition, on the relationship between THMs and diabetes mellitus, some scholars have different opinions. On the one hand, in diabetic rats with diet and alloxan-induced diabetes, the chloroform fraction of plants (such as *Anthocleista vogelii* Planch root bark) has antidiabetic effects (14). On the other hand, it has been shown that brominated trihalomethanes (Br-THMs) are a risk factor for diabetes, contributing to related diabetic events through leptin and liver damage (15, 16). The barriers to scholars' views give us enough motivation to further explore the relationship between trihalomethanes in human blood and diabetes mellitus. The determination of trihalomethane concentrations requires consideration of several factors, and other exposure pathways may have been overlooked in previous determinations of THMs in tap water. Blood trihalomethane concentrations represent a more integrated measurement of multiple exposure routes and sources (17). Steady-state blood concentrations generally depend on the frequency of exposure events. The time spent swimming in a chlorinated swimming pool is generally positively correlated with blood trihalomethane concentrations. Showering, washing dishes by hand, and ingestion of hot beverages made with tap water are associated with higher blood THMs (18). In addition, there are no research evaluating the relationship between blood trihalomethanes and diabetes mellitus in older adults. The immune system of older adults may be more fragile than the rest of the population. Therefore, to further explore the association of trihalomethanes with diabetes mellitus, we used the National Health and Nutrition Examination Study (NHANES) database and selected older adults as our study group.

2 Methods

2.1 Study population

In this cross-sectional study, data were collected from the 2013–2018 survey cycle in the NHANES database ($N = 29,400$). Participants aged no more than 60 years were excluded ($N = 23,508$). Meanwhile, there are no missing data for people with diabetes ($N = 5,892$). Subsequently, we removed the data with missing or zero weights ($N = 280$). In addition, we excluded missing data for trihalomethanes [including chloroform, bromodichloromethane, dibromochloromethane, bromoform, total trihalomethanes (TTHMs), and Br-THMs; $N = 3101$]. Finally, 2,511 participants were eligible for this study (Figure 1). Based on a population cross-sectional survey, the NHANES collects information on the health and nutrition of households in America. Each participant in the interview and evaluation provided informed consent. The National Health Statistics Research Ethics Review Board approved this biennial data collection. Likewise, the Centers for Disease Control and Prevention's (CDC's) Institutional Review Board also approved the protocol for the study.

2.2 Blood THM measurement

According to previous studies, the procedure for the determination of trihalomethanes is blood sampling by venipuncture, storing, determination, quality assurance (QA), and quality control (QC) (19, 20). Trihalomethanes are highly volatile and need to be stored in the room at 4°C. There are three methods for determining the concentration of trihalomethanes in blood, namely, solid-phase microextraction, gas chromatography, and mass spectrometry (21–23). BDCM, DBCM, and TBM were summed as Br-THMs, and TCM, BDCM, TBM, and DBCM were summed as TTHMs (13). In our research, values below the limit of detection (LOD) have been replaced by LOD/$\sqrt{2}$.

2.3 Determination of diabetes mellitus

According to the latest update of the diagnostic criteria for diabetes mellitus and the CDC's undiagnosed diabetes definition (24), diabetes was defined as fasting plasma glucose (FPG) >7.0 mmol/L or 2 h postprandial >11.1 mmol/L in the oral glucose tolerance test (OGTT), or random blood glucose ≥11.1 mmol/L, HbA1C ≥ 6.5%, or self-reported. The diabetes population in this study was identified based on the above conditions' diagnosis.

2.4 Definition of covariates

Factors that we considered may influence the relationship between blood trihalomethane concentrations and diabetes mellitus in diabetes as covariates. Information regarding patients' age, sex, race, hyperlipidemia, marriage, poverty-to-income ratio (PIR), education, smoke status, body mass index, alcohol user status, and hypertension was collected. Ethnic groups include Mexican-Americans, non-Hispanic whites, non-Hispanic blacks, and other races. Marital information includes married/living with partner, widowed/divorced/separated, and never married. Educational level is categorized as below senior high school, senior high school, and above senior high school. BMI was calculated as weight/(height)^2 kg/m^2. The conditions for smokers include never smoked, used to smoke, and currently smoking. Alcohol user status was categorized as never drank, used to drink, low to moderate drinking (defined as ≤2 cups per day for women and ≤3

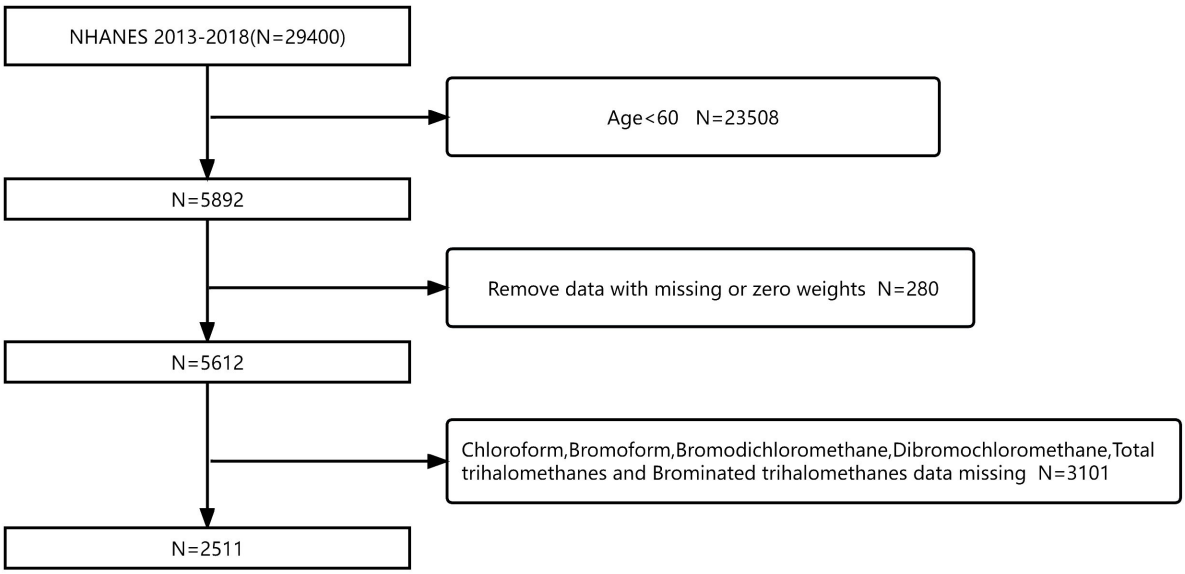

FIGURE 1
Flowchart of participant screening based on the NHANES database for the relationship between blood trihalomethane concentrations and diabetes mellitus from 2013 to 2018.

cups per day or ≤4 days of drinking per month for men), and heavy drinking (defined as ≥3 cups per day for women or ≥4 cups per day or ≥5 days of drinking per month for men). We defined hypertension as a systolic blood pressure (SBP) ≥130 mm Hg or diastolic blood pressure (DBP) ≥80 mm Hg or the presence of antihypertensive drug treatment or self-reported (Whelton et al., 2018). The PIR is divided into three levels, namely, PIR ≤ 1 (low income), PIR 1–3 (middle income), and PIR > 3 (high income). Participants were considered to have diabetes mellitus when they had a fasting glucose level >7 mmol/L, or a random glucose >11 mmol/L, or a glycated hemoglobin >6.5%, or 2 h postprandial >11.1 mmol/L in OGTT, or self-reported (24). The definition of hyperlipemia was triglyceride (TG) > 200 mg/dL, total cholesterol (TC) > 200 mg/dL, low-density lipoprotein (LDL) > 130 mg/dL, high-density lipoprotein (HDL)< 40 mg/dL (men)/50 mg/dL (women), or taking hypolipidemic drugs. Among the covariates, we found no statistically significant differences between diabetic and non-diabetic populations in age, marital, and smoking status ($p > 0.05$).

2.5 Statistical analysis

NHANES adopted a complex multi-stage probability sampling design; thus, appropriate weighting was used in our study. In our study, we described continuous variables (e.g., age) as mean ± standard deviation and categorical variables as percentages. In order to compare the differences among the groups, we used weighted ANOVA and chi-square test. Meanwhile, the multivariate logistic regression was conducted to explore the relationship between blood trihalomethane concentrations and diabetes mellitus. The older adults were assigned to quartile for TTHMs, whereas five groups were created for TCM (<75th, 75–87.5th, and ≥87.5th), BDCM (≤50th, 50–75th, and >75th), DBCM (≤25th, 25–75th, and >75th), TBM (≤25th, 25–75th, and >75th), and Br-THMs (<75th, 75–87.5th, and ≥87.5th). In order to reduce the influence of confounding factors on our result, we conducted model adjustments, Model 1: adjusted for age, race, and sex, and Model 2: adjusted for all covariates (age +sex +race + smoke+ alcohol user status + hypertension + marriage+ education + BMI + hyperlipidemia+ PIR). Subsequently, restricted cubic splines were used to further evaluate the blood concentration–response relationship between blood trihalomethane concentrations and diabetes mellitus, and the blood trihalomethane concentration–response curves were plotted clearly and show the relationship between blood trihalomethane concentrations and diabetes mellitus. To explore the contribution of trihalomethanes in reducing the incidence of diabetes, we used WQS. Finally, we also conducted a stratified analysis. Subgroups include race, sex, smoke, alcohol user status, marriage, education, PIR, hypertension, hyperlipidemia, and body mass index. The purpose was to explore the stability of the association between blood trihalomethane concentrations and diabetes mellitus in different subgroups. To explore multicollinearity in trihalomethanes, we plot a correlation heatmap. R-Version 4.21 is used to complete all our data analysis.

3 Results

3.1 Baseline information and correlation analysis

The study had a total of 29,400 participants and ultimately included 2,511 members. The average age of most members is 69 years old (Table 1). In our study, the proportion of men and women was approximately identical. Over half of the participants had been educated in senior high school education or even obtained advanced degrees. Approximately 26.0% of participants had a high school diploma, and 15.7% of participants did not receive a high school education. Whether participants had diabetes or not, non-Hispanic whites make up most of our research group (75.7% of participants), most participants are low to moderate drinkers (67.5% of participants), most participants have hyperlipidemia (84.5% of participants), and most people suffer from hypertension (76.5% of participants). In addition, half of the participants had never smoked and more than half of those with diabetes had a body mass index above 30 kg/m^2. We also found that the concentrations of TCM and BDCM in the blood of most participants were Q1, while others were Q2. In the correlation analysis (Figure 2), TBM and TCM have the strongest correlation (correlation coefficient: 0.79). The correlation coefficients between most trihalomethanes are less than 0.2.

3.2 Association between blood trihalomethane concentrations and diabetes mellitus

We conducted multivariate logistic regression analysis (Table 2). The results on blood levels of chloroform and diabetes mellitus are shown in model 1 (adjusted for covariates including age, sex, and race, OR = 0.71; 95% CI: 0.50–1.02; $p = 0.068$; p for trend = 0.094) and model 2 (adjusted for all covariates, OR = 0.68; 95% CI: 0.48–0.96; $p = 0.029$; p for trend = 0.061). For bromodichloromethane, the results are shown in model 1 (adjusted for covariates including age, OR = 0.54; 95% CI: 0.35–0.82; $p = 0.005$; p for trend = 0.002) and model 2(adjusted for all covariates, OR = 0.54; 95% CI: 0.35–0.82; $p = 0.003$; p for trend = 0.002). In the study of bromoform, dibromochloromethane, TTHMs, and Br-THMs, we did not find a statistically significant correlation with diabetes mellitus ($p > 0.05$). Meanwhile, we plotted restricted cubic spline curves to further evaluate the blood concentration–response relationship between blood trihalomethane concentrations and diabetes mellitus (Figure 3). Apart from the non-linear relationship in BDCM (p for nonlinear = 0.0047), we found a linear relationship in blood concentrations of all trihalomethanes. Moreover, blood chloroform, bromodichloromethane concentrations, and diabetes mellitus events in older adults in the US are negatively correlated (p overall = 0.0027; p overall< 0.01). Most members have lower concentrations of chloroform and bromodichloromethane in their blood than other types of trihalomethanes. Based on the results that we have obtained, we speculated that the protective effects of

10.3389/fendo.2024.1401131

TABLE 1 Baseline information, weighted, NHANES 2013–2018.

Characteristic	Trihalomethane			
	Overall	Non-diabetic	Diabetes	*p*
N	2,511	1,630	881	
Age (years)	69.88 ± 6.72	69.91 ± 6.77	69.84 ± 6.59	0.819
GFR (mL/1.73 m^2)	102.02 ± 28.59	101.81 ± 29.15	102.4 ± 27.20	0.616
Gender, *n* (%)				0.003
Male	1,260 (45.9)	782 (43.1)	478 (52.6)	
Female	1,251 (54.1)	848 (56.9)	403 (47.4)	
Race, *n* (%)				<0.001
Mexican American	328 (4.6)	170 (3.5)	158 (7.4)	
Other races	556 (11.2)	345 (10.1)	221 (14.1)	
Non-Hispanic white	1,116 (75.8)	792 (78.8)	324 (68.3)	
Non-Hispanic blacks	501 (8.4)	323 (7.6)	178 (10.2)	
Marriage, *n* (%)				0.296
Married/living with partner	1,448 (62.5)	925 (63.0)	523 (61.3)	
Widowed/divorced/separated	900 (32.6)	602 (32.8)	298 (32.3)	
Never married	163 (4.9)	103 (4.3)	60 (6.4)	
Education, *n* (%)				<0.001
<High school	667 (15.7)	397 (14.3)	270 (19.3)	
High school	609 (26.0)	388 (25.3)	221 (27.6)	
>High school	1,235 (58.3)	845 (60.4)	390 (53.1)	
Alcohol user status, *n* (%)				0.01
Never	401 (12.3)	243 (10.2)	158 (17.5)	
Former	419 (14.0)	252 (13.2)	167 (16.0)	
Low to moderate	1,511 (67.5)	1,017 (70.2)	494 (61.1)	
Heavy	180 (6.1)	118 (6.4)	62 (5.4)	
Smoke, *n* (%)				0.456
Never	1,301 (51.8)	849 (51.9)	452 (51.6)	
Former	892 (38.6)	567 (38.2)	325 (39.5)	
Currently	318 (9.6)	214 (9.9)	104 (8.9)	
BMI, kg/m^2, *n* (%)				<0.001
≤25 kg/m^2	616 (22.5)	475 (26.7)	141 (12.3)	
25–30 kg/m^2	942 (37.8)	637 (40.0)	305 (32.6)	
≥30 kg/m^2	953 (39.7)	518 (33.4)	435 (55.1)	
Hypertension, *n* (%)				<0.001
Yes	1,998 (76.5)	1,247 (73.3)	751 (84.3)	
No	513 (23.5)	383 (26.7)	130 (15.7)	
Hyperlipidemia, *n* (%)				<0.001
Yes	2,102 (84.5)	1,323 (82.4)	779 (89.5)	
No	409 (15.5)	307 (17.6)	102 (10.5)	

(Continued)

TABLE 1 Continued

Characteristic	Trihalomethane			
	Overall	Non-diabetic	Diabetes	*p*
Chloroform, *n* (%)				0.035
Q1 (<0.016 ng/mL)	1,867 (74.2)	1,185 (73.0)	682 (77.2)	
Q2 (0.016 to 0.024 ng/mL)	312 (12.9)	214 (13.1)	98 (12.3)	
Q3 (≥0.024 ng/mL)	332 (12.9)	231 (13.9)	101 (10.5)	
Bromodichloromethane, *n* (%)				<0.001
Q1 (≤0.004 ng/mL)	1,462 (57.4)	903 (55.3)	559 (62.8)	
Q2 (0.004 to 0.0042 ng/mL)	685 (27.4)	460 (27.6)	225 (26.7)	
Q3 (>0.0042 ng/mL)	364 (15.2)	267 (17.1)	97 (10.5)	
Dibromochloromethane, *n* (%)				0.084
Q1 (≤0.0035 ng/mL)	695 (28.5)	471 (29.0)	224 (27.1)	
Q2 (0.0035 to 0.0040 ng/mL)	1,511 (61.7)	955 (60.7)	556 (64.1)	
Q3 (>0.0040 ng/mL)	305 (9.8)	204 (10.2)	101 (8.9)	
Bromoform, *n* (%)				0.04
Q1 (≤0.0057 ng/mL)	743 (29.8)	510 (30.9)	233 (27.2)	
Q2 (0.0057 to 0.0060 ng/mL)	1,591 (64.2)	1,008 (63.3)	583 (66.4)	
Q3 (>0.0060 ng/mL)	177 (5.9)	112 (5.8)	65 (6.4)	
Total trihalomethane, *n* (%)				0.001
Q1 (<0.02 ng/mL)	332 (13.3)	215 (13.3)	117 (13.4)	
Q2 (0.02 to 0.028 ng/mL)	1,338 (53.7)	829 (52.4)	509 (56.8)	
Q3 (≥0.028 ng/mL)	841 (33.0)	586 (34.3)	255 (29.8)	
Brominated trihalomethane, *n* (%)				0.01
Q1 (<0.014 ng/mL)	627 (25.5)	422 (26.0)	205 (24.3)	
Q2 (0.014 to 0.018 ng/mL)	1,558 (62.0)	978 (60.8)	580 (64.9)	
Q3 (≥0.018 ng/mL)	326 (12.5)	230 (13.2)	96 (10.8)	

BMI, body mass index; GFR, glomerular filtration rate.

chloroform and bromodichloromethane on diabetes may be realized at low concentrations.

3.3 Trihalomethane exposure and diabetes mellitus in the WQS model

We used the WQS model to examine the relationship between the combined effects of these four tri-halomethanes and the incidence of diabetes. In terms of co-exposures, the WQS model found that trihalomethanes are inversely associated with diabetes (Model: OR = 0.51; 95% CI: 0.37–0.7; $p < 0.001$), with the top weight contributions from BDCM (79.2%) and TCM (12.2%). Positive WQS regression analysis showed no association between trihalomethanes and diabetes (Model: OR = 0.7; 95% CI: 0.43–1.13; $p = 0.144$), as shown in Table 2 and Figure 4.

3.4 Subgroup analysis

Our purpose was to explore the stability of the association between blood trihalomethane concentrations and diabetes mellitus in different subgroups (Tables 3, 4). In the results, we found that the *p* for interaction in most subgroups is higher than 0.1, indicating that the negative association between blood trihalomethane concentrations (chloroform and bromodichloromethane) and diabetes mellitus is robust. This means that these factors do not influence our results, such as gender, race, and education.

4 Discussion

This cross-sectional analysis of older adults in the US showed that blood BDCM and TCM concentrations were associated with

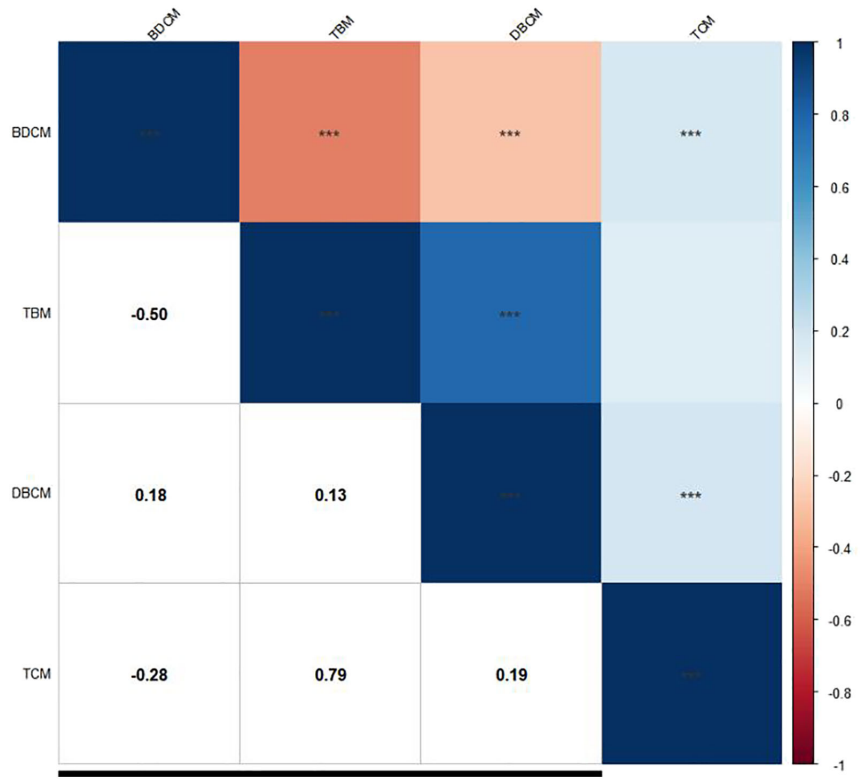

FIGURE 2
Exploring the correlation between trihalomethanes. ***means *P*<0.001.

TABLE 2 Results of multiple logistic regression analysis of the association between trihalomethane and diabetes mellitus in older adults, weighted.

Chloroform	Model 1	*p*-value	Model 2	*p*-value
	OR (95% CI)		OR (95% CI)	
Q1	Ref	Ref	Ref	Ref
Q2	0.92 (0.62,1.36)	0.658	0.99 (0.66,1.50)	0.965
Q3	0.71 (0.50,1.02)	0.068	0.68 (0.48,0.96)	0.029
***p* for trend**	0.094		0.061	
Dibromochloromethane	**OR (95% CI)**	***p*-value**	**OR (95% CI)**	***p* value**
Q1	Ref	Ref	Ref	Ref
Q2	1.11 (0.88,1.39)	0.361	1.11 (0.89,1.39)	0.34
Q3	0.84 (0.54,1.29)	0.407	0.84 (0.55,1.28)	0.404
***p* for trend**	0.137		0.77	
Bromodichloromethane	**OR (95% CI)**	***p*-value**	**OR (95% CI)**	***p*-value**
Q1	Ref	Ref	Ref	Ref
Q2	0.87 (0.67,1.14)	0.305	0.89 (0.69,1.15)	0.374
Q3	0.54 (0.35,0.82)	0.005	0.54 (0.36,0.81)	0.003
***p* for trend**	0.002		0.002	
Bromoform	**OR (95% CI)**	***p*-value**	**OR (95% CI)**	***p*-value**

(Continued)

TABLE 2 Continued

Chloroform	Model 1	*p*-value	Model 2	*p*-value
	OR (95% CI)		OR (95% CI)	
Bromoform	**OR (95% CI)**	***p*-value**	**OR (95% CI)**	***p*-value**
Q1	Ref	Ref	Ref	Ref
Q2	1.17 (0.92,1.48)	0.193	1.15 (0.91,1.46)	0.228
Q3	1.16 (0.60,2.24)	0.648	1.12 (0.59,2.11)	0.731
***p* for trend**	0.335		0.403	
Total trihalomethane	**OR (95% CI)**	***p*-value**	**OR (95% CI)**	***p*-value**
Q1	Ref	Ref	Ref	Ref
Q2	1.05 (0.71,1.55)	0.796	1.05 (0.72,1.53)	0.803
Q3	0.85 (0.55,1.33)	0.473	0.83 (0.54,1.27)	0.39
***p* for trend**	0.302		0.211	
Brominated trihalomethane	**OR (95% CI)**	***p*-value**	**OR (95% CI)**	***p*-value**
Q1	Ref	Ref	Ref	Ref
Q2	1.11 (0.83,1.49)	0.464	1.09 (0.81,1.47)	0.575
Q3	0.83 (0.51,1.35)	0.442	0.81 (0.50,1.32)	0.388
***p* for trend**	0.302		0.562	
WQS (Negative)			0.51 (0.37,0.7)	<0.001
WQS (Positive)			0.7 (0.43,1.13)	0.144

OR, odds ratio; 95% CI, 95% confidence interval. WQS, weighted quantile sum.
Model 1: Adjusted for covariates (age, race, and sex).
Model 2: Adjust for all confounding factors (age, sex, race, hyperlipidemia, marriage, poverty-to-income ratio, education, smoke status, body mass index, alcohol user status, and hypertension).
Chloroform: Q1 (<0.016 ng/mL), Q2 (0.016 to 0.024 ng/mL), Q3 (≥0.024 ng/mL).
Bromodichloromethane: Q1 (≤0.004 ng/mL), Q2 (0.004 to 0.0042 ng/mL), Q3 (>0.0042 ng/mL).
Dibromochloromethane: Q1 (≤0.0035 ng/mL), Q2 (0.0035 to 0.0040 ng/mL), Q3 (>0.0040 ng/mL).
Bromoform: Q1 (≤0.0057 ng/mL), Q2 (0.0057 to 0.0060 ng/mL), Q3 (>0.0060 ng/mL).
Total trihalomethane: Q1 (<0.02 ng/mL), Q2 (0.02 to 0.028 ng/mL), Q3 (≥0.028 ng/mL).
Brominated trihalomethane: Q1 (<0.014 ng/mL), Q2 (0.014 to 0.018 ng/mL), Q3 (≥0.018 ng/mL).

diabetes mellitus. Furthermore, we believe that this relationship is negatively correlated, indicating that BDCM and TCM may play a protective role in diabetes mellitus development. These associations, however, were not observed in other trihalomethanes (DBCM, TTHMs, TBM, and Br-THMs). Most members had lower concentrations of chloroform and bromodichloromethane in their blood than other types of trihalomethanes. We speculate that the protective effects of chloroform and bromodichloromethane on diabetes may be realized at low concentrations.

Previous population studies have shown that all trihalomethanes, with the exception of TBMs, have protective effects in the diabetic population (18), which seems to contradict our conclusions. In fact, our study does not deny this conclusion. It is well known that the pathogenesis of diabetes mellitus is associated with abnormalities in immune system and metabolism. Metabolic abnormalities, such as insulin resistance, are critical in the development of diabetes mellitus. The immune system and metabolic function are often two-way linked. On the one hand, inflammation can promote metabolic abnormalities such as obesity and diabetes. On the other hand, the metabolic factors, in turn, may regulate immune cell function (25). Our study was conducted in older adults in the US of the diabetic population. We considered that older adults might be a representative group with immunometabolism disorders. Older adults usually have a low level of immune system and tend to show chronic low-grade inflammation, which is related to the pathogenesis of many age-related diseases (atherosclerosis, Alzheimer's disease, osteoporosis, and diabetes) (26). In addition, it has been reported that trihalomethanes also play a role in the development of asthma and other diseases (27). It is well known that the pathogenicity of trihalomethanes is inevitable. Therefore, we consider that studying lower concentrations of trihalomethanes is more meaningful in exploring their role for diabetes mellitus. Compared with the younger group with good body management and love of sports, the living habits of older adults are usually reducing physical activity (PA) and exercise, which means less exposure. In 2006, the standard for DBPs in water has been revised by the United States Environmental Protection Agency (28). Compared to Rieder's study of NHANES from the 1999–2006 survey cycle, the information for the 2013–2018 survey cycle was collected according to the new standards. The World Health Organization's guidelines on drinking water also require limiting the concentration of trihalomethanes in daily water (WHO G, (29)).

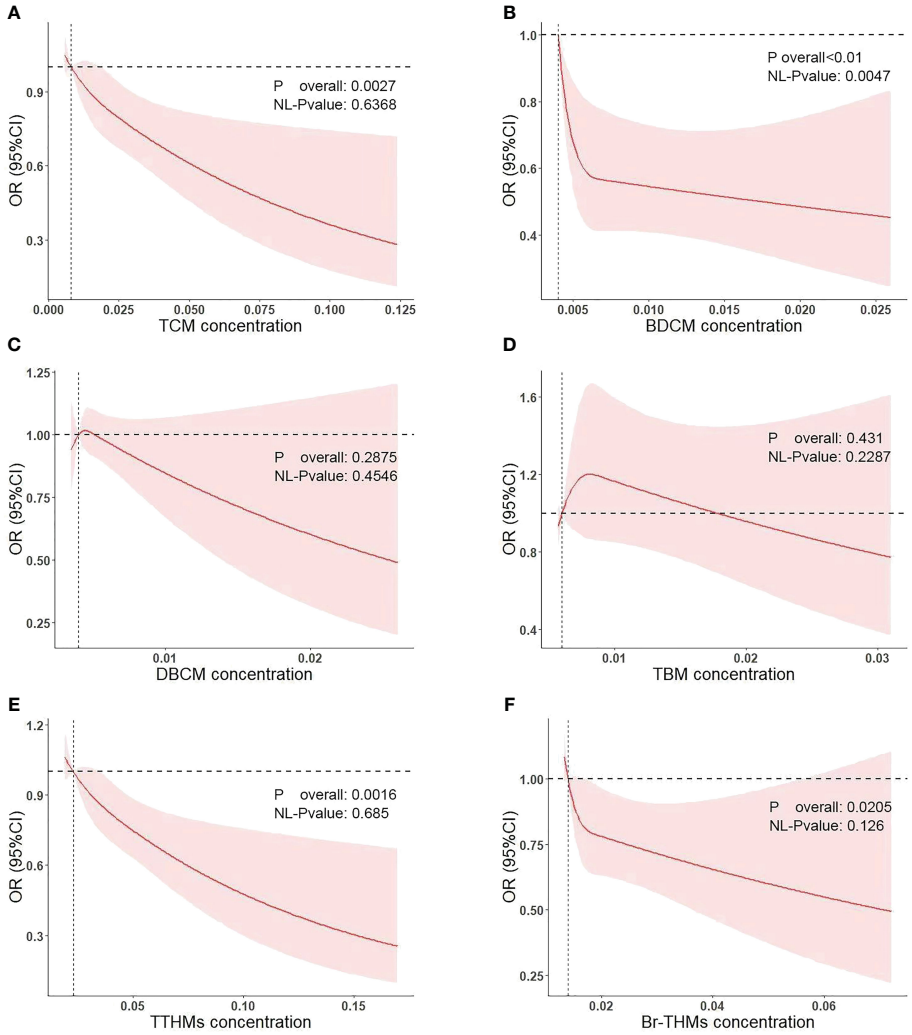

FIGURE 3
Association of diabetes mellitus with the TCM **(A)**, BDCM **(B)**, DBCM **(C)**, TBM **(D)**, TTHMs **(E)**, and Br-THMs **(F)** performed by restricted cubic spline analysis.

Unfortunately, we have not explored the specific THM concentration that can exhibit antidiabetic activity without causing other diseases, which is the direction of our next research.

According to previous studies, the chloroform fraction of plants (such as *A. vogelii* Planch root bark) can exhibit antidiabetic activity in rats with diet- and alloxan-induced obesity–diabetes (14), which may be related to the extracted components of chloroform fraction, including quebrachitol (QCT), loganin, sweroside, oleoside 11methyl ester, and ferulic acid (30). QCT can act as a β-glucosidase inhibitor and thus resist diabetes (31). Sweroside can the regulation of phosphoenolpyruvate carboxykinase gene expression and then mimic insulin to resist diabetes (32). Loganin, oleoside 11-methyl, and ferulic acid ameliorates hyperglycemia by reducing oxidative stress levels (33–35). Most components are associated with oxidative stress levels. This is robust evidence that chloroform may be a protective factor for diabetes. Unfortunately, no extracts of BDCM have been reported for their antidiabetic effects in animal models of diabetes. Our research can be supplementary to the antidiabetic effects of chloroform and it can also stimulate the development of animal models to validate the antidiabetic effects of BDCM.

In addition, some studies have concluded that Br-THMs are a risk factor for diabetes (15, 16). We believe that their study may have some limitations that lead to the opposite conclusion from ours. Firstly, the study is not in a larger sample size population to validate the accuracy of conclusion. Secondly, based on multivariate logistic regression models for T2DM, we found that none of their trihalomethane-related data was statistically significant ($p > 0.05$). However, we also agree with another view that exposure of Br-THM can modulate leptin and insulin sensitivity; thus, we do not completely reject the conclusions of these two studies. Further experiments are still needed to demonstrate the complex mechanisms.

Finally, our study inevitably has some limitations. First, we cannot avoid the shortcomings of reverse causality in cross-sectional studies. Second, we may also be affected by non-measured or uncontrolled covariates. Third, because the intake of trihalomethanes causes various systemic diseases, we were not able to provide a definite concentration as an indicator of anti-diabetes. Fourth, we do not consider the impact

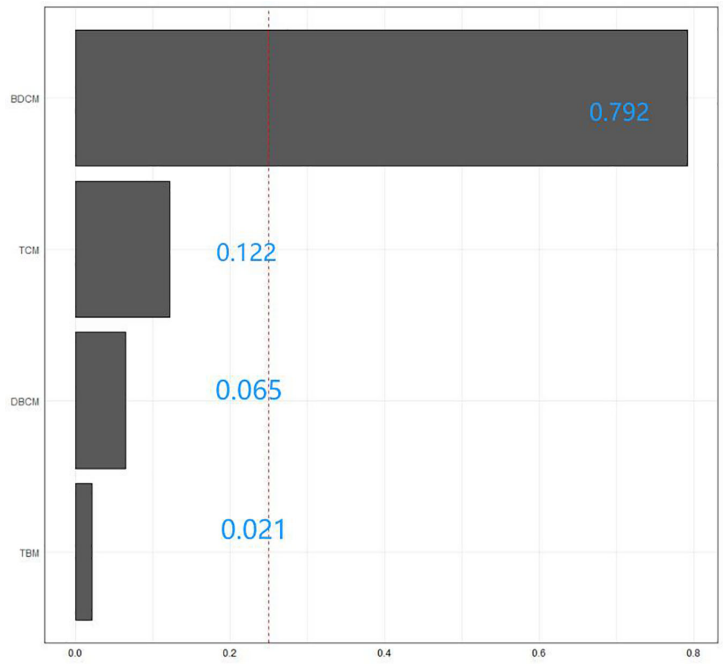

FIGURE 4
The WQS model weights of trihalomethanes on the prevalence of diabetes mellitus in the negative direction.

TABLE 3 Chloroform subgroup analysis.

Character	Q1	Q2	*p*	Q3	*p*	*p* for trend	*p* for interaction
Sex							0.449
Male	Ref	1.188 (0.574,2.462)	0.635	0.694 (0.415,1.163)	0.161	0.347	
Female	Ref	0.712 (0.393,1.288)	0.254	0.739 (0.457,1.193)	0.210	0.165	
Race							0.941
Mexican American	Ref	0.592 (0.177,1.982)	0.373	1.020 (0.393,2.646)	0.966	0.689	
Other races	Ref	1.043 (0.597,1.821)	0.879	0.776 (0.484,1.244)	0.283	0.321	
Non-Hispanic white	Ref	0.916 (0.546,1.539)	0.735	0.684 (0.430,1.087)	0.105	0.16	
Non-Hispanic blacks	Ref	0.742 (0.392,1.405)	0.348	0.648 (0.335,1.252)	0.189	0.152	
Marriage							0.078
Married/living with partner	Ref	1.216 (0.709,2.085)	0.469	0.648 (0.401,1.048)	0.076	0.224	
Widowed/ divorced/separated	Ref	0.442 (0.224,0.871)	0.020	0.650 (0.366,1.154)	0.138	0.048	
Never married	Ref	1.353 (0.285,6.422)	0.695	1.923 (0.479,7.725)	0.345	0.322	
Education							0.372
<High school	Ref	0.615 (0.315,1.199)	0.149	0.634 (0.324,1.241)	0.178	0.119	
High school	Ref	1.470 (0.620,3.485)	0.373	1.109 (0.614,2.003)	0.727	0.477	
>High school	Ref	0.756 (0.373,1.532)	0.429	0.603 (0.332,1.093)	0.094	0.068	
Smoke							0.058
Never	Ref	0.620 (0.408,0.943)	0.026	0.560 (0.331,0.948)	0.032	0.016	

(Continued)

TABLE 3 Continued

Character	Q1	Q2	*p*	Q3	*p*	*p* for trend	*p* for interaction
Former	Ref	1.116 (0.633,1.967)	0.698	1.008 (0.543,1.874)	0.978	0.873	
Now	Ref	2.602 (0.908,7.453)	0.074	0.816 (0.282,2.359)	0.700	0.778	
Alcohol user status							0.172
Never	Ref	0.794 (0.390,1.616)	0.516	0.455 (0.179,1.158)	0.096	0.081	
Former	Ref	1.009 (0.541,1.880)	0.978	0.501 (0.210,1.199)	0.116	0.166	
Low to moderate	Ref	0.852 (0.532,1.365)	0.497	0.720 (0.460,1.127)	0.147	0.124	
Heavy	Ref	2.707 (0.629,11.655)	0.173	2.777 (0.836, 9.226)	0.092	0.032	
BMI							0.229
≤25 kg/m^2	Ref	0.787 (0.281,2.203)	0.641	0.937 (0.423,2.076)	0.871	0.676	
25–30 kg/m^2	Ref	0.619 (0.322,1.192)	0.147	0.586 (0.370,0.928)	0.024	0.011	
≥30 kg/m^2	Ref	1.502 (0.806,2.799)	0.194	0.823 (0.474,1.432)	0.483	0.919	
Hyperlipidemia							0.218
Yes	Ref	0.634 (0.190,2.114)	0.449	1.533 (0.540,4.352)	0.412	0.533	
No	Ref	0.884 (0.594,1.315)	0.534	0.627 (0.427,0.919)	0.018	0.02	
PIR							0.744
Low income	Ref	1.447 (0.662,3.161)	0.345	1.032 (0.475,2.244)	0.934	0.713	
Middle income	Ref	0.854 (0.589,1.240)	0.399	0.716 (0.416,1.234)	0.223	0.182	
High income	Ref	0.868 (0.430,1.751)	0.686	0.563 (0.295,1.076)	0.081	0.106	
Hypertension	Ref						0.956
Yes	Ref	0.783 (0.315,1.946)	0.591	0.693 (0.307,1.568)	0.370	0.361	
No	Ref	0.889 (0.603,1.312)	0.546	0.696 (0.476,1.018)	0.061	0.075	

Subgroup analyses were performed on the following covariates: age, sex, race, hyperlipidemia, marriage, poverty-to-income ratio, education, smoke status, body mass index, alcohol user status, and hypertension.

TABLE 4 Bromodichloromethane subgroup analysis.

Character	Q1	Q2	*p*	Q3	*p*	*p* for trend	*p* for interaction
Sex							0.823
Male	Ref	0.802 (0.524,1.230)	0.304	0.567 (0.310,1.036)	0.065	0.041	
Female	Ref	0.901 (0.641,1.268)	0.542	0.483 (0.256,0.910)	0.025	0.022	
Race							0.789
Mexican American	Ref	0.692 (0.346,1.385)	0.279	0.389 (0.173,0.872)	0.025	0.026	
Other races	Ref	0.999 (0.612,1.632)	0.998	0.772 (0.452,1.320)	0.335	0.413	
Non-Hispanic white	Ref	0.837 (0.578,1.212)	0.338	0.508 (0.289,0.891)	0.019	0.014	
Non-Hispanic blacks	Ref	1.088 (0.728,1.628)	0.670	0.589 (0.271,1.281)	0.175	0.239	

(Continued)

TABLE 4 Continued

Character	Q1	Q2	*p*	Q3	*p*	*p* for trend	*p* for interaction
Marriage							0.61
Married/living with partner	Ref	0.797 (0.558,1.139)	0.207	0.613 (0.314,1.197)	0.147	0.097	
Widowed/ divorced/separated	Ref	0.993 (0.633,1.557)	0.975	0.502 (0.262,0.961)	0.038	0.073	
Never married	Ref	0.772 (0.309,1.928)	0.569	0.211 (0.054,0.826)	0.027	0.061	
Education							0.745
<High school	Ref	1.118 (0.627,1.993)	0.700	0.781 (0.396,1.543)	0.468	0.844	
High school	Ref	0.746 (0.443,1.254)	0.261	0.429 (0.216,0.852)	0.017	0.012	
>High school	Ref	0.813 (0.571,1.157)	0.243	0.574 (0.274,1.199)	0.136	0.1	
Smoke							0.313
Never	Ref	0.957 (0.679,1.347)	0.795	0.413 (0.250,0.683)	<0.001	0.003	
Former	Ref	0.726 (0.441,1.195)	0.202	0.698 (0.383,1.274)	0.235	0.115	
Now	Ref	0.776 (0.310,1.943)	0.578	0.698 (0.321,1.518)	0.354	0.318	
Alcohol user status							0.276
Never	Ref	0.766 (0.458,1.281)	0.301	0.454 (0.151,1.358)	0.153	0.153	
Former	Ref	0.656 (0.316,1.362)	0.247	0.287 (0.154,0.535)	<0.001	0.007	
Low to moderate	Ref	0.784 (0.562,1.092)	0.146	0.570 (0.374,0.867)	0.010	0.006	
Heavy	Ref	1.931 (0.663,5.622)	0.217	1.554 (0.480,5.037)	0.448	0.305	
BMI							0.278
≤25 kg/m^2	Ref	1.363 (0.803,2.311)	0.244	0.539 (0.230,1.266)	0.152	0.546	
25–30 kg/m^2	Ref	0.717 (0.471,1.092)	0.118	0.417 (0.204,0.854)	0.018	0.01	
≥30 kg/m^2	Ref	0.893 (0.626,1.275)	0.526	0.701 (0.395,1.246)	0.220	0.156	
Hyperlipidemia							0.55
Yes	Ref	0.697 (0.349,1.391)	0.297	0.363 (0.130,1.010)	0.052	0.05	
No	Ref	0.893 (0.674,1.183)	0.421	0.568 (0.395,0.817)	0.003	0.002	
PIR							0.402
Low income	Ref	1.112 (0.659,1.878)	0.683	0.804 (0.353,1.829)	0.594	0.727	
Middle income	Ref	0.782 (0.487,1.257)	0.303	0.363 (0.218,0.604)	<0.001	<0.001	

(Continued)

TABLE 4 Continued

Character	Q1	Q2	*p*	Q3	*p*	*p* for trend	*p* for interaction
High income	Ref	0.837 (0.534,1.310)	0.427	0.689 (0.361,1.316)	0.252	0.217	
Hypertension	Ref						0.683
Yes	Ref	1.030 (0.500,2.123)	0.934	0.784 (0.300,2.050)	0.612	0.72	
No	Ref	0.821 (0.584,1.154)	0.248	0.487 (0.309,0.767)	0.003	<0.001	

Subgroup analyses were performed on the following covariates: age, sex, race, hyperlipidemia, marriage, poverty-to-income ratio, education, smoke status, body mass index, alcohol user status, and hypertension.

of living habits on data measurement. For example, some people love swimming while others do not. Finally, although NHANES measured a large amount of data on trihalomethanes, we did not explore the accuracy of our conclusions in the context of co-exposure to other DBPs, and the steady-state exposures of different DBPs may be inconsistent; thus, it is not possible to control for co-exposure under the same variable. Meanwhile, for older adults, it is still worth considering whether it is necessary to increase water-use activities to increase the concentration of trihalomethanes in the blood. These activities (such as swimming and sauna) are strongly related to blood THM concentrations in the older adults, which means that they may also experience other diseases. Investigating the antidiabetic effects of trihalomethanes at specified levels in the context of not causing other diseases is a new research direction, which is indicated by our study.

5 Conclusions

Our study demonstrated a negative correlation between blood concentrations of chloroform and bromodichloromethane and the incidence of diabetes in older adults in the US, which indicates that they may reduce the incidence of diabetes. Compared to other trihalomethanes, chloroform and bromodichloromethane concentrations in older adults in the US are lower. This greatly reduces the potential for other diseases. The pathogenicity of trihalomethanes is not negligible, and our study provides a new reference for standards for chlorinating water for disinfection, but the necessity of increased water use activities in older adults in the US is worth considering. Investigating the antidiabetic effects of specific levels of trihalomethanes without causing other diseases is a new direction for research.

Data availability statement

Publicly available datasets were analyzed in this study. This data can be found here: https://www.cdc.gov/nchs/nhanes/index.htm.

Ethics statement

The studies involving humans were approved by NCHS Research Ethics Review Board. The studies were conducted in accordance with the local legislation and institutional requirements. The participants provided their written informed consent to participate in this study.

Author contributions

TC: Writing – review & editing, Writing – original draft, Investigation, Data curation. HH: Writing – review & editing, Investigation. WT: Writing – review & editing, Data curation. HZ: Writing – review & editing, Supervision, Resources, Project administration, Funding acquisition. ZL: Writing – review & editing, Validation, Software, Methodology, Formal analysis, Conceptualization.

Funding

The author(s) declare financial support was received for the research, authorship, and/or publication of this article. This research was supported by the Changsha Natural Science Foundation of China(kq2208331).

Acknowledgments

The authors thank Lihua Xiao (The Second Xiangya Hospital) for her work in the NHANES R package, which made it easier for us to explore the NHANES databases.

Conflict of interest

The authors declare that the research was conducted in the absence of any commercial or financial relationships that could be construed as a potential conflict of interest.

Publisher's note

References

1. American Diabetes Association. Diagnosis and classification of diabetes mellitus. *Diabetes Care*. (2013) 36 Suppl 1:S67–74. doi: 10.2337/dc13-S067

2. Goldstein AS, Janson BJ, Skeie JM, Ling JJ, Greiner MA. The effects of diabetes mellitus on the corneal endothelium: A review. *Surv Ophthalmol*. (2020) 65:438–50. doi: 10.1016/j.survophthal.2019.12.009

3. Yang Z, Tan T-E, Shao Y, Wong TY, Li X. Classification of diabetic retinopathy: Past, present and future. *Front Endocrinol (Lausanne)*. (2022) 13:1079217. doi: 10.3389/fendo.2022.1079217

4. Selby NM, Taal MW. An updated overview of diabetic nephropathy: Diagnosis, prognosis, treatment goals and latest guidelines. *Diabetes Obes Metab*. (2020) 22 Suppl 1:3–15. doi: 10.1111/dom.14007

5. Selvarajah D, Kar D, Khunti K, Davies MJ, Scott AR, Walker J, et al. Diabetic peripheral neuropathy: advances in diagnosis and strategies for screening and early intervention. *Lancet Diabetes Endocrinol*. (2019) 7:938–48. doi: 10.1016/S2213-8587(19)30081-6

6. Sloan G, Selvarajah D, Tesfaye S. Pathogenesis, diagnosis and clinical management of diabetic sensorimotor peripheral neuropathy. *Nat Rev Endocrinol*. (2021) 17:400–20. doi: 10.1038/s41574-021-00496-z

7. Ritchie RH, Abel ED. Basic mechanisms of diabetic heart disease. *Circ Res*. (2020) 126:1501–25. doi: 10.1161/CIRCRESAHA.120.315913

8. Cho NH, Shaw JE, Karuranga S, Huang Y, da Rocha Fernandes JD, Ohlrogge AW, et al. IDF Diabetes Atlas: Global estimates of diabetes prevalence for 2017 and projections for 2045. *Diabetes Res Clin Pract*. (2018) 138:271–81. doi: 10.1016/j.diabres.2018.02.023

9. Bellary S, Kyrou I, Brown JE, Bailey CJ. Type 2 diabetes mellitus in older adults: clinical considerations and management. *Nat Rev Endocrinol*. (2021) 17:534–48. doi: 10.1038/s41574-021-00512-2

10. Srivastav AL, Patel N, Chaudhary VK. Disinfection by-products in drinking water: Occurrence, toxicity and abatement. *Environ pollut*. (2020) 267:115474. doi: 10.1016/j.envpol.2020.115474

11. Chaves RS, Guerreiro CS, Cardoso VV, Benoliel MJ, Santos MM. Hazard and mode of action of disinfection by-products (DBPs) in water for human consumption: Evidences and research priorities. *Comp Biochem Physiol C Toxicol Pharmacol*. (2019) 223:53–61. doi: 10.1016/j.cbpc.2019.05.015

12. Burch JB, Everson TM, Seth RK, Wirth MD, Chatterjee S. Trihalomethane exposure and biomonitoring for the liver injury indicator, alanine aminotransferase, in the United States population (NHANES 1999-2006). *Sci Total Environ*. (2015) 521–522:226–34. doi: 10.1016/j.scitotenv.2015.03.050

13. Sun Y, Wang Y-X, Mustieles V, Shan Z, Zhang Y, Messerlian C. Blood trihalomethane concentrations and allergic sensitization: A nationwide cross-sectional study. *Sci Total Environ*. (2023) 871:162100. doi: 10.1016/j.scitotenv.2023.162100

14. Anyanwu GO, Iqbal J, Khan SU, Zaib S, Rauf K, Onyeneke CE, et al. Antidiabetic activities of chloroform fraction of Anthocleista vogelii Planch root bark in rats with diet- and alloxan-induced obesity-diabetes. *J Ethnopharmacol*. (2019) 229:293–302. doi: 10.1016/j.jep.2018.10.021

15. Makris KC, Andrianou XD, Charisiadis P, Burch JB, Seth RK, Ioannou A, et al. Association between exposures to brominated trihalomethanes, hepatic injury and type II diabetes mellitus. *Environ Int*. (2016) 92–93:486–93. doi: 10.1016/j.envint.2016.04.012

16. Andra SS, Charisiadis P, Makris KC. Obesity-mediated association between exposure to brominated trihalomethanes and type II diabetes mellitus: an exploratory analysis. *Sci Total Environ*. (2014) 485–486:340–7. doi: 10.1016/j.scitotenv.2014.03.075

17. Blount BC, Backer LC, Aylward LL, Hays SM, LaKind JS. Human exposure assessment for DBPs: factors influencing blood trihalomethane levels. In: Nriagu JO, editor. *Encyclopedia of Environmental Health*. Elsevier, Burlington (2011). p. 100–7. doi: 10.1016/B978-0-444-52272-6.00103-3

18. Riederer AM, Dhingra R, Blount BC, Steenland K. Predictors of blood trihalomethane concentrations in NHANES 1999-2006. *Environ Health Perspect*. (2014) 122:695–702. doi: 10.1289/ehp.1306499

19. Sun Y, Chen C, Mustieles V, Wang L, Zhang Y, Wang Y-X, et al. Association of blood trihalomethane concentrations with risk of all-cause and cause-specific mortality in U.S. Adults: A prospective cohort study. *Environ Sci Technol*. (2021) 55:9043–51. doi: 10.1021/acs.est.1c00862

20. Sun Y, Xia P-F, Korevaar TIM, Mustieles V, Zhang Y, Pan X-F, et al. Relationship between blood trihalomethane concentrations and serum thyroid function measures in U.S. Adults. *Environ Sci Technol*. (2021) 55:14087–94. doi: 10.1021/acs.est.1c04008

21. Bonin MA, Silva LK, Smith MM, Ashley DL, Blount BC. Measurement of trihalomethanes and methyl tert-butyl ether in whole blood using gas chromatography with high-resolution mass spectrometry. *J Anal Toxicol*. (2005) 29:81–9. doi: 10.1093/jat/29.2.81

22. Cardinali FL, Ashley DL, Morrow JC, Moll DM, Blount BC. Measurement of trihalomethanes and methyl tertiary-butyl ether in tap water using solid-phase microextraction GC-MS. *J Chromatogr Sci*. (2004) 42:200–6. doi: 10.1093/chromsci/42.4.200

23. Stack MA, Fitzgerald G, O'Connell S, James KJ. Measurement of trihalomethanes in potable and recreational waters using solid phase micro extraction with gas chromatography-mass spectrometry. *Chemosphere*. (2000) 41:1821–6. doi: 10.1016/S0045-6535(00)00047-3

24. ElSayed NA, Aleppo G, Aroda VR, Bannuru RR, Brown FM, Bruemmer D, et al. 2. Classification and diagnosis of diabetes: standards of care in diabetes-2023. *Diabetes Care*. (2023) 46:S19–40. doi: 10.2337/dc23-S002

25. Daryabor G, Atashzar MR, Kabelitz D, Meri S, Kalantar K. The effects of type 2 diabetes mellitus on organ metabolism and the immune system. *Front Immunol*. (2020) 11:1582. doi: 10.3389/fimmu.2020.01582

26. Castelo-Branco C, Soveral I. The immune system and aging: a review. *Gynecol Endocrinol*. (2014) 30:16–22. doi: 10.3109/09513590.2013.852531

27. Sun Y, Xia P-F, Xie J, Mustieles V, Zhang Y, Wang Y-X, et al. Association of blood trihalomethane concentrations with asthma in US adolescents: nationally representative cross-sectional study. *Eur Respir J*. (2022) 59:2101440. doi: 10.1183/13993003.01440-2021

28. Ashley DL, Smith MM, Silva LK, Yoo YM, De Jesús VR, Blount BC. Factors associated with exposure to trihalomethanes, NHANES 2001–2012. *Environ Sci Technol*. (2020) 54:1066–74. doi: 10.1021/acs.est.9b05745

29. *Guidelines for drinking-water quality: Fourth edition incorporating the first and second addenda* (2022). Geneva: World Health Organization. Available online at: http://www.ncbi.nlm.nih.gov/books/NBK579461/ (Accessed July 6, 2023).

30. Wang D, Zhang S, Chang Z, Kong D-X, Zuo Z. Quebrachitol: global status and basic research. *Nat Prod Bioprospect*. (2017) 7:113–22. doi: 10.1007/s13659-017-0120-3

31. Rines AK, Sharabi K, Tavares CDJ, Puigserver P. Targeting hepatic glucose metabolism in the treatment of type 2 diabetes. *Nat Rev Drug Discovery*. (2016) 15:786–804. doi: 10.1038/nrd.2016.151

32. Huang X-J, Li J, Mei Z-Y, Chen G. Gentiopicroside and sweroside from Veratrilla baillonii Franch. induce phosphorylation of Akt and suppress Pck1 expression in hepatoma cells. *Biochem Cell Biol*. (2016) 94:270–8. doi: 10.1139/bcb-2015-0173

33. Castejón ML, Montoya T, Alarcón-de-la-Lastra C, Sánchez-Hidalgo M. Potential protective role exerted by secoiridoids from olea europaea L. @ in cancer, cardiovascular, neurodegenerative, aging-related, and immunoinflammatory diseases. *Antioxidants (Basel)*. (2020) 9:149. doi: 10.3390/antiox9020149

34. Cheng Y-C, Chu L-W, Chen J-Y, Hsieh S-L, Chang Y-C, Dai Z-K, et al. Loganin attenuates high glucose-induced schwann cells pyroptosis by inhibiting ROS generation and NLRP3 inflammasome activation. *Cells*. (2020) 9:1948. doi: 10.3390/cells9091948

35. Li X, Wu J, Xu F, Chu C, Li X, Shi X, et al. Use of ferulic acid in the management of diabetes mellitus and its complications. *Molecules*. (2022) 27:6010. doi: 10.3390/molecules27186010

frontiers | Frontiers in Physiology

TYPE Review
PUBLISHED 16 July 2024
DOI 10.3389/fphys.2024.1426244

OPEN ACCESS

EDITED BY
Curtis C. Hughey,
University of Minnesota Twin Cities, United States

REVIEWED BY
Roxana Carbó,
Instituto Nacional de Cardiología Ignacio Chávez, Mexico
Yujun Cai,
Yale University, United States

*CORRESPONDENCE
Fubiao Shi,
fubiao.shi@vumc.org

RECEIVED 01 May 2024
ACCEPTED 26 June 2024
PUBLISHED 16 July 2024

CITATION
Shi F (2024), Understanding the roles of salt-inducible kinases in cardiometabolic disease. *Front. Physiol.* 15:1426244.
doi: 10.3389/fphys.2024.1426244

Understanding the roles of salt-inducible kinases in cardiometabolic disease

Fubiao Shi*

Department of Medicine, Division of Cardiovascular Medicine, Vanderbilt University Medical Center, Nashville, TN, United States

Salt-inducible kinases (SIKs) are serine/threonine kinases of the adenosine monophosphate-activated protein kinase family. Acting as mediators of a broad array of neuronal and hormonal signaling pathways, SIKs play diverse roles in many physiological and pathological processes. Phosphorylation by the upstream kinase liver kinase B1 is required for SIK activation, while phosphorylation by protein kinase A induces the binding of 14-3-3 protein and leads to SIK inhibition. SIKs are subjected to auto-phosphorylation regulation and their activity can also be modulated by Ca^{2+}/calmodulin-dependent protein kinase in response to cellular calcium influx. SIKs regulate the physiological processes through direct phosphorylation on various substrates, which include class IIa histone deacetylases, cAMP-regulated transcriptional coactivators, phosphatase methylesterase-1, among others. Accumulative body of studies have demonstrated that SIKs are important regulators of the cardiovascular system, including early works establishing their roles in sodium sensing and vascular homeostasis and recent progress in pulmonary arterial hypertension and pathological cardiac remodeling. SIKs also regulate inflammation, fibrosis, and metabolic homeostasis, which are essential pathological underpinnings of cardiovascular disease. The development of small molecule SIK inhibitors provides the translational opportunity to explore their potential as therapeutic targets for treating cardiometabolic disease in the future.

KEYWORDS

salt-inducible kinases, cardiovascular disease, metabolic syndrome, inflammation, fibrosis, SIK inhibitors

Abbreviations: SIKs, salt-inducible kinases; SNF1, sucrose-nonfermenting 1; HDACs, histone deacetylases; CREB, cAMP responsive element binding protein; CRTCs, CREB-regulated transcriptional coactivators; MEF2, myocyte enhancer factor 2; LKB1, liver kinase B1; PKA, protein kinase A; AMPK, adenosine monophosphate-activated protein kinase; CaMK, Ca2+/calmodulin dependent kinase; PKD, protein kinase D; TGFβ, transforming growth factor β; PI3K, phosphoinositide 3-kinase; NKA, Na+/K+-ATPase; NCX, Na+/Ca2+ exchanger, VDCC, voltage-dependent Ca2+ channels; HAT, histone acetyltransferase; MI, myocardial infarction; PAH, pulmonary arterial hypertension; ECM, extracellular matrix; PAECs, pulmonary artery endothelial cells; PASMCs, pulmonary artery smooth muscle cells; SREBP-1c, sterol regulatory element-binding protein 1c; ChREBP, carbohydrate response element binding protein; MHC, myosin heavy chain; NF-κB, nuclear factor-κB; PME-1, phosphatase methylesterase-1, NRVMs, neonatal rat ventricular myocytes.

Introduction

Salt-inducible kinases (SIKs), including SIK1, SIK2, and SIK3, are serine/threonine kinases of the adenosine monophosphate-activated protein kinase (AMPK) family (Jagannath et al., 2023). The founding member SIK1 was first described as a myocardial sucrose-nonfermenting 1 (SNF1)-like kinase (*msk*) involving mouse heart development (Ruiz et al., 1994). It was cloned later as a protein kinase of 776 amino acids from rats adrenal gland after high-salt diet treatment (Wang et al., 1999), thereby the name of *salt-inducible kinase* was first devised. The two additional members SIK2 and SIK3 were identified later through *in silicon* studies based on protein sequence similarity (Horike et al., 2003; Katoh et al., 2004a).

The three SIK isoforms are broadly expressed in vertebrate tissues. Based on the transcriptomic data from human and mouse tissues, SIK1, SIK2, and SIK3 are mostly enriched in the adrenal gland, the adipose tissue, and the brain, respectively (Fagerberg et al., 2014; Yue et al., 2014). SIK activities are dynamically regulated by multiple physiological cues through both transcriptional and post-translational mechanisms. SIK1 expression is regulated by cyclic AMP (cAMP) through the action of the cAMP responsive element binding (CREB) protein (Jagannath et al., 2013). The mRNA expression of SIK1 can be induced by many physiological cues, such as high-salt dietary intake (Wang et al., 1999), membrane depolarization (Feldman et al., 2000), adrenocorticotropic hormone (Lin et al., 2001), fasting (Koo et al., 2005), adrenergic stimulations (Kanyo et al., 2009), transforming growth factor β (TGFβ) signaling (Lönn et al., 2012), circadian clock (Jagannath et al., 2013), and hypertrophic cardiac stresses (Hsu et al., 2020). In contrast, SIK2 and SIK3 are constitutively expressed but their expression can be modulated under certain pathophysiological conditions. For example, SIK2 and SIK3 mRNA expression are downregulated in the adipose tissue of diabetic and obese individuals (Säll et al., 2016).

SIK proteins process an N-terminal serine/threonine kinase domain (KD), followed by a ubiquitin-associated (UBA) domain, and a C-terminal domain (CTD) (Figure 1). The KD is well-conserved among the three isoforms. It contains a liver kinase B1 (LKB1) phosphorylation threonine site in the activation loop (T-loop). The UBA domain is located within a SNF1 homolog (SNH) region following the KD. The regulatory CTD varies in length among the three isoforms and contains multiple protein kinase A (PKA) phosphorylation sites. SIK1 also has nuclear localization sequences (NLS) (Katoh et al., 2002) and it can repress CREB activity both in the nucleus and cytoplasm (Katoh et al., 2004b).

SIK activities are tightly regulated through post-translational modification in response to hormonal stimulation and physiological alternations (Figure 1). The activation of SIK kinase activity requires the phosphorylation by LKB1 in the activation loop near the substrate binding sites (SIK1 Thr182, SIK2 Thr175, and SIK3 Thr221). The UBA domain assists the LKB1 phosphorylation and SIK kinase activation, potentially by preventing the binding of SIKs with the 14-3-3 phospho-binding proteins (Al-Hakim et al., 2005; Jaleel et al., 2006). Activation by LKB1 stimulates the autophosphorylation in the activation loop of SIK1 (Ser186) and SIK2 (Ser179), which are important for sustained kinase activity (Hashimoto et al., 2008). SIK2 can also be auto-phosphorylated at Ser358, which regulates it protein stability (Henriksson et al., 2012). SIK1 and SIK2 can be phosphorylated by Ca^{2+}/calmodulin dependent kinase (CaMK). Intracellular sodium-mediated SIK1 activation requires its phosphorylation by

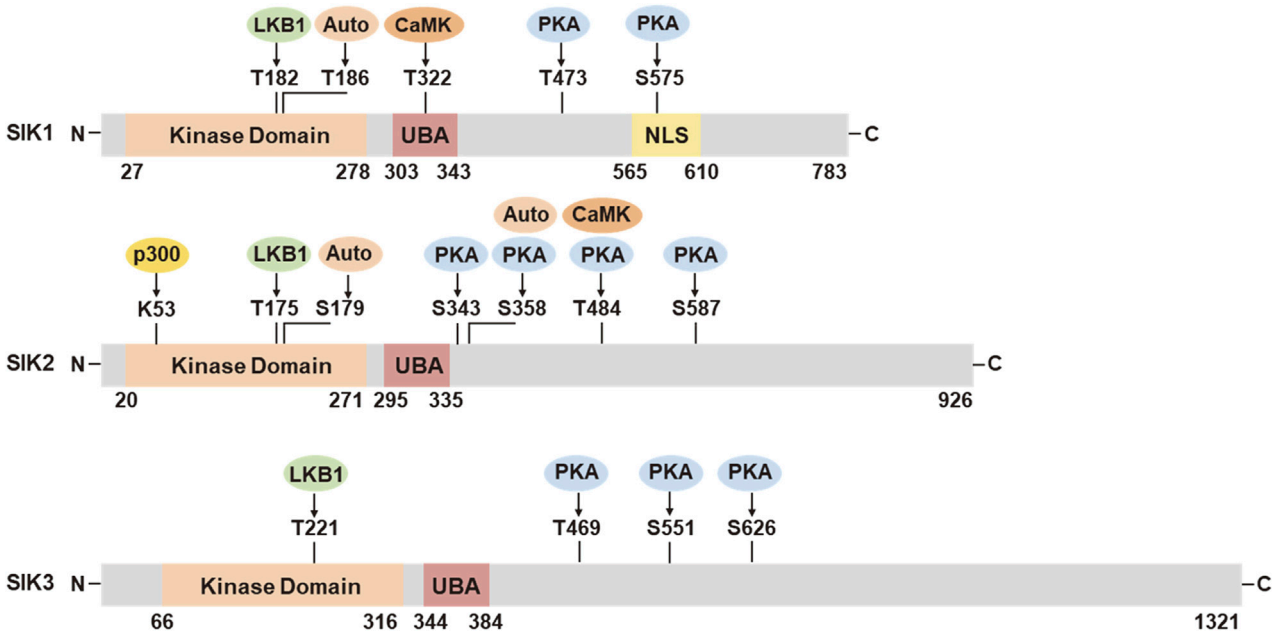

FIGURE 1
Functional domains and post-translational modifications in SIK1, SIK2, and SIK3. UBA, ubiquitin associated domain; NLS, nuclear location sequences; LKB1, liver kinase B1; Auto, autocatalysis; PKA, protein kinase A; CaMK, Ca^{2+}/calmodulin dependent kinase; p300, histone acetyltransferase. The numbers of amino acid residues refer to human proteins SIK1 (NP_775490.2), SIK2 (NP_056006.1), and SIK3 (NP_079440.3), respectively.

CaMK I at Thr322 (Sjöström et al., 2007; Bertorello and Zhu, 2009). Phosphorylation of SIK2 by CaMK I/V at Ser484 promotes its protein degradation (Sasaki et al., 2011). PKA phosphorylation sites have been identified in SIK1 (Thr473, Ser575), SIK2 (Ser343, Ser358, Thr484, Ser587), and SIK3 (Thr469, Ser551, Ser626) (Sonntag et al., 2018). PKA phosphorylation facilitates the binding of 14-3-3 protein and leads to SIK inhibition. PKA-mediated SIK inhibition is underpinning a variety of neuronal and hormonal factor actions, such as glucagon, prostaglandins, parathyroid hormone, and α-melanocyte stimulation hormone (Sakamoto et al., 2018; Wein et al., 2018). SIKs are also subjected to additional post-translational modification (Sun et al., 2020), such as histone acetyltransferase (HAT) p300-mediated inhibitory acetylation and HDAC6-mediated deacetylation in SIK2 at Lys53 (K53) (Bricambert et al., 2010; Yang et al., 2013), and E3 ligase RNF2-mediated ubiquitination in SIK1 (Qu and Qu, 2017).

SIKs regulates physiological processes through direct phosphorylation of their substrates. The SIK phosphorylation sites have been defined through *in vitro* studies as a motif of LXB(S/T)XS*XXXL (B, basic amino acid; X, any amino acid) (Screaton et al., 2004). SIK phosphorylation leads to 14-3-3 binding and cytoplasmic retention of their substrates. Following PKA-mediated SIK inhibition, SIK substrates will become dephosphorylated and translocated to the nucleus to control the target gene program. The most well-characterized SIK substrates include the class IIa histone deacetylases (HDACs, HDAC4, 5, 7 and 9) and the CREB-regulated transcriptional coactivators (CRTCs, CRTC1, 2 and 3). Despite their name, the histone deacetylation activity of class IIa HDACs towards histones are relatively weak. This is due to the differences in amino acid composition in their active site as compared to the *bona fide* HDACs (Asfaha et al., 2019; Park and Kim, 2020). Instead, they can interact and remove the acetylation marks in a variety of non-histone proteins or transcriptional coregulators and hereby control the transcriptional activity of these targets. In addition, class IIa HDACs may associate with HDAC3 (a member of the class I HDACs that possesses *bona fide* histone deacetylation activity) and nuclear co-repressors and transcription factors NCoR/SMRT as an active complex that can drive epigenetic changes (Fischle et al., 2002). In their dephosphorylated states, CRTCs are translocated to the nucleus and interact with CREB via the basic leucine zipper (bZIP) domain to promote the CREB-dependent transcriptional gene program (Altarejos and Montminy, 2011). Mechanistically, the interaction with CRTCs increase the stability of CREB and binding to target gene promoters (Katoh et al., 2006). CRTCs also facilitate the recruitment of HAT p300 for CREB transcription activity (Altarejos and Montminy, 2011).

In response to external hormonal and neuronal factor stimulation, the second messenger cAMP signaling stimulates PKA-mediated phosphorylation and leads to SIK inhibition. This will release the cytosolic retention of SIK substrates and facilitate their nuclear translocation to control target gene program. Class IIa HDACs functions as a potent suppressor of the myocyte enhancer factor 2 (MEF2)-dependent gene program, which controls a variety of pathological and developmental processes, including cardiac hypertrophy (Zhang et al., 2002), muscle development and fiber-type formation (Edmondson et al., 1994; Handschin et al., 2003), myocyte survival and growth (Shen et al., 2006; Berdeaux et al., 2007; Stewart et al., 2012), craniofacial development (Verzi et al., 2007), and bone formation (Arnold et al., 2007; Collette et al., 2012). CRTCs functions as a coactivator to promote the CREB-dependent gene program, which involves in many metabolic pathways, such as the glucose uptake (Qi et al., 2009; Weems et al., 2012; Henriksson et al., 2015; Nixon et al., 2015), lipogenesis (Yoon et al., 2009; Bricambert et al., 2010; Park et al., 2014), gluconeogenesis (Patel et al., 2014; Itoh et al., 2015), steroidogenesis (Doi et al., 2002; Lee et al., 2016), and inflammatory cytokine production (Clark et al., 2012; MacKenzie et al., 2012). Furthermore, the transcription of *Sik1* mRNA is regulated in a CREB-dependent manner (Jagannath et al., 2013), suggesting a negative feedback regulation between SIK1 and the CRTCs-CREB pathway.

Although HDACs and CRTCs are well-described SIK substrates, additional substrates have been identified. SIK1 can phosphorylate phosphatase methylesterase-1 (PME-1) of the protein phosphatase 2A (PP2A) complex to activate the activity of Na^+/K^+-ATPase (NKA) (Sjöström et al., 2007) (more details in next section). SIK1 functions downstream of TGFβ to negatively regulate type I receptor kinase signaling (Kowanetz et al., 2008; Lönn et al., 2012). Mechanistically, SIK1 forms a complex with SMAD7 (mothers against decapentaplegic homolog 7) and the E3 ubiquitin-protein ligase SMURF2 (SMAD-specific E3 ubiquitin-protein ligase 2) to promotes protein degradation of the activated type-I TGFβ receptor (TGFBR1 or ALK5) (Kowanetz et al., 2008; Lönn et al., 2012). SIK1 can phosphorylate the polarity protein PAR3 (Partitioning defective 3) to regulate tight junction assembly (Vanlandewijck et al., 2017). SIK1 can phosphorylate and activate the nucleotide release channel Pannexin 1 (PANX1) at Ser205, which involves the inflammatory responses of T cell to restrict the severity of allergic airway inflammation (Medina et al., 2021). In addition, SIK2 can form a complex with the cyclin-dependent kinase 5 (CDK5) regulatory subunit 1 (CDK5R1, also known as p35) and the E3 ligase PJA2 (praja ring finger ubiquitin ligase 2) to promotes insulin secretion (Sakamaki et al., 2014).

Acting as mediators of a broad array of neuronal and hormonal signaling pathways, SIKs play diverse roles in many physiological and pathological processes. Earlier studies and recent progress have demonstrated that they are critical regulators of the pathophysiological processes in cardiovascular and metabolic disease. This review will summarize our current understanding of the cardiovascular function of SIKs, with a focus on their pathophysiological roles in sodium handling, vascular remodeling, pulmonary arterial hypertension, cardiac hypertrophy and ischemia, inflammation, and fibrosis (Figure 2).

Sodium sensing and salt intake

The Na^+/K^+-ATPase (NKA) is a sodium/potassium-transporting ATPase wildly expressed on the outer plasma membrane. For each ATP consumed per transport cycle, NKA transports 3 sodium out of the cell and 2 potassium into the cell (Pirahanchi et al., 2024). Structurally, the NKA is composed of three subunits assembled in a 1:1:1 stoichiometry–the catalytic alpha (α)-subunit, the extracellular beta (β)-subunit, and the regulatory FXYD subunit (Nguyen et al., 2022). NKA activity helps to maintain the ion

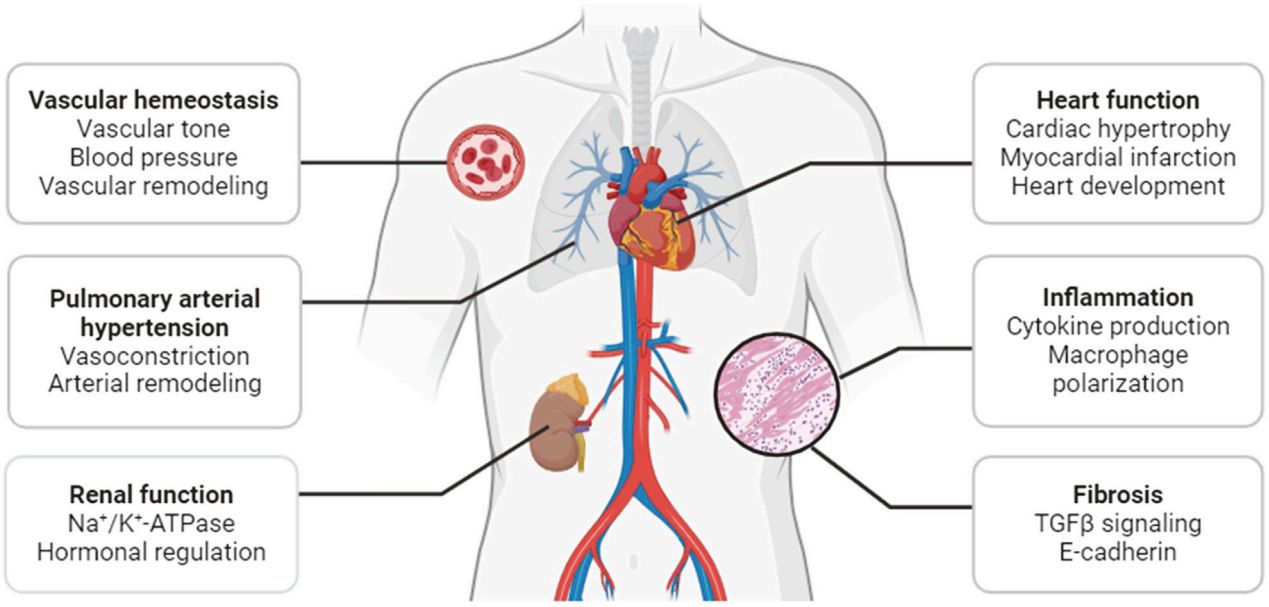

FIGURE 2
Functions of SIKs in the cardiovascular system.

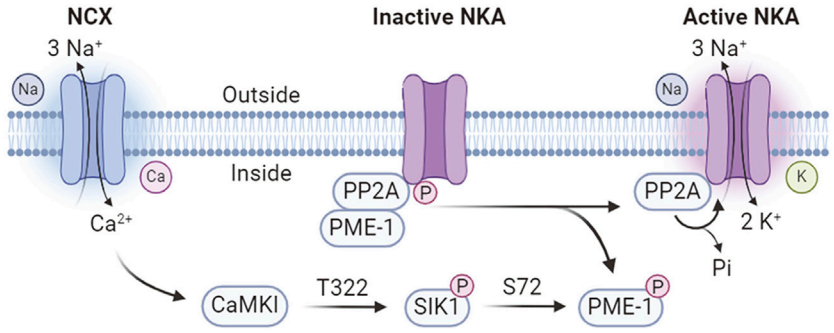

FIGURE 3
Calcium-dependent SIK1 regulation of NKA activity. NCX, $Na^+/Ca2^+$ exchanger; NKA, Na^+/K^+-ATPase; PP2A, protein phosphatase 2A; PME-1, phosphatase methylesterase-1; CaMKI, Ca2+/calmodulin dependent kinase I.

concentration gradient and cellular membrane potential, hereby the sodium and potassium gradients across the plasma membrane can be utilized by animal cells in various physiological processes for specialized functions (Jaitovich and Bertorello, 2010). As such, the range of the gradient demands requires NKA activity to be fine-tuned to coordinate different cellular needs (Jaitovich and Bertorello, 2010).

SIK1 involves in an intracellular sodium sensing network that controls NKA activity through a calcium-dependent process (Sjöström et al., 2007) (Figure 3). SIK1 was associated with NKA in the renal epithelium cells and participates in the regulation of NKA activity in response to sodium changes (Sjöström et al., 2007). Increases in intracellular sodium are coupled with calcium influx through the reversible $Na^+/Ca2^+$ exchanger (NCX), which is co-localized with NKA (Moore et al., 1993; Dostanic et al., 2004; Iwamoto et al., 2004). The sodium-induced calcium influx leads to the activation of SIK1 by CaMK-dependent phosphorylation at Thr322 (Sjöström et al., 2007). In its inactive form, the NKA catalytic α-subunit is constitutively associates with the protein phosphatase 2A (PP2A)/phosphatase methylesterase-1 (PME-1) complex (Sjöström et al., 2007). Activated SIK1 phosphorylates PME-1 possibly at Ser72 (Jaitovich and Bertorello, 2010), leading to its dissociation from the NKA/PP2A complex and allowing the dephosphorylation of NKA by PP2A to attain its catalytic activity (Sjöström et al., 2007). In addition, NKA activity can be regulated at the gene expression levels (Taub, 2018). The expression of *ATP1B1* gene, encoding the NKA β1-subunit, is transcriptionally regulated by CRTCs (Taub, 2018). SIKs promote the cytoplasmic retention of CRTCs and hereby negatively regulates *ATP1B1* expression (Taub et al., 2010). Extracellular stimulations by renal effectors such as

norepinephrine, dopamine, and prostaglandins leads to the inhibition of SIK1 and nuclear translocation of CRTCs to promote *ATP1B1* transcription via CREB (Taub et al., 2015). Furthermore, SIK1 also involves in sodium-independent hormonal regulation of NKA activity such as the dopamine and angiotensin pathways to control blood pressure homeostasis (Jaitovich and Bertorello, 2010).

Genetic knockout mouse models have demonstrated the important roles of SIK1 in the pathological vascular adaptations to high-salt (HS) intake. HS intake induces *Sik1* expression in the vascular smooth muscle cell (VSMCs) layer of the aorta (Bertorello et al., 2015). Under normal salt condition, *Sik1* deletion does not affect blood pressure (BP) but increase collagen deposition in the aorta (Bertorello et al., 2015). On HS condition, *Sik1* deletion leads to increased BP and vascular remodeling, as indicated by higher systolic BP, upregulation of TGFβ1 signaling, increased expression of endothelin-1 and genes related to VSMC contraction, and signs of cardiac hypertrophy (Bertorello et al., 2015). In *in vitro* cell models, *Sik1* knockdown increases collagen in aortic adventitial fibroblasts and enhances the expression of endothelin-1 and contractile markers in VSMCs (Bertorello et al., 2015). These data suggested that vascular SIK1 prevents salt-induced hypertension by regulating vasoconstriction via downregulation of TGFβ1 signaling (Bertorello et al., 2015). Furter study showed that HS intake induced hypertension in *Sik1*$^{-/-}$ mice is associated with overactivity of the sympathetic nervous system (SNS), as indicated by increased levels of urinary L-3,4-dihydroxyphenylalanine (L-DOPA) and noradrenaline, and higher adrenal dopamine β-hydroxylase (DβH) activity (Pires et al., 2019). Preadministration of etamicastat, a peripheral reversible DβH inhibitor, prevents the HS-induced systolic BP increase, suggesting that SNS overactivity is a key mediator of salt-induced hypertension in *Sik1*$^{-/-}$ mice (Pires et al., 2019).

SIK1 and SIK2 play distinct roles in mediating the HS-induced high BP and cardiac hypertrophy in mouse models. *Sik2* deletion does not affect the BP but prevents the development of left ventricular hypertrophy (LVH) on chronic HS intake (Popov et al., 2014). Instead, combined *Sik1/2* deletion leads to higher BP but does not alter LVH on chronic HS intake, suggesting that SIK1 is required for maintaining normal BP while SIK2 is required for HS-induced cardiac hypertrophy independent of high BP (Pires et al., 2021). Further evidence also supports a pathological role for SIK2 in cardiac hypertrophy. For example, the hypertensive variant of α-adducin is associated with higher *Sik2* expression and LVH in hypertensive Milan rats (Popov et al., 2014). In addition, the mRNA expression of *SIK2*, α-adducin, and genes related to cardiac hypertrophy are also positively correlated in human cardiac biopsies (Popov et al., 2014).

Vascular remodeling

The blood vessel is an autocrine-paracrine complex composed of VSMCs, endothelium cells, and fibroblasts (Gibbons and Dzau, 1994). In response to the hemodynamic alterations, the blood vessels undergo a structural remodeling processes involving in cell growth, death, migration, and production or degradation of the extracellular matrix (ECM) (Gibbons and Dzau, 1994). SIK1 plays an important role in maintaining vascular homeostasis. SIK1 is localized in human VSMCs and endothelial cells (Popov et al., 2011). Lower SIK1 activity leads to decreased NKA activity in VSMCs and is associated with increased vascular tone (Popov et al., 2011; Bertorello et al., 2015). A polymorphism in SIK1 gene encoding a Gly15 to Ser (G15S) missense mutation increases plasma membrane NKA activity in cultured VSMCs and is associated with lower blood pressure and reduced left ventricle (LV) mass in two separate Swedish and Japanese cohorts (Popov et al., 2011). In addition, SIK1 also involves in the negative feedback regulation of the TGFβ1 signaling and SIK1 deletion increases the expression of genes related to ECM remodeling (Bertorello et al., 2015). Furthermore, SIK1 regulates the expression of E-cadherin and contribute to LKB1-mediated regulation of cell polarity and intercellular junction stability (Eneling et al., 2012).

SIKs have been implicated in the pathological vascular remodeling process. Vascular calcification is a pathologic osteochondrogenic process of the blood vessels and is widely used as a clinical indicator of atherosclerosis (Abedin et al., 2004). SIKs promote vascular calcification by inducing cytoplasmic retention of HDAC4 (Abend et al., 2017). HDAC4 is induced in early calcification process, and it acts with the cytoplasmic adaptor protein ENIGMA (Pdlim7) to promote the VSMC calcification phenotypes (Abend et al., 2017). Pharmacologic SIK inhibition facilitates HDAC4 nuclear translocation and leads to the suppression of calcification process (Abend et al., 2017). Arterial restenosis is a pathological arterial narrowing process that results from a combination of elastic recoil, thrombosis, remodeling and intimal hyperplasia (Kenagy, 2011). SIK3 promotes arterial restenosis by stimulating VSMC proliferation and neointima formation (Cai et al., 2021). SIK3 is highly expressed in proliferating VSMCs and is also highly induced by growth medium *in vitro* and in neointimal lesions *in vivo* (Cai et al., 2021). Inactivation of SIKs attenuates the proliferation and migration of VSMCs, and reduced neointima formation and vascular inflammation in a femoral artery wire injury model (Cai et al., 2021).

Pulmonary arterial hypertension

Pulmonary arterial hypertension (PAH) is a high blood pressure condition in the arteries of lung. The pathogenesis of PAH involves in progressive narrowing of the arteries due to vasoconstriction, thrombosis, and vascular remodeling (Lan et al., 2018). Narrowing of the pulmonary arteries induces higher flow resistance and arterial pressure which cause right ventricle (RV) overload and ultimately lead to RV failure (António et al., 2022). Vascular remodeling is a hallmark feature in PAH and is characterized by excessive cell proliferation, abnormal release of inflammatory cytokines such as interleukin 1 (IL-1), IL-6, and tumor necrosis factor alpha (TNFα), and the upregulation of growth factors such as TGFβ (António et al., 2022). PAH is a multifactorial disease. The familiar form of PAH has been linked with mutations in genes of the TGFβ signaling pathway (Liu et al., 2011; Reynolds et al., 2011; Frydman et al., 2012) and mutations in ion channels such as KCNK3 (K^+ channel subfamily K member 3) (Ma et al., 2013) and ATP1A2 (NKA α2-subunit) (Montani et al., 2013). As SIKs coordinate signaling pathways

implicated in vasoconstriction, inflammation, and vascular remodeling, it has been proposed that the dysregulation of SIK pathways might underpin the pathophysiology of PAH (António et al., 2022).

Aberrant proliferation of the pulmonary artery endothelial cells (PAECs) plays an important role in the pathogenesis of PAH. It has been shown that the transcriptional factor MEF2 regulates expression of a number of transcriptional targets involved in pulmonary vascular homeostasis (Kim et al., 2014). The activity of MEF2 is significantly impaired in the PAECs derived from subjects with PAH due to the excess nuclear accumulation of HDAC4 and HDAC5 (Kim et al., 2014). Pharmacological inhibition by a selective class IIa HDACs inhibitor MC1568 restores MEF2 activity and transcriptional target expression, suppresses cell migration and proliferation, and rescues pulmonary hypertension in experimental mouse models (Kim et al., 2014). As SIKs are known to inhibit type IIa HDACs and able to restore MEF2-mediated transcription, it has been proposed that maneuvers that upregulate SIK activity could offer new opportunity to explore disease-modifying strategy for PAH (António et al., 2022).

Arterial remodeling in PAH also involves in the excessive proliferation and migration of pulmonary artery smooth muscle cells (PASMCs). A recent study showed that SIK1 deficiency stimulates PASMC proliferation via upregulation of the yes-associated protein (YAP) pathway and promotes vascular remodeling in PAH (Pu et al., 2022). The expression of SIK1, but not SIK2 or SIK3, is suppressed in the lung tissues of experimental PAH mice and in cultured human PASMCs under hypoxia (Pu et al., 2022). Pharmacological SIK inhibition or AAV9-mediated *Sik1* knockdown in smooth muscles aggravates RV hypertrophy and pulmonary arterial remodeling in a hypoxia-induced PAH mouse model (Pu et al., 2022). *Sik1* knockdown or inhibition promote the nuclear accumulation of YAP and stimulate proliferation and migration of human PASMCs under hypoxia condition (Pu et al., 2022). This study supported an anti-proliferative role for SIK1 in hypoxia-induced PAH remodeling and suggested that SIK1 might be a potential target for the treatment of PAH (Pu et al., 2022). However, the pathological role for SIK1 in alternative PAH models and in PAH patients is yet to be further explored.

Cardiac hypertrophy and ischemia

SIK1 was originally identifies as a myocardial SNF1-like kinase (*msk*) in a screen for novel protein kinases involving mouse heart development (Ruiz et al., 1994). *Sik1* mRNA expression is restricted in the myocardial progenitor cells and marks the promotive ventricle and atrium in the developing heart (Ruiz et al., 1994), suggesting a possible role for SIK1 in embryonic myocardial cell differentiation and primitive heart formation (Ruiz et al., 1994). A later study further showed that *Sik1* deletion in mouse embryonic stem cells postpones cardiomyocyte differentiation possibly by downregulation of the cyclin-dependent kinase inhibitor protein (Romito et al., 2010).

SIKs involve in high-salt (HS)-induced cardiac hypertrophy. HS intake is associated with cardiac hypertrophy both in humans (Du Cailar et al., 1992; Frohlich and Varagic, 2004) and animal models (Ferreira et al., 2010). A HS diet is associated with hallmark features of pathological cardiac remodeling, such as alterations in myocardial mechanical performance, dysregulation of the α/β-myosin heavy chain (MHC) expression, and alterations in calcium homeostasis and myocardial contractility (Patel and Joseph, 2020). Increases in intracellular sodium activates SIK1 and increases MEF2 transcriptional activity and cardiac hypertrophy signature gene expression in myocardial cells (Popov et al., 2012). The salt-induced activation of SIK1 and MEF2 is coupled by intracellular calcium influx through the NCX and activation of CaMKI (Popov et al., 2012). In addition, systemic hypertension also leads to a shift in the isoform distribution towards a decrease in the α/β-MHC ratio (Patel and Joseph, 2020). Cardiac hypertrophy of the spontaneous hypertensive rats is associated with decreased cardiac expression of SIK1 and SIK3 (Pinho et al., 2012). In contrast, SIK2 activation has been implicated in cardiac hypertrophy. SIK2 deletion prevents HS-induced cardiac hypertrophy independent of high BP (Pires et al., 2021). In hypertensive Milan rats, the hypertensive variant of α-adducin is associated with higher *Sik2* expression and LVH (Popov et al., 2014). Furthermore, the mRNA expression of *SIK2*, α-adducin, and genes related to cardiac hypertrophy are positively correlated in human cardiac biopsies (Popov et al., 2014).

SIKs have been implicated in pressure overload-induced hypertrophic cardiac remodeling. In adult mice, *Sik1* deletion protects against hypertrophic cardiac remodeling and heart failure following pressure overload via transverse aortic constriction (Hsu et al., 2020). Mechanistically, SIK1 phosphorylates and stabilizes HDAC7 to increase the expression of c-Myc, which in turn promotes the pro-hypertrophic gene program (Hsu et al., 2020) (Figure 4). In contrast, other class IIa HDACs, including HDAC4, HDAC5, and HDAC9, are regulated by stress-induced CaMKII and protein kinase D (PKD) phosphorylation for nuclear export in cardiomyocytes, which will de-suppress MEF2 to stimulate pro-hypertrophic gene expression (Zhang et al., 2002; Chang et al., 2004; Lehmann et al., 2017; Travers et al., 2020) (Figure 4). This suggests the functional divergence of HDAC7 from the other class IIa HDACs in cardiomyocyte remodeling (Hsu et al., 2020; Travers et al., 2020). A recent study further reported that the SIK1 expression is potentially regulated by the master circadian rhythm factor BMAL1 and *Sik1* knockdown in neonatal rat ventricular myocytes (NRVMs) reduces myocyte size and hypertrophic gene expression in response to phenylephrine stimulation (Arrieta et al., 2023). Unlike the pro-hypertrophic role of SIK1, SIK3 functions as a suppressor of cardiac hypertrophy (Hsu, 2022). Loss of SIK3 induces hypertrophic phenotypes in cultured NRVMs and in adult mouse hearts (Hsu, 2022). Mechanically, SIK3 deletion reduces ARHGAP21 (Rho GTPase activating protein 21) protein and promotes the nuclear translocation of MRTF-A (myocardin related transcription factor A) to stimulate hypertrophic gene program (Hsu, 2022).

SIKs also involve in the pathological cardiac remodeling following myocardial infarction (MI). A recent study reported that intramyocardial transplantation of embryonic cardiopulmonary progenitors can target the SIK1-CREB1 axis via exosomal transfer of miR-27b-3p to facilitate cardiac repair and improve cardiac function in a mouse model of MI (Xiao et al., 2024). Ischemia-reperfusion (IR) injury induces the expression of SIK2 in myocardial tissues (Liu et al., 2022). Overexpression of SIK2 in NRVMs increases AKT phosphorylation but suppresses the activity

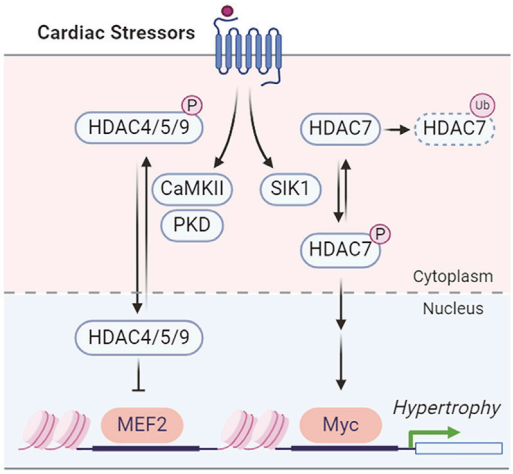

FIGURE 4
SIK1 and CaMKII/PKD regulation of HDACs in cardiac hypertrophy.

of YAP, one of the downstream effectors of Hippo pathway (Facchi et al., 2022). However, SIK2 overexpression does not impact NRVM proliferation or survival, but leads to an increase in cardiomyocyte hypertrophy (Facchi et al., 2022). *Sik2* deletion suppresses hypertrophic response and reduces infarct area and cardiac fibrosis in MI induced by coronary artery ligation, suggesting that SIK2 deficiency protects against cardiac ischemia (Facchi et al., 2022). However, the detailed mechanisms by which SIK2 promotes the hypertrophic gene program is yet to be revealed.

Inflammation

Inflammation is a coordinated immune response of the body to defense against injuries, infection, and stress (Pahwa et al., 2024). It is an essential pathological component closely associated with cardiovascular disease. For example, atherogenesis is a process associated with endothelial cell dysfunction that leads to atherosclerotic plaque formation and coronary arterial heart disease (Alfaddagh et al., 2020). It is considered that these pathological processes are driven by the cytokines, interleukins (ILs), and cellular constituents of the inflammatory response (Alfaddagh et al., 2020). Pathological cardiac remodeling is a process involving cardiac myocyte growth and death, vascular rarefaction, fibrosis, inflammation, and electrophysiological remodeling (Burchfield et al., 2013). There are growing evidences showing that elevated inflammatory biomarkers, implicating innate immune cells such as macrophages, are associated with worsened clinical outcomes in heart failures (HF) (Kalogeropoulos et al., 2010; Chen and Frangogiannis, 2016; Hage et al., 2017; DeBerge et al., 2019).

SIKs regulate the production of inflammatory cytokines, such as TNFα and ILs, to coordinate the innate immune responses (Figure 5). The endogenous SIK activity suppresses the anti-inflammatory signaling in macrophages. Pharmacological SIK inhibition increases secretion of anti-inflammatory cytokine IL-10 but suppresses proinflammatory cytokines TNFα, IL-6, and IL-12 in macrophage after toll-like receptor (TLR) stimulation by lipopolysaccharide (LPS) (Clark et al., 2012). The anti-inflammatory IL-10 expression depends on the CRTC3-CREB transcription activity (Clark et al., 2012), while the proinflammatory cytokine expression depends on HDAC4-mediated regulation of the nuclear factor-κB (NF-κB) pathway (Luan et al., 2014). SIKs mediate the prostaglandin E2 (PGE_2) signaling to promote IL-10 production and macrophage polarization (MacKenzie et al., 2012). Combined stimulation with PGE_2 and LPS leads to IL-10 expression and an anti-inflammatory phenotype in macrophages (Darling et al., 2016). Similarly, PGE_2 stimulates IL-10 mRNA expression through CRTC3-CREB-mediated transcription and either genetic or pharmacological SIK inhibition mimics the effect of PGE_2 on IL-10 production (Darling et al., 2016). Characterization of the primary macrophages carrying a catalytically inactive mutation in individual SIK gene further revealed that all three SIK isoforms contribute to macrophage polarization, with a major role for SIK2 and SIK3 (Darling et al., 2016). However, conflicting results have shown that SIKs act to suppress the pro-inflammatory signaling in Raw 264.7 macrophage cells. Overexpression of SIK1 and SIK3, but not SIK2, inhibits LPS-induced NF-κB activity and impacts proinflammatory cytokine expression (Kim et al., 2013). Knockdown of SIK1 and SIK3 in Raw 264.7 cells leads to activation of NF-κB pathway (Kim et al., 2013). Another study reported that SIK3 deficiency exacerbates LPS-induced endotoxicity and is associated with higher expression of proinflammatory cytokines (Sanosaka et al., 2015). Thus, it remains to be understood for the isoform specific function of endogenous SIKs in regulating the proinflammatory cytokine expression (Jagannath et al., 2023).

In addition to their immunoregulatory roles in macrophages, SIKs also involve in zymosan-stimulated cytokine production in mouse bone marrow-derived dendritic cells (Sundberg et al., 2014), LPS or IL-1β induced cytokine modulation in human myeloid cells (Lombardi et al., 2016), and IL-33-stumulated cytokine secretion in mast cells (Darling et al., 2021). Furthermore, SIKs also modulate adaptive immunity by regulating T cell lineage commitment, differentiation, and survival via a MEF2C-dependent mechanism (Nefla et al., 2021; Canté-Barrett et al., 2022).

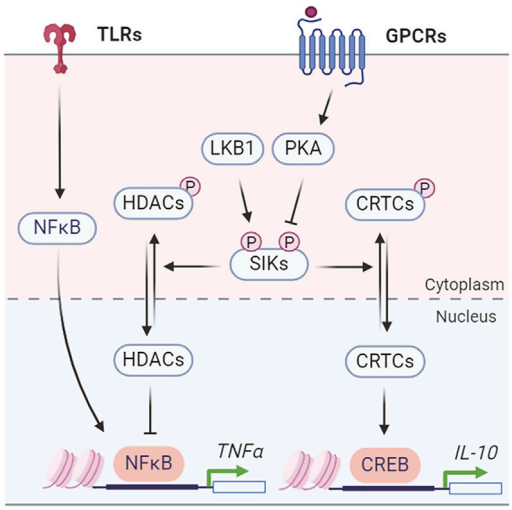

FIGURE 5
SIK regulation of inflammatory cytokine production.

Fibrosis

Fibrosis is a pathological process resulted from tissue injury or chronic inflammation (Henderson et al., 2020). It is characterized by the activation of fibroblasts and access accumulation of ECM proteins such as collagen and glycosaminoglycans (Henderson et al., 2020). Fibrosis is a hallmark feature of many cardiovascular disease. In pathological cardiac remodeling, myocardial fibrosis occurs as deposition of ECM proteins by activated fibroblast, which results in the expansion of cardiac interstitium and ultimately leads to systolic and diastolic dysfunction (Frangogiannis, 2021). Fibrogenic growth factors such as TGFβ, cytokines including TNF-α, IL-1, IL-6, IL-10, and IL-4, and neurohormonal pathways play essential roles in the pathogenesis of fibrosis (Frangogiannis, 2021).

SIK1 involves in a negative feedback regulation of the TGFβ signaling (Figure 6). TGFβ signals through type I and type II receptor serine/threonine kinases and intracellular Smad proteins to ultimately regulate the transcriptional program (Kowanetz et al., 2008). SIK1 is an inducible target of TGFβ pathway and acts to negatively regulate type I receptor kinase signaling (Kowanetz et al., 2008). Mechanistically, SIK1 forms a complex with Smad7 to downregulate the activated type I receptor TGFBR1 (ALK5) by increasing ubiquitination dependent receptor degradation (Kowanetz et al., 2008). Further study showed that TGFβ can direct regulate the transcription of *Sik1*, which involves in the binding of SMAD protein to the promoter of *Sik1* (Lönn et al., 2012). SIK1 forms a complex with the ubiquitin ligase Smurf2 to regulate type I receptor turnover (Lönn et al., 2012). *Sik1* deletion in mice induces collagen deposition and expression of genes related to ECM remodeling in the aorta (Bertorello et al., 2015). Furthermore, SIKs also regulate the TGFβ-targeted transcriptional gene program. Small molecule SIK inhibition or genetic SIK inactivation attenuates TGFβ-mediated transcription of PAI-1 (plasminogen activator inhibitor-1) and enhances cell apoptosis response (Hutchinson et al., 2020).

Pharmacological SIK inhibitors have demonstrated anti-fibrosis effects in mouse models. Earlier studies showed that dasatinib attenuates pulmonary fibrosis in bleomycin-exposed mice (Yilmaz et al., 2015) and in acute experimental silicosis (Cruz et al., 2016). However, whether the anti-fibrosis of dasatinib depends on SIKs is unclear. A recently study showed that SIK2 expression and activity is increased in fibrotic lung tissues and activated fibroblasts (Zou et al., 2022). A selective SIK2 inhibitor ARN-3236 restricts fibroblasts differentiation and ECM gene expression in human fetal lung fibroblasts and attenuates bleomycin-induced pulmonary fibrosis in mice (Zou et al., 2022), supporting as pathological role for SIK2 in pulmonary fibrosis.

Metabolic syndrome

As major risk factors for cardiovascular disease, diabetes, obesity, and metabolic syndrome negatively impact cardiovascular function (Strain and Paldánius, 2018; Powell-Wiley et al., 2021). The sodium/glucose cotransporter 2 (SGLT2) inhibitor empagliflozin and glucagon-like peptide-1 receptor (GLP1R) agonist semaglutide, medications originally developed to treat diabetes and/or obesity, have demonstrated clinically significant cardiovascular benefits (Cowie and Fisher, 2020; Sattar et al., 2021; Lincoff et al., 2023). It has been increasingly appreciated that targeting diabetes, obesity, and related metabolic dysfunction could be a disease modifying strategy for cardiovascular disease. SIKs are broadly expressed in the metabolic relevant tissues and play essential roles in mediating insulin action, maintaining glucose hemostasis, and controlling lipid metabolism (Figure 7). It has been appreciated that dysregulation of SIK function could underpin the pathophysiology of insulin resistance, dyslipidemia, and metabolic syndrome. In addition, SIKs are also expressed in the central nervous system and play essential roles in the regulation of circadian rhythm, sleep needs, and many other

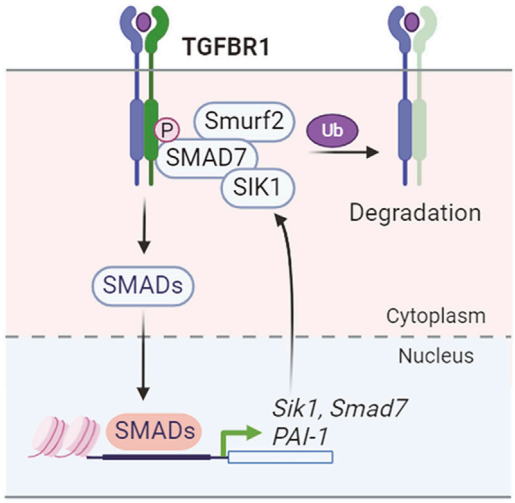

FIGURE 6
SIK1 regulation of TGFβ signaling.

neurophysiological functions (Jagannath et al., 2023). Dysregulation of these neurophysiological processes could also have major impacts on systemic metabolic homeostasis and potentially contributes the cardiometabolic disease (Chellappa et al., 2019; Fagiani et al., 2022).

SIKs are critical regulators of hepatic gluconeogenesis. After feeding, insulin-stimulated FOXO (forkhead box O) phosphorylation by AKT leads to 14-3-3 binding and cytoplasmic restriction of FOXO, and thus inhibits the gluconeogenesis gene program (Wein et al., 2018). Under fasting condition, glucagon induces the PKA-mediated phosphorylation of CREB and recruitment of the p300 HAT and CREB binding protein (p300/CBP) to activate the gluconeogenesis gene expression (Wein et al., 2018). Glucagon action leads to PKA-mediated phosphorylation and inactivation of SIKs, which results in the dephosphorylation and nuclear translocation of CRTCs and class IIa HDACs. CRTCs bind to CREB and act as coactivator to stimulate the gluconeogenesis gene expression. Class IIa HDACs can recruit HDAC3 to the target gene promoters to regulate the acetylation of FOXO, which further activate the transcription of gluconeogenesis genes (Wein et al., 2018). In mouse models, liver specific ablation of LKB1, the upstream activating kinase for SIKs, leads to increased glucose production in hepatocytes. Pharmacological pan-SIK inhibition phenocopies LKB1 deficient hepatocytes, including the dephosphorylations in CRTC2/3 and HDAC4/5 and increased gluconeogenesis gene expression and glucose production (Foretz et al., 2010; Patel et al., 2014). However, deleting either *Sik1* or *Sik2* alone in the liver does not impact hepatic gluconeogenesis (Patel et al., 2014; Nixon et al., 2015), suggesting SIKs play redundant roles in hepatic gluconeogenesis.

SIKs also control hepatic lipogenesis. Hepatic lipogenesis gene expression is controlled by master transcription factors, including SREBP-1c (sterol regulatory element-binding protein 1c) and ChREBP (carbohydrate response element binding protein) (Wang et al., 2015). Hepatic *Sik1* knockdown increases lipogenic gene expression (Yoon et al., 2009). SIK1 suppresses hepatic lipogenesis gene expression by inhibitory phosphorylation of SREBP-1c at Ser329 (Yoon et al., 2009). *Sik2* knockdown in the liver also increases hepatic lipogenesis gene expression and steatosis (Bricambert et al., 2010). Mechanistically, SIK2 suppresses p300 HAT activity by inhibitory phosphorylation at Ser89, which in turn leads to decreased acetylation in ChREBP and reduced transcriptional activity of lipogenesis genes (Bricambert et al., 2010). Global *Sik3* deletion leads to neonatal death and skeletal malformations in survived adults (Uebi et al., 2012). The survived adult *Sik3* knockout mice show lipodystrophy phenotypes with altered cholesterol and bile acid metabolism in the liver (Uebi et al., 2012), indicating the involvement of SIK3 in lipid metabolism.

SIKs control a broad array of metabolic pathways in the adipose tissue. Among all the three SIK isoforms, SIK2 is the most abundant both in rodent and human adipocytes (Horike et al., 2003; Säll et al., 2016). SIK2 expression is robustly induced during adipocyte differentiation and its deletion leads to increased adipocyte differentiation in cell culture (Horike et al., 2003; Du et al., 2008; Gormand et al., 2014; Park et al., 2014). SIK2 can directly phosphorylates IRS-1 (insulin receptor substrate 1) *in vitro* and in cultured adipocytes, suggesting its involvement in insulin signaling (Horike et al., 2003). Insulin-stimulated AKT phosphorylation is reduced in the adipose tissue of global *Sik2* knockout mice (Park et al., 2014) and in human adipocytes treated with pan-SIK inhibitor (Säll et al., 2016). *SIK2* activity is increased in the adipose tissues from diabetic *db/db* mice (Du et al., 2008). However, *SIK2* mRNA expression and activity is downregulated in the adipose tissue of obese individuals (Säll et al., 2016). Global *Sik2* knockout mice show impaired glucose and insulin tolerance, hypertriglyceridemia, and adipose tissue dysfunction, such as increased lipolysis and macrophage infiltration and decreased GLUT4 and adiponectin expression (Park et al., 2014). The downstream molecular targets of SIK2 include HDAC4, CRTC2, and CRTC3 in adipocytes and

FIGURE 7
SIK regulation of glucose homeostasis and lipid metabolism.

support a role for SIK2 in regulating GLUT4 expression and adipocyte glucose uptake (Park et al., 2014; Henriksson et al., 2015). Lipogenesis gene expression is increased in the adipose tissue of *Sik2* knockout mice (Park et al., 2014). It has been shown that SIK2 inhibits the expression of lipogenic genes potentially by regulating SREBP1c in adipocytes (Du et al., 2008).

SIKs play redundant roles as suppressors of the adipocyte thermogenic program. The adipocyte thermogenic program is orchestrated by the β-adrenergic receptor signaling cascade to drive the transcriptional machinery for thermogenic gene expression (Shi and Collins, 2017; 2023). Combined deletion of *Sik1* and *Sik2*, but not deletion of *Sik1* or *Sik2* alone, increases the expression of thermogenic gene uncoupling protein 1 (*Ucp1*) in subcutaneous inguinal while adipose tissue (iWAT) (Wang et al., 2017). Knockdown of either *Sik1*, *Sik2*, or *Sik3* increases *Ucp1* expression in mouse brown adipocytes (Shi et al., 2023). In addition, treatment with a pan-SIK inhibitor YKL-05-099 in mice stimulates the thermogenic gene expression in iWAT (Shi et al., 2023). Furthermore, adipose tissue specific ablation of LKB1, the upstream kinase for SIK activation, promotes brown fat expansion and WAT browning (Shan et al., 2016; Wang et al., 2017). The adipose browning phenotypes of LKB1 adipose knockout mice are mediated by the action of SIK substrates CRTC3 and HDAC4 (Shan et al., 2016; Wang et al., 2017).

SIK1 involves in the CREB-dependent myogenic gene program. SIK1 is induced by the CREB transcription activity in skeletal myocytes and it promotes MEF2-dependent myogenic program by suppressing the class IIa HDAC activity (Berdeaux et al., 2007). SIK1 protein abundance is also dynamically controlled in response to cAMP stimulation during myogenesis (Stewart et al., 2012). *Sik1* depletion in myogenic precursors profoundly impairs MEF2 protein accumulation and myogenesis (Stewart et al., 2012). Overexpression of SIK1 reduces the muscle dystrophy caused by a dominant negative A-CREB mutation (Berdeaux et al., 2007). In adult mice, skeletal muscle *Sik1* expression can be induced by exercise training (Bruno et al., 2014), acute muscle injury (Stewart et al., 2011), and obesity (Horike et al., 2003; Nixon et al., 2015). Interestingly, global *Sik1* knockout mice are protected against high-fat diet induced insulin resistance (Nixon et al., 2015). *Sik1* deletion in skeletal muscle, but not liver or adipose tissue phenocopies the whole-body knockout mice, suggesting skeletal muscle *Sik1* contribute to diet-induced insulin resistance through a tissue autonomous mechanism (Nixon et al., 2015).

SIKs involve in the regulation of insulin secretion in pancreatic β-cells. *Sik1* deletion enhances glucose-stimulated insulin secretion in β-cells (Kim et al., 2015). Mechanistically, *Sik1* directly phosphorylates phosphodiesterase 4D (PDE4D) at Ser136/Ser141, which leads to reduction in cellular cAMP and attenuation of insulin secretion (Kim et al., 2015). In contrast, β-cell specific *Sik2* deletion reduces glucose-stimulated insulin secretion (Sakamaki et al., 2014). SIK2 phosphorylates CDK5R1 (p35) to induce its ubiquitination and proteasomal degradation, which leads to the suppression of CDK5 activity and activation of the voltage-dependent Ca^{2+} channels (VDCC) (Sakamaki et al., 2014). VDCC activation in turn induces Ca^{2+} influx and potentiates exocytosis and insulin vesicle release (Sakamaki et al., 2014). It was also proposed that SIK2 is involved in the β-cell compensation during hyperglycemia and loss of SIK2 contributes to β-cell failure and diabetes (Sakamaki et al., 2014).

Development of SIK inhibitors

Small molecule SIK inhibitors (SIKi) have been developed as tools to probe the function of SIKs and have also shown therapeutic potential in various disease models, including osteoporosis, leukemia, inflammatory and fibrotic disease, and certain types of cancer (Wein et al., 2018; Sun et al., 2020; Darling and Cohen, 2021; António et al., 2022; Jagannath et al., 2023). HG-9-91-01 is the first widely used pan-SIKi for *in vitro* models as it can be rapidly degraded by mouse liver microsomes (Sundberg et al., 2016). HG-9-91-01 targets a hydrophobic pocket created by the presence of a small amino acid residue at the gatekeeper site in the SIK kinase domain (Clark et al., 2012). Mutation of threonine residue within the gatekeeper sites impairs the accessibility of inhibitor and confers resistance to HG-9-91-01 inhibition (Clark et al., 2012). Using HG-9-91-01 as a starting point, YKL-05-099 was development and it shows increased selectivity for SIKs and enhanced pharmacokinetic properties (Sundberg et al., 2016). A well-tolerated dose of YKL-05-099 *in vivo* achieves free serum concentrations above its IC_{50} for SIK2 inhibition for >16 h, making it the first pan-SIKi widely used for *in vivo* studies (Sundberg et al., 2016). YKL-05-099 has been shown to modulate immunoregulatory cytokine production (Sundberg et al., 2016), suppress acute myeloid leukemia progression (Tarumoto et al., 2020), and increase bone formation (Wein et al., 2016; Tang et al., 2021). Our group showed that YKL-05-099 stimulates

TABLE 1 Cardiovascular and metabolic phenotypes of *Siks* deficient mouse models.

Mice	Disease models	Phenotypes	References
Sik1 KO	High-salt intake	Higher blood pressure, increased vasoconstriction, sympathetic nerve system activity, and cardiac hypertrophy	Bertorello et al. (2015), Pires et al. (2019), Pires et al. (2021), António et al. (2022)
Sik2 KO	High-salt intake	Prevents LV hypertrophy, normal blood pressure and plasma electrolytes homeostasis	Pires et al. (2021), Popov et al. (2014)
Sik1/2 KO	High-salt intake	Higher blood pressure, prevents LV hypertrophy	António et al. (2022)
Sik1 KO	Transverse aortic constriction	Improves LV systolic function, reduces cardiac hypertrophy and LV fibrosis	Hsu et al. (2020)
Sik3 cmKO	Transverse aortic constriction	Exhibits cardiomegaly, increases cardiac hypertrophy and LV fibrosis	Hsu (2022)
Sik2 KO	Myocardial infarction	Reduces hypertrophic response, infarct area and fibrosis	Liu et al. (2022)
Sik1 smKD	Hypoxia-induced PAH	Increases RV hypertrophy and pulmonary arterial remodeling	Pu et al. (2022)
Pan-SIK inhibition	Femoral artery wire injury	Reduces neointima formation and vascular inflammation, attenuates vascular SMC proliferation	Cai et al. (2021)
Sik1 KO	High fat diet	Normoglycemic on chow diet, prevents high-fat diet induced insulin resistance	Nixon et al. (2015)
Sik2 KO	Chow diet	Hypertriglyceridemia, impaired glucose and insulin tolerance, adipose tissue dysfunction	Park et al. (2014)
Sik3 KO	Chow diet	Postnatal lethality, skeletal malformation, dysregulation in glucose and lipid metabolism	Uebi et al. (2012)

Note: KO, knockout; KD, knockdown; cm, cardiomyocyte; sm, smooth muscle; LV, left ventricle; RV, right ventricle; PAH, Pulmonary arterial hypertension.

adipocyte thermogenic gene expression and promotes adipose tissue browning *in vivo* (Shi et al., 2023), suggesting a role for SIKs in regulating energy hemostasis and their potential as therapeutic targets of obesity.

The three SIK isoforms are broadly expressed. Each SIK isoform could have both unique and redundant functions in a variety of physiological processes (Wein et al., 2018; Sun et al., 2020; Darling and Cohen, 2021; António et al., 2022; Jagannath et al., 2023). As such, both pan and isoform specific SIKi are desired to better approach these targets in specific disease contexts. Newer SIKi with better potency, specificity and oral bioavailability have been developed. GLPG3312 is a pan-SIKi developed by Galapagos NV that demonstrated both anti-inflammatory and immunoregulatory activities *in vitro* in human primary myeloid cells and *in vivo* in mouse models (Temal-Laib et al., 2023). JRD-SIK1/2i-4 is a selective SIK1/2 inhibitor that modulates innate immune activation and suppresses intestinal inflammation (Babbe et al., 2024). SK-124 is an orally available SIK2/3 inhibitor that stimulates bone formation without evidence of short-term toxicity in mice (Sato et al., 2022). GLPG3970 is a SIK2/3 inhibitor developed by Galapagos NV for the treatment of auto-immune and inflammatory diseases (Peixoto et al., 2024). Selective SIK2 inhibitors have been developed based on the binding pose of GLPG-3970 by the application of AlphaFold structures and generative models (Zhu et al., 2023).

ARN-3236 is an orally active and selective SIK2 inhibitor (Lombardi et al., 2016; Zhou et al., 2017). ARN-3236 induces an anti-inflammatory phenotype in human myeloid cells by modulating cytokine production after TLR agonist stimulation (Lombardi et al., 2016). ARN-3236 has also been shown to inhibit ovarian cancer growth and enhancing paclitaxel chemosensitivity in preclinical models (Zhou et al., 2017). Pterosin B is an indanone found in bracken fern (pteridium aquilinum) and a selective SIK3 inhibitor (Itoh et al., 2015; Yahara et al., 2016). It has been shown that pterosin B stimulates hepatic glucose production (Itoh et al., 2015) and prevents chondrocyte hypertrophy and osteoarthritis in mice (Yahara et al., 2016). However, our knowledge on the *in vivo* effects of pterosin B is very limited. More recently, OMX-0407 was reported as an orally available, single-digit nanomolar inhibitor of SIK3 (Hartl et al., 2022). OMX-0407 suppresses intratumoral NF-κB activity and inhibits tumor cell growth *in vivo* (Hartl et al., 2022). Inhibition of SIK1 activity is considered undesirable due to its essential role in blood pressure control and vascular remodeling (Bertorello et al., 2015). However, selective SIK1 inhibition might be beneficial in certain disease conditions (Kim et al., 2015; Hsu et al., 2020). Instead, phanginin A, a diterpenoid from the seeds of Caesalpinia sappan Linn (Yodsaoue et al., 2008), has been reported as a SIK1 activator to inhibit hepatic gluconeogenesis by increasing PDE4 activity and suppressing the cAMP signaling pathway (Liu et al., 2020).

Conclusion remarks

Studies of genetic mouse models have demonstrated that SIKs are important regulators in the cardiovascular system and metabolic pathways (summarized in Table 1). It has been appreciated that SIKs could have both redundant and isoform-distinct functions in these pathophysiological processes. As such, the *in vivo* studies of genetic mouse models with SIK deletions might be challenging as efforts have to be made to delineate the

redundant and distinct roles of each SIK protein in each tissue. These studies could be further complicated by the additional efforts required to identify the specific SIK substrate and their mechanisms of regulation in each physiological context. It has also been proposed that dysregulation of SIKs is associated with cardiometabolic disease. As mentioned above, a polymorphism in SIK1 gene encoding a G15S missense mutation is associated with lower blood pressure and reduced cardiac hypertrophy in humans (Popov et al., 2011; Bertorello et al., 2015). The expression and activity of SIK2 and SIK3 are downregulated in the adipose tissue of people with obesity and diabetes (Säll et al., 2016). Genetic variants in SIK genes also have been linked with alterations in blood lipid panels, suggesting the potential clinical relevance of SIK genes for dyslipidemia (Chasman et al., 2008; Teslovich et al., 2010; Braun et al., 2012; Willer and Mohlke, 2012; Ko et al., 2014; Karjalainen et al., 2020). For the translational development of SIKi, their cardiovascular and metabolic effects need to be considered and carefully evaluated. Understanding the cardiometabolic function of SIKs would not only offer new knowledge but also provide opportunity to better approach these targets and pathways for intervention and treatment of disease in the future.

Author contributions

FS: Conceptualization, Funding acquisition, Visualization, Writing–original draft, Writing–review and editing.

Funding

The author(s) declare that financial support was received for the research, authorship, and/or publication of this article. FS is supported by the American Heart Association Career Development Award 23CDA1048341.

Acknowledgments

The figures were created with BioRender.com.

Conflict of interest

The author declares that the research was conducted in the absence of any commercial or financial relationships that could be construed as a potential conflict of interest.

Publisher's note

References

Abedin, M., Tintut, Y., and Demer, L. L. (2004). Vascular calcification: mechanisms and clinical ramifications. *Arterioscler. Thromb. Vasc. Biol.* 24 (7), 1161–1170. doi:10.1161/01.Atv.0000133194.94939.42

Abend, A., Shkedi, O., Fertouk, M., Caspi, L. H., and Kehat, I. (2017). Salt-inducible kinase induces cytoplasmic histone deacetylase 4 to promote vascular calcification. *EMBO Rep.* 18 (7), 1166–1185. doi:10.15252/embr.201643686

Alfaddagh, A., Martin, S. S., Leucker, T. M., Michos, E. D., Blaha, M. J., Lowenstein, C. J., et al. (2020). Inflammation and cardiovascular disease: from mechanisms to therapeutics. *Am. J. Prev. Cardiol.* 4, 100130. doi:10.1016/j.ajpc.2020.100130

Al-Hakim, A., Göransson, O., Deak, M., Toth, R., Campbell, D. G., Morrice, N. A., et al. (2005). 14-3-3 cooperates with LKB1 to regulate the activity and localization of QSK and SIK. *J. Cell Sci.* 118 (23), 5661–5673. doi:10.1242/jcs.02670

Altarejos, J. Y., and Montminy, M. (2011). CREB and the CRTC co-activators: sensors for hormonal and metabolic signals. *Nat. Rev. Mol. Cell Biol.* 12 (3), 141–151. doi:10.1038/nrm3072

António, T., Soares-da-Silva, P., Pires, N. M., and Gomes, P. (2022). Salt-inducible kinases: new players in pulmonary arterial hypertension? *Trends Pharmacol. Sci.* 43 (10), 806–819. doi:10.1016/j.tips.2022.06.008

Arnold, M., Kim, Y., Czubryt, M. P., Phan, D., McAnally, J., Qi, X., et al. (2007). MEF2C transcription factor controls chondrocyte hypertrophy and bone development. *Dev. Cell* 12 (3), 377–389. doi:10.1016/j.devcel.2007.02.004

Arrieta, A., Chapski, D., Reese, A., Rosa-Garrido, M., and Vondriska, T. M. (2023). Abstract P1133: bmal1 drives postnatal cardiac hypertrophy via circadian chromatin remodeling of the pro-hypertrophic gene Sik1. *Circulation Res.* 133 (1), AP1133. doi:10.1161/res.133.suppl_1.P1133

Asfaha, Y., Schrenk, C., Alves Avelar, L. A., Hamacher, A., Pflieger, M., Kassack, M. U., et al. (2019). Recent advances in class IIa histone deacetylases research. *Bioorg Med. Chem.* 27 (22), 115087. doi:10.1016/j.bmc.2019.115087

Babbe, H., Sundberg, T. B., Tichenor, M., Seierstad, M., Bacani, G., Berstler, J., et al. (2024). Identification of highly selective SIK1/2 inhibitors that modulate innate immune activation and suppress intestinal inflammation. *Proc. Natl. Acad. Sci. U. S. A.* 121 (1), e2307086120. doi:10.1073/pnas.2307086120

Berdeaux, R., Goebel, N., Banaszynski, L. A., Takemori, H., Wandless, T. J., Shelton, G. D., et al. (2007). SIK1 is a class II HDAC kinase that promotes survival of skeletal myocytes. *Nat. Med.* 13 (5), 597–603. doi:10.1038/nm1573

Bertorello, A. M., Pires, N., Igreja, B., Pinho, M. J., Vorkapic, E., Wågsäter, D., et al. (2015). Increased arterial blood pressure and vascular remodeling in mice lacking salt-inducible kinase 1 (SIK1). *Circ. Res.* 116 (4), 642–652. doi:10.1161/circresaha.116.304529

Bertorello, A. M., and Zhu, J.-K. (2009). SIK1/SOS2 networks: decoding sodium signals via calcium-responsive protein kinase pathways. *Pflugers Archiv Eur. J. physiology* 458 (3), 613–619. doi:10.1007/s00424-009-0646-2

Braun, T. R., Been, L. F., Singhal, A., Worsham, J., Ralhan, S., Wander, G. S., et al. (2012). A replication study of GWAS-derived lipid genes in Asian Indians: the chromosomal region 11q23.3 harbors loci contributing to triglycerides. *PloS one* 7 (5), e37056–NA. doi:10.1371/journal.pone.0037056

Bricambert, J., Miranda, J., Benhamed, F., Girard, J., Postic, C., and Dentin, R. (2010). Salt-inducible kinase 2 links transcriptional coactivator p300 phosphorylation to the prevention of ChREBP-dependent hepatic steatosis in mice. *J. Clin. investigation* 120 (12), 4316–4331. doi:10.1172/jci41624

Bruno, N. E., Kelly, K. A., Hawkins, R., Bramah-Lawani, M., Amelio, A. L., Nwachukwu, J. C., et al. (2014). Creb coactivators direct anabolic responses and enhance performance of skeletal muscle. *Embo J.* 33 (9), 1027–1043. doi:10.1002/embj.201386145

Burchfield, J. S., Xie, M., and Hill, J. A. (2013). Pathological ventricular remodeling: mechanisms: part 1 of 2. *Circulation* 128 (4), 388–400. doi:10.1161/circulationaha.113.001878

Cai, Y., Wang, X. L., Lu, J., Lin, X., Dong, J., and Guzman, R. J. (2021). Salt-inducible kinase 3 promotes vascular smooth muscle cell proliferation and arterial restenosis by regulating AKT and PKA-CREB signaling. *Arterioscler. Thromb. Vasc. Biol.* 41 (9), 2431–2451. doi:10.1161/atvbaha.121.316219

Canté-Barrett, K., Meijer, M. T., Cordo, V., Hagelaar, R., Yang, W., Yu, J., et al. (2022). MEF2C opposes Notch in lymphoid lineage decision and drives leukemia in the thymus. *JCI insight* 7 (13), e150363–NA. doi:10.1172/jci.insight.150363

Chang, S., McKinsey, T. A., Zhang, C. L., Richardson, J. A., Hill, J. A., and Olson, E. N. (2004). Histone deacetylases 5 and 9 govern responsiveness of the heart to a subset of

stress signals and play redundant roles in heart development. *Mol. Cell. Biol.* 24 (19), 8467–8476. doi:10.1128/mcb.24.19.8467-8476.2004

Chasman, D. I., Paré, G., Zee, R. Y., Parker, A. N., Cook, N. R., Buring, J. E., et al. (2008). Genetic loci associated with plasma concentration of low-density lipoprotein cholesterol, high-density lipoprotein cholesterol, triglycerides, apolipoprotein A1, and Apolipoprotein B among 6382 white women in genome-wide analysis with replication. *Circ. Cardiovasc Genet.* 1 (1), 21–30. doi:10.1161/circgenetics.108.773168

Chellappa, S. L., Vujovic, N., Williams, J. S., and Scheer, F. (2019). Impact of circadian disruption on cardiovascular function and disease. *Trends Endocrinol. Metab.* 30 (10), 767–779. doi:10.1016/j.tem.2019.07.008

Chen, B., and Frangogiannis, N. G. (2016). Macrophages in the remodeling failing heart. *Circ. Res.* 119 (7), 776–778. doi:10.1161/circresaha.116.309624

Clark, K., MacKenzie, K. F., Petkevicius, K., Kristariyanto, Y. A., Zhang, J., Choi, H. G., et al. (2012). Phosphorylation of CRTC3 by the salt-inducible kinases controls the interconversion of classically activated and regulatory macrophages. *Proc. Natl. Acad. Sci. U. S. A.* 109 (42), 16986–16991. doi:10.1073/pnas.1215450109

Collette, N. M., Genetos, D. C., Economides, A. N., Xie, L., Shahnazari, M., Yao, W., et al. (2012). Targeted deletion of Sost distal enhancer increases bone formation and bone mass. *Proc. Natl. Acad. Sci. U. S. A.* 109 (35), 14092–14097. doi:10.1073/pnas.1207188109

Cowie, M. R., and Fisher, M. (2020). SGLT2 inhibitors: mechanisms of cardiovascular benefit beyond glycaemic control. *Nat. Rev. Cardiol.* 17 (12), 761–772. doi:10.1038/s41569-020-0406-8

Cruz, F. F., Horta, L. F., Maia Lde, A., Lopes-Pacheco, M., da Silva, A. B., Morales, M. M., et al. (2016). Dasatinib reduces lung inflammation and fibrosis in acute experimental silicosis. *PLoS One* 11 (1), e0147005. doi:10.1371/journal.pone.0147005

Darling, N. J., Arthur, J. S. C., and Cohen, P. (2021). Salt-inducible kinases are required for the IL-33-dependent secretion of cytokines and chemokines in mast cells. *J. Biol. Chem.* 296 (NA), 100428. doi:10.1016/j.jbc.2021.100428

Darling, N. J., and Cohen, P. (2021). Nuts and bolts of the salt-inducible kinases (SIKs). *Biochem. J.* 478 (7), 1377–1397. doi:10.1042/bcj20200502

Darling, N. J., Toth, R., Arthur, J. S. C., and Clark, K. (2016). Inhibition of SIK2 and SIK3 during differentiation enhances the anti-inflammatory phenotype of macrophages. *Biochem. J.* 474 (4), 521–537. doi:10.1042/bcj20160646

DeBerge, M., Shah, S. J., Wilsbacher, L., and Thorp, E. B. (2019). Macrophages in heart failure with reduced versus preserved ejection fraction. *Trends Mol. Med.* 25 (4), 328–340. doi:10.1016/j.molmed.2019.01.002

Doi, J., Takemori, H., Lin, X. Z., Horike, N., Katoh, Y., and Okamoto, M. (2002). Salt-inducible kinase represses cAMP-dependent protein kinase-mediated activation of human cholesterol side chain cleavage cytochrome P450 promoter through the CREB basic leucine zipper domain. *J. Biol. Chem.* 277 (18), 15629–15637. doi:10.1074/jbc.m109365200

Dostanic, I., Schultz Jel, J., Lorenz, J. N., and Lingrel, J. B. (2004). The alpha 1 isoform of Na,K-ATPase regulates cardiac contractility and functionally interacts and co-localizes with the Na/Ca exchanger in heart. *J. Biol. Chem.* 279 (52), 54053–54061. doi:10.1074/jbc.M410737200

Du, J., Chen, Q., Takemori, H., and Xu, H. (2008). SIK2 can be activated by deprivation of nutrition and it inhibits expression of lipogenic genes in adipocytes. *Obes. (Silver Spring)* 16 (3), 531–538. doi:10.1038/oby.2007.98

Du Cailar, G., Ribstein, J., Daures, J. P., and Mimran, A. (1992). Sodium and left ventricular mass in untreated hypertensive and normotensive subjects. *Am. J. physiology* 263 (1), H177–H181. doi:10.1152/ajpheart.1992.263.1.h177

Edmondson, D. G., Lyons, G. E., Martin, J. F., and Olson, E. N. (1994). Mef2 gene expression marks the cardiac and skeletal muscle lineages during mouse embryogenesis. *Development* 120 (5), 1251–1263. doi:10.1242/dev.120.5.1251

Eneling, K., Brion, L., Pinto, V., Pinho, M. J., Sznajder, J. I., Mochizuki, N., et al. (2012). Salt-inducible kinase 1 regulates E-cadherin expression and intercellular junction stability. *FASEB J.* 26 (8), 3230–3239. doi:10.1096/fj.12-205609

Facchi, C., Zi, M., Prehar, S., King, K., Njegic, A., Wang, X., et al. (2022). Salt-inducible kinase 2 (SIK2) modulates cardiac remodeling following ischemic pathological stress. *J. Mol. Cell. Cardiol.* 173, S39. doi:10.1016/j.yjmcc.2022.08.077

Fagerberg, L., Hallström, B. M., Oksvold, P., Kampf, C., Djureinovic, D., Odeberg, J., et al. (2014). Analysis of the human tissue-specific expression by genome-wide integration of transcriptomics and antibody-based proteomics. *Mol. Cell Proteomics* 13 (2), 397–406. doi:10.1074/mcp.M113.035600

Fagiani, F., Di Marino, D., Romagnoli, A., Travelli, C., Voltan, D., Di Cesare Mannelli, L., et al. (2022). Molecular regulations of circadian rhythm and implications for physiology and diseases. *Signal Transduct. Target Ther.* 7 (1), 41. doi:10.1038/s41392-022-00899-y

Feldman, J. D., Vician, L., Crispino, M., Hoe, W., Baudry, M., and Herschman, H. R. (2000). The salt-inducible kinase, SIK, is induced by depolarization in brain. *J. Neurochem.* 74 (6), 2227–2238. doi:10.1046/j.1471-4159.2000.0742227.x

Ferreira, D. N., Katayama, I. A., Oliveira, I. B., Rosa, K. T., Furukawa, L. N. S., Coelho, M. S., et al. (2010). Salt-induced cardiac hypertrophy and interstitial fibrosis are due to a blood pressure–independent mechanism in Wistar rats. *J. Nutr.* 140 (10), 1742–1751. doi:10.3945/jn.109.117473

Fischle, W., Dequiedt, F., Hendzel, M. J., Guenther, M. G., Lazar, M. A., Voelter, W., et al. (2002). Enzymatic activity associated with class II HDACs is dependent on a multiprotein complex containing HDAC3 and SMRT/N-CoR. *Mol. Cell* 9 (1), 45–57. doi:10.1016/s1097-2765(01)00429-4

Foretz, M., Hébrard, S., Leclerc, J., Zarrinpashneh, E., Soty, M., Mithieux, G., et al. (2010). Metformin inhibits hepatic gluconeogenesis in mice independently of the LKB1/AMPK pathway via a decrease in hepatic energy state. *J. Clin. investigation* 120 (7), 2355–2369. doi:10.1172/jci40671

Frangogiannis, N. G. (2021). Cardiac fibrosis. *Cardiovasc Res.* 117 (6), 1450–1488. doi:10.1093/cvr/cvaa324

Frohlich, E. D., and Varagic, J. (2004). The role of sodium in hypertension is more complex than simply elevating arterial pressure. *Nat. Clin. Pract. Cardiovasc. Med.* 1 (1), 24–30. doi:10.1038/ncpcardio0025

Frydman, N., Steffann, J., Girerd, B., Frydman, R., Munnich, A., Simonneau, G., et al. (2012). Pre-implantation genetic diagnosis in pulmonary arterial hypertension due to BMPR2 mutation. *Eur. Respir. J.* 39 (6), 1534–1535. doi:10.1183/09031936.00185011

Gibbons, G. H., and Dzau, V. J. (1994). The emerging concept of vascular remodeling. *N. Engl. J. Med.* 330 (20), 1431–1438. doi:10.1056/nejm199405193302008

Gormand, A., Berggreen, C., Amar, L., Henriksson, E., Lund, I., Albinsson, S., et al. (2014). LKB1 signalling attenuates early events of adipogenesis and responds to adipogenic cues. *J. Mol. Endocrinol.* 53 (1), 117–130. doi:10.1530/jme-13-0296

Hage, C., Michaëlsson, E., Linde, C., Donal, E., Daubert, J. C., Gan, L. M., et al. (2017). Inflammatory biomarkers predict heart failure severity and prognosis in patients with heart failure with preserved ejection fraction: a holistic proteomic approach. *Circ. Cardiovasc Genet.* 10 (1), e001633. doi:10.1161/circgenetics.116.001633

Handschin, C., Rhee, J., Lin, J., Tarr, P. T., and Spiegelman, B. M. (2003). An autoregulatory loop controls peroxisome proliferator-activated receptor gamma coactivator 1alpha expression in muscle. *Proc. Natl. Acad. Sci. U. S. A.* 100 (12), 7111–7116. doi:10.1073/pnas.1232352100

Hartl, C., Maser, I.-P., Michels, T., Milde, R., Klein, V., Beckhove, P., et al. (2022). Abstract 3708: OMX-0407, a highly potent SIK3 inhibitor, sensitizes tumor cells to cell death and eradicates tumors in combination with PD-1 inhibition. *Cancer Res.* 82 (12), 3708. doi:10.1158/1538-7445.Am2022-3708

Hashimoto, Y. K., Satoh, T., Okamoto, M., and Takemori, H. (2008). Importance of autophosphorylation at Ser186 in the A-loop of salt inducible kinase 1 for its sustained kinase activity. *J. Cell. Biochem.* 104 (5), 1724–1739. doi:10.1002/jcb.21737

Henderson, N. C., Rieder, F., and Wynn, T. A. (2020). Fibrosis: from mechanisms to medicines. *Nature* 587 (7835), 555–566. doi:10.1038/s41586-020-2938-9

Henriksson, E., Jones, H. A., Patel, K. A., Peggie, M., Morrice, N. A., Sakamoto, K., et al. (2012). The AMPK-related kinase SIK2 is regulated by cAMP via phosphorylation at Ser358 in adipocytes. *Biochem. J.* 444 (3), 503–514. doi:10.1042/bj20111932

Henriksson, E., Säll, J., Gormand, A., Wasserstrom, S., Morrice, N. A., Fritzen, A. M., et al. (2015). SIK2 regulates CRTCs, HDAC4 and glucose uptake in adipocytes. *J. Cell Sci.* 128 (3), 472–486. doi:10.1242/jcs.153932

Horike, N., Takemori, H., Katoh, Y., Doi, J., Min, L., Asano, T., et al. (2003). Adipose-specific expression, phosphorylation of Ser794 in insulin receptor substrate-1, and activation in diabetic animals of salt-inducible kinase-2. *J. Biol. Chem.* 278 (20), 18440–18447. doi:10.1074/jbc.m211770200

Hsu, A. (2022). "*Identifying Signaling and gene regulatory Mechanisms of pathologic cardiac Remodeling and heart failure pathogenesis*,". Ph.D. (San Francisco: University of California).

Hsu, A., Duan, Q., McMahon, S., Huang, Y., Wood, S. A., Gray, N. S., et al. (2020). Salt-inducible kinase 1 maintains HDAC7 stability to promote pathologic cardiac remodeling. *J. Clin. Invest.* 130 (6), 2966–2977. doi:10.1172/jci133753

Hutchinson, L. D., Darling, N. J., Nicolaou, S., Gori, I., Squair, D. R., Cohen, P., et al. (2020). Salt-inducible kinases (SIKs) regulate TGFβ-mediated transcriptional and apoptotic responses. *Cell death Dis.* 11 (1), 49. doi:10.1038/s41419-020-2241-6

Itoh, Y., Sanosaka, M., Fuchino, H., Yahara, Y., Kumagai, A., Takemoto, D., et al. (2015). Salt-inducible kinase 3 signaling is important for the gluconeogenic programs in mouse hepatocytes. *J. Biol. Chem.* 290 (29), 17879–17893. doi:10.1074/jbc.M115.640821

Iwamoto, T., Kita, S., Zhang, J., Blaustein, M. P., Arai, Y., Yoshida, S., et al. (2004). Salt-sensitive hypertension is triggered by Ca2+ entry via Na+/Ca2+ exchanger type-1 in vascular smooth muscle. *Nat. Med.* 10 (11), 1193–1199. doi:10.1038/nm1118

Jagannath, A., Butler, R., Sih, G., Couch, Y., Brown, L. A., Vasudevan, S. R., et al. (2013). The CRTC1-SIK1 pathway regulates entrainment of the circadian clock. *Cell* 154 (5), 1100–1111. doi:10.1016/j.cell.2013.08.004

Jagannath, A., Taylor, L., Ru, Y., Wakaf, Z., Akpobaro, K., Vasudevan, S., et al. (2023). The multiple roles of salt-inducible kinases in regulating physiology. *Physiol. Rev.* 103 (3), 2231–2269. doi:10.1152/physrev.00023.2022

Jaitovich, A., and Bertorello, A. M. (2010). Intracellular sodium sensing: SIK1 network, hormone action and high blood pressure. *Biochimica biophysica acta* 1802 (12), 1140–1149. doi:10.1016/j.bbadis.2010.03.009

Jaleel, M., Villa, F., Deak, M., Toth, R., Prescott, A. R., van Aalten, D. M. F., et al. (2006). The ubiquitin-associated domain of AMPK-related kinases regulates conformation and LKB1-mediated phosphorylation and activation. *Biochem. J.* 394 (3), 545–555. doi:10.1042/bj20051844

Kalogeropoulos, A., Georgiopoulou, V., Psaty, B. M., Rodondi, N., Smith, A. L., Harrison, D. G., et al. (2010). Inflammatory markers and incident heart failure risk in older adults: the Health ABC (Health, Aging, and Body Composition) study. *J. Am. Coll. Cardiol.* 55 (19), 2129–2137. doi:10.1016/j.jacc.2009.12.045

Kanyo, R., Price, D. M., Chik, C. L., and Ho, A. K. (2009). Salt-inducible kinase 1 in the rat pinealocytes: adrenergic regulation and role in arylalkylamine N-acetyltransferase gene transcription. *Endocrinology* 150 (9), 4221–4230. doi:10.1210/en.2009-0275

Karjalainen, M. K., Holmes, M. V., Wang, Q., Anufrieva, O., Kähönen, M., Lehtimäki, T., et al. (2020). Apolipoprotein A-I concentrations and risk of coronary artery disease: a Mendelian randomization study. *Atherosclerosis* 299, 56–63. doi:10.1016/j.atherosclerosis.2020.02.002

Katoh, Y., Takemori, H., Doi, J., and Okamoto, M. (2002). Identification of the nuclear localization domain of salt-inducible kinase. *Endocr. Res.* 28 (4), 315–318. doi:10.1081/erc-120016802

Katoh, Y., Takemori, H., Horike, N., Doi, J., Muraoka, M., Min, L., et al. (2004a). Salt-inducible kinase (SIK) isoforms: their involvement in steroidogenesis and adipogenesis. *Mol. Cell. Endocrinol.* 217 (1), 109–112. doi:10.1016/j.mce.2003.10.016

Katoh, Y., Takemori, H., Lin, X.-z., Tamura, M., Muraoka, M., Satoh, T., et al. (2006). Silencing the constitutive active transcription factor CREB by the LKB1-SIK signaling cascade. *FEBS J.* 273 (12), 2730–2748. doi:10.1111/j.1742-4658.2006.05291.x

Katoh, Y., Takemori, H., Min, L., Muraoka, M., Doi, J., Horike, N., et al. (2004b). Salt-inducible kinase-1 represses cAMP response element-binding protein activity both in the nucleus and in the cytoplasm. *Eur. J. Biochem.* 271 (21), 4307–4319. doi:10.1111/j.1432-1033.2004.04372.x

Kenagy, R. D. (2011). "Biology of restenosis and targets for intervention," in *Mechanisms of vascular disease: a reference book for vascular specialists*. Editors R. Fitridge and M. Thompson (Adelaide (AU): University of Adelaide Press).

Kim, J., Hwangbo, C., Hu, X., Kang, Y., Papangeli, I., Mehrotra, D., et al. (2014). Restoration of impaired endothelial myocyte enhancer factor 2 function rescues pulmonary arterial hypertension. *Circulation* 131 (2), 190–199. doi:10.1161/circulationaha.114.013339

Kim, M. J., Park, S. K., Lee, J. H., Jung, C. Y., Sung, D. J., Park, J.-H., et al. (2015). Salt-inducible kinase 1 terminates cAMP signaling by an evolutionarily conserved negative-feedback loop in β-cells. *Diabetes* 64 (9), 3189–3202. doi:10.2337/db14-1240

Kim, S. Y., Jeong, S., Chah, K.-H., Jung, E., Baek, K.-H., Kim, S.-T., et al. (2013). Salt-inducible kinases 1 and 3 negatively regulate Toll-like receptor 4-mediated signal. *Mol. Endocrinol.* 27 (11), 1958–1968. doi:10.1210/me.2013-1240

Ko, A., Cantor, R. M., Weissglas-Volkov, D., Nikkola, E., Reddy, P. M., Sinsheimer, J. S., et al. (2014). Amerindian-specific regions under positive selection harbour new lipid variants in Latinos. *Nat. Commun.* 5, 3983. doi:10.1038/ncomms4983

Koo, S. H., Flechner, L., Qi, L., Zhang, X., Screaton, R. A., Jeffries, S., et al. (2005). The CREB coactivator TORC2 is a key regulator of fasting glucose metabolism. *Nature* 437 (7062), 1109–1111. doi:10.1038/nature03967

Kowanetz, M., Lönn, P., Vanlandewijck, M., Kowanetz, K., Heldin, C.-H., and Moustakas, A. (2008). TGFbeta induces SIK to negatively regulate type I receptor kinase signaling. *J. Cell Biol.* 182 (4), 655–662. doi:10.1083/jcb.200804107

Lan, N. S. H., Massam, B. D., Kulkarni, S. S., and Lang, C. C. (2018). Pulmonary arterial hypertension: pathophysiology and treatment. *Diseases* 6 (2), 38. doi:10.3390/diseases6020038

Lee, J., Yamazaki, T., Dong, H., and Jefcoate, C. R. (2016). A single cell level measurement of StAR expression and activity in adrenal cells. *Mol. Cell. Endocrinol.* 441 (NA), 22–30. doi:10.1016/j.mce.2016.08.015

Lehmann, L. H., Jebessa, Z. H., Kreusser, M. M., Horsch, A., He, T., Kronlage, M., et al. (2017). A proteolytic fragment of histone deacetylase 4 protects the heart from failure by regulating the hexosamine biosynthetic pathway. *Nat. Med.* 24 (1), 62–72. doi:10.1038/nm.4452

Lin, X.-z., Takemori, H., Katoh, Y., Doi, J., Horike, N., Makino, A., et al. (2001). Salt-inducible kinase is involved in the ACTH/cAMP-dependent protein kinase signaling in Y1 mouse adrenocortical tumor cells. *Mol. Endocrinol.* 15 (8), 1264–1276. doi:10.1210/mend.15.8.0675

Lincoff, A. M., Brown-Frandsen, K., Colhoun, H. M., Deanfield, J., Emerson, S. S., Esbjerg, S., et al. (2023). Semaglutide and cardiovascular outcomes in obesity without diabetes. *N. Engl. J. Med.* 389 (24), 2221–2232. doi:10.1056/NEJMoa2307563

Liu, D., Qq, L., Eyries, M., Wu, W.-H., Yuan, P., Zhang, R., et al. (2011). Molecular genetics and clinical features of Chinese idiopathic and heritable pulmonary arterial hypertension patients. *Eur. Respir. J.* 39 (3), 597–603. doi:10.1183/09031936.00072911

Liu, S., Huang, S., Wu, X., Feng, Y., Shen, Y., Zhao, Q. S., et al. (2020). Activation of SIK1 by phanginin A inhibits hepatic gluconeogenesis by increasing PDE4 activity and suppressing the cAMP signaling pathway. *Mol. Metab.* 41, 101045. doi:10.1016/j.molmet.2020.101045

Liu, X., Xu, L., Wu, J., Zhang, Y., Wu, C., and Zhang, X. (2022). Down-regulation of SIK2 expression alleviates myocardial ischemia-reperfusion injury in rats by inhibiting autophagy through the mTOR-ULK1 signaling pathway. *Nan Fang. Yi Ke Da Xue Xue Bao* 42 (7), 1082–1088. doi:10.12122/j.issn.1673-4254.2022.07.18

Lombardi, M. S., Gilliéron, C., Dietrich, D., and Gabay, C. (2016). SIK inhibition in human myeloid cells modulates TLR and IL-1R signaling and induces an anti-inflammatory phenotype. *J. Leukoc. Biol.* 99 (5), 711–721. doi:10.1189/jlb.2A0715-307R

Lönn, P., Vanlandewijck, M., Raja, E., Kowanetz, M., Watanabe, Y., Kowanetz, K., et al. (2012). Transcriptional induction of salt-inducible kinase 1 by transforming growth factor β leads to negative regulation of type I receptor signaling in cooperation with the Smurf2 ubiquitin ligase. *J. Biol. Chem.* 287 (16), 12867–12878. doi:10.1074/jbc.m111.307249

Luan, B., Goodarzi, M. O., Phillips, N. G., Guo, X., Chen, Y.-D. I., Yao, J., et al. (2014). Leptin-mediated increases in catecholamine signaling reduce adipose tissue inflammation via activation of macrophage HDAC4. *Cell metab.* 19 (6), 1058–1065. doi:10.1016/j.cmet.2014.03.024

Ma, L., Roman-Campos, D., Austin, E. D., Eyries, M., Sampson, K. J., Soubrier, F., et al. (2013). A novel channelopathy in pulmonary arterial hypertension. *N. Engl. J. Med.* 369 (4), 351–361. doi:10.1056/nejmoa1211097

MacKenzie, K. F., Clark, K., Naqvi, S., McGuire, V. A., Nöehren, G., Kristariyanto, Y. A., et al. (2012). PGE2 induces macrophage IL-10 production and a regulatory-like phenotype via a protein kinase A–SIK–CRTC3 pathway. *J. Immunol.* 190 (2), 565–577. doi:10.4049/jimmunol.1202462

Medina, C. B., Chiu, Y.-H., Stremska, M. E., Lucas, C. D., Poon, I. K. H., Tung, K. S. K., et al. (2021). Pannexin 1 channels facilitate communication between T cells to restrict the severity of airway inflammation. *Immunity* 54 (8), 1715–1727.e7. doi:10.1016/j.immuni.2021.06.014

Montani, D., Girerd, B., Günther, S., Riant, F., Tournier-Lasserve, E., Magy, L., et al. (2013). Pulmonary arterial hypertension in familial hemiplegic migraine with ATP1A2 channelopathy. *Eur. Respir. J.* 43 (2), 641–643. doi:10.1183/09031936.00147013

Moore, E. D., Etter, E. F., Philipson, K. D., Carrington, W. A., Fogarty, K. E., Lifshitz, L. M., et al. (1993). Coupling of the Na+/Ca2+ exchanger, Na+/K+ pump and sarcoplasmic reticulum in smooth muscle. *Nature* 365 (6447), 657–660. doi:10.1038/365657a0

Nefla, M., Darling, N. J., van Gijsel Bonnello, M., Cohen, P., and Arthur, J. S. C. (2021). Salt inducible kinases 2 and 3 are required for thymic T cell development. *Sci. Rep.* 11 (1), 21550–NA. doi:10.1038/s41598-021-00986-0

Nguyen, P. T., Deisl, C., Fine, M., Tippetts, T. S., Uchikawa, E., Bai, X. C., et al. (2022). Structural basis for gating mechanism of the human sodium-potassium pump. *Nat. Commun.* 13 (1), 5293. doi:10.1038/s41467-022-32990-x

Nixon, M., Stewart-Fitzgibbon, R., Fu, J., Akhmedov, D., Rajendran, K., Mendoza-Rodriguez, M. G., et al. (2015). Skeletal muscle salt inducible kinase 1 promotes insulin resistance in obesity. *Mol. Metab.* 5 (1), 34–46. doi:10.1016/j.molmet.2015.10.004

Pahwa, R., Goyal, A., and Jialal, I. (2024). "Chronic inflammation," in *StatPearls* (Treasure Island (FL): StatPearls Publishing).

Park, J.-Y., Yoon, Y. S., Han, H. S., Kim, Y.-H., Ogawa, Y., Park, K.-G., et al. (2014). SIK2 is critical in the regulation of lipid homeostasis and adipogenesis *in vivo*. *Diabetes* 63 (11), 3659–3673. doi:10.2337/db13-1423

Park, S. Y., and Kim, J. S. (2020). A short guide to histone deacetylases including recent progress on class II enzymes. *Exp. Mol. Med.* 52 (2), 204–212. doi:10.1038/s12276-020-0382-4

Patel, K. A., Foretz, M., Marion, A., Campbell, D. G., Gourlay, R., Boudaba, N., et al. (2014). The LKB1-salt-inducible kinase pathway functions as a key gluconeogenic suppressor in the liver. *Nat. Commun.* 5 (1), 4535. doi:10.1038/ncomms5535

Patel, Y., and Joseph, J. (2020). Sodium intake and heart failure. *Int. J. Mol. Sci.* 21 (24), 9474. doi:10.3390/ijms21249474

Peixoto, C., Joncour, A., Temal-Laib, T., Tirera, A., Dos Santos, A., Jary, H., et al. (2024). Discovery of clinical candidate GLPG3970: a potent and selective dual SIK2/SIK3 inhibitor for the treatment of autoimmune and inflammatory diseases. *J. Med. Chem.* 67, 5233–5258. doi:10.1021/acs.jmedchem.3c02246

Pinho, M. J., Bertorello, A. M., and Silva, P.S.-d.-. (2012). Abstract 325: cardiac hypertrophy in spontaneous hypertensive rats (SHR) is associated with decreased cardiac expression of SIK1 and SIK3 isoforms. *Hypertension* 60 (1), A325. doi:10.1161/hyp.60.suppl_1.A325

Pirahanchi, Y., Jessu, R., and Aeddula, N. R. (2024). "Physiology, sodium potassium pump," in *StatPearls* (Treasure Island (FL): Ineligible companies).

Pires, N., Igreja, B., and Soares-da-Silva, P. (2021). Antagonistic modulation of SIK1 and SIK2 isoforms in high blood pressure and cardiac hypertrophy triggered by high-salt intake. *Clin. Exp. Hypertens.* 43 (5), 428–435. doi:10.1080/10641963.2021.1896728

Pires, N. M., Igreja, B., Serrão, M. P., Matias, E. F., Moura, E., António, T., et al. (2019). Acute salt loading induces sympathetic nervous system overdrive in mice lacking salt-inducible kinase 1 (SIK1). *Hypertens. Res.* 42 (8), 1114–1124. doi:10.1038/s41440-019-0249-z

Popov, S., Silveira, A., Wågsäter, D., Takemori, H., Oguro, R., Matsumoto, S., et al. (2011). Salt-inducible kinase 1 influences Na(+),K(+)-ATPase activity in vascular smooth muscle cells and associates with variations in blood pressure. *J. Hypertens.* 29 (12), 2395–2403. doi:10.1097/hjh.0b013e32834d3d55

Popov, S., Takemori, H., Tokudome, T., Mao, Y., Otani, K., Mochizuki, N., et al. (2014). Lack of salt-inducible kinase 2 (SIK2) prevents the development of cardiac hypertrophy in response to chronic high-salt intake. *PLoS One* 9 (4), e95771. doi:10.1371/journal.pone.0095771

Popov, S., Venetsanou, K., Chedrese, P. J., Pinto, V., Takemori, H., Franco-Cereceda, A., et al. (2012). Increases in intracellular sodium activate transcription and gene expression via the salt-inducible kinase 1 network in an atrial myocyte cell line. *Am. J. physiology. Heart circulatory physiology* 303 (1), H57–H65. doi:10.1152/ajpheart.00512.2011

Powell-Wiley, T. M., Poirier, P., Burke, L. E., Després, J. P., Gordon-Larsen, P., Lavie, C. J., et al. (2021). Obesity and cardiovascular disease: a scientific statement from the American heart association. *Circulation* 143 (21), e984–e1010. doi:10.1161/cir.0000000000000973

Pu, J., Wang, F., Ye, P., Jiang, X., Zhou, W., Gu, Y., et al. (2022). Salt-inducible kinase 1 deficiency promotes vascular remodeling in pulmonary arterial hypertension via enhancement of yes-associated protein-mediated proliferation. *Heliyon* 8 (10), e11016. doi:10.1016/j.heliyon.2022.e11016

Qi, L., Saberi, M., Zmuda, E., Wang, Y., Altarejos, J. Y., Zhang, X., et al. (2009). Adipocyte CREB promotes insulin resistance in obesity. *Cell metab.* 9 (3), 277–286. doi:10.1016/j.cmet.2009.01.006

Qu, C., and Qu, Y. (2017). Down-regulation of salt-inducible kinase 1 (SIK1) is mediated by RNF2 in hepatocarcinogenesis. *Oncotarget* 8 (2), 3144–3155. doi:10.18632/oncotarget.13673

Reynolds, A. M., Holmes, M., Danilov, S. M., and Reynolds, P. N. (2011). Targeted gene delivery of BMPR2 attenuates pulmonary hypertension. *Eur. Respir. J.* 39 (2), 329–343. doi:10.1183/09031936.00187310

Romito, A., Lonardo, E., Roma, G., Minchiotti, G., Ballabio, A., and Cobellis, G. (2010). Lack of sik1 in mouse embryonic stem cells impairs cardiomyogenesis by down-regulating the cyclin-dependent kinase inhibitor p57kip2. *PLoS One* 5 (2), e9029. doi:10.1371/journal.pone.0009029

Ruiz, J. C., Conlon, F. L., and Robertson, E. J. (1994). Identification of novel protein kinases expressed in the myocardium of the developing mouse heart. *Mech. Dev.* 48 (3), 153–164. doi:10.1016/0925-4773(94)90056-6

Sakamaki, J., Fu, A., Reeks, C., Baird, S., Depatie, C., Al Azzabi, M., et al. (2014). Role of the SIK2-p35-PJA2 complex in pancreatic β-cell functional compensation. *Nat. Cell Biol.* 16 (3), 234–244. doi:10.1038/ncb2919

Sakamoto, K., Bultot, L., and Goransson, O. (2018). The salt-inducible kinases: emerging metabolic regulators. *Trends Endocrinol. Metab.* 29 (12), 827–840. doi:10.1016/j.tem.2018.09.007

Säll, J., Pettersson, A. M. L., Björk, C., Henriksson, E., Wasserstrom, S., Linder, W., et al. (2016). Salt-inducible kinase 2 and -3 are downregulated in adipose tissue from obese or insulin-resistant individuals: implications for insulin signalling and glucose uptake in human adipocytes. *Diabetologia* 60 (2), 314–323. doi:10.1007/s00125-016-4141-y

Sanosaka, M., Fujimoto, M., Ohkawara, T., Nagatake, T., Itoh, Y., Kagawa, M., et al. (2015). Salt-inducible kinase 3 deficiency exacerbates lipopolysaccharide-induced endotoxin shock accompanied by increased levels of pro-inflammatory molecules in mice. *Immunology* 145 (2), 268–278. doi:10.1111/imm.12445

Sasaki, T., Takemori, H., Yagita, Y., Terasaki, Y., Uebi, T., Horike, N., et al. (2011). SIK2 is a key regulator for neuronal survival after ischemia via TORC1-CREB. *Neuron* 69 (1), 106–119. doi:10.1016/j.neuron.2010.12.004

Sato, T., Andrade, C. D. C., Yoon, S. H., Zhao, Y., Greenlee, W. J., Weber, P. C., et al. (2022). Structure-based design of selective, orally available salt-inducible kinase inhibitors that stimulate bone formation in mice. *Proc. Natl. Acad. Sci. U. S. A.* 119 (50), e2214396119. doi:10.1073/pnas.2214396119

Sattar, N., Lee, M. M. Y., Kristensen, S. L., Branch, K. R. H., Del Prato, S., Khurmi, N. S., et al. (2021). Cardiovascular, mortality, and kidney outcomes with GLP-1 receptor agonists in patients with type 2 diabetes: a systematic review and meta-analysis of randomised trials. *Lancet Diabetes Endocrinol.* 9 (10), 653–662. doi:10.1016/s2213-8587(21)00203-5

Screaton, R. A., Conkright, M. D., Katoh, Y., Best, J. L., Canettieri, G., Jeffries, S., et al. (2004). The CREB coactivator TORC2 functions as a calcium- and cAMP-sensitive coincidence detector. *Cell* 119 (1), 61–74. doi:10.1016/j.cell.2004.09.015

Shan, T., Xiong, Y., Zhang, P., Li, Z., Jiang, Q., Bi, P., et al. (2016). Lkb1 controls brown adipose tissue growth and thermogenesis by regulating the intracellular localization of CRTC3. *Nat. Commun.* 7, 12205. doi:10.1038/ncomms12205

Shen, H., McElhinny, A. S., Cao, Y., Gao, P., Liu, J., Bronson, R. T., et al. (2006). The Notch coactivator, MAML1, functions as a novel coactivator for MEF2C-mediated transcription and is required for normal myogenesis. *Genes and Dev.* 20 (6), 675–688. doi:10.1101/gad.1383706

Shi, F., and Collins, S. (2017). Second messenger signaling mechanisms of the brown adipocyte thermogenic program: an integrative perspective. *Horm. Mol. Biol. Clin. Investig.* 31 (2). doi:10.1515/hmbci-2017-0062

Shi, F., and Collins, S. (2023). Regulation of mTOR signaling: emerging role of cyclic nucleotide-dependent protein kinases and implications for cardiometabolic disease. *Int. J. Mol. Sci.* 24 (14), 11497. doi:10.3390/ijms241411497

Shi, F., de Fatima Silva, F., Liu, D., Patel, H. U., Xu, J., Zhang, W., et al. (2023). Salt-inducible kinase inhibition promotes the adipocyte thermogenic program and adipose tissue browning. *Mol. Metab.* 74, 101753. doi:10.1016/j.molmet.2023.101753

Sjöström, M., Stenström, K., Eneling, K., Zwiller, J., Katz, A. I., Takemori, H., et al. (2007). SIK1 is part of a cell sodium-sensing network that regulates active sodium transport through a calcium-dependent process. *Proc. Natl. Acad. Sci. U. S. A.* 104 (43), 16922–16927. doi:10.1073/pnas.0706838104

Sonntag, T., Vaughan, J., and Montminy, M. (2018). 14-3-3 proteins mediate inhibitory effects of cAMP on salt-inducible kinases (SIKs). *FEBS J.* 285 (3), 467–480. doi:10.1111/febs.14351

Stewart, R., Akhmedov, D., Robb, C., Leiter, C., and Berdeaux, R. (2012). Regulation of SIK1 abundance and stability is critical for myogenesis. *Proc. Natl. Acad. Sci. U. S. A.* 110 (1), 117–122. doi:10.1073/pnas.1212676110

Stewart, R., Flechner, L., Montminy, M., and Berdeaux, R. (2011). CREB is activated by muscle injury and promotes muscle regeneration. *PLoS One* 6 (9), e24714. doi:10.1371/journal.pone.0024714

Strain, W. D., and Paldánius, P. M. (2018). Diabetes, cardiovascular disease and the microcirculation. *Cardiovasc Diabetol.* 17 (1), 57. doi:10.1186/s12933-018-0703-2

Sun, Z., Jiang, Q., Li, J., and Guo, J. (2020). The potent roles of salt-inducible kinases (SIKs) in metabolic homeostasis and tumorigenesis. *Signal Transduct. Target Ther.* 5 (1), 150. doi:10.1038/s41392-020-00265-w

Sundberg, T. B., Choi, H. G., Song, J. H., Russell, C. N., Hussain, M. M., Graham, D. B., et al. (2014). Small-molecule screening identifies inhibition of salt-inducible kinases as a therapeutic strategy to enhance immunoregulatory functions of dendritic cells. *Proc. Natl. Acad. Sci. U. S. A.* 111 (34), 12468–12473. doi:10.1073/pnas.1412308111

Sundberg, T. B., Liang, Y., Wu, H., Choi, H. G., Kim, N. D., Sim, T., et al. (2016). Development of chemical probes for investigation of salt-inducible kinase function *in vivo*. *ACS Chem. Biol.* 11 (8), 2105–2111. doi:10.1021/acschembio.6b00217

Tang, C. C., Castro Andrade, C. D., O'Meara, M. J., Yoon, S. H., Sato, T., Brooks, D. J., et al. (2021). Dual targeting of salt inducible kinases and CSF1R uncouples bone formation and bone resorption. *Elife* 10, e67772. doi:10.7554/eLife.67772

Tarumoto, Y., Lin, S., Wang, J., Milazzo, J. P., Xu, Y., Lu, B., et al. (2020). Salt-inducible kinase inhibition suppresses acute myeloid leukemia progression *in vivo*. *Blood* 135 (1), 56–70. doi:10.1182/blood.2019001576

Taub, M. (2018). Gene level regulation of Na,K-ATPase in the renal proximal tubule is controlled by two independent but interacting regulatory mechanisms involving salt inducible kinase 1 and CREB-regulated transcriptional coactivators. *Int. J. Mol. Sci.* 19 (7), 2086. doi:10.3390/ijms19072086

Taub, M., Garimella, S., Kim, D., Rajkhowa, T., and Cutuli, F. (2015). Renal proximal tubule Na,K-ATPase is controlled by CREB-regulated transcriptional coactivators as well as salt-inducible kinase 1. *Cell. Signal.* 27 (12), 2568–2578. doi:10.1016/j.cellsig.2015.09.015

Taub, M., Springate, J. E., and Cutuli, F. (2010). Targeting of renal proximal tubule Na,K-ATPase by salt-inducible kinase. *Biochem. biophysical Res. Commun.* 393 (3), 339–344. doi:10.1016/j.bbrc.2010.02.037

Temal-Laib, T., Peixoto, C., Desroy, N., De Lemos, E., Bonnaterre, F., Bienvenu, N., et al. (2023). Optimization of selectivity and pharmacokinetic properties of salt-inducible kinase inhibitors that led to the discovery of pan-SIK inhibitor GLPG3312. *J. Med. Chem.* 67, 380–401. doi:10.1021/acs.jmedchem.3c01428

Teslovich, T. M., Musunuru, K., Smith, A. V., Edmondson, A. C., Stylianou, I. M., Koseki, M., et al. (2010). Biological, clinical and population relevance of 95 loci for blood lipids. *Nature* 466 (7307), 707–713. doi:10.1038/nature09270

Travers, J. G., Hu, T., and McKinsey, T. A. (2020). The black sheep of class IIa: HDAC7 SIKens the heart. *J. Clin. Invest.* 130 (6), 2811–2813. doi:10.1172/jci137074

Uebi, T., Itoh, Y., Hatano, O., Kumagai, A., Sanosaka, M., Sasaki, T., et al. (2012). Involvement of SIK3 in glucose and lipid homeostasis in mice. *PloS one* 7 (5), e37803–NA. doi:10.1371/journal.pone.0037803

Vanlandewijck, M., Dadras, M. S., Lomnytska, M., Mahzabin, T., Miller, M. L., Busch, C., et al. (2017). The protein kinase SIK downregulates the polarity protein Par3. *Oncotarget* 9 (5), 5716–5735. doi:10.18632/oncotarget.23788

Verzi, M. P., Agarwal, P., Brown, C., McCulley, D. J., Schwarz, J. J., and Black, B. L. (2007). The transcription factor MEF2C is required for craniofacial development. *Dev. Cell* 12 (4), 645–652. doi:10.1016/j.devcel.2007.03.007

Wang, Y., Paulo, E., Wu, D., Wu, Y., Huang, W., Chawla, A., et al. (2017). Adipocyte liver kinase b1 suppresses beige adipocyte renaissance through class IIa histone deacetylase 4. *Diabetes* 66 (12), 2952–2963. doi:10.2337/db17-0296

Wang, Y., Viscarra, J., Kim, S. J., and Sul, H. S. (2015). Transcriptional regulation of hepatic lipogenesis. *Nat. Rev. Mol. Cell Biol.* 16 (11), 678–689. doi:10.1038/nrm4074

Wang, Z. n., Takemori, H., Halder, S. K., Nonaka, Y., and Okamoto, M. (1999). Cloning of a novel kinase (SIK) of the SNF1/AMPK family from high salt diet-treated rat adrenal. *FEBS Lett.* 453 (1), 135–139. doi:10.1016/s0014-5793(99)00708-5

Weems, J. C., Griesel, B. A., and Olson, A. L. (2012). Class II histone deacetylases downregulate GLUT4 transcription in response to increased cAMP signaling in cultured adipocytes and fasting mice. *Diabetes* 61 (6), 1404–1414. doi:10.2337/db11-0737

Wein, M. N., Foretz, M., Fisher, D. E., Xavier, R. J., and Kronenberg, H. M. (2018). Salt-inducible kinases: physiology, regulation by cAMP, and therapeutic potential. *Trends Endocrinol. Metab.* 29 (10), 723–735. doi:10.1016/j.tem.2018.08.004

Wein, M. N., Liang, Y., Goransson, O., Sundberg, T. B., Wang, J., Williams, E. A., et al. (2016). SIKs control osteocyte responses to parathyroid hormone. *Nat. Commun.* 7, 13176. doi:10.1038/ncomms13176

Willer, C. J., and Mohlke, K. L. (2012). Finding genes and variants for lipid levels after genome-wide association analysis. *Curr. Opin. Lipidol.* 23 (2), 98–103. doi:10.1097/MOL.0b013e328350fad2

Xiao, Y. Y., Xia, L. X., Jiang, W. J., Qin, J. F., Zhao, L. X., Li, Z., et al. (2024). Cardiopulmonary progenitors facilitate cardiac repair via exosomal transfer of miR-27b-3p targeting the SIK1-CREB1 axis. *Cell Prolif.* 57, e13593. doi:10.1111/cpr.13593

Yahara, Y., Takemori, H., Okada, M., Kosai, A., Yamashita, A., Kobayashi, T., et al. (2016). Pterosin B prevents chondrocyte hypertrophy and osteoarthritis in mice by inhibiting Sik3. *Nat. Commun.* 7, 10959. doi:10.1038/ncomms10959

Yang, F.-C., Tan, B.C.-M., Chen, W. H., Lin, Y. H., Huang, J. Y., Chang, H. Y., et al. (2013). Reversible acetylation regulates salt-inducible kinase (SIK2) and its function in autophagy. *J. Biol. Chem.* 288 (9), 6227–6237. doi:10.1074/jbc.m112.431239

Yilmaz, O., Oztay, F., and Kayalar, O. (2015). Dasatinib attenuated bleomycin-induced pulmonary fibrosis in mice. *Growth factors* 33 (5-6), 366–375. doi:10.3109/08977194.2015.1109511

Yodsaoue, O., Cheenpracha, S., Karalai, C., Ponglimanont, C., Chantrapromma, S., Fun, H. K., et al. (2008). Phanginin A-K, diterpenoids from the seeds of Caesalpinia sappan Linn. *Phytochemistry* 69 (5), 1242–1249. doi:10.1016/j.phytochem.2007.11.013

Yoon, Y. S., Seo, W. Y., Lee, M. W., Kim, S.-T., and Koo, S. H. (2009). Salt-inducible kinase regulates hepatic lipogenesis by controlling SREBP-1c phosphorylation. *J. Biol. Chem.* 284 (16), 10446–10452. doi:10.1074/jbc.m900096200

Yue, F., Cheng, Y., Breschi, A., Vierstra, J., Wu, W., Ryba, T., et al. (2014). A comparative encyclopedia of DNA elements in the mouse genome. *Nature* 515 (7527), 355–364. doi:10.1038/nature13992

Zhang, C. L., McKinsey, T. A., Chang, S., Antos, C. L., Hill, J. A., and Olson, E. N. (2002). Class II histone deacetylases act as signal-responsive repressors of cardiac hypertrophy. *Cell* 110 (4), 479–488. doi:10.1016/s0092-8674(02)00861-9

Zhou, J., Alfraidi, A., Zhang, S., Santiago-O'Farrill, J. M., Yerramreddy Reddy, V. K., Alsaadi, A., et al. (2017). A novel compound ARN-3236 inhibits salt-inducible kinase 2 and sensitizes ovarian cancer cell lines and xenografts to paclitaxel. *Clin. Cancer Res.* 23 (8), 1945–1954. doi:10.1158/1078-0432.Ccr-16-1562

Zhu, W., Liu, X., Li, Q., Gao, F., Liu, T., Chen, X., et al. (2023). Discovery of novel and selective SIK2 inhibitors by the application of AlphaFold structures and generative models. *Bioorg Med. Chem.* 91, 117414. doi:10.1016/j.bmc.2023.117414

Zou, L., Hong, D., Li, K., and Jiang, B. (2022). Salt-inducible kinase 2 (SIK2) inhibitor ARN-3236 attenuates bleomycin-induced pulmonary fibrosis in mice. *BMC Pulm. Med.* 22 (1), 140–NA. doi:10.1186/s12890-022-01940-0

frontiers | Frontiers in Pharmacology

TYPE Original Research
PUBLISHED 12 August 2024
DOI 10.3389/fphar.2024.1445975

OPEN ACCESS

EDITED BY
Lin Zhu,
Vanderbilt University Medical Center,
United States

REVIEWED BY
Sumita Dutta,
Cleveland Clinic, United States
Kakali Ghoshal,
Vanderbilt University Medical Center,
United States

*CORRESPONDENCE
Xiao-Jiao Cui,
cuixiaojiao@med.uestc.edu.cn
Min Chen,
bear_min@163.com

†These authors share first authorship

RECEIVED 08 June 2024
ACCEPTED 29 July 2024
PUBLISHED 12 August 2024

CITATION
Yi X-Q, Xie B, Hu Y, Gong T-J, Chen M and Cui X-J (2024) Association between acetaminophen administration and outcomes in critically ill patients with gout and hypertension.
Front. Pharmacol. 15:1445975.
doi: 10.3389/fphar.2024.1445975

Association between acetaminophen administration and outcomes in critically ill patients with gout and hypertension

Xiao-Qing Yi[1†], Bo Xie[2†], Yuan Hu[1], Tian-Jiao Gong[1], Min Chen[1*] and Xiao-Jiao Cui[1*]

[1]Department of Pharmacy, Personalized Drug Therapy Key Laboratory of Sichuan Province, Sichuan Academy of Medical Sciences and Sichuan Provincial People's Hospital, School of Medicine, University of Electronic Science and Technology of China, Chengdu, China, [2]Department of Cardiology, Chengdu First People's Hospital, Chengdu, China

Background: Acetaminophen is a commonly used medication, yet its recommendation for patients with comorbid conditions of gout and hypertension is contradictory, and the impact of its usage on clinical outcomes in real-world practical settings remains uncertain. The aim of this study was to investigate the association between acetaminophen administration and clinical outcomes in critically ill patients with gout and hypertension, utilizing real-world data.

Methods: A retrospective cohort study was conducted based on the MIMIC-IV (Medical Information Mart in Intensive Care-IV) database. Adult critically ill patients with gout and hypertension were included in the analysis. The exposure was acetaminophen use during ICU stay. The primary outcome was in-hospital mortality. The secondary endpoints were frequent hospitalization, 30-day, and 60-day all-cause mortality, and incidence of hypertensive emergencies. Propensity score matching (PSM) was conducted at a 1:1 ratio. Multivariable analyses were used to adjust for confounders.

Results: The pre-matched and propensity score-matched cohorts included 2448 and 1012 patients, respectively. In the PSM analysis, in-hospital mortality was 9.7% (49/506) in the acetaminophen use group and 12.1% (61/506) in the no use group. Acetaminophen use was associated with a decrease in-hospital mortality (hazard ratio [HR], 0.62; 95% CI, 0.41–0.92; P = 0.018). In terms of secondary endpoints, after PSM, there was no statistically significant difference for both 30-day and 60-day all-cause mortality reductions in the acetaminophen use group, and HRs were 0.78 (95% CI 0.55–1.11; P = 0.175), and 0.75 (95% CI 0.55–1.02; P = 0.069), respectively. According to the analysis of dosage and treatment group, the use of APAP within the dosage range of 2–4 g and within 3–5 days of treatment significantly reduced the mortality rate of the entire cohort and PSM cohort, with statistical differences. Subgroup analysis demonstrated that lower in-hospital mortality was consistent across different baselines (age, gender,

BMI, liver disease, and renal disease), with no interactions in all subgroups (interaction *p*-values >0.05), thereby affirming the robustness and reliability of the findings.

Conclusion: Acetaminophen use was associated with lower in-hospital mortality in critically ill patients with gout and hypertension. Prospective studies are needed to verify this finding.

KEYWORDS

critical illness, mortality, acetaminophen, gout, hypertension

1 Introduction

Gout is the most common inflammatory arthritis in adults, affecting approximately 41.2 million adults worldwide (Danve et al., 2021). It is precipitated by sustained hyperuricemia, leading to the deposition of monosodium urate crystals in joints, tendons, and other tissues. This accumulation triggers recurrent bouts of acute inflammation, known as gout flares (Dehlin et al., 2020). Hypertension and cardiovascular diseases are among the most common comorbidities of gout and hyperuricaemia (Kuwabara et al., 2017; Sandoval-Plata et al., 2021), which are associated with increased morbidity and mortality risk (Singh and Gaffo, 2020). Hypertension predisposes to gout by reducing renal urate excretion due to glomerular arteriolar damage and glomerulosclerosis, and studies have shown that hypertension is an independent risk factor for gout (Kuo et al., 2016; Evans et al.,

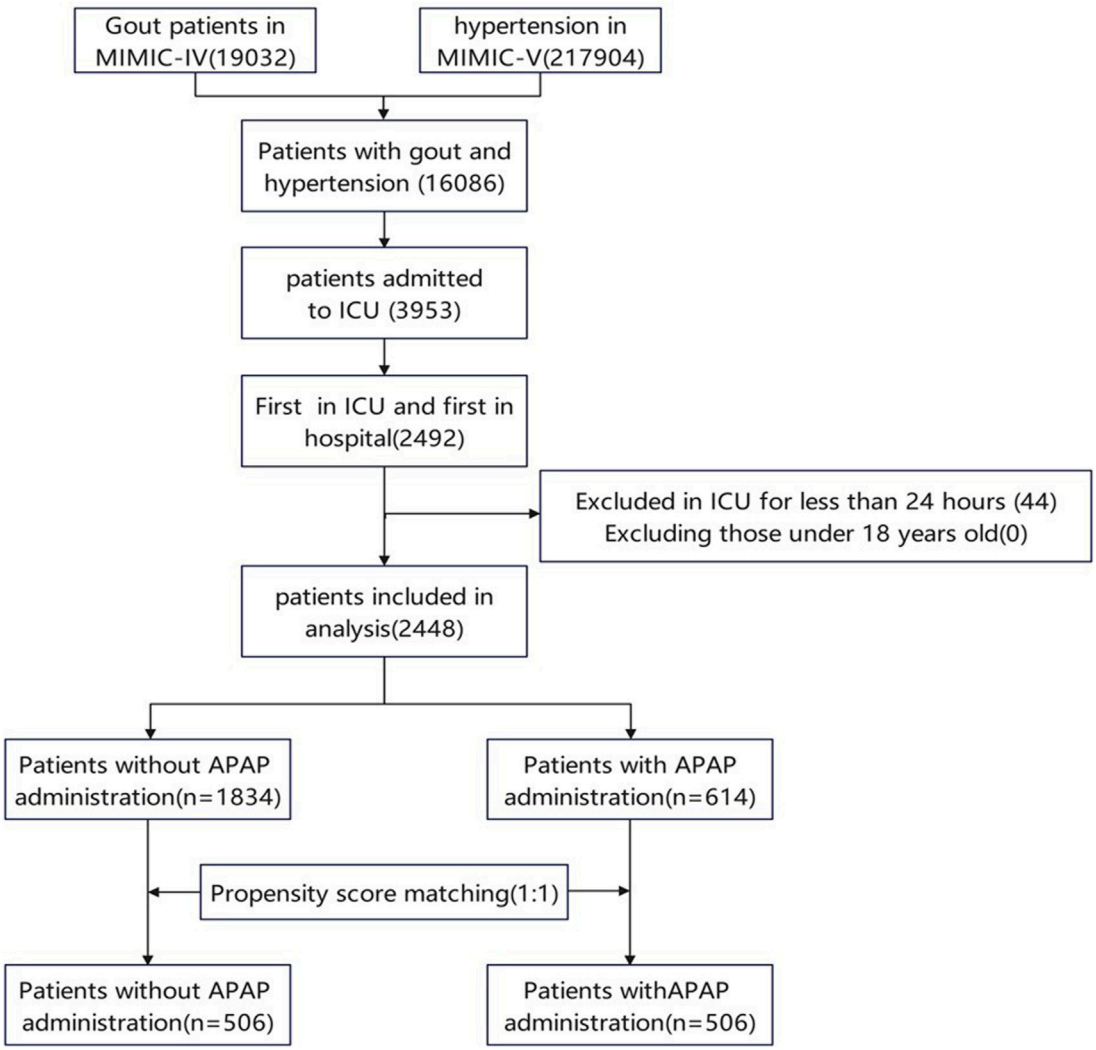

FIGURE 1
Flow chart of patient selection. MIMIC IV, Multiparameter Intelligent Monitoring in Intensive Care Database IV; ICU, intensive care unit; PSM, propensity-score matching.

TABLE 1 Baseline characteristics before and after propensity score matching.

Variables	Entire cohort (n = 2448)		SMD	PSM cohort (n = 1012)		SMD
	No-APAP (n = 1834)	APAP (n = 614)		No-APAP (n = 506)	APAP (n = 506)	
Demographics						
Age, year	73.5 ± 12.1	71.9 ± 10.6	0.134	72.8 ± 11.4	72.3 ± 11.1	0.044
Gender, Male, n (%)	1326 (72.3)	491 (80)	0.181	389 (76.9)	390 (77.1)	0.005
Race, white, n (%)	1275 (69.5)	413 (67.3)	0.049	362 (71.5)	341 (67.4)	0.09
BMI, kg/m2	30.9 ± 7.8	31.1 ± 7.1	0.022	30.8 ± 7.3	31.1 ± 7.1	0.047
Laboratory Examination						
WBC, K/μL	10.1 (7.6, 13.6)	12.6 (9.6, 15.9)	0.184	11.1 (8.1, 14.5)	12.6 (9.5, 15.8)	0.012
Platelet, K/μL	185.1 (141.4, 242.0)	156.3 (126.3, 204.2)	0.338	167.5 (125.0, 212.6)	159.5 (129.1, 212.8)	0.012
ALT, U/L	25.0 (16.0, 49.0)	23.8 (15.0, 46.4)	0.027	25.0 (16.0, 50.5)	25.0 (16.0, 49.0)	0.08
AST, U/L	32.5 (21.0, 60.0)	35.0 (22.0, 61.9)	0.044	35.0 (21.0, 64.0)	35.0 (22.0, 63.6)	0.054
Serum creatinine, mg/dL	1.4 (1.0, 2.3)	1.2 (0.9, 1.7)	0.23	1.3 (1.0, 2.0)	1.3 (1.0, 1.8)	0.054
Serum glucose, mg/dL	130.5 (108.5, 162.9)	128.0 (109.0, 152.5)	0.113	129.0 (108.1, 158.9)	129.2 (110.2, 153.4)	0.012
Concomitant Medication						
βblocker, n (%)	1443 (78.7)	557 (90.7)	0.339	460 (90.9)	453 (89.5)	0.047
ACEI, n (%)	561 (30.6)	167 (27.2)	0.075	154 (30.4)	141 (27.9)	0.057
ARB, n (%)	242 (13.2)	76 (12.4)	0.024	66 (13)	64 (12.6)	0.012
CCB, n (%)	488 (26.6)	222 (36.2)	0.207	172 (34)	168 (33.2)	0.017
Diuretics, n (%)	1211 (66)	508 (82.7)	0.39	400 (79.1)	403 (79.6)	0.015
Colchicine, n (%)	317 (17.3)	75 (12.2)	0.143	65 (12.8)	70 (13.8)	0.029
NSAIDs, n (%)	84 (4.6)	29 (4.7)	0.007	23 (4.5)	24 (4.7)	0.009
Glucocorticoids, n (%)	295 (16.1)	85 (13.8)	0.063	88 (17.4)	77 (15.2)	0.059
antibiotic	1075 (58.6)	549 (89.4)	0.75	438 (86.6)	441 (87.2)	0.018
Vasoactive drugs	513 (28)	398 (64.8)	0.795	294 (58.1)	295 (58.3)	0.004
Comorbidities						
Myocardial infarct, n (%)	441 (24)	154 (25.1)	0.024	127 (25.1)	127 (25.1)	<0.001
Congestive heart failure, n (%)	862 (47)	226 (36.8)	0.208	204 (40.3)	199 (39.3)	0.02
Peripheral vascular disease, n (%)	313 (17.1)	106 (17.3)	0.005	82 (16.2)	86 (17)	0.021
Cerebrovascular disease, n (%)	282 (15.4)	93 (15.1)	0.006	88 (17.4)	82 (16.2)	0.032
Chronic pulmonary disease, n (%)	500 (27.3)	151 (24.6)	0.061	115 (22.7)	128 (25.3)	0.06
Rheumatic disease, n (%)	82 (4.5)	22 (3.6)	0.045	21 (4.2)	19 (3.8)	0.02
Peptic ulcer disease, n (%)	64 (3.5)	9 (1.5)	0.13	7 (1.4)	8 (1.6)	0.016
Diabetes, n (%)	799 (43.6)	233 (37.9)	0.115	202 (39.9)	202 (39.9)	<0.001
Renal disease, n (%)	973 (53.1)	244 (39.7)	0.269	222 (43.9)	219 (43.3)	0.012
Liver disease, n (%)	175 (9.5)	37 (6)	0.132	32 (6.3)	36 (7.1)	0.032
Vital signs						
Heart rate	81.4 ± 15.2	82.4 ± 13.4	0.069	82.4 ± 14.6	82.6 ± 13.9	0.019
SBP, mmHg	121.3 ± 17.1	116.0 ± 13.9	0.335	117.3 ± 15.5	116.8 ± 14.4	0.036

(Continued on following page)

TABLE 1 (*Continued*) Baseline characteristics before and after propensity score matching.

Variables	Entire cohort (n = 2448)		SMD	PSM cohort (n = 1012)		SMD
	No-APAP (n = 1834)	APAP (n = 614)		No-APAP (n = 506)	APAP (n = 506)	
DBP, mmHg	62.4 ± 11.3	59.2 ± 9.6	0.314	59.3 ± 9.6	59.6 ± 9.9	0.026
Respiratory rate	19.3 ± 3.6	18.7 ± 3.1	0.186	18.7 ± 3.5	18.9 ± 3.2	0.066
Temperature (°C)	36.7 ± 0.5	36.8 ± 0.5	0.176	36.8 ± 0.5	36.8 ± 0.5	0.005
Spo2	96.6 ± 2.2	97.2 ± 1.9	0.291	97.2 ± 1.7	97.1 ± 2.0	0.059
Scoring systems						
SOFA	4.0 (2.0, 6.0)	6.0 (4.0, 8.0)	0.458	6.0 (4.0, 8.0)	6.0 (4.0, 8.0)	0.029
Outcome						
In-hospital mortality, n (%)	160 (8.7)	55 (9)		61 (12.1)	49 (9.7)	
LOS hospital, days	7.0 (4.3, 11.4)	8.7 (6.1, 13.9)		8.6 (5.3, 13.0)	8.7 (6.1, 14.2)	
30-day mortality, n (%)	229 (12.5)	66 (10.7)		72 (14.2)	63 (12.5)	
60-day mortality, (%)	312 (17)	84 (13.7)		98 (19.4)	77 (15.2)	
Hypertensive emergencie, (%)	309 (16.8)	111 (18.1)		99 (19.6)	96 (19)	

APAP, acetaminophen; SMD, standardised mean difference.

2018). A survey found that among the 3.9% of surveyed individuals with gout, 74% had hypertension (Zhu et al., 2012).

Acetaminophen (also known as paracetamol) is widely used worldwide, it has a spectrum of action similar to that of NSAIDs and resembles particularly the COX-2 selective inhibitors (Graham et al., 2013). Due to its weak anti-inflammatory activity (Graham et al., 2013), acetaminophen is usually not recommended as the main treatment for gout (Richette et al., 2017; FitzGerald et al., 2020; Richette et al., 2020; Neilson et al., 2022), but some gout patients may need it to relieve pain or reduce fever when taking other gout medications. Acetaminophen is often preferred because it is generally well tolerated and considered safer than other analgesics (Graham et al., 2013; Alchin et al., 2022), especially previous researches have shown that NSAIDs increase cardiovascular risk (McGettigan and Henry, 2011; Coxib and traditional NSAID Trialists' CNT Collaboration et al., 2013). The guideline of the American Heart Association recommends the use of acetaminophen in hypertension patients with pain (Whelton et al., 2018). However, and recent research reports that acetaminophen increases hypertension (Dawson et al., 2013; Benitez-Camps et al., 2018; MacIntyre et al., 2022), and increases the risk of cardiovascular adverse consequences (Zeng et al., 2022). Meanwhile, another multicenter cohort study targeting the ICU population showed that half of patients receiving intravenous injection of acetaminophen experienced hypotension, and up to one-third of observed episodes required therapeutic intervention (Cantais et al., 2016). There has been no further research evaluating the impact of acetaminophen on the mortality of critically ill patients with gout and hypertension. The aim of this study was to investigate the actual use of acetaminophen in gout patients with hypertension admitted to ICU, and further evaluates the impact of acetaminophen use on mortality in this patient population.

2 Methods

2.1 Data source

This study was a retrospective cohort study based on the MIMIC-IV database (Johnson and Bulgarelli, 2024). MIMIC-IV is a publicly available database sourced from the electronic health record of the Beth Israel Deaconess Medical Center and record dataset covering a decade of admissions between 2008 and 2019. The Institutional Review Board at the Beth Israel Deaconess Medical Center granted a waiver of informed consent and approved the sharing of the research resource. Author Yi passed the online training courses and exams (certification number: 59888607). MIMIC-IV establishes a modular organization of the constituent data allowing linking of the database to external departments and distinct modalities of data which allowed us to explore the availability of out-of-hospital mortality.

2.2 Study population

Patients whose diagnostic description included both "Gout" and "Hypertension" were enrolled in the study. A total of 16086 hospitalization records of patients with Gout and hypertension were collected in the MIMIC-IV database. We excluded patients who were under 18 years of age, were not admitted to the ICU, or had an ICU stay of less than 24 h. If the patient had multiple ICU admissions, only the first ICU admission was analysed.

TABLE 2 Analysis of the impact of potential confounders of in-hospital mortality association.

	HR (95% CI)	P (Wald's test)
Age	1.04 (1.02,1.06)	<0.001
Male	0.94 (0.62,1.45)	0.792
White	0.7 (0.48,1.03)	0.068
BMI	0.97 (0.94,0.99)	0.015
WBC	1.01 (1,1.02)	0.001
Platelet	0.9994 (0.9972,1.0015)	0.557
ALT	1.0005 (0.9999,1.0012)	0.131
AST	1.0003 (1,1.0006)	0.091
Serum creatinine	1.14 (1.04,1.25)	0.003
Serum glucose	1.0029 (0.9998,1.0059)	0.063
βblocker	0.35 (0.22,0.56)	<0.001
ACEI	0.53 (0.32,0.87)	0.013
ARB	0.05 (0.01,0.34)	0.002
CCB	0.52 (0.33,0.79)	0.003
Diuretics	0.61 (0.38,0.96)	0.034
Colchicine	0.42 (0.2,0.87)	0.019
NSAIDs	0.43 (0.11,1.75)	0.238
Glucocorticoids	1.02 (0.65,1.59)	0.936
antibiotic	0.95 (0.53,1.69)	0.852
Vasoactive drugs	1.64 (1.09,2.48)	0.018
Myocardial infarct	1.15 (0.76,1.74)	0.513
Congestive heart failure	1.53 (1.04,2.24)	0.031
Peripheral vascular disease	0.73 (0.42,1.29)	0.28
Cerebrovascular disease	1.23 (0.79,1.91)	0.357
Chronic pulmonary disease	0.54 (0.33,0.9)	0.018
Rheumatic disease	1.04 (0.42,2.55)	0.937
Peptic ulcer disease	0.66 (0.16,2.7)	0.568
Diabetes	0.8 (0.55,1.19)	0.272
Renal disease	1.36 (0.94,1.99)	0.106
Liver disease	1.68 (0.99,2.84)	0.053
Heart rate	1.01 (1,1.02)	0.078
SBP	0.97 (0.96,0.98)	<0.001
DBP	0.98 (0.96,1)	0.021
Respiratory rate	1.1 (1.04,1.15)	<0.001
Temperature	0.92 (0.64,1.34)	0.668
Spo2	0.95 (0.88,1.03)	0.245
SOFA	1.14 (1.08,1.19)	<0.001
APAP	0.67 (0.46,0.98)	0.041

2.3 Exposure and outcomes

The exposure of interest was the use of acetaminophen during the ICU stay, without any restrictions. Acetaminophen use was extracted from the prescriptions table. The primary outcome was in-hospital mortality. Secondary outcomes included 30-day all-cause mortality, 60-day all-cause mortality, and length of stay at the hospital (LOS), and incidence of hypertensive emergencies. According to the guidelines of the ESC Hypertension Committee (van den Born et al., 2019), we consider the occurrence of systolic blood pressure >200 mmHg or diastolic blood pressure >120 mmHg during ICU hospitalization as hypertensive emergencies.

2.4 Data extraction

Baseline variables for the first 24 h of ICU admission were gathered from the MIMIC-IV database. Patient characteristics, including age, gender, race, and BMI, were collected. We extracted information on concomitant medications, including β-blockers, angiotensin-converting enzyme inhibitors (ACEI), angiotensin receptor blockers (ARB), calcium channel blockers (CCB), diuretics, colchicine, NSAIDs, glucocorticoids, antibiotics and Vasoactive drugs. We extracted information on comorbidities, such as myocardial infarction, congestive heart failure, peripheral vascular disease, cerebrovascular disease, chronic pulmonary disease, rheumatic disease, peptic ulcer disease, diabetes, renal disease, malignant cancer, and liver disease. The following variables were extracted, and for variables with multiple measured values, calculate the average value within 24 h to reduce the impact of their variation: systolic blood pressure (SBP), diastolic blood pressure (DBP), heart rate, respiratory rate, temperature, pulse oxygen saturation (SpO2), sequential organ failure assessment (SOFA), WBC, platelet, ALT, AST, serum creatinine, and serum glucose.

2.5 Statistical analysis

The study cohort was divided into two groups: those who received acetaminophen (APAP group) and those who did not (no-APAP group). A patient with a serum glucose value of 143054 and 171 patients with a BMI greater than 100 or less than 10 were considered as outliers. Multiple imputation was used to estimate missing values for each variable in our study (Sterne et al., 2009; Mackinnon, 2010). Mean (standard deviation [SD]) and median (interquartile range [IQR]) should be used for description of normally and non-normally distributed data, respectively (Habibzadeh, 2017). Categorical variables were presented as counts and percentages, which compared by Pearson's chi-squared test. We used propensity score matching (PSM) to adjust variables according to the recommendations in the literature (Lonjon et al., 2017). The matching was constructed based on a 1:1 ratio using the nearest neighbour method with a calliper width of 0.05 without replacement. The balance of variables between the groups before and after matching was assessed using standardised mean difference (SMD), with a value of less than

TABLE 3 Multivariable Cox regression analysis for mortality.

Categories	Model I		Model II		Model III	
	HR (95% CI)	*p*-value	HR (95% CI)	*p*-value	HR (95% CI)	*p*-value
primary outcome						
In-hospital mortality						
Entire cohort (APAP)	0.73 (0.54–0.99)	0.044	0.74 (0.54–1.01)	0.062	0.62 (0.45–0.86)	0.005
PSM cohort (APAP)	0.67 (0.46–0.98)	0.041	0.66 (0.45–0.96)	0.03	0.62 (0.41–0.92)	0.018
second outcome						
30-day mortality						
Entire cohort (APAP)	0.85 (0.65–1.12)	0.258	0.96 (0.73–1.27)	0.77	0.78 (0.58–1.05)	0.103
PSM cohort (APAP)	0.87 (0.62–1.22)	0.407	0.9 (0.64–1.26)	0.542	0.78 (0.55–1.11)	0.175
60-day mortality						
Entire cohort (APAP)	0.79 (0.62–1.01)	0.06	0.88 (0.69–1.13)	0.317	0.72 (0.55–0.94)	0.014
PSM cohort (APAP)	0.77 (0.57–1.04)	0.093	0.81 (0.6–1.09)	0.159	0.75 (0.55–1.02)	0.069
Hypertensive emergencies						
Entire cohort (APAP)	0.73 (0.58–0.9)	0.004	0.72 (0.58–0.9)	0.004	0.81 (0.64–1.03)	0.081
PSM cohort (APAP)	0.76 (0.57–1.01)	0.058	0.71 (0.54–0.95)	0.022	0.68 (0.5–0.92)	0.013

Model I: did not adjust any variables.
Model II: adjusted for age, gender, race, BMI.
Model III: adjusted for model II, covariates, βblocker, ACEI, ARB, CCB, diuretics, colchicine, vasoactive drugs, congestive heart failure, chronic pulmonary disease, SBP, DBP, respiratory rate; WBC, serum creatinine, SOFA.

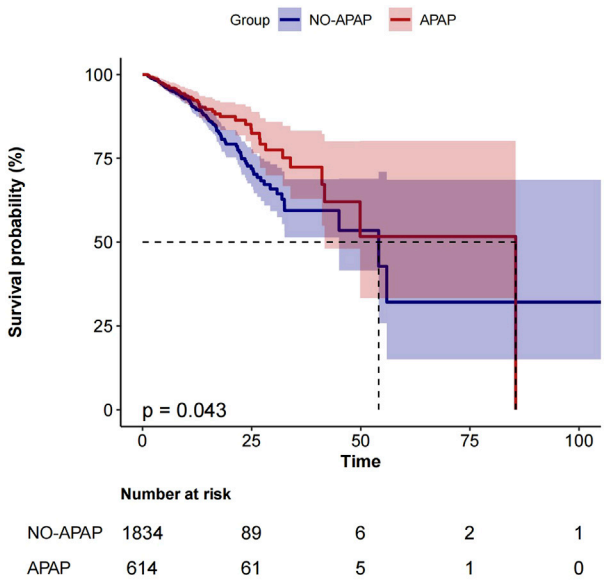

FIGURE 2
Kaplan–Meier curve for in-hospital mortality according to APAP use in the entire cohort.

0.10 indicating balance (Austin, 2009). Univariate analyses were used to explore the variables associated with death. Statistically significant variables ($p < 0.05$) were brought into multivariate analysis as covariates for further analysis. Multivariate Cox regression analyses with results expressed as hazard ratios (HR) with 95% CI were used to assess the relationship between acetaminophen and mortality. Three multivariate models were used. Cumulative incidence of in-hospital mortality was analysed with the Kaplan-Meier method and evaluated by the log-rank test. Subgroup analyses were performed for the PSM cohort based on age, sex, race, BMI, liver disease, and kidney disease.

All the analyses were performed with the statistical software packages R (http://www.R-project.org, The R Foundation) and Free Statistics software versions 1.9.

3 Results

3.1 Patient selection

The initial search from the MIMIC-IV database identified 16086 patients with gout and hypertension. 3953 cases were admitted to the ICU. The final study population consisted of 2448 patients, with 614 using acetaminophen and 1834 not using it. This population retained their first stay in the ICU, excluding patients under 18 years old and those who had been in the ICU for less than 24 h (Figure 1).

3.2 Baseline characteristics

Table 1 shows the baseline characteristics before and after matching. In the entire cohort, patients who received acetaminophen tended to be younger (see additional file: Supplementary Table S2). Patients who received treatment with acetaminophen upon admission

TABLE 4 Multivariable Cox regression analysis of daily dose on in-hospital mortality rate.

Daily dose(g)	n.total	n.event_%	crude.HR (95%CI)	crude.*p*-value	adj.HR (95%CI)	adj.*p*-value
Entire cohort (APAP)						
Not used	1834	160 (8.7)	1(Ref)		1(Ref)	
≤2 g	427	41 (9.6)	0.86 (0.61–1.22)	0.403	0.7 (0.49–1.01)	0.058
2~4 g	182	14 (7.7)	0.52 (0.3–0.89)	0.018	0.47 (0.26–0.83)	0.01
>4 g	5	0 (0)	0 (0~Inf)	0.99	0 (0~Inf)	0.994
P for trend	2448	215 (8.8)	0.75 (0.61–0.94)	0.012	0.69 (0.54–0.87)	0.002
PSM cohort (APAP)						
Not used	506	61 (12.1)	1(Ref)		1(Ref)	
≤2 g	355	37 (10.4)	0.78 (0.52–1.18)	0.24	0.7 (0.45–1.08)	0.107
2~4 g	146	12 (8.2)	0.49 (0.26–0.92)	0.025	0.47 (0.25–0.9)	0.023
>4 g	5	0 (0)	0 (0~Inf)	0.993	0 (0~Inf)	0.994
P for trend	1012	110 (10.9)	0.71 (0.54–0.93)	0.012	0.68 (0.51–0.91)	0.009

Adj: adjusted for age, gender, race, BMI, β-blocker, ACEI, ARB, CCB, diuretics, colchicine, vasoactive drugs, congestive heart failure, chronic pulmonary disease, SBP, DBP, respiratory rate; WBC, serum creatinine, SOFA.

TABLE 5 Multivariable Cox regression analysis of in-hospital mortality rate using APAP treatment course.

Course of treatment (day)	n.total	n.Event_%	crude.HR (95%CI)	crude.*p*-value	adj.HR (95%CI)	adj.*p*-value
Entire cohort (APAP)						
Not used	1834	160 (8.7)	1(Ref)		1(Ref)	
≤3d	538	47 (8.7)	0.84 (0.6–1.16)	0.279	0.74 (0.53–1.04)	0.088
3~5d	49	4 (8.2)	0.4 (0.15–1.08)	0.072	0.25 (0.09–0.7)	0.009
>5d	27	4 (14.8)	0.42 (0.15–1.13)	0.087	0.33 (0.12–0.93)	0.035
P for trend	2448	215 (8.8)	0.75 (0.61–0.94)	0.011	0.66 (0.53–0.84)	0.001
PSM cohort (APAP)						
Not used	506	61 (12.1)	1(Ref)		1(Ref)	
≤3d	453	44 (9.7)	0.76 (0.52–1.12)	0.169	0.71 (0.47–1.07)	0.101
3~5d	35	2 (5.7)	0.24 (0.06–0.97)	0.045	0.17 (0.04–0.75)	0.019
>5d	18	3 (16.7)	0.44 (0.14–1.42)	0.17	0.39 (0.11–1.34)	0.135
P for trend	1012	110 (10.9)	0.7 (0.53–0.93)	0.013	0.65 (0.48–0.88)	0.005

Adj: adjusted for age, gender, race, BMI, β-blocker, ACEI, ARB, CCB, diuretics, colchicine, vasoactive drugs, congestive heart failure, chronic pulmonary disease, SBP, DBP, respiratory rate; WBC, serum creatinine, SOFA.

had a higher WBC, a lower platelet, and a lower serum glucose value (see additional file: Supplementary Table S2). In terms of vital signs, compared to the no-APAP group, the APAP group had higher body temperature and SOFA scores, while SBP and DBP were lower. Patients receiving acetaminophen treatment have fewer comorbidities but more concomitant medications, especially the proportion of antibiotics and vasoactive drugs used, which was significantly higher in the APAP group. (see additional file: Supplementary Table S2). In general, patients in the APAP group were likely more severe.

After PSM, 1012 patients were enrolled, with 506 patients receiving acetaminophen treatment matched to 506 patients who did not receive acetaminophen treatment. The SMD of all variables was<0.1, indicating a similar distribution of baseline variables between the two groups (Table 1).

3.3 Relationship between acetaminophen and mortality rate

The overall in-hospital mortality was 8.8% (215/2448). The in-hospital mortality of the APAP group was 9% (55/614), compared with 8.7% (160/1834) for the no-APAP group in Table 1.

In the multivariate Cox regression analysis, we adjusted three models, which included covariates that showed significant

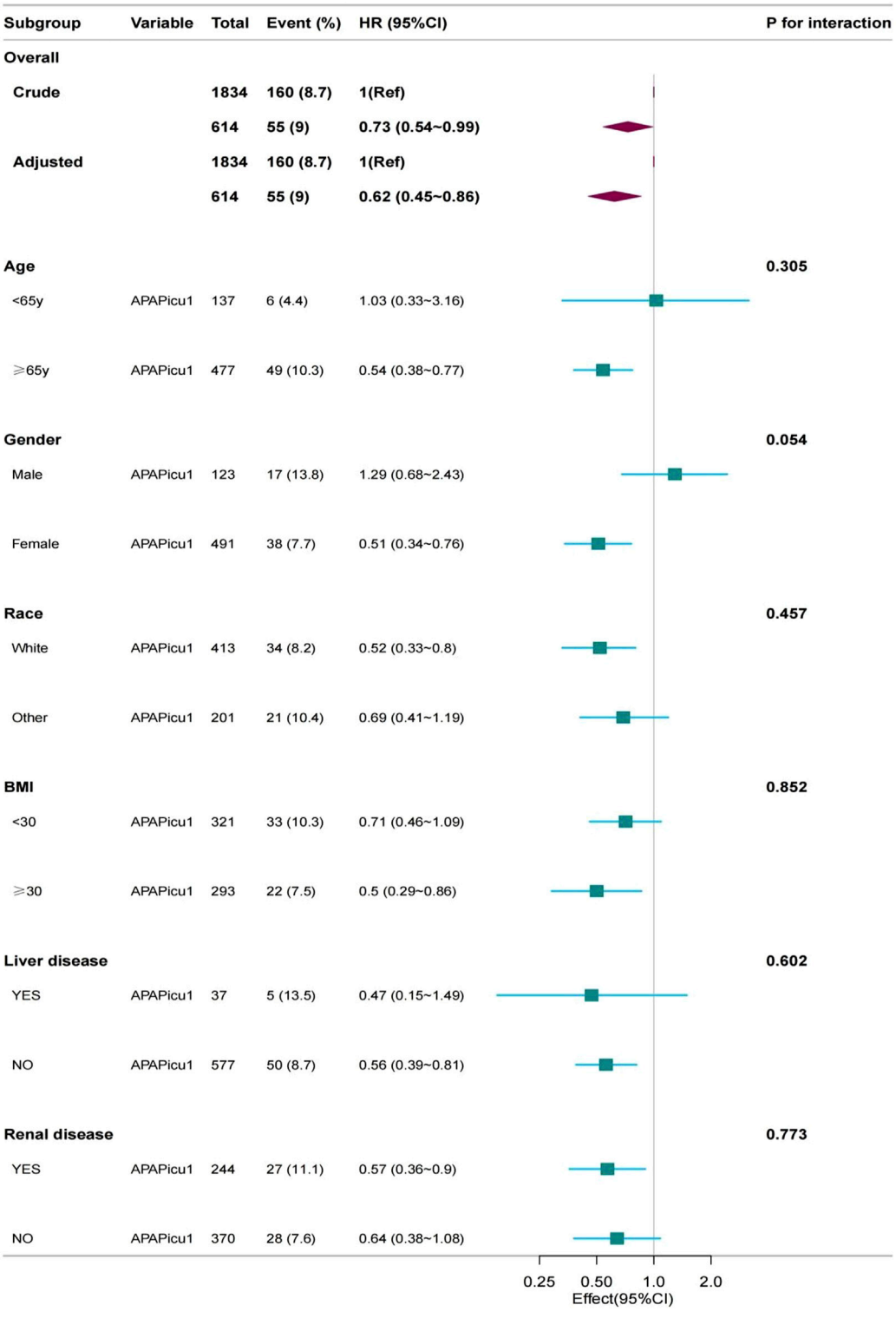

FIGURE 3
Subgroup analyses for in-hospital mortality. The multivariable Cox proportional hazards model was adjusted for βblocker, ACEI, ARB, CCB, diuretics, colchicine, vasoactive drugs, congestive heart failure, chronic pulmonary disease, SBP, DBP, respiratory rate, WBC, serum creatinine, SOFA. CI, confidence interval; HR, hazard ratio; APAPicu1, acetaminophen was used in the ICU.

differences (P < 0.05) in the univariate analysis. Compared with patients who were not administered APAP, patients who received APAP during ICU stay were associated with a 33% decrease in the risk of in-hospital mortality in the unadjusted model (HR, 0.67; 95% CI, 0.46–0.98; P = 0.041) (Table2). After adjusting for confounding factors, the HR for APAP administration in the multivariate analysis was 0.62 (95% CI, 0.45–0.86; p = 0.005) (Table3). The results of the IPTW (HR: 0.67%, 95% CI 0.5–0.91, p = 0.048) and PSM (HR:

0.62%, 95% CI 0.41–0.92, p = 0.018) models demonstrated a significant beneficial effect of APAP use on in-hospital mortality among ICU patients (see additional file: Supplementary Table S3). At the same time, there was a significant difference in the reduction of hypertensive emergencies in the acetaminophen group (HR: 0.68%, 95% CI 0.5–0.92; p = 0.013) (Table 3). In terms of secondary endpoints, after PSM, in the multivariate Cox regression analysis, there was no statistically significant difference for both 30-day and 60-day all-cause mortality reductions in the acetaminophen use group, and HRs were 0.78 (95% CI 0.55–1.11; p = 0.175) and 0.75 (95% CI 0.55–1.02; p = 0.069), respectively (Table 3). Another secondary endpoint showed a correlation between acetaminophen use and prolonged hospital stay in the multivariate analysis. (see additional file: Supplementary Table S4).

Figure 2 shows the Kaplan-Meier curve for in-hospital mortality according to acetaminophen use in the entire cohort.

We analyzed the effect of APAP dosage on in-hospital mortality, and divided the daily dose into three groups: ≤2 g, 2 g ~ 4 g and >4 g.The results showed that in the entire cohort (HR, 0.47; 95% CI, 0.26–0.83; p = 0.01) and PSM cohort (HR, 0.47; 95% CI, 0.25–0.9; p = 0.023), the use of 2–4 g doses of acetaminophen can reduce in-hospital mortality, with statistical differences (Table 4). In addition, we analyzed the impact of APAP treatment duration on in-hospital mortality, dividing treatment duration into three groups: ≤3 days, 3–5 days, and>5 days. In the entire cohort (HR, 0.25; 95% CI, 0.09–0.7; p = 0.009) and the post PSM cohort (HR, 0.17; 95% CI: 0.04–0.75; p = 0.019), treatment with acetaminophen for 3–5 days reduced in-hospital mortality with statistical differences (Table 5).

3.4 Subgroup analyses

A subgroup analysis was performed on the PSM cohort. We used age (<65, ≥65 years), gender (female, male), race (white, other, BMI (<30, ≥30), liver disease, and renal disease as stratification variables to observe the effect values and generate a forest plot of data (Figure 3).We did not observe any significant interactions in all subgroups (p-values of interactions were>0.05). Subgroup analysis showed that the relationship remained robust and reliable.

4 Discussion

Our study shows that acetaminophen administration is associated with lower in-hospital mortality in ICU patients with gout and hypertension. Even after adjusting for risk factors and applying Cox regression, these results still maintain their strength. The association between acetaminophen use and mortality was broadly consistent across subgroups. The use of acetaminophen is associated with prolonged hospital stay, possibly due to the fact that patients in the acetaminophen group have a relatively more severe initial condition and may have longer hospital stays, resulting in a higher probability of using acetaminophen. The use of acetaminophen reduced all-cause mortality by 30 and 60 days, but there was no significant difference, possibly because 75% of patients in both groups had a total hospital stay within 15 days. Therefore, we believe that the use of acetaminophen in the acute phase has greater benefits. Currently, there are no studies on the impact of acetaminophen use on mortality in ICU populations with gout and hypertension.

There is limited research on acetaminophen in adult ICU patients, and previous studies mainly focused on sepsis patients (Selladurai et al., 2011; Sun et al., 2024). In our study, patients with gout and hypertension who used acetaminophen during ICU stays were included. The usage rate of acetaminophen in this study was 33.5%, which is lower than previous studies (approximately 58%–70%) (Selladurai et al., 2011; Niven et al., 2013), and is related to differences in the study population, as most sepsis patients have fever and higher usage rates. It is worth noting that the use of colchicine and glucocorticoids in the combined medication information of the two groups in the entire queue is significantly higher than that of NSAIDs, and the use of these two types of drugs in the APAP group is relatively lower than that in the no-APAP group. It may be generally believed that acetaminophen is safer, and doctors are more inclined to choose this drug when combined with hypertension. In addition, throughout the entire queue, during the ICU period, the proportion of antibacterial and vasoactive drugs used in the APAP group was significantly higher than that in the non APAP group, possibly due to the poorer general condition of patients in the APAP group. In this study, we corrected for bias caused by factors such as the above and analyzed in-hospital mortality after PSM.

The analgesic and antipyretic effects of acetaminophen are well-established, but the underlying mechanisms of its potential protective effect on mortality are not fully understood. The analgesic and antipyretic effects of acetaminophen are due to its selective action on cyclooxygenase in the central and peripheral nervous system, which inhibits the conversion of arachidonic acid into prostaglandins, thromboxanes, and prostacyclins (Warner and Mitchell, 2004). Acetaminophen reinforces descending inhibitory pain pathways (Pickering et al., 2008), and a study has confirmed that the analgesic mechanism of acetaminophen may involve the serotonin system (Pickering et al., 2006), while the anti-inflammatory activity is very weak, and the guidelines do not specify the use of acetaminophen for gout patients. Glucocorticoid is the first-line treatment recommended by the guidelines, but long-term high-dose use of glucocorticoid has many side effects (such as Cushing's syndrome, osteoporosis, diabetes and hypertension). Some studies suggest that moderate doses of oral prednisolone plus oral acetaminophen should be used as the first-line treatment for acute gout (Man et al., 2007). Compared with NSAIDs, acetaminophen has higher overall gastrointestinal safety (Hinz et al., 2008). Our study corrected the influencing factors of patients with concomitant peptic ulcer disease.

Acetaminophen is an effective and specific blood protein reducing agent that can block cell-free hemoglobin induced lipid and other substrate oxidation, reducing oxidative damage (Boutaud et al., 2010; Boutaud and Roberts, 2011). Cell-free hemoglobin is an important new predictive factor for survival in patients with severe sepsis and ARDS (40, 41), as it increases inflammation, pulmonary edema, and microvascular permeability (Adamzik et al., 2012; Shaver et al., 2017; Kerchberger et al., 2019; Meegan et al., 2020), and its elevated plasma concentration has been also identified as an independent risk factor for AKI(44) (Graw et al., 2022). This may be one of the reasons for the reduced in-hospital mortality rate in critically ill patients with gout and hypertension in this study.

Because after PSM, nearly 90% of the two groups of patients were treated with antibiotics and nearly 60% were treated with vasoactive drugs, there is a higher possibility of sepsis or septic shock in the ICU. The use of APAP weakened the oxidative damage of acellular hemoglobin, thus reducing hospitalization mortality. In addition, acetaminophen can inhibit other peroxidase including myeloperoxidase, reduce the formation of halogenated oxidants (such as hypochlorite and hypobromous acid), and may slow down the development of atherosclerosis and other diseases (Graham et al., 2013).

COXs are highly expressed in renal structures related to volume and pressure control, including cortical and medullary collecting ducts, mesangial cells and dense plaques, as well as medullary interstitial cells in the glomerular vascular system (Francois and Coffman, 2004; Hao and Breyer, 2008). NSAIDs induce hypertension, sodium retention and edema by inhibiting COXs in the kidney (Grosser et al., 2017). There is a similar mechanism for acetaminophen, although its inhibitory activity is weaker compared to NSAIDs. Research reports indicate that acetaminophen, like most other NSAIDs, increases blood pressure. A retrospective observational study reported that among 2754 hypertensive patients treated with acetaminophen, there was a slight increase in blood pressure during treatment with acetaminophen, while the antihypertensive treatment regimen remained unchanged (Dawson et al., 2013). A double-blind, crossover study targeting hypertensive patients with osteoarthritis showed that both acetaminophen and naproxen can have varying degrees of impact on the treatment of hypertension with ramipril, valsartan, or aligilem (Gualtierotti et al., 2013). A double-blind, placebo-controlled, crossover study published in 2022 showed that administering 4 g of Acetaminophen to 110 hypertensive patients for 14 consecutive days increased systolic blood pressure by 4.7 mmHg compared to placebo (MacIntyre et al., 2022). Existing research supports the long-term and regular use of acetaminophen to have an impact on blood pressure. However, perhaps the most important is whether these BP effects translate to increased cardiovascular risk (Smith and Cooper-DeHoff, 2022). There is not enough high-quality data to evaluate the cardiovascular risk of acetaminophen. In a large number of hypertensive patients, the use of acetaminophen is not associated with an increased risk of myocardial infarction or stroke (Fulton et al., 2015). Our study included a critically ill population diagnosed with gout and hypertension, with the primary endpoint set as in-hospital mortality, which better reflects the safety of acetaminophen in this population and suggests a reduction in in-hospital mortality. In addition, we further analyzed the effects of the dosage and duration of acetaminophen on in-hospital mortality and the occurrence of hypertension emergencies. Based on our research results, using a daily dosage range of 2–4 g acetaminophen and a short course of 3–5 days resulted in greater benefits than risks.

4.1 Study limitations

The current study has several key limitations. Firstly, because of its retrospective observational design, the results are subject to residual bias and unmeasured confounders despite propensity score matching and multivariable analyses. Secondly, the cause-effect relationship could not be established. Thirdly, due to the significant absence of serum uric acid values and the lack of information related to febuxostat, allopurinol, and benzbromarone, the impact of blood uric acid was not analyzed. Finally, the population we included in the study was predominantly white individuals, and further observations of other populations are needed in the future.

5 Conclusion

Acetaminophen use was associated with lower in-hospital mortality in critically ill patients with gout and hypertension. Prospective studies are needed to verify this retrospective finding.

Data availability statement

The original contributions presented in the study are included in the article/Supplementary Material, further inquiries can be directed to the corresponding authors.

Ethics statement

The studies involving humans were approved by the Institutional Review Board at the Beth Israel Deaconess Medical Center granted a waiver of informed consent and approved the sharing of the research resource. Author Yi passed the online training courses and exams (certification number: 59888607). The studies were conducted in accordance with the local legislation and institutional requirements. Written informed consent for participation was not required from the participants or the participants' legal guardians/next of kin in accordance with the national legislation and institutional requirements.

Author contributions

X-QY: Writing–review and editing, Writing–original draft, Conceptualization, Data curation, Formal Analysis, Investigation, Methodology, Project administration. BX: Conceptualization, Data curation, Formal Analysis, Investigation, Methodology, Project administration, Writing–original draft, Writing–review and editing. YH: Writing–review and editing, Data curation, Formal Analysis. T-JG: Data curation, Formal Analysis, Writing–review and editing. MC: Conceptualization, Data curation, Formal Analysis, Methodology, Project administration, Supervision, Writing–review and editing. X-JC: Conceptualization, Data curation, Formal Analysis, Investigation, Methodology, Project administration, Supervision, Validation, Writing–original draft, Writing–review and editing.

Funding

The author(s) declare that no financial support was received for the research, authorship, and/or publication of this article.

Conflict of interest

The authors declare that the research was conducted in the absence of any commercial or financial relationships that could be construed as a potential conflict of interest.

Publisher's note

All claims expressed in this article are solely those of the authors and do not necessarily represent those of their affiliated organizations, or those of the publisher, the editors and the reviewers. Any product that may be evaluated in this article, or claim that may be made by its manufacturer, is not guaranteed or endorsed by the publisher.

Supplementary material

The Supplementary Material for this article can be found online at: https://www.frontiersin.org/articles/10.3389/fphar.2024.1445975/full#supplementary-material

References

Adamzik, M., Hamburger, T., Petrat, F., Peters, J., de Groot, H., and Hartmann, M. (2012). Free hemoglobin concentration in severe sepsis: methods of measurement and prediction of outcome. *Crit. Care* 16, R125. doi:10.1186/cc11425

Alchin, J., Dhar, A., Siddiqui, K., and Christo, P. J. (2022). Why paracetamol (acetaminophen) is a suitable first choice for treating mild to moderate acute pain in adults with liver, kidney or cardiovascular disease, gastrointestinal disorders, asthma, or who are older. *Curr. Med. Res. Opin.* 38, 811–825. doi:10.1080/03007995.2022.2049551

Austin, P. C. (2009). Balance diagnostics for comparing the distribution of baseline covariates between treatment groups in propensity-score matched samples. *Stat. Med.* 28, 3083–3107. doi:10.1002/sim.3697

Benitez-Camps, M., Morros Padrós, R., Pera-Pujadas, H., Dalfó Baqué, A., Bayó Llibre, J., Rebagliato Nadal, O., et al. (2018). Effect of effervescent paracetamol on blood pressure: a crossover randomized clinical trial. *J. Hypertens.* 36, 1656–1662. doi:10.1097/HJH.0000000000001733

Boutaud, O., Moore, K. P., Reeder, B. J., Harry, D., Howie, A. J., Wang, S., et al. (2010). Acetaminophen inhibits hemoprotein-catalyzed lipid peroxidation and attenuates rhabdomyolysis-induced renal failure. *Proc. Natl. Acad. Sci. U S A.* 107, 2699–2704. doi:10.1073/pnas.0910174107

Boutaud, O., and Roberts, L. J. (2011). Mechanism-based therapeutic approaches to rhabdomyolysis-induced renal failure. *Free Radic. Biol. Med.* 51, 1062–1067. doi:10.1016/j.freeradbiomed.2010.10.704

Cantais, A., Schnell, D., Vincent, F., Hammouda, Z., Perinel, S., Balichard, S., et al. (2016). Acetaminophen-induced Changes in systemic blood pressure in critically ill patients: results of a multicenter cohort study. *Crit. Care Med.* 44, 2192–2198. doi:10.1097/CCM.0000000000001954

Coxib and traditional NSAID Trialists' (CNT) Collaboration, Bhala, N., Emberson, J., Merhi, A., Abramson, S., Arber, N., Baron, J. A., et al. (2013). Vascular and upper gastrointestinal effects of non-steroidal anti-inflammatory drugs: meta-analyses of individual participant data from randomised trials. *Lancet* 382, 769–779. doi:10.1016/S0140-6736(13)60900-9

Danve, A., Sehra, S. T., and Neogi, T. (2021). Role of diet in hyperuricemia and gout. *Best. Pract. Res. Clin. Rheumatol.* 35, 101723. doi:10.1016/j.berh.2021.101723

Dawson, J., Fulton, R., McInnes, G. T., Morton, R., Morrison, D., Padmanabhan, S., et al. (2013). Acetaminophen use and change in blood pressure in a hypertensive population. *J. Hypertens.* 31, 1485–1490. ; discussion 1490. doi:10.1097/HJH.0b013e328360f6f8

Dehlin, M., Jacobsson, L., and Roddy, E. (2020). Global epidemiology of gout: prevalence, incidence, treatment patterns and risk factors. *Nat. Rev. Rheumatol.* 16, 380–390. doi:10.1038/s41584-020-0441-1

Evans, P. L., Prior, J. A., Belcher, J., Mallen, C. D., Hay, C. A., and Roddy, E. (2018). Obesity, hypertension and diuretic use as risk factors for incident gout: a systematic review and meta-analysis of cohort studies. *Arthritis Res. Ther.* 20, 136. doi:10.1186/s13075-018-1612-1

FitzGerald, J. D., Dalbeth, N., Mikuls, T., Brignardello-Petersen, R., Guyatt, G., Abeles, A. M., et al. (2020). 2020 American college of rheumatology guideline for the management of gout. *Arthritis & Rheumatology* 72, 879–895. doi:10.1002/art.41247

Francois, H., and Coffman, T. M. (2004). Prostanoids and blood pressure: which way is up? *J. Clin. Invest* 114, 757–759. doi:10.1172/JCI22929

Fulton, R. L., Walters, M. R., Morton, R., Touyz, R. M., Dominiczak, A. F., Morrison, D. S., et al. (2015). Acetaminophen use and risk of myocardial infarction and stroke in a hypertensive cohort. *Hypertension* 65, 1008–1014. doi:10.1161/HYPERTENSIONAHA.114.04945

Graham, G. G., Davies, M. J., Day, R. O., Mohamudally, A., and Scott, K. F. (2013). The modern pharmacology of paracetamol: therapeutic actions, mechanism of action, metabolism, toxicity and recent pharmacological findings. *Inflammopharmacology* 21, 201–232. doi:10.1007/s10787-013-0172-x

Graw, J. A., Hildebrandt, P., Krannich, A., Balzer, F., Spies, C., Francis, R. C., et al. (2022). The role of cell-free hemoglobin and haptoglobin in acute kidney injury in critically ill adults with ARDS and therapy with VV ECMO. *Crit. Care* 26, 50. doi:10.1186/s13054-022-03894-5

Grosser, T., Ricciotti, E., and FitzGerald, G. A. (2017). The cardiovascular pharmacology of nonsteroidal anti-inflammatory drugs. *Trends Pharmacol. Sci.* 38, 733–748. doi:10.1016/j.tips.2017.05.008

Gualtierotti, R., Zoppi, A., Mugellini, A., Derosa, G., D'Angelo, A., and Fogari, R. (2013). Effect of naproxen and acetaminophen on blood pressure lowering by ramipril, valsartan and aliskiren in hypertensive patients. *Expert Opin. Pharmacother.* 14, 1875–1884. doi:10.1517/14656566.2013.816286

Habibzadeh, F. (2017). Statistical data editing in scientific articles. *J. Korean Med. Sci.* 32, 1072–1076. doi:10.3346/jkms.2017.32.7.1072

Hao, C.-M., and Breyer, M. D. (2008). Physiological regulation of prostaglandins in the kidney. *Annu. Rev. Physiol.* 70, 357–377. doi:10.1146/annurev.physiol.70.113006.100614

Hinz, B., Cheremina, O., and Brune, K. (2008). Acetaminophen (paracetamol) is a selective cyclooxygenase-2 inhibitor in man. *FASEB J.* 22, 383–390. doi:10.1096/fj.07-8506com

Johnson, A. E. W., and Bulgarelli, L. (2024). *MIMIC-IV, a freely accessible electronic health record dataset*. Scientific Data. https://www.nature.com/articles/s41597-022-01899-x (Accessed April 11, 2024).

Kerchberger, V. E., Bastarache, J. A., Shaver, C. M., Nagata, H., McNeil, J. B., Landstreet, S. R., et al. (2019). Haptoglobin-2 variant increases susceptibility to acute respiratory distress syndrome during sepsis. *JCI Insight* 4, e131206. doi:10.1172/jci.insight.131206

Kuo, C.-F., Grainge, M. J., Mallen, C., Zhang, W., and Doherty, M. (2016). Comorbidities in patients with gout prior to and following diagnosis: case-control study. *Ann. Rheum. Dis.* 75, 210–217. doi:10.1136/annrheumdis-2014-206410

Kuwabara, M., Niwa, K., Hisatome, I., Nakagawa, T., Roncal-Jimenez, C. A., Andres-Hernando, A., et al. (2017). Asymptomatic hyperuricemia without comorbidities predicts cardiometabolic diseases: Five-Year Japanese cohort study. *Hypertension* 69, 1036–1044. doi:10.1161/HYPERTENSIONAHA.116.08998

Lonjon, G., Porcher, R., Ergina, P., Fouet, M., and Boutron, I. (2017). Potential pitfalls of reporting and bias in observational studies with propensity score analysis assessing a surgical procedure: a methodological systematic review. *Ann. Surg.* 265, 901–909. doi:10.1097/SLA.0000000000001797

MacIntyre, I. M., Turtle, E. J., Farrah, T. E., Graham, C., Dear, J. W., Webb, D. J., et al. and (2022). Regular acetaminophen use and blood pressure in people with hypertension: the PATH-BP trial. *Circulation* 145, 416–423. doi:10.1161/CIRCULATIONAHA.121.056015

Mackinnon, A. (2010). The use and reporting of multiple imputation in medical research - a review. *J. Intern Med.* 268, 586–593. doi:10.1111/j.1365-2796.2010.02274.x

Man, C. Y., Cheung, I. T. F., Cameron, P. A., and Rainer, T. H. (2007). Comparison of oral prednisolone/paracetamol and oral indomethacin/paracetamol combination therapy in the treatment of acute goutlike arthritis: a double-blind, randomized, controlled trial. *Ann. Emerg. Med.* 49, 670–677. doi:10.1016/j.annemergmed.2006.11.014

McGettigan, P., and Henry, D. (2011). Cardiovascular risk with non-steroidal anti-inflammatory drugs: systematic review of population-based controlled observational studies. *PLoS Med.* 8, e1001098. doi:10.1371/journal.pmed.1001098

Meegan, J. E., Shaver, C. M., Putz, N. D., Jesse, J. J., Landstreet, S. R., Lee, H. N. R., et al. (2020). Cell-free hemoglobin increases inflammation, lung apoptosis, and microvascular permeability in murine polymicrobial sepsis. *PLoS One* 15, e0228727. doi:10.1371/journal.pone.0228727

Neilson, J., Bonnon, A., Dickson, A., Roddy, E., and Guideline Committee (2022). Gout: diagnosis and management-summary of NICE guidance. *BMJ* 378, o1754. doi:10.1136/bmj.o1754

Niven, D. J., Stelfox, H. T., and Laupland, K. B. (2013). Antipyretic therapy in febrile critically ill adults: a systematic review and meta-analysis. *J. Crit. Care* 28, 303–310. doi:10.1016/j.jcrc.2012.09.009

Pickering, G., Estève, V., Loriot, M.-A., Eschalier, A., and Dubray, C. (2008). Acetaminophen reinforces descending inhibitory pain pathways. *Clin. Pharmacol. Ther.* 84, 47–51. doi:10.1038/sj.clpt.6100403

Pickering, G., Loriot, M.-A., Libert, F., Eschalier, A., Beaune, P., and Dubray, C. (2006). Analgesic effect of acetaminophen in humans: first evidence of a central serotonergic mechanism. *Clin. Pharmacol. Ther.* 79, 371–378. doi:10.1016/j.clpt.2005.12.307

Richette, P., Doherty, M., Pascual, E., Barskova, V., Becce, F., Castaneda, J., et al. (2020). 2018 updated European League against Rheumatism evidence-based recommendations for the diagnosis of gout. *Ann. Rheum. Dis.* 79, 31–38. doi:10.1136/annrheumdis-2019-215315

Richette, P., Doherty, M., Pascual, E., Barskova, V., Becce, F., Castañeda-Sanabria, J., et al. (2017). 2016 updated EULAR evidence-based recommendations for the management of gout. *Ann. Rheum. Dis.* 76, 29–42. doi:10.1136/annrheumdis-2016-209707

Sandoval-Plata, G., Nakafero, G., Chakravorty, M., Morgan, K., and Abhishek, A. (2021). Association between serum urate, gout and comorbidities: a case-control study using data from the UK Biobank. *Rheumatol. Oxf.* 60, 3243–3251. doi:10.1093/rheumatology/keaa773

Selladurai, S., Eastwood, G. M., Bailey, M., and Bellomo, R. (2011). Paracetamol therapy for septic critically ill patients: a retrospective observational study. *Crit. Care Resusc.* 13, 181–186. doi:10.1016/s1441-2772(23)01633-2

Shaver, C. M., Wickersham, N., McNeil, J. B., Nagata, H., Sills, G., Kuck, J. L., et al. (2017). Cell-free hemoglobin-mediated increases in vascular permeability. A novel mechanism of primary graft dysfunction and a new therapeutic target. *Ann. Am. Thorac. Soc.* 14, S251–S252. doi:10.1513/AnnalsATS.201609-693MG

Singh, J. A., and Gaffo, A. (2020). Gout epidemiology and comorbidities. *Seminars Arthritis Rheumatism* 50, S11–S16. doi:10.1016/j.semarthrit.2020.04.008

Smith, S. M., and Cooper-DeHoff, R. M. (2022). Acetaminophen-induced hypertension: where have all the "safe" analgesics gone? *Circulation* 145, 424–426. doi:10.1161/CIRCULATIONAHA.121.058068

Sterne, J. A. C., White, I. R., Carlin, J. B., Spratt, M., Royston, P., Kenward, M. G., et al. (2009). Multiple imputation for missing data in epidemiological and clinical research: potential and pitfalls. *BMJ* 338, b2393. doi:10.1136/bmj.b2393

Sun, S., Liu, H., Liang, Q., Yang, Y., Cao, X., and Zheng, B. (2024). Association between acetaminophen administration and clinical outcomes in patients with sepsis admitted to the ICU: a retrospective cohort study. *Front. Med. (Lausanne)* 11, 1346855. doi:10.3389/fmed.2024.1346855

van den Born, B.-J. H., Lip, G. Y. H., Brguljan-Hitij, J., Cremer, A., Segura, J., Morales, E., et al. (2019). ESC Council on hypertension position document on the management of hypertensive emergencies. *Eur. Heart J. Cardiovasc Pharmacother.* 5, 37–46. doi:10.1093/ehjcvp/pvy032

Warner, T. D., and Mitchell, J. A. (2004). Cyclooxygenases: new forms, new inhibitors, and lessons from the clinic. *FASEB J.* 18, 790–804. doi:10.1096/fj.03-0645rev

Whelton, P. K., Carey, R. M., Aronow, W. S., Casey, D. E., Collins, K. J., Dennison Himmelfarb, C., et al. (2018). 2017 ACC/AHA/AAPA/ABC/ACPM/AGS/APhA/ASH/ASPC/NMA/PCNA guideline for the prevention, detection, evaluation, and management of high blood pressure in adults: executive summary: a report of the American college of cardiology/American heart association task force on clinical practice guidelines. *Hypertension* 71, 1269–1324. doi:10.1161/HYP.0000000000000066

Zeng, C., Rosenberg, L., Li, X., Djousse, L., Wei, J., Lei, G., et al. (2022). Sodium-containing acetaminophen and cardiovascular outcomes in individuals with and without hypertension. *Eur. Heart J.* 43 (43), 1743–1755. doi:10.1093/eurheartj/ehac059

Zhu, Y., Pandya, B. J., and Choi, H. K. (2012). Comorbidities of gout and hyperuricemia in the US general population: NHANES 2007-2008. *Am. J. Med.* 125, 679–687.e1. doi:10.1016/j.amjmed.2011.09.033

frontiers | Frontiers in Physiology

TYPE Original Research
PUBLISHED 21 August 2024
DOI 10.3389/fphys.2024.1423989

OPEN ACCESS

EDITED BY
Sonia Michael Najjar,
Ohio University, United States

REVIEWED BY
Georgios A. Christou,
University of Ioannina, Greece
Hsiang-Chun Lee,
Kaohsiung Medical University, Taiwan

*CORRESPONDENCE
John M. Stafford,
john.stafford@vumc.org

RECEIVED 26 April 2024
ACCEPTED 29 July 2024
PUBLISHED 21 August 2024

CITATION
Zhu L, An J, Luu T, Reyna SM, Tantiwong P, Sriwijitkamol A, Musi N and Stafford JM (2024) Short-term HIIT impacts HDL function differently in lean, obese, and diabetic subjects. *Front. Physiol.* 15:1423989.
doi: 10.3389/fphys.2024.1423989

Short-term HIIT impacts HDL function differently in lean, obese, and diabetic subjects

Lin Zhu[1,2], Julia An[2], Thao Luu[2], Sara M. Reyna[3,4], Puntip Tantiwong[3], Apiradee Sriwijitkamol[3], Nicolas Musi[3,5] and John M. Stafford[1,2,6]*

[1]Tennessee Valley Health System, Veterans Affairs, Nashville, TN, United States, [2]Department of Medicine, Division of Diabetes, Endocrinology and Metabolism, Vanderbilt University Medical Center, Nashville, TN, United States, [3]Diabetes Division, University of Texas Health Science Center at San Antonio, San Antonio, TX, United States, [4]Division of Human Genetics, School of Medicine, The University of Texas at Rio Grande Valley, Edinburg, TX, United States, [5]Department of Medicine, Cedars-Sinai Medical Center, Los Angeles, CA, United States, [6]Department of Molecular Physiology and Biophysics, Vanderbilt University, Nashville, TN, United States

Introduction: High density lipoproteins (HDL) exert cardiovascular protection in part through their antioxidant capacity and cholesterol efflux function. Effects of exercise training on HDL function are yet to be well established, while impact on triacylglycerol (TG)-lowering has been often reported. We previously showed that a short-term high-intensity interval training (HIIT) program improves insulin sensitivity but does not inhibit inflammatory pathways in immune cells in insulin-resistant subjects. The purpose of this study is to evaluate HDL function along with changes of lipoproteins after the short-term HIIT program in lean, obese nondiabetic, and obese type 2 diabetic (T2DM) subjects.

Methods: All individuals underwent a supervised 15-day program of alternative HIIT for 40 minutes per day. VO_{2peak} was determined before and after this training program. A pre-training fasting blood sample was collected, and the post-training fasting blood sample collection was performed 36 hours after the last exercise session.

Results: Blood lipid profile and HDL function were analyzed before and after the HIIT program. Along with improved blood lipid profiles in obese and T2DM subjects, the HIIT program affected circulating apolipoprotein amounts differently. The HIIT program increased HDL-cholesterol levels and improved the cholesterol efflux capacity only in lean subjects. Furthermore, the HIIT program improved the antioxidant capacity of HDL in all subjects. Data from multiple logistic regression analysis showed that changes in HDL antioxidant capacity were inversely associated with changes in atherogenic lipids and changes in HDL-TG content.

Discussion: We show that a short-term HIIT program improves aspects of HDL function depending on metabolic contexts, which correlates with improvements in blood lipid profile. Our results demonstrate that TG content in HDL particles may play a negative role in the anti-atherogenic function of HDL.

KEYWORDS

HIIT exercise training, hyperlipidemia, HDL function, obese, antioxidant capacity, cholesterol efflux

1 Introduction

Heart disease is the leading cause of death worldwide, and coronary artery disease (CAD) is the most common type of heart disease (Tsao et al, 2023). Atherosclerosis is the fundamental cause of CAD, and insulin resistance, dyslipidemia, and chronic inflammation are risk factors that drive the initiation and progression of atherosclerosis. Lifestyles, including daily physical activity, diet, and smoking independently regulate the metabolic risk factors for atherosclerosis. Evidence from cross-sectional studies shows that CAD is delayed in athletes compared to general populations, and CAD risk is lower in physically active than in sedentary individuals (Lee et al., 2012). However, the mechanisms for CAD protective effects of exercise training are not yet well established.

Dyslipidemia comprises multiple aspects, including hyperlipidemia, high lipid content in atherogenic lipoprotein particles (i.e., VLDL and LDL), and low HDL-cholesterol (HDL-C) levels. Regular exercise training improves hyperglycemia and hyperlipidemia by increasing energy expenditure and insulin sensitivity with or without changing body weight (Kraus et al, 2002; Stolinski et al, 2008). The improvement in hyperlipidemia severity is primarily attributed to decreases in lipid contents in VLDL and LDL particles because circulating cholesterol and triacylglycerol (TG) are mainly distributed in those particles compared to HDL particles in humans. The effects of exercise training on HDL-C concentrations reported in prospective studies are controversial. The variability observed may be related to the subjects' age and baseline lipid status, the amount of fat lost with exercise, and the volume of exercise training (Franczyk et al, 2023).

Aggressively increasing HDL-C concentrations has been an appealing target to reduce CAD events since a Framingham study reported low HDL-C concentrations as a CAD risk (Castelli, 1988). However, clinical trials have not shown promising effects on reducing CAD events by pharmaceutical approaches to increase HDL-C, shifting the focus on HDL function regarding CAD risk. LDL particles retained in the subendothelial space during hyperlipidemia are prone to oxidation (Linton et al, 2023). In response to the oxidized LDL, endothelial cells secrete cytokines to recruit inflammatory cells to the arterial wall to promote atherosclerosis progression. Apolipoproteins associated with HDL particles protect LDL from oxidation to prevent endothelial cells from inflammation (Linton et al., 2023). In addition, HDL particles accept cholesterols transported from the arterial wall and deliver the cholesterols to the liver to favor their secretion (Linton et al., 2023).

Studies have indicated that exercise training at high intensities or training for long periods is likely to increase HDL-C concentrations (Kraus et al., 2002; Valimaki et al, 2016; Wood et al, 2023). The impact of exercise training on HDL function is not yet well studied. High-intensity interval training (HIIT) involves exercise performed at more than 80% VO_{2peak} and interspersed by rest or lower-intensity exercise. HIIT programs often improve cardiometabolic health in less time when measured against high volume continuous exercise (Gillen and Gibala, 2014). In the current study, we examine the impact of an HIIT program on lipid profiles and HDL function in lean, obese, and type 2 diabetic (T2DM) subjects. We show that a short-term HIIT program improves the antioxidant capacity of HDL in all subjects from different metabolic groups and increases the cholesterol efflux capacity in lean subjects.

2 Methods and materials

2.1 Exercise participants and training

Participants and the exercise training regime have been reported previously (Reyna et al, 2013). Due to the limited availability of fasting blood samples, six samples were randomly used from each group in the current study. All subjects were sedentary and had stable body weight for 3 months before the study. The T2DM subjects were diagnosed no longer than 2 months, and one T2DM subject took a sulfonylurea, which was stopped 2 days before any study procedure. The anthropometric and geographic data for subjects used in the current analysis are shown in Supplement Table 1. Subjects undertook a supervised 15-day program of alternative HIIT for 40 min per day. VO_{2peak} was determined using a cycle ergometer before and after the HIIT program. The HIIT consisted of four identical 10-min periods, which included 8 min of cycle ergometer exercise at 70% of VO_{2peak} followed by 2 min at 90% of VO_{2peak}. Each of these 10-min sets was followed by 2 min of complete rest (Reyna et al., 2013). The study was approved by the Institute Review Board of the University of Texas Health Science Center at San Antonio and all participants gave written consent (Reyna et al., 2013). Plasma used in the current analysis was from blood samples collected before the insulin clamp study pre- and post-exercise training. To minimize the influence of acute physical exercise on blood lipid and other laboratory test results (Christou et al, 2017), the post-exercise training insulin clamp and blood sample collection were performed 36 h after the last exercise session (Reyna et al., 2013).

2.2 Blood lipid analysis

VLDL, LDL, and HDL particles were separated from plasma using fast performance liquid chromatography (FPLC) (Zhu et al, 2016; Zhu et al, 2018b). Cholesterol and triglycerides in serum and FPLC fractions were determined by enzymatic colorimetric assays with Cholesterol Reagent and Triglycerides GPO Reagent Kits from Infinity (Zhu et al., 2016; Zhu et al., 2018b).

2.3 Immunoblotting with plasma samples

For serum proteins, 2 μL (μL) of serum for each sample were denatured in loading buffer (Invitrogen) containing reducing buffer (Invitrogen) and phospholipase and protease inhibitors (Sigma). Serum proteins were separated with gel electrophoresis and transferred to nitrocellulose membranes (Zhu et al., 2016; Mueller et al, 2018). Membranes were incubated with primary antibody (1:1,000) at 4°C overnight, and with secondary antibody (1:20,000) at room temperature for 1 h. ApoB antibody (LS-C20729) was from Lifespan Biosciences; apoA1 antibody (K23500R) was from Biodesign Meridian LifeScience; apoE (ab150032) antibody was from Amcam; apoC2 (PA1-16813) and apoC3 (PA5-78802) antibodies were from Invitrogen. IRDye 800CW goat anti-rabbit IgG was from LI-COR Biosciences. Blot densities were analyzed with ImageJ.

2.4 Antioxidant assays

The antioxidant capacity of HDL particles was first assayed by examining their ability to protect LDL from oxidation using kinetics of LDL oxidation in the presence of copper with the protocol we reported previously (Zhu et al, 2018a). ApoB-free serum was prepared as we reported before (Zhu et al., 2018b). One μg of apoB-free serum purified from each sample was added in 300 μL of reaction mix containing 30 μg of LDL (Alfa Aesar) and 20 μM CuSO4 in DPBS. Human HDL particles from Cell Biolabs (Cat# STA-243) were used for the dose-response curve and as positive control, the reaction without HDL was used as blank. Reaction solutions were incubated at 37°C for 3 h in a plate reader. The absorbance readings at 234 nm (A234) were taken every minute to measure the formation of conjugated dienes.

The antioxidant capacity of HDL particles was also investigated by quantifying the ability to reduce copper II to copper I using an OxiSelect Total Antioxidant Capacity Assay Kit (Cell Biolabs, Cat# STA-360) following the manufacturer's introduction. The total antioxidant power of each sample was converted and presented as Copper Reducing Equivalence (CRE) according to Trachootham et al (2008).

Plasma paraoxonase activity was examined using an EnzCheck Paraoxonase Assay Kit from Invitrogen (Cat# E33702) according to Jarvik et al (2003).

2.5 Cholesterol efflux assays

The cholesterol efflux capacity of HDL was assayed with apoB-free serum from each sample using a protocol we had reported previously (Zhu et al., 2018a; Zhu et al., 2018b). Briefly, human THP-1 monocytes were differentiated into macrophages after culturing with DMEM containing phorbol myristate acetate (PMA) for 48 h. Cells were then incubated with ^{3}H-acylated-LDL particles for 48 h. These labeled foam cells were washed twice and equilibrated in DMEM with 0.2% BSA overnight. The following day, a set of cells were collected and lysed to determine the baseline ^{3}H-radioactivities in cells. The remaining cells were treated with 1% of the initial serum level of pooled plasma of each group for 4 h. Cells treated with DMEM with 0.2% BSA were used as negative controls, and cells treated with apoA1 (50 mg/mL, Meridian) as positive controls. ^{3}H-radioactivities in media and baseline cells were determined using liquid scintillation counting and used for cholesterol efflux calculation. The efflux rates were calculated as the portion of ^{3}H-radioactivities in media to the ^{3}H-radioactivities in the baseline cells.

2.6 Statistical analysis

Data are shown with pre- and post-exercise training results for individual subjects in each metabolic group. Statistical analysis was performed with one-way or two-way ANOVA with Tukey's multiple comparison test as indicated in each figure legend. p-values <0.05 were considered statistically significant.

3 Results

3.1 The short-term HIIT modified apolipoproteins differently in lean, obese, and T2DM subjects.

To understand the beneficial effects of exercise training regarding CAD risk, we performed a 15-day high intensity interval training (HIIT) program with lean, obese, and T2DM subjects. In addition to the physiological parameters of participants previously reported (Reyna et al., 2013), we show that the short-term HIIT reduced fasting plasma cholesterol levels in T2DM subjects and fasting TG levels in subjects from obese and T2DM groups (Supplemental Table 1).

To better understand the changes in plasma lipids modified by the HIIT, we examined protein amounts of circulating apolipoproteins that are known to regulate lipid delivery and lipolysis. ApoB is the structural protein of atherogenic particles of VLDL and LDL, with a ratio of 1:1 for each particle. The HIIT reduced plasma apoB proteins in lean ($p < 0.05$) participants but not significantly in T2DM ($p = 0.06$) or in obese participants (Figures 1A, B). Plasma apoE protein concentrations have been reported to be higher in T2DM patients than in healthy controls (Franczyk et al., 2023), and plasma cholesterol ester transport protein (CETP) amounts are reportedly higher in hyperlipidemia individuals and considered atherogenic (McPherson et al, 1991). In the current study, plasma apoE protein amounts were not different between lean and obese participants but were increased in T2DM participants compared to lean ($p < 0.05$) and obese participants ($p < 0.05$, Figure 1C). Plasma CETP amounts were higher in T2DM subjects than in lean and obese participants (Figures 1A, D). The HIIT showed a trend to reduce apoE ($p = 0.053$) and reduced CETP proteins ($p < 0.01$) in T2DM participants (Figure 1C).

ApoA1 is the structural protein for HDL particles. Plasma apoA1 protein amounts were not significantly different between metabolic groups or changed by the HIIT in any group (Figure 1E). The human apoCs play an important role in regulating lipoprotein lipase (LPL) activity. ApoC2 is an activator for LPL activity, and decreased apoC2 activities are inversely associated with hypertriglyceridemia in humans (Jong et al, 1999). ApoC3 is an inhibitor for LPL-mediated lipolysis, and increases in apoC3 activity contribute to the development of hyperglyceridemia (Jong et al., 1999). We observed that plasma apoC2 amounts were not different between groups, and the short-term HIIT significantly increased apoC2 only in obese subjects ($p < 0.01$, Figure 1F). Plasma apoC3 amounts were not different between lean and obese subjects and were higher in T2DM than in lean and obese participants (Figures 1A, G). The HIIT program did not significantly change plasma apoC3 in either lean, obese, or T2DM participants (Figure 1G). Interestingly, multiple logistic regression analysis showed that changes in apoC2 were inversely associated with changes in atherogenic factors, including fasting cholesterol, apoB, and insulin levels, while changes in plasma apoC3 proteins positively correlated with changes in fasting cholesterol, TG, and CETP (Supplemental Figure 1).

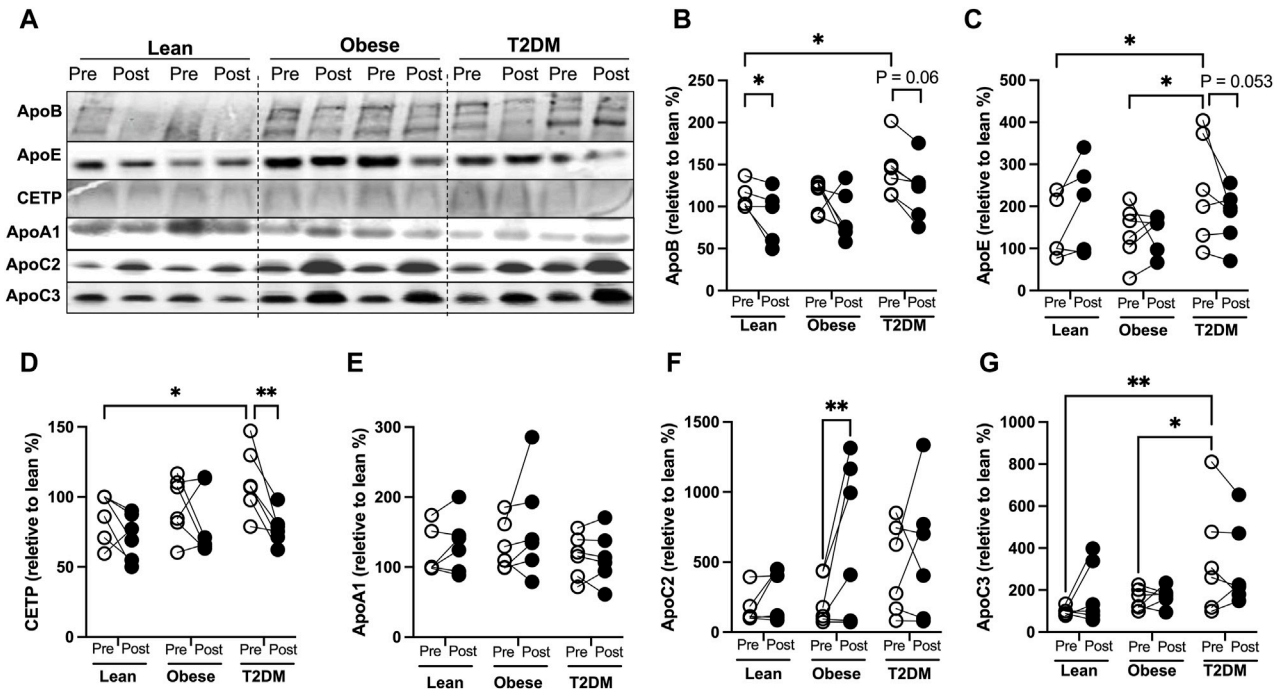

FIGURE 1
Changes of circulating apolipoproteins by the HIIT program in lean, obese, and T2DM subjects. **(A)** Representative Western blots (WB) for apolipoproteins in plasma pre- and post-exercise training from each subject in lean, obese, and T2DM subjects. All the samples were divided into three groups for WB with each group composed of two leans, two obese, and two T2DM subjects. **(B–G)** Blots was quantified as changes relative to pre-exercise training of lean subjects (first lane) on each WB gel. Open circles represent pre-exercise training expression and dark filled circles represent post-exercise training expression of proteins. Statistical analysis were performed with 2-way ANOVA with Tukey's multiply comparison analysis, $p < 0.05$ were considered statistically significant.

3.2 The short-term HIIT improved different aspects of lipid distribution in plasma lipoproteins in obese and T2DM subjects

Plasma lipoproteins were separated with fast performance liquid chromatography (FPLC), and lipoprotein-cholesterol and -TG contents were determined for lean, obese, and T2DM subjects (Figures 2A–C). VLDL-cholesterol (VLDL-C) concentrations were higher in obese and T2DM subjects than in lean subjects; the short-term HIIT reduced VLDL-C only in T2DM subjects (Figure 2D). The average LDL-C content was about 2-fold higher in obese and T2DM subjects than in lean subjects; the HIIT significantly reduced LDL-C in obese and T2DM subjects (Figure 2E). HDL-C content was slightly but significantly higher in obese than in lean subjects; the HIIT increased HDL-C only in lean subjects (Figure 2F). While hypercholesterolemia is atherogenic, HDL-C has been considered "good cholesterol" regarding CAD. The ratio of total cholesterol to HDL-C (TC/HDL-C) has been used to predict future CAD events in the clinic, and a ratio number higher than four is considered a high risk for heart disease (Lemieux et al, 2001). The ratio of TC/HDL-C was 4.079 ± 0.344 and 4.952 ± 0.339 in obese and T2DM subjects, respectively, which was higher than in lean subjects (3.014 ± 0.169, Figure 3G). The HIIT did not significantly reduce HC/HDL-C ratios in any group except for a trend of decrease in the T2DM group ($p = 0.0658$, Figure 3G).

The distribution of TG in lipoproteins was similar to the distribution of cholesterol in lipoproteins. VLDL-TG concentrations were not different between lean and obese subjects before and after the HIIT program (Figure 3). VLDL-TG concentrations were higher in T2DM than in lean and obese subjects before the HIIT and were maintained at higher levels compared to lean subjects after the exercise training (Figure 3D). LDL- and HDL-TG levels were higher in obese and T2DM than in lean subjects before and after the HIIT program (Figure 3). The short-term HIIT did not significantly change TG distribution in lipoproteins in any group except for a trend of decrease in HDL-TG in obese subjects (Figures 3A–F). While TC/HDL-C ratios are used to predict CAD risk, TG/HDL-C ratios are considered indicators for metabolic disorders and insulin resistance (Iwani et al, 2017; Liu et al, 2022). TG/HDL-C ratios range between 0.5–1.9 for healthy people, and ratios above 3.0 indicate significant insulin resistance and CAD risk (Iwani et al., 2017; Liu et al., 2022). The TG/HDL-C ratios were higher in obese than in lean subjects (2.197 ± 0.073 vs. 1.124 ± 0.092, $p < 0.01$) and were further increased in T2DM subjects compared to obese subjects (3.995 ± 0.486 vs. 2.197 ± 0.073, $p < 0.0001$, Figure 3G). The HIIT significantly reduced TG/HDL-C ratios only in T2DM subjects to 2.512 ± 0.218 ($p < 0.001$, Figure 3G).

3.3 The HIIT program improved the antioxidant capacity of HDL in all subjects and increased cholesterol efflux capacity in lean subjects

While the short-term HIIT program improved many aspects of lipid profile in obese and T2DM subjects, HDL-C levels were

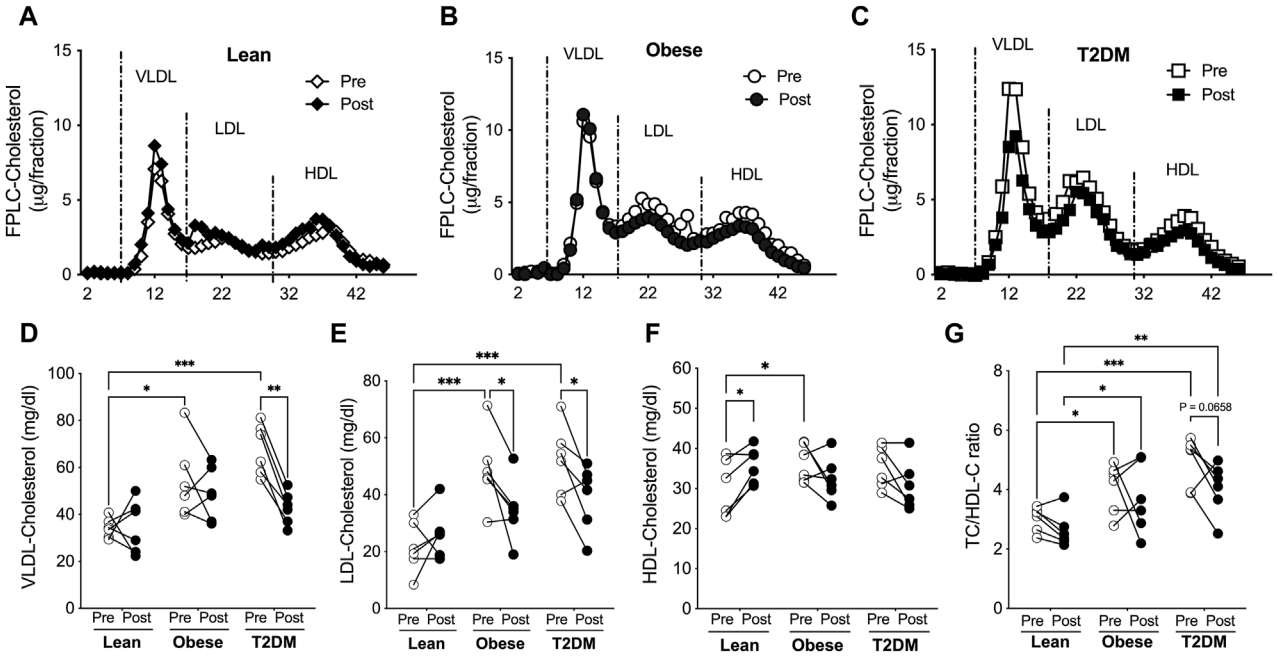

FIGURE 2
Short-term HIIT modified plasma cholesterol distribution in lipoproteins differently in lean, obese, and T2DM subjects. Plasma lipoproteins were saperated with FPLC and lipoprotein cholesterol levels were determined for lean **(A)**, obese **(B)**, and T2DM **(C)** subjects. **(D)** VLDL-cholesterol levels were higher in obese and T2DM subjects compared to lean subjects and the HIIT reduced VLDL-cholesterol in T2DM subjects. **(E)** LDL-cholesterol levels were higher in obese and T2DM subjects, which was reduced by the HIIT. **(F)** HDL-cholesterol levels were higher in obese subjects than in lean subjects, and were increased by the HIIT only in lean subjects. **(G)** The total plasma cholesterol to HDL-cholesterol (TC/HDL-C) ratios were significantly higher in obese and further higher in T2DM than in lean group and were in a trend of reduction by the HIIT in T2DM subjects. Statistical analysis were performed with 2-way ANOVA with Tukey's multiply comparison analysis *$p < 0.05$; **$p < 0.01$; ***$p < 0.001$.

unaffected. Given that HDL function is essential for delaying CAD, we next performed functional assays with HDL particles isolated from the plasma samples before and after the HIIT program.

The antioxidant capacity of HDL is important to suppress LDL oxidation and retention in the subendothelial space during atherosclerosis progression (Linton et al., 2023). To examine the antioxidant capacity of HDL, we first performed the kinetic assays for LDL oxidation in the presence of HDL particles isolated from plasma samples pre- and post-HIIT. HDL particles from post-HIIT plasma of all subjects delayed LDL oxidation by shifting the curves for the formation of conjugated diene, an oxidative product of LDL, toward the right (Figure 4A). These results indicate that the short-term HIIT improved the antioxidant capacity of HDL in all participants from lean, obese, and T2DM groups. To further quantify the antioxidant capacity, the reduction of copper oxidation was evaluated in the presence of HDL particles (Trachootham et al., 2008). The capacity of HDL to reduce copper oxidization was not significantly different between groups before the exercise training and was improved by the HIIT in lean and T2DM subjects (Figure 4B). Evidence from pre-clinical and clinical studies shows that the antioxidant capacity of HDL is largely accounted to the enzymatic activity of paraoxonase 1 (PON1) (Shokri et al, 2020). Plasma PON activities were examined, and the results showed that plasma PON activities were not different between lean and obese subjects but were higher in obese than in T2DM subjects before and after the exercise training (Figure 4C). The short-term HIIT increased PON activity in lean and obese subjects but not in T2DM participants (Figure 4C).

HDL particles accept cholesterol transported from the arterial wall and deliver cholesterol either back to the liver or to LDL particles in a process termed reverse cholesterol transport (RCT) (Linton et al., 2023). Impaired RCT is associated with increased CAD events (Zhu et al., 2018b). To examine the cholesterol efflux capacity, HDL particles from each sample before and after the HIIT program were added in the medium for culturing macrophages that were loaded with ^{3}H-acylated-LDL. The cholesterol efflux capacity of HDL was presented as the percentage of ^{3}H-radioactivity transported to HDL particles from macrophages (Zhu et al., 2018a; Zhu et al., 2018b). The cholesterol efflux capacity was not different between lean, obese, and T2D subjects before the exercise training, and was increased by the short-term HIIT program only in lean subjects (Figure 4D).

To better understand the improvement in HDL function by the HIIT program, we performed multiple logistic regression analysis for changes in HDL antioxidant capacity with the changes in other metabolic parameters (Table 1; Supplemental Figure 1). In addition to the inverse correlations with changes in atherogenic lipids, the improvement in HDL antioxidant capacity was inversely correlated with changes in HDL-TGs. Furthermore, changes in plasma PON activity were associated with changes in apoC2 and HDL-C but inversely correlated with changes in LDL-TG and HDL-TG (Supplemental Figure 1). These results together indicate that

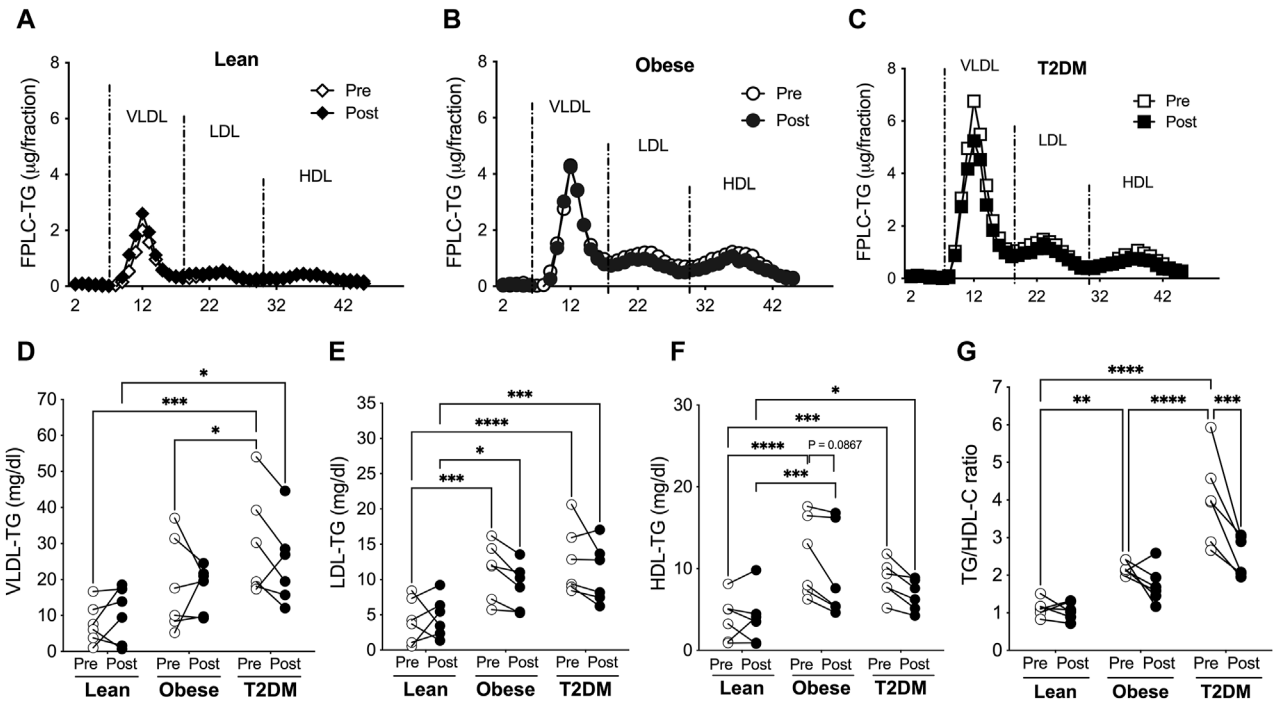

FIGURE 3
VLDL-, LDL-, and HDL-TG contents were higher in obese and T2DM subjects than in lean subjects, and the short-term HIIT reduced LDL- and HDL-TGs only in obese subjects. Blood lipoproteins were saperated with FPLC and lipoprotein TGs were determined for lean **(A)**, obese **(B)**, and T2DM **(C)** subjects. **(D)** VLDL-TG contens were higher in T2DM subjects than in lean and obese subjects before the HIIT program, and stayed higher in T2DM than in lean subjects after the HIIT program. **(E)** LDL-TG levels were higher in obese and T2DM individuals than in lean subjects before and after the HIIT program. **(F)** HDL-TG levels were higher in obese and T2DM subjects than in lean subjects before and after the HIIT program, and there was a trend of reduction in HDL-TG only in obese subjects by the HIIT. **(G)** The total plasma TG to HDL-cholesterol (TG/HDL-C) ratios were significantly higher in obese and further higher in T2DM than in lean subjects and were reduced by the HIIT program only in T2DM subjects. Statistical analysis were performed with 2-way ANOVA with Tukey's multiply comparison analysis *$p < 0.05$; **$p < 0.01$; ***$p < 0.001$; ****$p < 0.0001$.

hyperlipidemia, especially the TG content in HDL particles, may have negative impact on HDL function by interrupting the enzyme activities of apolipoproteins.

4 Discussion

In this study, we report that a short-term HIIT program reversed plasma TG levels in obese subjects and partially reversed plasma TG and cholesterol levels in T2DM subjects. While TG contents in lipoproteins were not significantly changed, the HIIT program reduced VLDL-C and LDL-C concentrations in T2DM subjects and increased HDL-C concentrations in lean subjects. The improvement in lipid profile was in line with our previous report that the HIIT increased VO_{2peak} associated with increased insulin sensitivity in subjects from all three groups (Reyna et al., 2013). Furthermore, we show that the short-term HIIT program improved the antioxidant capacity of HDL in all subjects and increased the cholesterol efflux capacity in lean subjects. The impact of the HIIT on HDL functions is metabolic context dependent and associated with a reduction in atherogenic lipids in the plasma.

We report that the short-term HIIT program increased cholesterol efflux capacity of HDL and HDL-C in lean subjects. Studies have shown that changes in HDL-C concentrations by exercise training depend on subjects' baseline lipid profiles, and training programs with extended periods are required for subjects with hyperlipidemia to increase HDL-C (Franczyk et al., 2023). Although HIIT is an efficient training for reducing hyperlipidemia, a 15-day continuous training may not be sufficient to improve HDL-C in obese and T2DM subjects. It is worth noticing that the clinical practice of HIIT for patients with dyslipidemia may need to be limited to once per week to minimize the symptoms related to overreaching (Gottschall et al, 2020). We also show that the increase in HDL-C in lean subjects was associated with increased cholesterol efflux capacity but disassociated with changes in circulating apoA1 or CETP amounts. This observation indicates that the short-term HIIT program modified additional regulatory steps in RCT to steps regulated by ApoA1 and CETP to increase HDL-C. In line with our observations, in a study with prolonged exercise training, HDL-C was modestly increased without any change in apoA1 protein amounts (Thompson et al, 1988). Furthermore, HDL-C concentrations are reported to be higher in trained subjects, and changes in HDL-C are positively correlated with increases in aerobic capacity by exercise training (Schwartz, 1988). We were unable to perform a correlation analysis between the changes in HDL-C and VO2peak due to the missing values for three subjects after the HIIT training. Christou et al (2024) reported that oxygen uptake at the first ventilatory threshold (VO2VT1) is more accurate than VO2peak for aerobic capacity in heart failure patients, and VO2VT1 should be considered in future studies for

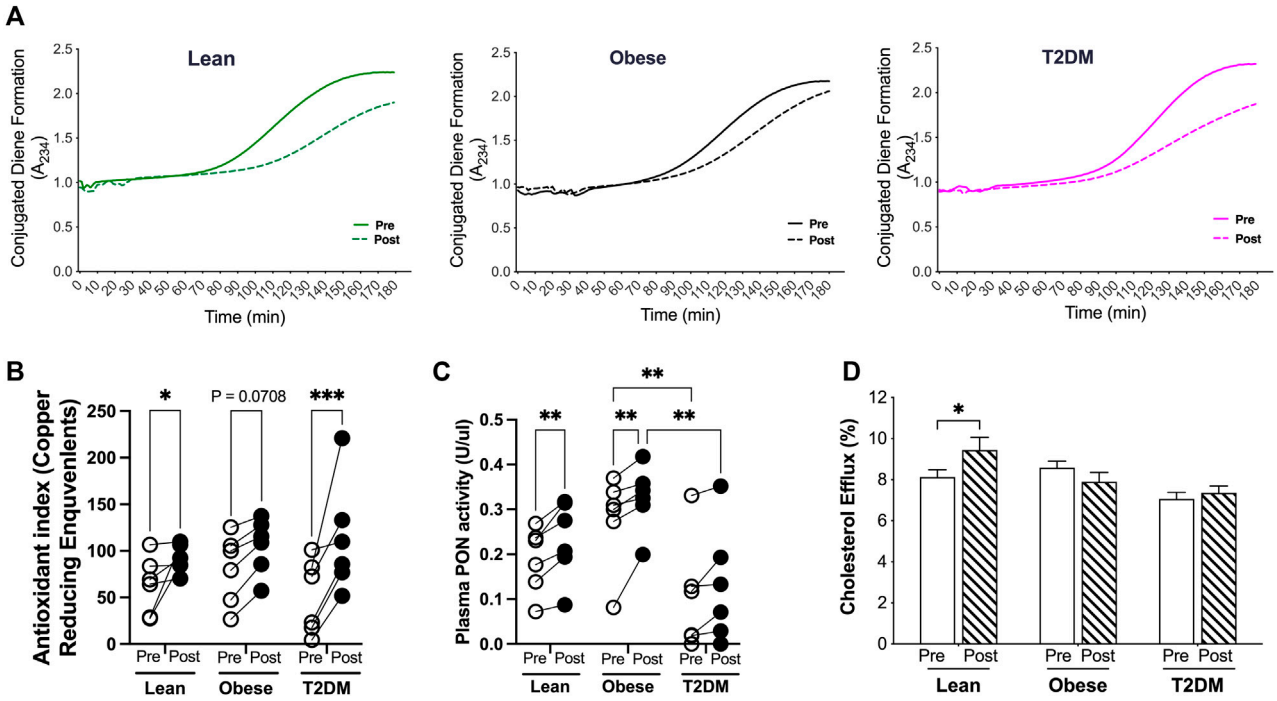

FIGURE 4
Antioxidant and cholesterol efflux capacities of HDL were changed by the HIIT in lean, obese, and T2DM subjects. ApoB-free serum of each sample was used for the function assays to exame the antioxidant and cholesterol efflux capacities as discribed in the Methods and Material section. **(A)** HDL particles isolated from post-HIIT plasma samples of all subjects impleded copper-induced LDL oxidation. **(B)** The capacity of reduction of copper II to copper I by HDL particles was inproved by the HIIT program in lean and T2DM subjects. **(C)** Plasma total paraoxonase (PON) activities were higher in obese than in T2DM subjects before and after the exercise training, and the HIIT program improved the PON activities in lean and obese subjects. **(D)** Cholesterol efflux capacity was improved by the HIIT only in lean subjects. Statistical analysis were performed with 2-way ANOVA with Tukey's multiply comparison analysis *$p < 0.05$; **$p < 0.01$; ***$p < 0.001$.

TABLE 1 Metabolic factors whose changes significantly correlate with the change in HDL capacity for antioxidant function by multiple logistic regression analysis (more data shown in Supplemental Figure 1).

	ΔPON activity	ΔTC	ΔTG	ΔVLDL-TG	ΔLDL-TG	ΔHDL-TG	ΔVLDL-C	ΔTG/HDL-C
95% Confidence interval of R	−0.050 to 0.745	−0.846 to −0.227	−0.897 to −0.418	−0.812 to −0.121	−0.844 to −0.220	−0.799 to −0.084	−0.868 to −0.304	−0.832 to −0.179
Pearson R value	0.427	−0.627	−0.741	−0.557	−0.623	−0.530	−0.675	−0.596
p-value	0.77	0.005	<0.001	0.016	0.006	0.024	0.002	0.009

PON, paraoxonase; TC, total cholesterol; TG, triacylglycerol; VLDL-C, very low-density lipoprotein cholesterol; HDL-C, high density lipoproteins cholesterol.

evaluating the impact of exercise training on HDL functions. The disassociation between HDL-C concentrations and apoA1 was also seen in obese subjects in the current study. HDL-C concentrations were higher in obese than lean subjects at the baseline but were disassociated with higher functional quality, such as the cholesterol efflux capacity. Notably, HDL-TG content was higher in the obese than in lean subjects at the baseline. Our analysis showed that reduction in HDL-TG was associated with improvements in atherogenic blood lipid concentrations and correlated with increases in HDL antioxidant capacity. Clinical studies have shown that HDL-TG content is positively associated with the risk of myocardial infarction (Lamarche et al, 1999; Holmes et al, 2018; Ito and Ito, 2020). Observations from our study and others' indicate that TG enrichment in HDL may impair their function of HDL particles.

The short-term HIIT improved the antioxidant capacity of HDL in all subjects from different metabolic groups. Paraoxonase proteins (PON1 and PON3) in HDL particles play a key role in hydrolyzing and clearing lipid peroxides in circulation (Soran et al, 2015; Ruiz-Ramie et al, 2019). Increases in the antioxidant property of HDL in lean and obese subjects were associated with the increases in PON activities by the HIIT program. Other apolipoproteins, such as apoA1, apoA2, or CETP, are required for PON1 impeding lipid peroxide accumulation on LDL because highly purified PON1 proteins isolated from HDL could

not reduce lipid peroxides (Draganov et al, 2005; Kontush and Chapman, 2010). These studies indicate that modification of other apolipoproteins by the HIIT contributed to the enhancement in the antioxidant capacity of HDL in T2DM subjects where PON activities were not significantly increased (Figures 4B, C). In agreement with our observation, evidence from independent studies has shown that exercise training promotes the antioxidant capacity of HDL in subjects of different metabolic contexts. Valimaki et al. (2016) reported that lipid peroxide clearing by HDL was elevated after an incremental maximal treadmill run to exhaustion. Roberts et al (2006) showed that a 21-day program of daily moderate-intensity exercise and dietary modification improved the antioxidant effect of HDL and reduced lipid peroxides in subjects with obesity and metabolic syndrome. Furthermore, a 3-month moderate-intensity exercise training program increased the HDL subfractions' oxidative capacity and PON1 activity without significant changes in HDL-C (Casella-Filho et al, 2011). In another study with obese subjects, a 12-week exercise training program improved PON activities without affecting HDL-C content or cholesterol efflux capacity (Woudberg et al, 2018).

There were several limitations in our study. The sample size was small, especially for obese subjects whose metabolic regulations may span a wide range. A bigger sample size would better show metabolic significance between groups. In addition, lecithin cholesterol acyl transferase (LCAT) esterifies cholesterol and facilitates the transport of cholesterol esters to HDL particles, and phospholipid transport proteins (PLTP) are also involved in the regulation of HDL-C concentrations (Rousset et al, 2011). It would be interesting to investigate the regulation of LCAT and PLTP activities by exercise training in lean, obese, and T2DM subjects in future studies. Regarding HDL function, we could not examine the anti-inflammatory capacity of HDL with *in vitro* functional assays due to the limited amounts of plasma samples. We speculate that the HIIT improved the HDL capacity to protect endothelial cell injury from oxidized LDL, at least in lean and T2DM subjects, given that the ability of HDL particles to reduce the oxidized copper was improved in those subjects (Figure 4B).

In summary, our results show that a short-term HIIT program is sufficient to improve hyperlipidemia and HDL capacity of antioxidant function in obese and T2DM subjects, which might not be associated with increases in HDL-C concentrations. In addition to enhancing the antioxidant capacity, a short-term HIIT program could increase HDL-C concentrations and cholesterol efflux function in subjects without metabolic disorders. Furthermore, our data indicate that the TG content in HDL particles may play a negative role in the anti-atherogenic function of HDL.

Data availability statement

Publicly available datasets were analyzed in this study. This data can be found here: https://www.hindawi.com/journals/jdr/2013/107805/.

Ethics statement

The studies involving humans were approved by the Institutional Review Board of the University of Texas Health Science Center at San Antonio. The studies were conducted in accordance with the local legislation and institutional requirements. The participants provided their written informed consent to participate in this study.

Author contributions

LZ: Conceptualization, Data curation, Formal Analysis, Funding acquisition, Investigation, Methodology, Project administration, Writing–original draft, Writing–review and editing. JA: Data curation, Investigation, Writing–review and editing. TL: Data curation, Investigation, Writing–review and editing. SR: Data curation, Funding acquisition, Resources, Writing–review and editing. PT: Data curation, Ivestigation, Writing–review and editing. AS: Data curation, Investigation, Writing–review and editing. NM: Funding acquisition, Project administration, Resources, Supervision, Writing–review and editing. JS: Funding acquisition, Project administration, Resources, Supervision, Writing–review and editing.

Funding

The author(s) declare that financial support was received for the research, authorship, and/or publication of this article. The NIA (K01AG077038) provided support to LZ. The NHLBI (F32HL086089) and NIGMS (SC2GM127272) provided support to SR. The Department of Veterans Affairs (BX002223) and NIH (R01DK109102, R01HL144846) provided support to JS. The content is solely the responsibility of the authors and does not necessarily represent the official views of the National Institutes of Health.

Conflict of interest

The authors declare that the research was conducted in the absence of any commercial or financial relationships that could be construed as a potential conflict of interest.

Publisher's note

Supplementary material

The Supplementary Material for this article can be found online at: https://www.frontiersin.org/articles/10.3389/fphys.2024.1423989/full#supplementary-material

References

Casella-Filho, A., Chagas, A. C., Maranhao, R. C., Trombetta, I. C., Cesena, F. H., Silva, V. M., et al. (2011). Effect of exercise training on plasma levels and functional properties of high-density lipoprotein cholesterol in the metabolic syndrome. *Am. J. Cardiol.* 107, 1168–1172. doi:10.1016/j.amjcard.2010.12.014

Castelli, W. P. (1988). Cholesterol and lipids in the risk of coronary artery disease--the Framingham Heart Study. *Can. J. Cardiol.* 4 (Suppl. A), 5A–10A.

Christou, G. A., Christou, M. A., Davos, C. H., Markozannes, G., Christou, K. A., Mantzoukas, S., et al. (2024). Ergophysiological evaluation of heart failure patients with reduced ejection fraction undergoing exercise-based cardiac rehabilitation: a systematic review and meta-analysis. *Hell. J. Cardiol.* 77, 106–119. doi:10.1016/j.hjc.2024.01.004

Christou, G. A., Kouidi, E. J., Deligiannis, A. P., and Kiortsis, D. N. (2017). Diagnosis and treatment of dyslipidaemias in athletes. *Curr. Vasc. Pharmacol.* 15, 238–247. doi:10.2174/1570161115666170127162526

Draganov, D. I., Teiber, J. F., Speelman, A., Osawa, Y., Sunahara, R., and La Du, B. N. (2005). Human paraoxonases (PON1, PON2, and PON3) are lactonases with overlapping and distinct substrate specificities. *J. Lipid Res.* 46, 1239–1247. doi:10.1194/jlr.M400511-JLR200

Franczyk, B., Gluba-Brzozka, A., Cialkowska-Rysz, A., Lawinski, J., and Rysz, J. (2023). The impact of aerobic exercise on HDL quantity and quality: a narrative review. *Int. J. Mol. Sci.* 24, 4653. doi:10.3390/ijms24054653

Gillen, J. B., and Gibala, M. J. (2014). Is high-intensity interval training a time-efficient exercise strategy to improve health and fitness? *Appl. Physiol. Nutr. Metab.* 39, 409–412.

Gottschall, J. S., Davis, J. J., Hastings, B., and Porter, H. J. (2020). Exercise time and intensity: how much is too much? *Int. J. Sports Physiol. Perform.* 15, 808–815. doi:10.1123/ijspp.2019-0208

Holmes, M. V., Millwood, I. Y., Kartsonaki, C., Hill, M. R., Bennett, D. A., Boxall, R., et al. (2018). Lipids, lipoproteins, and metabolites and risk of myocardial infarction and stroke. *J. Am. Coll. Cardiol.* 71, 620–632. doi:10.1016/j.jacc.2017.12.006

Ito, F., and Ito, T. (2020). High-density lipoprotein (HDL) triglyceride and oxidized HDL: new lipid biomarkers of lipoprotein-related atherosclerotic cardiovascular disease. *Antioxidants (Basel)* 9, 362. doi:10.3390/antiox9050362

Iwani, N. A., Jalaludin, M. Y., Zin, R. M., Fuziah, M. Z., Hong, J. Y., Abqariyah, Y., et al. (2017). Triglyceride to HDL-C ratio is associated with insulin resistance in overweight and obese children. *Sci. Rep.* 7, 40055. doi:10.1038/srep40055

Jarvik, G. P., Hatsukami, T. S., Carlson, C., Richter, R. J., Jampsa, R., Brophy, V. H., et al. (2003). Paraoxonase activity, but not haplotype utilizing the linkage disequilibrium structure, predicts vascular disease. *Arterioscler. Thromb. Vasc. Biol.* 23, 1465–1471. doi:10.1161/01.ATV.0000081635.96290.D3

Jong, M. C., Hofker, M. H., and Havekes, L. M. (1999). Role of ApoCs in lipoprotein metabolism: functional differences between ApoC1, ApoC2, and ApoC3. *Arterioscler. Thromb. Vasc. Biol.* 19, 472–484. doi:10.1161/01.atv.19.3.472

Kontush, A., and Chapman, M. J. (2010). Antiatherogenic function of HDL particle subpopulations: focus on antioxidative activities. *Curr. Opin. Lipidol.* 21, 312–318. doi:10.1097/MOL.0b013e32833bcdc1

Kraus, W. E., Houmard, J. A., Duscha, B. D., Knetzger, K. J., Wharton, M. B., McCartney, J. S., et al. (2002). Effects of the amount and intensity of exercise on plasma lipoproteins. *N. Engl. J. Med.* 347, 1483–1492. doi:10.1056/NEJMoa020194

Lamarche, B., Uffelman, K. D., Carpentier, A., Cohn, J. S., Steiner, G., Barrett, P. H., et al. (1999). Triglyceride enrichment of HDL enhances *in vivo* metabolic clearance of HDL apo A-I in healthy men. *J. Clin. Invest* 103, 1191–1199. doi:10.1172/JCI5286

Lee, I. M., Shiroma, E. J., Lobelo, F., Puska, P., Blair, S. N., Katzmarzyk, P. T., et al. (2012). Effect of physical inactivity on major non-communicable diseases worldwide: an analysis of burden of disease and life expectancy. *Lancet* 380, 219–229. doi:10.1016/S0140-6736(12)61031-9

Lemieux, I., Lamarche, B., Couillard, C., Pascot, A., Cantin, B., Bergeron, J., et al. (2001). Total cholesterol/HDL cholesterol ratio vs LDL cholesterol/HDL cholesterol ratio as indices of ischemic heart disease risk in men: the Quebec Cardiovascular Study. *Arch. Intern Med.* 161, 2685–2692. doi:10.1001/archinte.161.22.2685

Linton, M. F., Yancey, P. G., Tao, H., and Davies, S. S. (2023). HDL function and atherosclerosis: reactive dicarbonyls as promising targets of therapy. *Circulation Res.* 132, 1521–1545. doi:10.1161/CIRCRESAHA.123.321563

Liu, H., Liu, J., Liu, J., Xin, S., Lyu, Z., and Fu, X. (2022). Triglyceride to high-density lipoprotein cholesterol (TG/HDL-C) ratio, a simple but effective indicator in predicting type 2 diabetes mellitus in older adults. *Front. Endocrinol. (Lausanne)* 13, 828581. doi:10.3389/fendo.2022.828581

McPherson, R., Mann, C. J., Tall, A. R., Hogue, M., Martin, L., Milne, R. W., et al. (1991). Plasma concentrations of cholesteryl ester transfer protein in hyperlipoproteinemia. Relation to cholesteryl ester transfer protein activity and other lipoprotein variables. *Arteriosclerosis thrombosis a J. Vasc. Biol./Am. Heart Assoc.* 11, 797–804. doi:10.1161/01.atv.11.4.797

Mueller, P. A., Zhu, L., Tavori, H., Huynh, K., Giunzioni, I., Stafford, J. M., et al. (2018). Deletion of macrophage low-density lipoprotein receptor-related protein 1 (LRP1) accelerates atherosclerosis regression and increases C-C chemokine receptor type 7 (CCR7) expression in plaque macrophages. *Circulation* 138, 1850–1863. doi:10.1161/CIRCULATIONAHA.117.031702

Reyna, S. M., Tantiwong, P., Cersosimo, E., Defronzo, R. A., Sriwijitkamol, A., and Musi, N. (2013). Short-term exercise training improves insulin sensitivity but does not inhibit inflammatory pathways in immune cells from insulin-resistant subjects. *J. Diabetes Res.* 2013, 107805. doi:10.1155/2013/107805

Roberts, C. K., Ng, C., Hama, S., Eliseo, A. J., and Barnard, R. J. (2006). Effect of a short-term diet and exercise intervention on inflammatory/anti-inflammatory properties of HDL in overweight/obese men with cardiovascular risk factors. *J. Appl. Physiol.* 101, 1727–1732. doi:10.1152/japplphysiol.00345.2006

Rousset, X., Shamburek, R., Vaisman, B., Amar, M., and Remaley, A. T. (2011). Lecithin cholesterol acyltransferase: an anti- or pro-atherogenic factor? *Curr. Atheroscler. Rep.* 13, 249–256. doi:10.1007/s11883-011-0171-6

Ruiz-Ramie, J. J., Barber, J. L., and Sarzynski, M. A. (2019). Effects of exercise on HDL functionality. *Curr. Opin. Lipidol.* 30, 16–23. doi:10.1097/MOL.0000000000000568

Schwartz, R. S. (1988). Effects of exercise training on high density lipoproteins and apolipoprotein A-I in old and young men. *Metabolism* 37, 1128–1133. doi:10.1016/0026-0495(88)90188-6

Shokri, Y., Variji, A., Nosrati, M., Khonakdar-Tarsi, A., Kianmehr, A., Kashi, Z., et al. (2020). Importance of paraoxonase 1 (PON1) as an antioxidant and antiatherogenic enzyme in the cardiovascular complications of type 2 diabetes: genotypic and phenotypic evaluation. *Diabetes Res. Clin. Pract.* 161, 108067. doi:10.1016/j.diabres.2020.108067

Soran, H., Schofield, J. D., and Durrington, P. N. (2015). Antioxidant properties of HDL. *Front. Pharmacol.* 6, 222. doi:10.3389/fphar.2015.00222

Stolinski, M., Alam, S., Jackson, N. C., Shojaee-Moradie, F., Pentecost, C., Jefferson, W., et al. (2008). Effect of 6-month supervised exercise on low-density lipoprotein apolipoprotein B kinetics in patients with type 2 diabetes mellitus. *Metabolism* 57, 1608–1614. doi:10.1016/j.metabol.2008.06.018

Thompson, P. D., Cullinane, E. M., Sady, S. P., Flynn, M. M., Bernier, D. N., Kantor, M. A., et al. (1988). Modest changes in high-density lipoprotein concentration and metabolism with prolonged exercise training. *Circulation* 78, 25–34. doi:10.1161/01.cir.78.1.25

Trachootham, D., Lu, W., Ogasawara, M. A., Nilsa, R. D., and Huang, P. (2008). Redox regulation of cell survival. *Antioxid. Redox Signal* 10, 1343–1374. doi:10.1089/ars.2007.1957

Tsao, C. W., Aday, A. W., Almarzooq, Z. I., Anderson, C. A. M., Arora, P., Avery, C. L., et al. (2023). Heart disease and stroke statistics-2023 update: a report from the American heart association. *Circulation* 147, e93–e621. doi:10.1161/CIR.0000000000001123

Valimaki, I. A., Vuorimaa, T., Ahotupa, M., and Vasankari, T. J. (2016). Strenuous physical exercise accelerates the lipid peroxide clearing transport by HDL. *Eur. J. Appl. Physiol.* 116, 1683–1691. doi:10.1007/s00421-016-3422-y

Wood, G., Taylor, E., Ng, V., Murrell, A., Patil, A., van der Touw, T., et al. (2023). Estimating the effect of aerobic exercise training on novel lipid biomarkers: a systematic review and multivariate meta-analysis of randomized controlled trials. *Sports Med.* 53, 871–886. doi:10.1007/s40279-023-01817-0

Woudberg, N. J., Mendham, A. E., Katz, A. A., Goedecke, J. H., and Lecour, S. (2018). Exercise intervention alters HDL subclass distribution and function in obese women. *Lipids Health Dis.* 17, 232. doi:10.1186/s12944-018-0879-1

Zhu, L., Giunzioni, I., Tavori, H., Covarrubias, R., Ding, L., Zhang, Y., et al. (2016). Loss of macrophage low-density lipoprotein receptor-related protein 1 confers resistance to the antiatherogenic effects of tumor necrosis factor-α inhibition. *Arterioscler. Thromb. Vasc. Biol.* 36, 1483–1495. doi:10.1161/ATVBAHA.116.307736

Zhu, L., Luu, T., Emfinger, C. H., Parks, B. A., Shi, J., Trefts, E., et al. (2018a). CETP inhibition improves HDL function but leads to fatty liver and insulin resistance in CETP-expressing transgenic mice on a high-fat diet. *Diabetes* 67, 2494–2506. doi:10.2337/db18-0474

Zhu, L., Shi, J., Luu, T. N., Neuman, J. C., Trefts, E., Yu, S., et al. (2018b). Hepatocyte estrogen receptor alpha mediates estrogen action to promote reverse cholesterol transport during Western-type diet feeding. *Mol. Metab.* 8, 106–116. doi:10.1016/j.molmet.2017.12.012

frontiers | Frontiers in Pharmacology

TYPE Review
PUBLISHED 06 September 2024
DOI 10.3389/fphar.2024.1451445

OPEN ACCESS

EDITED BY
Lin Zhu,
Vanderbilt University Medical Center,
United States

REVIEWED BY
Sumita Dutta,
Cleveland Clinic, United States
Mena Abdelsayed,
Lankenau Institute for Medical Research,
United States

*CORRESPONDENCE
Sheng Zhou,
lzzs@sina.com

†These authors have contributed equally to this work

RECEIVED 19 June 2024
ACCEPTED 29 August 2024
PUBLISHED 06 September 2024

CITATION
Lu Y, Li D-H, Xu J-M and Zhou S (2024) Role of naringin in the treatment of atherosclerosis. *Front. Pharmacol.* 15:1451445. doi: 10.3389/fphar.2024.1451445

Role of naringin in the treatment of atherosclerosis

Yan Lu[1†], De-Hong Li[1†], Ji-Mei Xu[2†] and Sheng Zhou[3*]

[1]Department of Clinical Laboratory, Gansu Provincial Hospital, Lanzhou, China, [2]Department of General Surgery, Gansu Provincial Hospital, Lanzhou, China, [3]Department of Radiology, Gansu Provincial Hospital, Lanzhou, China

Atherosclerosis (AS) is a major pathological basis of coronary heart disease. However, the currently available medications are unable to effectively reduce the incidence of cardiovascular events in the majority of patients with AS. Therefore, naringin has been attracting considerable attention owing to its anti-AS effects. Naringin can inhibit the growth, proliferation, invasion, and migration of vascular smooth muscle cells, ameliorate endothelial cell inflammation and apoptosis, lower blood pressure, halt the cell cycle at the G1 phase, and impede growth via its antioxidant and free radical scavenging effects. These activities suggest the potential anti-AS effects of naringin. In this review article, we comprehensively summarized the latest findings on the anti-AS effects of naringin and their underlying mechanisms, providing a crucial reference for future research on the anti-AS potential of this agent.

KEYWORDS

naringin, atherosclerosis, vascular smooth muscle cell, endothelial cell, inflammation, antioxidant

1 Introduction

Atherosclerosis (AS) is a chronic inflammatory cardiovascular disease characterized by lipid deposition in the vascular wall and immune cell recruitment. This condition is a major risk factor for chronic heart disease (Liu et al., 2023). According to World Health Organization data, coronary heart disease accounts for seven million deaths worldwide annually (Liu et al., 2023). The main strategies for the prevention and treatment of arteriosclerosis include a balanced diet (Przybylska and Tokarczyk, 2022), body mass management (Hwang et al., 2023), smoking cessation and limited consumption of alcohol, regular physical activity (Xu et al., 2022), control of blood pressure, regulation of serum sugar and blood lipid levels, and anti-platelet therapy (Virani et al., 2023). However, the use of currently available medication can effectively reduce cardiovascular events in only 40% of patients with AS (Parsamanesh et al., 2019). An increasing number of studies focus on traditional Chinese medicine and its active ingredients due to their lipid-lowering and anti-AS effects.

Naringin is a flavonoid abundantly found in fruits and vegetables (particularly grapefruit and tomatoes) (Memariani et al., 2021; Viswanatha et al., 2017), which exists in two forms (i.e., naringenin and naringin). Naringenin is formed through rapid glycosylation of naringin by the liver enzyme naringinase. It has been established that the sour and bitter taste of citrus fruits is attributed to naringin rather than naringenin. Most clinical studies have shown that the main pharmacological effects of grapefruit are produced by naringin (Adetunji et al., 2023; Bailey et al., 2007). Moreover, evidence indicates that, in addition to the liver enzyme naringinase, intestinal bacteria possess the capability to hydrolyze naringin into naringenin. This process has the potential to generate

hypoglycemic and hypolipidemic effects (Xulu and Oroma Owira, 2012). Due to the inhibitory effects of naringin on liver enzymes (cytochrome P450 enzymes), the consumption of grapefruit juice can reduce or increase the concentration of drugs that are metabolized in the liver, thereby altering their pharmacokinetics and potentially leading to toxicity (Heidary Moghaddam et al., 2020). Naringin exhibits various pharmacological activities, namely, antioxidant (Balachandran et al., 2023), anti-inflammatory (Zhang et al., 2022), anti-apoptotic (Zhao et al., 2020), anti-ulcer (Wang et al., 2023), and anti-osteoporotic (Pi et al., 2023), among others. Thus, increasing attention has been focused on the anti-AS effects of naringin. Naringin inhibits vascular smooth muscle cell (VSMC) proliferation (Lee et al., 2009) and ameliorates endothelial cell inflammation and apoptosis (Zhao et al., 2020) by exerting antioxidant effects and scavenging free radicals (Zhang et al., 2022; Amini et al., 2022). In this review, we summarized the latest available information on the anti-AS effects of naringin and their underlying mechanisms, providing a reference for future research on the anti-atherosclerotic properties of naringin.

Hypertension (Global Cardiovascular Risk et al., 2023), dyslipidemia (Global Cardiovascular Risk et al., 2023; Capra et al., 2023), endothelial cell injury (Li et al., 2014; Li et al., 2017), and smooth muscle proliferation are pivotal factors in the pathogenesis of AS (Feng and Xu, 2023). Naringin exerts anti-atherosclerotic effects by intervening in hypertension, ameliorating lipid disorders, safeguarding against endothelial cell damage, inhibiting smooth muscle proliferation, regulating the cell cycle, and modulating other mechanisms. The underlying mechanism may involve antioxidation, anti-inflammation, regulation of autophagy, and modulation of other pathways.

2 Naringin prevents AS by lowering blood pressure

Hypertension is associated with up to 13.5% of all deaths annually worldwide, and is the leading risk factor for cardiovascular disease, including AS (Global Cardiovascular Risk et al., 2023). Strict control of blood pressure significantly decreases the rates of cardiovascular events and all-cause mortality (Yntema et al., 2023; Virani et al., 2021). Findings have demonstrated the significant blood pressure-lowering effects of naringin in hypertensive rats with renal artery occlusion, potentially through the inhibition of oxidative stress (Visnagri et al., 2015). Additionally, naringin reduces systolic blood pressure in rats fed a high-carbohydrate and -fat diet, and improves both vascular and ventricular diastolic dysfunction (Alam et al., 2013). Its antihypertensive effects may be associated with the reduction of inflammatory cell infiltration, oxidative stress, plasma lipid concentrations, and improvement of hepatic mitochondrial function in rats (Alam et al., 2013). In another study, naringenin (a metabolite of naringin) significantly decreased cerebral glutathione S-transferase (GST) and superoxide dismutase (SOD) activity as well as the levels of glutathione (GSH) in rats with hypertension induced by oral administration of L-N^G-Nitro arginine methyl ester (L-NAME) (Oyagbemi et al., 2020). Moreover, it restored the activity of renal catalase, SOD, GST, glutathione peroxidase (GPX), and glutathione reductase (GSR). Additionally, naringenin significantly decreased the expression of renal angiotensin-converting enzyme (ACE) and mineralocorticoid receptor (MCR) (Oyagbemi et al., 2020). These observations indicate that the hypotensive effect of naringenin is mediated by modulation of the MCR/ACE/kidney injury molecule 1 (MCR/ACE/KIM1) signaling pathway, and by its antioxidative properties (Oyagbemi et al., 2020). Other studies have demonstrated that naringin reduces angiotensin II receptor type 2 (AT2R) mRNA expression in the medulla and the ratio of AT1R/AT2R, while increasing ACE expression and the ACE/ACE2 ratio in the cortex and medulla. These findings propose a potential mechanism underlying the beneficial effects of naringenin on hypertensive nephropathy (Wang et al., 2019), as it restores the ACE/ACE2 imbalance and normalizes the renal AGTR1/AGTR2 protein ratio in hypertensive rats (Wang et al., 2019). However, contrasting evidence from the two-kidney, one-clip (2K1C) hypertension rat model suggests that naringenin does not affect blood pressure. This indicates that its antihypertensive effects might be specific to different models of hypertension (Wang et al., 2019) (Figure 1; Table 1). Naringin has demonstrated efficacy in reducing blood pressure in hypertensive rats with renal artery occlusion-induced renovascular dysfunction (Visnagri et al., 2015) and in rats fed a high-carbohydrate and high-fat diet (Alam et al., 2013). However, in two-kidney one-clip (2K1C) (Wang et al., 2019) and NG-nitro-L-arginine methyl ester (L-NAME)-induced hypertensive left ventricular hypertrophy models (Gao et al., 2018), naringin was found to reduce ACE 1 expression; however, it did not significantly affect blood pressure. We had initially attributed the inconsistent impact of naringin on blood pressure in hypertensive animal models to variations in dosage and administration methods. However, a detailed review of the literature showed that all four modes of administration involved intra-intestinal delivery with similar dose ranges. This controlled for the potential influence of drug dosage and administration routes on the antihypertensive efficacy of naringin. We believe that the inconsistent effects of naringin on blood pressure in hypertensive rats may be attributed to the pathogenesis of hypertension and factors related to the animal model. In rats with L-NAME-induced hypertension, a reduction in nitric oxide (NO) is primarily involved; the mechanism underlying hypertension induced by both the 2K1C model and renal artery obstruction appears similar. However, the degree of renal artery occlusion may vary. In both 2K1C and renal artery obstruction rat models, naringin decreased ACE1 expression; this was possibly caused by inconsistent reductions in ACE1 levels within each model. Blood pressure therefore remained unaffected despite an improvement in the kidney lesions. The effects of naringin on blood pressure in hypertensive rat models warrant further investigation.

3 Naringin prevents AS by ameliorating dyslipidemia

Dyslipidemia is widely recognized as an important risk factor associated with the morbidity and mortality caused by AS (Yu et al., 2022; Hong et al., 2022; Capra et al., 2023). Dyslipidemia is a metabolic disorder characterized by elevated levels of serum

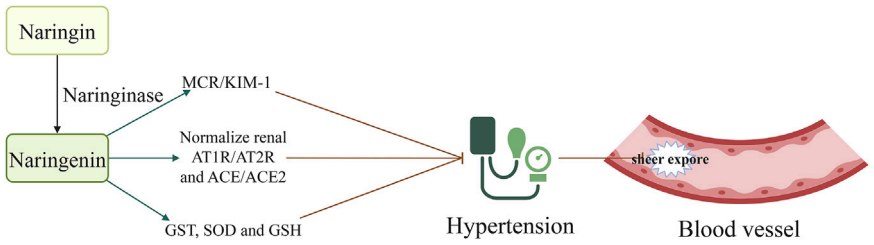

FIGURE 1
Naringin decreased sheer stress injury by lowering blood pressure; this effect was mediated by the attenuation of MCR/KIM1, and normalization of AT1R/AT2R and ACE/ACE2 ratios. Naringin is rapidly metabolized by the liver enzyme naringinase to produce naringenin. Naringenin decreased blood pressure and reduced vascular shear stress injury. Consequently, it decreased the occurrence of tissue atherosclerosis by adjusting the MCR/KIM1, AT1R/AT2R, and ACE/ACE2 ratios, and increasing the levels of GST, SOD, and GSH. Abbreviations: AT1R, angiotensin II type 1 receptor; AT2R, angiotensin II receptor type 2; ACE: angiotensin converting enzyme; GSH, reduced glutathione; GST, glutathione S-transferase; KIM, kidney injury molecule; MCR, mineralocorticoid receptor; SOD, superoxide dismutase.

cholesterol, triglycerides, low-density lipoprotein, and very-low-density lipoprotein, as well as decreased levels of high-density lipoprotein cholesterol (Hong et al., 2022). Increasing evidence suggests that naringin exerts inhibitory effects on the progression of AS by ameliorating dyslipidemia (Pu et al., 2012). Naringin attenuates foam cell infiltration into plaques and reduces lesion areas in the aortic sinus (Li et al., 2014). Intragastric administration of naringin significantly reduced total cholesterol and triglyceride levels, while increasing high-density lipoprotein cholesterol levels in mice fed a high-fat diet (Yu et al., 2022). In type I diabetic rats, naringin did not significantly alter hyperglycemia; however, it effectively improved atherogenic dyslipidemia by increasing the levels of high-density lipoprotein cholesterol (Xulu and Oroma Owira, 2012). Moreover, in rabbits fed a 0.25% cholesterol diet, naringin reduced serum cholesterol levels and demonstrated remarkable efficacy in reducing the area of fatty streaks in the thoracic aorta and subintimal foam cell infiltration (Choe et al., 2001). Additionally, naringin inhibited the hypercholesterolemia-induced expression of intercellular adhesion molecule 1 (ICAM1) on endothelial cells, suggesting that the suppression of ICAM1 contributes to its anti-atherogenic effect (Choe et al., 2001).

Non-target metabolomics analysis showed that naringin modulates the hepatic levels of cholesterol derivatives and bile acids (Wang F. et al., 2020) by inhibiting 3-hydroxy-3-methylglutaryl-CoA reductase (HMGCR) and acyl-coenzyme cholesterol acyltransferase (ACCA), respectively. Further investigation suggested that the gut microbiota-liver-cholesterol axis may represent the primary potential pathway through which naringin exerts its anti-atherosclerotic effects. Naringin alters the abundance of bacteria producing bile salt hydrolase and 7α-dehydroxylase, thereby promoting bile acid synthesis from cholesterol. This is achieved by upregulating cholesterol 7α-hydroxylase (cytochrome P450 family 7 subfamily A member 1 [CYP7A1]) expression via suppression of the farnesoid X receptor/fibroblast growth factor 15 (FXR/FGF15) pathway (Wang F. et al., 2020). Through oral administration, naringin predominantly localizes in the intestine due to the high solubility of 7-O-nohesperidoside. It exerts its anti-atherosclerotic effects primarily by augmenting bile acid synthesis through modulation of the gut microbiota-FXR/FGF15-CYP7A1 pathway (Wang F. et al., 2020). Naringin modulates the composition of gut microbiota by reducing the relative abundance of *Bacteroides*, *Bifidobacterium*, and *Clostridium* genera, which are associated with bile acid metabolism, while increasing that of *Eubacterium* genus that possesses bile acid-hydrolyzing activity and reduces the levels of bile acids (Wang F. et al., 2020). The administration of naringin facilitates the accumulation of conjugated bile acids, including tauro-α/β-muricholic acid, while concurrently inhibiting the expression of FGF15 through the inactivation of FXR. The expression of CYP7A1, which encodes the rate-limiting enzyme in the biosynthesis of bile acids from cholesterol, was enhanced by downregulation of the FXR/FGF pathway (Wang F. et al., 2020). Modulation of gut microbiota remodeling by naringin (a natural polyphenolic compound) has a profound impact on cholesterol metabolism and AS. In addition, recent findings have shown that naringin supplementation increases the abundance of Bifidobacterium and Lachnospiraceae bacterium 28–4, while reducing that of Lachnospiraceae bacterium DW59 and Dubosiella newyorkensis. Naringin supplementation has also been found to alter the fecal metabolite profile by significantly promoting the production of taurine, tyrosol, and thymol, which offers benefits in atherosclerosis by reducing oxidative stress, inflammation, hyperlipidemia, and lipid lesions in the aortic intima (Zoubdane et al., 2024; Yu et al., 2016).

In addition, naringin suppressed the expression of proprotein convertase subtilisin/kexin type 9 (PCSK9) and an inducible degrader of low-density lipoprotein receptor (IDOL), thereby promoting reverse cholesterol transport to the liver from peripheral tissues. The excretion of cholesterol from the liver to the gallbladder was also enhanced, as was that via the enterohepatic circulation. These mechanisms collectively decrease the cholesterol levels, thus alleviating AS. Notably, the expression of genes in the FXR/FGF15 pathway, particularly CYP7A1, was significantly inhibited by gut microbiota remodeling. Therefore, modulation of cholesterol metabolism by gut microbiota remodeling may be implicated in the effect of naringin on AS (Figure 2; Table 1).

Furthermore, naringin promotes reverse cholesterol transport by downregulating the expression of PCSK9/IDOL (Wang F. et al., 2020). Clinical investigations revealed that naringin significantly reduces the body mass index, total cholesterol, and low-density lipoprotein cholesterol, whereas it concurrently elevates the levels of adiponectin in adult patients diagnosed with dyslipidemia. These findings suggest that naringin holds potential as a therapeutic agent

TABLE 1 Main opinions regarding the mode of action of naringin in the treatment of atherosclerosis.

	Reference	Mode	Main opinion
1	Zhao and Zhao (2022)	HUVEC damage induced by TMAO	Naringin inhibited endothelial inflammation, oxidative stress, and degradation of tight junction proteins, such as ZO-2, OCLN, and vascular endothelial-cadherin. Furthermore, it promoted NO release, thereby restoring the functional and structural integrity of the endothelium and inactivating MAPK signaling.
2	Wang et al. (2020a)	$ApoE^{-/-}$ mice fed a high-fat diet	Naringin increased the excretion of bile acids and neutral sterols mainly by modulating the abundance of bile salt hydrolase- and 7α-dehydroxylase-producing bacteria. This led to the promotion of bile acid synthesis from cholesterol by upregulating CYP7A1 via suppression of the FXR/FGF15 pathway. In addition, naringin facilitated reverse cholesterol transport by downregulating PCSK9/IDOL.
3	Chanet et al. (2012)	Wild-type mice fed a high-fat/high-cholesterol diet, ApoE-deficient mice fed a semisynthetic diet	Naringin supplementation reduced plaque progression and the levels of plasma non-high-density lipoprotein cholesterol. It limited atherosclerosis progression by preventing immune cell adhesion and infiltration in the intima of the vascular wall, as well as smooth muscle cell proliferation.
4	Lee et al. (2008)	VSMCs	Naringin inhibited growth and induced cell cycle arrest at the G1 phase (mediated by induction of p53-independent p21WAF1 expression), downregulated the expression of CCNs and CDKs by inhibiting ERK function and p21WAF1 expression, and increased the activation of both Ras and Raf by the Ras/Raf/ERK pathway.
5	Lee et al. (2009)	VSMCs	Naringin impeded the TNF-α-induced expression of MMP9 in VSMCs, as well as invasion and migration. It also inhibited the TNF-α-mediated release of IL6 and IL8. Following administration to VSMCs in the presence of TNF-α, naringin did not affect cell growth and apoptosis. Furthermore, naringin reduced the transcriptional activity of AP-1 and NF-κB, and blocked the PI3K/AKT/mTOR/p70S6K pathway in TNF-α-induced VSMCs. These findings suggest that naringin repressed the PI3K/AKT/mTOR/p70S6K pathway in TNF-α-induced VSMCs, as well as invasion and migration. This was followed by suppression of MMP9 expression through transcription factors NF-κB and AP-1.
6	Zhao et al. (2020)	ox-LDL-induced HUVECs	Pretreatment with naringin inhibited ox-LDL-induced cell injury and apoptosis, and restored the integrity of the endothelial barrier by preventing vascular endothelial-cadherin disassembly and F-actin remodeling in HUVECs. Additionally, treatment with naringin downregulated the expression of pro-inflammatory factors, such as IL1β, IL6, and IL18, in these cells. Naringin-induced YAP downregulation was restored, as demonstrated by the attenuation of the cytoprotective effect of naringin on ox-LDL-induced endothelial cell injury and apoptosis by YAP-shRNA.
7	Pengnet et al. (2019)	Hypercholesterolaemic rats	In hypercholesterolaemic rats, treatment with naringin enhanced aortic NO levels, restored endothelium-dependent responses to acetylcholine, and reduced the levels of O_2^-, LOX-1, NOX subunits ($p47^{phox}$, NOX2, and NOX4), and iNOS, as well as the expression of oxidative damage markers (3-nitrotyrosine and 4-hydroxynonenal) in aortic tissues.
8	Mao et al. (2017)	Thoracic aortas vascular ring	Naringin inhibited the expression of VEGF, CRP, JNK2, p38, and the MAPK pathway. These effects resulted in the decrease of NO synthesis, VEGF expression, and endothelial adhesion factor expression.
9	Bi et al. (2016)	LPS-induced damage in HUVECs	Naringin enhanced the survival rate of HUVECs, concurrently reducing LPS-induced ROS generation and intracellular Ca (2+) levels. Moreover, it exhibited a significant reduction in cytochrome C release from mitochondria to the cytosol. This phytochemical agent downregulated the protein or mRNA levels of IL1, IL6, TNF-α, VCAM1, ICAM1, NF-κB, AP-1, cleaved-CASP3/7/9, p53, BAK, and BAX, while

(Continued on following page)

TABLE 1 (*Continued*) Main opinions regarding the mode of action of naringin in the treatment of atherosclerosis.

	Reference	Mode	Main opinion
			upregulating the expression of BCL-xl and BCL2 to suppress inflammation and apoptosis. Additionally, naringin demonstrated a notable inhibitory effect on the phosphorylation levels of JNK, ERK, and p38 MAPK.
10	Hsueh et al. (2016)	HUVECs	Naringin impeded the adhesion of THP-1 monocytes to TNF-α-stimulated HUVECs, and suppressed the expression of cell adhesion molecules (VCAM-1, ICAM1, and SELE) induced by TNF-α. Furthermore, naringin inhibited the mRNA and protein levels of chemokines, including fractalkine/CX3CL1, MCP-1, and RANTES, stimulated by TNF-α. Significantly, naringin obstructed the nuclear translocation of NF-κB induced by TNF-α, which arises from the inhibited phosphorylation of IKKα/β, IκB-α, and NF-κB.
11	Li et al. (2014)	TNF-α induced HUVECs	Naringin impeded the generation of ROS and the overexpression of NOX4 and $p22^{phox}$ triggered by TNF-α. Furthermore, naringin obstructed the TNF-α induced overexpression of ICAM1 and VCAM-1 (mRNA and protein). Lastly, naringin also suppressed the activation of the NF-κB and PI3K/Akt signaling pathways.
12	Xulu and Oroma Owira (2012)	Diabetes rats induced by streptozotocin intraperitoneally	Naringin reduced the levels of blood LDL, elevated HDL, and decreased hepatic total cholesterol and triglycerides in diabetic rats. It inhibited hepatic HMGCR and Acyl-CoA: cholesterol acyltransferase activities. Naringin modulated the plasma low-density lipoprotein to high-density lipoprotein ratio.
13	Chanet et al. (2012)	Mouse models of hypercholesterolemia, wild-type mice fed a high-fat/high-cholesterol diet and ApoE-deficient mice fed a semisynthetic diet	Naringin decreased the plasma levels of non-high-density lipoprotein cholesterol and modulated biomarkers of endothelial dysfunction. Consequently, the alterations in gene expression induced by naringin imply a restricted progression of atherosclerosis by inhibiting immune cell adhesion and infiltration within the intima of vascular walls, as well as suppressing the proliferation of smooth muscle cells. Additionally, naringenin efficiently mitigated monocyte adhesion to endothelial cells and smooth muscle cell proliferation.
14	Jeon et al. (2001)	Male rabbits were fed a high-cholesterol diet (0.5%, w/w) and naringin (0.05%, w/w) or lovastatin (0.03%) supplemented high-cholesterol diet.	Naringin significantly increased the concentration of plasma vitamin E, and upregulated the mRNA expression of SOD, catalase, and GSH-Px. These results indicate that naringin plays an important role in regulating antioxidative capacities.
15	Choe et al. (2001)	New Zealand white rabbits were fed a 0.25% cholesterol diet	Naringin effectively reduced the size of fatty streak lesions in the thoracic aorta, inhibited subintimal foam cell infiltration, and suppressed hypercholesterolemia-induced ICAM1 expression on endothelial cells. Furthermore, it demonstrated potent protection against hypercholesterolemia-induced fatty liver and elevations in the levels of liver enzymes.
16	Lee et al. (2009)	TNF-α-induced invasion and migration of VSMCs	In VSMCs, naringin exhibited a suppressive effect on TNF-α-induced MMP9 expression, inhibited invasion and migration, and reduced the release of IL6 and IL8 mediated by TNF-α. However, it did not influence cell growth and apoptosis. Furthermore, in additional experiments, naringin demonstrated the ability to reduce the transcriptional activity of AP-1 and NF-κB, and inhibited the PI3K/AKT/mTOR/p70S6K pathway.
14	Wu et al. (2021)	Monocrotaline administration (60 mg/kg) was delivered for the induction of PAH in rats, HUVECs	Naringin significantly inhibited endothelial-to-mesenchymal transition and alleviated PAH progression induced by treatment with TGFβ1, enhanced endothelial marker expression, and inhibited the activation of the ERK and NF-κB signaling pathways.
17	Shangguan et al. (2017)	Vascular endothelial cells	Naringin markedly stimulated vascular endothelial cell proliferation, significantly inhibited serum starvation-induced apoptosis in endothelial cells, and suppressed GRP78, CHOP, CASP12, and cytochrome C protein expression. Additionally,

(Continued on following page)

TABLE 1 (*Continued*) Main opinions regarding the mode of action of naringin in the treatment of atherosclerosis.

	Reference	Mode	Main opinion
			it reduced the mitochondrial membrane potential and the activities of CASP3 and CASP9. Naringin also potently inhibited EDN1, while enhancing NO synthesis. Assessment of the distal femoral microvascular density revealed that the naringin treatment group exhibited a significantly higher number of microvessels compared with the ovariectomized group, as well as a positive correlation between microvascular density and bone mineral density.

Abbreviations: Acyl-CoA, acyl-coenzyme A; AKT, protein kinase B; AP-1, activator protein-1; ApoE$^{-/-}$, apolipoprotein E$^{-/-}$; BAK, BCL2 antagonist/killer; BAX, BCL2 associated X; BCL-xL, BCL-extra large; CASP, caspase; CDKs, cyclin-dependent kinases; CCNs, cyclins; CHOP, C/EBP, homologous protein; CRP, C-reactive protein; CX3CL1, C-X3-C motif chemokine ligand 1; CYP7A1, cytochrome P450 family 7 subfamily A member 1; EDN1, endothelin 1; ERK, extracellular signal-regulated kinase; FXR/FGF15, farnesoid X receptor/fibroblast growth factor 15; GSH-Px, glutathione peroxidase; GRP78, glucose-regulated protein, 78 kDa; HDL, high-density lipoprotein; HMGCR, 3-hydroxy-3-methylglutaryl CoA reductase; HUVECs, human umbilical vein endothelial cells; ICAM1, intercellular adhesion molecule 1; IDOL, E3 ubiquitin ligase-inducible degrader of the low density lipoprotein receptor; IL, interleukin; iNOS, inducible nitric oxide synthase; IKKα/β, IκB kinase α/β; JNK, JUN N-terminal kinase; LDL, low-density lipoprotein; LOX-1, lectin-like oxidized low-density lipoprotein receptor-1; LPS, lipopolysaccharide; MAPK, mitogen-activated protein kinase; MCP-1, monocyte chemoattractant protein-1; MMP9, matrix metalloproteinase 9; mTOR, mechanistic target of rapamycin kinase; NF-κB, nuclear factor-kappa B; NO, nitric oxide; NOX, NADPH, oxidase; O_2^-, superoxide anion; OCLN, occludin; ox-LDL, oxidized-low-density lipoprotein; PAH, pulmonary arterial hypertension; PCSK9, proprotein convertase subtilisin/kexin type 9; PI3K, phosphatidylinositol 3 kinase; RANTES, regulated upon activation, normally T-expressed, and presumably secreted; ROS, reactive oxygen species; SELE, selectin E; SOD, superoxide dismutase; TGFβ1, transforming growth factor β1; TMAO, trimethylamine-N-oxide; TNF-α, tumor necrosis factor-alpha; VCAM1, vascular cell adhesion molecule 1; VEGF, vascular endothelial growth factor; VSMCs, vascular smooth muscle cells; WAF1, wild-type p53 activated fragment-1; YAP, yes-associated protein; ZO-2, zona occludens-2.

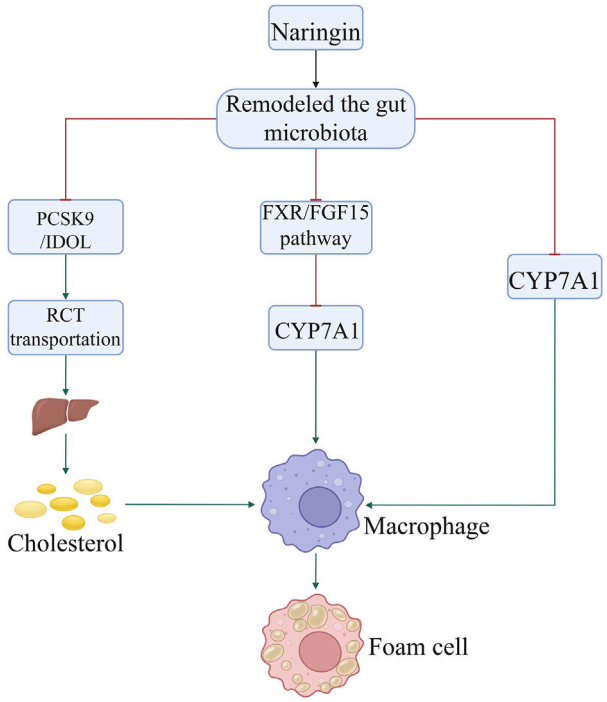

FIGURE 2
Naringin inhibited the formation of foam cells by decreasing the uptake of cholesterol by macrophages through regulation of the gut microbiota. Naringin suppressed the expression of PCSK9, IDOL, FXR/FGF15 pathway, and HMGCR by gut microbiota remodeling, thereby promoting RCT to the liver from peripheral tissues. Abbreviations: CYP7A1, cholesterol 7α-hydroxylase; FXR/FGF15, farnesoid X receptor/fibroblast growth factor 15; HMGCR, 3-hydroxy-3-methylglutaryl-CoA reductase; IDOL, inducible degrader of low-density lipoprotein receptor; PCSK, proprotein convertase subtilisin/kexin type; RCT, reverse cholesterol transport.

in the management of metabolic disorders (Barajas-Vega et al., 2022). The findings were further validated by the inclusion of bergamot juice extract, which contains naringin as one of its primary bioactive constituents. Supplementation with this extract has been shown to effectively lower blood lipid levels, and thereby offer potential benefits for individuals with dyslipidemia (Toth et al., 2015).

4 Naringin attenuates progression of AS by safeguarding endothelial dysfunction

Naringin enhances the survival rate of human umbilical vein endothelial cells (HUVECs) and preserves the functional and structural integrity of the endothelium, which plays a crucial role in inhibiting the advancement of AS. Thus, the preventive effect of naringin on endothelial dysfunction could potentially delay the progression of AS (Li et al., 2014). Pretreatment with naringin attenuates endothelial inflammation, reduces oxidative stress, enhances NO release, and inhibits the degradation of zona occludens 2 (ZO-2), occludin (OCLN), and vascular endothelial-cadherin. These effects preserve the functional and structural integrity of the endothelium (Zhao and Zhao, 2022). It has been demonstrated that the therapeutic effects of naringin are mediated through the inhibition of trimethylamine-N-oxide (TMAO)-stimulated mitogen-activated protein kinase (MAPK) signaling in HUVECs (Zhao and Zhao, 2022). In another investigation, naringin augmented the survival rate of HUVECs and mitigated the elevations in the levels of reactive oxygen species (ROS) and intracellular Ca^{2+} induced by lipopolysaccharide in comparison to the control group (Bi et al., 2016). Moreover, naringin impedes cytochrome C release from mitochondria to cytosol, notably represses the protein or mRNA expression of interleukin 1 (IL1), IL6, tumor necrosis factor-alpha (TNF-α), vascular cell adhesion molecule 1 (VCAM1), ICAM1, nuclear factor-kappa B (NF-κB), activator protein-1 (AP-1), cleaved caspase 3/7/9 (CASP3/7/9), p53, and BCL2 associated X (BAX), and enhances the expression of BCL-extra large (BCL-xl) and BCL2 to curtail inflammation and apoptosis (Zhao and Zhao, 2022). Additionally, naringin robustly inhibits the phosphorylation levels of JUN N-terminal kinase (JNK), extracellular signal-regulated kinase (ERK), and p38 MAPK (Bi et al., 2016), and reduces the expression

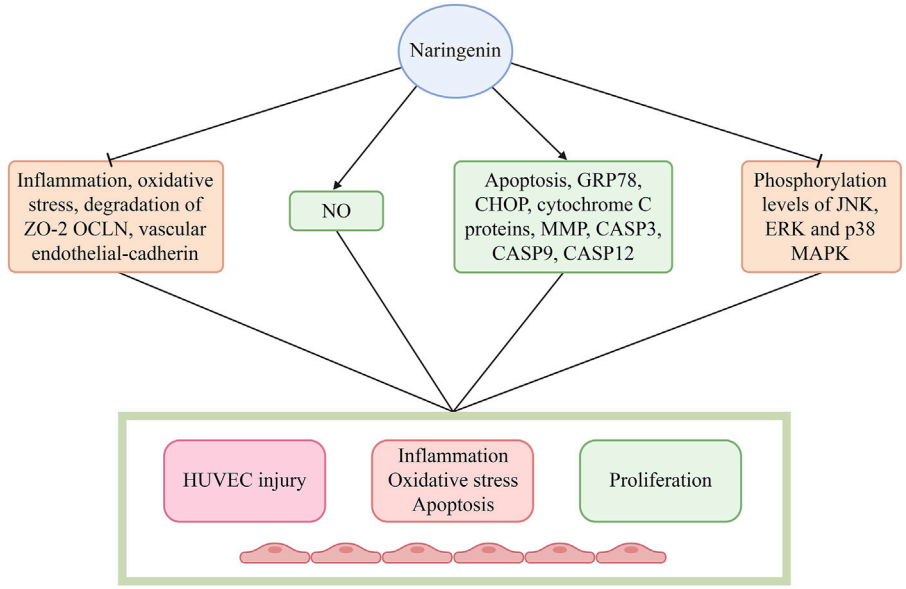

FIGURE 3
Naringin restored the functional and structural integrity of the endothelium by decreasing endothelial inflammation, reducing oxidative stress, increasing NO release, and inhibiting the degradation of zona occludens-2 (ZO-2), occludin (OCLN), and vascular endothelial-cadherin. Naringin obviously inhibited the phosphorylation of JNK, ERK, and p38 MAPK, and decreased the expression of cell adhesion molecules (VCAM-1, ICAM1, and SELE), which are related with the adhesion of THP-1 monocytes to HUVECs induced by TNF-α. Abbreviations: CASP3/9/12, caspase 3/9/12; CHOP, C/EBP homologous protein; ERK, extracellular signal-regulated kinase; GRP78, glucose-regulated protein, 78 kDa; HUVECs: human umbilical vein endothelial cells; ICAM1: intercellular cell adhesion molecule-1; JNK, JUN N-terminal kinase; MAPK, mitogen-activated protein kinase; NO, nitric oxide; SELE, selectin E; TNF-α, tumor necrosis factor-α; VCAM-1, vascular cell adhesion molecule-1.

of cell adhesion molecules (VCAM1, ICAM1, and selectin E [SELE]), which are associated with the adhesion of THP-1 monocytes to HUVECs induced by TNF-α (Li et al., 2014). In addition, naringin markedly reduced the mRNA and protein levels of chemokines, such as fractalkine/C-X3-C motif chemokine ligand 1 (fractalkine/CX3CL1), and monocyte chemoattractant protein-1 (MCP-1), and regulated the activation of normal T cell expressed and secreted, induced by TNF-α (Hsueh et al., 2016). This effect is attributed to the potent inhibition of TNF-α-induced nuclear translocation of NF-κB by naringin, which is mediated by the suppression of IκB kinase α/β (IKKα/β), IκB-α, and NF-κB phosphorylation (Hsueh et al., 2016). These findings indicate that naringin exerts an anti-atherosclerotic effect by modulating the expression of cell adhesion molecules and chemokines. This is achieved by inhibiting the activation of the IKK/NF-κB signaling pathway induced by TNF-α (Hsueh et al., 2016). Naringin inhibits the production of ROS and the overexpression of NADPH oxidase 4 (NOX4) and $p22^{phox}$ induced by TNF-α. Furthermore, it suppresses the activation of the NF-κB and phosphatidylinositol 3 kinase/protein kinase B (PI3K/AKT) signaling pathways. These findings suggest that naringin exerts preventive effects on HUVEC injury induced by alleviated oxidative stress and the inflammatory response. The potential mechanisms underlying these effects may involve inhibition of the NOX4 and NF-κB pathways, as well as activation of the PI3K/AKT pathway (Wang K. et al., 2020). Naringin inhibits the expression of vascular endothelial growth factor (VEGF), C-reactive protein (CRP), JNK2, p38, and NO, indicating that it reduces CRP expression, curtails the activity of JNK2 and p38 kinases, and represses the MAPK pathway. This leads to a decline in NO synthesis, VEGF levels, and endothelial adhesion factor expression (Pengnet et al., 2019). These observations suggest that naringin regulates the inactivation of NO and shields endothelial function from ROS through its potent antioxidant properties (Ikemura et al., 2012).

Naringin also significantly reduced serum starvation-induced apoptosis in endothelial cells (Shangguan et al., 2017). Moreover, it promotes the proliferation of lung vascular endothelial cells in newborn rats, downregulates the expression of glucose-regulated protein, 78 kDa (GRP78), C/EBP homologous protein (CHOP), CASP12, and cytochrome C proteins, reduces the mitochondrial membrane potential, and decreases the activities of CASP3 and CASP9 (Shangguan et al., 2017). In addition, naringin exhibits dual functionality *in vitro* and *in vivo* by suppressing endothelin and enhancing NO synthesis. In summary, naringin exerts its anti-apoptotic effect on vascular endothelial cells by inhibiting the endoplasmic reticulum stress- and mitochondria-mediated pathways, thereby regulating endothelial cell function. Furthermore, naringin promotes angiogenesis, thus exerting its anti-osteoporotic effect (Shangguan et al., 2017) (Figure 3; Table 1).

5 Naringin inhibits the growth, proliferation, invasion, and migration of VSMCs, and induces cell cycle arrest at the G1 phase, demonstrating its potential utility in the prevention of AS

Naringin exerts a significant inhibitory effect on cell growth and triggers VSMCs in response to TNF-α. The inhibitory mechanisms of naringin on TNF-α-induced VSMC proliferation, invasion, and

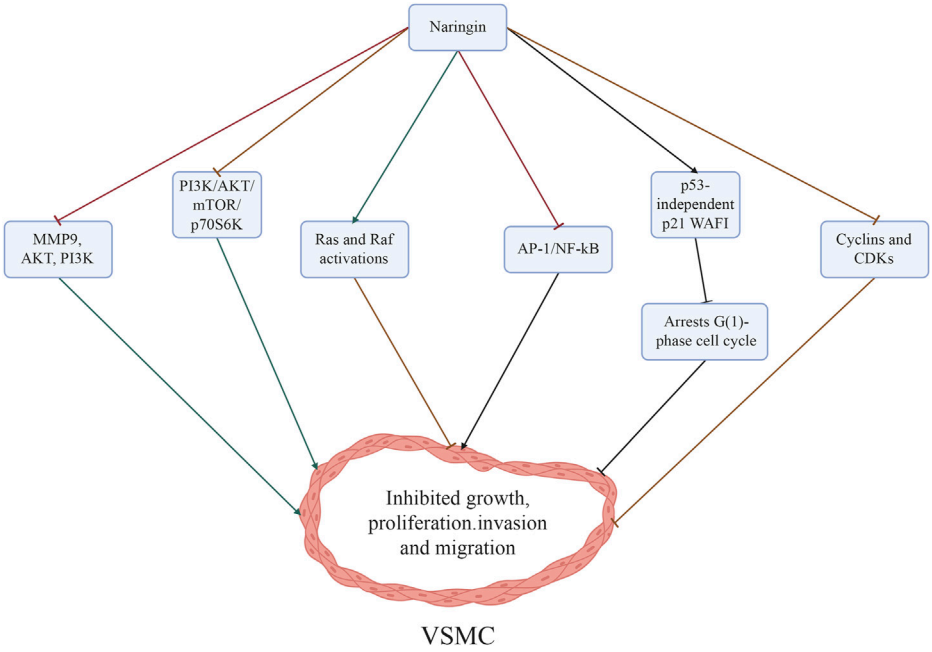

FIGURE 4
Mechanisms through which naringin inhibited the proliferation, invasion, and migration of VSMCs induced by TNF-α. The inhibitory effects of naringin on atherosclerosis were mediated by its ability to downregulate MMP9 and AKT phosphorylation (a downstream effector of PI3K), and reduce NF-κB activity, while also inhibiting the PI3K/AKT/mTOR/p70S6K axis. Naringin resulted in significant inhibition of growth and induced cell cycle arrest at the G1 phase by triggering p53-independent p21WAF1 induction, while concurrently downregulating the expression of cyclins (CCNs) and CDKs in VSMCs. In addition, blockage of ERK function repressed naringin-dependent p21WAF1 expression and concurrently enhanced the activation of Ras and Raf. Abbreviations: AKT, protein kinase B; AP-1, activator protein-1; CDKs, cyclin-dependent kinases; ERK, extracellular signal-regulated kinase; MMP, matrix metalloproteinases; mTOR, mammalian target of rapamycin; NF-κB, nuclear factor-κB; PI3K, phosphatidylinositol 3 kinase; VSMCs, vascular smooth muscle cells; WAF1, wild-type p53 activated fragment-1.

migration might be mediated by the downregulation of matrix metalloproteinase 9 (MMP9) and AKT phosphorylation, which acts as a downstream effector of PI3K (Lee et al., 2009). Besides, treatment with naringin reduced TNF-α-induced MMP9 secretion by decreasing the binding of transcription factors NF-kB and AP-1 to DNA (Lee et al., 2009). Naringin also inhibited TNF-α-induced AKT, mechanistic target of rapamycin kinase (mTOR), and p70S6K phosphorylation (Lee et al., 2009). These results corroborate the notion that naringin inhibits the PI3K/AKT/mTOR/p70S6K pathway (Lee et al., 2009), which could potentially explain the mechanisms underlying the inhibitory effects of naringin on TNF-α induced proliferation, invasion, and migration of VSMCs.

It was demonstrated that treatment with naringin significantly inhibited cell growth and induced cell cycle arrest at the G1 phase. These effects were mediated by the induction of p21 wild-type p53 activated fragment-1 (WAF1) expression independent of p53. Furthermore, it was found that naringin downregulated the expression of cyclins (CCNs) and cyclin-dependent kinases (CDKs) in VSMCs (Lee et al., 2008; Li et al., 2014). Inhibition of ERK function promotes naringin-dependent p21WAF1 expression, counteracts naringin-mediated suppression of cell proliferation, and reduces the levels of cell cycle proteins. Concurrently, treatment with naringin augments the activation of both Ras and Raf. Transfection of cells with dominant negative Ras (RasN17) and Raf (RafS621A) mutant genes impedes naringin-induced ERK activity and p21WAF1 expression. Attenuation of naringin-induced reduction in cell proliferation and cell cycle proteins was observed in the presence of RasN17 and RafS621A mutant genes. The involvement of the Ras/Raf/ERK pathway in p21WAF1 induction was demonstrated, resulting in a decline of CCND1/CDK4 and CCNE/CDK2 complexes and naringin-dependent inhibition of cell growth (Lee et al., 2008). Naringin (10–25 μM) exhibits inhibitory effects on TNF-α-induced MMP9 expression in VSMCs, as well as on invasion and migration. Additionally, it mitigates the TNF-α-mediated release of IL6 and IL8. However, treatment of VSMCs with naringin in the presence of TNF-α does not affect cell growth and apoptosis. In additional experiments, naringin suppressed the transcriptional activity of AP-1 and NF-κB, which are two crucial nuclear transcription factors implicated in MMP9 expression. Moreover, treatment with naringin inhibited the PI3K/AKT/mTOR/p70S6K pathway in TNF-α-induced VSMCs. These results suggest that naringin antagonizes the PI3K/AKT/mTOR/p70S6K pathway, thereby suppressing invasion and migration, and downregulating MMP9 expression through the transcription factors NF-κB and AP-1 in TNF-α-induced VSMCs (Lee et al., 2009) (Figure 4; Table 1).

6 Summary

In recent years, a growing body of evidence has corroborated the anti-atherosclerotic activity of naringin. These effects are attributable to its antioxidant capability, regulation of autophagy, amelioration of blood lipid disorders, inhibition of endothelial cell inflammation and vascular smooth muscle proliferation, reduction

of the entry of low-density lipoprotein into macrophages, and suppression of foam cell formation (All views have been summarized in Table 1). However, most research has focused on fundamental inquiries, with relatively fewer clinical studies conducted thus far. Additional clinical trials are warranted to validate the therapeutic efficacy and potential adverse effects of naringin. In this context, the toxicity of naringin has been evaluated extensively; data from available studies have unequivocally demonstrated the toxic effects to be negligible. In their study, Li et al. (2014) found that naringin did not demonstrate any significant acute or chronic oral toxicity in SD rats. They also found the no-observed-adverse-effect-level in beagle dogs to be at least 500 mg/kg body weight per day, on oral administration for 3 and 6 consecutive months. These studies provide evidence of the favorable safety profile of naringin (Li et al., 2020). Such knowledge would assist in effectively utilizing naringin in clinical practice against AS. In its native state, naringin displays limited water solubility and weak efficacy. Thus, the application of nanoparticle formulation technology should be considered to alter the structure of naringin, with the aim to enhance its water solubility, bioavailability, and pharmacological activity (Dashputre et al., 2023). Additionally, a comprehensive assessment of its pharmacokinetic properties is crucial to fully investigate the potential benefits offered by this intriguing phytochemical.

Author contributions

YL: Writing–original draft, Writing–review and editing, Conceptualization. D-HL: Writing–review and editing, Writing–original draft. J-MX: Formal Analysis, Writing–review and editing. SZ: Formal Analysis, Supervision, Writing–review and editing.

Funding

The author(s) declare that financial support was received for the research, authorship, and/or publication of this article. This work was supported by the Natural Science Foundation of Gansu Province (grant number: 23JRRA1282) and Postgraduate Tutors Fund of Gansu Provincial Hospital (grant number: 22GSSYB-3).

Conflict of interest

The authors declare that the research was conducted in the absence of any commercial or financial relationships that could be construed as a potential conflict of interest.

Publisher's note

All claims expressed in this article are solely those of the authors and do not necessarily represent those of their affiliated organizations, or those of the publisher, the editors and the reviewers. Any product that may be evaluated in this article, or claim that may be made by its manufacturer, is not guaranteed or endorsed by the publisher.

References

Adetunji, J. A., Fasae, K. D., Awe, A. I., Paimo, O. K., Adegoke, A. M., Akintunde, J. K., et al. (2023). The protective roles of citrus flavonoids, naringenin, and naringin on endothelial cell dysfunction in diseases. *Heliyon* 9, e17166. doi:10.1016/j.heliyon.2023.e17166

Alam, M. A., Kauter, K., and Brown, L. (2013). Naringin improves diet-induced cardiovascular dysfunction and obesity in high carbohydrate, high fat diet-fed rats. *Nutrients* 5, 637–650. doi:10.3390/nu5030637

Amini, N., Maleki, M., and Badavi, M. (2022). Nephroprotective activity of naringin against chemical-induced toxicity and renal ischemia/reperfusion injury: a review. *Avicenna J. Phytomed.* 12, 357–370. doi:10.22038/AJP.2022.19620

Bailey, D. G., Dresser, G. K., Leake, B. F., and Kim, R. B. (2007). Naringin is a major and selective clinical inhibitor of organic anion-transporting polypeptide 1A2 (OATP1A2) in grapefruit juice. *Clin. Pharmacol. Ther.* 81, 495–502. doi:10.1038/sj.clpt.6100104

Balachandran, A., Choi, S. B., Beata, M. M., Małgorzata, J., Froemming, G. R. A., Lavilla, C. A., Jr., et al. (2023). Antioxidant, wound healing potential and *in silico* assessment of naringin, eicosane and octacosane. *Molecules* 28, 1043. doi:10.3390/molecules28031043

Barajas-Vega, J. L., Raffoul-Orozco, A. K., Hernandez-Molina, D., Ávila-González, A. E., García-Cobian, T. A., Rubio-Arellano, E. D., et al. (2022). Naringin reduces body weight, plasma lipids and increases adiponectin levels in patients with dyslipidemia. *Int. J. Vitam. Nutr. Res.* 92, 292–298. doi:10.1024/0300-9831/a000658

Bi, C., Jiang, Y., Fu, T., Hao, Y., Zhu, X., and Lu, Y. (2016). Naringin inhibits lipopolysaccharide-induced damage in human umbilical vein endothelial cells via attenuation of inflammation, apoptosis and MAPK pathways. *Cytotechnology* 68, 1473–1487. doi:10.1007/s10616-015-9908-3

Capra, M. E., Biasucci, G., Crivellaro, E., Banderali, G., and Pederiva, C. (2023). Dietary intervention for children and adolescents with familial hypercholesterolaemia. *Ital. J. Pediatr.* 49, 77. doi:10.1186/s13052-023-01479-8

Chanet, A., Milenkovic, D., Deval, C., Potier, M., Constans, J., Mazur, A., et al. (2012). Naringin, the major grapefruit flavonoid, specifically affects atherosclerosis development in diet-induced hypercholesterolemia in mice. *J. Nutr. Biochem.* 23, 469–477. doi:10.1016/j.jnutbio.2011.02.001

Choe, S. C., Kim, H. S., Jeong, T. S., Bok, S. H., and Park, Y. B. (2001). Naringin has an antiatherogenic effect with the inhibition of intercellular adhesion molecule-1 in hypercholesterolemic rabbits. *J. Cardiovasc. Pharmacol.* 38, 947–955. doi:10.1097/00005344-200112000-00017

Dashputre, N. L., Laddha, U. D., Darekar, P. P., Kadam, J. D., Patil, S. B., Sable, R. R., et al. (2023). Potential therapeutic effects of naringin loaded PLGA nanoparticles for the management of alzheimer's disease: *in vitro*, *ex vivo* and *in vivo* investigation. *Heliyon* 9, e19374. doi:10.1016/j.heliyon.2023.e19374

Feng, Y., and Xu, D. (2023). Short-chain fatty acids are potential goalkeepers of atherosclerosis. *Front. Pharmacol.* 14, 1271001. doi:10.3389/fphar.2023.1271001

Gao, Y., Wang, Z., Zhang, Y., Liu, Y., Wang, S., Sun, W., et al. (2018). Naringenin inhibits N(G)-nitro-L-arginine methyl ester-induced hypertensive left ventricular hypertrophy by decreasing angiotensin-converting enzyme 1 expression. *Exp. Ther. Med.* 16, 867–873. doi:10.3892/etm.2018.6258

Global Cardiovascular Risk Consortium, Magnussen, C., Ojeda, F. M., Leong, D. P., Alegre-Diaz, J., Amouyel, P., et al. (2023). Global effect of modifiable risk factors on cardiovascular disease and mortality. *N. Engl. J. Med.* 389, 1273–1285. doi:10.1056/NEJMoa2206916

Heidary Moghaddam, R., Samimi, Z., Moradi, S. Z., Little, P. J., Xu, S., and Farzaei, M. H. (2020). Naringenin and naringin in cardiovascular disease prevention: a preclinical review. *Eur. J. Pharmacol.* 887, 173535. doi:10.1016/j.ejphar.2020.173535

Hong, N., Lin, Y., Ye, Z., Yang, C., Huang, Y., Duan, Q., et al. (2022). The relationship between dyslipidemia and inflammation among adults in east coast China: a cross-sectional study. *Front. Immunol.* 13, 937201. doi:10.3389/fimmu.2022.937201

Hsueh, T. P., Sheen, J. M., Pang, J. H., Bi, K. W., Huang, C. C., Wu, H. T., et al. (2016). The anti-atherosclerotic effect of naringin is associated with reduced expressions of cell adhesion molecules and chemokines through NF-κB pathway. *Molecules* 21, 195. doi:10.3390/molecules21020195

Hwang, I. C., Kim, C. H., Kim, J. Y., Choi, H. M., Yoon, Y. E., and Cho, G. Y. (2023). Rate of change in 10-year atherosclerotic cardiovascular disease risk and its implications for primary prevention. *Hypertension* 80, 1697–1706. doi:10.1161/HYPERTENSIONAHA.122.20678

Ikemura, M., Sasaki, Y., Giddings, J. C., and Yamamoto, J. (2012). Preventive effects of hesperidin, glucosyl hesperidin and naringin on hypertension and cerebral thrombosis in stroke-prone spontaneously hypertensive rats. *Phytother. Res.* 26, 1272–1277. doi:10.1002/ptr.3724

Jeon, S. M., Bok, S. H., Jang, M. K., Lee, M. K., Nam, K. T., Park, Y. B., et al. (2001). Antioxidative activity of naringin and lovastatin in high cholesterol-fed rabbits. *Life Sci.* 69, 2855–2866. doi:10.1016/s0024-3205(01)01363-7

Lee, E. J., Kim, D. I., Kim, W. J., and Moon, S. K. (2009). Naringin inhibits matrix metalloproteinase-9 expression and AKT phosphorylation in tumor necrosis factor-alpha-induced vascular smooth muscle cells. *Mol. Nutr. Food Res.* 53, 1582–1591. doi:10.1002/mnfr.200800210

Lee, E. J., Moon, G. S., Choi, W. S., Kim, W. J., and Moon, S. K. (2008). Naringin-induced p21WAF1-mediated G(1)-phase cell cycle arrest via activation of the ras/raf/ERK signaling pathway in vascular smooth muscle cells. *Food Chem. Toxicol.* 46, 3800–3807. doi:10.1016/j.fct.2008.10.002

Li, G., Xu, Y., Sheng, X., Liu, H., Guo, J., Wang, J., et al. (2017). Naringin protects against high glucose-induced human endothelial cell injury via antioxidation and CX3CL1 downregulation. *Cell Physiol. biochem.* 42, 2540–2551. doi:10.1159/000480215

Li, P., Wang, S., Guan, X., Cen, X., Hu, C., Peng, W., et al. (2014). Six months chronic toxicological evaluation of naringin in Sprague-Dawley rats. *Food Chem. Toxicol.* 66, 65–75. doi:10.1016/j.fct.2014.01.023

Li, P., Wu, H., Wang, Y., Peng, W., and Su, W. (2020). Toxicological evaluation of naringin: acute, subchronic, and chronic toxicity in Beagle dogs. *Regul. Toxicol. Pharmacol.* 111, 104580. doi:10.1016/j.yrtph.2020.104580

Li, W., Wang, C., Peng, J., Liang, J., Jin, Y., Liu, Q., et al. (2014). Naringin inhibits TNF-α induced oxidative stress and inflammatory response in HUVECs via Nox4/NF-κB and PI3K/Akt pathways. *Curr. Pharm. Biotechnol.* 15 (12), 1173–1182. doi:10.2174/1389201015666141111114442

Liu, S., Liu, Y., Liu, Z., Hu, Y., and Jiang, M. (2023). A review of the signaling pathways of aerobic and anaerobic exercise on atherosclerosis. *J. Cell. Physiol.* 238, 866–879. doi:10.1002/jcp.30989

Mao, Z., Gan, C., Zhu, J., Ma, N., Wu, L., Wang, L., et al. (2017). Anti-atherosclerotic activities of flavonoids from the flowers of *Helichrysum arenarium* L. MOENCH through the pathway of anti-inflammation. *Bioorg. Med. Chem. Lett.* 27, 2812–2817. doi:10.1016/j.bmcl.2017.04.076

Memariani, Z., Abbas, S. Q., Ul Hassan, S. S., Ahmadi, A., and Chabra, A. (2021). Naringin and naringenin as anticancer agents and adjuvants in cancer combination therapy: efficacy and molecular mechanisms of action, a comprehensive narrative review. *Pharmacol. Res.* 171, 105264. doi:10.1016/j.phrs.2020.105264

Oyagbemi, A. A., Omobowale, T. O., Adejumobi, O. A., Owolabi, A. M., Ogunpolu, B. S., Falayi, O. O., et al. (2020). Antihypertensive power of naringenin is mediated via attenuation of mineralocorticoid receptor (MCR)/angiotensin converting enzyme (ACE)/Kidney injury molecule (Kim-1) signaling pathway. *Eur. J. Pharmacol.* 880, 173142. doi:10.1016/j.ejphar.2020.173142

Parsamanesh, N., Moossavi, M., Bahrami, A., Fereidouni, M., Barreto, G., and Sahebkar, A. (2019). NLRP3 inflammasome as a treatment target in atherosclerosis: a focus on statin therapy. *Int. Immunopharmacol.* 73, 146–155. doi:10.1016/j.intimp.2019.05.006

Pengnet, S., Prommaouan, S., Sumarithum, P., and Malakul, W. (2019). Naringin reverses high-cholesterol diet-induced vascular dysfunction and oxidative stress in rats via regulating LOX-1 and NADPH oxidase subunit expression. *Biomed. Res. Int.* 2019, 3708497. doi:10.1155/2019/3708497

Pi, Y., Liang, Z., Jiang, Q., Chen, D., Su, Z., Ouyang, Y., et al. (2023). The role of PIWI-interacting RNA in naringin pro-angiogenesis by targeting HUVECs. *Chem. Biol. Interact.* 371, 110344. doi:10.1016/j.cbi.2023.110344

Przybylska, S., and Tokarczyk, G. (2022). Lycopene in the prevention of cardiovascular diseases. *Int. J. Mol. Sci.* 23, 1957. doi:10.3390/ijms23041957

Pu, P., Gao, D. M., Mohamed, S., Chen, J., Zhang, J., Zhou, X. Y., et al. (2012). Naringin ameliorates metabolic syndrome by activating AMP-activated protein kinase in mice fed a high-fat diet. *Arch. Biochem. Biophys.* 518, 61–70. doi:10.1016/j.abb.2011.11.026

Shangguan, W. J., Zhang, Y. H., Li, Z. C., Tang, L. M., Shao, J., and Li, H. (2017). Naringin inhibits vascular endothelial cell apoptosis via endoplasmic reticulum stress and mitochondrial mediated pathways and promotes intraosseous angiogenesis in ovariectomized rats. *Int. J. Mol. Med.* 40, 1741–1749. doi:10.3892/ijmm.2017.3160

Toth, P. P., Patti, A. M., Nikolic, D., Giglio, R. V., Castellino, G., Biancucci, T., et al. (2015). Bergamot reduces plasma lipids, atherogenic small dense LDL, and subclinical atherosclerosis in subjects with moderate hypercholesterolemia: A 6 months prospective study. *Front Pharmacol.* 6, 299. doi:10.3389/fphar.2015.00299

Virani, S. S., Alonso, A., Aparicio, H. J., Benjamin, E. J., Bittencourt, M. S., Callaway, C. W., et al. (2021). Heart disease and stroke statistics-2021 update: a report from the American heart association. *Circulation* 143, e254–e743. doi:10.1161/CIR.0000000000000950

Virani, S. S., Newby, L. K., Arnold, S. V., Bittner, V., Brewer, L. C., Demeter, S. H., et al. (2023). 2023 AHA/ACC/ACCP/ASPC/NLA/PCNA guideline for the management of patients with chronic coronary disease: a report of the American heart association/American college of cardiology oint committee on clinical practice guidelines. *Circulation* 148, e148. doi:10.1161/cir.0000000000001168

Visnagri, A., Adil, M., Kandhare, A. D., and Bodhankar, S. L. (2015). Effect of naringin on hemodynamic changes and left ventricular function in renal artery occluded renovascular hypertension in rats. *J. Pharm. Bioallied Sci.* 7, 121–127. doi:10.4103/0975-7406.154437

Viswanatha, G. L., Shylaja, H., and Moolemath, Y. (2017). The beneficial role of naringin-a citrus bioflavonoid, against oxidative stress-induced neurobehavioral disorders and cognitive dysfunction in rodents: a systematic review and meta-analysis. *Biomed. Pharmacother.* 94, 909–929. doi:10.1016/j.biopha.2017.07.072

Wang, F., Zhao, C., Tian, G., Wei, X., Ma, Z., Cui, J., et al. (2020a). Naringin alleviates atherosclerosis in ApoE−/− mice by regulating cholesterol metabolism involved in gut microbiota remodeling. *J. Agric. Food Chem.* 68, 12651–12660. doi:10.1021/acs.jafc.0c05800

Wang, K., Peng, S., Xiong, S., Niu, A., Xia, M., Xiong, X., et al. (2020b). Naringin inhibits autophagy mediated by PI3K-Akt-mTOR pathway to ameliorate endothelial cell dysfunction induced by high glucose/high fat stress. *Eur. J. Pharmacol.* 874, 173003. doi:10.1016/j.ejphar.2020.173003

Wang, Y., Li, X., Lv, H., Sun, L., Liu, B., Zhang, X., et al. (2023). Therapeutic potential of naringin in improving the survival rate of skin flap: a review. *Front. Pharmacol.* 14, 1128147. doi:10.3389/fphar.2023.1128147

Wang, Z., Wang, S., Zhao, J., Yu, C., Hu, Y., Tu, Y., et al. (2019). Naringenin ameliorates renovascular hypertensive renal damage by normalizing the balance of renin-angiotensin system components in rats. *Int. J. Med. Sci.* 16, 644–653. doi:10.7150/ijms.31075

Wu, Y., Cai, C., Xiang, Y., Zhao, H., Lv, L., and Zeng, C. (2021). Naringin ameliorates monocrotaline-induced pulmonary arterial hypertension through endothelial-to-mesenchymal transition inhibition. *Front. Pharmacol.* 12, 696135. doi:10.3389/fphar.2021.696135

Xu, Z., Zhang, M., Li, X., Wang, Y., and Du, R. (2022). Exercise ameliorates atherosclerosis via up-regulating serum β-hydroxybutyrate levels. *Int. J. Mol. Sci.* 23, 3788. doi:10.3390/ijms23073788

Xulu, S., and Oroma Owira, P. M. (2012). Naringin ameliorates atherogenic dyslipidemia but not hyperglycemia in rats with type 1 diabetes. *J. Cardiovasc. Pharmacol.* 59, 133–141. doi:10.1097/FJC.0b013e31823827a4

Yntema, T., Koonen, D. P. Y., and Kuipers, F. (2023). Emerging roles of gut microbial modulation of bile acid composition in the etiology of cardiovascular diseases. *Nutrients* 15, 1850. doi:10.3390/nu15081850

Yu, X., Meng, X., Yan, Y., Wang, H., and Zhang, L. (2022). Extraction of naringin from pomelo and its therapeutic potentials against hyperlipidemia. *Molecules* 27, 9033. doi:10.3390/molecules27249033

Yu, Y. M., Chao, T. Y., Chang, W. C., Chang, M. J., and Lee, M. F. (2016). Thymol reduces oxidative stress, aortic intimal thickening, and inflammation-related gene expression in hyperlipidemic rabbits. *J. Food Drug Anal.* 24, 556–563. doi:10.1016/j.jfda.2016.02.004

Zhang, H. H., Zhou, X. J., Zhong, Y. S., Ji, L. T., Yu, W. Y., Fang, J., et al. (2022). Naringin suppressed airway inflammation and ameliorated pulmonary endothelial hyperpermeability by upregulating Aquaporin1 in lipopolysaccharide/cigarette smoke-induced mice. *Biomed. Pharmacother.* 150, 113035. doi:10.1016/j.biopha.2022.113035

Zhao, H., Liu, M., Liu, H., Suo, R., and Lu, C. (2020). Naringin protects endothelial cells from apoptosis and inflammation by regulating the hippo-YAP pathway. *Biosci. Rep.* 40, BSR20193431. doi:10.1042/BSR20193431

Zhao, H., and Zhao, J. (2022). Study on the role of naringin in attenuating trimethylamine-N-Oxide-induced human umbilical vein endothelial cell inflammation, oxidative stress, and endothelial dysfunction. *Chin. J. Physiol.* 65, 217–225. doi:10.4103/0304-4920.359796

Zoubdane, N., Abdo, R. A., Nguyen, M., Bentourkia, M., Turcotte, E. E., Berrougui, H., et al. (2024). High tyrosol and hydroxytyrosol intake reduces arterial inflammation and atherosclerotic lesion microcalcification in healthy older populations. *Antioxidants (Basel)* 13, 130. doi:10.3390/antiox13010130

Glossary

2K1C	two-kidney one clip
ACE	angiotensin-converting enzyme
AP-1	activating protein-1
CDKs	cyclin-dependent kinases
CX3CL1	fractalkine
GRP78	glucose regulated protein 78
HDL-C	high-density lipoprotein cholesterol
ICAM-1	intercellular adhesion molecule-1
IDOL	low-density lipoprotein receptor
IKK	IκB kinase
LDL	low-density lipoprotein
LPS	lipopolysaccharide
MCR	mineralocorticoid receptor
NF-kB	nuclear factor-kB
PCSK9	proprotein convertase subtilisin/kexin type
RCT	reverse cholesterol transport
SMC	smooth muscle cell
TNF-α	tumor necrosis factor-alpha
VEC	vascular endothelial cell
VLDL	very-low-density lipoprotein
WAF1	wild-type p53 activated fragment-1
AS	atherosclerosis
AKT	protein kinase B
ATR	angiotensin receptor
CHOP	C/EBP-homologous protein
ERK	extracellular signal-regulated kinase
GST	glutathione S-transferase
HUVEC	human umbilical vein endothelial cell
ICAM-1	intercellular cell adhesion molecule-1
MMP	matrix metalloproteinase
Kim	kidney injury molecule
L-NAME	L-NG-nitro arginine methyl ester
MAPK	mitogen-activated protein kinase
mTOR	mammalian target of rapamycin
NO	Nitric oxide
PI3	phosphatidylinositol 3 kinase
ROS	reactive oxygen species
SOD	superoxide dismutase
VCAM-1	vascular cell adhesion molecule-1
VEGF	vascular endothelial growth factor
VSMC	vascular smooth muscle cell

frontiers | Frontiers in Physiology

TYPE Original Research
PUBLISHED 24 September 2024
DOI 10.3389/fphys.2024.1452986

OPEN ACCESS

EDITED BY
Bakovic Marica,
University of Guelph, Canada

REVIEWED BY
Dengbao Yang,
University of Texas Southwestern Medical Center, United States
Timothy Allerton,
Pennington Biomedical Research Center, United States

*CORRESPONDENCE
Craig Porter,
cporter@uams.edu

RECEIVED 21 June 2024
ACCEPTED 26 August 2024
PUBLISHED 24 September 2024

CITATION
Sadler DG, Landes RD, Treas L, Sikes J and Porter C (2024) Protonophore treatment augments energy expenditure in mice housed at thermoneutrality.
Front. Physiol. 15:1452986.
doi: 10.3389/fphys.2024.1452986

Protonophore treatment augments energy expenditure in mice housed at thermoneutrality

Daniel G. Sadler[1,2,3], Reid D. Landes [2,4], Lillie Treas[1,2], James Sikes[1,2] and Craig Porter[1,2,3]*

[1]Arkansas Children's Nutrition Center, Little Rock, AR, United States, [2]Arkansas Children's Research Institute, Little Rock, AR, United States, [3]Department of Pediatrics, Univesrity of Arkansas for Medical Sciences, Little Rock, AR, United States, [4]Departments of Biostatistics, University of Arkansas for Medical Sciences, Little Rock, AR, United States

Background: Sub-thermoneutral housing increases facultative thermogenesis in mice, which may mask the pre-clinical efficacy of anti-obesity strategies that target energy expenditure (EE). Here, we quantified the impact of protonophore treatment on whole-body energetics in mice housed at 30°C.

Methods: C57BL/6J mice (n = 48, 24M/24F) were housed at 24°C for 2 weeks; 32 (16M/16F) were then transitioned to 30°C for a further 4 weeks. Following 2 weeks acclimation at 30°C, mice (n = 16 per group, 8M/8F) received either normal (0 mg/L; Control) or supplemented (400 mg/L; 2,4-Dinitrophenol [DNP]) drinking water. Mice were singly housed in metabolic cages to determine total EE (TEE) and its components via respiratory gas exchange. Mitochondrial respiratory function of permeabilized liver tissue was determined by high-resolution respirometry.

Results: Transitioning mice from 24°C to 30°C reduced TEE and basal EE (BEE) by 16% and 41%, respectively (both $P < 0.001$). Compared to 30°C controls, TEE was 2.6 kcal/day greater in DNP-treated mice (95% CI: 1.6–3.6 kcal/day, $P < 0.001$), which was partly due to a 1.2 kcal/day higher BEE in DNP-treated mice (95% CI: 0.6–1.7 kcal/day, $P < 0.001$). The absolute TEE of 30°C DNP-treated mice was lower than that of mice housed at 24°C in the absence of DNP (DNP: 9.4 $\pm$ 0.7 kcal/day vs. 24°C control: 10.4 $\pm$ 1.5 kcal/day). DNP treatment reduced overall body fat of females by 2.9 percentage points versus sex-matched controls (95% CI: 1.3%–4.5%, $P < 0.001$), which was at least partly due to a reduction in inguinal white fat mass.

Conclusion: Protonophore treatment markedly increases EE in mice housed at 30°C. The magnitude of change in TEE of mice receiving protonophore treatment at 30°C was smaller than that brought about by transitioning mice from 24°C to 30°C, emphasizing that housing temperature must be considered when assessing anti-obesity strategies that target EE in mice.

KEYWORDS

protonophores, energy expenditure, thermoneutral, mitochondria, mouse models

Introduction

The obesity pandemic affects more than 4 in 10 adults in the United States. Upward of $150 billion is spent annually to treat acute and chronic conditions related to obesity (Finkelstein et al., 2009). Despite this, there are very few drugs approved for obesity treatment. Currently available pharmacotherapy regimens rarely achieve weight loss of

greater than 10% and often fail to provide patients with long-term weight control (Calderon et al., 2022; Rucker et al., 2007). The limited availability of effective drugs that target obesity is likely explained by the complex multifaceted nature of the disease. Indeed, until the recent development of the GLP1 agonist Semaglutide, only bariatric surgery was capable of bringing about significant and sustained weight loss in individuals with obesity.

The paucity of anti-obesity drugs may also be related to the failure of some pre-clinical obesity models to accurately recapitulate human obesity. Indeed, laboratory mice housed under standard vivarium temperatures (20°C–26°C) are relatively resistant to diet-induced obesity (Feldmann et al., 2009; Keipert et al., 2020; Liu et al., 2003) and exhibit a total-to-basal energy expenditure (EE) ratio 2–3 times greater than that of humans (Fischer et al., 2018; Keijer et al., 2019). This reflects the fact that sub-thermoneutral housing temperatures impose thermal stress on mice that can induce significant non-shivering thermogenesis (Fischer et al., 2018; Keijer et al., 2019; Škop et al., 2020) and changes in the proteomic signatures of adipose tissue depots (Sadler et al., 2022). Accordingly, the outcome(s) of rodent studies investigating anti-obesity therapies may be influenced by housing temperature.

Protonophores have long been considered anti-obesity agents given their ability to potently uncouple mitochondria. The protonophore 2,4-dinitrophenol (DNP) was known to augment EE as early as the 1890's (Dunlop, 1934), which resulted in its use as a weight loss drug in the 1930's (Tainter et al., 1934). However, DNP was withdrawn from patient use due to unfavorable side effects (Grundlingh et al., 2011). Despite this, mitochondrial uncoupling through DNP treatment has been demonstrated to improve glucose tolerance and reduce adiposity without causing toxicity in pre-clinical models of obesity (Goldgof et al., 2014; Perry et al., 2013). Further studies have demonstrated improved metabolic health with alternative protonophores (Alexopoulos et al., 2020; Kalinovich et al., 2005; Tao et al., 2014), renewing interests in the anti-obesity effects of mitochondrial uncouplers.

Given the renewed interest in the anti-obesity potential of drugs such as protonophores, it is important to study the efficacy and safety of these compounds using preclinical models that are not already hypermetabolic. Indeed, DNP's ability to increase EE and lower adiposity in mice at 30°C is diminished at 22°C (Goldgof et al., 2014). However, there is limited data available on how protonophores impact total energy expenditure (TEE) and its components in male and female mice housed at thermoneutrality. To this end, we investigated the impact of housing temperature and protonophore treatment on whole-body energetics in male and female mice.

Methods

Animals

Male and female C57Bl/6J (#000664, Jackson Laboratories, Bar Harbor, ME, United States) mice (6–8 weeks old) were individually housed at 24°C on a standard light cycle (light 7am–7pm) with *ad libitum* access to a standard chow diet (TD.95092 [18.8% protein, 17.2% kcal fat, 63.9% kcal carbohydrate, 3.8 kcal/G] Envigo Teklad Diets, Madison, WI, United States). After ~2 weeks of acclimation, one group of animals were maintained at 24°C (n = 16) and the remaining two groups were transitioned to 30°C (n = 32) for a total of 4 weeks. After 2 weeks of acclimation at the assigned housing temperature, the two groups of mice (n = 16 per group, 8 male/8 female) housed at 30°C were further randomized to receive either normal drinking water (0 mg/L; Control) or DNP-supplemented (400 mg/L; DNP) drinking water for a further 2 weeks. Animal weights and body composition were recorded before and after 2 weeks of DNP treatment. At conclusion of the study, all animals were euthanized in a rising concentration of CO_2, and tissue samples were collected. This protocol was approved by the Institutional Animal Care and Use Committee at the University of Arkansas for Medical Sciences. The experimental approaches used in preliminary studies to determine the DNP dose (400 mg/L) used in the current study are described in the Supplementary Material. Due to the nature of the current studies (i.e., housing temperature changes and administration of a hazardous compound via drinking water) research staff were not blinded to group allocation. Whenever possible, the collation and analysis of raw data was performed by researchers that were blinded to group allocation.

Body composition analysis

Body composition was measured by quantitative magnetic resonance imaging (qMRI) using the EchoMRI-1100 (EchoMRI, Houston, Texas, United States). Fat free mass (FFM) was calculated as the difference between body weight and fat mass (FM).

Metabolic and activity phenotyping

From days 12–16 and 37–41 of the 6-week study, all mice underwent metabolic and activity phenotyping. Mice were individually housed for 5-6 consecutive days in specialized cages that allowed rates of oxygen consumption (VO_2) and carbon dioxide production (VCO_2) to be continuously measured to calculate total energy expenditure and its components (Sable Systems International, Las Vegas, NV, United States). During this time, food and water intake, activity, and voluntary wheel running were also continuously recorded. Animals were housed in environmental cabinets to control ambient temperature for metabolic phenotyping experiments. For mice transitioned from 24°C to 30°C, cabinet temperature was increased from 24°C to 30°C by 1°C per hour on day 3 of metabolic data collection (days 12–16 of the study).

Data files from metabolic phenotyping experiments were processed using macros to distill data into hourly averages/totals and provided circadian reports for each 12-h light cycle (Sable Systems International, Las Vegas, NV, United States). Rates of EE were calculated from VO_2 and VCO_2 using the Weir equation:

$$EE\left(\frac{kcal}{hr}\right) = 60 \times (0.003941 \times VO_2) + (0.001106 \times VCO_2)$$

TEE was calculated by summing average rates of EE for the light and dark cycle (kcal/cycle). Basal EE (BEE) was calculated from the 30-min period with the lowest average EE (kcal/hour) in the light

cycle and extrapolated to 24 h. Resting EE (REE) was calculated from the 30-min activity period with the lowest average EE (kcal/hour) in the light cycle and extrapolated to 24 h. Energy expenditure of individual wheel running bouts were calculated as the EE exceeding the BEE associated with each individual running bout. Total daily wheel EE was calculated by summing the EE of all wheel running bouts for each day and averaging across the measurement period. Peak activity EE (AEE) was calculated as the highest EE (kcal/hour) over a 15-min period in the dark cycle. All data were averaged over two consecutive days. Daily energy intake was calculated by summing the total food consumed by the mouse during the experimental period and multiplying that sum by the diet energy density, before dividing by the number of days in the experimental period. All meters were the measurement of cage ambulation that included all gross and fine movements but excluded any meters ran directly on the running wheel. Wheel meters for two male (24°C) and one female (30°C), and all meters for one male (30°C + DNP) and one female (30°C) were excluded due to technical issues pertaining to the collection of running wheel use data.

Tissue collection

Mice were euthanized in a rising concentration of CO_2. Subsequently, liver, interscapular brown adipose tissue (iBAT) and inguinal white adipose tissue (iWAT) depots were excised and weighed. Liver tissue was then immediately placed in ice-cold BIOPS preservation buffer (10 mM Ca-EGTA buffer, 0.1 μM free calcium, 20 mM imidazole, 20 mM taurine, 50 mM K-MES, 0.5 mM DTT, 6.56 mM $MgCl_2$, 5.77 mM ATP, 15 mM phosphocreatine, pH 7.1) for respirometry measures. Remaining tissue was frozen and stored at −80°C for further analyses.

High resolution respirometry

Liver tissue was stored in ice-cold BIOPS preservation buffer from the time of sample collection until it was analyzed by high resolution respirometry. Liver tissue was minced into in BIOPS buffer before being blotted on filter paper briefly prior to being weighed. Approximately 1–2 mg (wet weight) of liver was transferred into the chamber of an Oxygraph-2K (O2k) high-resolution respirometer (Oroboros Instruments, Innsbruck, Austria) containing 2 mL of buffer (MiR05 composition: 0.5 mM EGTA; 3 mM MgCl2; 0.5 M K–lactobionate; 20 mM taurine; 10 mM KH_2PO_4; 20 mM HEPES; 110 mM sucrose; and 1 mg/mL essential fatty acid free bovine serum albumin) for assessment of mitochondrial bioenergetics. High resolution respirometry analysis was performed on the same day of sample collection, typically within 2–4 h of euthanasia. Temperature was maintained at 37°C and O_2 concentration within the range of 200–400 nmol/mL for all respirometry analyses. O_2 concentration within the Oxygraph chamber was recorded at 2–4 s intervals (DatLab, Oroboros Instruments, Innsbruck, Austria) and used to calculate respiration per milligram of wet tissue weight.

Upon loading into the chamber, liver was permeabilized by the addition of digitonin (2 μM). Mitochondrial respiration in the leak state was subsequently assayed following the addition of saturating concentrations of substrates (20 mM pyruvate, 2 mM malate, 10 mM glutamate and 20 mM succinate). Thereafter, saturating concentrations of ADP (7.5 mM) and oligomycin (OMY; 15 μM) were added to determine maximal respiration rates linked to ATP production (OXPHOS) and proton leak, respectively. Finally, carbonyl cyanide m-chlorophenylhydrazone (CCCP; 20 μM) was titrated into the chamber to determine maximal electron transfer capacity. Where measured electron transfer capacity was lower than OXPHOS, values of OXPHOS were used in place of electron transfer capacity. Respiratory (RCR) and flux (FCR) control ratios were calculated from respirometry data as qualitative indices of mitochondrial respiratory function.

Statistical analysis

Outcomes from individual animals are presented in the figures and are summarized with the groups' means and standard deviations (SDs). When evaluating the effects of transitioning mice from 24°C to 30°C, the outcomes were analyzed with a repeated measures ANOVA having sex, time, and their interaction as factors. There was evidence that the variability differed between pre- and post-transition for all outcomes examined; hence the within-animal covariance matrix was assumed to be general. The primary comparison of interest was between pre- and post-transition (the time main effect). When there was evidence of a time× sex interaction at the $P < 0.20$ level, then the pre- vs. post-transition comparison was made within each sex, and the results adjusted for these 2 comparisons with Bonferroni's method.

When evaluating DNP effects, the outcomes were analyzed with a two-factor ANOVA having DNP administration, sex, and their interaction as factors. Normal and constant variance assumptions were checked. Normal assumptions were violated for only one outcome (body mass). For this one outcome, we performed a nonparametric analysis to determine whether the inferences based on the normal assumptions differed. Constant variance assumptions were violated for several outcomes. In those instances, we allowed variances among select groups to differ, and we estimated the error of degrees of freedom with the Kenward-Roger method (Kenward and Roger, 2009). Our primary comparison of interest was the main effect of DNP. If, however, the DNP sex interaction was significant at the $P < 0.20$ level, we present the sex-specific DNP effects, and adjust these comparisons with Bonferroni's method. For significant sex-dependent results, we report the interaction effect, which compares the DNP effect in females to that in males. Our significance level was 0.05. The models described above were fitted with the MIXED procedure in SAS/STAT© version 9.4 (SAS Institute, Cary, NC). Though outcomes from the control animals housed continuously at 24°C are included in the figures, these data were not included in the statistical models; they are for visual comparison purposes only. The data and software code producing the results are provided in the Supplementary Material.

Sample size considerations

We wanted to be able to detect a difference in means of total energy expenditure between DNP-treated and control animals of size 1.4 SD, where SD is assumed constant between populations. The sample size was calculated for detecting a main effect of DNP with 0.90 power on a 0.01 level test in the two-factor ANOVA described above. The DNP group size was calculated to be 16 (8 males); thus 32 total animals that

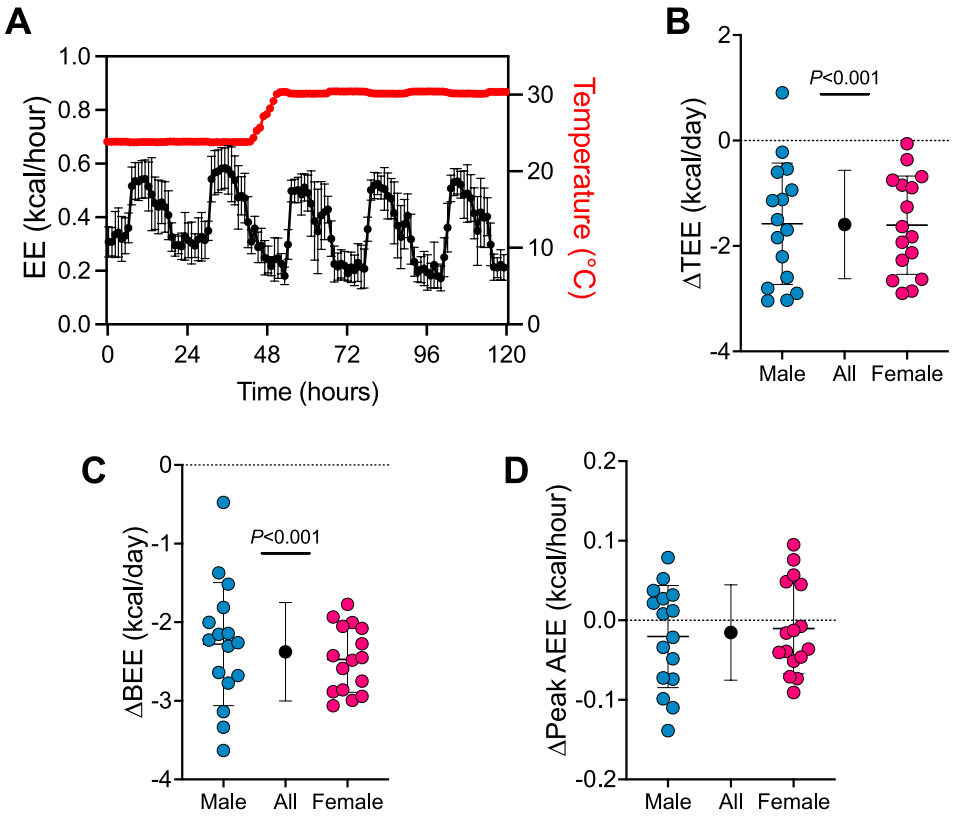

FIGURE 1
Energy expenditure rapidly changes upon the transition from 24°C to 30°C. **(A)** Representative energy expenditure trace upon the transition from 24°C to 30°C housing (n = 32). Change in **(B)** TEE, **(C)** BEE and **(D)** peak AEE from pre- to post- transition from 24°C to 30°C. Blue and red circles represent male and female animals (n = 16), respectively. Black points represent group means when male and female data combined. Data are mean ± SD.

were to be transitioned to 30°C. We also used n = 16 (8 males) for the control animals continuously housed at 24°C. Altogether we used 48 animals to evaluate transition and DNP effects.

Results

Dose-response to DNP treatment

To determine the optimal concentrations of DNP to administer in this study, a pilot study was performed where mice received DNP-supplemented drinking water ranging from 0 to 1,400 mg/L (in 200 mg/L increments, n = 4 mice per group) at 24°C. Concentrations of DNP >400 mg/L acutely attenuated mouse TEE (despite increased BEE), which was the result of reduced food and water intake, as well as a marked reduction in wheel running (Supplementary Figure S1). In contrast, a dose of 400 mg/L did not markedly affect animal behavior but did augment BEE and TEE.

Transitioning mice from 24°C to 30°C lowers energy expenditure

First, we determined how the transition from 24°C to 30°C affects TEE and its components (see Figure 1; Supplementary Figure S2). A trace of EE during the transition from 24°C to 30°C is presented in Figure 1A. Transitioning mice from 24°C to 30°C reduced TEE by 1.6 kcal/day (95% CI: 1.2–2.0 kcal/day, P < 0.001; Figure 1B) and BEE by 2.4 kcal/day (95% CI: 2.1–2.6 kcal/day, P < 0.001; Figure 1C). Peak AEE was similar in all mice pre- and post-temperature transition (Figure 1D). There was no evidence that transition effects depended on sex (all 3 time×sex interactions P > 0.390).

DNP treatment augments energy expenditure in male and female mice housed at 30°C

After establishing the impact of transitioning mice from 24°C to 30°C on TEE and its components, we assessed how DNP affects these parameters in mice acclimated to 30°C. TEE was 2.6 kcal/day greater in all DNP-treated mice (95% CI: 1.6–3.6 kcal/day, P < 0.001) when compared to all 30°C control mice (Figure 2A). Of interest, though TEE in mice treated with DNP was significantly higher than the 30°C control mice, their mean was still lower than that of mice housed at 24°C in the absence of DNP (DNP: 9.4 ± 0.7 kcal/day vs. 24°C control: 10.4 ± 1.5 kcal/day). BEE was 1.2 kcal/day greater in DNP-treated mice (95% CI: 0.6–1.7 kcal/day, P < 0.001) when compared to the 30°C control mice (Figure 2B). Daily food intake of DNP-treated mice was 5.1 kcal/day higher than controls (95% CI: 2.8–7.3 kcal/day, P < 0.001; Figure 2C). DNP treatment did not alter wheel running activity compared to 30°C control mice; though,

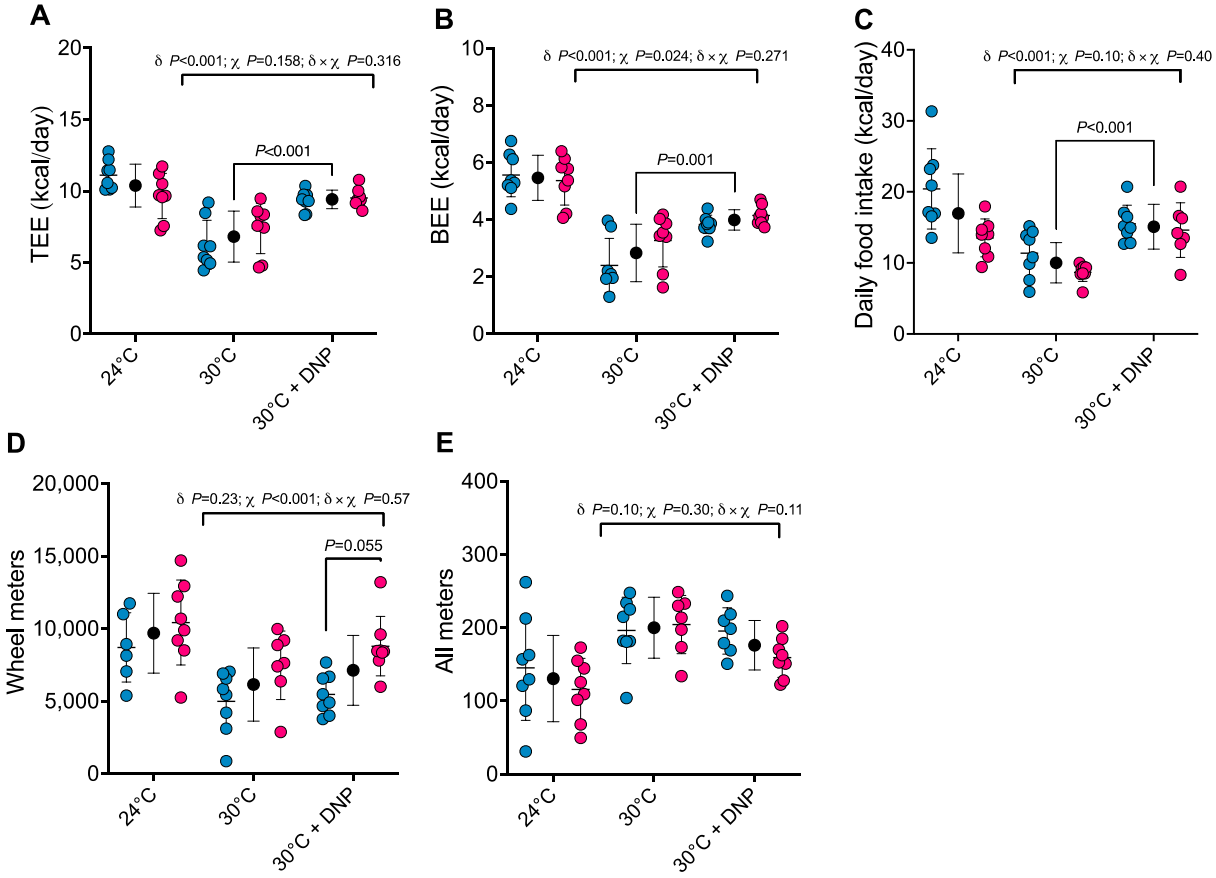

FIGURE 2
DNP treatment augments energy expenditure. **(A)** TEE. **(B)** BEE. **(C)** daily food intake. **(D)** Wheel meters. **(E)** all meters. Blue, red, and black circles represent males, females and males/female combined, respectively. Data are values ± SD (n = 8 per group; total n = 48). δ main effect of DNP treatment. χ main effect sex. δ × χ DNP and sex interaction. Protonophore treatment alters body composition of mice housed at thermoneutrality in a sex-dependent manner.

females ran more than males averaged over both 30°C conditions (Figure 2D). For all meters (ambulation), there was some evidence that the DNP effect depended on sex (DNP×sex interaction p = 0.110). The 30°C DNP females moved 45 m/day less than the 30°C control females (95% CI: 0–90 m/day; Figure 2E), whereas there was little difference between the DNP and control males at 30°C.

Next, we determined how DNP affects body composition. Body mass of male and female mice was similar between DNP and 30°C control groups (Figure 3A). DNP effects on body composition were sex dependent (Figures 3B, C): DNP decreased relative fat mass in females by 2.9 percentage points (P < 0.001), and the female's DNP-decrease was 2.7 percentage points more (95% CI: 0.8 to 4.7 percentage points, interaction p = 0.007, Figure 3C) than the non-significant DNP-decrease of 0.2 percentage points experienced by males. Likewise, DNP decreased relative iWAT mass by 0.34 percentage points in females (P < 0.001; Figure 3D), and the female's DNP-decrease was 0.25 percentage points more (95% CI: 0.08 to 0.43 percentage points, interaction p = 0.006) than the non-significant DNP-decrease of 0.08 percentage points experienced by males (Figure 3D). Compared to 30°C control mice, DNP treatment increased iBAT mass by 0.05 percentage points (95% CI: 0.01 to 0.09, p = 0.017; Figure 3E); the DNP effect did not depend on sex (interaction p = 0.626).

Protonophore treatments alters hepatic bioenergetics in a sex-dependent manner

To establish whether DNP alters the respiratory capacity and coupling control of hepatic mitochondria, we performed high-resolution respirometry on digitonin permeabilized liver tissue. No effects of DNP were found in PGMS-driven respiration, OMY-sensitive respiration, or OMY flux control (Figure 4A/B/C). However, DNP effects were present in OMY-insensitive respiration, OXPHOS, and ETC., and the DNP effects statistically differed between the sexes. For OMY-insensitive respiration, DNP increased O_2 flux in females by 7.4 pmol/O_2/mg (p = 0.026) and decreased O_2 flux in males by 15.7 pmol/O_2/mg (p = 0.005): thus a 23.1 pmol/O_2/mg difference in DNP effects between the sexes (95% CI: 12.8, 33.4 pmol/O_2/mg, P < 0.001, Figure 4D). For OXPHOS, DNP increased O_2 flux in females by 19.0 pmol/O_2/mg (p = 0.033) and decreased O_2 flux in males by 20.9 pmol/O_2/mg (p = 0.207): thus a 40.0 pmol/O_2/mg difference in DNP effects between the sexes (95% CI: 11.2–68.8 pmol/O_2/mg, p = 0.009, Figure 4E). Finally, for, ETC., DNP increased O_2 flux in females by 39.2 pmol/O_2/mg (p = 0.016) and decreased O_2 flux in males by 33.5 pmol/O_2/mg (p = 0.042): thus a 72.8 pmol/O_2/mg difference in DNP effects between the sexes (95% CI: 33.0–112.6 pmol/O_2/mg, P < 0.001, Figure 4F).

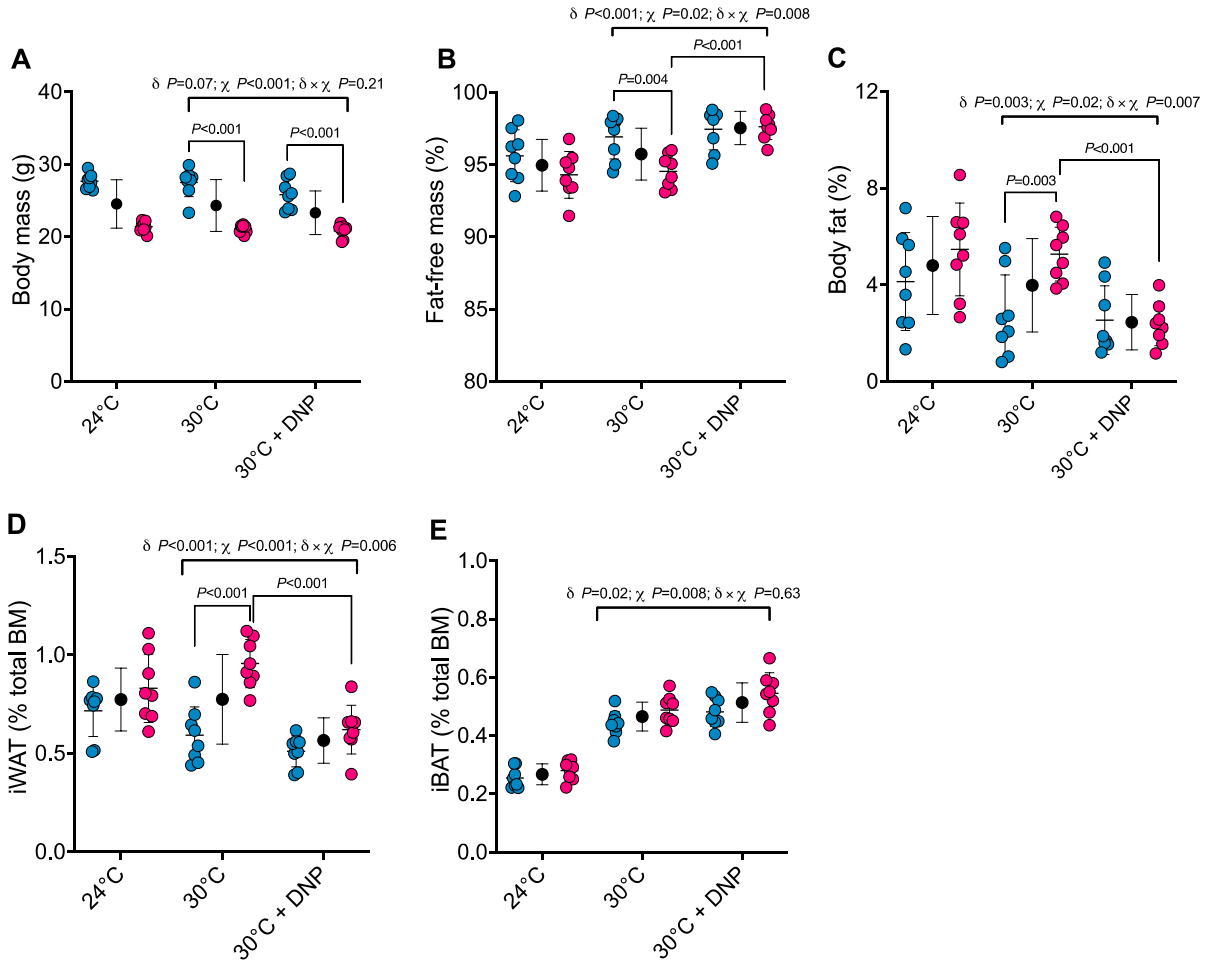

FIGURE 3
DNP treatment alters body composition in a sex-dependent manner. **(A)** Body mass. **(B)** Percent fat-free mass. **(C)** Percent body fat. **(D)** Relative iWAT mass. **(E)** Relative iBAT mass. Blue, red, and black circles represent males, females and males/female combined, respectively. Data are values ± SD (n = 8 per group; total n = 48). δ main effect of DNP treatment. χ main effect sex. δ × χ DNP and sex interaction.

Discussion

We investigated how housing temperature and protonophore treatment impact whole body EE and behavior in mice. We demonstrate that chronic protonophore treatment augments the TEE of mice housed at 30˚C by augmenting BEE. Of interest, TEE of protonophore-treated mice housed at 30˚C were still lower than those of mice housed at 24˚C in the absence of protonophores. This emphasizes the impact of housing temperature on facultative thermogenesis in mice and highlights the need to consider housing temperature when investigating drugs that target EE.

It has long been known that protonophores such as DNP augment EE in humans (Dunlop, 1934). More recent work has demonstrated that DNP treatment elevates EE of mice housed at thermoneutrality, although this effect is lost in mice housed at 22˚C (Goldgof et al., 2014). Similarly, we observed a robust increase in the basal, and therefore, TEE of male and female mice treated with DNP when housed at 30˚C. These findings suggest that protonophores can potently augment murine TEE in the absence of cold-induced non-shivering thermogenesis. Interestingly, the magnitude of change in TEE we observed with DNP treatment at 30˚C was smaller than the change evoked in the temperature transition from 24˚C to 30˚C. This highlights the importance of considering housing temperature when designing experiments to study drugs that target EE. Furthermore, our findings underscore the ability of protonophores to alter bioenergetics independent of cold-induced UCP1 mediated uncoupling (Bertholet et al., 2022).

Our finding that energy intake increases concurrently with EE following protonophore treatment supports the notion that mammalian energy intake is somewhat coupled to EE (Ono-Moore et al., 2020) – at least in the paradigm of a significant hypermetabolic response to protonophore treatment. However, this observation contrasts previous studies reporting unaltered energy intake and elevated EE in rodents following protonophore treatment (Goldgof et al., 2014; Alexopoulos et al., 2020; Axelrod et al., 2020). Perhaps, the discrepancies between these findings and those in the present study are due to the methods used to quantify animal energy intake–one study assessed energy intake biweekly in group housed animals, whereas we quantified daily energy intake in singly housed mice by real-time food intake measures, where animals also had access to running wheels. These discrepancies may also be explained by the use of high versus low-fat diets. Moreover, in the present study we did not directly measure dietary absorption efficiency, which could have been influenced by protonophore

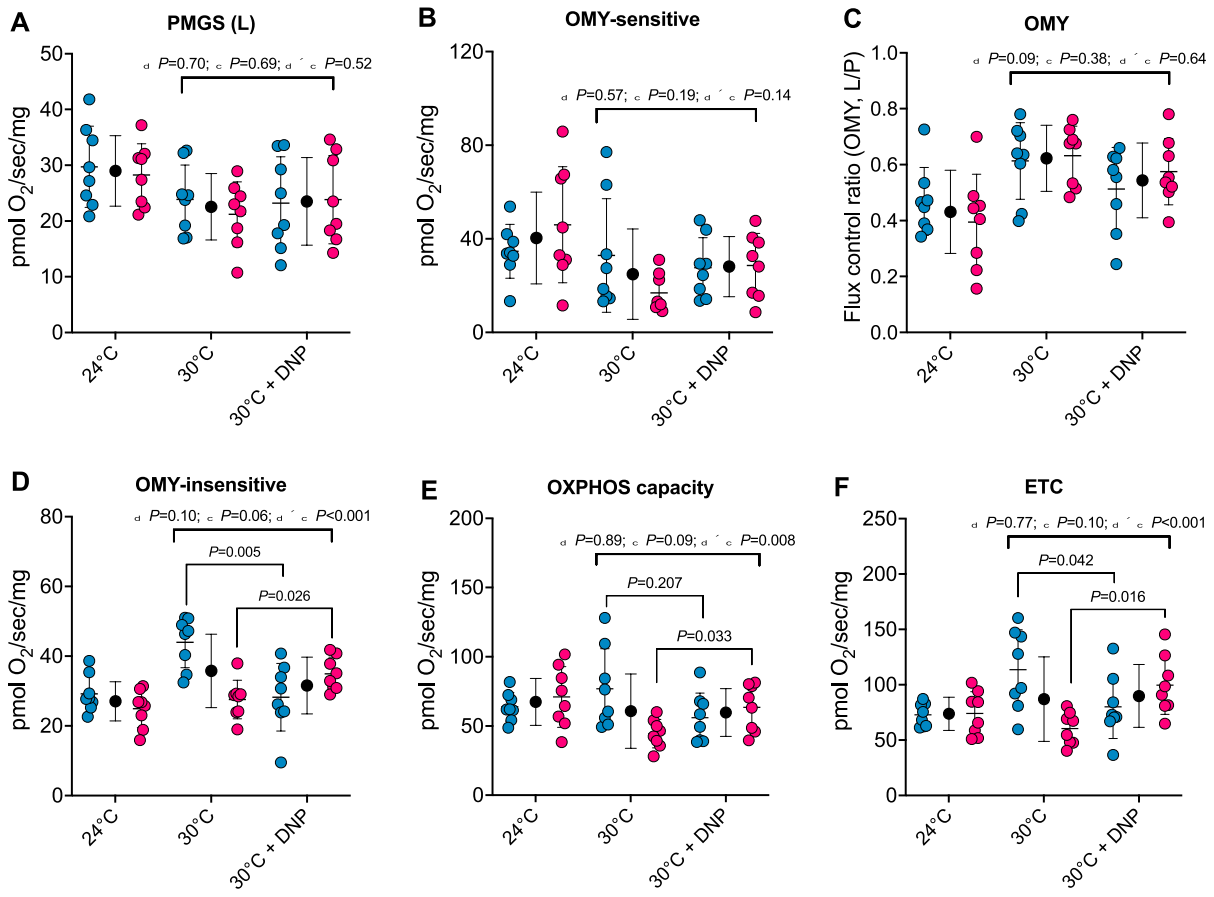

FIGURE 4
Protonophore treatment alters liver bioenergetics in a sex-dependent manner. Hepatic bioenergetics in response to substrates, uncoupler and inhibitors. **(A)** PGMS-driven leak respiration; **(B)** OMY-sensitive respiration; **(C)** Flux control ratio for respiration in the presence of OMY (L/P); **(D)** OMY-insensitive respiration; **(E)** OXPHOS capacity **(F)** Electron transfer capacity (ETC.). PGMS = Pyruvate/glutamate/malate/succinate. OMY = oligomycin. (L), leak state; **(E)**, electron transfer. Blue, red, and black circles represent males, females and males/female combined, respectively. Values are means ± SD (n = 8 per group; total n = 48). δ main effect of DNP treatment. χ main effect sex. δ × χ DNP and sex interaction.

treatment. Since we observed reductions in body fat mass in females in response to protonophore treatment, despite no changes in total body mass, this suggests that despite a matching between TEE and energy intake, protonophore treatment altered body composition.

At thermoneutrality, brown adipose tissue activation is minimal in rodents (Fischer et al., 2018; Keijer et al., 2019). Given that mice were housed at approximately thermoneutrality (30°C) in this study, it is likely that other tissues contributed to the DNP-mediated increase in TEE. It has been suggested that the liver may be a key site of DNP-mediated mitochondrial uncoupling based on reported elevations in circulating β-hydroxybutyrate (Goldgof et al., 2014). Indeed, DNP treatment has been reported to increase state 4 respiration of isolated liver mitochondria (Perry et al., 2013). We demonstrated that noncoupled respiration of female, but not male livers were elevated in response to DNP, which might partly explain why DNP attenuated adiposity in only female mice. What explains this sex-specific bioenergetic response to protonophore treatment remains unclear. However, there is apparent sexual dimorphism in weight gain and adipose tissue mitochondrial uncoupling protein expression following a high-fat diet in mice (Norheim et al., 2019; MacCannell et al., 2021). One consideration for these findings is that liver tissue was minced and kept in an ice-cold preservation buffer for ~1–2 h prior to analysis, where it is possible that residual DNP was removed from liver tissue. Nevertheless, mitochondria from livers of both control and DNP-treated mice responded robustly to protonophore titration, suggesting that liver mitochondria are likely more uncoupled *in-vivo* in protonophore treated mice.

Another key observation of the current study was that liver bioenergetics exhibited sexual dimorphism. We observed greater hepatic respiratory capacity in both the coupled and uncoupled state in males versus females in the absence of DNP. These data are in contrast to previous studies reporting greater hepatic maximal oxidative capacity and maximal electron transfer capacity in female versus male rodents (Justo et al., 2005; Schulze et al., 2018; Valle et al., 2007), although the experiments performed in these studies used isolated mitochondria, compared to permeabilized tissue in the current report. As previous studies have demonstrated, bioenergetic data interpretation may be influenced by whether one is studying isolated mitochondria or permeabilized tissue (Picard et al., 2010).

It is well known that DNP has a narrow therapeutic window. The 400 mg/L dose of DNP was chosen as an experimental dose here because of its ability to increase basal and TEE, which was not observed with doses >400 mg/L in an acute pilot study. Although we did not assess drug toxicity, it is unlikely our chosen dose caused acute toxicity given a previous report documenting 800 mg/L DNP (twice that of the present

study) treatment did not affect plasma alanine aminotransferase levels or liver histology (Goldgof et al., 2014). In this study by Goldgof and colleagues, 800 mg/L daily DNP treatment of female C57BL/6J mice housed at 30°C caused mild weight reduction over 1–2 weeks and did not affect food intake (Goldgof et al., 2014). The greater dose used in this previous study likely contributed to reduced body mass–a finding not reproduced in this investigation. However, it should be noted that in the current study we provided mice with running wheels during DNP treatment. Given that mice voluntarily run ~5–10 km daily when provided with wheels, running wheel provision can have a marked impact on energy balance experiments. In preliminary studies, escalating DNP doses (particularly >400 mg/L) significantly reduced voluntary wheeling running, to an extent that DNP doses of 600 mg/L or greater did not significantly increase TEE, despite having a marked impact on BEE. Thus, we chose a dose that had the least impact on running behavior while still augmenting REE (i.e., 400 mg/L). Consideration of baseline physical activity and it's modulation by protonophore therapy may be useful in terms of providing a more holistic understanding of the impact of mitochondrial uncouplers on TEE.

Though some doses of DNP may be tolerable and acutely non-toxic in rodents, DNP is still unsuitable for the treatment of human obesity (Grundlingh et al., 2011). Nevertheless, the data in the present study underscore the utility of protonophores as agents that induce hypermetabolism, supporting a role for protonophores as potential treatments for obesity. Recent advancements involving DNP analogues and alternative protonophores with improved safety profiles show promise in animal models of obesity (Perry et al., 2013; Alexopoulos et al., 2020; Axelrod et al., 2020). Our data emphasize the importance of assessing the preclinical safety and efficacy of such compounds in rodents housed at temperatures that thwart facultative thermogenesis, while also taking into consideration other important variables such as biological sex and physical activity levels.

Overall, we have demonstrated that protonophore treatment augments TEE and, in a sex-dependent manner, reduces adiposity in mice housed at 30°C. Together, these findings underscore the efficacy of compounds that uncouple mitochondria–such as protonophores–in the context of augmenting energy expenditure. However, our current data highlight the critical importance of studying rodents at appropriate housing temperatures when assessing the impact of compounds that target energy metabolism.

Data availability statement

The datasets presented in this study can be found in online repositories. The names of the repository/repositories and accession number(s) can be found below: https://doi.org/10.6084/m9.figshare.20397468.

Ethics statement

The animal study was approved by University of Arkansas for Medical Sciences. The study was conducted in accordance with the local legislation and institutional requirements.

Author contributions

DS: Data curation, Formal Analysis, Investigation, Methodology, Writing–original draft, Writing–review and editing. RL: Data curation, Formal Analysis, Methodology, Writing–original draft, Writing–review and editing, Conceptualization, Visualization. LT: Data curation, Formal Analysis, Methodology, Visualization, Writing–review and editing, Investigation. JS: Data curation, Investigation, Methodology, Writing–review and editing. CP: Data curation, Investigation, Methodology, Writing–review and editing, Conceptualization, Formal Analysis, Funding acquisition, Project administration, Supervision, Visualization, Writing–original draft.

Funding

The author(s) declare that financial support was received for the research, authorship, and/or publication of this article. This study was supported by NIGMS through a Center of Biomedical Research Excellence pilot project (5P20GM109096). CP is supported by an NIGMS MIRA award (R35GM142744). Support was also provided by the Arkansas Biosciences Institute and the USDA-ARS (USDA ARS 6026-51000-012-06S).

Acknowledgments

We acknowledge the technical support of Trae Pittman, Bobby Fae and Taylor Ross.

Conflict of interest

The authors declare that the research was conducted in the absence of any commercial or financial relationships that could be construed as a potential conflict of interest.

Publisher's note

Supplementary material

The Supplementary Material for this article can be found online at: https://www.frontiersin.org/articles/10.3389/fphys.2024.1452986/full#supplementary-material

References

Alexopoulos, S. J., Chen, S.-Y., Brandon, A. E., Salamoun, J. M., Byrne, F. L., Garcia, C. J., et al. (2020). Mitochondrial uncoupler BAM15 reverses diet-induced obesity and insulin resistance in mice. *Nat. Commun.* 11, 2397. doi:10.1038/s41467-020-16298-2

Axelrod, C. L., King, W. T., Davuluri, G., Noland, R. C., Hall, J., Hull, M., et al. (2020). BAM15-mediated mitochondrial uncoupling protects against obesity and improves glycemic control. *EMBO Mol. Med.* 12, e12088. doi:10.15252/emmm.202012088

Bertholet, A. M., Natale, A. M., Bisignano, P., Suzuki, J., Fedorenko, A., Hamilton, J., et al. (2022). Mitochondrial uncouplers induce proton leak by activating AAC and UCP1. *Nature* 606, 180–187. doi:10.1038/s41586-022-04747-5

Calderon, G., Gonzalez-Izundegui, D., Shan, K. L., Garcia-Valencia, O. A., Cifuentes, L., Campos, A., et al. (2022). Effectiveness of anti-obesity medications approved for long-term use in a multidisciplinary weight management program: a multi-center clinical experience. *Int. J. Obes.* 46, 555–563. doi:10.1038/s41366-021-01019-6

Dunlop, D. M. (1934). The use of 2:4-dinitrophenol as a metabolic stimulant. *BMJ* 1, 524–527. doi:10.1136/bmj.1.3820.524

Feldmann, H. M., Golozoubova, V., Cannon, B., and Nedergaard, J. (2009). UCP1 ablation induces obesity and abolishes diet-induced thermogenesis in mice exempt from thermal stress by living at thermoneutrality. *Cell Metab.* 9, 203–209. doi:10.1016/j.cmet.2008.12.014

Finkelstein, E. A., Trogdon, J. G., Cohen, J. W., and Dietz, W. (2009). Annual medical spending attributable to obesity: payer-and service-specific estimates. *Health Aff. Proj. Hope* 28, w822–w831. doi:10.1377/hlthaff.28.5.w822

Fischer, A. W., Cannon, B., and Nedergaard, J. (2018). Optimal housing temperatures for mice to mimic the thermal environment of humans: an experimental study. *Mol. Metab.* 7, 161–170. doi:10.1016/j.molmet.2017.10.009

Goldgof, M., Xiao, C., Chanturiya, T., Jou, W., Gavrilova, O., and Reitman, M. L. (2014). The chemical uncoupler 2,4-dinitrophenol (DNP) protects against diet-induced obesity and improves energy homeostasis in mice at thermoneutrality. *J. Biol. Chem.* 289, 19341–19350. doi:10.1074/jbc.M114.568204

Grundlingh, J., Dargan, P. I., El-Zanfaly, M., and Wood, D. M. (2011). 2,4-dinitrophenol (DNP): a weight loss agent with significant acute toxicity and risk of death. *J. Med. Toxicol. Off. J. Am. Coll. Med. Toxicol.* 7, 205–212. doi:10.1007/s13181-011-0162-6

Justo, R., Boada, J., Frontera, M., Oliver, J., Bermúdez, J., and Gianotti, M. (2005). Gender dimorphism in rat liver mitochondrial oxidative metabolism and biogenesis. *Am. J. Physiol-Cell Physiol.* 289, C372–C378. doi:10.1152/ajpcell.00035.2005

Kalinovich, A. V., Mattsson, C. L., Youssef, M. R., Petrovic, N., Ost, M., Skulachev, V. P., et al. (2005). Mitochondria-targeted dodecyltriphenylphosphonium (C12TPP) combats high-fat-diet-induced obesity in mice. *Int. J. Obes.* 40, 1864–1874. doi:10.1038/ijo.2016.146

Keijer, J., Li, M., and Speakman, J. R. (2019). What is the best housing temperature to translate mouse experiments to humans? *Mol. Metab.* 25, 168–176. doi:10.1016/j.molmet.2019.04.001

Keipert, S., Lutter, D., Schroeder, B. O., Brandt, D., Ståhlman, M., Schwarzmayr, T., et al. (2020). Endogenous FGF21-signaling controls paradoxical obesity resistance of UCP1-deficient mice. *Nat. Commun.* 11, 624. doi:10.1038/s41467-019-14069-2

Kenward, M. G., and Roger, J. H. (2009). An improved approximation to the precision of fixed effects from restricted maximum likelihood. *Comput. Stat. Data Anal.* 53, 2583–2595. doi:10.1016/j.csda.2008.12.013

Liu, X., Rossmeisl, M., McClaine, J., Riachi, M., Harper, M.-E., and Kozak, L. P. (2003). Paradoxical resistance to diet-induced obesity in UCP1-deficient mice. *J. Clin. Invest* 111, 399–407. doi:10.1172/JCI15737

MacCannell, A. D. V., Futers, T. S., Whitehead, A., Moran, A., Witte, K. K., and Roberts, L. D. (2021). Sexual dimorphism in adipose tissue mitochondrial function and metabolic flexibility in obesity. *Int. J. Obes.* 45, 1773–1781. doi:10.1038/s41366-021-00843-0

Norheim, F., Hasin-Brumshtein, Y., Vergnes, L., Chella Krishnan, K., Pan, C., Seldin, M. M., et al. (2019). Gene-by-Sex interactions in mitochondrial functions and cardio-metabolic traits. *Cell Metab.* 29, 932–949. doi:10.1016/j.cmet.2018.12.013

Ono-Moore, K. D., Rutkowsky, J. M., Pearson, N. A., Williams, D. K., Grobe, J. L., Tolentino, T., et al. (2020). Coupling of energy intake and energy expenditure across a temperature spectrum: impact of diet-induced obesity in mice. *Am. J. Physiol-Endocrinol Metab.* 319, E472-E484–E484. doi:10.1152/ajpendo.00041.2020

Perry, R. J., Kim, T., Zhang, X.-M., Lee, H.-Y., Pesta, D., Popov, V. B., et al. (2013). Reversal of hypertriglyceridemia, fatty liver disease, and insulin resistance by a liver-targeted mitochondrial uncoupler. *Cell Metab.* 18, 740–748. doi:10.1016/j.cmet.2013.10.004

Picard, M., Ritchie, D., Wright, K. J., Romestaing, C., Thomas, M. M., Rowan, S. L., et al. (2010). Mitochondrial functional impairment with aging is exaggerated in isolated mitochondria compared to permeabilized myofibers. *Aging Cell.* 9, 1032–46. doi:10.1111/j.1474-9726.2010.00628.x

Rucker, D., Padwal, R., Li, S. K., Curioni, C., and Lau, D. C. W. (2007). Long term pharmacotherapy for obesity and overweight: updated meta-analysis. *BMJ* 335, 1194–1199. doi:10.1136/bmj.39385.413113.25

Sadler, D. G., Treas, L., Sikes, J. D., and Porter, C. (2022). A modest change in housing temperature alters whole body energy expenditure and adipocyte thermogenic capacity in mice. *Am J Physiol Endocrinol Metab*. doi:10.1152/ajpendo.00079.2022

Schulze, A., McCoin, C. S., Onyekere, C., Allen, J., Geiger, P., Dorn, G. W., et al. (2018). Hepatic mitochondrial adaptations to physical activity: impact of sexual dimorphism, PGC1α and BNIP3-mediated mitophagy. *J. Physiol.* 596, 6157–6171. doi:10.1113/JP276539

Škop, V., Guo, J., Liu, N., Xiao, C., Hall, K. D., Gavrilova, O., et al. (2020). Mouse thermoregulation: introducing the concept of the thermoneutral point. *Cell Rep.* 31, 107501. doi:10.1016/j.celrep.2020.03.065

Tainter, M. L., Cutting, W. C., and Stockton, A. B. (1934). Use of dinitrophenol in nutritional disorders: a critical survey of clinical results. *Am. J. Public Health Nations Health* 24, 1045–1053. doi:10.2105/ajph.24.10.1045

Tao, H., Zhang, Y., Zeng, X., Shulman, G. I., and Jin, S. (2014). Niclosamide ethanolamine-induced mild mitochondrial uncoupling improves diabetic symptoms in mice. *Nat. Med.* 20, 1263–1269. doi:10.1038/nm.3699

Valle, A., Guevara, R., García-Palmer, F. J., Roca, P., and Oliver, J. (2007). Sexual dimorphism in liver mitochondrial oxidative capacity is conserved under caloric restriction conditions. *Am. J. Physiol-Cell Physiol.* 293, C1302–C1308. doi:10.1152/ajpcell.00203.2007

frontiers | Frontiers in Physiology

TYPE Original Research
PUBLISHED 14 November 2024
DOI 10.3389/fphys.2024.1358177

OPEN ACCESS

EDITED BY
Bakovic Marica,
University of Guelph, Canada

REVIEWED BY
Rodríguez-Antolín Jorge,
Autonomous University of Tlaxcala, Mexico
Lin Zhu,
Vanderbilt University Medical Center, United States

*CORRESPONDENCE
Ahmed El Sayed Nour El-Deen,
drnoor83@hotmail.com
Reda Samir Taha,
rtaha@zu.edu.jo

RECEIVED 19 December 2023
ACCEPTED 22 May 2024
PUBLISHED 14 November 2024

CITATION
Nour El-Deen AES, Taha AM, Elsayed A, Ali AN and Taha RS (2024), Impact of co-administration of apricot kernels and caffeine on adult male diabetic albino rats. *Front. Physiol.* 15:1358177. doi: 10.3389/fphys.2024.1358177

Impact of co-administration of apricot kernels and caffeine on adult male diabetic albino rats

Ahmed El Sayed Nour El-Deen[1,2]*, Ahmad Mohamad Taha[1,3], Almoatazbellah Elsayed[1,4], Ahmed Noaman Ali[1,5] and Reda Samir Taha[1,6]*

[1]Department of Basic Medical and Dental Sciences, Faculty of Dentistry, Zarqa University, Zarqa, Jordan, [2]Department of Physiology, Faculty of Medicine, Al-Azhar University, Assiut, Egypt, [3]Department of Physiology, Faculty of Medicine, Port Said University, Port Said, Egypt, [4]Department of Pathology, Faculty of Medicine, Al-Azhar University, Assiut, Egypt, [5]Department of Oral Pathology, Faculty of Dentistry, Tanta University, Tanta, Egypt, [6]Department of Anatomy, Faculty of Medicine in Damietta, Al-Azhar University, Assiut, Egypt

The purpose of this study is to evaluate the impacts of apricot kernels and caffeine on blood glucose, lipid profile, insulin secretion, and antioxidant effect in diabetic rats. Forty adult male albino rats were divided into five groups: normal control, diabetic control, diabetic rats treated with apricot kernels, diabetic rats treated with caffeine, and diabetic rats treated with apricot kernels plus caffeine. Fasting samples were collected at the end of the study for analysis, and pieces of liver and pancreatic tissues were removed for histological analysis. There was a significant decrease in blood glucose, glycated hemoglobin, body weight, total cholesterol, triglyceride, and low-density lipoprotein cholesterol (LDL-C) levels and a significant increase in insulin and high-density lipoprotein cholesterol (HDL-C) levels in the kernel and caffeine-treated groups. However, there was little histological alteration in the liver or pancreas, and no significant differences were observed in the histological findings between groups. Overall, it can be concluded that apricot kernel and caffeine had a positive effect in decreasing blood glucose and harmful lipid profile and that caffeine had a synergistic effect on the apricot kernel.

KEYWORDS

type 2 diabetes mellitus, apricot kernels, caffeine, Antioxidant, nutritarian

1 Introduction

Diabetes mellitus (DM) is a fast-growing health problem that causes significant economic burden worldwide, especially the adult-onset or type 2 diabetes mellitus (T2DM) (Arokiasamy et al., 2021). It was reported that the global prevalence of diabetes among adults has reached alarming levels all over the world; it was nearly 9.4% in the year 2019, which indicated approximately 462 million adults had DM worldwide, and this number would increase to 700 million in 2045 (Alp et al., 2023).

The increased incidence of known risk factors for T2DM, such as physical inactivity, obesity, and unhealthy diet, increased the morbidity and mortality of the world population (Arokiasamy et al., 2021).

In the early stages of T2DM, oxidative stress, together with other factors, upregulated the activation of AMP-activated protein kinase (AMPK) and enhanced pancreatic beta cell survival and function. However, in chronic cases, chronic oxidative stress conditions can be

the result of the continuous production of reactive oxygen species that chronically activate AMPK and result in damage to pancreatic beta cells with repressed insulin release (Fu et al., 2013). Therefore, reducing inflammation and oxidative stress can be one of the main therapeutic objectives for managing T2DM (Vivó-Barrachina et al., 2022). Seeds and nuts can be useful sources for the aforementioned therapeutic targets for T2DM. Their bioactive components have high nutraceutical and medicinal value (Shalaby et al., 2015; El-Deen et al., 2018; El-Deen et al., 2019; El-Deen et al., 2024). They proved to be beneficial in controlling body weight, blood glucose levels, and blood pressure, along with reduction of coronary heart disease and levels of blood cholesterol and triacylglycerol (Sater et al., 2016; Shalaby et al., 2016; El-Deen et al., 2018; Jugran et al., 2021).

Apricot (*Prunus armeniaca* L.) is a fruit that belongs to the genus *Prunus* of the Rosaceae family. The fruits contain a kernel enclosed in a stone seed. The kernel can be a food by-product for its high content of dietary protein (14%–45%), oil (28%–66.7%), and phytochemicals such as phenolic compounds, carotene, phytosterols, and tocopherol (Mohamed et al., 2021). Apricot kernel contains caffeic acid and gallic acid, which are used in anti-asthmatic, antiseptic, sedative, emetic, and laxative medicinal preparations. It can also be beneficial in the treatment of various diseases such as cardiovascular disease and breast cancer (Akhone et al., 2022; Hamid et al., 2022). They can also be used in developing a source of antioxidant biocompounds and some hypoglycemic agents like anthocyanin (Akbari et al., 2022).

Caffeine (1,3,7-trimethylxanthine) is present in different sources, mainly coffee, tea, and soft drinks (Heckman et al., 2010). Coffee contains several bioactive compounds that are well known for being antioxidants (Cämmerer and Kroh, 2006; Neves et al., 2018). Antioxidants have been shown to reduce diabetes complications by improving cell function in animal models, suggesting that enhancing antioxidant defense mechanisms in pancreatic islets may be a valuable pharmacologic approach to managing diabetes. Several studies have demonstrated that a higher consumption of coffee is associated with a lower risk of developing T2DM (Huxley et al., 2009; Muley et al., 2012; Bidel and Tuomilehto, 2013).

Our hypothesis is that apricot kernel can reduce the blood glucose concentration in type 2 diabetic patients and may also reduce complications resulting from chronic uncontrolled diabetes because it contains antioxidants and some hypoglycemic agents. So, the aim of this work was to study the effect of apricot kernel with or without caffeine on blood glucose concentration and lipid and antioxidant profiles in diabetic rats.

2 Materials and methods

2.1 Preparation of apricot kernel and caffeine

Apricot kernels were collected from an Egyptian local market during the fruit-ripening season. Fruits were washed thoroughly under running tap water, and then kernels were removed from the fruits; the kernels were dried in an air oven at 50°C for 24 h and ground to obtain fine powder using an air mill according to the method described by Musa and Sciences (2010). Then, the powder was stored in dark glass bottles at normal room temperature until further use. Caffeine (1,3,7-trimethylxanthine) was obtained from local Egyptian markets.

2.2 Experimental animals

Forty adult male albino rats of the local strain weighing 150 ± 20 g were purchased from the animal house of Assiut University. All animal procedures were conducted in strict conformity with the Ethical Committee Guidelines for the Care and Use of Laboratory Animals of the Faculty of Medicine, Al-Azhar University.

Animals were kept in suitable cages (20 × 32 × 20 cm for every 3 rats) in an environmentally controlled breeding room (temperature: 22°C ± 2°C, humidity: 60% ± 5%, 12 h dark/light cycle); the animals were maintained on a standard diet of commercial rat food formula (El-Nasr-Pharmaceutical Co., Cairo, Egypt) and tap water.

T2DM was induced in male albino rats fed with a high-fat diet for 3 weeks, followed by intraperitoneal injection of a low-dose streptozotocin (40 mg/kg/body weight daily for five successive days) from the 22nd day of treatment with a high-fat diet (Akbarzadeh et al., 2007). Rats with fasting blood glucose level (FBG) > 200 mg/dL were selected as diabetic and were included in this study (Furman, 2015). Blood glucose levels were estimated.

2.3 Experimental design

All procedures were conducted at Al-Azhar University, Assuit, Egypt. Rats were weighed at the beginning and the end of the experiment.

Animals were randomly divided into 5 groups ($n = 8$) as follows:

(Group1) Normal control rat treated with normal saline: received daily 1 mL/kg of sterile saline by gavage for 1 month.
(Group 2) Type 2 diabetic control rats treated with normal saline, received daily 1 mL/kg of sterile saline by gavage for 1 month.
(Group 3) Type 2 diabetic rats treated with apricot kernels as powder, received daily as 5% of the diet for 1 month.
(Group 4) Type 2 diabetic rats treated with caffeine, received daily 20 mg/kg by gavage.
(Group 5) Type 2 diabetic rats treated with apricot kernels as powder, received daily as 5% of the diet plus received daily 20 mg/kg by gavage.

2.4 Blood sampling

After 30 days of treatment, the rats were sacrificed by cervical dislocation. Blood was immediately collected from the aorta into a dry clean glass heparinized centrifuge tube and centrifuged for 15 min at 5,000 rpm to separate the plasma, which was carefully aspirated and transferred into a clean cuvette tube and stored in a deep freezer for further biochemical assays.

2.5 Biochemical analysis

2.5.1 Glycated hemoglobin (HbA1c)

HbA1c was measured with the help of BioRad D10-HbA1c analyzer, CAL-REMEDIES (Shoaib et al., 2020).

2.5.2 Lipid profile

Total cholesterol (TC), high-density lipoprotein cholesterol (HDL-C), low-density lipoprotein cholesterol (LDL-C), and triglycerides (TG) were measured in sera using enzymatic colorimetric kits (Stanbio Laboratory, United States, and ELITech Group, France) according to Tietz (1990).

2.5.3 Insulin level

The levels of insulin in plasma were estimated by a commercial rat enzyme-linked immunosorbent assay kit (Abnova, Germany) according to the enclosed manufacturer's protocol.

2.5.4 Antioxidant profile analysis

Lipid peroxidation was estimated by measuring malondialdehyde (MDA) levels according to the method described (Ohkawa et al., 1979). Using commercially available kits from Biodiagnostic Chemical Company (Cairo, Egypt), glutathione peroxidase (GPx) activity was estimated according to Rotruck et al. (1973). To estimate the rate of glutathione oxidation by H_2O_2, one unit of GPx activity per minute is defined as the amount of enzyme needed for the conversion of 1 µmol of reduced glutathione to its oxidized form. Catalase (CAT) activity was estimated in the plasma according to the method described by Aebi (1984) (HADWAN et al., 2018) using commercially available kits from Biodiagnostic Chemical Company (Cairo, Egypt).

2.6 Histopathology

At the end of the experiment, after scarification, a small piece of liver and pancreatic tissue were removed for histological analysis. The tissues were fixed in 10% formalin (diluted to 10% with normal saline). The tissues were dehydrated in graded concentrations of ethyl alcohol and cleared with xylene, embedded in molten paraffin wax, and sectioned at 5 µ. Tissue sections were fixed on glass slides and stained with hematoxylin and eosin for light microscopy (Kilari et al., 2020).

The histological changes were evaluated in nonconsecutive, randomly chosen × 200 histological fields using a light microscope (the Nikon Eclipse E200 student microscope).

2.7 Statistical analysis

We used R software version 4.1.1 (Packages: tidyverse, ggpubr, and rstatix) to perform biomedical analysis. We applied one-way ANOVA followed by Tukey's post hoc test to compare different parameters. Mean ± SD described our results. p-value < 0.05) was considered a statistically significant value.

3 Results

3.1 Kernels and caffeine decreased blood glucose level in diabetic rats

The results of the current study showed a significant increase in blood glucose levels (mg/dL) in diabetic rats when compared to normal control rats. The results also showed that ingesting kernels or caffeine caused a significant decrease in blood glucose levels compared to the diabetic group, and the effect of their combination showed a more substantial impact on lowering blood glucose levels in diabetic rats. The changes in blood glucose levels in different experimental groups are presented in Figure 1A.

3.2 Kernel increased insulin levels in diabetic rats more efficiently than caffeine

The induced diabetic rats exhibited a significant decrease in insulin levels (mIU/L) compared to normal control rats. The administration of kernel alone and caffeine alone increased insulin levels; however, kernel showed a better result than caffeine when compared with the diabetic group. The addition of caffeine to the kernel displayed a more significant effect on increasing insulin levels in diabetic rats. The changes in insulin levels in different experimental groups are shown in Figure 1B.

3.3 Addition of caffeine to kernel had the most effect in decreasing hemoglobin A1c

Hemoglobin A1c (%) is the percentage of glucose-coated hemoglobin in red blood cells. It shows the average blood sugar level over the length of the experiment. There was a statistically significant difference in the average HbA1c% between the five groups of mice. The highest value of HbA1c% was found in the induced diabetic rats, while the greatest decrease compared to the normal group was found in type 2 diabetic rats treated with apricot kernels plus caffeine. The changes in hemoglobin A1c percentage in different experimental groups are shown in Figure 1C.

3.4 Kernel and caffeine decreased body weight in diabetic rats

The body weights of rats at the end of the experiment are shown in Figure 1D and Table 1. There was a statistically significant difference in the mean body weight at the end of the experiment between the five groups, and after conducting Tukey's *post hoc* test, the highest rate of decrease in body weight was in the induced diabetic group, while the lowest decrease in weight was in the type 2 diabetic rats treated with apricot kernels plus caffeine.

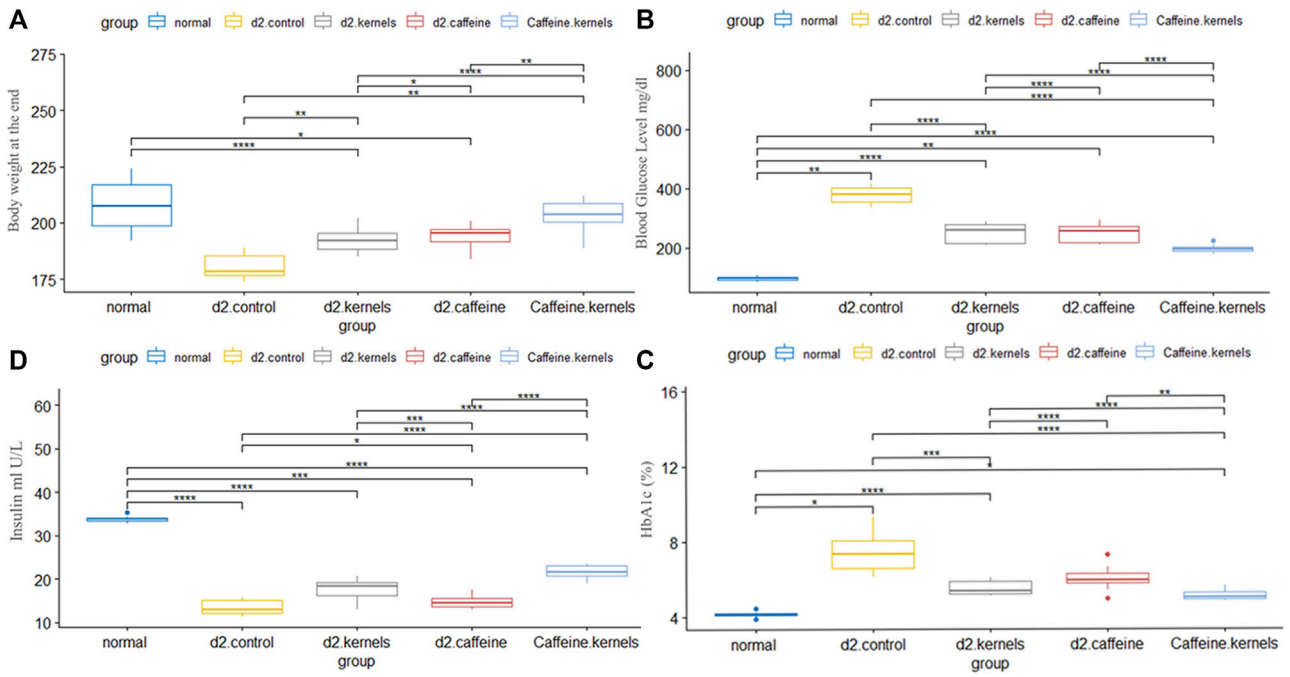

FIGURE 1
Administration of apricot kernel and caffeine improved blood glucose level and related factors in diabetic rats. **(A)** Body weight differences between groups at the end of the experiment. **(B)** Glucose concentration. **(C)** HbA1c level in different groups. **(D)** Insulin level in diabetic rats after different treatments. Healthy control rats (normal), control diabetic rats (d2.control), diabetic rats treated with apricot kernel (d2.kernels), diabetic rats treated with caffeine (d2.caffeine), and diabetic rats treated with both caffeine and apricot kernel (Caffeine.kernels). One-way ANOVA and *post hoc* test, *p*-value* <0.05, **<0.01, ***<0.001, ****<0.0001.

TABLE 1 Histological pattern of the Liver.

	Portal tract			CV	Hepatocyte	Blood sinusoids	Intra-lobular inflammatory infiltrate
	PV	Inflammatory infiltrate	Edema				
Group 1	0	0	0	0	0	0	0
Group 2	++	0	+	++	++	0	0
Group 3	++	0	+	0	0	0	0
Group 4	+	+	0	+	++	0	+
Group 5	+	0	0	++	+	+	0

❖ Portal tract.
- Portal vein (PV): 0: average; +: mildly dilated/congested; ++: markedly dilated/congested.
- Inflammatory infiltrate: 0: no; +: mild; ++: moderate/marked.
- Edema: 0: no; +: present.

❖ Central vein (CV): 0: average; +: dilated/congested; ++: markedly dilated/detached lining.
❖ Hepatocytes: 0: average; +: hydropic change; ++: apoptotic/necrotic.
❖ Blood sinusoids: 0: average; +: mildly dilated/congested; ++: markedly dilated/congested.
❖ Intra-lobular inflammatory infiltrate: 0: no; +: mild; ++: moderate/marked.

3.5 Improvement of lipid profile in diabetics after administration of kernel

In T2DM, hyperglycemia is accompanied by an abnormal lipid profile characterized by imbalances in lipoproteins and cholesterol levels. In the current study, there was a significant increase in the level of TC, triglycerides (TG), and low-density lipoprotein cholesterol (LDL-C). In contrast, high-density lipoprotein cholesterol (HDL-C) was decreased in the diabetic control group in comparison with normal control rats. Kernel or/and caffeine administration showed a significant decrease in the levels of TC, TG, and LDL-C in type 2 diabetic rats. There was also a significant increase in HDL-C in type 2 diabetic rats treated with apricot kernels plus caffeine. The changes in lipid profiles in different experimental groups are shown in Figure 2.

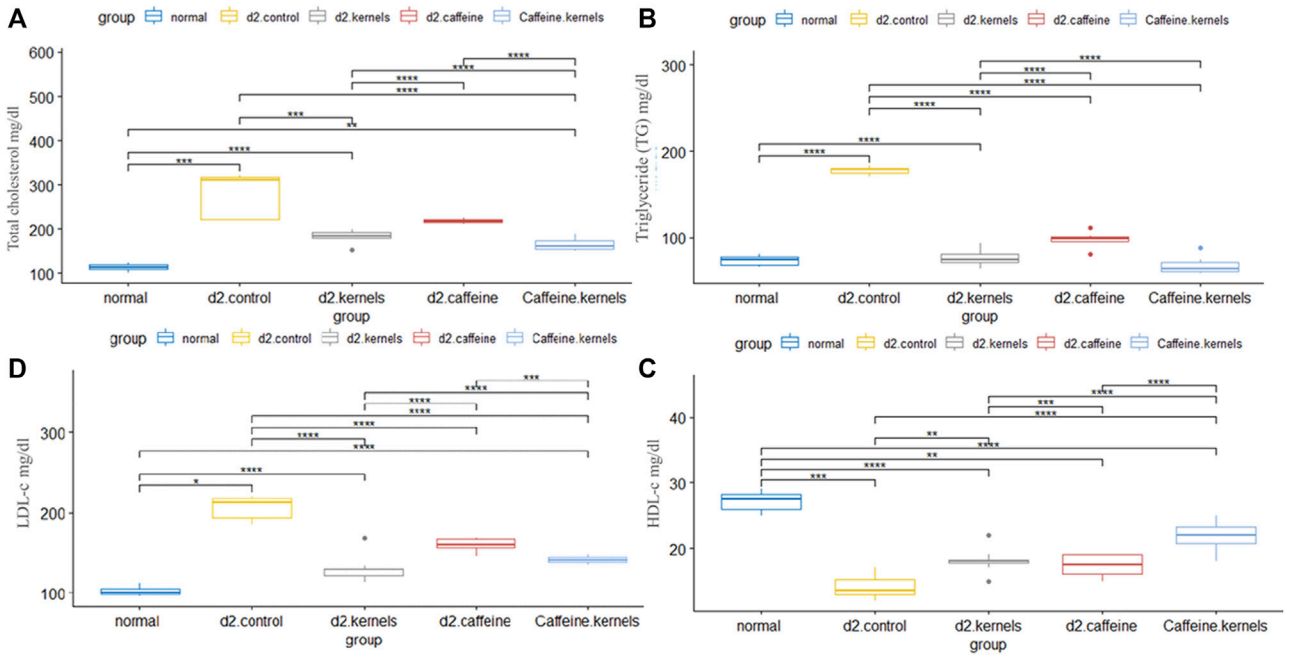

FIGURE 2
Apricot kernel and caffeine had a positive effect on lipid profile of diabetic rats. **(A)** Total cholesterol level in diabetic rats after different treatments. **(B)** Triglyceride (TG) level in different groups. **(C)** High-density lipoprotein cholesterol (HDL-C). **(D)** Low-density lipoprotein cholesterol (LDL-C). Healthy control rats (normal), control diabetic rats (d2.control), diabetic rats treated with apricot kernel (d2.kernels), diabetic rats treated with caffeine (d2.caffeine), and diabetic rats treated with both caffeine and apricot kernel (Caffeine.kernels). One-way ANOVA and *post hoc* test, *p*-value* <0.05, **<0.01, ***<0.001, ****<0.0001.

3.6 Administration of both kernel and caffeine enhanced antioxidant profile in diabetic rats

Antioxidants play a crucial role in maintaining overall health and may have specific benefits for managing diabetes type 2. Malondialdehyde (MDA), glutathione peroxidase activity GPX (U/mL), and catalase activity CAT (U/mL) are important markers of lipid peroxidation. There was a statistically significant difference in the mean MDA, GPX, and CAT between the five groups, and after performing Tukey's *post hoc* test, the significance among all groups was significant ($p < 0.001$), except it was not significant between the caffeine and the control group. In contrast, the type 2 diabetic rats treated with apricot kernels plus caffeine had the highest increase in MDA and GPX, while there was a significant decrease in the level of level CAT, approaching the normal level. The changes in antioxidant levels in different experimental groups are shown in Figure 3.

3.7 Histopathological analysis

3.7.1 Liver tissue

The liver of the normal control showed average portal tracts with average portal veins, average bile ducts, and average hepatocytes in the peri-portal area, and average central veins with average hepatocytes arranged in single-cell cords with average intervening blood sinusoids (Figure 4, G1). However, in the induced diabetes group, mildly edematous portal areas with markedly dilated congested portal veins, markedly dilated central venules with detached lining, and scattered hepatocytes in the peri-portal and peri-portal regions showed pathological changes caused by the induction of diabetes in rats; in turn, these changes reduced the liver's consumption of glucose, contributing greatly to high blood glucose levels and disturbances in lipid profile and antioxidants as described above (Figure 4, G2). In diabetic rats treated with apricot kernels, the liver showed markedly edematous portal spaces with markedly dilated congested portal venules, intermediate central venules, and intermediate hepatocytes in the peri-portal and peri-venous areas (Figure 4, G3). In diabetic rats treated with caffeine, the liver showed average portal tracts with mild portal inflammatory infiltrate and mildly dilated congested portal veins, mildly dilated congested central veins, and scattered apoptotic hepatocytes in a peri-venular area with intra-lobular inflammatory infiltrate (Figure 4, G4). In diabetic rats treated with apricot kernels plus caffeine, the liver showed average portal tracts with mildly congested portal veins, markedly dilated central veins with mildly congested blood sinusoids, a hydropic change of hepatocytes, and mild micro-vesicular steatosis in the peri-venular area. This necessarily means an improvement in the condition of the liver cells compared to the diabetic control group, as well as an improvement in the rate of glucose consumption by the liver cells, which led to a noticeable decrease in the level of glucose in the blood and an improvement in the lipid profile and antioxidants as described above (Figure 4, G5). The changes in histological structures of different experimental groups are shown in Figure 4 and Table 1.

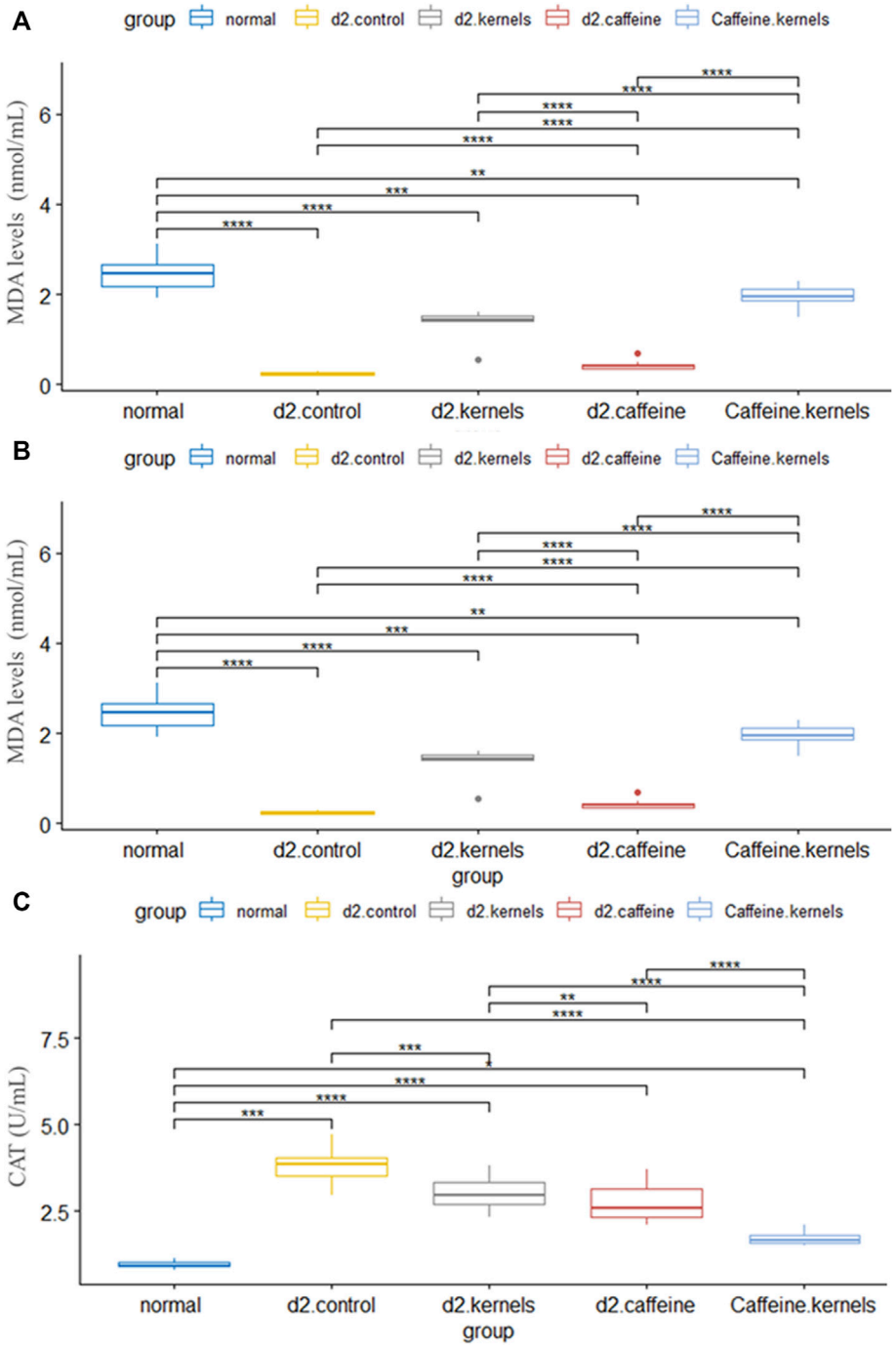

FIGURE 3
Antioxidant profile in diabetic rats improved after the administration of apricot kernel and caffeine. **(A)** Malondialdehyde (MDA) level in diabetic rats after different treatments. **(B)** Glutathione peroxidase activity (GP_x). **(C)** Catalase activity (CAT) level in diabetic rats after different treatments. Healthy control rats (normal), control diabetic rats (d2.control), diabetic rats treated with apricot kernel (d2.kernels), diabetic rats treated with caffeine (d2.caffeine), and diabetic rats treated with both caffeine and apricot kernel (Caffeine.kernels). One-way ANOVA and *post hoc* test, *p*-value* <0.05, **<0.01, ***<0.001, ****<0.0001.

3.7.2 Pancreas tissue

In the normal control, the pancreas showed average-sized pale-staining islets of Langerhans composed of predominating beta cells with pale blue cytoplasm, and less frequently alpha cells with pink cytoplasm separated by average thin-walled blood capillaries, average exocrine areas, and average ducts (Figure 4, G1). In the induced diabetes group, the pancreas showed small-sized islets of Langerhans with scattered apoptotic beta cells, mildly dilated overlapping capillaries, moderately dilated interstitial blood vessels, intermediate exocrine zones, and intermediate ducts. This severe inflammation of the pancreatic cells led, of course, to decreased insulin secretion by beta cells and thus a significant

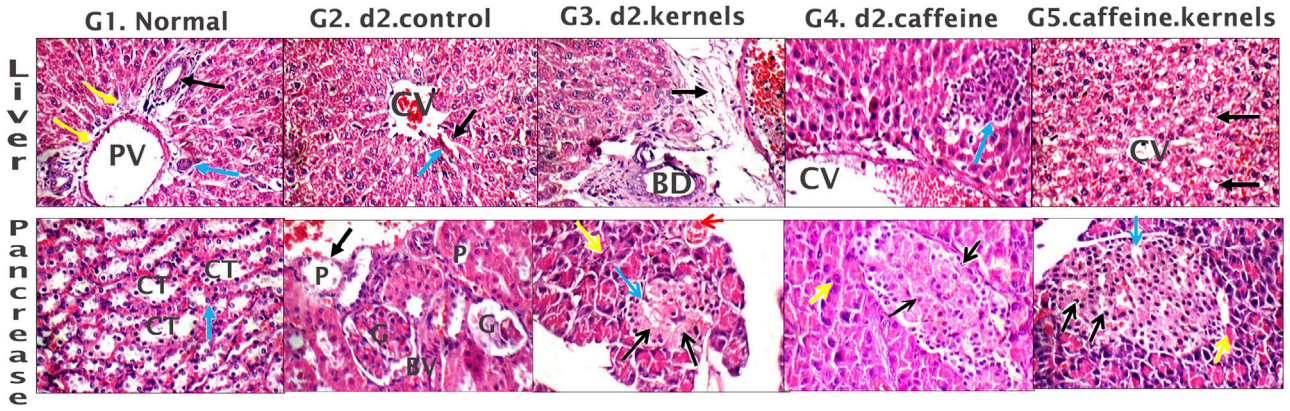

FIGURE 4
Histological sections of the liver and pancreas. Liver tissue: G1. Control group displays average portal tract size with average portal vein (PV) size, average bile ducts (black arrow), average hepatic artery (blue arrow), and average hepatocytes in peri-portal area (yellow arrow). G2. Diabetic rats treated with normal saline group shows liver with mildly edematous portal tract (black arrow), markedly dilated congested PV, dilated congested central veins (CV), and average hepatocytes (blue arrow). G3. Diabetic rats treated with apricot kernels group exhibits markedly edematous portal tract (black arrow) with markedly dilated congested PV, average bile ducts (BD), and average hepatocytes in peri-portal area (blue arrows). G4. Diabetic rats treated with caffeine group showed mildly dilated congested CV with scattered apoptotic hepatocytes in peri-venular area (black arrow), and intra-lobular inflammatory infiltrate (blue arrow). G5. Diabetic rats treated with apricot kernels plus caffeine group displays average CV with mild micro-vesicular steatosis of hepatocytes in peri-venular area (black arrow). Pancreatic tissue: G1. Control group displays predominating beta cells with pale blue cytoplasm (black arrows) and less frequently alpha cells with pink cytoplasm (blue arrows) separated by average thin-walled blood capillaries (red arrow), and average exocrine areas (yellow arrow). G2. Diabetic rats treated with normal saline group displays hypocellular islets with scattered apoptotic beta cells (black arrow) and mildly congested intervening blood capillaries (blue arrow), average exocrine areas (yellow arrows), and average ducts (red arrow). G3. Diabetic rats treated with apricot kernels group exhibits hypocellular islets with scattered apoptotic beta cells (black arrows) and mildly dilated intervening blood capillaries (blue arrow), average exocrine areas (yellow arrows), and mildly congested interstitial blood vessels (red arrow). G4. Diabetic rats treated with caffeine group show hypocellular islets with scattered apoptotic beta cells (black arrow) and mildly dilated intervening blood capillaries (blue arrow), and average exocrine areas (yellow arrow). G5. Diabetic rats treated with apricot kernels plus caffeine group displays average islets with predominating beta cells (black arrows), mildly dilated congested intervening blood capillaries (blue arrow), and average exocrine areas (yellow arrow) (H&E X 400).

increase in blood glucose levels (Figure 4, G2). In diabetic rats treated with apricot kernels, the pancreas showed small-sized hypocellular islets of Langerhans with scattered apoptotic beta cells and mildly dilated congested intervening blood capillaries, mildly congested interstitial blood vessels, average exocrine areas, and average ducts (Figure 4, G3). In diabetic rats treated with caffeine, the pancreas showed average-sized hypocellular islets of Langerhans with scattered apoptotic beta cells and mildly dilated intervening blood capillaries, average exocrine areas, and average ducts (Figure 4, G4). In diabetic rats treated with apricot kernels plus caffeine, the pancreas showed moderately sized islets of Langerhans with predominant beta cells, mildly dilated interstitial capillaries, mildly dilated interstitial blood vessels, moderate exocrine zones, and mesenchymal ducts. This means a significant improvement in the condition of pancreatic cells when compared to the diabetic control group. This improvement in the morphology of the cells led to a clear improvement in the level of glucose in the blood (Figure 4, G5). The changes in histological structures of different experimental groups were shown in Figure 4 and Table 2.

4 Discussion

In this study, T2DM was induced in male albino rats fed with a high-fat diet for 3 weeks, followed by a low dose of streptozotocin (Nath et al., 2017). Low streptozotocin doses partially damage pancreatic beta cells and cause the breakage of DNA strands (Szkudelski, 2001). The alkylation of DNA is followed by cell death, and then consequently, an increase in blood sugar levels. Both a high-fat diet and streptozotocin mimic the human syndrome T2DM (Rais et al., 2022). Apricot kernel oil contains some biologically active substances, such as β-carotene, phenolic compounds, campesterol, stigmasterol, sitosterol, and provitamin A (Fratianni et al., 2018). The presence of tocopherols, vitamin C, saponins, oleic acid, and amygdalin in apricot kernel boosts its antioxidant activity and anti-lipemic capacity (Dawod and Ahmed, 2021). Specifically, 100 mg/kg of amygdalin can increase gene expression of glutathione peroxidase and superoxide dismutase in the hepatic tissue of mice (Dawod and Ahmed, 2021).

The reduction of blood glucose levels is the primary therapeutic goal for controlling diabetes (Ceriello et al., 2022). In the present study, the blood glucose level of diabetic rats was significantly decreased when treated with apricot kernels, and this effect was synergized when the kernel was combined with caffeine. The reduction of blood glucose may be either due to the increased level of plasma insulin in diabetic rats, which may influence the stimulation of pancreatic insulin secretion from beta cells in islets of Langerhans, or due to the enhanced transport of blood glucose to peripheral tissue. The mass loss and functionality of pancreatic beta cells have been the major concerns in the pathogenesis of T2DM (Dawood et al., 2023). Functional improvement by increasing the expression of genes linked to beta cell function and insulin biogenesis is one of the mechanisms of the apricot kernel in boosting insulin secretion (Anwar et al., 2018) and improving insulin sensitivity, which is an important therapeutic approach to treating T2DM (Blahova et al., 2021). It could also improve glucose

TABLE 2 Histological pattern of the pancreas.

	Pancreatic islets				Ducts	Exocrine area	BV
	Islet size	Cellularity	Beta cells	Capillaries			
Group 1	0	0	0	0	0	0	0
Group 2	+	+	+	+	0	0	+
Group 3	+	+	+	+	0	0	+
Group 4	0	+	+	+	0	0	0
Group 5	0	0	0	+	0	0	+

❖ Islet size: 0: average; +: small; ++: atrophied.
❖ Cellularity: 0: average; +: hypocellular; ++: acellular.
❖ Beta cells: 0: average; +: few/apoptotic; ++: necrotic/absent.
❖ Capillaries: 0: average; +: mildly dilated; ++: markedly dilated/congested.
❖ Ducts: 0: average; +: dilated; ++: atrophied.
❖ Exocrine area: 0: average acini; +: small acini; ++: atrophied acini.
Interstitial BV: 0: average; +: mildly dilated; ++: markedly dilated/congested.

tolerance, augment energy expenditure, and reduce adiposity (Szkudelski, 2001); apricot kernels can be considered a hypoglycemic agent, protecting beta cells, improving their function ability, and acting as hepatoprotective agents (Peng et al., 2023).

Hyperglycemia is accompanied by dyslipidemia, characterized by an increase in TC, LDL, and TG and a fall in HDL. This altered serum lipid profile was reversed to normal after treatment with metformin, as mentioned by Mullugeta et al. (2012). In this study, there was an increase in plasma TG, TC, and LDL-C fractions along with a decreased HDL-C level in the diabetic control group. The HDL-C levels in diabetic and non-diabetic rats fed with apricot kernels were found to be higher compared to the diabetic control group, an indication of a beneficial effect of the apricot kernels, while TG, TC, and LDL levels were decreased in both diabetic and non-diabetic rats fed with apricot kernels. Similarly, consumption of apricot kernels daily had a positive effect on lowering plasma TC and LDL-C in patients with dyslipidemia without a significant effect on plasma cholesterol levels (Zibaeenezhad et al., 2017; Kopčeková et al., 2021; Kopčeková et al., 2022). Furthermore, it reduced hepatic lipid synthesis by decreasing the activity of lipogenic enzymes and increasing hepatic lipolytic enzymes, consequently lowering plasma TG (Sun et al., 2020; Dinda and Dinda, 2022; Kopčeková et al., 2022). The possible mechanism of the anti-hyperlipidemic effect of caffeine might include the changed activity of cholesterol biosynthesis enzymes and/or the changed level of lipolysis, which are under the control of insulin, as mentioned by Zhang et al. (2013). It is reported that caffeine treatment could decrease the capacity of LDL to carry free cholesterol to various tissues without affecting the capacity of HDL to carry cholesterol back to the liver in rats (Ontawong et al., 2019). In addition, apricot kernel treatment can correct hyperlipidemia in rats, as reported by Kutlu et al. (2009). Our results indicated that the lipid-lowering effect could be an indirect consequence of amelioration of insulin resistance or a direct hypolipidemic effect mediated through other mechanisms.

Apricot mostly contains phytochemicals that reduce the risk of free radicals, which cause oxidative damage in living cells and common degenerative disorders such as cancer and cardiovascular diseases; the major anti-inflammatory compounds are acetylcholinesterase (Vahedi-Mazdabadi et al., 2020). Cyclooxygenase, interleukin 6, prostaglandin, Toll-like receptors, and tumor necrosis factor alpha (Huang et al., 2011). The antioxidant potential of apricot has been repeatedly investigated through different *in vitro* systems by measuring its ability to reduce free radicals and comparing it with standard reference compounds (Arora et al., 2017). Tissue MDA content, the final product of lipid breakdown caused by oxidative stress, is an important indicator of free radical-induced lipid peroxidation (Tsikas, 2017). In our study, there was a significant decrease in MDA in diabetic rats treated with apricot and caffeine, which indicates the positive effect of apricot kernels as an antioxidant. MDA is one of the final products of polyunsaturated fatty acid peroxidation in the cells (Tsikas, 2017). An increase in free radicals causes overproduction of MDA. Therefore, it is commonly known as a marker of oxidative stress and the antioxidant status in patients (Demirci-Cekic et al., 2022). There was a significant increase in GPx in diabetic rats treated with apricot and caffeine, which are the most important selenoenzymes due to their role in a diverse range of biological functions, including the detoxification of H_2O_2 and hydroperoxides (Lima-Cabello et al., 2023). The catalase activity was significantly increased in diabetic rats treated with apricot and caffeine. Measurements of catalase activity function as a good evaluating tool for assessing the liver's capacity to attenuate the inclination toward oxidative stress (Sousa et al., 2020).

Caffeine had a similar effect to kernel on blood glucose level, HDL-C, HbA1c, and GPX; conversely, the kernel has a better effect on other parameters such as lipid profile and insulin. Caffeine did not exceed kernel in any tested parameter; however, the addition of caffeine to kernel improved its effect in all tested parameters.

In the study of Ramli et al. (2021), caffiene was shown to reduce the risk of metabolic syndrome. It was found to reduce waist circumference, triglyceride levels, low-density lipoprotein-cholesterol levels, and blood pressure. In a systematic review of the effect of caffeine therapy on cardiometabolic markers in rat models of the metabolic syndrome, out of 228 studies retrieved from the search, caffeine was found to favorably reduce obesity and insulin resistance in the rat model of the

metabolic syndrome (Alhadi et al., 2023). In the current study, caffeine had a similar effect to kernel on blood glucose level, HDL-C, HbA1c, and GPX; conversely, kernel has a better effect on another parameter, although caffeine yielded no better result than kernel in any parameter. The addition of caffeine to kernel improved its effect on all tested parameters. The study of caffeine and kernel needs more advanced and deeper research.

In conclusion, apricot kernel helped reduce blood glucose levels and lipid content and increase plasma insulin, in addition to its antioxidant effect. The addition of caffeine augments its beneficial properties. The apricot kernel has excellent therapeutic properties and can be considered a potential ingredient in many drugs and food supplements due to its cost effective and ecofriendly nature. Moreover, further work is necessary to elucidate in detail the mechanism of action of the apricot kernel at the cellular and molecular levels.

Data availability statement

The original contributions presented in the study are included in the article/Supplementary Material; further inquiries can be directed to the corresponding author.

Ethics statement

The animal studies were approved by the ethical comity of the faculty of medicine, Al-azhar University, Assuit, Egypt.

Author contributions

ANE-D: Conceptualization, Data curation, Formal Analysis, Funding acquisition, Investigation, Methodology, Project administration, Resources, Software, Supervision, Validation, Visualization, Writing–original draft, Writing–review and editing. AT: Conceptualization, Data curation, Formal Analysis, Funding acquisition, Investigation, Methodology, Project administration, Resources, Software, Supervision, Validation, Visualization, Writing–original draft, Writing–review and editing. AE: Conceptualization, Data curation, Formal Analysis, Funding acquisition, Investigation, Methodology, Project administration, Resources, Software, Supervision, Validation, Visualization, Writing–original draft, Writing–review and editing. AA: Conceptualization, Data curation, Formal Analysis, Funding acquisition, Investigation, Methodology, Project administration, Resources, Software, Supervision, Validation, Visualization, Writing–original draft, Writing–review and editing. RT: Conceptualization, Data curation, Formal Analysis, Funding acquisition, Investigation, Methodology, Project administration, Resources, Software, Supervision, Validation, Visualization, Writing–original draft, Writing–review and editing.

Funding

The author(s) declare that no financial support was received for the research, authorship, and/or publication of this article.

Acknowledgments

We wish to express our highest appreciation and ever-lasting gratitude to Prof. Dr. Adel Shalaby Abdullatif, Professor of Physiology, Faculty of Medicine, Al-Azhar University (Cairo) for his kind supervision, moral support, and great effort in supervising the whole work and in teaching me perseverance and patience. We would also like to extend our great thanks to Dr. Fatima Mohamed Rashed Associated Professor, Department of Basic Medical and Dental Sciences, Faculty of Dentistry, Zarqa University, Jordan for the great effort in reviewing and contacting with the journal during my absence. We would also like to thank Dr. Ahmed Gad Allah, Professor of Physiology, Faculty of Medicine, Al-Azhar University (Assuit) for his continuous efforts in reviewing, supporting, and advising until this work was completed.

Conflict of interest

The authors declare that the research was conducted in the absence of any commercial or financial relationships that could be construed as a potential conflict of interest.

Publisher's note

All claims expressed in this article are solely those of the authors and do not necessarily represent those of their affiliated organizations, or those of the publisher, the editors, and the reviewers. Any product that may be evaluated in this article, or claim that may be made by its manufacturer, is not guaranteed or endorsed by the publisher.

References

Arora, M., Moser, J., Phadke, H., Basha, AA., Basha, A. A., and Spencer, S. L. (2017). Endogenous replication stress in mother cells leads to quiescence of daughter cells. *Cell Rep.* 19 (7), 1351–1364. doi:10.1016/j.celrep.2017.04.055

Akbari, B., Baghaei-Yazdi, N., Bahmaie, M., and Mahdavi Abhari, F. (2022). The role of plant-derived natural antioxidants in reduction of oxidative stress. *Biofactors* 48 (3), 611–633. doi:10.1002/biof.1831

Akbarzadeh, A., Norouzian, D., Mehrabi, M. R., Jamshidi, S., Farhangi, A., Verdi, A. A., et al. (2007). Induction of diabetes by streptozotocin in rats. *Indian J. Clin. biochem.* 22, 60–64. doi:10.1007/BF02913315

Akhone, M. A., Bains, A., Tosif, M. M., Chawla, P., Fogarasi, M., and Fogarasi, S. (2022). Apricot kernel: bioactivity, characterization, applications, and health attributes. *Foods* 11 (15), 2184. doi:10.3390/foods11152184

Alhadi, I. A., Al Ansari, A. M., AlSaleh, A. F. F., and Alabbasi, A. M. A. (2023). Systematic review of the effect of caffeine therapy effect on cardiometabolic markers in rat models of the metabolic syndrome. *BMC Endocr. Disord.* 23 (1), 34. doi:10.1186/s12902-023-01288-4

Alp, H., Sahin, A., Karabagli, P., Karaburgu, S., Yılmaz Sanal, B., Yuksel, E. B., et al. (2023) *Current perspective on diabetes mellitus in clinical sciences*. Nobel Tıp Bookstores, 1–502.

Anwar, H., Hussain, G., and Mustafa, I. (2018). Antioxidants from natural sources. *Antioxidants foods its Appl.*, 3–28. doi:10.5772/intechopen.75961

Arokiasamy, P., Salvi, S., and Selvamani, Y. (2021). "Global burden of diabetes mellitus," in *Canada International Conference on Education (CICE-2010)* (Toronto, OA, Canada: Infonomics Society, World Scientific).

Bidel, S., and Tuomilehto, J. J. E. e. (2013). The emerging health benefits of coffee with an emphasis on type 2 diabetes and cardiovascular disease. *Eur. Endocrinol.* 9 (2), 99–106. doi:10.17925/EE.2013.09.02.99

Blahova, J., Martiniakova, M., Babikova, M., Kovacova, V., Mondockova, V., and Omelka, R. (2021). Pharmaceutical drugs and natural therapeutic products for the treatment of type 2 diabetes mellitus. *Pharmaceuticals* 14 (8), 806. doi:10.3390/ph14080806

Cämmerer, B., and Kroh, L. W. J. E. F. R. (2006). Antioxidant activity of coffee brews. *Eur. Food Res. Technol.* 223, 469–474. doi:10.1007/s00217-005-0226-4

Ceriello, A., Prattichizzo, F., Phillip, M., Hirsch, I. B., Mathieu, C., and Battelino, T. (2022). Glycaemic management in diabetes: old and new approaches. *Lancet Diabetes and Endocrinol.* 10 (1), 75–84. doi:10.1016/S2213-8587(21)00245-X

Dawod, B. K., and Ahmed, M. A. (2021). Evaluation various doses of apricot kernels effect on antioxidant system and hepatic tissue in female albino rats. *Ann. Romanian Soc. Cell Biol.* 25 (6), 1694–1701.

Dawood, D.A.-J., Rasheed, E. M., and Hassan, A. S. (2023). Detection of preptin and megalin in type 2 diabetic patients in baghdad city. *Acta Biomed.* 94. doi:10.62940/als.v10i0.1990

Demirci-Cekic, S., Özkan, G., Avan, A. N., Uzunboy, S., Çapanoğlu, E., and Apak, R. (2022). Biomarkers of oxidative stress and antioxidant defense. *J. Pharm. Biomed. Anal.* 209, 114477. doi:10.1016/j.jpba.2021.114477

Dinda, B., and Dinda, M. (2022). "Natural products, a potential source of new drugs discovery to combat obesity and diabetes: their efficacy and multi-targets actions in treatment of these diseases," in *Natural products in obesity and diabetes* (Germany: Springer), 101–275.

El-Deen, A. E., Taha, A., Fahmy, E. M., and Mansour, A. E. (2024). Effects of oral zinc supplementation in early neonatal live on development of obesity and metabolic syndrome in albino rats. *Dep. Physiology* 12, 1433. doi:10.13040/IJPSR.0975-8232.12(3).1433-41

El-Deen, A.E.-S. N., Mansour, A.E.-M., and Taha, A. (2018). High protein diet that cause weight loss and lower blood glucose level have a serious impact on the kidney functions of male diabetic obese albino rats. *Food Nutr. Sci.* 9 (10), 1174–1191. doi:10.4236/fns.2018.910085

El-Deen, A.E.-S. N., Mansour, A. E. M., Taha, A., and Fahmy, E. M. (2019). Effect of green coffee on cisplatin induced renal apoptosis in adult male albino rats. *Food Nutr. Sci.* 10 (04), 358–368. doi:10.4236/fns.2019.104028

Fratianni, F., Ombra, M. N., d'Acierno, A., Cipriano, L., and Nazzaro, F. (2018). Apricots: biochemistry and functional properties. *Curr. Opin. Food Sci.* 19, 23–29. doi:10.1016/j.cofs.2017.12.006

Fu, Z., Gilbert, E. R., and Liu, D. J. C. d.r. (2013). Regulation of insulin synthesis and secretion and pancreatic Beta-cell dysfunction in diabetes. *Curr. Diabetes Rev.* 9 (1), 25–53. doi:10.2174/15733998130104

Furman, B. L. J. C. p.i.p. (2015). Streptozotocin-induced diabetic models in mice and rats. *Curr. Protoc. Pharmacol.* 70 (1), 5.47. 1–5.47. 20. doi:10.1002/0471141755.ph0547s70

Hadwan, M. H., Khabt, H. J. J. o.C., and Research, D., Simple spectrophotometric method for analysis of serum catalase activity. 2018. 12, doi:10.7860/jcdr/2018/35014.120119).

Hamid, A., Anker, M. S., Ruckdeschel, J. C., Khan, M. S., Tharwani, A., Oshunbade, A. A., et al. (2022). Cardiovascular safety reporting in contemporary breast cancer clinical trials. *J. Am. Heart Assoc.* 11 (15), e025206. doi:10.1161/JAHA.121.025206

Heckman, M. A., Weil, J., and De Mejia, E. G. J. J. o.f.s. (2010). Caffeine (1, 3, 7-trimethylxanthine) in foods: a comprehensive review on consumption, functionality, safety, and regulatory matters. *J. Food Sci.* 75 (3), R77–R87. doi:10.1111/j.1750-3841.2010.01561.x

Huang, H., Zhao, N., Xu, X., Xu, Y., Li, S., Zhang, J., et al. (2011). Dose-specific effects of tumor necrosis factor alpha on osteogenic differentiation of mesenchymal stem cells. *Cell Prolif.* 44 (5), 420–427. doi:10.1111/j.1365-2184.2011.00769.x

Huxley, R., Lee, C. M. Y., Barzi, F., Timmermeister, L., Czernichow, S., Perkovic, V., et al. (2009). Coffee, decaffeinated coffee, and tea consumption in relation to incident type 2 diabetes mellitus: a systematic review with meta-analysis. *Arch. Intern. Med.* 169 (22), 2053–2063. doi:10.1001/archinternmed.2009.439

Jugran, A. K., Rawat, S., Devkota, H. P., Bhatt, I. D., and Rawal, R. S. (2021). Diabetes and plant-derived natural products: from ethnopharmacological approaches to their potential for modern drug discovery and development. *Phytother. Res.* 35 (1), 223–245. doi:10.1002/ptr.6821

Kilari, E. K., Putta, S., and Silakabattini, K. (2020). Effect of gymnema sylvestre on insulin receptor (IR) and proglucagon gene expression in streptozotocin induced diabetic rats. *Indian J. Pharm. Educ. Res.* 54 (2), s277–s284. doi:10.5530/ijper.54.2s.84

Kopčeková, J., Kolesárová, A., Schwarzová, M., Kováčik, A., Mrázová, J., Gažarová, M., et al. (2022). Phytonutrients of bitter apricot seeds modulate human lipid profile and LDL subfractions in adults with elevated cholesterol levels. *Int. J. Environ. Res. Public Health* 19 (2), 857. doi:10.3390/ijerph19020857

Kopčeková, J., Kováčiková, E., Kováčik, A., Kolesárová, A., Mrázová, J., Chlebo, P., et al. (2021). Consumption of bitter apricot seeds affects lipid and endocrine profile in women. *J. Environ. Sci. Health, Part B* 56 (4), 378–386. doi:10.1080/03601234.2021.1890513

Kutlu, T., Durmaz, G., Ates, B., and Erdogan, A. (2009). Protective effect of dietary apricot kernel oil supplementation on cholesterol levels and antioxidant status of liver in hypercholesteremic rats. *J. Food Agric. Environ.* 7, 61–65.

Lima-Cabello, E., Escudero-Feliu, J., Peralta-Leal, A., Garcia-Fernandez, P., Siddique, K. H. M., Singh, K. B., et al. (2023). β-Conglutins' unique mobile arm is a key structural domain involved in molecular nutraceutical properties of narrow-leafed lupin (lupinus angustifolius L.). *Int. J. Mol. Sci.* 24 (8), 7676. doi:10.3390/ijms24087676

Mohamed, D. A., Hamed, I., and Mohammed, S. (2021). Utilization of grape and apricot fruits by-products as cheap source for biologically active compounds for health promotion. *Egypt. J. Chem.* 64 (4), 2–3. doi:10.21608/ejchem.2021.54427.3132

Muley, A., Muley, P., and Shah, M. J. C. (2012). Coffee to reduce risk of type 2 diabetes?a systematic review. *Curr. Diabetes Rev.* 8 (3), 162–168. doi:10.2174/157339912800564016

Mullugeta, Y., Chawla, R., Kebede, T., and Worku, Y. (2012). Dyslipidemia associated with poor glycemic control in type 2 diabetes mellitus and the protective effect of metformin supplementation. *Indian J. Clin. biochem.* 27, 363–369. doi:10.1007/s12291-012-0225-8

Musa, M. J. F., and Sciences, N. (2010). Properties of apricot kernel and oils as fruit juice processing waste. *Food Nutr. Sci.* 1, 31–37. doi:10.4236/fns.2010.12006

Nath, S., Ghosh, S. K., and Choudhury, Y. (2017). A murine model of type 2 diabetes mellitus developed using a combination of high fat diet and multiple low doses of streptozotocin treatment mimics the metabolic characteristics of type 2 diabetes mellitus in humans. *J. Pharmacol. Toxicol. Methods* 84, 20–30. doi:10.1016/j.vascn.2016.10.007

Neves, J. S., Leitão, L., Magriço, R., Bigotte Vieira, M., Viegas Dias, C., Oliveira, A., et al. (2018). Caffeine consumption and mortality in diabetes: an analysis of NHANES 1999–2010. *Front. Endocrinol.* 9, 547. doi:10.3389/fendo.2018.00547

Ohkawa, H., Ohishi, N., and Yagi, K. (1979). Assay for lipid peroxides in animal tissues by thiobarbituric acid reaction. *Anal. Biochem.* 95 (2), 351–358. doi:10.1016/0003-2697(79)90738-3

Ontawong, A., Duangjai, A., Muanprasat, C., Pasachan, T., Pongchaidecha, A., Amornlerdpison, D., et al. (2019). Lipid-lowering effects of Coffea arabica pulp aqueous extract in Caco-2 cells and hypercholesterolemic rats. *Phytomedicine* 52, 187–197. doi:10.1016/j.phymed.2018.06.021

Peng, Y., Zhang, Z., Chen, W., Zhao, S., Pi, Y., and Yue, X. (2023). Structural characterization, α-glucosidase inhibitory activity and antioxidant activity of neutral polysaccharide from apricot (Armeniaca Sibirica L. Lam) kernels. *Int. J. Biol. Macromol.* 238, 124109. doi:10.1016/j.ijbiomac.2023.124109

Rais, N., Ved, A., Ahmad, R., Parveen, K., Gautam, G. K., Bari, D. G., et al. (2022). Model of streptozotocin-nicotinamide Induced Type 2 diabetes: a comparative review. *Curr. Diabetes Rev.* 18 (8), e171121198001–e171121198069. doi:10.2174/1573399818666211117123358

Ramli, N. N. S., Alkhaldy, A. A., and Mhd Jalil, A. M. J. M. (2021). Effects of caffeinated and decaffeinated coffee consumption on metabolic syndrome parameters: a systematic review and meta-analysis of data from randomised controlled trials. *Medicina* 57(9), 957. doi:10.3390/medicina57090957

Rotruck, J., Pope, A. L., Ganther, H. E., Swanson, A. B., Hafeman, D. G., and Hoekstra, W. G. (1973). Selenium: biochemical role as a component of glutathione peroxidase. *Science* 179 (4073), 588–590. doi:10.1126/science.179.4073.588

Sater, K. A., Shalaby, A., Abdel-Hamid, G. E. D., Hassan, A. M., and El-Deen, A. S. N. (2016). Hepatorenal changes by nigella sativa seeds powder in diabetic rats. *Pak. J. Physiology* 12 (2), 3–7.

Shalaby, A., Abd-El-Sater, K., El-Din Abdel-Hamid, G., Mostafa Mahmoud, A., and S. S.Nour El-Deen, A. (2016). Changes in lipid profile, ast, alt, urea, and creatinine by nigella sativa seeds powder in adult male albino diabetic rats. *Al-Azhar Med. J.* 45 (1), 13–22. doi:10.12816/0026262

Shalaby, A., Abd El-Sater, K., El-Din Abdel-Hamid, G., Basma Kamal, R., and Nour El-Deen, A. S. S (2015). Effects of nigella sativa seeds powder in body weight, insulin, C-peptides and blood indices in adult diabetic male rats. *Al-Azhar Med. J.* 44, 4.

Shoaib, A., Salem-Bekhit, M. M., Siddiqui, H. H., Dixit, R. K., Bayomi, M., Khalid, M., et al. (2020). Antidiabetic activity of standardized dried tubers extract of Aconitum napellus in streptozotocin-induced diabetic rats. *3 Biotech.* 10 (2), 56–58. doi:10.1007/s13205-019-2043-7

Sousa, B., Pereira, J., Marques, R., Grilo, L. F., Pereira, S. P., Sardão, V. A., et al. (2020). P-cadherin induces anoikis-resistance of matrix-detached breast cancer cells by promoting pentose phosphate pathway and decreasing oxidative stress. *Biochim. Biophys. Acta. Mol. Basis Dis.* 1866 (12), 165964. doi:10.1016/j.bbadis.2020.165964

Sun, C., Zhao, C., Guven, E. C., Paoli, P., Simal-Gandara, J., Ramkumar, K. M., et al. (2020). Dietary polyphenols as antidiabetic agents: advances and opportunities. *Food Front.* 1 (1), 18–44. doi:10.1002/fft2.15

Szkudelski, T. J. P. r. (2001). The mechanism of alloxan and streptozotocin action in B cells of the rat pancreas. *Physiol. Res.* 50 (6), 537–546.

Tietz, N. (1990) *Clinical guide to laboratory tests*, 554. Philadelphia, USA: WB Saunders Company, 556.

Tsikas, D. J. A. (2017). Assessment of lipid peroxidation by measuring malondialdehyde (MDA) and relatives in biological samples: analytical and biological challenges. *Anal. Biochem.* 524, 13–30. doi:10.1016/j.ab.2016.10.021

Vahedi-Mazdabadi, Y., Karimpour-Razkenari, E., Akbarzadeh, T., Lotfian, H., Toushih, M., Roshanravan, N., et al. (2020). Anti-cholinesterase and neuroprotective activities of sweet and bitter apricot kernels (prunus armeniaca L.). *Iran. J. Pharm. Res.* 19 (4), 216–224. doi:10.22037/ijpr.2019.15514.13139

Vivó-Barrachina, L., Rojas-Chacón, M. J., Navarro-Salazar, R., Belda-Sanchis, V., Pérez-Murillo, J., Peiró-Puig, A., et al. (2022). The role of natural products on diabetes mellitus treatment: a systematic review of randomized controlled trials. *Pharmaceutics* 14 (1), 101. doi:10.3390/pharmaceutics14010101

Zhang, X., Wu, C., Wu, H., Sheng, L., Su, Y., Zhang, X., et al. (2013). Anti-hyperlipidemic effects and potential mechanisms of action of the caffeoylquinic acid-rich Pandanus tectorius fruit extract in hamsters fed a high fat-diet. *PLoS One* 8 (4), e61922. doi:10.1371/journal.pone.0061922

Zibaeenezhad, M. J., Shahamat, M., Mosavat, S. H., Attar, A., and Bahramali, E. (2017). Effect of Amygdalus scoparia kernel oil consumption on lipid profile of the patients with dyslipidemia: a randomized, open-label controlled clinical trial. *Oncotarget* 8 (45), 79636–79641. doi:10.18632/oncotarget.18956

Frontiers in Physiology

Understanding how an organism's components work together to maintain a healthy state

The second most-cited physiology journal, promoting a multidisciplinary approach to the physiology of living systems - from the subcellular and molecular domains to the intact organism and its interaction with the environment.

Discover the latest Research Topics

See more →

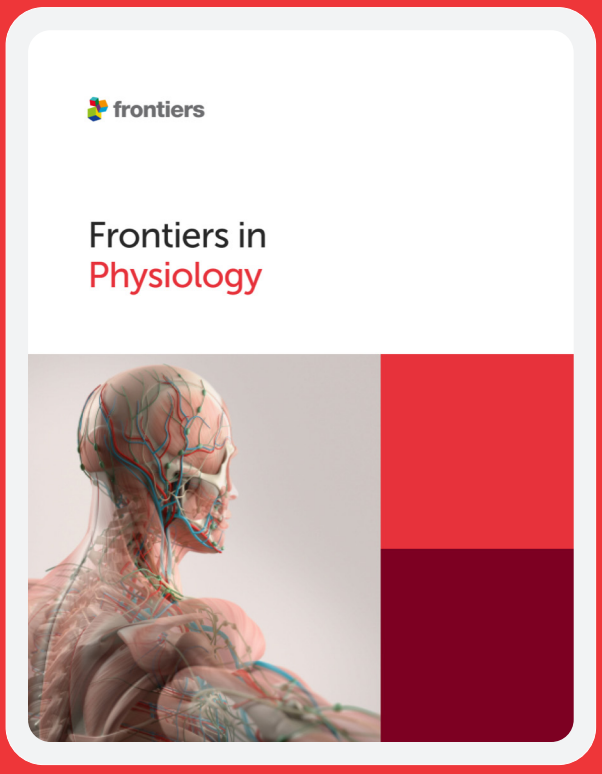

Frontiers

Avenue du Tribunal-Fédéral 34
1005 Lausanne, Switzerland
frontiersin.org

Contact us

+41 (0)21 510 17 00
frontiersin.org/about/contact